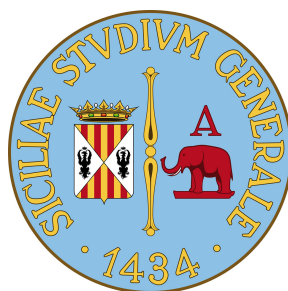


Perturbative methods in non-perturbative Quantum Chromodynamics

Giorgio Comitini

Dissertation presented in partial fulfillment of the requirements for the
degree of Doctor of Physics/Doctor of Science (PhD) in Physics

Supervisors: Prof. Dr. F. Siringo and Prof. Dr. D. Dudal



Department of Physics and Astronomy “E. Majorana”
Università degli Studi di Catania
Italy

KU LEUVEN

Department of Physics and Astronomy, Faculty of Science
KU Leuven – Campus Kortrijk
Belgium

January 2023

A Cinzia

Contents

Abstract	ix
Abstract (Italian)	xi
Abstract (Dutch)	xiii
Introduction	xv
I Quantum Chromodynamics and its infrared regime	1
1 The standard formulation of QCD	3
1.1 Action functionals for QCD and their symmetries	3
1.1.1 The classical action	3
1.1.2 Quantizing QCD: the Faddeev-Popov action	6
1.1.3 The partition function and the quantum effective action	9
1.1.4 BRST symmetry, the Slavnov-Taylor identities and the Nielsen identities	12
1.2 Ordinary perturbation theory, the strong coupling constant and the infrared breakdown of perturbative QCD	19
1.2.1 The standard perturbative expansion and Feynman rules of QCD . .	19
1.2.2 Regularization and renormalization	24
1.2.3 The Renormalization Group, the running coupling constant and the Landau pole	27
2 Non-perturbative techniques and results in Quantum Chromodynamics	33
2.1 Lattice QCD	33
2.1.1 Set-up	33
2.1.2 Results	35
2.2 The Operator Product Expansion	37
2.2.1 Set-up	37
2.2.2 Results	38
2.3 The Gribov-Zwanziger approach	40
2.3.1 Set-up and results	40
2.4 The Curci-Ferrari model	43
2.4.1 Set-up	43
2.4.2 Results	44

II	Massive perturbative models for infrared QCD	47
3	The Screened Massive Expansion	49
3.1	Motivation, definition and first results	51
3.1.1	Dynamical mass generation and perturbation theory: the set-up of the Screened Massive Expansion	51
3.1.2	General properties of the Screened Massive Expansion	55
3.1.3	The ghost propagator	58
3.1.4	The gluon propagator	61
3.2	Optimization of the Screened Massive Expansion	67
3.2.1	The gluon poles and the Nielsen identities in the context of the Screened Massive Expansion	68
3.2.2	The phases of the residues of the gluon propagator: restoring the predictivity of the Screened Massive Expansion in the gluon sector	71
3.2.3	The optimized gluon and ghost propagators	77
3.3	Renormalization Group analysis of the Screened Massive Expansion in the Landau gauge	83
3.3.1	MOM-Taylor-scheme renormalization of the Screened Massive Expansion	84
3.3.2	The SME strong running coupling and RG-improved propagators	87
3.3.3	Intermediate-energy matching with the fixed-scale optimized results and comparison with the lattice data	92
3.4	Conclusions	99
4	Applications of the Screened Massive Expansion	101
4.1	The Screened Massive Expansion at finite temperature	101
4.1.1	The Gaussian Effective Potential at finite temperature and the deconfinement phase transition	101
4.1.2	The Landau-gauge gluon propagator and its poles at finite temperature	104
4.2	The Screened Massive Expansion of full QCD	110
4.2.1	Dynamical mass generation in the quark sector	110
4.2.2	The massive shift of the quark Lagrangian	112
4.2.3	The quark propagator in the Landau gauge	114
4.2.4	Conclusions	120
5	The Dynamical Model	121
5.1	The BRST-invariant quadratic gluon condensate	123
5.1.1	A note on the conventions	123
5.1.2	The field A^h and its quadratic condensate	123
5.1.3	Calculation of the condensate's effective action	125
5.1.4	Dynamical mass generation: the gap equation	131
5.2	Dynamical Model: the propagators in the Landau gauge	133
5.2.1	Renormalization and Feynman rules	133
5.2.2	The gluon and ghost propagators	135
5.2.3	RG improvement of the Dynamical Model in the Dynamically Infrared-Safe scheme	139
5.2.4	Comparison with the lattice data	143
5.3	Conclusions	147
6	Conclusions and outlook	149

Appendices	155
A Canonical quantization of the Faddeev-Popov action	157
B Perturbative decoupling of the determinant $\det(\Lambda(\xi))$ within dimensional regularization in the Dynamical Model	159
C Published papers	163
C.1 G. Comitini and F. Siringo, Phys. Rev. D 97 (2018)	164
C.2 F. Siringo and G. Comitini, Phys. Rev. D 98 (2018)	184
C.3 G. Comitini and F. Siringo, Phys. Rev. D 102 (2020)	202
C.4 F. Siringo and G. Comitini, Phys. Rev. D 103 (2021)	227
C.5 G. Comitini, D. Rizzo, M. Battello, and F. Siringo, Phys. Rev. D 104 (2021)	260
C.6 F. Siringo and G. Comitini, Phys. Rev. D 106 (2022)	288
Bibliography	307
A note on the figures	327
Acknowledgments	329

Abstract

The objective of this thesis is to present two new perturbative frameworks for the study of low-energy Quantum Chromodynamics (QCD), termed the Screened Massive Expansion and the Dynamical Model. Both the frameworks paint a picture of the infrared regime of QCD which is consistent with the current knowledge provided by the lattice calculations and by other non-perturbative methods, displaying dynamical mass generation in the gluon sector and a massless ghost propagator. The Screened Massive Expansion achieves this by operating a shift of the QCD perturbative series, performed by adding a mass term for the transverse gluons in the kinetic part of the Faddeev-Popov Lagrangian and subtracting it back from its interaction part so that the total action remains unchanged. The Dynamical Model, on the other hand, interprets the generation of a dynamical mass for the gluons as being triggered by a non-vanishing condensate of the form $\langle (A^h)^2 \rangle$, where A^h is a gauge- and BRST-invariant non-local version of the gluon field, and explores the consequences of the inclusion of the former in the partition function of the theory. Since the main focus of this thesis is on the gauge sector of QCD, most of our calculations will be carried out in the context of pure Yang-Mills theory. There we will show that the gluon and the ghost propagator derived by making use of the two frameworks are in good agreement with the Euclidean Landau-gauge lattice data, within the limits of a one-loop approximation. During the course of the thesis we will address topics such as the first-principles status of the two methods, the absence of Landau poles from the strong running coupling constant and the extension of the Screened Massive Expansion to finite temperatures and to full QCD. Future research prospects are discussed in the Conclusions.

Abstract (Italian)

L'obiettivo di questa tesi è presentare due nuovi framework perturbativi per lo studio della Cromodinamica Quantistica (QCD) alle basse energie, denominati Sviluppo Perturbativo Massivo (Screened Massive Expansion) e Modello Dinamico (Dynamical Model). Entrambi i framework forniscono un quadro del regime infrarosso della QCD in accordo con le conoscenze attuali ottenute grazie a calcoli su reticolo e ad altri metodi non perturbativi, mostrando generazione dinamica di massa nel settore gluonico e un propagatore ghost non massivo. Lo Sviluppo Perturbativo Massivo perviene a tale risultato attraverso una modifica della serie perturbativa della QCD, operata aggiungendo un termine di massa per i gluoni trasversali nella parte cinetica della Lagrangiana di Faddeev-Popov e sottraendo lo stesso termine dalla parte di interazione, in modo che l'azione totale rimanga inalterata. Il Modello Dinamico, per contro, interpreta la generazione di una massa dinamica per i gluoni come innescata da un condensato non nullo della forma $\langle(A^h)^2\rangle$, dove A^h è una versione non-locale gauge e BRST invariante del campo gluonico, ed esplora le conseguenze della sua introduzione nella funzione di partizione della teoria. Poiché il focus di questa tesi è sul settore di gauge della QCD, la maggior parte dei nostri calcoli saranno condotti nel contesto della teoria di Yang-Mills pura. In esso mostreremo che i propagatori gluonico e ghost derivati nell'ambito dei due framework sono in buon accordo con i dati euclidei sul reticolo nella gauge di Landau, entro i limiti di un'approssimazione a one loop. Nel corso della tesi affronteremo argomenti quali lo status da principi primi dei due metodi, l'assenza di poli di Landau nella costante di accoppiamento forte e l'estensione dello Sviluppo Perturbativo Massivo a temperature finite e alla QCD completa. Nelle Conclusioni verranno discusse alcune prospettive di ricerca future.

Abstract (Dutch)

Het doel van deze thesis is om 2 nieuwe perturbatieve raamwerken voor te stellen om lage energie Kwantumchromodynamica (QCD) te bestuderen: de Gescreende Massieve Expansie (Screened Massive Expansion) en het Dynamisch Model (Dynamical Model). Beide raamwerken schetsen een beeld van het infrarood regime van QCD dat consistent is met onze huidige kennis zoals aangeleverd door roostersimulaties en andere niet-perturbatieve methodes: dynamische massageneratie in de gluonsector en een massaloos spookdeeltje. De Gescreende Massieve Expansie bekommt dit door een gepaste shift van de QCD perturbatiereeks, meerbepaald door een nieuwe massaterm toe te voegen in de kinetische term voor de transversale gluonenn op het niveau van de Faddeev Popov Lagrangiaan, waarbij deze nieuwe term dan weer wordt afgetrokken in het interactiegedeelte. Daardoor blijft de totale actie wel onveranderd. Het Dynamisch Model daarentegen bekommt een gluonmassageneratie als een gevolg van een niet-verdwijvend massacondensaat van de vorm $\langle(A^h)^2\rangle$, waarbij A^h een ijk- en BRST-invariante niet-lokale versie van het gluonveld is. Verschillende niet-triviale consequenties van het toevoegen van deze laatste aan de partitiefunctie van de theorie worden uitvoerig besproken. Vermits het hoofddoel van deze thesis de ijksector van QCD is, zullen we de meeste berekeningen in de context van pure ijktheorieën uitvoeren. We zullen daarbij aantonen dat de gluon- en spookpropagator, zoals deze kunnen bepaald worden vanuit beide raamwerken, in goede overeenkomst zijn met de Euclidische Landau-ijk roosterdata en dat binnen de beperkingen van een één-lus benadering. In de loop van de thesis zullen we verschillende onderwerpen bespreken zoals daar zijn de ab initio status van beide methodieken, het ontbreken van een Landau-pool in de sterke koppelingsconstante en de veralgemening van de Gescreende Massieve Expansie naar eindige temperatuur en naar volledige QCD. Toekomstige onderzoeksuitbreidingen bespreken we tenslotte in de Conclusies.

Introduction

Quantum Chromodynamics as the theory of the strong interactions

Quantum Chromodynamics was born in 1973 with the publication of three seminal papers by D. J. Gross and F. Wilczek [GW73], H. D. Politzer [Pol73], and H. Fritzsch, M. Gell-Mann and H. Leutwyler [FGML73]. During the late '60s and early '70s, evidence had begun accumulating [Pan68, BCD⁺69, BFK⁺69, Tay69, MP71, FK72, MBB⁺72, Per72, BBB⁺75] that the *quarks*, fermionic degrees of freedom originally devised as a mathematically convenient tool for explaining the observed hadron spectrum [GM61, Ne'61, Gre64, HN65, GM64, Zwe64a, Zwe64b], might have more physical significance than was initially attributed to them. Experiments on deep inelastic electron-proton scattering carried out at SLAC [Pan68, BCD⁺69, BFK⁺69, Tay69, FK72, MBB⁺72], together with later experiments on neutrinos [MP71, Per72, BBB⁺75], painted a picture of the nucleon structure which was in general agreement with the theoretical predictions obtained by J. D. Bjorken, R. P. Feynman and others [Bjo69, BP69, Fey69a, Fey69b] using the *parton* model. The latter regarded the nucleons as loosely bound conglomerates of more elementary components – the partons – unable to exchange large momenta via their reciprocal non-electromagnetic interactions.

While the scientific community started to get accustomed with the idea that the quarks might in fact exist as elementary particles, the proponents of the quark model maintained a more abstract, algebraic point of view [FGM71, FGM72]. The reason for this was the complete lack of evidence for the existence of free quarks, combined with the fact that no explanation had yet been given for the curious “switching-off” of the strong interactions at large momentum transfers. It is in this spirit of abstraction that in 1973 Fritzsch, Gell-Mann and Leutwyler advocated that the strong interactions inside the hadrons could be modeled by an octet of massless *gluon* fields carrying color charge [FGML73]. In their paper, they argued that the coloredness of the gluons – along with the established postulate that any physical state be colorless – might explain why the gluons were not observed as free particles, just like the quarks were not. This property of the strong interactions is today known as *confinement*. The color octet gluon picture would also lead to other physically meaningful consequences, such as the fact that quark-antiquark bound pairs are preferably created in colorless states (in compliance with the aforementioned principle of color-neutrality for physical states) and the existence of eight instead of nine massless pseudoscalar mesons in the limit of zero mass for the constituent quarks. These would be the charged and neutral pions and kaons plus the lighter neutral eta meson, if nature had not decided to go its own way and provide the quarks with a mass.

In the meantime, the solution to the problem of the switching-off of the strong interactions at high energies had been given by Gross and Wilczek and Politzer [GW73, Pol73]. Using the Renormalization Group (RG) approach of Gell-Mann, F. E. Low, C. G. Callan

and K. Symanzik [GML54, Cal70, Sym70], Gross, Wilczek and Politzer showed that the non-abelian gauge theory formulated by C. N. Yang and R. Mills in 1954 [YM54] possesses the property of *asymptotic freedom*: in the limit of high energies – provided that the number of fermions coupled to the gauge bosons is not too large – the running coupling constant of the Yang-Mills (YM) theory tends to zero, thus making the theory effectively free at sufficiently large energies. In particular, modeling the strong interactions as a Yang-Mills theory with gauge group $SU(3)$ – in which the gluons were to be identified with the massless (color-charged) gauge bosons – would be sufficient to explain the success that the parton model had in describing the scaling properties exhibited by the deep inelastic scattering cross-sections. Such an approach also predicted violations to scaling, which would be subsequently observed in the experiments [BDD⁺78, dGHH⁺79a, dGHH⁺79b, dGHH⁺79c].

With the theoretical machinery in place for turning ideas into numbers, the following years were spent verifying the hypothesis that Quantum Chromodynamics was the right theory of the strong interactions. By 1975, little doubt was left that quarks were true dynamical degrees of freedom of the hadrons. In addition to the deep inelastic scattering data, this was confirmed by the first measurements of the hadronic cross-section in e^+e^- collisions [Ric74, SBB⁺75] and by the discovery of 2-jet events at SLAC [HAB⁺75]. The latter were interpreted as the product of the hadronization of a quark-antiquark pair, created by a single virtual photon in the process $e^+e^- \rightarrow (\gamma) \rightarrow q\bar{q} \rightarrow 2 \text{ jets}$.

The discovery of the gluon, on the other hand, had to wait until the end of the decade. The first indirect evidence for the existence of the gluon had been obtained in 1970-1971 by measuring the structure function of the nucleons [LS70, KW71, LS71]. Then it was observed that the quarks and antiquarks inside the nucleons did not exhaust the momentum sum rules of the structure functions, which would therefore also need to receive contributions from flavorless partons yet to be seen. The obvious candidate for the fulfillment of the sum rules was, of course, the gluon. Conclusive proof of its existence, however, only came in 1979, when four different collaborations – MARK-J, JADE, PLUTO and TASSO – working at the PETRA electron-positron collider detected the occurrence of 3-jet events in the hadronic channel of e^+e^- annihilation [BBB⁺79, BBG⁺79, BGG⁺79, BCD⁺80]. Since the quarks were fermions, the third jet in the event could not possibly stem from the hadronization of a quark. Instead, it had to originate from a boson. Interpreting the third jet as due to gluon bremsstrahlung in the QED/QCD process $e^+e^- \rightarrow (\gamma) \rightarrow q\bar{q}g \rightarrow 3 \text{ jets}$ was sufficient (albeit far from trivial in terms of the model employed for jet formation) to match the experimental data on the cross section of the channel and on the momentum distribution of the decay products. Soon enough, analyses of the angular distribution of the three jets confirmed the spin-1 nature of the gluon [BBG⁺80, BCF⁺80, BGG⁺80].

Since the '60s and '70s, the amount of evidence in favor of QCD being the true theory of the strong interactions has multiplied to the point that nobody today questions the validity of the model. From a mathematical perspective, QCD is a non-abelian gauge theory of Yang-Mills type with gauge group $SU(3)$. The global charges associated to the local $SU(3)$ symmetry are identified with the color charge carried by the gluons and quarks, the latter taken to be Dirac fields living in the fundamental representation of the gauge group.

Thanks to the asymptotic freedom typical of non-abelian gauge theories, the high-energy regime of QCD has been tested to an astonishing degree of precision using ordinary methods of perturbation theory. Theoretical results have been derived up to fifth order in the strong coupling constant α_s [vRVL97, Cza05, LMMS16, BCK17, CFHV17, HRU⁺17], and the fundamental parameters of the theory – that is, the coupling constant itself and the quark masses – have been measured extensively [HRZ22, LMQ22, MLB22].

Unfortunately, the other side of the coin of ultraviolet (UV) asymptotic freedom is the unbounded increase of the value of the strong coupling the infrared (IR). Since the beta-function coefficients computed in perturbative QCD (pQCD) turn out to be negative up to the current reaches of the perturbative calculations [HRU⁺17], perturbation theory predicts that, at low energies, the strong coupling constant grows to infinity at a finite, non-zero scale, thus developing an *infrared Landau pole*. While a strongly-coupled IR regime is perfectly consistent with the experimental observations, the fact that pQCD – whose applicability rests precisely on the smallness of α_s – yields an infinite IR coupling marks the breakdown of the method at low energies. In particular, the existence itself of the Landau pole cannot be trusted, being derived in a domain in which the assumptions of perturbation theory are invalid.

In order to extract predictions from low-energy QCD, one has to resort to *non-perturbative* methods, the most common of which are lattice QCD, the Dyson-Schwinger Equations and the Operator Product Expansion and Gribov-Zwanziger approaches. In the next section we will give a brief introduction to these techniques.

Non-perturbative methods in Quantum Chromodynamics

The term “non-perturbative”, in general, can be understood to have two meanings. First of all, it can mean *methodologically* non-perturbative – that is, not making use of any form of perturbative expansion. Second, it can mean *intrinsically* non-perturbative – i.e., able to incorporate features which cannot be described at any finite order in ordinary perturbation theory. Needless to say, calculational techniques which are methodologically non-perturbative are usually employed to study features of the theory which are intrinsically non-perturbative. Broadly speaking, lattice QCD and the Dyson-Schwinger equation approach are methodologically non-perturbative techniques, whereas the Operator Product Expansion and Gribov-Zwanziger approaches are intrinsically non-perturbative techniques.

In lattice QCD (LQCD) [Cre85, IM97, DD06, GL10, LM15, HSL22], the fundamental fields of the theory – that is, the gluon and quark fields – are defined on a discrete lattice of finite volume. Ordinary (continuum) QCD is then recovered by extrapolating the lattice results towards the limit of zero lattice spacing and infinite volume. Since the number of sites in the lattice is finite, the number of degrees of freedom of LQCD is also finite. As a result, the Green functions of the theory can be computed numerically by averaging over the values of finitely many variables.

For a typical state-of-the-art lattice calculation, the number of lattice sites can be as large as $128^4 \sim 3 \cdot 10^8$. Since the gluon has 4×8 degrees of freedom per site, while a single quark has 4, performing a LQCD calculation requires to evaluate integrals with as many as $\sim 10^{10}$ variables of integration. Clearly, this can only be done on extremely powerful supercomputers using Monte Carlo techniques.

In the intermediate- to high-energy regime, LQCD provides us with an independent determination of the values of the strong coupling constant α_s [ABC⁺22, HRZ22] and of the quark masses [ABC⁺22, MLB22] which is in excellent agreement with the results of perturbation theory. At low energy, amongst the most notable achievements of the lattice approach, we mention the calculation of the decay constants of the pseudoscalar mesons [BBB⁺15, FIK⁺15, CDK⁺16, GLT⁺18, DCMG⁺19, ABC⁺22, RSVdW22] – which, in addition to being significant in its own right, is also essential for measuring the elements of the Cabibbo-Kobayashi-Maskawa (CKM) quark-mixing matrix [CLS22] – and the (partial) determination of the hadron spectrum [ABD⁺04, DFF⁺08, AII⁺09, BTB⁺10,

CDI⁺10, LLOWL10, BBG⁺11, BDDP⁺11, DEJ⁺11, GDK⁺11, MW11, BnLB12, DDHH12, GIRM12, MOU13, NAI⁺13, ADJ⁺14, BDMO14, PEMP14, PRCB15, AK17, DKL⁺19, ADK22]. The fact that the lattice calculations are able to predict the lighter hadron masses within an error of a few percent from their experimentally measured values is arguably the most compelling proof that QCD truly provides a complete description of the strong interactions, from the TeV scales reached at the hadron colliders, down to the MeV scales typical of low-energy hadronic processes.

In contrast to lattice QCD, the Gribov-Zwanziger (GZ) approach is a continuum method whose main concern is to address the existence of *Gribov copies* in the configurations of the gluon field. In order to fully contextualize the method, we must first take a step back and discuss some of the issues that arise when quantizing a gauge theory.

The local gauge invariance that characterizes the theories like QCD causes some of the degrees of freedom of theory to be redundant, in the sense that field configurations which are related to one another via a gauge transformation describe the very same underlying physics. In order to extract physical predictions from a gauge theory, one must first dispose of such a redundancy by *fixing a gauge* – that is, by choosing a gauge in which to carry out the calculations.

In continuum quantum field theories, the gauge is usually fixed by employing a procedure devised by L. D. Faddeev and V. Popov (FP) [FP67]. The FP procedure consists in integrating out the redundant degrees of freedom from the partition function of the theory while introducing fictitious *ghost fields* whose role is to remove any leftover unphysical contribution from the computed gauge-invariant quantities. The resulting FP action is no longer gauge invariant, but possesses instead a fermionic global symmetry known as BRST symmetry from the names of their discoverers, C. Becchi, A. Rouet and R. Stora [BRS75, BRS76] and I. V. Tyutin [Tyu75]. Being realized through global transformations, BRST symmetry does not pose any obstacle to the proper calculation of physical quantities. On the contrary, it is nowadays used as the customary starting point for proving a large number of properties of the gauge theories, such as their perturbative renormalizability [Wei96].

In 1978, V. N. Gribov [Gri78] observed that, at the non-perturbative level, the FP procedure fails to fully fix the gauge of the non-abelian theories due to the existence of zero modes of the so-called *Faddeev-Popov operator* $-\partial^\mu D_\mu$ [FP67]. These zero modes can be used to construct gauge transformations which relate distinct field configurations of the FP partition function – the Gribov copies – to one another. As a result, the FP procedure is invalidated.

In order to solve this issue, Gribov proposed to restrict the Faddeev-Popov partition function to the configurations belonging to the domain since known as the *Gribov region* [Gri78], defined by the requirement that their associated Faddeev-Popov operator be positive. A local and renormalizable action capable of implementing the Gribov constraint was discovered in 1989 by D. Zwanziger [Zwa89], paving the way for the systematic study of the gauge sector of QCD under the lens of the Gribov hypothesis.

Since the eigenvalues of the Faddeev-Popov operator are strictly positive for small enough values of the gauge fields, the Gribov copies have no effect on the perturbative (UV) regime of QCD. In the deep infrared, on the other hand, the restriction of the fields to the Gribov region turns out to considerably alter the dynamics of the gluons: in [Gri78, Zwa89] it was shown that, within the GZ approach, instead of growing to infinity as is typical of massless fields, the zero-order gluon propagator vanishes at zero momentum.

Nowadays, thanks to relatively recent lattice calculations, a consensus has been reached that the IR behavior displayed by the standard GZ gluon propagator is not the correct one (we shall have more to say on this topic in the following section). Nonetheless, extensions of the GZ framework that take into account the non-perturbative effects brought by the *vacuum condensates*, like the Refined Gribov-Zwanziger approach of [DGS⁺08, DSVV08, DOV10, DSV11], do manage to reproduce the exact low-energy dynamics of the theory. These extensions shed light on key aspects of QCD such as the analytical structure of the propagators, and provide us with important benchmarks for the quantitative study of its infrared regime.

Vacuum condensates – that is, vacuum expectation values of products of operators evaluated at the same spacetime point – play a central role in the approach known as the Operator Product Expansion (OPE). First proposed by K. G. Wilson in 1969 [Wil69] and put on firm mathematical grounds by W. Zimmermann in 1970 [Zim70], the OPE allows us to compute the first non-perturbative corrections to the behavior of the Green functions due to the non-vanishing of the condensates. Such corrections have been calculated for quantities like the strong coupling constant α_s , the heavy quark-antiquark effective potential and numerous cross-sections – see e.g. [PS95, IFL10] for an overview.

While strictly valid only at intermediate- to high-energy scales, the OPE can be used at all scales as a tool to prove that terms which – often for dimensional reasons – would be forbidden to enter the perturbative series of a Green function can nonetheless emerge from non-perturbative contributions. A classic example of this is the appearance of a mass term in the quark propagator due to the non-vanishing of the quark condensate $\langle \bar{\psi}\psi \rangle$ even in the limit of zero quark mass, where such a term could never arise by plain perturbation theory.

Within the functional approach to the quantization of the field theories, it is possible to derive integral equations that describe the exact behavior of the n -point Green functions in terms of higher-point Green functions. Such equations are known as the Dyson-Schwinger Equations (DSE) from the names of their discoverers, F. J. Dyson and J. Schwinger [Dys49, Sch51], and are customarily used to investigate the non-perturbative behavior of QCD.

In order to solve the DSE, one has to truncate the infinite tower of equations by making assumptions on the form of the higher-point Green functions. A solution is then searched for in a self-consistent way, by improving the accuracy of the approximation step-by-step in the calculation until convergence is achieved.

One specific instance of a DSE, the Bethe-Salpeter equation [SB51], is the standard tool for the study of bound states in relativistic quantum field theory.

Lattice QCD, the Schwinger-Dyson Equations and the Gribov-Zwanziger approach all predict that, in the deep infrared, the dynamics of the gluons is substantially different from what is expected from the calculations carried out in ordinary perturbation theory. The low-energy behavior of the gluons in Quantum Chromodynamics is the subject of the next section.

The mass of the gluon

While at high energies the experimental observations are consistent with the ordinary perturbative picture of gluons as massless particles, it has been suggested in the literature that a non-vanishing gluon mass could help explain some of the data gathered on the

low energy behavior of QCD. Studies have been carried out on processes such as the decay and formation of the pseudoscalar and vector mesons [PP80, JA90, CF94, LW96, CF97, MN00, Fie02, Nat09], e^+e^- annihilation into hadrons [Fie94, LW96] and pp and $p\bar{p}$ scattering [HKN93, LMM⁺05, Nat09], all of which show that the IR data are better fitted by assuming that the gluon possesses a mass in the range ≈ 500 -1000 MeV. The gluon mass was included in the theoretical predictions by making use of a multitude of techniques, ranging from the calculation of phase-space effects [PP80, CF94, LW96, CF97, MN00, Fie02], to the implementation of the solutions of the Dyson-Schwinger Equations [Nat09], to the calculation of non-perturbative corrections due to the quadratic $\langle F^2 \rangle$ gluon condensate [JA90, LW96] which in papers such as [Cor82] were linked to dynamical mass generation in the gluon sector.

At the turn of the century, numerical simulations performed on larger and larger lattices [LSWP98a, LSWP98b, BBLW00, BBL⁺01] made it possible to explore the deep infrared regime of pure Yang-Mills theory – that is, QCD in the absence of quarks. The lattice data clearly showed that, in the limit of vanishing momentum, the gluon propagator does not grow to infinity as would be expected from a massless field, but saturates instead to a finite, non-zero value, just like the propagator of a massive particle. This was not completely unexpected, as approaches like that of Gribov and Zwanziger [Gri78, Zwa89] or the discovery of the so-called *scaling* solutions of the Dyson-Schwinger Equations [vSHA97, AB98] had already pointed out that non-perturbative effects could lead to the strong suppression of the gluon propagator in the IR; moreover, the possibility that the gluons might acquire a mass due to the strong interactions had already been investigated in studies such as [Cor82] and in some of the previously mentioned phenomenological analyses. Nonetheless, the results of the lattice calculations marked a turning point in the field of low-energy QCD both by providing the first clear evidence of the occurrence of dynamical mass generation for the gluons and by revealing that the zero-momentum limit of the gluon propagator is in fact finite, instead of vanishing, as had been predicted within the GZ and DSE frameworks. The massiveness and the zero-momentum finiteness of the gluon propagator have since been confirmed by a number of lattice studies carried out both in pure Yang-Mills theory [SIMPS05, CM08, BIMPS09, ISI09, BMMP10, BLLY⁺12, OS12, BBC⁺15, DOS16] and in full QCD [BHL⁺04, BHL⁺07, IMPS⁺07, SO10, ABB⁺12], and by the discovery of the so-called *decoupling* solutions of the DSE [AN04, AP06, ABP08, AP08, HvS13], to the point that, today, they are regarded as established facts by the low-energy QCD community.

The occurrence of dynamical mass generation (DMG) in the gluon sector of QCD has far-reaching implications both on the phenomenology and on the theoretical investigation of the strong interactions in the infrared regime. From a phenomenological perspective, as shown e.g. by the aforementioned [PP80, JA90, HKN93, CF94, Fie94, LW96, CF97, MN00, Fie02, LMM⁺05, Nat09], it is clear that a non-vanishing gluon mass does indeed affect the outcome of the experiments carried out at low energies. Nonetheless, we should remark that the relation of the lattice/DSE findings to the empirical data is far from clear at present: since the gluon propagator is a gauge-dependent quantity which must necessarily enter the physical predictions in a gauge-invariant way, it is not straightforward to spell out the influence of the saturation of the propagator on the QCD observables in the absence of a complete theory of the gluon mass.

From a theoretical perspective, on the other hand, dynamical mass generation is crucial to our understanding of the strong interactions, given that ordinary perturbation theory forbids the gluons to acquire a mass to any finite order in the coupling constant: it can be shown that the radiative corrections to the zero-momentum limit of the

gluon propagator vanish in pQCD, so that a singular gluon polarization *à la* Schwinger [Sch62a, Sch62b, ABP16, ADSF⁺22] yielding a finite propagator can never be obtained by ordinary perturbative methods. Of course, it could be argued that, since pQCD breaks down in the infrared regime, it makes little sense to try to extract predictions on the low-energy behavior of the strong interactions by making use of perturbation theory. And indeed, we will see that the issue of gluon DMG and that of the formation of a Landau pole in the strong coupling constant are deeply related, to the extent that succeeding in describing the first also manages to solve the second. Nonetheless, the fact remains that the failure of standard pQCD to account for DMG in the gluon sector leaves us with little to no fully analytical tools to explore the correct low-energy limit of QCD starting from its ordinary formulation, and creates the need to look for alternative computational methods.

At the beginning of the last decade, M. Tissier and N. Wschebor [TW10, TW11] showed that, by adding a mass term for the gluons in the Landau-gauge Faddeev-Popov Lagrangian of pure Yang-Mills theory, one could perturbatively derive a gluon and a ghost propagator that accurately reproduced the infrared lattice data already to one loop, while yielding a strong coupling constant with no Landau poles. Since the gluon mass term breaks the BRST invariance of the FP action¹, their *Curci-Ferrari (CF) model* – so named after its original proponents G. Curci and R. Ferrari [CF76] – was to be regarded as an effective description of the strong interactions. Following the publication of [TW10, TW11], the CF model was used to compute the three-point gauge vertices [PTW13], extended to full QCD [PTW14, PTW15, PRS⁺17, RSTT17, PRS⁺21a] and to finite temperatures [RSTW14, RST15, RSTW15a, RSTW15b, RSTW16], worked out to two loops [GPRT19, BPRW20, BGPR21] and employed to study the analytical structure of the propagators [HK19, HK20] – see also [RSTW17, PRS⁺21b]. In all cases, the CF technique provided essential insights both into the viability of perturbative techniques in Quantum Chromodynamics and into the IR behavior of QCD itself. The results obtained by making use of the model showed a remarkable agreement with the available lattice data, which only improved by going to higher order in perturbation theory.

The success of the Curci-Ferrari model in describing the low-energy regime of the strong interactions suggested that treating the gluons as massive at tree level could be sufficient to restore the validity of perturbation theory in the infrared, yielding a perturbative series that correctly displays dynamical mass generation in the gluon sector while at the same time remaining self-consistent thanks to the absence of Landau poles in the coupling constant. This suggestion prompted the research of further perturbative techniques by which a gluon mass term could be introduced in the expansion of the Green functions, without however changing the content of the Faddeev-Popov Lagrangian. The Screened Massive Expansion and the Dynamical Model are two examples of such techniques.

Massive perturbative formulations of Quantum Chromodynamics and the outline of this thesis

The objective of this thesis is to present the main results obtained by making use of two new perturbative frameworks for Quantum Chromodynamics, termed the Screened Massive Expansion and the Dynamical Model. In this section we give a brief overview of the two methods and of the contents of the thesis.

¹Although the action still possesses a generalized, non-nilpotent BRST symmetry that can be exploited to prove the renormalizability of the corresponding quantum theory – see [CF76].

The Screened Massive Expansion (SME) was formulated in 2015 by F. Siringo [Sir15a, Sir15b, Sir16b] in the context of pure Yang-Mills theory with the aim of providing a massive perturbation theory for QCD *à la* Curci-Ferrari without modifying the overall Faddeev-Popov action. This was achieved by adding a transverse mass term for the gluons in the kinetic part of the Lagrangian and subtracting it back from its interaction part, so that the transverse gluons would propagate as massive at order zero in the perturbative expansion while preserving the total action of the theory. As a result of the subtraction of the mass term from the interaction Lagrangian, a new two-point interaction vertex – termed the *gluon mass counterterm* – must be included in the Feynman rules of the expansion, giving rise to new Feynman diagrams which are not present in the perturbative series of the Curci-Ferrari model. To any order in the gluon mass counterterm, these diagrams can be shown to be equal to derivatives of corresponding Curci-Ferrari diagrams with respect to the gluon mass parameter. When all the new diagrams are resummed, the ordinary, massless perturbative series of QCD is recovered, proving that the SME is indeed perturbatively equivalent to pQCD. For obvious reasons, such a resummation is not performed in practice.

The Screened Massive Expansion neglects the existence of Gribov copies in the configuration space of QCD. The rationale for this is that the massiveness of the gluon – which is already taken care of by the SME – suppresses the large field configurations, so that the dynamical effects of the copies are expected to be suppressed not only in the UV – where the SME reproduces the results of ordinary perturbation theory – but also in the IR.

The gluon and ghost propagators computed within the SME are found to be in excellent agreement with the lattice data already at one loop [Sir15a, Sir15b, Sir16b, Sir17d], displaying mass generation in the gluon sector. Within the SME, the latter occurs in a non-trivial way: the tree-level mass term introduced in the gluon propagator by shifting the expansion point of perturbation theory cancels with an opposite term in the gluon polarization, so that the gluon mass only survives inside the loops of the expansion. In other words, the saturation of the gluon propagator at zero momentum is a truly dynamical effect of the interactions.

The SME was extended to the chiral limit of full QCD and used to study the analytic structure of the propagators in [Sir16b, Sir17a, Sir17b]. There it was shown that the one-loop gluon propagators possesses a pair of complex-conjugate poles and a spectral function which violates the positivity conditions that must hold for physical particles. This can be interpreted as evidence for gluon confinement. In the quark sector, an analogous finding was made for the quark spectral functions, pointing to quark confinement, but a single real quark pole was observed instead. Recent calculations, first presented in [CRBS21] and carried out with the aid of more accurate lattice data, show that, on the contrary, the poles of the quark propagator are actually complex conjugate like in the gluon sector. The quark mass functions computed in [CRBS21] turn out to be in very good agreement with the lattice, whereas the quark Z -functions display the wrong behavior due to the limitations of the one-loop approximation.

In [Sir17c, SC21] the Screened Massive Expansion of pure Yang-Mills theory was extended to non-zero temperatures with the aim of studying the temperature-dependence of the gluon propagator and of deriving dispersion relations for the gluon quasi-particles. A comparison with the lattice data yielded good results in the (spatially) transverse sector and mixed results in the (spatially) longitudinal sector, the latter accounted for by the fact that a 4-dimensionally transverse gluon mass term for the gluons might be sub-optimal at high temperatures. The finite-temperature behavior of YM theory was

also investigated under the lens of the Gaussian Effective Potential in [CS18], where it was shown that a discontinuity in the optimal value of the SME gluon mass parameter produces a corresponding discontinuity in the entropy density, marking the occurrence of the deconfinement phase transition.

The topic of the predictiveness of the Screened Massive Expansion was addressed in [SC18], where an optimization procedure based on the Nielsen identities – see also [SC22b] – was formulated with the aim of reducing the number of free parameters of the expansion. By enforcing the gauge-parameter independence of the position of the poles and of the phases of the residues of the gluon propagator, it was possible to obtain an expression for the propagator which – modulo multiplicative renormalization – only depends on the value of the gluon mass parameter. When compared to the lattice results, it was found that the optimized propagator was indistinguishable from one obtained by a full fit of the lattice data, thus demonstrating the soundness of the method. The optimization of the two-point sector of pure Yang-Mills theory was completed in [Sir19a, Sir19b] with the determination of the parameters of the ghost propagator. The results of [SC18] were used as a starting point for the studies carried out in [CRBS21, SC21].

In [CS20] the one-loop pure Yang-Mills gluon and ghost propagators were improved by making use of Renormalization Group methods. For not-too-large initial values of the coupling constant, the Taylor-scheme running coupling was shown to be free of Landau poles and to remain moderately small at all energy scales, thus confirming that the SME is self-consistent in the infrared. As in most massive models of QCD, the finiteness of the coupling is made possible by the fact that the gluon mass parameter provides the beta function with a scale at which the RG flow is allowed to slow down. While the RG-improved propagators display a good agreement with the lattice data at intermediate- to high-energy energy scales, essentially reducing to their ordinary pQCD analogues in the deep UV, the SME running coupling turns out to be too large at its maximum for the one-loop approximation to be sufficiently accurate in the deep IR, below momenta of approximately 500 MeV. At such low energies, the optimized fixed-scale results of [SC18] still constitute our best estimate of the behavior of the Yang-Mills propagators.

While the Screened Massive Expansion does not explicitly address the origin of the gluon mass, the Dynamical Model (DM) – born from studies carried out in the framework of the Gribov-Zwanziger approach [CDF⁺15, CDF⁺16a, CDF⁺16b, CDP⁺17, CFPS17, CDG⁺18, MPPS19, DFP⁺19] –, advances the hypothesis that dynamical mass generation might be triggered by a non-vanishing BRST-invariant quadratic gluon condensate of the form $\langle (A^h)^2 \rangle$, where A^h is a gauge-invariant version of the gluon field A . The formation of such a condensate can be proved to be energetically favored in pure Yang-Mills theory by making use of Local Composite Operator methods, which allow us to include the operator $(A^h)^2$ in the Faddeev-Popov Lagrangian from first principles, without changing the physical content of the theory. An effective potential for the condensate can then be derived and minimized to provide the on-shell value of $\langle (A^h)^2 \rangle$, which is found to be different from zero.

In the process of deriving the effective potential, successive transformations of the Faddeev-Popov action yield a new action I in which the condensate is coupled to the quadratic operator $(A^h)^2$. Since to lowest order in perturbation theory $(A^h)^2$ reduces to the square A^2 of the gluon field, the non-vanishing condensate generates a mass term for the gluons, with a mass parameter proportional to the condensate itself. We remark that the action I and the Faddeev-Popov action are dynamically equivalent on the shell of the gap equation – that is, on the minima of the effective potential. I is taken to be the

defining action of the Dynamical Model.

The renormalizability of the Dynamical Model was proved in [CFG⁺16, CvEP⁺18]. The first preliminary results on the DM gluon and ghost propagators in the Landau gauge, on the other hand, were obtained in [DM20], where it was shown that the propagators have the same expressions as in the Curci-Ferrari model, with the notable exception that the tree-level mass term in the gluon propagator disappears once the gap equation is enforced. This feature shows that the description of the IR dynamics of Yang-Mills theory provided by the DM lies somewhere in between the Curci-Ferrari model and the Screened Massive Expansion. Like in the latter, DMG in the Dynamical Model is a result of the radiative corrections brought by the interactions alone.

A new renormalization scheme for the RG analysis of the Dynamical Model in the Landau gauge, termed the Dynamically Infrared-Safe (DIS) scheme, is presented in this thesis. Within the DIS scheme, it is possible to derive a finite running coupling and one-loop RG-improved propagators which display a very good agreement with the lattice data over a wide range of momenta, only failing below approximately 500 MeV just like in the SME.

As a final note, we should mention that the Dynamical Model was recently extended to finite temperature in [DvERV22] with the aim of probing the deconfinement transition of pure Yang-Mills theory.

In this thesis we will give a theoretical overview of the Screened Massive Expansion and of the Dynamical Model and present the main results that have been obtained within the two frameworks. In detail, its contents are as follows. In Chapter 1 we review the formalism of Quantum Chromodynamics and its ordinary perturbative formulation and discuss the breakdown of the latter in the infrared. In Chapter 2 we review some of the non-perturbative results obtained by lattice QCD, the Operator Product Expansion and Gribov-Zwanziger approaches and the Curci-Ferrari model, upon which we will rely during the rest of the thesis. In Chapter 3 we discuss the set-up of the Screened Massive Expansion of pure Yang-Mills theory, report explicit expressions for the one-loop gluon and ghost SME propagators, describe the optimization procedure by which the spurious free parameters of the expansion are fixed from principles of gauge invariance and perform the RG improvement of the propagators. In Chapter 4 we present two applications of the Screened Massive Expansion – namely, its extension to finite temperature and to the quark sector of full QCD. In Chapter 5 we define the gauge-invariant gluon field A^h , derive the one-loop effective potential for its quadratic condensate $\langle (A^h)^2 \rangle$ and the action I of the Dynamical Model, report expressions for the one-loop DM gluon and ghost propagators and perform their RG improvement in the DIS scheme. The results of the lattice calculations are used throughout Chapters 3 to 5 as a benchmark for the validity of our calculations. In Chapter 6 we present our conclusions and discuss potential future developments of the Screened Massive Expansion and of the Dynamical Model.

Part I

Quantum Chromodynamics and its infrared regime

1

The standard formulation of QCD

In this first chapter we start by reviewing the definition of Quantum Chromodynamics. The main objective of our review is to fix the notation and highlight some of the properties of QCD which are assumed to be valid at all scales. We will discuss the symmetries of the theory, its quantization in the functional formalism and the issue of gauge fixing. Thanks to the BRST symmetry which survives the fixing of the gauge, we will be able to derive the general form of the well-known Slavnov-Taylor identities and that of the lesser-known Nielsen identities. The latter of these will play a fundamental role in obtaining some of the results presented in Chapter 3.

Next, we move on to the standard perturbative formulation of QCD. Although not suitable for studying the infrared dynamics of the strong interactions, standard perturbation theory remains the most important benchmark for any analytical treatment of QCD. Going through the derivation of the perturbative series for an arbitrary Green function will allow us to introduce the Feynman rules of standard perturbation theory, to discuss the validity of the approximation and to show how the formalism leaves the doors open to possible modifications of the series. By making use of the Renormalization Group, we will address the asymptotic freedom typical of the non-abelian gauge theories and illustrate the breakdown of the method at low energy.

1.1 Action functionals for QCD and their symmetries

1.1.1 The classical action

Quantum Chromodynamics is a Yang-Mills theory [YM54] with gauge group $SU(3)$ minimally coupled to quarks in the fundamental representation. In the presence of a single quark, its Lagrangian density \mathcal{L}_{QCD} takes the form

$$\mathcal{L}_{\text{QCD}} = -\frac{1}{4} F_{\mu\nu}^a F^{a\mu\nu} + \bar{\psi}(i\gamma^\mu D_\mu - M)\psi . \quad (1.1)$$

Here ψ – the quark field – is a triplet of Dirac fields, $\bar{\psi} = \psi^\dagger \gamma^0$ is its Dirac conjugate, M is its mass, the γ^μ 's are matrices satisfying the Dirac algebra

$$\{\gamma_\mu, \gamma_\nu\} = 2\eta_{\mu\nu} \mathbb{1} , \quad (1.2)$$

where $\eta = \text{diag}(+1, -1, -1, -1)$ is the Minkowski metric, and the covariant derivative $D_\mu = D_\mu(A)$ acting on the fundamental representation is defined as

$$D_\mu = \partial_\mu - igA_\mu^a T_a . \quad (1.3)$$

In the above equation, g is the strong coupling constant, the T_a 's ($a = 1, \dots, 8$) are the generators of the Lie algebra $\mathfrak{su}(3)$ of $SU(3)$ – that is, they are 8 linearly independent traceless 3×3 matrices –, chosen so as to satisfy the normalization condition

$$\text{Tr} \{T_a T_b\} = \frac{1}{2} \delta_{ab} , \quad (1.4)$$

and A_μ^a – the gluon field – is an octet of vector fields also known as the gauge potential. The gluon field-strength tensor $F_{\mu\nu}^a = F_{\mu\nu}^a[A]$ is defined as

$$F_{\mu\nu}^a = \partial_\mu A_\nu^a - \partial_\nu A_\mu^a + g f_{bc}^a A_\mu^b A_\nu^c , \quad (1.5)$$

where the f_{ab}^c 's – the structure constants – define the commutation relations of $\mathfrak{su}(3)$,

$$[T_a, T_b] = i f_{ab}^c T_c ; \quad (1.6)$$

$F_{\mu\nu} = F_{\mu\nu}^a T_a$ can equivalently be expressed in terms of the commutator of two covariant derivatives as

$$F_{\mu\nu} = \frac{i}{g} [D_\mu, D_\nu] . \quad (1.7)$$

Clearly, $f_{ab}^c = -f_{ba}^c$ and $F_{\mu\nu}^a = -F_{\nu\mu}^a$. The Jacobi identity $[X, [Y, Z]] + [Y, [Z, X]] + [Z, [X, Y]] = 0$, valid for any triplet of square matrices X, Y, Z , translates into the relation

$$f_{bc}^a f_{de}^c + f_{dc}^a f_{eb}^c + f_{ec}^a f_{bd}^c = 0 \quad (1.8)$$

for the structure constants.

In its full glory, the QCD Lagrangian can be expanded as

$$\begin{aligned} \mathcal{L}_{\text{QCD}} = & -\frac{1}{2} \partial_\mu A_\nu^a (\partial^\mu A^{a\nu} - \partial^\nu A^{a\mu}) - g f_{bc}^a \partial_\mu A_\nu^a A^{b\mu} A^{c\nu} + \\ & -\frac{1}{4} g^2 f_{bc}^a f_{de}^a A_\mu^b A_\nu^c A^{d\mu} A^{e\nu} + \bar{\psi} (i\gamma^\mu \partial_\mu - M) \psi + g \bar{\psi} \gamma^\mu T_a \psi A_\mu^a . \end{aligned} \quad (1.9)$$

The classical field equations of QCD can be obtained by functionally differentiating the action S_{QCD} ,

$$S_{\text{QCD}} = \int d^4x \mathcal{L}_{\text{QCD}} , \quad (1.10)$$

with respect to the gluon and quark fields. They read

$$(i\gamma^\mu D_\mu - M)\psi = 0 , \quad (1.11)$$

$$D_\mu F^{a\mu\nu} + g \bar{\psi} \gamma^\nu T^a \psi = 0 , \quad (1.12)$$

where the covariant derivative D_μ acts on $F_{\mu\nu}$ – and, more generally, on any object in the adjoint representation of $SU(3)$ – as

$$D_\mu F^{\sigma\nu} = \partial_\mu F^{\sigma\nu} - ig [A_\mu, F^{\sigma\nu}] , \quad (1.13)$$

so that

$$D_\mu F^{a\mu\nu} = \partial_\mu F^{a\mu\nu} + g f_{bc}^a A_\mu^b F^{c\mu\nu} . \quad (1.14)$$

QCD is a gauge theory in that it possesses a local symmetry – specifically, a local SU(3) symmetry. In order to see this, consider the transformation defined by $A_\mu = A_\mu^a T_a \rightarrow A_\mu^U$, $\psi \rightarrow \psi^U$, where

$$A_\mu^U = U \left(A_\mu + \frac{i}{g} \partial_\mu \right) U^\dagger, \quad \psi^U = U \psi, \quad (1.15)$$

and $U = U(x)$ is a function from Minkowski space to the group of 3×3 unitary matrices of determinant 1 – i.e., to the group SU(3). Using the transformation laws

$$\begin{aligned} D_\mu(A^U) \psi^U &= U D_\mu(A) \psi, & F_{\mu\nu}[A^U] &= U F_{\mu\nu}[A] U^\dagger, \\ \bar{\psi}^U &= \bar{\psi} U^\dagger, & F_{\mu\nu}^a F^{a\mu\nu} &= 2 \text{Tr} \{ F_{\mu\nu} F^{\mu\nu} \}, \end{aligned} \quad (1.16)$$

it is easy to show that \mathcal{L}_{QCD} remains invariant under the local SU(3) transformation in Eq. (1.15). In particular, the QCD Lagrangian is constant over the gauge orbits, i.e. over the sets of field configurations which are related to one-another via a gauge transformation (the “gauge-equivalent” configurations): given a solution of the QCD field equations (1.11) and (1.12), all of its gauge-equivalent configurations also solve the equations.

When globalized, the local SU(3) symmetry of the QCD action leads to the conservation of an octet J_a^μ of Noether currents,

$$J_a^\mu = \bar{\psi} \gamma^\mu T_a \psi + f_{abc} F^{b\mu\nu} A_\nu^c, \quad \partial_\mu J_a^\mu = 0. \quad (1.17)$$

Altogether, the J_a^μ 's form the color current. The color current corresponds to invariance under the infinitesimal global transformation

$$\delta A_\mu^a = g f_{bc}^a A_\mu^b \chi^c, \quad \delta \psi = i g \chi^a T_a \psi, \quad (1.18)$$

obtained by first setting $U = e^{ig\chi}$ with $\chi = \chi^a T_a$ infinitesimal in Eq. (1.15), so that

$$\delta A_\mu = D_\mu \chi = \partial_\mu \chi - i g [\chi, A_\mu], \quad \delta \psi = i g \chi \psi, \quad (1.19)$$

and then taking the χ^a 's to be constant. Observe that, in terms of the color current, the field equations for the gluon field read

$$\partial_\mu F^{a\mu\nu} = -g J^{a\nu}. \quad (1.20)$$

For future reference, we remark that the definitions presented in this section remain valid, with obvious modifications, for any Yang-Mills theory whose local symmetry group is a compact semi-simple group. In particular, they apply to arbitrary SU(N) Yang-Mills theories once we replace the quark triplet with an N -dimensional Dirac multiplet and the T^a 's with a set of $N_A = N^2 - 1$ linearly independent traceless $N \times N$ matrices ($a = 1, \dots, N_A$). Moreover, the definitions can be extended to multiple quark fields by simply taking the QCD Lagrangian to be

$$\mathcal{L}_{\text{QCD}} = -\frac{1}{4} F_{\mu\nu}^a F^{a\mu\nu} + \sum_f \bar{\psi}_f (i \gamma^\mu D_\mu - M_f) \psi_f, \quad (1.21)$$

where f denotes the flavor of the quark and M_f is the corresponding mass. The other equations must be changed accordingly. For example, in the presence of multiple quark fields, the color current becomes

$$J_a^\mu = \sum_f \bar{\psi}_f \gamma^\mu T_a \psi_f + f_{abc} F^{b\mu\nu} A_\nu^c. \quad (1.22)$$

In order to keep the expressions simple, in what follows we will restrict ourselves to a single flavor of quark.

1.1.2 Quantizing QCD: the Faddeev-Popov action

Quantum Chromodynamics is usually quantized by making use of the functional formalism. In the functional formalism, given any quantum operator \mathcal{O} , its vacuum expectation value (VEV) $\langle \mathcal{O} \rangle$ is computed by averaging its classical counterpart – which for simplicity we will also denote with \mathcal{O} – over the set of field configurations, using as the weighting factor the complex exponential e^{iS} of the classical action. In other words,

$$\langle \mathcal{O} \rangle = \frac{\int \mathcal{D}\mathcal{F} e^{iS[\mathcal{F}]} \mathcal{O}[\mathcal{F}]}{\int \mathcal{D}\mathcal{F} e^{iS[\mathcal{F}]}} , \quad (1.23)$$

where \mathcal{F} denotes a generic field and $\mathcal{D}\mathcal{F}$ is the measure over the complete set of fields. When working with gauge theories over a continuum spacetime, this definition has to be somewhat modified. The reason for this lies in the fact that, as remarked in the previous section, the action of any gauge theory is constant over the set of gauge-equivalent configurations. Since there are infinitely many such configurations, the integrand in the denominator of Eq. (1.23) is infinite. If, in addition, the operator \mathcal{O} is gauge invariant, then the integrand in the numerator of Eq. (1.23) will be infinite as well. In order to cure these infinities, one resorts to a procedure first devised by L. D. Faddeev and V. Popov (FP) [FP67]. In what follows, we will review the FP procedure in the context of QCD and of the covariant gauges.

Let us start from a generic QCD path integral I ,

$$I = \int \mathcal{D}A \mathcal{D}\bar{\psi} \mathcal{D}\psi e^{iS_{\text{QCD}}[A, \psi, \bar{\psi}]} \mathcal{O}[A, \psi, \bar{\psi}] . \quad (1.24)$$

If we assume \mathcal{O} to be gauge invariant, then I is infinite and thus ill-defined. Nonetheless, if we managed to factorize the infinity so that

$$I = \mathcal{C}_\infty \cdot I_{\text{finite}} , \quad (1.25)$$

where \mathcal{C}_∞ is an infinite constant and I_{finite} is finite, then the average of the operator \mathcal{O} ,

$$\langle \mathcal{O} \rangle = \frac{\mathcal{C}_\infty \cdot I_{\text{finite}}}{\int \mathcal{D}\mathcal{F} e^{iS[\mathcal{F}]}} , \quad (1.26)$$

would be well-defined provided that $\int \mathcal{D}\mathcal{F} e^{iS[\mathcal{F}]}$ contains the same infinite factor \mathcal{C}_∞ that appears in the numerator of Eq. (1.26).

In order to show that this factorization can indeed be performed, let us re-write I as

$$I = \mathcal{N}^{-1} \int \mathcal{D}A \mathcal{D}\bar{\psi} \mathcal{D}\psi \mathcal{D}F e^{iS_{\text{QCD}}[A, \psi, \bar{\psi}] - i \int d^4x \frac{1}{2\xi} F^a F^a} \mathcal{O}[A, \psi, \bar{\psi}] , \quad (1.27)$$

where F^a is a new set of integration fields, ξ is a (non-negative) constant and

$$\mathcal{N} = \int \mathcal{D}F e^{-i \int d^4x \frac{1}{2\xi} F^a F^a} . \quad (1.28)$$

Since the ill-definedness of I is caused by gauge invariance, meaning that

$$\begin{aligned} S_{\text{QCD}}[A^U, \psi^U, \bar{\psi}^U] &= S_{\text{QCD}}[A, \psi, \bar{\psi}] , & \mathcal{O}[A^U, \psi^U, \bar{\psi}^U] &= \mathcal{O}[A, \psi, \bar{\psi}] , \\ \mathcal{D}A^U \mathcal{D}\bar{\psi}^U \mathcal{D}\psi^U &= \mathcal{D}A \mathcal{D}\bar{\psi} \mathcal{D}\psi , \end{aligned} \quad (1.29)$$

where we denoted with A^U and ψ^U the gauge-transformed version of A and ψ as in Eq. (1.15), to make the integral well-defined we must manipulate the integrand in Eq. (1.27) so as to introduce in the action terms which break gauge symmetry. This can be achieved by changing variables of integration from F^a to λ^a , setting

$$F^a = F^a[\lambda] = \partial^\mu (A_\mu^{U(\lambda)})^a, \quad U(\lambda) = e^{ig\lambda^a T_a}. \quad (1.30)$$

The resulting integral reads

$$I = \mathcal{N}^{-1} \int \mathcal{D}A \mathcal{D}\bar{\psi} \mathcal{D}\psi \mathcal{D}\lambda e^{iS_{\text{QCD}}[A, \psi, \bar{\psi}] - i \int d^4x \frac{1}{2\xi} (\partial \cdot A^{U(\lambda)})^2} \det \left(\frac{\delta(\partial \cdot A^{U(\lambda)})}{\delta \lambda} \right) \mathcal{O}[A, \psi, \bar{\psi}], \quad (1.31)$$

where the determinant can be explicitly computed to be equal to¹

$$\det \left(\frac{\delta(\partial \cdot A^{U(\lambda)})}{\delta \lambda} \right) = \det \left(\partial^\mu D_\mu(A^{U(\lambda)}) \Lambda(\lambda) \right), \quad (1.32)$$

and, for each value of the index a , $\Lambda_a(\lambda)$ is the matrix

$$\Lambda_a(\lambda) = -\frac{i}{g} \frac{\partial e^{ig\lambda}}{\partial \lambda^a} e^{-ig\lambda}. \quad (1.33)$$

The latter lives in the adjoint representation; thus, its covariant derivative $D_\mu \Lambda$ reads

$$D_\mu(A) \Lambda_a = \partial_\mu \Lambda_a - ig[A_\mu, \Lambda_a]. \quad (1.34)$$

The crucial thing to notice about the determinant in Eq. (1.32) is that part of it decouples from the rest of the integral I thanks to gauge invariance itself. Indeed, factorizing the determinant as

$$\det \left(\partial^\mu D_\mu(A^{U(\lambda)}) \Lambda(\lambda) \right) = \det \left(\partial^\mu D_\mu(A^{U(\lambda)}) \right) \det(\Lambda(\lambda)) \quad (1.35)$$

and using the relations in Eq. (1.29), we can rewrite the integral I as

$$I = \mathcal{N}^{-1} \int \mathcal{D}A^U \mathcal{D}\bar{\psi}^U \mathcal{D}\psi^U \mathcal{D}\lambda e^{iS_{\text{QCD}}[A^U, \psi^U, \bar{\psi}^U] - i \int d^4x \frac{1}{2\xi} (\partial \cdot A^U)^2} \times \det(\partial^\mu D_\mu(A^U)) \det(\Lambda(\lambda)) \mathcal{O}[A^U, \psi^U, \bar{\psi}^U], \quad (1.36)$$

where $U = U(\lambda)$. A simple renaming of variables $A^U \rightarrow A$, $\psi^U \rightarrow \psi$ now yields

$$I = \mathcal{N}^{-1} \left(\int \mathcal{D}\lambda \det(\Lambda(\lambda)) \right) \times \left(\int \mathcal{D}A \mathcal{D}\bar{\psi} \mathcal{D}\psi e^{iS_{\text{QCD}}[A, \psi, \bar{\psi}] - i \int d^4x \frac{1}{2\xi} (\partial \cdot A)^2} \det(\partial^\mu D_\mu(A)) \mathcal{O}[A, \psi, \bar{\psi}] \right), \quad (1.37)$$

where the first line is a multiplicative constant which does not depend on the operator \mathcal{O} . On the second line, we see that the integrand is no longer gauge invariant: a transformation $A \rightarrow A^U$, $\psi \rightarrow \psi^U$, while still leaving the integration measure and the action S_{QCD}

¹It is precisely at this point in the derivation that the existence of Gribov copies – see the Introduction and Sec. 2.3 – spoils the validity of the Faddeev-Popov procedure. If the operator $\partial^\mu D_\mu$ has zero modes, then the determinant vanishes and the change of variables $F^a \rightarrow \lambda^a$ cannot be performed consistently. As discussed in our introduction to the Screened Massive Expansion, we will disregard this issue as it is not relevant in the UV, nor potentially in the IR once dynamical mass generation is accounted for.

invariant, changes the product $(\partial \cdot A)^2$ and the gauge potential inside the determinant. In particular, the second factor in brackets is finite. This is precisely what we were looking for: going back to Eq. (1.25), we can identify the constant \mathcal{C}_∞ with the \mathcal{O} -independent quantity

$$\mathcal{C}_\infty = \mathcal{N}^{-1} \left(\int \mathcal{D}\lambda \det(\Lambda(\lambda)) \right). \quad (1.38)$$

The operator $\partial^\mu D_\mu(A)$ in Eq. (1.37) and its determinant are respectively known as the Faddeev-Popov operator and the Faddeev-Popov determinant. The Faddeev-Popov determinant can be computed in terms of so-called *ghost fields* by observing that, given a pair of Grassmann – that is, anticommuting – fields c and \bar{c} and an operator \mathcal{M} ,

$$\int \mathcal{D}\bar{c}\mathcal{D}c \exp \left\{ i \int d^4x \bar{c} \mathcal{M} c \right\} \propto \det(-\mathcal{M}). \quad (1.39)$$

Therefore, by introducing two octets of Grassman fields c^a and \bar{c}^a , we can rewrite the finite part of the integral I in Eq. (1.37) as

$$I_{\text{finite}} = \int \mathcal{D}A \mathcal{D}\bar{\psi} \mathcal{D}\psi \mathcal{D}\bar{c} \mathcal{D}c e^{iS_{\text{FP}}[A, \psi, \bar{\psi}, c, \bar{c}]} \mathcal{O}[A, \psi, \bar{\psi}], \quad (1.40)$$

where S_{FP} is known as the Faddeev-Popov action and reads

$$S_{\text{FP}} = \int d^4x \mathcal{L}_{\text{FP}} = S_{\text{QCD}} + \int d^4x \left\{ -\frac{1}{2\xi} (\partial \cdot A)^2 + \partial^\mu \bar{c}^a D_\mu c^a \right\}. \quad (1.41)$$

We remark that, in order to obtain the last term, we have performed a partial integration.

The Faddeev-Popov action S_{FP} is not gauge invariant. Term by term, its Lagrangian is given by

$$\begin{aligned} \mathcal{L}_{\text{FP}} = & -\frac{1}{2} \partial_\mu A_\nu^a (\partial^\mu A^{a\nu} - \partial^\nu A^{a\mu}) - \frac{1}{2\xi} \partial^\mu A_\mu^a \partial^\nu A_\nu^a - g f_{bc}^a \partial_\mu A_\nu^a A^{b\mu} A^{c\nu} + \\ & -\frac{1}{4} g^2 f_{bc}^a f_{de}^a A_\mu^b A_\nu^c A^{d\mu} A^{e\nu} + \bar{\psi} (i\gamma^\mu \partial_\mu - M) \psi + g \bar{\psi} \gamma^\mu T_a \psi A_\mu^a + \\ & + \partial^\mu \bar{c}^a \partial_\mu c^a + g f_{bc}^a \partial^\mu \bar{c}^a A_\mu^b c^c. \end{aligned} \quad (1.42)$$

The fields c^a and \bar{c}^a are respectively known as Faddeev-Popov ghosts and antighosts. They are fermionic fields in that they anticommute with each other (and with the quark fields, which are also Grassmann/anticommuting fields); nonetheless, they have no spin structure, as can be seen from their kinetic term $\partial^\mu \bar{c}^a \partial_\mu c^a$, which is typical of a scalar field. Their role is to act as “negative” degrees of freedom by removing unphysical contributions to the computed physical quantities of the theory.

The constant ξ is known as the *gauge parameter* and it defines the *covariant gauge* in which the calculation is carried out. The VEV of any gauge-invariant operator which can be expressed solely in terms the gluon and the quark fields is easily seen to be independent of ξ . Indeed, since for any such operator \mathcal{O}

$$\langle \mathcal{O} \rangle = \frac{\int \mathcal{D}A \mathcal{D}\bar{\psi} \mathcal{D}\psi e^{iS_{\text{QCD}}} \mathcal{O}}{\int \mathcal{D}A \mathcal{D}\bar{\psi} \mathcal{D}\psi e^{iS_{\text{QCD}}}} = \frac{\int \mathcal{D}A \mathcal{D}\bar{\psi} \mathcal{D}\psi \mathcal{D}\bar{c} \mathcal{D}c e^{iS_{\text{FP}}} \mathcal{O}}{\int \mathcal{D}A \mathcal{D}\bar{\psi} \mathcal{D}\psi \mathcal{D}\bar{c} \mathcal{D}c e^{iS_{\text{FP}}}}, \quad (1.43)$$

where strict equalities hold between all of the members, the right-hand side of the equality must be ξ -independent because the middle average also is. On the other hand, the averages of operators which are not gauge invariant, or those of operators which also involve

the ghost and antighost fields, can – and in general do – depend on the gauge parameter. This is due to the fact that, since the FP procedure is only applicable to gauge-invariant operators, these averages are ill-defined with respect to the classical QCD action, and their calculation makes sense only a posteriori, by making use of the gauge-fixed, ξ -dependent Faddeev-Popov action.

In the quantum setting, the FP action replaces the classical QCD action. For future reference, let us write down its field equations. By functionally differentiating Eq. (1.42) with respect to the gluon, quark, ghost and antighost fields, we obtain

$$\begin{aligned} (i\gamma^\mu D_\mu - M)\psi &= 0, & \partial^\mu D_\mu c^a &= 0, & D_\mu \partial^\mu \bar{c}^a &= 0, & (1.44) \\ D_\mu F^{a\mu\nu} + \frac{1}{\xi} \partial^\nu \partial^\mu A_\mu^a + g \bar{\psi} \gamma^\nu T^a \psi - g f_{bc}^a \partial^\nu \bar{c}^b c^c &= 0. \end{aligned}$$

Observe that the field equations of the ghost and antighost fields do not coincide: in general, $\partial^\mu D_\mu \neq D_\mu \partial^\mu$.

To end this section, we should mention that the covariant gauges are not the only class of gauges used to quantize the QCD action. Two popular alternatives for fixing the gauge in QCD are the axial gauges, defined by choosing the functional F^a in Eq. (1.30) according to

$$F^a = n^\mu (A_\mu^U)^a, \quad (1.45)$$

where n^μ is a constant vector, and the Coulomb gauge, defined by the choice

$$F^a = \vec{\nabla} \cdot (\vec{A}^U)^a, \quad (1.46)$$

where only the spatial divergence of the (spatial component of the) gauge field is involved. Both of these have the disadvantage of making the calculations more difficult by breaking the Lorentz invariance of the action. A third alternative, the maximal abelian gauge, defined by

$$F^A = \partial^\mu A_\mu^A + g f_{IB}^A a^{I\mu} A_\mu^B, \quad F^I = \partial^\mu a_\mu^I, \quad (1.47)$$

where the a^I 's are the diagonal components of the gauge field $A_\mu = A_\mu^a T_a$, whereas the A^A 's are its off-diagonal components, breaks global SU(3) symmetry. We will go no further in discussing these alternatives.

1.1.3 The partition function and the quantum effective action

In this section we briefly review the definition of the partition function and of the quantum effective action and recall how these are used in quantum field theory. For the sake of definiteness, we will employ the Faddeev-Popov action of QCD for their formulation, although the same formalism applies to any field theory.

Consider the VEV of a time-ordered product $T\{A_{\mu_1}^{a_1}(x_1) \cdots A_{\mu_n}^{a_n}(x_n)\}$ of gluon field operators²,

$$\langle T \{A_{\mu_1}^{a_1}(x_1) \cdots A_{\mu_n}^{a_n}(x_n)\} \rangle = \frac{\int \mathcal{D}A \mathcal{D}\bar{\psi} \mathcal{D}\psi \mathcal{D}\bar{c} \mathcal{D}c e^{iS_{\text{FP}}} A_{\mu_1}^{a_1}(x_1) \cdots A_{\mu_n}^{a_n}(x_n)}{\int \mathcal{D}A \mathcal{D}\bar{\psi} \mathcal{D}\psi \mathcal{D}\bar{c} \mathcal{D}c e^{iS_{\text{FP}}}}. \quad (1.48)$$

²It can be proved – see e.g. [PS95], Chapter 9 – that the path integral of a product of fields computed at different spacetime points is actually equal to the quantum average of the time-ordered product of the corresponding quantum operators, rather than to the average of their simple product.

It is easy to see that, if we define a functional $Z[j]$ as

$$Z[j] = \int \mathcal{D}A \mathcal{D}\bar{\psi} \mathcal{D}\psi \mathcal{D}\bar{c} \mathcal{D}c e^{iS_{\text{FP}} + i \int d^4x A_\mu^a j_a^\mu}, \quad (1.49)$$

where the j_a^μ 's are classical external currents, then

$$\langle T \{ A_{\mu_1}^{a_1}(x_1) \cdots A_{\mu_n}^{a_n}(x_n) \} \rangle = \left[(-i)^n Z^{-1}[j] \frac{\delta^n Z[j]}{\delta j_{a_1}^{\mu_1}(x_1) \cdots \delta j_{a_n}^{\mu_n}(x_n)} \right]_{j=0}, \quad (1.50)$$

where $\delta/\delta j_a^\mu(x)$ denotes a functional derivative with respect to j_a^μ . More generally, we can define a *partition function* $Z[j, j^c, j^{\bar{c}}, j^\psi, j^{\bar{\psi}}]$ as

$$Z[j, j^c, j^{\bar{c}}, j^\psi, j^{\bar{\psi}}] = \int \mathcal{D}A \mathcal{D}\bar{\psi} \mathcal{D}\psi \mathcal{D}\bar{c} \mathcal{D}c e^{iS_{\text{FP}} + i \int d^4x (A_\mu^a j_a^\mu + c^a j_a^c + \bar{c}^a j_a^{\bar{c}} + \psi^A j_A^\psi + \bar{\psi}^A j_A^{\bar{\psi}})}, \quad (1.51)$$

where the external currents $j^{c, \bar{c}, \psi, \bar{\psi}}$ are Grassmann fields and the index A is a multi-index that enumerates the Dirac and color components of the quark field. The time-ordered product of gluon, ghost and quark operators can be computed by differentiating the partition function with respect to the corresponding external currents³, multiplying the result by the inverse of the partition function and by an appropriate power of i , and finally setting the currents to zero. Due to this property, the partition function is also known as the generator of the Green functions of the theory.

If we define a quantity $W[j]$ as

$$W[j] = -i \ln Z[j], \quad (1.52)$$

where with j we have collectively denoted the external currents corresponding to the gluon, ghost and quark fields, we find that, for example,

$$\begin{aligned} \left. \frac{\delta^2 W[j]}{\delta j_a^\mu(x) \delta j_b^\nu(y)} \right|_{j=0} &= i \left(\langle T \{ A_\mu^a(x) A_\nu^b(y) \} \rangle - \langle A_\mu^a(x) \rangle \langle A_\nu^b(y) \rangle \right) = \\ &= i \langle T \{ A_\mu^a(x) A_\nu^b(y) \} \rangle_{\text{conn.}}. \end{aligned} \quad (1.53)$$

In the general case, by differentiating the functional $W[j]$ with respect to the external currents, we obtain *connected* Green functions. Therefore, $W[j]$ is known as the generator of the connected Green functions of the theory.

An interesting application of the generator of the connected Green function is the computation of the VEV of the elementary quantum fields of the theory. For the gluon field, we have

$$\frac{\delta W[j]}{\delta j_a^\mu(x)} = \langle A_\mu^a(x) \rangle_j, \quad (1.54)$$

where the subscript j on the right-hand side denotes that the average is computed in the presence of the classical external currents. Similarly,

$$\begin{aligned} \frac{\delta_R W[j]}{\delta j_a^c(x)} &= \langle c^a(x) \rangle_j, & \frac{\delta_R W[j]}{\delta j_a^{\bar{c}}(x)} &= \langle \bar{c}^a(x) \rangle_j, \\ \frac{\delta_R W[j]}{\delta j_A^\psi(x)} &= \langle \psi^A(x) \rangle_j, & \frac{\delta_R W[j]}{\delta j_A^{\bar{\psi}}(x)} &= \langle \bar{\psi}^A(x) \rangle_j. \end{aligned} \quad (1.55)$$

³Care has to be taken when differentiating with respect to Grassmann variables such as the fermionic currents, since then the functional derivatives anticommute with the Grassmann fields. In what follows, we will distinguish between left and right derivatives as in [Wei96], denoting the first with a subscript L and the second with a subscript R .

By converse, we can define a set of currents $j_{\text{cl.}}[F_{\text{cl.}}] = j_{\text{cl.}}[A_{\text{cl.}}, \psi_{\text{cl.}}, \bar{\psi}_{\text{cl.}}, c_{\text{cl.}}, \bar{c}_{\text{cl.}}]$ such that

$$\begin{aligned} \left. \frac{\delta_R W[j]}{\delta j_{\mu}^a(x)} \right|_{j=j_{\text{cl.}}} &= A_{\text{cl.}, \mu}^a(x) , \\ \left. \frac{\delta_R W[j]}{\delta j_a^c(x)} \right|_{j=j_{\text{cl.}}} &= c_{\text{cl.}}^a(x) , & \left. \frac{\delta_R W[j]}{\delta j_a^{\bar{c}}(x)} \right|_{j=j_{\text{cl.}}} &= \bar{c}_{\text{cl.}}^a(x) , \\ \left. \frac{\delta_R W[j]}{\delta j_A^\psi(x)} \right|_{j=j_{\text{cl.}}} &= \psi_{\text{cl.}}^A(x) , & \left. \frac{\delta_R W[j]}{\delta j_A^{\bar{\psi}}(x)} \right|_{j=j_{\text{cl.}}} &= \bar{\psi}_{\text{cl.}}^A(x) \end{aligned} \quad (1.56)$$

for a given set of classical fields $A_{\text{cl.}, \mu}^a, c_{\text{cl.}}^a, \bar{c}_{\text{cl.}}^a, \psi_{\text{cl.}}, \bar{\psi}_{\text{cl.}}$. If we differentiate the functional $\Gamma[F_{\text{cl.}}]$ defined as

$$\Gamma[F_{\text{cl.}}] = W[j_{\text{cl.}}[F_{\text{cl.}}]] - \int d^4x \left\{ A_{\text{cl.}, \mu}^a j_{\text{cl.}, a}^{\mu} + c_{\text{cl.}}^a j_{\text{cl.}, a}^c + \bar{c}_{\text{cl.}}^a j_{\text{cl.}, a}^{\bar{c}} + \psi_{\text{cl.}}^A j_{\text{cl.}, A}^{\psi} + \bar{\psi}_{\text{cl.}}^A j_{\text{cl.}, A}^{\bar{\psi}} \right\} \quad (1.57)$$

with respect to the fields $F_{\text{cl.}}$, we obtain

$$\begin{aligned} \frac{\delta_L \Gamma[F_{\text{cl.}}]}{\delta A_{\text{cl.}, \mu}^a(x)} &= -j_{\text{cl.}, a}^{\mu}(x) , \\ \frac{\delta_L \Gamma[F_{\text{cl.}}]}{\delta c_{\text{cl.}}^a(x)} &= -j_{\text{cl.}, a}^c(x) , & \frac{\delta_L \Gamma[F_{\text{cl.}}]}{\delta \bar{c}_{\text{cl.}}^a(x)} &= -j_{\text{cl.}, a}^{\bar{c}}(x) , \\ \frac{\delta_L \Gamma[F_{\text{cl.}}]}{\delta \psi_{\text{cl.}}^A(x)} &= -j_{\text{cl.}, A}^{\psi}(x) , & \frac{\delta_L \Gamma[F_{\text{cl.}}]}{\delta \bar{\psi}_{\text{cl.}}^A(x)} &= -j_{\text{cl.}, A}^{\bar{\psi}}(x) , \end{aligned} \quad (1.58)$$

In particular, since $j_{\text{cl.}} = 0$ if and only if $A_{\text{cl.}, \mu}^a(x) = \langle A_{\mu}^a(x) \rangle_{j=0}$, $\psi_{\text{cl.}}(x) = \langle \psi(x) \rangle_{j=0}$, etc., we see that solving the equations

$$\frac{\delta_L \Gamma[F_{\text{cl.}}]}{\delta F_{\text{cl.}}(x)} = 0 \quad (1.59)$$

for the fields $F_{\text{cl.}}(x)$ is equivalent to finding the vacuum expectation values $\langle F(x) \rangle$ in the absence of external currents. For this reason, $\Gamma[F_{\text{cl.}}]$ is known as the *quantum effective action* – or, in brief, the *effective action* – of the theory. From now on, we will drop the “cl.” subscript from the arguments of Γ .

When differentiated three or more times, the quantum effective action can be shown to generate the 1-particle irreducible (1PI) Green functions of the theory [PS95]. For this reason, $\Gamma[F]$ is also known as the generator of the 1PI Green functions. The second derivatives of the effective action, on the other hand, are equal, modulo factors of i , to the functional inverses of the propagators of the fields [PS95]:

$$\int d^4z \langle T \{ F^A(x) F^C(z) \} \rangle_{j_{\text{cl.}}[F]} \frac{\delta_L^2 \Gamma[F]}{\delta F^C(z) \delta F^B(y)} = i \delta_B^A \delta(x - y) \quad (1.60)$$

where the indices A, B, C denote the different fields and their spacetime and color components.

The effective action can be used to study how the symmetries of a quantum field theory affect its Green functions. Indeed, it can be proved [PS95, Wei96] that, for any transformation δF^A of the fields,

$$\int d^4x \langle \delta F^A(x) \rangle_{j_{\text{cl.}}[F]} \frac{\delta_L \Gamma[F]}{\delta F^A(x)} = \langle \delta S_{\text{FP}} \rangle , \quad (1.61)$$

where δS_{FP} is the transformation of the action corresponding to δF^A . If the action is invariant under δF^A – that is, if $\delta S_{\text{FP}} = 0$ –, then the effective action will satisfy the invariance property

$$\int d^4x \langle \delta F^A(x) \rangle_{j_{\text{cl.}}[F]} \frac{\delta_L \Gamma[F]}{\delta F^A(x)} = 0 . \quad (1.62)$$

Relations of this kind are used to prove the renormalizability of QCD – and, more generally, of the Yang-Mills theories – in the covariant gauges, by exploiting a symmetry of the action known as BRST symmetry. The latter is the subject of the next section.

1.1.4 BRST symmetry, the Slavnov-Taylor identities and the Nielsen identities

In Section 1.1.2 we saw that in order to quantize QCD it is necessary to fix a gauge. By construction, the action that results from the Faddeev-Popov procedure is no longer gauge invariant; nonetheless, in 1975, C. Becchi, A. Rouet and R. Stora [BRS75] and I. V. Tyutin [Tyu75] showed that the FP action still possesses a symmetry which can be regarded as a remnant of the full gauge symmetry. This symmetry is today known as the BRST symmetry.

In order to define the BRST transformations, we first need to introduce a so-called Nakanishi-Lautrup (NL) field B^a [Lau66, Nak66] in the FP action. Observing that

$$e^{-\frac{i}{2\xi} \int d^4x (\partial \cdot A)^2} \propto \int \mathcal{D}B e^{i \int d^4x (\frac{\xi}{2} B^a B^a + B^a \partial \cdot A^a)} = \int \mathcal{D}B e^{i \int d^4x (\frac{\xi}{2} B^a B^a - \partial^\mu B^a A_\mu^a)} , \quad (1.63)$$

the FP Lagrangian can be rewritten as

$$\mathcal{L}_{\text{FP}} = -\frac{1}{4} F_{\mu\nu}^a F^{a\mu\nu} + \bar{\psi}(i\gamma^\mu D_\mu - M)\psi + \frac{\xi}{2} B^a B^a - \partial^\mu B^a A_\mu^a + \partial^\mu \bar{c}^a D_\mu c^a . \quad (1.64)$$

When using the above expression for \mathcal{L}_{FP} , it is understood that the path integrals are to be computed by also integrating over the configurations of the NL field.

Consider now the following set of transformations:

$$\begin{aligned} \delta A_\mu^a &= \epsilon D_\mu c^a , \\ \delta \psi &= i\epsilon g c^a T_a \psi , \\ \delta c^a &= -\frac{1}{2} \epsilon g f_{bc}^a c^b c^c , \\ \delta \bar{c}^a &= \epsilon B^a , \\ \delta B^a &= 0 , \end{aligned} \quad (1.65)$$

where ϵ is a constant Grassmann parameter. Going back to Eq. (1.19), we see that the first two lines in Eq. (1.65) are formally identical to an infinitesimal SU(3) gauge transformation of the gluon and quark fields with the transformation parameters $\chi^a(x)$ taken to be equal to $\epsilon c^a(x)$. It follows that the first two terms in Eq. (1.64) – that is, the terms which make up the classical QCD action – are left invariant by Eqs. (1.65). As for the other terms, we have

$$\begin{aligned} \delta \left(\frac{\xi}{2} B^a B^a - \partial^\mu B^a A_\mu^a + \partial^\mu \bar{c}^a D_\mu c^a \right) &= \\ &= -\epsilon \partial^\mu B^a D_\mu c^a + \epsilon \partial^\mu B^a D_\mu c^a + \partial^\mu \bar{c}^a \delta(D_\mu c^a) = \\ &= \partial^\mu \bar{c}^a \delta(D_\mu c^a) . \end{aligned} \quad (1.66)$$

The transformation of the covariant derivative $D_\mu c^a$ can be shown to vanish as a consequence of the Jacobi identity – Eq. (1.8) –,

$$\delta(D_\mu c^a) = 0 . \quad (1.67)$$

Therefore, we find that the FP Lagrangian – and the action S_{FP} with it – is invariant under the BRST transformations defined by Eqs. (1.65),

$$\delta\mathcal{L}_{\text{FP}} = 0 . \quad (1.68)$$

A second way to prove the invariance of the FP action under the BRST transformations is via the nilpotency of the latter. Let s be the operator such that $\delta F = \epsilon sF$, where F is one of the QCD fields. Explicitly,

$$\begin{aligned} sA_\mu^a &= D_\mu c^a , \\ s\psi &= ig c^a T_a \psi , \\ sc^a &= -\frac{g}{2} f_{bc}^a c^b c^c , \\ s\bar{c}^a &= B^a , \\ sB^a &= 0 . \end{aligned} \quad (1.69)$$

A straightforward calculation shows that $s^2 F = 0$ for every F . It follows that $s^2 = 0$, i.e., the BRST transformations are *nilpotent*. In terms of the BRST operator s , the FP Lagrangian can be rewritten as

$$\mathcal{L}_{\text{FP}} = \mathcal{L}_{\text{QCD}} + s \left(\frac{\xi}{2} B^a \bar{c}^a - A_\mu^a \partial^\mu \bar{c}^a \right) . \quad (1.70)$$

Since $s\mathcal{L}_{\text{QCD}} = 0$ and $s^2 = 0$, the BRST invariance of the FP Lagrangian follows.

Being global symmetries of the FP action, the BRST transformations have an associated conserved current j_B^μ , given by

$$j_B^\mu = -F^{a\mu\nu} D_\nu c^a + B^a D^\mu c^a - g \bar{\psi} \gamma^\mu T_a \psi c^a + \frac{g}{2} f_{bc}^a \partial^\mu \bar{c}^a c^b c^c , \quad \partial_\mu j_B^\mu = 0 . \quad (1.71)$$

The corresponding charge $Q_B = \int d^3x j_B^0$, called the BRST charge, is nilpotent and self-adjoint as a quantum operator⁴,

$$Q_B^2 = 0 , \quad Q_B^\dagger = Q_B . \quad (1.72)$$

Q_B generates the BRST transformations, in the sense that

$$[Q_B, F]_{\mp} = -isF , \quad (1.73)$$

where the commutator $[\cdot, \cdot]_- = [\cdot, \cdot]$ applies to bosonic operators, whereas the anticommutator $[\cdot, \cdot]_+ = \{\cdot, \cdot\}$ applies to fermionic operators. Using Eq. (1.73), the gluon field equations in Eq. (1.44) – which in the presence of the NL field read

$$D_\mu F^{a\mu\nu} - \partial^\nu B^a + g \bar{\psi} \gamma^\nu T^a \psi - g f_{bc}^a \partial^\nu \bar{c}^b c^c = 0 , \quad \xi B^a + \partial \cdot A^a = 0 \quad (1.74)$$

⁴In what follows, we will not delve into the fascinating subject of the canonical quantization of the FP action. The interested reader is referred to [KO78a, KO78b, Oji78, KO79a, KO79b, KO79c] for a complete treatment of the topic, and to Appendix A for a short summary of the formalism.

– can be rewritten as

$$\partial_\mu F^{a\mu\nu} + gJ^{a\nu} - i\{Q_B, D^\nu \bar{c}^a\} = 0, \quad (1.75)$$

where J_a^μ , the color current, now includes contributions from both from the ghost and NL fields,

$$J_a^\mu = \bar{\psi}\gamma^\mu T_a \psi + f_{abc} \left(F^{b\mu\nu} A_\nu^c + A^{b,\mu} B^c + \bar{c}^b D^\mu c^c - \partial^\mu \bar{c}^b c^c \right). \quad (1.76)$$

In particular, on the solutions of the field equations, the color charge $Q^a = \int d^3x j^{a0}$ can be evaluated as

$$\begin{aligned} Q^a &= \frac{1}{g} \int d^3x (\partial_i F^{a0i} + i\{Q_B, D_0 \bar{c}^a\}) = \\ &= \frac{1}{g} \oint d^2x_i F^{0i} + \frac{1}{g} \int d^3x \{Q_B, D_0 \bar{c}^a\}, \end{aligned} \quad (1.77)$$

where $i = 1, \dots, 3$ are spatial indices. In the literature, this expression for Q^a has been used to tentatively link the confinement of color charge to the asymptotic behavior of the gluon field strength tensor $F_{\mu\nu}^a$ as $|\vec{r}| \rightarrow \infty$ [Oji78, KO79a].

BRST symmetry is a powerful tool for exploring the properties of QCD and, more generally, of the gauge theories. Modern proofs of the perturbative renormalizability of the Yang-Mills theories in the covariant gauges exploit the BRST invariance of the FP action to determine which kind of divergences can appear in their Green functions [Wei96]. BRST symmetry is also used to prove the perturbative unitarity of the scattering matrix in the context of the gauge theories, once a gauge has been fixed [KO79a]. This is done by classifying the states of the theory according to the *cohomology* of the BRST charge Q_B : the physical states $|\text{phys}\rangle$ – that is, the states which can be realized in the physical world – are identified with the BRST-closed states of zero ghost charge Q_c ,

$$Q_B |\text{phys}\rangle = 0, \quad Q_c |\text{phys}\rangle = 0, \quad (1.78)$$

where Q_c generates the transformations $c^a \rightarrow e^\lambda c^a$, $\bar{c}^a \rightarrow e^{-\lambda} \bar{c}^a$, easily seen to be an additional symmetry of the FP Lagrangian. The physical Hilbert space, defined as the quotient $(\text{Ker}\{Q_B\} \cap \text{Ker}\{Q_c\})/\text{Im}\{Q_B\}$, can then be shown to carry a positive-definite inner product, a property which is essential for interpreting mathematical quantities such as $\langle \text{phys}' | \text{phys} \rangle$ as transition amplitudes from one physical state to another.

BRST symmetry imposes relations known as Slavnov-Taylor identities (STI) [Tay71, Sla72] between the Green functions of the gauge theories. The STI are often derived from Eq. (1.62) by choosing as δF the BRST transformations of the elementary fields F , $\delta F = sF$; nonetheless, they are easier to obtain using the operator formalism (see Appendix A).

Quite generally, we might say that any identity of the form

$$\langle 0 | [Q_B, \mathcal{O}]_{\mp} | 0 \rangle = 0, \quad (1.79)$$

where $|0\rangle$ is the vacuum state of the theory, \mathcal{O} is an arbitrary operator and the upper (resp. lower) sign applies to bosonic (resp. fermionic) operators, is a Slavnov-Taylor identity. That Eq. (1.79) is indeed an identity can be seen by explicitly writing out the anti/commutator and observing that, since the vacuum must be a physical state – i.e., $Q_B |0\rangle = 0$ –,

$$\langle 0 | [Q_B, \mathcal{O}]_{\mp} | 0 \rangle = \langle 0 | Q_B \mathcal{O} \pm \mathcal{O} Q_B | 0 \rangle = 0. \quad (1.80)$$

From Eqs. (1.73) and (1.79), it follows that the VEV of the BRST transformation of any operator \mathcal{O} vanishes,

$$\langle s\mathcal{O} \rangle = 0 . \quad (1.81)$$

As an example of a STI, consider the (time-ordered) BRST transformation of the product $B^a(x)\bar{c}^b(y)$. Since

$$0 = \left\langle T \left\{ s \left(B^a(x)\bar{c}^b(y) \right) \right\} \right\rangle = \left\langle T \left\{ B^a(x)B^b(y) \right\} \right\rangle , \quad (1.82)$$

BRST invariance tells us that the two-point function of the NL field vanishes exactly. A second STI is given by

$$0 = \left\langle T \left\{ s \left(A_\mu^a(x)\bar{c}^b(y) \right) \right\} \right\rangle = \left\langle T \left\{ D_\mu c^a(x)\bar{c}^b(y) + A_\mu^a(x)B^b(y) \right\} \right\rangle , \quad (1.83)$$

that is,

$$\left\langle T \left\{ A_\mu^a(x)B^b(y) \right\} \right\rangle = - \left\langle T \left\{ D_\mu c^a(x)\bar{c}^b(y) \right\} \right\rangle . \quad (1.84)$$

The content of the above identity can be unpacked by making use of the field equations and of the canonical anticommutation relations for the ghost fields. After taking the divergence of the right-hand side of the equation, we obtain

$$\partial_{(x)}^\mu \left\langle T \left\{ D_\mu c^a(x)\bar{c}^b(y) \right\} \right\rangle = \left\langle \left\{ D_0 c^a(x), \bar{c}^b(y) \right\} \right\rangle \delta(x^0 - y^0) = -i\delta^{ab}\delta(x - y) , \quad (1.85)$$

where the first delta distribution comes from the derivative of the time-ordering operator and we have used the operatorial identities

$$\partial^\mu D_\mu c^a = 0 , \quad \{ \bar{c}^a(\vec{x}, t), D_0 c^b(\vec{y}, t) \} = -i\delta^{ab}\delta^{(3)}(\vec{x} - \vec{y}) \quad (1.86)$$

(see Appendix A). By Lorentz symmetry, it follows that

$$\left\langle T \left\{ D_\mu c^a(x)\bar{c}^b(y) \right\} \right\rangle = \int \frac{d^4 p}{(2\pi)^4} e^{-ip \cdot (x-y)} \frac{p_\mu}{p^2} \delta^{ab} . \quad (1.87)$$

Eq. (1.84) thus tells us that the correlator between the A and the B field is given by

$$\left\langle T \left\{ A_\mu^a(x)B^b(y) \right\} \right\rangle = \int \frac{d^4 p}{(2\pi)^4} e^{-ip \cdot (x-y)} \frac{-p_\mu}{p^2} \delta^{ab} . \quad (1.88)$$

The last result can be used to derive a fundamental property of the gluon propagator. If in the last equation we replace the NL field with the gluon field by applying the field equation

$$B^a = -\frac{1}{\xi} \partial^\mu A_\mu^a , \quad (1.89)$$

we find that the following relation holds for the correlator of two gluon fields:

$$\left\langle T \left\{ A_\mu^a(x)\partial^\nu A_\nu^b(y) \right\} \right\rangle = \int \frac{d^4 p}{(2\pi)^4} e^{-ip \cdot (x-y)} \xi \frac{p_\mu}{p^2} \delta^{ab} . \quad (1.90)$$

Since the components of the gluon field commute with each other, the latter is equivalent to

$$\partial_{(y)}^\nu \left\langle T \left\{ A_\mu^a(x)A_\nu^b(y) \right\} \right\rangle = \int \frac{d^4 p}{(2\pi)^4} e^{-ip \cdot (x-y)} \xi \frac{p_\mu}{p^2} \delta^{ab} . \quad (1.91)$$

Let now $\Delta_{\mu\nu}^{ab}(p)$ be the Fourier-transform of the gluon propagator $\langle T \{ A_\mu^a(x) A_\nu^b(y) \} \rangle$,

$$\langle T \{ A_\mu^a(x) A_\nu^b(y) \} \rangle = \int \frac{d^4 p}{(2\pi)^4} e^{-ip \cdot (x-y)} \Delta_{\mu\nu}^{ab}(p) . \quad (1.92)$$

By Lorentz symmetry, $\Delta_{\mu\nu}^{ab}(p)$ can be expressed in terms of two scalar functions $\Delta_T^{ab}(p)$, $\Delta_L^{ab}(p)$, so that

$$\Delta_{\mu\nu}^{ab}(p) = \Delta_T^{ab}(p) t_{\mu\nu}(p) + \Delta_L^{ab}(p) \ell_{\mu\nu}(p) , \quad (1.93)$$

where $t_{\mu\nu}(p)$ and $\ell_{\mu\nu}(p)$ are, respectively, the transverse and longitudinal projectors

$$t_{\mu\nu}(p) = \eta_{\mu\nu} - \frac{p_\mu p_\nu}{p^2} , \quad \ell_{\mu\nu}(p) = \frac{p_\mu p_\nu}{p^2} . \quad (1.94)$$

Eq. (1.91) then tells us that $\Delta_L(p) = -i\xi/p^2$, that is

$$\Delta_{\mu\nu}^{ab}(p) = \Delta_T^{ab}(p) t_{\mu\nu}(p) + \frac{-i\xi}{p^2} \delta^{ab} \ell_{\mu\nu}(p) . \quad (1.95)$$

The longitudinal component of the gluon propagator is thus constrained by BRST symmetry to be proportional to the gauge parameter ξ and to have a pole at $p^2 = 0$.

The STI obtained from applying the BRST operator to polynomials of higher degree in the fields enforce relations between the higher-order Green functions. For instance, the vanishing of $\langle T \{ s(A_\mu^a(x) A_\nu^b(y) \bar{c}^c(z)) \} \rangle$ implies that

$$\langle T \{ A_\mu^a(x) A_\nu^b(y) B^c(z) \} \rangle + \langle T \{ D_\mu c^a(x) A_\nu^b(y) \bar{c}^c(z) \} \rangle + \langle T \{ A_\mu^a(x) D_\nu^b c(y) \bar{c}^c(z) \} \rangle = 0 , \quad (1.96)$$

whereas that of $\langle T \{ s(\psi(x) \bar{\psi}(y) \bar{c}^b(z)) \} \rangle$ yields

$$\langle T \{ \psi(x) \bar{\psi}(y) B^b(z) \} \rangle = -ig \langle T \{ T_a \psi(x) \bar{\psi}(y) c^a(x) \bar{c}^b(z) \} \rangle + ig \langle T \{ \psi(x) \bar{\psi}(y) T_a c^a(y) \bar{c}^b(z) \} \rangle . \quad (1.97)$$

In the context of the covariant gauges, BRST symmetry finds yet another application in the derivation of the so-called Nielsen identities (NI) [Nie75, PS85, BLS95]. The NI describe how the Green functions of a gauge theory vary with the gauge parameter ξ . They are extremely useful when studying features such as the gauge dependence of the poles of the propagators, or more generally of any Green function.

In order to derive the general form of the Nielsen identities, we start by observing that, being $\frac{i\xi}{2} \int d^4 x B^a B^a$ the only ξ -dependent term in the FP action, given an arbitrary operator \mathcal{O} ,

$$\frac{\partial}{\partial \xi} \langle \mathcal{O} \rangle = \frac{i}{2} \int d^4 x \langle T \{ \mathcal{O} B^a(x) B^a(x) \} \rangle , \quad (1.98)$$

where we have dropped a disconnected product of the form $\langle \mathcal{O} \rangle \langle B^a B^a \rangle$ since, as we saw earlier, $\langle T \{ B^a(x) B^b(y) \} \rangle = 0$. Thanks to BRST symmetry, the last equation can be rewritten as

$$\begin{aligned} \frac{\partial}{\partial \xi} \langle \mathcal{O} \rangle &= \frac{i}{2} \int d^4 x \langle T \{ \mathcal{O} s[B^a(x) \bar{c}^a(x)] \} \rangle = \\ &= \mp \frac{i}{2} \int d^4 x \langle T \{ (s\mathcal{O}) B^a(x) \bar{c}^a(x) \} \rangle , \end{aligned} \quad (1.99)$$

where the upper (resp. lower) sign applies to bosonic (resp. fermionic) operators. The Nielsen identity for the Green function $\langle \mathcal{O} \rangle$ is then obtained by writing out explicitly the

BRST variation of the operator \mathcal{O} in the above equation. For instance, the NI for the gluon propagator reads

$$\begin{aligned} \frac{\partial}{\partial \xi} \langle T \{ A_\mu^a(x) A_\nu^b(y) \} \rangle &= -\frac{i}{2} \int d^4 z \left[\langle T \{ D_\mu c^a(x) A_\nu^b(y) B^c(z) \bar{c}^c(z) \} \rangle + \right. \\ &\quad \left. + \langle T \{ A_\mu^a(x) D_\nu c^b(y) B^c(z) \bar{c}^c(z) \} \rangle \right], \end{aligned} \quad (1.100)$$

whereas the one for the quark propagator is given by

$$\begin{aligned} \frac{\partial}{\partial \xi} \langle T \{ \psi(x) \bar{\psi}(y) \} \rangle &= -\frac{1}{2} \int d^4 z \left[\langle T \{ T_a \psi(x) \bar{\psi}(y) c^a(x) B^b(z) \bar{c}^b(z) \} \rangle + \right. \\ &\quad \left. - \langle T \{ \psi(x) \bar{\psi}(y) T_a c^a(x) B^b(z) \bar{c}^b(z) \} \rangle \right]. \end{aligned} \quad (1.101)$$

By taking the Fourier transform of the Nielsen identities, one is able to study how the poles of the corresponding Green function vary with the gauge. Let us show how this works for the case of the gluon propagator. Let $\mathcal{F}_{\mu\nu}^{ab}(x)$ be the function defined by

$$\mathcal{F}_{\mu\nu}^{ab}(x-y) = \frac{i}{2} \int d^4 z \left\{ \langle T \{ D_\mu c^a(x) A_\nu^b(y) B^c(z) \bar{c}^c(z) \} \rangle + (x \leftrightarrow y, \mu \leftrightarrow \nu, a \leftrightarrow b) \right\}. \quad (1.102)$$

In terms of the Fourier transform $\mathcal{F}_{\mu\nu}^{ab}(p)$ of $\mathcal{F}_{\mu\nu}^{ab}(x)$, the NI in Eq. (1.100) can be expressed in momentum space as

$$\frac{\partial}{\partial \xi} \Delta_{\mu\nu}^{ab}(p) = -\mathcal{F}_{\mu\nu}^{ab}(p), \quad (1.103)$$

or, dropping the indices,

$$\frac{\partial}{\partial \xi} \Delta(p) = -\mathcal{F}(p). \quad (1.104)$$

A Nielsen identity for the inverse gluon propagator is then easily derived:

$$\frac{\partial}{\partial \xi} \Delta^{-1}(p) = \Delta^{-1}(p) \cdot \mathcal{F}(p) \cdot \Delta^{-1}(p). \quad (1.105)$$

Due to the orthogonality of the transverse and longitudinal projectors, $t(p) \cdot \ell(p) = 0$, the transverse and the longitudinal components of the above equation decouple: if we set

$$\Delta^{-1}(p) = \Delta_T^{-1}(p) t(p) + \Delta_L^{-1}(p) \ell(p), \quad \mathcal{F}(p) = \mathcal{F}_T(p) t(p) + \mathcal{F}_L(p) \ell(p), \quad (1.106)$$

using the idempotency relations $t(p) \cdot t(p) = t(p)$, $\ell(p) \cdot \ell(p) = \ell(p)$ and dropping the color structure, from Eq. (1.106) we obtain the two equations

$$\frac{\partial}{\partial \xi} \Delta_T^{-1}(p) = \mathcal{F}_T(p) \Delta_T^{-2}(p), \quad \frac{\partial}{\partial \xi} \Delta_L^{-1}(p) = \mathcal{F}_L(p) \Delta_L^{-2}(p). \quad (1.107)$$

It is quite simple to check that the longitudinal identity is indeed satisfied: to do this, it suffices to observe that⁵

$$\begin{aligned} \partial_{(x)}^\mu \langle T \{ D_\mu c^a(x) A_\nu^b(y) B^c(z) \bar{c}^c(z) \} \rangle &= -i\delta(x-z) \langle T \{ A_\nu^b(y) B^a(x) \} \rangle = \\ &= -i\delta(x-z) \int \frac{d^4 p}{(2\pi)^4} e^{-ip \cdot (x-y)} \frac{p_\nu}{p^2} \delta^{ab} \end{aligned} \quad (1.108)$$

⁵Here, like before, we use the ghost field equations and anticommutation relations.

implies

$$\mathcal{F}_L(p) = \frac{i}{p^2}, \quad (1.109)$$

so that, with $\Delta_L^{-1}(p) = ip^2/\xi$, the longitudinal identity explicitly reads

$$\frac{\partial}{\partial \xi} \left(\frac{ip^2}{\xi} \right) = \frac{i}{p^2} \left(\frac{ip^2}{\xi} \right)^2 = -\frac{ip^2}{\xi^2}. \quad (1.110)$$

Of more interest is the transverse identity, since in this case the exact expression of the transverse gluon propagator is not known a priori. To see how information on the gauge dependence of the transverse pole can be obtained from the first of Eq. (1.106), we start by noticing that, since the function $\mathcal{F}_{\mu\nu}^{ab}(x)$ can be rewritten as

$$\mathcal{F}_{\mu\nu}^{ab}(x-y) = -\frac{i}{2\xi} \int d^4z \left\{ \left\langle T \left\{ D_\mu c^a(x) A_\nu^b(y) \partial \cdot A^c(z) \bar{c}^c(z) \right\} \right\rangle + (x \leftrightarrow y, \mu \leftrightarrow \nu, a \leftrightarrow b) \right\}, \quad (1.111)$$

due to the presence of two A fields in its definition, the Fourier transform $\mathcal{F}_{\mu\nu}^{ab}(p)$ will contain the gluon propagator as a factor, that is

$$\mathcal{F}(p) = F_T(p) \Delta_T(p) t(p) + F_L(p) \Delta_L(p) \ell(p) \quad (1.112)$$

for a pair of functions $F_T(p)$ and $F_L(p)$ whose zeros and poles, in general, are different from the poles of $\Delta_T(p)$ and $\Delta_L(p)$. We have already verified that this is the case for the longitudinal component, for which $F_L(p) = -1/\xi$. If we plug the last equation into the first of Eq. (1.106), we now obtain

$$\frac{\partial}{\partial \xi} \Delta_T^{-1}(p, \xi) = F_T(p, \xi) \Delta_T^{-1}(p, \xi), \quad (1.113)$$

where we have made the gauge dependence of the transverse propagator and of the function F_T explicit.

Consider now what happens to the pole of Δ_T as ξ is changed. The transverse pole $p_0(\xi)$ is defined as the solution of the equation

$$\Delta_T^{-1}(p_0(\xi), \xi) = 0. \quad (1.114)$$

By taking the total derivative of this equation with respect to the gauge parameter, we find that

$$\begin{aligned} 0 &= \frac{d}{d\xi} \Delta_T^{-1}(p_0(\xi), \xi) = \frac{\partial}{\partial \xi} \Delta_T^{-1}(p_0(\xi), \xi) + \frac{\partial}{\partial p} \Delta_T^{-1}(p_0(\xi), \xi) \frac{dp_0}{d\xi}(\xi) = \\ &= F_T(p_0(\xi), \xi) \Delta_T^{-1}(p_0(\xi), \xi) + \frac{\partial}{\partial p} \Delta_T^{-1}(p_0(\xi), \xi) \frac{dp_0}{d\xi}(\xi) = \\ &= \frac{\partial}{\partial p} \Delta_T^{-1}(p_0(\xi), \xi) \frac{dp_0}{d\xi}(\xi). \end{aligned} \quad (1.115)$$

Since the momentum-derivative of Δ_T^{-1} , in general, is different from zero⁶, the last equation implies that

$$\frac{dp_0}{d\xi}(\xi) = 0, \quad (1.116)$$

that is, the position of the pole does not depend on the gauge parameter ξ . This exact property of the strong interactions will be extremely useful when formulating a possible modification of the QCD perturbative series in Chapter 3.

⁶Actually, it can be shown that the derivative vanishes if the pole is found at $p = 0$ for every value of the gauge parameter. However, if this is the case, the gauge-parameter independence of the pole holds trivially anyways, so this does not contradict our proof.

1.2 Ordinary perturbation theory, the strong coupling constant and the infrared breakdown of perturbative QCD

Having reviewed the definition of Quantum Chromodynamics, we are now in a position to discuss the merits and failures of its standard perturbative formulation. When dealing with a quantum field theory, one rarely knows how to exactly solve the equations which describe its underlying physics. Approximate methods must thus be devised in order to turn abstract expressions into physical predictions. Perturbation theory is one such method. By assuming that the interactions only slightly affect the behavior of an otherwise free theory, it provides an expansion of the quantities of interest in powers of the coupling constant. If this assumption is accurate, the higher-order terms in the expansion will make a negligible contribution to the overall result. The approximation then consists in truncating the perturbative series at some predefined, finite order.

In the context of Quantum Chromodynamics, the results obtained by employing ordinary perturbation theory have proved to be very accurate in the high-energy regime. This is made possible by the asymptotic freedom which is typical of the non-abelian gauge theories: given a suitable definition for the energy dependence of the coupling constant, it can be shown that, as the energy increases, the coupling decreases like the inverse of a logarithm. Thus, at very high energies, the non-abelian gauge theories resemble free theories of massless gauge bosons and Dirac fermions.

If we reverse our perspective, however, we see that the perturbative method necessarily entails an increase of the coupling constant at low energies. And as the coupling increases, perturbation theory no longer can be trusted, since – at the very least – the higher-order terms in the perturbative series will become less and less negligible. The situation is only made worse by the fact that, at low energies, the coupling computed within the standard perturbative framework increases so fast that it becomes infinite at a finite energy, thus developing what is known in the literature as an infrared Landau pole. The existence of an IR Landau pole in the strong coupling constant puts the final word on the validity of ordinary perturbative QCD (pQCD) at low energies.

In what follows, we will start our discussion by reviewing the standard set-up of perturbation theory in the context of QCD.

1.2.1 The standard perturbative expansion and Feynman rules of QCD

Let \mathcal{O} be an arbitrary operator and $\langle \mathcal{O} \rangle$ be its VEV. As we saw in Sec. 1.1.2, $\langle \mathcal{O} \rangle$ can be computed in the functional formalism as

$$\langle \mathcal{O} \rangle = \frac{\int \mathcal{D}\mathcal{F} e^{iS_{\text{FP}}} \mathcal{O}}{\int \mathcal{D}\mathcal{F} e^{iS_{\text{FP}}}} . \quad (1.117)$$

In the above equation, the Faddeev-Popov action can be naturally split into two terms,

$$S_{\text{FP}} = S_0 + S_{\text{int}} , \quad (1.118)$$

where the zero-order action S_0 and the interaction action S_{int} are defined as

$$S_0 = \lim_{g \rightarrow 0} S_{\text{FP}} , \quad S_{\text{int}} = S_{\text{FP}} - S_0 . \quad (1.119)$$

Explicitly,

$$S_0 = \int d^4x \left\{ -\frac{1}{2} \partial_\mu A_\nu^a (\partial^\mu A^{a\nu} - \partial^\nu A^{a\mu}) - \frac{1}{2\xi} \partial^\mu A_\mu^a \partial^\nu A_\nu^a + \bar{\psi} (i\gamma^\mu \partial_\mu - M) \psi + \partial^\mu \bar{c}^a \partial_\mu c^a \right\}, \quad (1.120)$$

$$S_{\text{int}} = \int d^4x \left\{ -g f_{bc}^a \partial_\mu A_\nu^a A^{b\mu} A^{c\nu} - \frac{1}{4} g^2 f_{bc}^a f_{de}^a A_\mu^b A_\nu^c A^{d\mu} A^{e\nu} + g \bar{\psi} \gamma^\mu T_a \psi A_\mu^a + g f_{bc}^a \partial^\mu \bar{c}^a A_\mu^b c^c \right\}. \quad (1.121)$$

If we assume that the interaction terms contained in S_{int} contribute to $\langle \mathcal{O} \rangle$ with a small correction over the corresponding zero-order result, that is, $\langle \mathcal{O} \rangle \approx \langle \mathcal{O} \rangle_0$, where

$$\langle \mathcal{O} \rangle_0 = \frac{\int \mathcal{D}\mathcal{F} e^{iS_0} \mathcal{O}}{\int \mathcal{D}\mathcal{F} e^{iS_0}}, \quad (1.122)$$

then it makes sense to seek an expansion of Eq. (1.117) in powers of g . Of course, such an hypothesis is sensible only provided that the coupling constant g is not too large.

The power-expansion of $\langle \mathcal{O} \rangle$ can be obtained as follows. We first rewrite the exponentials in Eq. (1.117) as

$$\begin{aligned} \langle \mathcal{O} \rangle &= \left(\frac{\int \mathcal{D}\mathcal{F} e^{iS_0} \mathcal{O} \sum_{n=0}^{+\infty} \frac{1}{n!} (iS_{\text{int}})^n}{\int \mathcal{D}\mathcal{F} e^{iS_0}} \right) \left(\frac{\int \mathcal{D}\mathcal{F} e^{iS_0} \sum_{n=0}^{+\infty} \frac{1}{n!} (iS_{\text{int}})^n}{\int \mathcal{D}\mathcal{F} e^{iS_0}} \right)^{-1} = \\ &= \left(\sum_{n=0}^{+\infty} \frac{1}{n!} \langle T \{ \mathcal{O} (iS_{\text{int}})^n \} \rangle_0 \right) \left(\sum_{n=0}^{+\infty} \frac{1}{n!} \langle T \{ (iS_{\text{int}})^n \} \rangle_0 \right)^{-1}, \end{aligned} \quad (1.123)$$

where, as in Eq. (1.122), the averages denoted with the subscript 0 are to be computed with respect to the zero-order action. Then, in order to evaluate the averages, we observe that the free action S_0 is quadratic in the fields. More precisely, in momentum space,

$$-iS_0 = \int \frac{d^4p}{(2\pi)^4} \left\{ \frac{1}{2} A_\mu^a(-p) [\Delta_0^{-1}(p)]_{ab}^{\mu\nu} A_\nu^b + \bar{\psi}(p) S_M^{-1}(p) \psi(p) + \bar{c}^a(p) [\mathcal{G}_0^{-1}(p)]_{ab} c^b(p) \right\}, \quad (1.124)$$

where $\Delta_0(p)$, $S_M(p)$ and $\mathcal{G}_0(p)$ are, respectively, the zero-order gluon, quark and ghost propagator,

$$\Delta_{0\mu\nu}^{ab}(p) = \int d^4x e^{ip \cdot x} \left\langle T \left\{ A_\mu^a(x) A_\nu^b(0) \right\} \right\rangle_0 = \frac{-i}{p^2} \delta^{ab} [t_{\mu\nu}(p) + \xi \ell_{\mu\nu}(p)], \quad (1.125)$$

$$S_M(p) = \int d^4x e^{ip \cdot x} \left\langle T \left\{ \psi(x) \bar{\psi}(0) \right\} \right\rangle_0 = \frac{i}{\not{p} - M} \mathbb{1}_{3 \times 3}, \quad (1.126)$$

$$\mathcal{G}_0^{ab}(p) = \int d^4x e^{ip \cdot x} \left\langle T \left\{ c^a(x) \bar{c}^b(0) \right\} \right\rangle_0 = \frac{i}{p^2} \delta^{ab}, \quad (1.127)$$

with $\not{p} = \gamma^\mu p_\mu$, and their inverses are given by

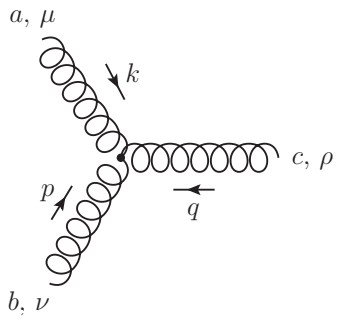
$$[\Delta_0^{-1}(p)]_{ab}^{\mu\nu}(p) = ip^2 \delta_{ab} \left(t^{\mu\nu}(p) + \frac{1}{\xi} \ell^{\mu\nu}(p) \right), \quad (1.128)$$

$$S_M^{-1}(p) = \int d^4x e^{ip \cdot x} \left\langle T \left\{ \psi(x) \bar{\psi}(0) \right\} \right\rangle_0 = -i(\not{p} - M) \mathbb{1}_{3 \times 3}, \quad (1.129)$$

$$[\mathcal{G}_0^{-1}(p)]_{ab} = \int d^4x e^{ip \cdot x} \left\langle T \left\{ c^a(x) \bar{c}^b(0) \right\} \right\rangle_0 = -ip^2 \delta_{ab}. \quad (1.130)$$

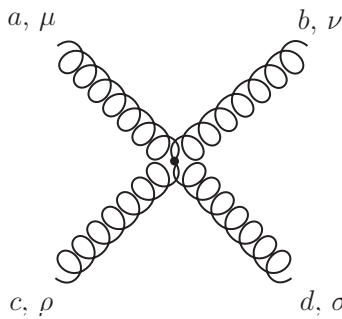
$$\longrightarrow = \frac{i}{\not{p} - M} \mathbb{1}_{3 \times 3}$$

Figure 1.3: Zero-order quark propagator



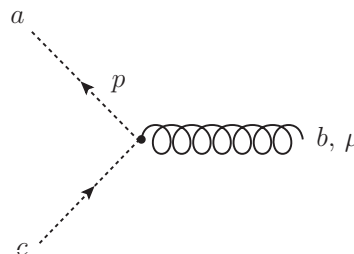
$$= g f^{abc} [\eta^{\mu\nu} (k - p)^\rho + \eta^{\nu\rho} (p - q)^\mu + \eta^{\rho\mu} (q - k)^\nu]$$

Figure 1.4: 3-gluon vertex



$$= -ig^2 [f^{abe} f^{cde} (\eta^{\mu\rho} \eta^{\nu\sigma} - \eta^{\mu\sigma} \eta^{\nu\rho}) + f^{ace} f^{bde} (\eta^{\mu\nu} \eta^{\rho\sigma} - \eta^{\mu\sigma} \eta^{\nu\rho}) + f^{ade} f^{bce} (\eta^{\mu\nu} \eta^{\rho\sigma} - \eta^{\mu\rho} \eta^{\nu\sigma})]$$

Figure 1.5: 4-gluon vertex



$$= -g f^{abc} p^\mu$$

Figure 1.6: Ghost-gluon vertex

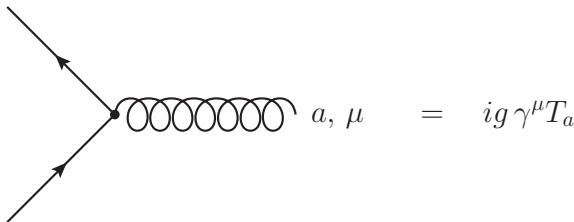


Figure 1.7: Quark-gluon vertex

As the last step in our derivation, a combinatorial argument [PS95] can be used to prove that

$$\sum_{n=0}^{+\infty} \frac{1}{n!} \langle T \{ \mathcal{O}(iS_{\text{int.}})^n \} \rangle_0 = \left(\sum_{n=0}^{+\infty} \frac{1}{n!} \langle T \{ \mathcal{O}(iS_{\text{int.}})^n \} \rangle_{0,\text{conn.}} \right) \left(\sum_{n=0}^{+\infty} \frac{1}{n!} \langle T \{ (iS_{\text{int.}})^n \} \rangle_0 \right), \quad (1.133)$$

where $\langle T \{ \mathcal{O}(iS_{\text{int.}})^n \} \rangle_{0,\text{conn.}}$ is given by the subset of diagrams in which all the interaction vertices coming from $(iS_{\text{int.}})^n$ are connected to at least one vertex coming from the “external” operator \mathcal{O} . Therefore, going back to Eq. (1.123), we obtain our final expression for $\langle \mathcal{O} \rangle$ in the form

$$\langle \mathcal{O} \rangle = \sum_{n=0}^{+\infty} \frac{1}{n!} \langle T \{ \mathcal{O}(iS_{\text{int.}})^n \} \rangle_{0,\text{conn.}}, \quad (1.134)$$

where we remark that the averages are to be computed diagrammatically using the Feynman rules of the theory. Clearly, with the exception of the $n = 0$ term which is equal to $\langle \mathcal{O} \rangle_0$, the remaining terms under the sign of summation will be proportional to powers of the coupling constant g .

Under what conditions does the power-expansion of the Green functions fail? The first and most obvious answer is that it fails when the coupling constant is too large. If this is the case, higher-order terms will generally be larger than the lower-order ones, and only retaining the first few terms of the expansion will yield a bad approximation.

Ordinary perturbation theory is also unsuitable for computing Green functions which receive non-negligible contributions from quantities which are not analytical in the coupling constant. An example of these are non-perturbative mass scales of the form

$$\Lambda = \mu e^{-\frac{\kappa}{g^2}}, \quad (1.135)$$

with κ a constant and μ a second mass scale, which cannot be expanded in powers of g .

A third situation in which the perturbative series is unable to capture the exact behavior of a Green function is when the latter has features that can only be described by resumming an infinite number of diagrams. This is what happens, for instance, when computing some four- and higher-point Green functions which contain information on bound states. The latter is lost when a purely perturbative truncation is performed.

Finally, perturbation theory can fail if the perturbative series does not converge. If this is the case, it may happen that adding higher-order terms to the perturbative series

improves the approximation up until some finite order, after which the higher-order corrections actually start to make the approximation worse. The worst-kept secret in quantum field theory is that perturbation theory is believed, in fact, not to converge⁸. Nonetheless, as far as Quantum Chromodynamics is concerned, going to higher perturbative orders has so far only improved the match with the experimental data.

To end this section, we make an observation that will be useful later on in Chapter 3. Going back to Eq. (1.131), we see that the correspondence between (perturbative) quantum averages and Feynman diagrams exists simply because the zero-order action S_0 , being quadratic in the fields, allows us to compute the former in terms of Gaussian integrals. Indeed, the derivation which brought us from the exact Green function $\langle \mathcal{O} \rangle$ to its perturbative expression only rests upon this basic property of S_0 . As a consequence, if instead of the S_0 given by Eq. (1.120) we had chosen any other quadratic action S'_0 , the procedure we followed in the previous pages would have yielded the same final result, with $S_{\text{int.}}$ replaced by $S'_{\text{int.}} = S_{\text{FP}} - S'_0$. Of course, such a result would no longer be an expansion of the Green function in powers of the coupling constant. In some situations, however, this may be precisely what we need in order to account for intrinsically non-perturbative effects.

1.2.2 Regularization and renormalization

When perturbation theory is used to compute the Green functions of a quantum field theory, it may happen that some of the integrals which appear in the expressions do not converge. The resulting divergences are called UV divergences if they arise from integrals I which in the high-momentum limit of their domain of integration behave like

$$I \sim \int \frac{d^4q}{(2\pi)^4} \frac{1}{q^{\kappa_{\text{UV}}}} \quad (1.136)$$

with $\kappa_{\text{UV}} \leq 4$, or IR divergences if they arise from integrals which in the low-momentum limit of the integration domain behave like

$$I \sim \int \frac{d^4q}{(2\pi)^4} \frac{1}{q^{\kappa_{\text{IR}}}} \quad (1.137)$$

with $\kappa_{\text{IR}} \geq 4$. Since in local quantum field theories such as QCD momenta with a negative power can enter the perturbative series only via the propagators, these theories are free of IR divergences when they describe fields which are all massive: if this is the case, then the low-energy limit of the propagators $\lim_{q \rightarrow 0} \pm i(q^2 - m^2)^{-1} = \mp i m^{-2}$ prevents the appearance of powers of momenta $\kappa_{\text{IR}} \geq 4$ as $q \rightarrow 0$. On the other hand, if the theory contains massless fields, then its Green functions can be IR-divergent.

As we saw in the last section, within the ordinary perturbative formulation of QCD the gluon and ghost fields are both treated as massless; IR divergences, thus, do indeed show up in the standard QCD perturbative series. The usual way to deal with these divergences is to limit oneself to the computation of quantities which are IR-finite⁹. In what follows, we will not discuss further the IR-finiteness of QCD, given that the non-perturbative generation of a mass for the gluon is expected to cure the IR divergences. Instead, we will give a brief overview of the status of QCD for what concerns its finiteness in the UV.

⁸And is actually *known* not to converge in the framework of Quantum Electrodynamics [Dys52].

⁹A comprehensive discussion of this topic in the context of standard perturbation theory can be found e.g. in [Wei95], Chapter 13.

By making use of dimensional arguments [Wei95], it can be shown that the Green functions of any quantum field theory whose coupling constants have non-positive mass dimension do contain UV divergences. QCD with its adimensional strong coupling g is, of course, no exception. In order to remove the divergences and obtain meaningful physical predictions, the perturbative series of QCD must undergo a procedure known as *renormalization*.

Renormalization is carried out in two steps. The first of these, called *regularization*, consists in redefining the perturbative series so that the UV divergences only appear when a suitable limit is taken. As a consequence of regularization, the series is made finite, but also dependent on a *regulator*, which needs to be removed at the end the calculation. The second step is the renormalization proper, and consists in absorbing the diverging terms into the free parameters of the theory. Once these terms disappear from the equations, the regulator can be removed safely, and the procedure as a whole will have left behind a finite expression.

The most commonly employed regularization scheme when dealing with gauge theories is *dimensional regularization* (dimreg). If we go back to Eq. (1.136), after generalizing from the 4-dimensional spacetime to a d -dimensional one,

$$I \sim \int \frac{d^d q}{(2\pi)^d} \frac{1}{q^{\kappa_{UV}}} , \quad (1.138)$$

we see that, if d strictly smaller than κ_{UV} , then the integral I does actually converge. In particular, we could compute I in an arbitrary dimension d and, as long as the latter is left undetermined, the resulting expression would remain finite. This is what dimreg does. By redefining the theory so that it fields live in $d = 4 - \epsilon$ dimensions, dimreg provides finite results which depend on the regulator ϵ . In the regularized expressions, the UV divergences appear as poles of the form $1/\epsilon^\kappa$ – with κ a positive integer – which must be removed by renormalization before taking the $\epsilon \rightarrow 0$ limit.

When dimensionally regularizing a theory, one must be careful in redefining any quantity in such a way that the corresponding 4-dimensional limit has the correct dimensions. This inevitably leads to the introduction of a mass scale μ into the expressions. For instance, since in d dimensions the strong coupling constant $g_{(d)}$ has mass dimension $(4-d)/2$, in going from 4 to d dimensions the coupling must be defined as $g_{(d)} = \mu^{\frac{4-d}{2}} g_{(4)}$, where the physical interpretation of the mass scale μ depends on the choice of renormalization scheme which is later made to remove the divergences.

Behind renormalization lies the observation that the parameters which are contained in the Lagrangian are not actually measured in the experiments; rather, what is measured are suitable combinations of Green functions. A similar argument can be made for the quantum fields. For instance, in the LSZ formula for the calculation of cross sections [PS95], the propagators – and thus the corresponding fields – appear in such a way that multiplying the latter by some constant does not change the result. Since neither the value of the parameters nor the normalization of the fields can be measured in the experiments, we are free to redefine both. The parameters and fields which were originally present in the Lagrangian are referred to as *bare* quantities, whereas their redefined versions are called *renormalized* quantities. Explicitly, in the context of QCD, one introduces a set of multiplicative constants $Z_A, Z_c, Z_\psi, Z_g, Z_\xi$ and Z_M such that¹⁰

¹⁰It can be proved that the ghost and antighost fields, as well as the different color components of the same field, can be renormalized using the same multiplicative factor, see e.g. [Wei96].

$$A_{B\mu}^a = Z_A^{1/2} A_{R\mu}^a, \quad c_B^a = Z_c^{1/2} c_R^a, \quad \bar{c}_B^a = Z_c^{1/2} \bar{c}_R^a, \quad \psi_B = Z_\psi^{1/2} \psi_R, \quad (1.139)$$

$$g_B = Z_g g_R, \quad \xi_B = Z_\xi \xi_R, \quad M_B = Z_M M_R,$$

where the subscripts B and R denote, respectively, bare and renormalized quantities. The Green functions are similarly renormalized. For instance, for the propagators, we have

$$\langle T \{ A_{R\mu}^a(x) A_{R\nu}^b(y) \} \rangle = Z_A^{-1} \langle T \{ A_{B\mu}^a(x) A_{B\nu}^b(y) \} \rangle, \quad (1.140)$$

$$\langle T \{ c_R^a(x) \bar{c}_R^b(y) \} \rangle = Z_c^{-1} \langle T \{ c_B^a(x) \bar{c}_B^b(y) \} \rangle, \quad (1.141)$$

$$\langle T \{ \psi_R(x) \bar{\psi}_R(y) \} \rangle = Z_\psi^{-1} \langle T \{ \psi_B(x) \bar{\psi}_B(y) \} \rangle. \quad (1.142)$$

Consider what happens if the bare propagators in the above equations contain UV divergences. If such divergences appear as multiplicative factors, then they can be absorbed into the renormalization factors Z_A , Z_c and Z_ψ , and the resulting renormalized propagators will be finite. In the process of factorizing the divergences, the bare couplings and masses may also need to be renormalized (and usually they do). The property of a theory by which all of its Green functions can be made UV-finite by a renormalization of the kind defined in Eq. (1.139) is called *multiplicative renormalizability*. By making use of BRST symmetry, it can be shown that QCD is indeed a multiplicatively renormalizable theory [Wei96].

While the diverging terms contained in the Z -factors are fixed by the requirement that the renormalized Green functions be finite, no such constraint exists with respect to the choice of the finite part of the renormalization factors. This has two implications. First of all, renormalization can be carried out in a multitude of schemes, depending on which *renormalization conditions* are chosen to fix the (finite terms of the) Z -factors. Second of all, the renormalized Green functions are renormalization-scheme-dependent. Thus, when comparing Green functions – or, more generally, any renormalized quantity – computed by different methods, one must be careful to take into account any difference in definition that might come from renormalization.

In QCD, there is no single universally adopted scheme for the renormalization of coupling, masses and fields. Nevertheless, three renormalization schemes are often used in the literature. These are the minimal-subtraction (MS), modified-minimal-subtraction ($\overline{\text{MS}}$) and momentum-subtraction (MOM) schemes.

The MS and $\overline{\text{MS}}$ schemes are defined specifically for dimensionally regularized quantities. In dimreg, it can be shown that, as $\epsilon = 4 - d \rightarrow 0$, the divergences take the general form

$$\left(\frac{2}{\epsilon} + \ln 4\pi - \gamma_E \right)^\kappa \quad (1.143)$$

for some positive integer κ , where $\gamma_E \approx 0.5772$ is the Euler-Mascheroni constant. In the MS scheme, the renormalization constants are chosen so that only the ϵ -poles are removed from the equations. In the $\overline{\text{MS}}$ scheme, on the other hand, also the $\ln 4\pi$ and γ_E constants are removed. The highest-order perturbative results obtained so far in QCD are computed in the MS and $\overline{\text{MS}}$ schemes.

In the MOM scheme, the Z -factors are chosen so that the renormalized Green functions are equal to some specified quantity at fixed spacelike momentum $p^2 = -\mu^2$ – often, to their tree-level value. For instance, the MOM-scheme gluon and ghost renormalization factors Z_A and Z_c are defined by the requirement that the exact transverse gluon and

ghost propagators $\Delta_T(p^2; \mu)$ and $\mathcal{G}(p^2; \mu)$ renormalized at the scale μ , when evaluated at $p^2 = -\mu^2$, be equal to

$$\Delta_T(p^2; \mu) \Big|_{p^2=-\mu^2} = \frac{-i}{-\mu^2}, \quad \mathcal{G}(p^2; \mu) \Big|_{p^2=-\mu^2} = \frac{i}{-\mu^2}. \quad (1.144)$$

The MOM scheme is especially suitable for situations in which finite-mass effects cannot be neglected when renormalizing the theory. We will explain precisely what this means in Chapter 3.

In the next section, we will see that renormalization causes the parameters of the theory to acquire a dependence on the energy scale. The analysis of the parameters' scale dependence is the subject of study of the Renormalization Group approach.

1.2.3 The Renormalization Group, the running coupling constant and the Landau pole

As we saw both in the context of dimensional regularization and in defining the MOM scheme, when renormalizing a quantum field theory one is forced to introduce a momentum scale into the expressions. Let us explore in more detail how this works and what use can be made of this aspect of renormalization.

In dimreg, in order for the fields, couplings and masses to have the correct mass dimension in the $\epsilon = 4 - d \rightarrow 0$ limit, their corresponding renormalized quantities must be defined as

$$A_{B\mu}^a = \mu^{-\frac{\epsilon}{2}} Z_A^{1/2} A_{R\mu}^a, \quad c_B^a = \mu^{-\frac{\epsilon}{2}} Z_c^{1/2} c_R^a, \quad \bar{c}_B^a = \mu^{-\frac{\epsilon}{2}} Z_c^{1/2} \bar{c}_R^a, \quad \psi_B = \mu^{-\frac{\epsilon}{2}} Z_\psi^{1/2} \psi_R, \quad (1.145)$$

$$g_B = \mu^{-\frac{\epsilon}{2}} Z_g g_R, \quad \xi_B = Z_\xi \xi_R, \quad M_B = Z_M M_R,$$

where μ is an energy scale. Since the bare quantities do not depend on μ , it follows that the Z -factors and the renormalized quantities, in general, are μ -dependent.

In the MS and $\overline{\text{MS}}$ scheme, by definition, the renormalization constants only contain ϵ -poles (plus μ -independent constants in the latter scheme); these poles, of course, are multiplied by factors of the coupling constant. Without loss of generality, we can assume that the coupling appears in the Z -factors in its renormalized form – i.e., as g_R –, for in any case g_B can be expressed in terms of the former. When the MS and $\overline{\text{MS}}$ renormalization constants are expressed as a series in ϵ^{-1} and g_R , they clearly depend on the scale μ only implicitly, through the coupling constant g_R . By looking at Eq. (1.145), then, we see that all of the renormalized quantities in the MS and $\overline{\text{MS}}$ schemes must have an explicit dependence on the dimreg scale μ . In particular, it makes sense to ask how they vary as functions of μ .

Consider the renormalized gluon propagator: in dimreg,

$$\Delta_{\mu\nu}^{ab}(x; \mu) = \left\langle T \left\{ A_{R\mu}^a(x) A_{R\nu}^b(0) \right\} \right\rangle = \mu^\epsilon Z_A^{-1} \left\langle T \left\{ A_{B\mu}^a(x) A_{B\nu}^b(0) \right\} \right\rangle. \quad (1.146)$$

Since in the MS/ $\overline{\text{MS}}$ schemes, as we just saw, the renormalized fields depend explicitly on the dimreg scale μ , the renormalized propagators do as well (hence the notation with μ as an argument of $\Delta_{\mu\nu}^{ab}$). By taking the total derivative of both members of Eq. (1.146) with respect to μ and switching to momentum space, we obtain the following equation for the renormalized gluon propagator:

$$\left(\mu \frac{\partial}{\partial \mu} + \beta_g \frac{\partial}{\partial g_R} + \gamma_M M_R \frac{\partial}{\partial M_R} + \gamma_\xi \xi_R \frac{\partial}{\partial \xi_R} + \gamma_A \right) \Delta_{\mu\nu}^{ab}(p; \mu) = 0, \quad (1.147)$$

where the *beta* and *gamma* functions – the latter being also known as *anomalous dimensions* – are defined as

$$\beta_g = \mu \frac{dg_R}{d\mu}, \quad \gamma_M = \frac{\mu}{M_R} \frac{dM_R}{d\mu}, \quad \gamma_\xi = \frac{\mu}{\xi_R} \frac{d\xi_R}{d\mu}, \quad \gamma_A = \frac{\mu}{Z_A} \frac{dZ_A}{d\mu}. \quad (1.148)$$

From the second line of Eq. (1.145), we compute that

$$\beta_g = \frac{\epsilon}{2} g_R - \frac{\mu}{Z_g} \frac{dZ_g}{d\mu} g_R, \quad \gamma_M = -\frac{\mu}{Z_M} \frac{dZ_M}{d\mu}, \quad \gamma_\xi = -\frac{\mu}{Z_\xi} \frac{dZ_\xi}{d\mu}. \quad (1.149)$$

Eq. (1.147) is called the Renormalization-Group (RG) equation for the gluon propagator (in the $\overline{\text{MS}}$ scheme).

By proceeding as we did for the gluon propagator, one can derive RG equations for any of the Green functions of the theory. These equations are generally used for improving the convergence of the perturbative series, so that the perturbative approximation remains valid over a wide range of momenta. Roughly speaking, since at order n the fixed-scale, renormalized perturbative expressions contain terms of the form

$$\left(g^2 \ln \frac{-p^2}{\mu^2} \right)^n, \quad (1.150)$$

perturbation theory breaks down when $\left| g^2 \ln \frac{-p^2}{\mu^2} \right| \sim 1$. This happens when the energy scale of the momenta is much larger or much smaller than that of the renormalization scale μ . A way to tame these large logs, thus improving the approximation, is to make use of a *sliding* renormalization scale. This is precisely what can be achieved by solving the RG equations.

As an example, let us go back to the gluon propagator. For simplicity, we will only consider its transverse component. The solution of the RG equation for the transverse gluon propagator, renormalized in the $\overline{\text{MS}}$ scheme at the scale μ , can be expressed as

$$\Delta_T(p^2; g_R(\mu), M_R(\mu), \xi_R(\mu), \mu) = e^{-\int_{\mu_0}^{\mu} \frac{d\mu'}{\mu'} \gamma_A(\mu')} \Delta_T(p^2; g_R(\mu_0), M_R(\mu_0), \xi_R(\mu_0), \mu_0), \quad (1.151)$$

where μ_0 is a second mass scale and we have written down explicitly all the parameters on which the propagator depends. If we take μ_0 to be equal to $p = \sqrt{-p^2}$, then we can put the last equation in the form

$$\Delta_T(p^2; g_R(\mu), M_R(\mu), \xi_R(\mu), \mu) = e^{\int_{\mu}^p \frac{d\mu'}{\mu'} \gamma_A(\mu')} \Delta_T(p^2; g_R(p), M_R(p), \xi_R(p), p). \quad (1.152)$$

Thus, by making use of the RG equations, the propagator evaluated at the momentum p and renormalized at the scale μ can be expressed as a function of the parameters renormalized at the scale p , rather than on those renormalized at the scale μ . Since at $p^2 = -\mu^2$ the logs of the form $\log(-p^2/\mu^2)$ vanish, the right-hand side of the equation does not contain large logs. As a result, the perturbative series will not break down when $\left| g^2 \ln \frac{-p^2}{\mu^2} \right| \sim 1$, but rather when $g^2(p) \sim 1$.

In the context of the MOM scheme, the RG improvement of the Green functions works in a slightly different, but non-dissimilar way. Going back to Eq. (1.145) and recalling that, in the MOM scheme, the renormalized quantities are defined by fixing their value at some specified momentum scale μ_{MOM} which bears no connection to the dimreg scale μ ,

we see that the renormalized fields, couplings and masses, together with the renormalization factors, must necessarily depend on μ_{MOM} . For instance, since the transverse gluon propagator's MOM renormalization condition reads

$$Z_A^{-1} D_{B,T}(p^2 = -\mu_{\text{MOM}}^2) = D_T(p^2 = -\mu_{\text{MOM}}^2; \mu_{\text{MOM}}) = \frac{i}{\mu_{\text{MOM}}^2} , \quad (1.153)$$

where we have denoted with $D_{B,T}(p^2)$ the bare transverse gluon propagator, it is clear that Z_A explicitly depends on μ_{MOM} :

$$Z_A = -i\mu_{\text{MOM}}^2 D_{B,T}(-\mu_{\text{MOM}}^2) . \quad (1.154)$$

This is at variance with what happens in the MS and $\overline{\text{MS}}$ schemes with respect to the dimreg scale μ . Then, since $A_{B\mu}^a = \mu^{-\frac{\epsilon}{2}} Z_A^{1/2} A_{R\mu}^a$, we see that the renormalized gluon field – and the renormalized gluon propagator with it – must explicitly depend on the MOM scale μ_{MOM} as well. The same applies to the other renormalized fields, parameters and Green functions. Thus, whereas in the MS and $\overline{\text{MS}}$ schemes we were interested in investigating the dependence of the Green functions on the dimreg scale μ , in the MOM scheme we study their dependence with respect to the MOM scale μ_{MOM} .

The derivation of the RG equations in the MOM scheme follows the same steps undertaken to derive those of the MS and $\overline{\text{MS}}$ schemes. The result is formally identical to its MS/ $\overline{\text{MS}}$ counterpart, with μ everywhere replaced by μ_{MOM} . The only formal difference with respect to the MS/ $\overline{\text{MS}}$ case is that, since in the MOM scheme we do not differentiate with respect to the dimreg scale μ , the MOM-scheme beta function loses an ϵ -term:

$$\beta_g|_{\text{MOM}} = -\frac{\mu_{\text{MOM}}}{Z_g} \frac{dZ_g}{d\mu_{\text{MOM}}} g_R . \quad (1.155)$$

Despite the similarities between the MS/ $\overline{\text{MS}}$ and MOM RG equations, we should notice that the beta functions and anomalous dimensions computed in these schemes are very different from each other. Indeed, as we remarked before, the MS/ $\overline{\text{MS}}$ Z -factors – and the beta and gamma functions with them – do not explicitly depend on the renormalization scale; the very opposite holds in the MOM scheme. Nonetheless, the solutions of the RG equations are formally the same in each of the three schemes. As a consequence, the removal of the large logs by the RG improvement of the perturbative series can be carried out in the MOM scheme as well.

From the perspective of the Renormalization Group, the strength of the interaction is measured in terms of the momentum-scale-dependent coupling¹¹ $g(\mu)$. The latter is known as the *running coupling constant* and is defined as the solution of the beta-function equation

$$\mu \frac{dg}{d\mu} = \beta_g , \quad (1.156)$$

where the explicit form of β_g depends on the renormalization scheme in which g is defined. What does the beta function of QCD look like in the MS/ $\overline{\text{MS}}$ scheme? An explicit one-loop calculation [PS95] carried out in ordinary perturbation theory shows that, for a Yang-Mills theory with gauge group SU(N) minimally coupled to n_f Dirac fields in the fundamental representation,

$$\beta_g = -\frac{\beta_0 g^3}{16\pi^2} , \quad (1.157)$$

¹¹From now on we drop the R subscript to denote renormalized quantities.

where the beta-function coefficient β_0 is given by

$$\beta_0 = \frac{11}{3}N - \frac{2}{3}n_f . \quad (1.158)$$

Clearly, as long as $n_f < \frac{11}{2}N$, the one-loop beta function is negative. As a consequence, the corresponding running coupling constant will decrease with the momentum scale. This behavior is known as asymptotic freedom, and is typical of the non-abelian gauge theories. For QCD we have $N = 3$ and n_f at most¹² equal to 6; therefore, $\beta_0 \geq 7$: QCD is an asymptotically free theory.

Asymptotic freedom is the reason why standard pQCD works so well in the UV regime. If we assume that there exists an energy scale at which the perturbative truncation of the QCD Green functions constitutes a good approximation, then the Renormalization Group tells us that at larger scales, being the coupling smaller, the perturbative series will converge even better. Higher orders in perturbation theory will become more and more negligible, and the behavior described by Eq. (1.157) will become (asymptotically) exact. Of course, the assumption is proved right by comparing the theoretical predictions to the experimental results.

The negativity of the beta function, however, also implies that at lower energies the coupling becomes larger. To one loop, we can exactly solve the beta-function equation and obtain

$$g^2(\mu) = \frac{g^2(\mu_0)}{1 + \frac{\beta_0 g^2(\mu_0)}{16\pi^2} \ln(\mu^2/\mu_0^2)} \quad (1.159)$$

for the one-loop running coupling of standard perturbation theory. Whereas in the $\mu \rightarrow \infty$ limit $g^2(\mu)$ goes to zero like the inverse of a logarithm, in the IR the coupling increases faster and faster, until it develops a pole at a finite scale Λ whose value is given by

$$\Lambda = \mu_0 \exp\left(-\frac{8\pi^2}{\beta_0 g^2(\mu_0)}\right) . \quad (1.160)$$

Such a singularity is known as an IR Landau pole, and outright invalidates the one-loop standard perturbative approximation of QCD at low energies. The situation does not improve at all when higher-order corrections are included in the perturbative series: if we express the beta function's power expansion as

$$\beta_g = -\frac{g^3}{16\pi^2} \sum_{n=0}^{+\infty} \beta_n \left(\frac{g^2}{16\pi^2}\right)^n , \quad (1.161)$$

then we find that, for QCD, $\beta_n > 0$ at least up to $n = 4$, which is the current limit of the perturbative calculations. As a result, as the perturbative order is increased, the running coupling diverges at scales which are even larger than the Λ defined by Eq. (1.160).

Does this mean that QCD ceases to be a self-consistent theory at low energies? Of course not. Before hitting the Landau pole, the running coupling computed in standard perturbation theory has long become too large for the ordinary perturbative approximation to be trusted. The Landau pole is, in fact, an artifact of standard pQCD: as we will see starting from the next chapter, other approaches allow us to compute running coupling constants which not only are finite in the IR, but also remain relatively small at low energies. We will review some of these approaches in the following chapters.

¹²We say ‘‘at most’’ because, as it turns out, the number n_f which must be plugged into the beta-function equation at the scale μ is actually equal to the number of fermions whose masses are smaller than μ .

In conclusion, while asymptotic freedom makes sure that ordinary perturbation theory constitutes a good approximation in the UV, the existence of an IR Landau pole in the pQCD running coupling constant signals the breakdown of the method in the low-energy regime. Due to the failure of pQCD at low energies, alternative approaches have to be devised for studying the IR dynamics of the strong interactions.

2

Non-perturbative techniques and results in Quantum Chromodynamics

In this chapter we will briefly review some of the techniques that are employed to study the non-perturbative regime of Quantum Chromodynamics and describe results upon which we will rely during the rest of this thesis. In Sec. 2.1 we will go over the definition of lattice QCD within the framework of pure Yang-Mills theory and report the results of [DOS16] regarding the Landau-gauge gluon propagator and the Taylor-scheme running coupling. In Sec. 2.2 we will formulate the Operator Product Expansion in a general setting and show how non-vanishing vacuum condensates can contribute to the Green functions of QCD with terms that cannot be derived by ordinary perturbative methods. In Sec. 2.3 we will review the Gribov-Zwanziger approach to the existence of the Gribov copies and discuss the analytical properties of the Gribov-Zwanziger zero-order gluon propagator both in the absence and in the presence of condensates. Finally, in Sec. 2.4 we will describe the set-up of the Curci-Ferrari model and report the one- and two-loop results of [GPRT19] concerning the RG-improved gluon propagator.

2.1 Lattice QCD

2.1.1 Set-up

Recall that the quantum average $\langle \mathcal{O} \rangle$ of an arbitrary operator \mathcal{O} can be computed as

$$\langle \mathcal{O} \rangle = \frac{\int \mathcal{D}\mathcal{F} e^{iS} \mathcal{O}}{\int \mathcal{D}\mathcal{F} e^{iS}}, \quad (2.1)$$

where S is the classical action of the theory and $\mathcal{D}\mathcal{F}$ is the measure over the field configurations. Due to the oscillatory nature of the exponential e^{iS} , the integrals in Eq. (2.1) converge very poorly when evaluated numerically by making use of Monte Carlo techniques. This can however be fixed by going from Minkowski spacetime to Euclidean spacetime¹.

The (4-dimensional) Euclidean spacetime is defined by taking the fourth component $\tau = x^4$ of the Euclidean position 4-vector to be equal to $it = ix^0$, where $t = x^0$ is the time component of the Minkowski position 4-vector. Despite being a real quantity by definition, τ is referred to as the *imaginary time*. In the action S of the theory, the integration measure, the spacetime derivatives and the fields can be replaced by corresponding quantities defined in Euclidean spacetime:

¹The dynamical content of the theory is then recovered by performing an analytic continuation of the Euclidean results back to Minkowski space.

$$\begin{aligned}
dx^0 dx^1 dx^2 dx^3 &= -i dx^4 dx^1 dx^2 dx^3 , \\
\partial_0 &= \partial/\partial x^0 = i\partial/\partial x^4 = i\partial_4 , \\
V^0 &= -iV^4 , \\
V_0 &= iV_4 ,
\end{aligned} \tag{2.2}$$

where V^0, V_0 and V^4, V_4 are, respectively, the time components of a Minkowski vector or covector and the imaginary-time components of a Euclidean vector or covector. In terms of its Lagrangian \mathcal{L} , the action then reads

$$S = \int dx^0 dx^1 dx^2 dx^3 \mathcal{L} = -i \int dx^4 dx^1 dx^2 dx^3 \mathcal{L}|_{x^0=-ix^4} = iS_E , \tag{2.3}$$

where S_E , defined as

$$S_E = - \int dx^4 dx^1 dx^2 dx^3 \mathcal{L}|_{x^0=-ix^4} \tag{2.4}$$

is the *Euclidean action* of the theory. As long as the energy density is positive-definite, S_E turns out to be a non-negative quantity. It follows that, in Euclidean space, the average

$$\langle \mathcal{O} \rangle = \frac{\int \mathcal{D}\mathcal{F} e^{-S_E} \mathcal{O}}{\int \mathcal{D}\mathcal{F} e^{-S_E}} \tag{2.5}$$

has nice convergence properties thanks to the damped nature of the real exponential e^{-S_E} . In practice, when Monte Carlo techniques are employed to compute averages like $\langle \mathcal{O} \rangle$, e^{-S_E} is used as the probability density for sampling the configuration space.

Dropping the label E , the Euclidean action S_{YM} of pure Yang-Mills theory reads

$$S_{\text{YM}} = \int d^4x \frac{1}{4} F_{\mu\nu}^a F^{a\mu\nu} , \tag{2.6}$$

where $d^4x = dx^4 dx^1 dx^2 dx^3$ and in terms of the component A_4^a and of derivatives with respect to x^4 the gluon field-strength tensor $F_{\mu\nu}^a$ is still defined as $F_{\mu\nu}^a = \partial_\mu A_\nu^a - \partial_\nu A_\mu^a + gf_{bc}^a A_\mu^b A_\nu^c$. In Eq. (2.6), the spacetime indices are raised and lowered using the Euclidean metric $\delta = \text{diag}(+1, +1, +1, +1)$ in place of the Minkowski metric. Clearly, $S_{\text{YM}} \geq 0$.

The Euclidean Yang-Mills action is discretized on the lattice [SO04] by defining group variables $U_\mu(x) \in \text{SU}(3)$ over the links that connect any pair of neighboring lattice sites, where the index μ refers to the direction of the link. $U_\mu(x)$ is then interpreted in terms of the (Euclidean) gauge field A_μ as

$$U_\mu(x) = e^{ig_0 a A_\mu(x + a\hat{e}_\mu/2)} + O(a^3) , \tag{2.7}$$

where g_0 is the bare lattice coupling, a is the lattice spacing, \hat{e}_μ is a unit spacetime vector in the direction μ and $A_\mu(x + a\hat{e}_\mu/2) = A_\mu^a(x + a\hat{e}_\mu/2) T_a$ is the gauge field evaluated midpoint in the link. By converse, up to higher-order corrections in the lattice spacing,

$$A_\mu(x + a\hat{e}_\mu/2) = \frac{1}{2ig_0 a} \left(U_\mu(x) - U_\mu^\dagger(x) \right) + O(a^2) . \tag{2.8}$$

The lattice action itself is defined in terms of so-called *Wilson loops* [Wil74] $U_{\mu\nu}(x)$,

$$U_{\mu\nu}(x) = U_\mu(x) U_\nu(x + a\hat{e}_\mu) U_\mu^\dagger(x + a\hat{e}_\nu) U_\nu^\dagger(x) . \tag{2.9}$$

It can be shown [Rot97] that, in the limit of vanishing lattice spacing a , the Wilson loops can be expanded as

$$U_{\mu\nu} = \mathbb{1} + ig_0 a^2 F_{\mu\nu} - \frac{g_0^2 a^4}{2} F_{\mu\nu} F_{\mu\nu} + O(a^6) , \quad (2.10)$$

where $F_{\mu\nu} = F_{\mu\nu}^a T_a$ and in the third term no sum is implied over the spacetime indices. In particular, by taking the trace of the above expression, we find that

$$\text{Tr} \{U_{\mu\nu}\} = 3 - \frac{g_0^2 a^4}{4} \sum_a F_{\mu\nu}^a F_{\mu\nu}^a + O(a^6) . \quad (2.11)$$

The *Wilson action* S_W , defined as

$$S_W = \frac{6}{g_0^2} \sum_{x, \mu < \nu} \left(1 - \frac{1}{3} \text{Tr} \{U_{\mu\nu}(x)\} \right) , \quad (2.12)$$

is then easily seen to reduce to the Yang-Mills action in the $a \rightarrow 0$ limit. Within the lattice approach, S_W is taken to be the defining action of pure Yang-Mills theory.

Since the number of integration variables – that is, of link variables $U_\mu(x)$ – is finite for a lattice of finite volume, the gauge invariance of the Wilson action² poses no issue of finiteness for averages computed by lattice methods. In particular, no analogue of the Faddeev-Popov procedure is strictly required to be performed when carrying out lattice calculations. Nonetheless, the gauge still needs to be fixed if one wants to evaluate the vacuum expectation values of gauge-dependent quantities such as the gluon or the ghost propagator. For the topics of covariant gauge fixing and of the effects of the Gribov copies within the lattice approach, we refer e.g. to [SO04, DOS16]; for the evaluation of the ghost propagator in covariant gauges, we refer to [BBC⁺15, CDM⁺18]. A review of some of the most common techniques employed to discretize the quark fields on the lattice can be found in [Rot97].

2.1.2 Results

In the Introduction we saw that the transverse component of the gluon propagator computed on the lattice is found to saturate to a finite, non-zero value in the limit of vanishing momenta, implying that in the infrared the gluons acquire a mass. In Fig. 2.1 we display an example of such behavior, provided to us by the Landau-gauge pure Yang-Mills results of [DOS16]. In order to push the calculations below the GeV scale, these need to be performed on lattices of very large volumes. In the figure, the results obtained for three such volumes, of sides 6.5, 8.1 and 13.0 fm at fixed lattice spacing $a = 0.10$ fm, are shown. Crucially, neither the finiteness of the gluon propagator, nor its saturation value are found to be strongly dependent on the volume. This proves that the massiveness of the propagator is not an artifact of the finite-volume approximation. An analogous conclusion can be reached with respect to the dependence on the lattice spacing [DOS16], which however turns out to be larger than the volume dependence.

In Fig. 2.2 we display the lattice data for the running coupling of pure Yang-Mills theory reported in [DOS16]. In the latter, as is customary for lattice calculations carried out in the Landau gauge, the coupling was computed from the gluon and the ghost propagators within the so-called *Taylor scheme*³. As we can see, instead of diverging at a finite scale as in in

²The gauge transformations act on the link variables as $U_\mu(x) \rightarrow g(x)U_\mu(x)g^\dagger(x + a\hat{e}_\mu)$, where the $g(x)$'s are SU(3) matrices defined at each lattice site [SO04].

³See Secs. 3.3.1 and 5.2.3.

ordinary pQCD, the Taylor coupling hits a maximum at $p \approx 0.6$ GeV and then decreases to zero in the limit of vanishing momenta. The fact that the coupling remains finite and moderately small at all scales proves on the one hand that the Landau pole predicted by ordinary pQCD is an artifact of the expansion, and on the other hand that a perturbation theory for infrared Quantum Chromodynamics may still be viable, provided that non-perturbative effects such as the dynamical generation of a gluon mass are accounted for.

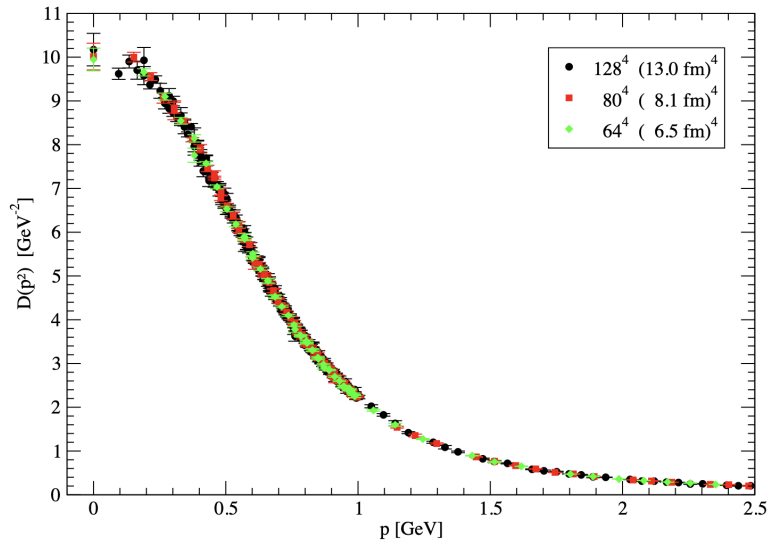


Figure 2.1: Euclidean Landau-gauge transverse gluon propagator computed on the lattice for different lattice volumes. Figure from [DOS16].

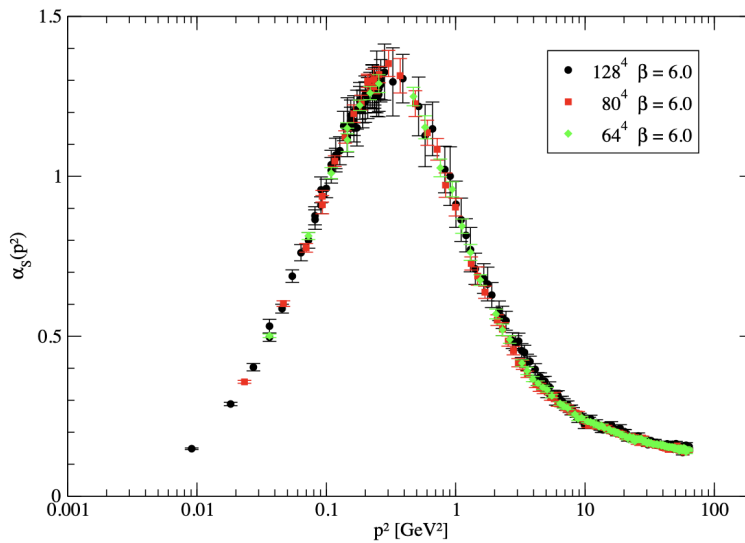


Figure 2.2: Taylor running coupling computed on the lattice and in the Landau gauge for different lattice volumes. Figure from [DOS16].

The lattice results show that Quantum Chromodynamics is infrared-finite, displaying dynamical mass generation in the gluon sector. While in this section we have only reported data obtained in the framework of pure Yang-Mills theory, similar calculations carried out while including the quarks [BHL⁺04, BHL⁺07, IMPS⁺07, SO10, ABB⁺12, BBDS⁺14, ZBDS⁺19, CZB⁺20] essentially paint the same picture of the low-energy dynamics of full QCD.

2.2 The Operator Product Expansion

2.2.1 Set-up

The Operator Product Expansion (OPE) approach⁴ assumes that the product of two local quantum operators $\mathcal{O}_1(x_1)$ and $\mathcal{O}_2(x_2)$ evaluated in the $x_1, x_2 \rightarrow x$ limit can be expressed as a linear combination of local operators $\mathcal{O}_n(x)$ evaluated at x ,

$$\mathcal{O}_1(x_1)\mathcal{O}_2(x_2) \rightarrow \sum_n C_{12}^n(x_1 - x_2) \mathcal{O}_n(x) , \quad (2.13)$$

where the coefficient functions $C_{12}^n(x_1 - x_2)$ only depend on the separation $x_1 - x_2 \rightarrow 0$. By making use of Eq. (2.13), one is able to compute the first non-perturbative contributions to the small-distance – equivalently, to the high-energy – behavior of the Green functions of QCD in terms of vacuum condensates. Let us see how this works.

For simplicity, let $x_2 = 0$ and rename x_1 as x . By taking the time-ordered VEV of Eq. (2.13), one obtains the OPE of the Green function corresponding to the operators \mathcal{O}_1 and \mathcal{O}_2 ,

$$\langle T \{ \mathcal{O}_1(x) \mathcal{O}_2(0) \} \rangle \rightarrow \sum_n C_{12}^n(x) \langle \mathcal{O}_n(0) \rangle \quad (x \rightarrow 0) . \quad (2.14)$$

Given an arbitrary local operator $\mathcal{O}_n(x) \not\propto \mathbb{1}$, where $\mathbb{1}$ is the identity operator, the VEV $\langle \mathcal{O}_n(x) \rangle = \langle \mathcal{O}_n(0) \rangle$ is known as a vacuum condensate. Condensates are intrinsically non-perturbative objects, in that their value depends on the low-energy content of the theory. On the contrary, the coefficient functions which multiply the condensates in the OPE, being evaluated at small separations x , are entirely determined by the high-energy behavior of the operators. In asymptotically free theories such as QCD, these coefficients can be computed explicitly by resorting to ordinary perturbative techniques which we will review shortly. Once the OPE coefficients have been computed, Eq. (2.14) provides us with a high-energy expression for the Green function $\langle T \{ \mathcal{O}_1(x) \mathcal{O}_2(0) \} \rangle$ that includes non-perturbative contributions due to the condensates.

In the $x \rightarrow 0$ limit, the dominant contributions to the OPE are given by the condensates of lower mass dimension. This is a consequence of the fact that the functions $C_{12}^n(x)$, having canonical mass dimension $\kappa_n = d_1 + d_2 - d_n$ – where $d_{1,2,n}$ are the mass dimensions of the operators $\mathcal{O}_{1,2,n}$ –, scale like $C_{12}^n(\lambda x) \approx \lambda^{-\kappa_n} C_{12}^n(x)$, and thus tend to zero more rapidly as the dimension d_n of the operator \mathcal{O}_n increases. For this reason, only the lower-dimensional condensates are usually retained in the OPE.

The OPE coefficients $C_{12}^n(x)$ can be computed as follows. Starting from the coefficient $C_{12}^{\mathbb{1}}(x)$ associated to the identity operator,

$$\langle T \{ \mathcal{O}_1(x) \mathcal{O}_2(0) \} \rangle \rightarrow C_{12}^{\mathbb{1}}(x) + \sum_{\mathcal{O}_n \neq \mathbb{1}} C_{12}^n(x) \langle \mathcal{O}_n(0) \rangle , \quad (2.15)$$

⁴The validity of the OPE in the context of asymptotically free theories was proved in 1970 by Zimmermann [Zim70].

we see that in the above expression $C_{12}^1(x)$ is the only term not to be multiplied by a condensate. Therefore it must be equal to the perturbative value of the Green function,

$$C_{12}^1(x) = \langle T \{ \mathcal{O}_1(x) \mathcal{O}_2(0) \} \rangle_{\text{pert.}} . \quad (2.16)$$

As for the other coefficients, these can be computed by multiplying the OPE of $\mathcal{O}_1(x) \mathcal{O}_2(0)$ to a product of operators $\mathcal{O}_3(x_3) \cdots \mathcal{O}_N(x_N)$ and then taking the time-ordered VEV of the resulting expression,

$$\langle T \{ \mathcal{O}_1(x) \mathcal{O}_2(0) \mathcal{O}_3(x_3) \cdots \mathcal{O}_N(x_N) \} \rangle \rightarrow \sum_n C_{12}^n(x) \langle T \{ \mathcal{O}_n(0) \mathcal{O}_3(x_3) \cdots \mathcal{O}_N(x_N) \} \rangle . \quad (2.17)$$

As long as the spacetime points x_3, \dots, x_N are kept sufficiently far from the origin, no new condensates arise in Eq. (2.17). In particular, we can evaluate both sides of the relation perturbatively in the limit of vanishing x and of very large x_3, \dots, x_N , and then determine the functions $C_{12}^n(x)$ by matching the x -dependence of the right-hand side to that of the left-hand side. In practice, this is usually done in momentum space, where the momenta associated to the operators $\mathcal{O}_3, \dots, \mathcal{O}_N$ are kept small while the expression is expanded in powers of the momentum p associated to the separation x as $p \rightarrow \infty$.

2.2.2 Results

By making use of the OPE formalism, one can show that, at high energies, a non-vanishing quark condensate $\langle \bar{\psi}\psi \rangle$ contributes to the quark propagator with a term that plays the role of a quark mass. To see this, assume that the quark is massless and consider the OPE of the product $\psi(x)\bar{\psi}(0)$,

$$\psi(x)\bar{\psi}(0) \rightarrow C_1(x) \mathbb{1} + C_{\bar{\psi}\psi}^-(x) \bar{\psi}\psi(0) + \cdots . \quad (2.18)$$

In the above expression, the dots denote contributions coming both from higher-dimensional local operators and from operators which vanish as soon as the time-ordered VEV of $\psi(x)\bar{\psi}(0)$ is taken⁵. The corresponding OPE for the quark propagator $S(x)$ reads

$$S(x) \rightarrow S_{\text{pert.}}(x) + C_{\bar{\psi}\psi}^-(x) \langle \bar{\psi}\psi \rangle \quad (x \rightarrow 0) , \quad (2.19)$$

or, in (Minkowski) momentum space,

$$S(p) \rightarrow \frac{iZ(p^2)}{\not{p}} + c_{\bar{\psi}\psi}^- \frac{\langle \bar{\psi}\psi \rangle}{(p^2)^2} \quad (p \rightarrow \infty) , \quad (2.20)$$

where $Z(p^2)$ is the perturbative quark Z -function and by dimensional counting $c_{\bar{\psi}\psi}^-$ is a dimensionless coefficient. To lowest order in the coupling, since $Z(p^2) = 1 + O(g^2)$ and $c_{\bar{\psi}\psi}^- = O(g^2)$, we can set $Z(p^2)c_{\bar{\psi}\psi}^- \approx c_{\bar{\psi}\psi}^-$, so that

$$S(p) \rightarrow \frac{iZ(p^2)}{\not{p}} \left(1 - \frac{ic_{\bar{\psi}\psi}^- \langle \bar{\psi}\psi \rangle}{\not{p} p^2} \right) \approx \frac{iZ(p^2)}{\not{p} \left(1 + \frac{ic_{\bar{\psi}\psi}^- \langle \bar{\psi}\psi \rangle}{\not{p} p^2} \right)} = \frac{iZ(p^2)}{\not{p} - \mathcal{M}(p^2)} , \quad (2.21)$$

⁵Also, in Eq. (2.18) we are disregarding the dimension-2 operators A^2 and $\bar{c}c$, since these do not contribute to the mass-like term under consideration. The former can be shown to correct the quark Z -function already to lowest order in perturbation theory – see e.g. [LS88].

where the mass function $\mathcal{M}(p^2)$ is given by

$$\mathcal{M}(p^2) = -i c_{\bar{\psi}\psi} \frac{\langle \bar{\psi}\psi \rangle}{p^2}. \quad (2.22)$$

The coefficient $c_{\bar{\psi}\psi}$ can be explicitly computed to lowest order in the coupling to yield [LS88]

$$c_{\bar{\psi}\psi} = -i \frac{3N_A g^2}{8N^2} \quad \Longrightarrow \quad \mathcal{M}(p^2) = -\frac{3N_A g^2}{8N^2} \frac{\langle \bar{\psi}\psi \rangle}{p^2} \quad (2.23)$$

in the Landau gauge, where $N_A = N^2 - 1$ is the dimension of the gauge group $SU(N)$. In particular, we see that, even when the quark is massless, a non-vanishing quark condensate $\langle \bar{\psi}\psi \rangle$ can provide its propagator with a mass function.

A word of caution is in order. As discussed in the last section, the OPE is only valid in the high-energy limit. That of being massive or massless, on the other hand, is a low-energy property of the fields. Therefore, the function $\mathcal{M}(p^2)$ defined by Eq. (2.23) should not be interpreted as a fully-fledged non-perturbative mass function, but rather as the high-energy limit of the actual mass function, which cannot be derived within the framework of the OPE. What is of interest to us here is that – at variance with ordinary perturbation theory – the OPE approach predicts that the mass of a massless quark can be different from zero as a non-perturbative consequence of the existence of condensates.

Like the quark propagator, the gluon propagator as well can be expanded by making use of a suitable OPE⁶,

$$A_\mu^a(x) A_\nu^b(0) \rightarrow C_1(x)_{\mu\nu}^{ab} \mathbb{1} + C_{A^2}(x)_{\mu\nu}^{ab} A^2(0) + \dots \quad (2.24)$$

The OPE for the (Minkowski) momentum-space gluon propagator $\Delta_{\mu\nu}^{ab}(p) = \Delta_{\mu\nu}(p) \delta^{ab}$ then reads

$$\Delta_{\mu\nu}(p) \rightarrow -\frac{iJ(p^2)}{p^2} t_{\mu\nu}(p) + c_{A^2} \frac{\langle A^2 \rangle}{(p^2)^2} t_{\mu\nu}(p) \approx -\frac{iJ(p^2)}{p^2 \left(1 - ic_{A^2} \frac{\langle A^2 \rangle}{p^2}\right)} t_{\mu\nu}(p), \quad (2.25)$$

where $J(p^2)$ is the perturbative gluon dressing function, c_{A^2} is a dimensionless coefficient, the calculations are carried out in the Landau gauge so that $\Delta_{\mu\nu}(p) \propto t_{\mu\nu}(p)$ and we have used $J(p^2)c_{A^2} \approx c_{A^2}$ to $O(g^2)$ in order to bring the condensate to the denominator. If we define a constant m^2 as

$$m^2 = ic_{A^2} \langle A^2 \rangle, \quad (2.26)$$

then the OPE tells us that in the high-energy limit

$$\Delta_{\mu\nu}(p) \rightarrow -\frac{iJ(p^2)}{p^2 - m^2} t_{\mu\nu}(p), \quad (2.27)$$

where in the Landau gauge the coefficient c_{A^2} is computed to be [LS88]

$$c_{A^2} = -i \frac{Ng^2}{4N_A} \quad \Longrightarrow \quad m^2 = \frac{Ng^2}{4N_A} \langle A^2 \rangle. \quad (2.28)$$

Like in the quark sector, we see that the OPE predicts that a high-energy mass term, proportional to $\langle A^2 \rangle$ [CNZ99, GSZ01, GZ01, BLYL⁺01], is generated for the gluon propagator which cannot be accounted for by ordinary perturbation theory. Nonetheless, there

⁶To leading order in the dimension of the condensates – that is, modulo condensates of dimension 3 and higher – no other terms are present in the gluon OPE as far as the propagator is concerned [LS88].

is one crucial difference between the $\langle A^2 \rangle$ and the $\langle \bar{\psi}\psi \rangle$ condensates: while $\bar{\psi}\psi$ is a gauge-invariant operator, the A^2 operator is not; it follows that the VEV $\langle A^2 \rangle$ may be expected to be non-zero only if gauge invariance is broken by the vacuum⁷. This would have disastrous consequences on the self-consistency of the theory. In Chapter 5 we will show that, thanks to the existence of a (non-local) gauge-invariant generalization of the operator A^2 , the condensate $\langle A^2 \rangle$ can actually be different from zero in the Landau gauge without spoiling any fundamental symmetry of the strong interactions⁸.

2.3 The Gribov-Zwanziger approach

2.3.1 Set-up and results

In Sec. 1.1.2 we saw that the Faddeev-Popov procedure routinely employed to fix a gauge for the QCD action involves the introduction of the determinant of the FP operator $\partial^\mu D_\mu$ in the path integrals of the theory. If the FP operator has zero modes, meaning that there exist algebra fields χ^a such that $\partial^\mu D_\mu \chi^a = 0$, then such a determinant vanishes; as a consequence, the FP procedure is invalidated⁹.

From the perspective of gauge invariance, the zero modes of the FP operator can be used to construct gauge transformations that relate different field configurations of the FP action to one another. Consider for instance the Landau gauge, defined by¹⁰

$$\xi = 0 \quad \Longrightarrow \quad \partial^\mu A_\mu^a = 0, \quad (2.29)$$

where ξ , like in Sec. 1.1.2, is the gauge parameter. An infinitesimal gauge transformation of the gluon field A_μ^a with parameters χ^a yields

$$A_\mu^a \rightarrow \tilde{A}_\mu^a = A_\mu^a + D_\mu \chi^a. \quad (2.30)$$

If χ^a is a zero mode of $\partial^\mu D_\mu$, then $\partial^\mu A_\mu = 0$ implies $\partial^\mu \tilde{A}_\mu = 0$, so that both A_μ^a and \tilde{A}_μ^a belong to the configuration space of the Landau-gauge FP action. In other words, the FP procedure fails to fix a gauge for QCD. Two or more field configurations related to each other by gauge transformations constructed by making use of zero modes of the FP operator are called Gribov copies.

The existence of zero modes of the FP operator was proved by Gribov in 1978 [Gri78]. In order to address the issue of the Gribov copies, he proposed that, in the Landau gauge, the Euclidean partition function of QCD be restricted to the so-called Gribov region, defined by the positive-definiteness of the FP operator $-\partial^\mu D_\mu$,

$$\int \mathcal{D}\mathcal{F} e^{-S_{\text{FP}}}|_{\xi=0} \rightarrow \int \mathcal{D}\mathcal{F} e^{-S_{\text{FP}}}|_{\xi=0} \Theta(-\partial^\mu D_\mu), \quad (2.31)$$

⁷Incidentally, as we will discuss in Chpt. 4, in the limit of zero quark mass the condensate $\langle \bar{\psi}\psi \rangle$ should vanish as well because of a global symmetry known as chiral symmetry. Such a symmetry is indeed known to be broken by the vacuum.

⁸We should remark, however, that condensates of non-local operators do not enter in the OPE of gauge-invariant operators.

⁹If the gauge field A is sufficiently small, the FP operator is just a perturbation of the Laplacian operator. Since the latter has no zero modes that vanish at large distances, the FP procedure remains valid in the perturbative regime.

¹⁰The implication is a consequence of the fact that the exponential $e^{-\frac{i}{2\xi} \int d^4x (\partial \cdot A)^2}$ that appears in the QCD path integral reduces to a delta functional $\delta(\partial \cdot A)$ in the limit of vanishing ξ .

where

$$\Theta(x) = \begin{cases} 1 & x > 0 \\ 0 & x < 0 \end{cases} \quad (2.32)$$

is the Heaviside function. A local and renormalizable action S_{GZ} that implements the Gribov condition was discovered by Zwanziger in 1989 [Zwa89]. In Euclidean space, the Gribov-Zwanziger (GZ) action S_{GZ} reads

$$S_{\text{GZ}} = S_{\text{FP}}|_{\xi=0} + \int d^4x \left(\bar{\phi}_\mu^{ac} K^{ab} \phi^{bc\mu} - \bar{\omega}_\mu^{ac} K^{ab} \omega^{bc\mu} + \gamma^2 g f_{abc} A^{a\mu} (\phi_\mu^{bc} + \bar{\phi}_\mu^{bc}) \right) + S_{\text{vac.}} , \quad (2.33)$$

where $K = -\partial^\mu D_\mu(A)$, the commuting $\phi_\mu^{ab}, \bar{\phi}_\mu^{ab}$ and anticommuting $\omega_\mu^{ab}, \bar{\omega}_\mu^{ab}$ are new auxiliary fields, γ is a variational parameter with the dimensions of a mass known as the *Gribov parameter* and the vacuum term $S_{\text{vac.}}$ is given by

$$S_{\text{vac.}} = -4\gamma^2 \mathcal{V}_4 N_A , \quad (2.34)$$

with \mathcal{V}_4 the volume of 4-dimensional Euclidean spacetime and $N_A = N^2 - 1$ the dimension of the gauge group $\text{SU}(N)$. The value of the Gribov parameter is fixed by the requirement that the effective action of QCD be minimal with respect to its variation. This can be easily shown to be equivalent to the *horizon condition*

$$\langle H[A] \rangle_\gamma = 4\mathcal{V}_4 N_A , \quad (2.35)$$

where $H[A]$ is the so-called *horizon functional*,

$$H[A] = g^2 \int d^4x f_{abc} f_{dec} A_\mu^b [K^{-1}(A)]^{ad} A^{c\mu} . \quad (2.36)$$

The horizon functional appears in the GZ action as soon as the auxiliary fields are integrated out:

$$S_{\text{GZ}} \rightarrow S_{\text{FP}}|_{\xi=0} + \gamma^4 (H[A] - 4\mathcal{V}_4 N_A) . \quad (2.37)$$

Since the derivative of the Euclidean effective action with respect to γ is equal to the derivative of $W = -\ln Z$, where Z is the Euclidean partition function of the theory, the horizon condition easily follows.

On the shell of Eq. (2.35), the extra terms in the GZ action can be shown [Zwa89] to enforce the Gribov condition $\det(-\partial^\mu D_\mu) > 0$ to every order in perturbation theory. At the perturbative level, the horizon functional modifies the zero-order gluon propagator due to the fact that the FP operator reduces to the Laplacian as $gA \rightarrow 0$,

$$K^{ad} \rightarrow -\partial^2 \delta^{ad} . \quad (2.38)$$

Indeed, by making use of the $\text{SU}(N)$ relation $f_{abc} f_{dbc} = N\delta_{ad}$, we see that, when expanded in powers of gA , the horizon functional contains a quadratic gluon term,

$$H[A] = N g^2 \int d^4x A_\mu^a \left(-\frac{1}{\partial^2} \right) A^{a\mu} + O(g^3 A^3) , \quad (2.39)$$

that shifts the zero-order gluon propagator from $\Delta_0(p^2) = 1/p^2$ to a GZ propagator $\Delta_{\text{GZ}}(p^2)$ whose inverse can be read out directly from the full action. Modulo color structure

$$\Delta_{\text{GZ}}^{-1}(p^2) = p^2 + \frac{2N g^2 \gamma^4}{p^2} , \quad (2.40)$$

leading to

$$\Delta_{\text{GZ}}(p^2) = \frac{p^2}{p^4 + 2Ng^2\gamma^4}. \quad (2.41)$$

We then see that $\Delta_{\text{GZ}}(p^2)$ vanishes in the $p^2 \rightarrow 0$ limit.

Gluon propagators with a vanishing zero-momentum limit have been derived in functional approaches such as the Dyson-Schwinger Equations (the so-called scaling solutions, [vSHA97, AB98]) and studied in relation to the phenomenon of confinement [Oji78, KO79a]. Today we know that the deep-infrared behavior of the propagator is less suppressed than predicted within the original GZ approach. To account for the zero-momentum finiteness of the propagator, in [DGS⁺08, DSVV08, DOV10, DSV11] it was shown that a condensate of the form $\langle \bar{\phi}_\mu^{ab} \phi^{ab\mu} - \bar{\omega}_\mu^{ab} \omega^{ab\mu} \rangle$ could provide the GZ action with an additional quadratic gluon term. The $p^2 \rightarrow 0$ limit of the resulting Refined Gribov-Zwanziger (RGZ) zero-order propagator $\Delta_{\text{RGZ}}(p^2)$,

$$\Delta_{\text{RGZ}}(p^2) = \frac{p^2 + M^2}{p^4 + M^2 p^2 + 2Ng^2\gamma^4}, \quad (2.42)$$

is controlled by a mass parameter M^2 whose value can be determined dynamically and was proved to be different from zero [DSV11]. Once the quadratic gluon condensate $\langle A^2 \rangle$ is included in the RGZ formalism, a modified propagator of the form

$$\Delta_{\text{RGZ}}^{\langle A^2 \rangle}(p^2) = \frac{p^2 + M^2}{p^4 + (M^2 + m^2)p^2 + 2Ng^2\gamma^4 + M^2 m^2} \quad (2.43)$$

with $m^2 \propto \langle A^2 \rangle$ can be derived that is found to be in very good agreement with the lattice data up to momenta $\approx 1\text{-}1.5$ GeV [DOV10].

The GZ and RGZ propagators reported in Eqs. (2.41)-(2.43) have the interesting property of possessing poles which, depending on the values of the parameters, can be complex conjugate. By looking at Eq. (2.43), we see that this happens when

$$(M^2 + m^2)^2 - 4M^2 m^2 - 8Ng^2\gamma^4 = (M^2 - m^2)^2 - 8Ng^2\gamma^4 < 0. \quad (2.44)$$

The GZ propagator clearly satisfies the above inequality, given that $M^2 = m^2 = 0$ in that case, yielding purely imaginary poles at $p^2 = \pm i\sqrt{2N}g\gamma^2$. As for the RGZ propagator, using the parameters

$$M^2 = 2.15 \pm 0.13 \text{ GeV}^2, \quad m^2 = -1.81 \pm 0.14 \text{ GeV}^2, \quad 2Ng^2\gamma^4 = 4.16 \pm 0.38 \text{ GeV}^4 \quad (2.45)$$

obtained in [DOV10] by fitting the lattice data, one finds that the poles are complex conjugate for the central values of the fit, although the upper and lower bounds of the parameters do not exclude that the propagator may have a pair of real poles.

To end this section, we mention that proposals have been recently made that aim to extend the GZ and RGZ formalisms to covariant gauges other than the Landau gauge in a way that complies with BRST invariance [CDF⁺15, CDF⁺16a, CDF⁺16b, CDP⁺17, CFPS17, CDG⁺18, MPPS19, DFP⁺19]. Such proposals reformulate the horizon condition – Eq. 2.35 – in terms of a gauge-invariant gluon field A^h which will be the subject of Chapter 5.

2.4 The Curci-Ferrari model

2.4.1 Set-up

The Curci-Ferrari (CF) model is defined by the Euclidean action S_{CF} [TW10, TW11]

$$S_{\text{CF}} = S_{\text{YM}} + S_{\text{g.f.}} + S_{m^2} , \quad (2.46)$$

where

$$S_{\text{g.f.}} = \int d^4x (iB^a \partial \cdot A^a + \bar{c}^a \partial^\mu D_\mu c^a) \quad (2.47)$$

is the Landau-gauge FP gauge-fixing term¹¹, whereas

$$S_{m^2} = \int d^4x \frac{1}{2} m^2 A_\mu^a A^{a\mu} \quad (2.48)$$

is a mass term for the gluons. Under an infinitesimal gauge transformation with parameters χ^a , the variation of the mass operator $A_\mu^a A^{a\mu}$ is given by $\delta(A_\mu^a A^{a\mu}) = 2\partial_\mu \chi^a A^{a\mu} \neq 0$. It follows that the gluon mass term must be interpreted as being added to the action *after* gauge fixing has been performed, for otherwise the lack of gauge invariance of $S_{\text{YM}} + S_{m^2}$ would forbid the FP procedure to be carried out in the first place.

Although the gluon mass term S_{m^2} breaks the BRST invariance of the FP action,

$$sS_{m^2} = -m^2 \int d^4x \partial_\mu c^a A^{a\mu} \neq 0 , \quad (2.49)$$

where s is the ordinary BRST operator,

$$sA_\mu^a = -D_\mu c^a , \quad sc^a = \frac{g}{2} f_{bc}^a c^b c^c , \quad s\bar{c}^a = iB^a , \quad sB^a = 0 , \quad (2.50)$$

the overall CF action still possesses a global symmetry which reduces to BRST symmetry in the limit of vanishing mass. The corresponding operator s_{m^2} reads [PRS⁺21b]

$$s_{m^2} A_\mu^a = -D_\mu c^a , \quad s_{m^2} c^a = \frac{g}{2} f_{bc}^a c^b c^c , \quad s_{m^2} \bar{c}^a = iB^a , \quad s_{m^2} B^a = im^2 c^a , \quad (2.51)$$

and acts on the sum $S_{\text{g.f.}} + S_{m^2}$ as

$$s_{m^2}(S_{\text{g.f.}} + S_{m^2}) = 0 . \quad (2.52)$$

Clearly, $\lim_{m^2 \rightarrow 0} s_{m^2} = s$. For $m^2 \neq 0$, since

$$s_{m^2}^2 \bar{c}^a , s_{m^2}^2 B^a \propto m^2 , \quad (2.53)$$

the extended BRST operator s_{m^2} is not nilpotent. While in general the lack of nilpotency of the BRST operator poses obstructions to the unitarity of a gauge theory, it has been argued in [PRS⁺21b] that, if the CF model displays color confinement, then it may still be possible to define a physical subspace with a positive-definite inner product within the CF Hilbert space as the kernel of $s_{m^2}^2$.

The invariance of S_{CF} under the extended BRST transformations in Eq. (2.51) can be exploited to prove that the CF model is perturbatively renormalizable. The divergent parts of the CF renormalization factors can be shown to satisfy the constraints [DVS03, TW11]

$$Z_g Z_A^{1/2} Z_c = 1 , \quad Z_{m^2} Z_A Z_c = 1 , \quad (2.54)$$

¹¹Note that the replacements $c^a \rightarrow -c^a$, $B^a \rightarrow iB^a$ and partial integrations with respect to Eq. (1.64) – which are customary in Euclidean space – do not change the outcome of gauge fixing.

where Z_{m^2} is the renormalization factor of the gluon mass parameter,

$$m_B^2 = Z_{m^2} m^2 . \quad (2.55)$$

The two-point sector of the Curci-Ferrari model is usually renormalized within the so-called Infrared-Safe (IRS) scheme [TW11], defined by extending the relations in Eq. (2.54) to the finite terms of the renormalization factor and by imposing the conditions

$$\Delta(\mu^2; \mu^2) = \frac{1}{\mu^2 + m^2(\mu^2)} , \quad \mathcal{G}(\mu^2; \mu^2) = \frac{1}{\mu^2} , \quad (2.56)$$

on the (transverse) gluon and ghost propagators $\Delta(p^2; \mu^2)$ and $\mathcal{G}(p^2; \mu^2)$ renormalized at the scale μ . The mass term in the first of Eqs. (2.56) is introduced in order to account for the presence of an analogous tree-level term in the fixed-scale CF gluon propagator,

$$\Delta(p^2) = \frac{1}{Z_A p^2 + Z_A Z_{m^2} m^2 + \Pi_T^{(\text{CF})}(p^2)} , \quad (2.57)$$

where $\Pi_T^{(\text{CF})}(p^2)$ is the transverse component of the CF gluon polarization.

2.4.2 Results

Within the IRS scheme, the running coupling $\alpha_s(\mu^2)$ of the CF model is found not to develop Landau poles provided that the value of $\alpha_s(\mu_0^2)$ at the initial renormalization scale μ_0 is not too large [GPRT19, PRS⁺21b]. For such values of the coupling, the model is finite and self consistent in the infrared, admitting a perturbative expansion which can be improved order by order.

In Fig. 2.3 we display the one- and two-loop RG-improved Euclidean gluon propagator and dressing function computed within the Curci-Ferrari model and renormalized in the IRS scheme. The figure is reported from [GPRT19] and features lattice data from [CMM08]. As we can see, the one-loop CF dressing function falls slightly above the lattice results in the UV and slightly below them at intermediate energies¹². Nonetheless, already at one loop the CF results accurately capture the behavior of the lattice propagator, displaying dynamical mass generation in the gluon sector and a non-zero saturation value for the propagator at vanishing momenta. Including the two-loop corrections sensibly improves the quantitative match with the lattice, bringing both the UV tail and the $p \approx 1\text{-}2$ GeV segment of the curve closer to the lattice results.

The lesson that can be learned from the achievements of the Curci-Ferrari model is that treating the gluons as massive at tree level yields a perturbative description of the infrared regime of QCD which agrees both qualitatively and quantitatively with the non-perturbative picture painted by the lattice calculations. The Screened Massive Expansion and the Dynamical Model, to be discussed in the next chapters, build on this notion to provide perturbative frameworks for low-energy QCD that accomplish the same objective without changing the overall Faddeev-Popov action.

¹²For future reference, we note that a simple multiplicative normalization of the CF one-loop dressing function can bring its UV tail to match the lattice data at the price of an over-suppressed zero-momentum limit for the propagator.

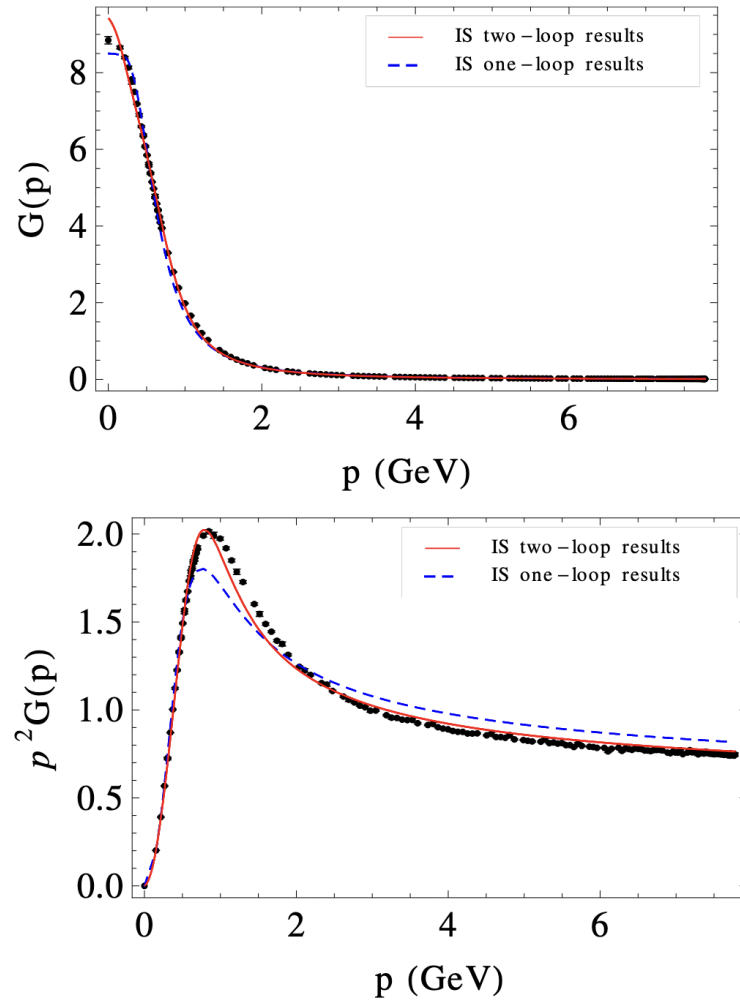


Figure 2.3: Euclidean Landau-gauge transverse gluon propagator (top) and dressing function (bottom) computed to one and two loops within the Curci-Ferrari model, together with the lattice data from [CMM08]. Figure from [GPRT19].

Part II

Massive perturbative models for infrared QCD

3

The Screened Massive Expansion

In Part I of this thesis we saw that the ordinary perturbation theory of Quantum Chromodynamics breaks down at low energies due to the presence of a Landau pole in its running coupling constant. In order to investigate the infrared regime of the strong interactions, one has to resort to alternative, non-perturbative computational methods, such as lattice QCD or the Dyson-Schwinger Equations. Both of these approaches offer a solid perspective on the low-energy behavior of the transverse gluon propagator. They clearly show that, in the infrared, instead of diverging as would be typical for a massless field, the propagator changes concavity and saturates to a finite value [LSWP98a, LSWP98b, BBLW00, BBL⁺01, AN04, AP06, ABP08, AP08, HvS13]. In other words, the gluons acquire a dynamically generated mass.

The occurrence of dynamical mass generation (DMG) in the gluon sector of QCD is a feature of primary interest both from a phenomenological and from a theoretical point of view. Phenomenologically, since in the IR a massive gluon behaves very differently from a massless one, we should expect the low-energy dynamics of the strong interactions to be deeply affected by DMG. For instance, as discussed in some early studies [PP80, CF94, LW96, CF97, MN00, Fie02, LMM⁺05], a gluon mass would bring about both phase-space effects and explicit modifications to the scattering amplitudes in the evaluation of the QCD cross sections. Some (non-conclusive) experimental evidence for the IR-massiveness of the gluon has been presented in the literature by now – see the Introduction for a brief review.

From a purely theoretical perspective, on the other hand, DMG poses new challenges to our understanding and ability to make analytical predictions in the context of QCD. In this respect, it is useful to take the Higgs mechanism of the electroweak interactions as a benchmark. In the electroweak sector of the Standard Model, the quarks and the charged leptons acquire a mass as a consequence of their being coupled to the Higgs field. The Higgs mechanism is triggered by the non-vanishing VEV of the latter, which is a direct consequence of the Higgs potential having a minimum for some non-zero value of the Higgs field. In particular, the magnitude of the quarks' and charged leptons' masses is in direct relation to the parameters which are present in the Higgs Lagrangian; moreover, the Higgs mechanism is mainly classical in nature, as it already occurs at the classical level, without the aid of quantum corrections. DMG for the quarks and charged leptons in the electroweak sector can be easily accommodated into the standard formalism (and studied with the ordinary computational methods) of the gauge theories, resulting in a dynamical symmetry breaking of the global gauge group which we know how to deal with analytically.

Conversely, the dynamical generation of a mass for the gluon is a genuinely quantum phenomenon. It is not caused by the interaction of the gluon field with the VEV of some other field, but rather it happens through self-interaction. The scale that sets the units

for the gluon mass cannot be read off directly from the QCD Lagrangian, but is itself generated by the strong interactions. In addition to there being no evidence that it leads to dynamical symmetry breaking, DMG for the gluons does not play well with the standard analytical method used in QCD – namely, with ordinary perturbation theory. Indeed, as we discussed in the Introduction, a mass for the gluons cannot be generated at any finite order in standard perturbation theory due to the constraints imposed by gauge invariance on the form of the radiative corrections which appear in the QCD perturbative series. In other words, it is an intrinsically non-perturbative effect of the strong interactions. We remark that this is a limitation of pQCD which is not directly related to its infrared breakdown: one could imagine that ordinary pQCD remained valid at arbitrarily low energies, and DMG in the gluon sector would still be perturbatively forbidden by gauge invariance.

In the early 2010s, Tissier and Wschebor [TW10, TW11] made a groundbreaking discovery: by adding a mass term for the gluons in the Landau-gauge Faddeev-Popov Lagrangian, they were able to derive propagators and vertices which accurately reproduced the lattice data in the deep-IR region of QCD (see e.g. Sec. 2.4.2). The strong running coupling computed in their so-called Curci-Ferrari (CF) model was furthermore shown to remain finite and moderately small down to arbitrarily small momenta – a feature that had already been anticipated by the results of the lattice calculations. What is perhaps most surprising about the achievements of the CF model is that, at the most basic level, the latter uses nothing more than standard perturbative techniques. Of course, since the inclusion of a gluon mass term constitutes a modification of the FP Lagrangian, the CF model must be interpreted as an effective theory; indeed, it is not clear whether the model can be derived from first-principles QCD. Nonetheless, the success of the Curci-Ferrari model strongly suggests that, once DMG for the gluons is taken into account by the formalism, the IR regime of the strong interactions might actually be accessible by simple perturbative calculations. This raises a crucial question: may it be that standard perturbation theory fails at low energies because it implicitly assumes that the gluons remain massless down to arbitrarily small scales? If this is so, can a change of the expansion point of the QCD perturbative series fix its IR behavior?

An answer to these questions was provided in 2015 with the formulation of the Screened Massive Expansion of QCD [Sir15a, Sir15b, Sir16b]. The SME is a simple modification of ordinary perturbation theory that consists in treating the transverse gluons as massive already at tree level, while leaving the Faddeev-Popov action unchanged. By expanding around massive, rather than massless transverse gluons, the SME implements DMG in the gluon sector from the get-go; the gluon mass itself can then be shown to screen the IR regime of QCD from the development of Landau poles, thus making the low-energy limit accessible to ordinary perturbative techniques.

The main objective of this chapter is to present the general features and main results of the Screened Massive Expansion with regard to the gauge sector of QCD. Since dynamical mass generation for the gluons occurs even in the absence of quarks, in what follows we will focus exclusively on pure Yang-Mills theory (YMT) – that is, on QCD with no quarks. Working within the framework of YMT allows us to investigate the overall dynamics of the gluons without having to worry about the values of the quark masses. Moreover, it provides for better benchmarks on the infrared regime of the strong interactions, given that the highest-quality lattice calculations which are currently available for the gluon and ghost propagators are carried out in YMT rather than in full QCD.

This chapter is organized as follows. In Sec. 3.1 we define the Screened Massive Expansion of YMT, discuss some of its features and present the first results for the one-loop gluon

and ghost propagators. In Sec. 3.2 we show how the SME can be optimized by making use of arguments based on gauge invariance. This will allow us to reduce the number of free parameters in the expressions and make predictions from first principles. In Sec. 3.3 we perform a Renormalization Group analysis and improvement of the Screened Massive Expansion. The strong running coupling constant $\alpha_s(p)$ computed in the SME will be shown to be free of Landau poles, provided that the value of the coupling at the initial renormalization scale is not too large. The absence of IR Landau poles in $\alpha_s(p)$ proves that the SME is indeed a self-consistent method, valid down to arbitrarily small energy scales.

Most of the contents of this chapter were originally presented in various papers published between 2016 and 2020. Specifically, the main sources for the three sections that make up the chapter are:

- Sec. 3.1: [Sir16b, CS18, SC18, Sir19b],
- Sec. 3.2: [SC18, SC22b, Sir19a, Sir19b],
- Sec. 3.3: [CS20].

Refs. [CS18], [SC18], [CS20] and [SC22b] are attached as an insert to this thesis, to be found in Appendix C.

3.1 Motivation, definition and first results

3.1.1 Dynamical mass generation and perturbation theory: the set-up of the Screened Massive Expansion

In our review of the set-up of ordinary perturbation theory (Sec. 1.2.1), we saw that the standard perturbative expansion of QCD is obtained by splitting the Faddeev-Popov action S_{FP} as

$$S_{\text{FP}} = S_0 + S_{\text{int}} , \quad (3.1)$$

where, in the absence of quarks, the zero-order action S_0 can be expressed in momentum space as

$$S_0 = i \int \frac{d^4p}{(2\pi)^4} \left\{ \frac{1}{2} A_\mu^a(-p) [\Delta_0^{-1}(p)]^{\mu\nu} A_\nu^b(p) + \bar{c}^a(p) [\mathcal{G}_0^{-1}(p)]_{ab} c^b(p) \right\} , \quad (3.2)$$

with the zero-order gluon and ghost propagators $\Delta_0(p)$ and $\mathcal{G}_0(p)$ given by

$$\Delta_{0\mu\nu}^{ab}(p) = \frac{-i}{p^2} \delta^{ab} (t_{\mu\nu}(p) + \xi \ell_{\mu\nu}(p)) , \quad \mathcal{G}_0^{ab}(p) = \frac{i}{p^2} \delta^{ab} , \quad (3.3)$$

whereas the interaction terms in S_{int} explicitly read

$$S_{\text{int}} = \int d^4x \left\{ -g f_{bc}^a \partial_\mu A_\nu^a A^{b\mu} A^{c\nu} - \frac{1}{4} g^2 f_{bc}^a f_{de}^a A_\mu^b A_\nu^c A^{d\mu} A^{e\nu} + g f_{bc}^a \partial^\mu \bar{c}^a A_\mu^b c^c \right\} . \quad (3.4)$$

Since $\Delta_0(p)$ and $\mathcal{G}_0(p)$ have a pole at $p^2 = 0$, Eq. (3.2) implies that at the tree level of standard perturbation theory the ghosts and the gluons are massless.

As we know by now, the strong interactions generate an infrared mass for the transverse gluons. However, in the framework of ordinary pQCD, gauge invariance prevents the quantum corrections from shifting the position of the transverse gluon pole to a non-zero value of p^2 . This makes the standard perturbative expansion of QCD especially unsuitable

to describe the low-energy limit of the strong interactions. In order to obtain a better approximation of the exact gluon propagator, we could try to reorganize the perturbative series in such a way that the transverse gluons are treated as massive already at tree level. In other words, we could look for a modification of perturbation theory capable of yielding a zero-order gluon propagator of the form

$$\Delta_{m\mu\nu}^{ab}(p) = \delta^{ab} \left(\frac{-it_{\mu\nu}(p)}{p^2 - m^2} + \xi \frac{-i\ell_{\mu\nu}(p)}{p^2} \right), \quad (3.5)$$

where the pole of the longitudinal component of $\Delta_m(p)$ is left unshifted from $p^2 = 0$, since we know that $\Delta_L^{ab}(p) = \ell^{\mu\nu}(p) \Delta_{\mu\nu}^{ab}(p) = -i\frac{\xi}{p^2} \delta^{ab}$ is an exact identity for the dressed gluon propagator – see Sec. 1.1.4.

At the end of the derivation of the Feynman rules for ordinary pQCD in Sec. 1.2.1, we observed that the perturbative expansion of QCD can be formally generalized to an arbitrary zero-order action, provided that the latter is chosen to be quadratic in the fields. This comes in very handy, since the $\Delta_m(p)$ in Eq. (3.5) can be obtained as the zero-order gluon propagator associated to the quadratic action S_m given by

$$S_m = i \int \frac{d^4p}{(2\pi)^4} \left\{ \frac{1}{2} A_\mu^a(-p) [\Delta_m^{-1}(p)]_{ab}^{\mu\nu} A_\nu^b(p) + \bar{c}^a(p) [\mathcal{G}_0^{-1}(p)]_{ab} c^b(p) \right\}. \quad (3.6)$$

In particular, a perturbative expansion of pure Yang-Mills theory around massive transverse gluons can be achieved by splitting the Faddeev-Popov action S_{FP} as¹

$$S_{\text{FP}} = S_m + S'_{\text{int.}}, \quad (3.7)$$

where S_m is given by Eq. (3.6), whereas by definition

$$S'_{\text{int.}} = S_{\text{FP}} - S_m. \quad (3.8)$$

Explicitly, since $S_m = S_0 + \delta S$ with

$$\delta S = i \int \frac{d^4p}{(2\pi)^4} \frac{1}{2} A_\mu^a(-p) [\Delta_m^{-1}(p) - \Delta_0^{-1}(p)]_{ab}^{\mu\nu} A_\nu^b(p), \quad (3.9)$$

the modified interaction action $S'_{\text{int.}}$ is equal to $S_{\text{int.}} - \delta S$, where

$$-\delta S = -i \int \frac{d^4p}{(2\pi)^4} \frac{1}{2} A_\mu^a(-p) \Gamma_{ab}^{\mu\nu}(p) A_\nu^b(p) \quad (3.10)$$

and the two-point gluon vertex $\Gamma_{ab}^{\mu\nu}(p)$ contained in the interaction term $-\delta S$ reads

$$\Gamma_{ab}^{\mu\nu}(p) = -im^2 t^{\mu\nu}(p) \delta_{ab}. \quad (3.11)$$

The Feynman rules associated to the split defined by Eq. (3.7) can be read off directly from the action terms S_m and $S'_{\text{int.}}$. By construction, the zero-order gluon propagator is given by Eq. (3.5) – see Fig. 3.1 –, whereas the zero-order ghost propagator and the 3-gluon, 4-gluon and ghost-gluon vertices are the same as those of standard perturbation theory – Figs. 1.2, 1.4, 1.5 and 1.6, respectively. In addition to the ordinary interaction vertices, a new 2-gluon vertex – depicted by a cross in Fig. 3.2 – must be included in the calculations; this is the vertex known as the *gluon mass counterterm*, and corresponds to

¹Similar ideas can be found in the literature, see e.g. [JP97, KPP97].

Here \mathcal{V}_4 is the four-dimensional volume of spacetime, I_0 is the zero-order action of the theory, $I_{\text{int.}}$ is the interaction action, the full action is given by the sum $I_0 + I_{\text{int.}}$ and the subscript 0 denotes that the VEV of $I_{\text{int.}}$ is to be computed with respect to the zero-order integration measure $\mathcal{D}F e^{iI_0}$. The crucial property of the GEP is that V_G can be shown to be greater than or equal to the exact energy density \mathcal{E} of the theory,

$$e^{-i\mathcal{E}\mathcal{V}_4} = \int \mathcal{D}F e^{i(I_0 + I_{\text{int.}})} . \quad (3.13)$$

This is a consequence of the so-called Jensen-Feynman inequality [Fey98], which holds for the Gaussian integrals if the elementary fields F are not Grassmann fields.

Since the zero-order and interaction terms I_0 and $I_{\text{int.}}$ in Eq. (3.12) are only restricted by the requirements that 1. they sum to the total action of the theory, and 2. that I_0 be quadratic in the fields, we are free to choose any quadratic zero-order action I_0 , define $I_{\text{int.}}$ as the difference between the full action and I_0 , and the inequality $V_G \geq \mathcal{E}$ will be fulfilled. In particular, in the context of pure Yang-Mills theory, we can take I_0 to be equal to S_m , $I_{\text{int.}} = S'_{\text{int.}}$, and the resulting GEP will be a function of the mass parameter m^2 which appears in the zero-order gluon propagator Δ_m . The best approximation to the vacuum energy density of Yang-Mills theory will then be provided by the value of the mass parameter which, by minimizing the GEP $V_G(m^2)$, pushes the value of the potential closer to the exact result \mathcal{E} ².

An explicit calculation shows that, in an arbitrary covariant gauge [Com19], the mass-dependent GEP for a pure Yang-Mills theory with gauge group SU(N) is given by [CS18]

$$V_G(m^2) = \frac{3N_A m^4}{128\pi^2} \left(\alpha \ln^2 \frac{m^2}{m_0^2} + 2 \ln \frac{m^2}{m_0^2} - 1 \right) , \quad (3.14)$$

where N_A is the dimension of the gauge group and α is a rescaled coupling defined by

$$\alpha = \frac{9N\alpha_s}{8\pi} , \quad \alpha_s = \frac{g^2}{4\pi} , \quad (3.15)$$

and m_0^2 is an arbitrary non-zero mass scale, generated by the renormalization of the potential, whose explicit value cannot be computed from first principles since pure Yang-Mills theory is scale-free at the classical level. We stress that in Eq. (3.14) there is nothing special about the scale m_0^2 , other than it being different from zero: we could redefine m_0^2 by multiplying it by some arbitrary constant, and the GEP would just acquire an additional term proportional to m^4 . Also, we observe that the GEP is gauge-independent, in the sense that $V_G(m^2)$ does not depend on the gauge parameter ξ despite having been computed in a general covariant gauge.

By differentiating V_G with respect to m^2 , we find that – regardless of the value of the coupling constant – the GEP has a local minimum at $m^2 = m_0^2 \neq 0$, where

$$V_G(m^2 = m_0^2) = -\frac{3N_A m_0^4}{128\pi^2} < 0 . \quad (3.16)$$

By contrast, at $m^2 = 0$ – which is also a local minimum for V_G – the GEP vanishes, thus attaining a value which is greater than $V_G(m^2 = m_0^2)$. This can be clearly seen in Fig. 3.3, where the GEP is plotted as a function of the ratio m/m_0 for different values of the coupling constant.

²Earlier we stated that the Jensen-Feynman inequality holds if the functional averages do not involve Grassmann fields. Of course, in the path integrals of pure Yang-Mills theory we do integrate over Grassmann fields – namely, the ghost and antighost fields. Nonetheless, it can be shown that in the framework of pure Yang-Mills theory the Jensen-Feynman inequality is saturated by *maximizing* the contribution due to the ghosts. This is equivalent to requiring that the latter do not acquire a mass in the infrared; see [CS18] for a detailed treatment of this technical aspect of the GEP.

The fact that the GEP is globally minimized by a non-zero value of the gluon mass parameter signals that a perturbative expansion that treats the transverse gluons as massive provides a better approximation to the vacuum energy density of pure Yang-Mills theory in comparison to one in which the gluons are massless. In other words, the true vacuum of pure Yang-Mills theory better resembles the vacuum of free massive transverse gluons, rather than that of free massless ones. In particular, we may expect the massive expansion defined by the split in Eq. (3.7) to reproduce more faithfully the infrared regime of the strong interactions at finite order in its perturbative series, when compared to the ordinary massless perturbation theory. As we will see in the following sections, this is indeed the case: the Screened Massive Expansion allows us to incorporate the phenomenon of dynamical mass generation non-trivially into the formalism of QCD, and to analytically compute gluon and ghost propagators which are in excellent agreement with the results of the lattice calculations down to the deep IR.

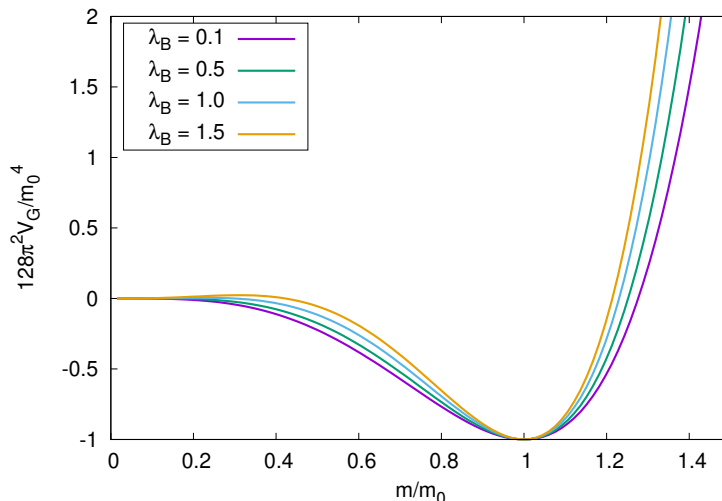


Figure 3.3: The Gaussian Effective Potential of pure Yang-Mills theory, normalized by a factor of $\frac{128\pi^2}{3N_A m_0^4}$ and computed for different values of $\lambda_B = 16\pi^2\alpha$. Figure from [CS18].

3.1.2 General properties of the Screened Massive Expansion

In the process of replacing the zero-order massless gluon propagator Δ_0 with a massive one, the Screened Massive Expansion introduces a gluon mass parameter m^2 in the perturbative series of QCD. As it stands, m^2 is a new free parameter whose value will need to be fixed in order to be able to make physical predictions. Since pure Yang-Mills theory is scale-free at the classical level, m^2 – together with the renormalization scale – is the only dimensionful parameter of the theory. Therefore, choosing a value for the gluon mass parameter is equivalent to setting the energy units of the theory³. Of course, this cannot be done from

³This is not the case for full QCD with massive quarks, as of course the quark masses are also dimensionful parameters. Nonetheless, the corrections to the gluon mass due to the presence of quarks turn out to be negligible as far as the overall scale of m is concerned [Sir16a]. Therefore, even in the context of full QCD, when discussing the deep IR behavior of the gluon propagator one can safely assume that m is the only relevant energy scale. The same holds true for the ghost propagator, since the corrections to the latter due to the quarks are higher-order in perturbation theory.

first principles, but must instead be done a posteriori by making comparisons with the experiments, or with the lattice data.

We should mention that m must not be interpreted as the actual mass of the gluon. Indeed, whereas at tree level the pole of the transverse gluon propagator is found at $p^2 = m^2$, the quantum corrections radically change the analytic structure of the dressed propagator already at the one-loop order. In particular, we shall see that the transverse gluon propagator computed in the SME possesses a pair of complex-conjugate poles. Within the Screened Massive Expansion, m must simply be regarded as a mass scale which determines the infrared behavior of the gluon propagator.

The presence of the new free parameter m^2 in the equations of the SME, when taken at face value, may seem to reduce the predictive power of the approximation. While this is certainly true if we limit ourselves to using the plain SME, we anticipate that optimization methods can be devised to fix the value of some of the free parameters of the expansion from first principles, thus restoring the predictivity of the technique. Interestingly, these methods are ultimately based on the delicate balance that exists between the massiveness of the gluon and the need to preserve gauge/BRST invariance. We will come back to this topic in both Sec. 3.2 and Sec. 3.3.

As a consequence of the massiveness of the zero-order gluon propagator Δ_m , some of the loop diagrams of the SME contain *mass divergences* – that is, diverging terms proportional to the gluon mass parameter m^2 . These divergences cannot be absorbed by the ordinary renormalization counterterms of QCD, since the total Faddeev-Popov action – which is left unchanged by the SME – contains no gluon mass term, and cannot therefore accommodate a gluon mass renormalization counterterm.

Nonetheless, the mass divergences can be shown to disappear as soon as a sufficient number of crossed diagrams is included in the equations. Heuristically, this can be explained by arguing that since $\Delta_m \rightarrow \Delta_0$ in the high-energy ($|p^2| \gg m^2$) limit, the Screened Massive Expansion cannot modify the UV behavior of QCD; in particular, it will not modify the structure of the UV-diverging terms in its perturbative series. If any of the diagrams is found to contain a mass divergence, then other diagrams must exist that contain opposite mass divergences to cancel it. This must be possible order by order in the coupling constant.

A more rigorous argument requires us to analyze the structure of the crossed diagrams which appear at a fixed order in g in the perturbative series of the SME. Let \mathcal{D}_0 be a diagram which does not contain gluon mass counterterms, and denote with \mathcal{D}_1 the sum of all of the diagrams which can be obtained from \mathcal{D}_0 by inserting a single gluon mass counterterm in one of its internal gluon lines. Clearly, \mathcal{D}_1 is of the same order in g as \mathcal{D}_0 . Now, observe that the insertion of a single gluon counterterm $\Gamma(p)$ into a gluon line $\Delta_m(p)$ can be achieved by replacing $\Delta_m(p) \rightarrow \Delta_m(p) \cdot \Gamma(p) \cdot \Delta_m(p)$ under the sign of integral; moreover,

$$\Delta_m(p) \cdot \Gamma(p) \cdot \Delta_m(p) = \frac{im^2}{(p^2 - m^2)^2} t(p) = -m^2 \frac{\partial}{\partial m^2} \Delta_m(p) . \quad (3.17)$$

It is then easy to see that

$$\mathcal{D}_1 = -m^2 \frac{\partial}{\partial m^2} \mathcal{D}_0 . \quad (3.18)$$

If \mathcal{D}_0 contains a mass divergence, then the sum $\mathcal{D}_0 + \mathcal{D}_1$, which thanks to the above equation can be expressed as

$$\mathcal{D}_0 + \mathcal{D}_1 = \left(1 - m^2 \frac{\partial}{\partial m^2} \right) \mathcal{D}_0 , \quad (3.19)$$

will not contain any, given that the operator $1 - m^2 \frac{\partial}{\partial m^2}$ kills any term linear in m^2 inside \mathcal{D}_0 . What about the other crossed diagrams, $\mathcal{D}_2, \mathcal{D}_3, \dots, \mathcal{D}_n$, which contain 2, 3, \dots, n gluon mass counterterms? Just like \mathcal{D}_1 , they are given by

$$\mathcal{D}_n = \frac{(-m^2)^n}{n!} \frac{\partial^n}{\partial (m^2)^n} \mathcal{D}_0. \quad (3.20)$$

In particular, since every $\partial/\partial m^2$ derivative increases the number of propagators under the sign of integral, the diagrams in \mathcal{D}_2 – which contain at least three gluon propagators – are superficially convergent, as well as any \mathcal{D}_n with $n \geq 3$. Therefore, once the mass divergences are cancelled in subdiagrams by summing the latter to their crossed counterparts, the rest of the perturbative series is also convergent, as far as the divergences proportional to m^2 are concerned.

Eq. (3.20) helps us understand the precise relation that exists between the SME and ordinary perturbation theory. Indeed, if we start from a single diagram $\mathcal{D}_0(m^2)$ – where the dependence on m^2 is made explicit for reasons that will become clear in a moment – and sum to it all of the diagrams $\mathcal{D}_n(m^2)$ that can be obtained by inserting n gluon mass counterterms in its internal gluon lines, we find that

$$\begin{aligned} \sum_{n=0}^{+\infty} \mathcal{D}_n(m^2) &= \left(\sum_{n=0}^{\infty} \frac{(-m^2)^n}{n!} \frac{\partial^n}{\partial (m^2)^n} \right) \mathcal{D}_0(m^2) = \\ &= e^{-\lambda \frac{\partial}{\partial m^2}} \Big|_{\lambda=m^2} \mathcal{D}_0(m^2) = \\ &= \mathcal{D}_0(m^2 - \lambda) \Big|_{\lambda=m^2} = \mathcal{D}_0(0). \end{aligned} \quad (3.21)$$

In other words, by summing an uncrossed diagram $\mathcal{D}_0(m^2)$ to all of its crossed counterparts $\mathcal{D}_n(m^2)$ ($n \geq 1$), we obtain the former computed in ordinary pQCD, $\mathcal{D}_0(0)$. This can be seen explicitly at the level of the single gluon line, for which an identity analogous to Eq. (3.21) reads

$$\sum_{n=0}^{+\infty} \Delta_m(p) \cdot [\Gamma(p) \cdot \Delta_m(p)]^n = \Delta_m(p) \cdot \frac{1}{\mathbb{1} - \Gamma(p) \cdot \Delta_m(p)} = \Delta_0(p), \quad (3.22)$$

where we have used

$$\frac{1}{\mathbb{1} - \Gamma(p) \cdot \Delta_m(p)} = \frac{1}{1 + \frac{m^2}{p^2 - m^2}} t(p) + \ell(p) = \frac{p^2 - m^2}{p^2} t(p) + \ell(p). \quad (3.23)$$

It is then clear that in the Screened Massive Expansion we are not interested in resumming all of the crossed diagrams: if we did so, we would be back to ordinary massless perturbation theory. On the contrary, at any finite order in the coupling constant g , we must choose a finite number of crossed diagrams to include in the calculation.

Unfortunately, to date, no first-principles argument has been found to constrain the maximum number of crossed diagrams that are to be retained in a fixed-loop-order calculation. Nonetheless, the principle of renormalizability, together with a principle of minimality, are still able to provide us with a useful criterion for the truncation of the SME perturbative series. At a fixed loop order ℓ , in order to obtain a renormalizable result, one must at the very least include all of the crossed diagrams which are needed to remove the mass divergences arising from the uncrossed diagrams. Among these crossed and uncrossed

diagrams, there will be a subset of diagrams with a maximal number of vertices N . In the spirit of perturbation theory, once some diagrams with $\ell' \leq \ell$ loops and $N' \leq N$ vertices are included, then *all* of the diagrams with the same properties should be included as well. Since there is no need to add other diagrams, by a principle of minimality we shall not do so. When following these criteria, the SME can be interpreted as a *double* expansion in both the number ℓ of loops and the number N of vertices.

In Secs. 3.1.3 and 3.1.4, the double expansion will be used to derive explicit expressions for the one-loop ghost and gluon propagators. There we will see that the uncrossed loops that contribute to the gluon propagator contain mass divergences which are removed by corresponding crossed loops with a maximum number of vertices $N = 3$. As a consequence, our calculations will include every diagram with at most 1 loop and at most 3 vertices.

3.1.3 The ghost propagator

In the present and in the following section we start reviewing some of the results which have been obtained to one-loop by making use of the Screened Massive Expansion of pure Yang-Mills theory. For the sake of conciseness, we will not go through the explicit derivation of the analytic expressions; the details of the calculations can be found in [Sir16b, SC18, Sir19b] (see Appendix C for [SC18]). Let us begin from the dressed ghost propagator.

The dressed ghost propagator $\mathcal{G}^{ab}(p)$, defined as the Fourier transform

$$\mathcal{G}^{ab}(p) = \int d^4x e^{ip \cdot x} \left\langle T \left\{ c^a(x) \bar{c}^b(0) \right\} \right\rangle, \quad (3.24)$$

can be expressed in terms of a single scalar function $\mathcal{G}(p^2)$ as

$$\mathcal{G}^{ab}(p) = \mathcal{G}(p^2) \delta^{ab}. \quad (3.25)$$

The function $\mathcal{G}(p^2)$, in turn, can be computed by resumming all the insertions of the one-particle-irreducible (1PI) ghost self-energy $\Sigma(p^2)$,

$$\mathcal{G}(p^2) = \frac{i}{Z_c p^2 - \Sigma(p^2)}, \quad (3.26)$$

where Z_c , the ghost field renormalization factor, is required for removing the diverging terms contained in $\Sigma(p^2)$.



Figure 3.4: Diagrams for the one-loop SME ghost self-energy

To one loop, the diagrams which contribute to the ghost self-energy are those displayed in Fig. 3.4 [Sir16b, Sir19b]. The crossed loop on the right of the figure is included in the calculation in order to be consistent with the choice of diagrams made for the computation

of the gluon propagator. More precisely, as anticipated in the last section, to obtain the one-loop gluon and ghost SME propagators we shall include every one-loop diagram which has a maximum of three interaction vertices. An explicit calculation carried out in a generic covariant gauge within the framework of the Screened Massive Expansion of pure Yang-Mills SU(N) theory yields [Sir16b, Sir19b]

$$\Sigma(p^2) = \frac{\alpha}{4} p^2 \left(1 - \frac{\xi}{3}\right) \left(\frac{2}{\epsilon} - \ln \frac{m^2}{\bar{\mu}^2}\right) - \alpha p^2 \left(G(s) - \frac{2}{3} - \frac{\xi}{12} \ln s\right) \quad (3.27)$$

for the one-loop, 1PI dimensionally regularized ghost self-energy. In the above equation, $\bar{\mu} = \sqrt{4\pi}\mu e^{-\gamma_E/2}$ is the energy scale generated by dimreg, α is a rescaled coupling constant defined as

$$\alpha = \frac{3N\alpha_s}{4\pi}, \quad \alpha_s = \frac{g^2}{4\pi}, \quad (3.28)$$

$s = -p^2/m^2$, and $G(s)$ is the function given by

$$G(s) = \frac{1}{12} \left[\frac{(1+s)^2(2s-1)}{s^2} \ln(1+s) - 2s \ln s + \frac{1}{s} + 2 \right]. \quad (3.29)$$

In order to remove the divergence in Eq. (3.27), we choose the ghost field renormalization factor Z_c to be equal to

$$Z_c = 1 + \frac{\alpha}{4} \left[\left(1 - \frac{\xi}{3}\right) \left(\frac{2}{\epsilon} - \ln \frac{m^2}{\bar{\mu}^2}\right) + \frac{8}{3} + 4g_0 \right], \quad (3.30)$$

where g_0 is an adimensional constant which selects the renormalization scheme for the ghost propagator. In the above equation, the ϵ -pole coincides with the one contained in the corresponding MS renormalization factor [IZ06]. This was to be expected, since – as discussed in Sec. 3.1.2 – the Screened Massive Expansion does not modify the UV behavior of the theory, and in particular its UV divergences.

To one loop, the renormalized ghost propagator, which reads

$$\mathcal{G}(p^2) = \frac{i}{p^2[1 + \alpha(G(s) - \xi \ln s/12 + g_0)]}, \quad (3.31)$$

can be rewritten in such a way that the coupling constant formally disappears from the equations. In order to do so, we define two adimensional constants G_0 and Z_G as

$$G_0 = \frac{1}{\alpha} + g_0, \quad Z_G = \frac{1}{\alpha}, \quad (3.32)$$

in terms of which $\mathcal{G}(p^2)$ can be expressed as

$$\mathcal{G}(p^2) = \frac{iZ_G}{p^2(G(s) - \xi \ln s/12 + G_0)}. \quad (3.33)$$

While in the context of the SME the multiplicative factor Z_G is given by Eq. (3.32), when comparing $\mathcal{G}(p^2)$ with ghost propagators computed by other methods we are free to interpret Z_G as an independent variable. This is a consequence of the arbitrariness in the choice of the normalization for the quantum fields, which makes the corresponding propagators comparable only modulo multiplicative factors. On the other hand, the additive constant G_0 contains information on both the value of the strong coupling constant and the renormalization scheme in which the one-loop ghost propagator is defined.

As the first step in our analysis of the SME ghost propagator, let us explore its asymptotic behavior⁴. At large and small momenta – corresponding, respectively, to $s \rightarrow \infty$ and $s \rightarrow 0^-$, the function $G(s)$ which appears in the denominator of the propagator $\mathcal{G}(p^2)$ has the following limits:

$$\lim_{s \rightarrow \infty} G(s) = \frac{1}{4} \ln s + \frac{1}{3}, \quad \lim_{s \rightarrow 0} G(s) = \frac{5}{24}. \quad (3.34)$$

By plugging the first of these into Eq. (3.27), we find that at high energies the ghost self-energy reduces to

$$\Sigma(p^2) \rightarrow \frac{\alpha}{4} p^2 \left(1 - \frac{\xi}{3}\right) \left(\frac{2}{\epsilon} - \ln \frac{-p^2}{\bar{\mu}^2}\right). \quad (3.35)$$

It should come as no surprise that this is the ghost self-energy computed in ordinary perturbation theory [IZ06]: again, as we said, the SME does not modify the high-energy limit of the theory. Because of Eq. (3.35), at large momenta the ghost propagator goes to zero like $1/p^2 \ln(-p^2)$.

At the other end of the spectrum, as $p^2 \rightarrow 0$, the function $G(s)$ approaches a constant. It follows that the ghost propagator diverges in the infrared:

$$\lim_{p^2 \rightarrow 0} \mathcal{G}(p^2) = \lim_{p^2 \rightarrow 0} \frac{iZ_{\mathcal{G}}}{p^2(5/24 - \xi \ln(-p^2/m^2)/12 + G_0)} = \infty. \quad (3.36)$$

In particular, in the framework of the SME, the ghosts remain massless. It is worth noticing that, whereas the masslessness of the ghost is independent of the gauge, the way in which $\mathcal{G}(p^2)$ tends to infinity as $p^2 \rightarrow 0$ very much is: while in the zero-momentum limit $p^2 \mathcal{G}(p^2)$ remains finite in the Landau gauge ($\xi = 0$), the same is not true in any other gauge, for then $p^2 \mathcal{G}(p^2)$ itself goes to zero like $1/\ln(-p^2)$ ⁵.

How does the ghost propagator computed in the Screened Massive Expansion compare with the lattice data? The answer is shown in Fig. 3.5, where we display a fit of the Euclidean ghost dressing function $p_E^2 \mathcal{G}_E(p_E^2)$ evaluated in the Landau gauge ($\xi = 0$) together with the lattice data of [DOS16]. We recall that $\mathcal{G}_E(p_E^2)$ is defined as

$$\mathcal{G}_E(p_E^2) = i\mathcal{G}(-p_E^2), \quad (3.37)$$

with the Euclidean momentum $p_E^2 \geq 0$.

The fit in Fig. 3.5 was performed by using as free parameters the multiplicative and additive renormalization constants $Z_{\mathcal{G}}$ and G_0 defined in Eq. (3.33), while fixing the gluon mass parameter m to 0.654 GeV. The latter was obtained by fitting the SME transverse gluon propagator, as described in the next section. Moreover, in order to avoid (at this stage) the use of the Renormalization Group, the data was cut at a momentum of 2 GeV. Finally, we should mention that the normalization of the ghost propagator is the one provided by the lattice data, that is, we did not perform a further re-normalization of the propagator. A summary of the values obtained from the fit is reported in Tab. 3.1.

As we can see, in the deep IR region the Screened Massive Expansion of the ghost propagator manages to accurately reproduce the Landau-gauge lattice results. At low

⁴We should remark that the true high-energy limit of the propagators can only be studied by improving their momentum behavior via the use of the Renormalization Group equations (Sec. 1.2.3). Thus, when in the context of a fixed-scale calculation we say that a propagator has a certain high-energy limit, we interpret this to be a formal, rather than an actual, property of the propagator.

⁵The infrared-suppression of the ghost dressing function in a general covariant gauge $\xi \neq 0$ compared to its Landau-gauge counterpart was observed in a recent lattice calculation [CDM⁺18].

momenta, the Euclidean ghost dressing function $p_E^2 \mathcal{G}_E(p_E^2)$ first changes concavity and then saturates to a finite value, implying that as $p^2 \rightarrow 0$ the ghost propagator diverges to infinity like $1/p^2$, as previously anticipated. This behavior is consistent with that of the decoupling solution obtained by solving the Dyson-Schwinger Equations for pure Yang-Mills theory [AN04, AP06, ABP08, AP08, HvS13].

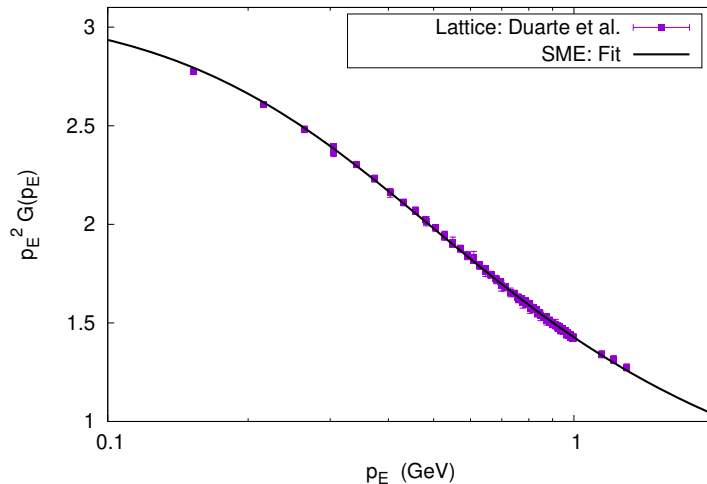


Figure 3.5: Euclidean ghost dressing function in the Landau gauge ($\xi = 0$). Solid curve: one-loop SME result with the parameters of Tab. 3.1. Squares: lattice data from [DOS16].

G_0	Z_G	m (GeV)
0.1464	1.0994	0.654

Table 3.1: Parameters obtained from fitting the lattice data of [DOS16] for the Landau-gauge Euclidean ghost propagator in the range 0-2 GeV at fixed $m = 0.654$ GeV.

3.1.4 The gluon propagator

The dressed gluon propagator $\Delta_{\mu\nu}^{ab}(p)$ is defined as the Fourier transform

$$\Delta_{\mu\nu}^{ab}(p) = \int d^4x e^{ip \cdot x} \langle T \{ A_\mu^a(x) A_\nu^b(0) \} \rangle. \quad (3.38)$$

Since – as we saw in Sec. 1.1.4 – the longitudinal projection of $\Delta_{\mu\nu}^{ab}(p)$ is exactly equal to $-i\xi/p^2$, the gluon propagator can be expressed in terms of a single unknown scalar function $\Delta(p^2)$:

$$\Delta_{\mu\nu}^{ab}(p) = \left(\Delta(p^2) t_{\mu\nu}(p) + \frac{-i\xi}{p^2} \ell_{\mu\nu}(p) \right) \delta^{ab}. \quad (3.39)$$

Modulo the color structure, $\Delta(p^2)$ is the transverse component of the gluon propagator.

$\Delta(p^2)$ can be computed by resumming all the insertions of the 1PI gluon polarization⁶, whose transverse component we denote by $\Pi(p^2)$:

$$\Delta(p^2) = \frac{-i}{Z_A p^2 - m^2 - \Pi(p^2)}. \quad (3.40)$$

In the above equation, the gluon field renormalization factor Z_A is needed to absorb the diverging terms in $\Pi(p^2)$, whereas the presence of the mass term m^2 is a consequence of the massiveness of the zero-order SME propagator.

To one loop, the 1PI gluon polarization receives contributions from the diagrams shown in Figs. 3.6 and 3.7. The single-counterterm diagram in Fig. 3.6 is easily computed to be equal to $-m^2$. It follows that the 1PI gluon polarization can be expressed as

$$\Pi(p^2) = -m^2 + \Pi_{\text{loop}}(p^2), \quad (3.41)$$

where the function $\Pi_{\text{loop}}(p^2)$ collects the contributions to $\Pi(p^2)$ due to the loops of the perturbative series. By plugging the last equation into Eq. (3.40), we see that the transverse gluon propagator can be written as

$$\Delta(p^2) = \frac{-i}{Z_A p^2 - \Pi_{\text{loop}}(p^2)}. \quad (3.42)$$

The expression (3.42) for $\Delta(p^2)$ is especially important, since it proves that, in the framework of the Screened Massive Expansion, the generation of a gluon mass is not the trivial consequence of having forced a mass term into the zero-order gluon propagator. Indeed, if $\Pi_{\text{loop}}(p^2)$ vanished in the zero-momentum limit, then the gluon propagator – having a pole at $p^2 = 0$ – would remain massless. Instead, as we shall see in a moment, $\Pi_{\text{loop}}(p^2)$ actually turns out to be proportional to the gluon mass parameter m^2 when computed at $p^2 = 0$. As a result, the propagator is finite in the zero-momentum limit and a mass is generated for the gluon. Coming from the loops of the expansion, such a mass is a truly dynamical effect of the interactions.



Figure 3.6: Single-counterterm diagram

The diagrams which make up $\Pi_{\text{loop}}(p^2)$ at the one-loop order are depicted in Fig. 3.7. Those denoted by (1), (2a) and (3a) are just the ordinary one-loop diagrams of standard perturbation theory, although we should keep in mind that – at variance with pQCD – diagrams (2a) and (3a) are computed by making use of the massive gluon propagator Δ_m ⁷. Due to the mass which runs inside the loops, both of these diagrams can be shown to contain mass divergences. As discussed in Sec. 3.1.2, these divergences cannot be renormalized by making use of the gluon field renormalization factor Z_A ⁸. In order to eliminate the mass

⁶At variance with ordinary pQCD, the SME gluon polarization can develop a longitudinal component $\Pi_L(p^2) \neq 0$ when computed to finite order in the gluon mass counterterm. Nonetheless, we have seen that by resumming all the crossed diagrams associated to an uncrossed SME diagram the ordinary pQCD result is recovered. Therefore, we can assume that such a resummation has been performed and set $\Pi_L(p^2) = 0$.

⁷As such, diagrams (2a) and (3a) can also be found in the gluon polarization of the Curci-Ferrari model.

⁸That Z_A is only able to absorb divergences proportional to the momentum squared p^2 is clear from Eq. (3.42).

divergences, the crossed diagrams (2b) and (3b) must also be included in the calculation. This is sufficient because, as we saw in Sec. 3.1.2,

$$\Pi_{(2b/3b)}(p^2) = -m^2 \frac{\partial}{\partial m^2} \Pi_{(2a/3a)}(p^2) , \quad (3.43)$$

so that if the polarization term $\Pi_{(2a/3a)}(p^2)$ associated to diagram (2a/3a) contains a divergence proportional to m^2 , then the sum

$$\Pi_{(2a/3a)}(p^2) + \Pi_{(2b/3b)}(p^2) = \left(1 - m^2 \frac{\partial}{\partial m^2} \right) \Pi_{(2a/3a)}(p^2) \quad (3.44)$$

does not. Finally, since diagram (3b) is a one-loop, three-vertex diagram, we also include the only other diagram which has these properties – namely, diagram (2c).

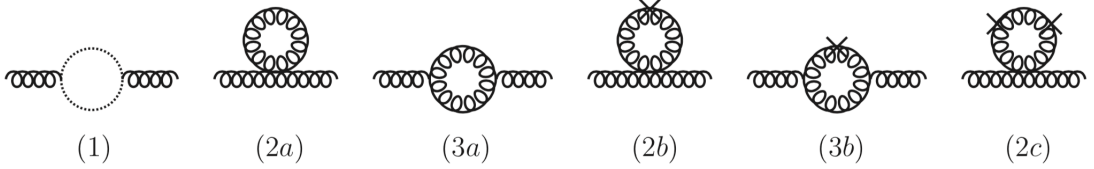


Figure 3.7: Loop diagrams for the one-loop SME gluon polarization

An explicit calculation carried out in a general covariant gauge within the framework of the Screened Massive Expansion of pure Yang-Mills SU(N) theory shows that, to one loop and in dimensional regularization [Sir16b, SC18],

$$\Pi_{\text{loop}}(p^2) = \frac{\alpha}{3} \left(\frac{13}{6} - \frac{\xi}{2} \right) p^2 \left(\frac{2}{\epsilon} - \ln \frac{m^2}{\bar{\mu}^2} \right) - \alpha p^2 (F(s) + \xi F_\xi(s) + \mathcal{C}) . \quad (3.45)$$

In the above equation, like in the last section, $\bar{\mu} = \sqrt{4\pi} \mu e^{-\gamma_E/2}$ is the energy scale generated by dimreg, $\alpha = \frac{3N\alpha_s}{4\pi}$ is a rescaled coupling constant and $s = -p^2/m^2$. Moreover, \mathcal{C} is an unessential constant which disappears after renormalization, and $F(s)$ and $F_\xi(s)$ are the functions defined as

$$F(s) = \frac{5}{8s} + \frac{1}{72} [L_a(s) + L_b(s) + L_c(s) + R_a(s) + R_b(s) + R_c(s)] , \quad (3.46)$$

$$F_\xi(s) = \frac{1}{4s} - \frac{1}{12} \left[2s \ln s - \frac{2(1-s)(1-s^3)}{s^3} \ln(1+s) + \frac{3s^2 - 3s + 2}{s^2} \right] , \quad (3.47)$$

where the logarithmic functions $L_a(s)$, $L_b(s)$ and $L_c(s)$ and the rational functions $R_a(s)$, $R_b(s)$ and $R_c(s)$ are given by

$$\begin{aligned} L_a(s) &= \frac{3s^3 - 34s^2 - 28s - 24}{s} \sqrt{\frac{4+s}{s}} \ln \left(\frac{\sqrt{4+s} - \sqrt{s}}{\sqrt{4+s} + \sqrt{s}} \right) , \\ L_b(s) &= \frac{2(1+s)^2}{s^3} (3s^3 - 20s^2 + 11s - 2) \ln(1+s) , \\ L_c(s) &= (2 - 3s^2) \ln s , \end{aligned} \quad (3.48)$$

$$\begin{aligned}
R_a(s) &= -\frac{4+s}{s} (s^2 - 20s + 12) , \\
R_b(s) &= \frac{2(1+s)^2}{s^2} (s^2 - 10s + 1) , \\
R_c(s) &= \frac{2}{s^2} + 2 - s^2 .
\end{aligned} \tag{3.49}$$

In order to remove the divergence in $\Pi_{\text{loop}}(p^2)$, the gluon field renormalization constant Z_A must be chosen according to

$$Z_A = 1 + \frac{\alpha}{3} \left(\frac{13}{6} - \frac{\xi}{2} \right) \left(\frac{2}{\epsilon} - \ln \frac{m^2}{\mu^2} \right) + \alpha(f_0 - \mathcal{C}) , \tag{3.50}$$

where f_0 is an adimensional constant that selects the renormalization scheme for the gluon propagator. Just like in the ghost sector, the ϵ -pole in Z_A is the one that appears in the MS gluon field renormalization constant [IZ06], yet again confirming that the SME does not modify the UV behavior of the theory.

As we did for the ghost propagator, we can rewrite the transverse gluon propagator,

$$\Delta(p^2) = \frac{-i}{p^2[1 + \alpha(F(s) + \xi F_\xi(s) + f_0)]} , \tag{3.51}$$

in such a way that the coupling constant disappears from the equation. To do so, we define two adimensional constants F_0 and Z_Δ as

$$F_0 = \frac{1}{\alpha} + f_0 , \quad Z_\Delta = \frac{1}{\alpha} , \tag{3.52}$$

in terms of which

$$\Delta(p^2) = \frac{-iZ_\Delta}{p^2(F(s) + \xi F_\xi(s) + F_0)} . \tag{3.53}$$

Again, Z_Δ can be taken to be a free constant when the SME gluon propagator is compared to one computed by different methods (see Sec. 3.1.4), whereas F_0 contains information on both the coupling constant and the renormalization scheme in which $\Delta(p^2)$ is defined.

In the high- and low-momentum limits $s \rightarrow \infty$ and $s \rightarrow 0$, the functions $F(s)$ and $F_\xi(s)$ have the asymptotic behavior

$$\lim_{s \rightarrow \infty} F(s) = \frac{17}{18} + \frac{13}{18} \ln s , \quad \lim_{s \rightarrow 0} F(s) = \frac{5}{8s} , \tag{3.54}$$

$$\lim_{s \rightarrow \infty} F_\xi(s) = -\frac{1}{6} \ln s - \frac{1}{12} , \quad \lim_{s \rightarrow 0} F_\xi(s) = \frac{1}{4s} . \tag{3.55}$$

As a consequence, in the UV, the SME gluon polarization $\Pi(p^2)$ reduces to

$$\Pi(p^2) \rightarrow \frac{\alpha}{3} \left(\frac{13}{6} - \frac{\xi}{2} \right) p^2 \left(\frac{2}{\epsilon} - \ln \frac{-p^2}{\mu^2} \right) , \tag{3.56}$$

which is the same expression that is obtained in standard perturbation theory [IZ06]. In particular, just like the ghost propagator, the transverse gluon propagator tends to zero as $1/p^2 \ln(-p^2)$ in the high-energy limit (see Note 4 in Sec. 3.1.4). On the other hand, at vanishing momentum,

$$\Delta(0) = \frac{-iZ_\Delta}{-M_\xi^2} , \tag{3.57}$$

where M_ξ^2 is the ξ -dependent mass scale given by

$$M_\xi^2 = \frac{5m^2}{8} \left(1 + \frac{2\xi}{5} \right) . \quad (3.58)$$

Since $\Delta(0)$ is finite, the gluon propagator is evidently massive.

In order to investigate the origin of the gluon mass in the framework of the SME, it is interesting to analyze what kind of contributions are made to the scale M_ξ^2 – equivalently, to the polarization term $\Pi_{\text{loop}}(0)$ – by the loop diagrams in Fig. 3.7. As we stated earlier, diagram (1) is just an ordinary pQCD diagram. For this reason, we do not expect it to generate a mass for the gluon, and indeed we find that $\Pi_{(1)}(p^2 = 0) = 0$. On the other hand, diagrams (2a), (2b), (3a) and (3b) are all computed by making use of the massive propagator Δ_m , and all of them contain mass divergences. As a consequence, their $p^2 \rightarrow 0$ limits are UV-divergent, and to quantify their contribution to M_ξ^2 it only makes sense to consider the sums (2a+2b) and (3a+3b). This being said, we find that the mass scale M_ξ^2 is distributed as follows between the one-loop diagrams (1) to (3c):

$$\Pi_{(1)}(0) = 0 , \quad (3.59)$$

$$\begin{aligned} \Pi_{(2a)}(0) + \Pi_{(2b)}(0) &= -\frac{3\alpha}{4} m^2 , \\ \Pi_{(2c)}(0) &= \frac{3\alpha}{8} m^2 , \end{aligned} \quad (3.60)$$

$$\Pi_{(3a)}(0) + \Pi_{(3b)}(0) = \alpha \left(1 + \frac{\xi}{4} \right) m^2 .$$

All of the one-loop diagrams, with the exception of the ordinary ghost loop, contribute to the zero-momentum finiteness of the gluon propagator. Notably, the diagrams which do not vanish in the $p^2 \rightarrow 0$ limit all involve the self-interaction of gluons, be it mediated by 3-gluon or by 4-gluon vertices. The breakdown of the contributions to $\Pi_{\text{loop}}(0)$ clearly illustrates that the generation of a dynamical mass for the gluons in QCD – as described within the framework of the SME – is the consequence of the non-abelian nature of the interaction between the gauge fields.

We remark that this would still hold true had we included the quarks in the calculation. Indeed, the quark loop which in full QCD contributes to the gluon polarization to lowest order in the coupling (Fig. 3.8), not containing internal gluon lines, has the same expression both in the SME and in ordinary perturbation theory; hence it vanishes in the limit $p^2 \rightarrow 0$, just like the ghost loop $\Pi_{(1)}(p^2)$. As an aside, we note that the vanishing of the quark loop at $p^2 = 0$, combined with the lack of the necessary gauge self-interaction vertices, also implies that the SME would not predict the occurrence of DMG for the photons if it were applied to Quantum Electrodynamics. This is further confirmation of the non-triviality of DMG in the framework of the Screened Massive Expansion of QCD.

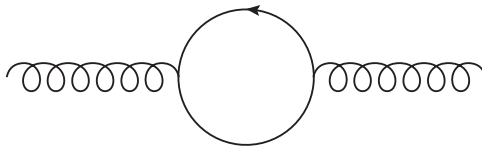


Figure 3.8: Quark loop (lowest-order full-QCD gluon polarization)

Having discussed the main features of the SME gluon propagator, it is now time to compare our results with the lattice data. In Fig. 3.9 we show the Landau-gauge ($\xi = 0$) Euclidean transverse gluon propagator $\Delta_E(p_E^2)$, defined as⁹

$$\Delta_E(p_E^2) = -i\Delta(-p_E^2) \quad (p_E^2 \geq 0), \quad (3.61)$$

together with the lattice data of [DOS16]. The plot was obtained by fitting the free parameters F_0 , Z_Δ and m in Eq. (3.53) over the Euclidean momentum range $p_E \in [0, 4]$ GeV; this is at variance with the ghost dressing function, for which we had cut the data at $p_E = 2$ GeV. Like in the previous section, we did not perform a further re-normalization of the propagator, using instead the normalization provided by the lattice. The outcome of the fit is reported in Tab. 3.2. For future reference, we note that the fitted value of the parameter F_0 is -0.8872 .

As we can see from the figure, the SME gluon propagator accurately reproduces the lattice data down to very small momenta. As the momentum decreases, the propagator changes concavity and saturates to a finite value $\approx 10 \text{ GeV}^{-2}$, corresponding to $\Delta^{-1/2}(0) \approx 0.3 \text{ GeV}$. The energy units are set by the gluon mass parameter, whose fitted value is found to be $m \approx 0.654 \text{ GeV}$, in general agreement with values derived by other methods – see e.g. [Fie02].

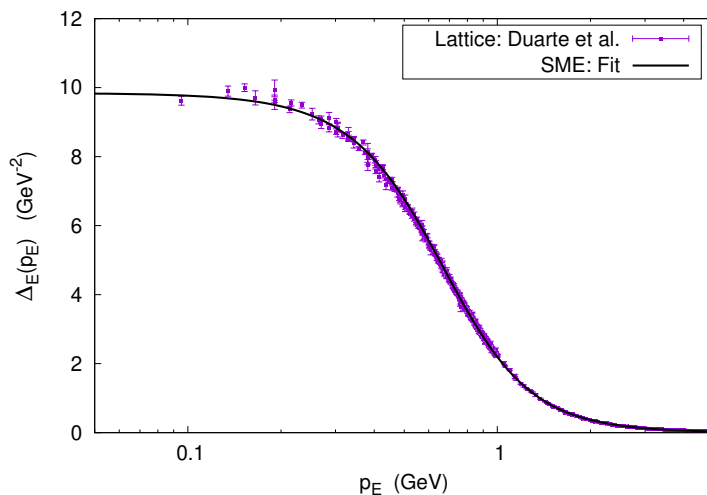


Figure 3.9: Euclidean transverse gluon propagator in the Landau gauge ($\xi = 0$). Solid line: one-loop SME result with the parameters of Tab. 3.2. Squares: lattice data from [DOS16].

F_0	m (GeV)	Z_Δ
-0.8872	0.6541	2.6308

Table 3.2: Parameters obtained by fitting the lattice data of [DOS16] for the Landau-gauge Euclidean transverse gluon propagator in the range 0-4 GeV.

⁹We should mention that the analytic continuation of results obtained in Minkowski space to the Euclidean space and vice-versa is far from being as trivial as Eq. (3.61) suggests [SC22a]. This is especially true for the gluon propagator, which – as we will see in Sec. 3.2 – possesses a pair of complex-conjugate poles. In what follows we will disregard this issue and take Eq. (3.61) as a definition.

The remarkable precision with which the infrared behavior of the gluon propagator is predicted by the SME substantiates the hypothesis that a shift of the expansion point of QCD is able both to incorporate dynamical mass generation and to avoid the low-energy breakdown of perturbation theory, yielding results which remain valid down into the deep IR. Nonetheless, up to this point, all of our predictions required the fitting of free parameters which do not exist in standard perturbation theory. In the next section, we will discuss how principles of gauge invariance can be exploited to fix some of their values a priori, thus restoring the predictive power of the Screened Massive Expansion.

3.2 Optimization of the Screened Massive Expansion

In order to compare the one-loop ghost and gluon propagators computed in the Screened Massive Expansion with the results of the Landau-gauge lattice calculations, in Secs. 3.1.3 and 3.1.4 we performed fits which made use of a number of free parameters. For the gluon propagator, these were the gluon mass parameter m^2 , the multiplicative renormalization constant Z_Δ and the additive renormalization constant F_0 ; for the gluon dressing function, they were the multiplicative renormalization constant Z_G and the additive renormalization constant G_0 . In total, these add up to one dimensionful parameter (m^2) plus *four* adimensional renormalization constants. By comparison, the ordinary perturbative expressions contain far fewer free parameters. Indeed, going back to Eqs. (3.31) and (3.51), we see that, in the absence of the gluon mass parameter m^2 , the one-loop analytical expressions for the ghost and gluon propagators would be determined in terms of the value of the coupling constant α (equivalently, α_s) and of *two* additive renormalization constants, one for each propagator. The latter are usually fixed by choosing appropriate renormalization conditions.

Where do the additional SME free parameters come from? The gluon mass parameter, of course, arises from the shift $\Delta_0 \rightarrow \Delta_m$ that defines the Screened Massive Expansion. The additive renormalization constants F_0 and G_0 , on the other hand, were introduced with the double purpose of keeping the renormalization of the propagators fully general and of removing the coupling constant from the expressions¹⁰, thus reducing the number of parameters. As a by-product of this reparametrization, new multiplicative renormalization constants Z_Δ and Z_G appeared as factors in $\Delta(p^2)$ and $\mathcal{G}(p^2)$. When comparing the propagators with the results obtained by other methods (such as lattice QCD), the arbitrariness in the choice of the ghost and gluon fields' normalization, together with our decision not to fix the renormalization conditions for the SME expressions, allows us to interpret Z_Δ and Z_G as new free parameters.

As we saw in Secs. 3.1.3 and 3.1.4, when expressed in terms of m^2 , F_0 , G_0 , Z_Δ and Z_G , the SME ghost and gluon propagators turn out to accurately reproduce the infrared lattice data. So accurately, in fact, that we may say that, at low energies, the parametrization introduced in the last section effectively incorporates most of the corrections coming from the higher orders in the perturbative series. Nonetheless, the number of free parameters in the expressions is far too large to interpret our results as first-principles analytical predictions. If we could somehow fix the values of the constants F_0 and G_0 , then the predictive power of the expansion would be restored, leaving Z_Δ and Z_G as the only renormalization parameters and the gluon's m^2 as the scale that sets the physical units

¹⁰We remark that, formally, the removal of α is only possible at the one-loop order, since higher-order corrections to the ghost self-energy/gluon polarization – being proportional to powers α^k with $k \geq 2$ – would make it impossible to redefine the additive renormalization constants like we did in Eqs. (3.32) and (3.52), while yielding α -independent propagators.

of the expansion. In this scenario, m^2 would play a role similar to that of the scale¹¹ introduced in pQCD by the coupling constant $\alpha_s(\mu^2)$.

The objective of this section is to show that the number of parameters of the SME can indeed be reduced by resorting to principles of gauge invariance [SC18]. More precisely, we will exploit the gauge-parameter independence of the position of the poles of the gluon propagator in a general covariant gauge – see the discussion on the Nielsen identities in Sec. 1.1.4 – to fix the free gluon constant F_0 . The latter can then be used to determine the ghost constant G_0 based on principles of minimal sensitivity. In what follows, we will not go into the details of the determination of G_0 , limiting ourselves to present the main results of [Sir19a, Sir19b] in Sec. 3.2.3.

The *optimized* one-loop expressions obtained by enforcing the gauge-parameter independence of the analytical structure of the gluon propagator will be shown to reproduce the infrared lattice data just as well as the fits of Secs. 3.1.3 and 3.1.4. However, at variance with the fits, this will be achieved from first principles, with no external inputs other than a required energy scale in the form of the gluon mass parameter m^2 .

3.2.1 The gluon poles and the Nielsen identities in the context of the Screened Massive Expansion

By making use of the Nielsen identities, in Sec. 1.1.4 we showed that the position p_0^2 of the poles of the transverse gluon propagator, defined as the solution to the equation

$$\Delta^{-1}(p_0^2, \xi) = 0 , \quad (3.62)$$

does not depend on the gauge parameter ξ . While this is a trivial property for massless propagators, since in that case $p_0^2 = 0$ for any ξ , if the gluon develops a mass its poles are shifted from the origin and, in principle, can be found at any non-zero value of the complex- p^2 plane; therefore, the gauge-parameter independence of the poles acquires a new significance in the presence of dynamical mass generation. Gauge-independent gluon poles are likely to play an important role in the evaluation of gauge-invariant physical quantities, which can be directly measured in the experiments¹².

From an analytical perspective, the only constraint that the gluon poles must satisfy is that they either be real, or appear in complex-conjugate (c.c.) pairs. This is a direct consequence of the identity

$$\Delta(\overline{p^2}) = \overline{\Delta(p^2)} , \quad (3.63)$$

where the overline denotes complex-conjugation, which holds for $\Delta(p^2)$ since the latter is real for $p^2 \in \mathbb{R}$, $p^2 \leq 0$ and analytic away from its singularities. From Eq. (3.63) it follows that if $\Delta^{-1}(p_0^2) = 0$, then also $\Delta^{-1}(\overline{p_0^2}) = 0$, implying that p_0^2 and $\overline{p_0^2}$ are both poles of the propagator.

The existence of c.c. poles in the propagators of interacting quantum fields has been linked in the literature to the phenomenon of confinement. This is due to the fact that, in the presence of c.c. poles, the Källén-Lehman spectral representation which is derived by ordinary quantum-field-theoretical methods for the propagators of physical particles is invalidated [Sir17b]: first of all, the spectral representation acquires an anomalous rational part which describes the contribution coming from the c.c. poles [Sir17b, SC18]; additionally, the spectral function associated to the propagator is negative at both low and high

¹¹That is, either the renormalization scale μ itself or the value of the QCD scale Λ_{QCD} , $\Lambda_{\text{QCD}} = \mu \exp(-8\pi^2/\beta_0 g^2(\mu))$ – see Sec. 1.2.3.

¹²We should remark, however, that the Nielsen identities do not guarantee that the poles of the propagator do not depend on the gauge; technically speaking, they only prove that their position does not depend on the gauge parameter *in a general covariant gauge*.

momenta [SC18, HK19], in violation of the positivity constraints which hold for physical particles. From a dynamical perspective, the imaginary part of the c.c. poles causes an exponential damping of the coordinate-space Minkowski propagator at large times $|t| \rightarrow \infty$, a symptom that the degrees of freedom described by the propagator are removed from the asymptotic states of the theory [SC22a].

What does the Screened Massive Expansion tell us about the analytic structure of the transverse gluon propagator? If we take the parameters in Tab. 3.2 as an example, we find that – as predicted by the Gribov-Zwanziger and Refined Gribov-Zwanziger approaches (Sec. 2.3) – the Landau-gauge ($\xi = 0$) gluon propagator computed in the SME indeed possesses a pair of complex conjugate poles at

$$p_0^2 = (0.4487 \pm 1.0209 i) m^2 , \quad (3.64)$$

which, with $m = 0.654$ GeV, correspond to

$$p_0 = (\pm 0.5784 \pm 0.3776 i) \text{ GeV} , \quad (3.65)$$

the four \pm signs being independent from each other. More generally, since

$$\Delta^{-1}(p^2, \xi) = i Z_{\Delta}^{-1} p^2 J^{-1}(-p^2/m^2, \xi) , \quad (3.66)$$

where the inverse dressing function $J^{-1}(s, \xi)$ reads

$$J^{-1}(s, \xi) = F(s) + \xi F_{\xi}(s) + F_0 \quad (3.67)$$

and is singular at $s = 0$, the gluon poles are given by the zeros of $J^{-1}(-p^2/m^2, \xi)$,

$$J^{-1}(-p_0^2/m^2, \xi) = 0 , \quad (3.68)$$

the latter being equivalent to the pair of coupled equations

$$\text{Re} \{ F(-p_0^2/m^2) + \xi F_{\xi}(-p_0^2/m^2) \} + F_0 = 0 , \quad \text{Im} \{ F(-p_0^2/m^2) + \xi F_{\xi}(-p_0^2/m^2) \} = 0 . \quad (3.69)$$

Observe that the imaginary part of $J^{-1}(s, \xi)$ does not depend on the additive renormalization constant F_0 , since the latter is a real quantity; moreover, $\text{Im}\{J^{-1}(s, \xi)\}$ does not vanish for arbitrary s , despite $J(s, \xi)$ being a real function for $s \in \mathbb{R}$, as the domain of p^2 – equivalently, of s – is the whole complex plane, $p^2 \in \mathbb{C}$.

In order to solve Eqs. (3.69), it is understood that one must first fix a gauge ξ ; the solution p_0^2 will then be a function of the parameters m^2 , F_0 and ξ :

$$p_0^2 = p_0^2(m^2, F_0, \xi) . \quad (3.70)$$

As ξ varies, we are actually allowed to change the values of both F_0 and m^2 . Indeed, F_0 is a renormalization constant for the gluon propagator; since the latter is gauge dependent, F_0 also generally depends on ξ . m^2 , on the other hand, is a mass parameter which is introduced in the Faddeev-Popov action *after* fixing the gauge of the QCD Lagrangian. As such, there is no reason to force it to be a gauge-invariant parameter. With $F_0 = F_0(\xi)$ and $m^2 = m^2(\xi)$, the solutions of Eqs. (3.69) take the form

$$p_0^2(\xi) = p_0^2(m^2(\xi), F_0(\xi), \xi) . \quad (3.71)$$

Are there solutions of Eqs. (3.69) such that $dp_0^2/d\xi \neq 0$? The answer is yes. For general values of the functions $m^2(\xi)$ and $F_0(\xi)$, the gluon propagator computed in the SME has

poles which depend on the gauge parameter, in violation of the Nielsen identities. This happens because the massive shift that defines the SME breaks BRST symmetry at any finite order in perturbation theory, unless all the gluon mass counterterms are resummed. As a result, the Nielsen identities are not automatically satisfied [SC22b], and the position of the gluon poles can depend on ξ .

Nonetheless, since the shift does not change the total Faddeev-Popov Lagrangian, we should expect the gauge-parameter independence of the gluon poles to be recovered also in the framework of the SME. And indeed, the freedom in the choice of the functions $F_0(\xi)$ and $m^2(\xi)$ in Eqs. (3.69) and (3.71) enables us to *enforce* the ξ -independence of the poles. This can be done as follows. Suppose that we know that, in a gauge ξ_1 , the exact gluon propagator has a pole at $p_0^2 = p_0^2(\xi_1)$. The Nielsen identities then tell us that in a gauge ξ_2 the propagator will have a pole at the same position $p_0^2(\xi_2) = p_0^2(\xi_1)$. In order for this to be true at one loop in the SME, the values of the parameters $m^2(\xi_2)$ and $F_0(\xi_2)$ need to be chosen so that

$$p_0^2(m^2(\xi_2), F_0(\xi_2), \xi_2) = p_0^2(m^2(\xi_1), F_0(\xi_1), \xi_1) , \quad (3.72)$$

where $m^2(\xi_1)$ and $F_0(\xi_1)$ are the parameters by which $p_0^2 = p_0^2(\xi_1)$ in the gauge ξ_1 . In terms of Eq. (3.69), this means that the value of the gluon mass parameter $m^2(\xi_2)$ must be such that

$$\text{Im} \{ F(-p_0^2/m^2(\xi_2)) + \xi_2 F_\xi(-p_0^2/m^2(\xi_2)) \} = 0 . \quad (3.73)$$

If this equation has a solution, then – again by Eq. (3.69) – $F_0(\xi_2)$ will be given by

$$F_0(\xi_2) = -\text{Re} \{ F(-p_0^2/m^2(\xi_2)) + \xi_2 F_\xi(-p_0^2/m^2(\xi_2)) \} . \quad (3.74)$$

The requirement that the gluon poles be gauge-parameter independent allows us to fix the value of $F_0(\xi)$ and $m^2(\xi)$ in any covariant gauge ξ starting from their values $F_0(\xi_0)$ and $m^2(\xi_0)$ in an initial gauge ξ_0 . To do so, one first computes the position of the pole $p_0^2 = p_0^2(\xi_0)$ in the gauge ξ_0 by solving the equation $J^{-1}(-p_0^2/m^2(\xi_0), \xi_0) = 0$ for p_0^2 , and then uses the steps described above to obtain $F_0(\xi)$ and $m^2(\xi)$.

As an example of the application of this method, in Fig. 3.10 we show the ratio $m^2(\xi)/m^2(0)$ and the function $F_0(\xi)$ computed from the Landau-gauge ($\xi = 0$) lattice fit values of Tab. 3.2, Sec. 3.1.4 – namely, $F_0(0) = -0.8872$ and $m(0) = 0.6541$ GeV. As we can see, the gluon mass parameter decreases with the gauge, whereas the additive renormalization constant $F_0(\xi)$ is a non-monotonic function of ξ . So long as $m^2(\xi)$ and $F_0(\xi)$ are chosen like in the figure, the gluon poles computed in an arbitrary covariant gauge remain fixed at their $\xi = 0$ value, $p_0 = (\pm 0.5784 \pm 0.3776 i)$ GeV. We remark that Eqs. (3.73) and (3.74) are automatically satisfied by $\overline{p_0^2}$ if they are by p_0^2 , explaining how invariance is achieved for both the c.c. gluon poles by a single choice of the functions $m^2(\xi)$ and $F_0(\xi)$.

Interestingly, the method we just described for determining $m^2(\xi)$ and $F_0(\xi)$ only works if the poles of the gluon propagator have a non-zero imaginary part (and thus appear in c.c. pairs), for otherwise Eq. (3.73) would be trivially solved by an arbitrary function $m^2(\xi)$ and we would be left with an infinite number of corresponding $F_0(\xi)$'s by Eq. (3.74). On the other hand, if the propagator has more than one pair of c.c. poles, then it may be impossible to enforce the gauge-parameter independence of *all* the poles by making use of unique functions $m^2(\xi)$ and $F_0(\xi)$. It is remarkable that the single pair of c.c. poles found by fitting the lattice data prevents these issues from arising.

Once the gluon mass parameter and additive renormalization constant are fixed in an arbitrary covariant gauge by enforcing the gauge-parameter independence of the position

of the poles, the SME expression for the gluon propagator is left to depend – modulo multiplicative renormalization – on just two real numbers: $m^2(\xi_0)$ and $F_0(\xi_0)$, both evaluated at an initial gauge ξ_0 . By pushing forward with requirements of gauge invariance, it can be shown that the constant $F_0(\xi_0)$ also can be fixed from first principles, thus completing the reduction of the number of free parameters needed to restore the predictivity of the SME in the gluon sector. This will be the subject of the next section.

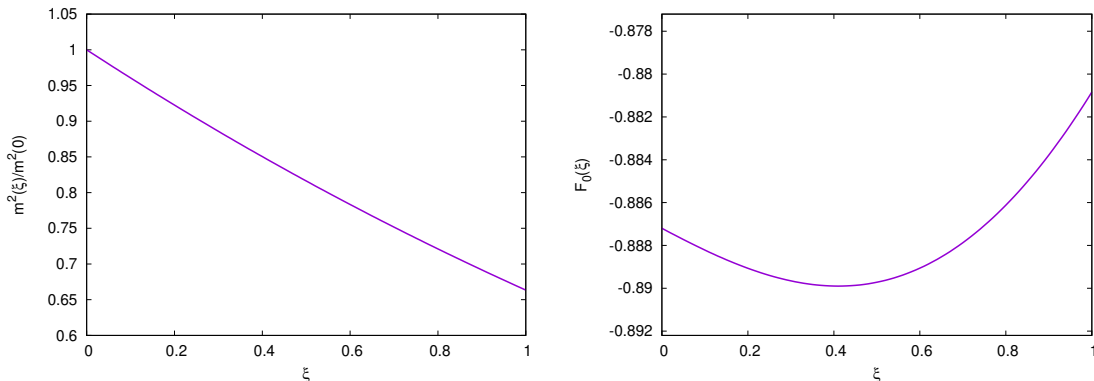


Figure 3.10: Ratio $m^2(\xi)/m^2(0)$ (left) and function $F_0(\xi)$ (right) computed from the Landau-gauge ($\xi = 0$) lattice fit values of Tab. 3.2 using Eqs. (3.73) and (3.74).

3.2.2 The phases of the residues of the gluon propagator: restoring the predictivity of the Screened Massive Expansion in the gluon sector

While investigating the properties of the SME gluon propagator evaluated on the fit parameters of Tab. 3.2, an unexpected discovery was made regarding the behavior of the residues at its poles: if the propagator is extended to an arbitrary covariant gauge by enforcing the gauge-parameter independence of the poles as described in Sec. 3.2.1, then the *phases* of the its residues depend on the gauge parameter ξ so slightly that they may also be regarded to be invariant.

In more detail, the functions $m^2(\xi)$ and $F_0(\xi)$ were derived by making use of Eqs. (3.73) and (3.74) with the Landau-gauge parameters of Tab. 3.2 as an input (see Fig. 3.10). The residue $R(\xi)$ of the gluon propagator at $p_0^2 = (0.4487 + 1.0209i) m^2(0)$, defined in terms of the Euclidean propagator as

$$R(\xi) = \lim_{p_E^2 \rightarrow -p_0^2} (p_E^2 + p_0^2) \Delta_E(p_E^2, \xi) = |R(\xi)| e^{i\theta(\xi)}, \quad (3.75)$$

was then calculated as a function of the gauge parameter ξ . Over the range $\xi \in [0, 1]$, the phase $\theta(\xi)$ was found to attain values

$$\theta(\xi) = 1.262_{-0.24\%}^{+0.09\%}, \quad (3.76)$$

where the quoted value is the Landau-gauge phase, $\theta(0) = 1.262$, whereas the maximum and minimum values were found at $\xi \approx 0.9$ and $\xi \approx 0.3$, respectively. In modulus, these are equal to $\theta(0)$ to within less than 2.5 parts in 1000. For reference, the function $\theta(\xi)$ is shown on an enlarged scale in Fig. 3.11. Due to the analytical properties of the gluon

propagator, these results also hold – with obvious modifications – for the conjugated pole $p_0^2 = (0.4487 - 1.0209i) m^2(0)$, which has residue $\overline{R(\xi)}$ and phase $-\theta(\xi)$.

If the gauge-parameter independence of the phases of gluon residues were an *exact* property of the covariant gauges, this finding could hint to some degree of physical significance for the angle θ . Such a notion is strengthened by the observation that θ does not depend on the renormalization of the propagator. Indeed, while the residue $R(\xi)$ can always be redefined by multiplying the propagator $\Delta(p^2, \xi)$ by a (generally ξ -dependent) renormalization factor $Z(\xi)$, so that the absolute value $|R(\xi)|$ is both gauge and renormalization dependent, the same is not true for the phase $\theta(\xi)$: given that $Z(\xi)$ must be chosen real, the renormalization of the propagator cannot change the phase θ , nor its gauge dependence.

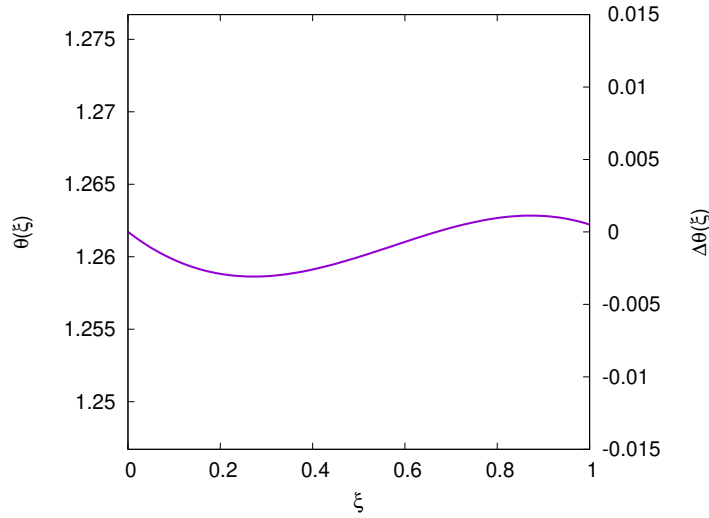


Figure 3.11: Phase of the residue $\theta(\xi)$ (left axis) and phase difference $\Delta\theta(\xi) = \theta(\xi) - \theta(0)$ (right axis) as functions of the gauge ξ computed by enforcing the gauge-parameter independence of the gluon poles obtained from the fitted Landau-gauge parameters of Tab. 3.2. $\theta(0) \approx 1.2617$.

Interestingly, in the context of the Screened Massive Expansion, the assumption that $\theta(\xi)$ be exactly gauge-parameter independent provides us with a criterion for fixing the value of the renormalization constant $F_0(\xi_0)$ at some initial gauge ξ_0 [SC18]. The idea that underlies this kind of optimization is that, if the phases of the residues of the exact gluon propagator do not depend on ξ , then the best approximation of the propagator is the one for which $\theta(\xi)$ varies the least with the gauge parameter. That this can be achieved by an appropriate choice of $F_0(\xi_0)$ can be shown as follows. Going back to the definition of the residue – Eq. (3.75) –, we see that

$$\begin{aligned} R(\xi) &= \lim_{p_E^2 \rightarrow -p_0^2} (p_E^2 + p_0^2) \Delta_E(p_E^2, \xi) = \\ &= \lim_{p_E^2 \rightarrow -p_0^2} \frac{p_E^2 + p_0^2}{\Delta_E^{-1}(p_E^2, \xi) - \Delta_E^{-1}(-p_0^2, \xi)} = \left(\frac{\partial \Delta_E^{-1}}{\partial p_E^2} \Big|_{p_E^2 = -p_0^2} \right)^{-1}. \end{aligned} \quad (3.77)$$

In terms of the inverse dressing function $J^{-1}(s)$,

$$\Delta_E^{-1}(p_E^2, \xi) = Z_\Delta^{-1} p_E^2 J^{-1}(p_E^2/m^2(\xi)), \quad J^{-1}(-p_0^2/m^2(\xi)) = 0, \quad (3.78)$$

Eq. (3.77) reads

$$R(\xi) = \frac{Z_\Delta m^2(\xi)}{-p_0^2} \left(\frac{\partial J^{-1}}{\partial s} \Big|_{s=-\frac{p_0^2}{m^2(\xi)}} \right)^{-1}. \quad (3.79)$$

By denoting the adimensional ratios $m^2(\xi)/m^2(\xi_0)$ and $-p_0^2/m^2(\xi_0)$ respectively with $a(\xi)$ and z_0 , the residue can be put in the form

$$R(\xi) = \frac{Z_\Delta a(\xi)}{z_0} \left(\frac{\partial J^{-1}}{\partial s} \Big|_{s=\frac{z_0}{a(\xi)}} \right)^{-1}. \quad (3.80)$$

In particular, $R(\xi)$ depends on Z_Δ , z_0 and $a(\xi)$, and also on $F_0(\xi)$ and ξ through $J^{-1}(s)$.

Now, at $\xi = \xi_0$, as detailed in Sec. 3.2.1, the position of the poles is found by solving the equation

$$J^{-1}(-p_0^2/m^2(\xi_0)) = 0 \quad \Longleftrightarrow \quad J^{-1}(z_0) = 0. \quad (3.81)$$

Therefore, one does not need the mass parameter $m^2(\xi_0)$ to compute z_0 : the adimensional pole z_0 only depends on $F_0(\xi_0)$ and on the gauge ξ_0 itself,

$$z_0 = z_0(F_0(\xi_0), \xi_0). \quad (3.82)$$

Moreover, in a general gauge $\xi \neq \xi_0$, to find $m^2(\xi)$ and $F_0(\xi)$ one needs to solve the equation

$$J^{-1}(-p_0^2/m^2(\xi)) = 0 \quad \Longleftrightarrow \quad J^{-1}(z_0/a(\xi)) = 0, \quad (3.83)$$

i.e.

$$F(z_0/a(\xi)) + \xi F_\xi(z_0/a(\xi)) + F_0(\xi) = 0. \quad (3.84)$$

The imaginary part of Eq. (3.84) allows us to determine $a(\xi)$,

$$\text{Im} \{F(z_0/a(\xi)) + \xi F_\xi(z_0/a(\xi))\} = 0, \quad (3.85)$$

which therefore only depends on the gauge ξ and on the parameters $F_0(\xi_0)$, ξ_0 through z_0 ,

$$a(\xi) = a(\xi; F_0(\xi_0), \xi_0). \quad (3.86)$$

The real part of Eq. (3.84), on the other hand, allows us to determine $F_0(\xi)$,

$$F_0(\xi) = -\text{Re} \{F(z_0/a(\xi)) + \xi F_\xi(z_0/a(\xi))\}, \quad (3.87)$$

which therefore also only depends on $F_0(\xi_0)$ and ξ_0 :

$$F_0(\xi) = F_0(\xi; F_0(\xi_0), \xi_0). \quad (3.88)$$

In other words, $a(\xi)$ and $F_0(\xi)$, as functions of ξ , are determined by the single constant $F_0(\xi_0)$, and not by the mass scale $m^2(\xi_0)$. This could have been anticipated by observing that $a(\xi)$ and $F_0(\xi)$ are adimensional parameters, while $m^2(\xi_0)$ is a dimensionful scale.

Since z_0 , $a(\xi)$ and $F_0(\xi)$ are all functions of $F_0(\xi_0)$ and ξ_0 alone, then the residue $R(\xi)$ also is:

$$R(\xi) = R(\xi; F_0(\xi_0), \xi_0) \quad (3.89)$$

(here we have suppressed the dependence of $R(\xi)$ on Z_Δ , since the latter does not affect the value of the phase $\theta(\xi)$). In particular, if the gauge-parameter independence of the position of the gluon poles is enforced by the method of Sec. 3.2.1, then phases of the

residues in any covariant gauge are completely determined by the value of the additive renormalization constant $F_0(\xi_0)$ at the gauge ξ_0 . In what follows, we will take ξ_0 to be equal to the Landau gauge, $\xi_0 = 0$.

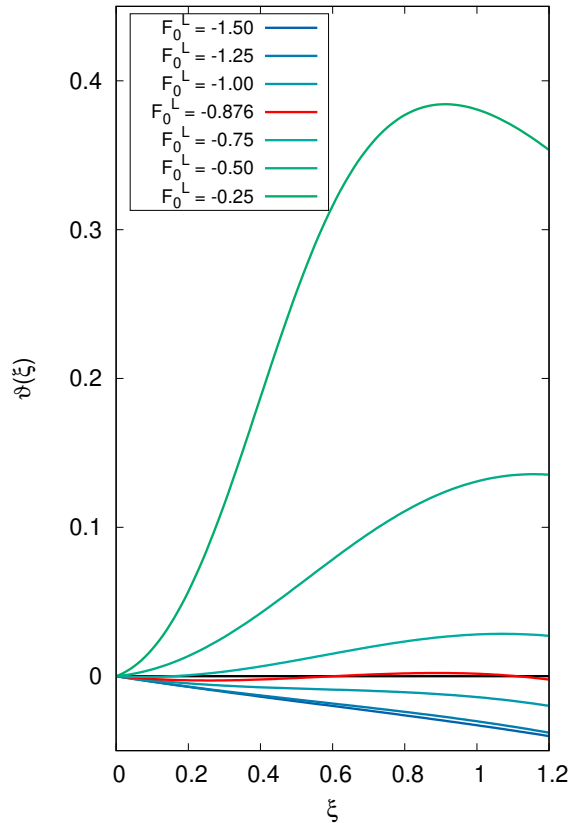


Figure 3.12: Phase difference $\Delta\theta(\xi) = \theta(\xi) - \theta(0)$ as a function of ξ for different values of $F_0(0)$ in the range $[-1.5, -0.25]$. $F_0^L = F_0(0)$.

In Fig. 3.12 we show the phase differences $\Delta\theta(\xi) = \theta(\xi) - \theta(0)$ of the residues at the gluon pole p_0^2 as functions of the gauge parameter ξ for different values of the additive renormalization constant $F_0(0)$ at $\xi = 0$. We remark that, as $F_0(0)$ varies, the position of the pole p_0^2 also changes due to Eq. (3.81); in Fig. 3.13 we display the adimensional poles $p_0^2/m^2(0)$ for different values of $F_0(0)$, with the understanding that the corresponding $\overline{p_0^2}$'s are also poles of the transverse gluon propagator.

As we can see from Fig. 3.12, the deviation of the phase $\theta(\xi)$ from its Landau-gauge value $\theta(0)$ is approximately zero only in a neighborhood of the fitted parameter $F_0(0) \approx -0.9$. This indicates that, analytically, the near gauge-parameter independence of the phase is a non-trivial feature of the one-loop SME approximation which is realized only when the SME propagator accurately reproduces the lattice result. It thus makes sense to seek a value of $F_0(0)$ that minimizes the dependence of $\theta(\xi)$ on the gauge parameter.

In order to determine the optimal value for the additive renormalization constant $F_0(0)$, in [SC18] the maximum value of the difference $|\Delta\theta(\xi)|$ was minimized over the range $\xi \in [0, 1.2]$. The resulting $F_0(0)$ was found to be equal to

$$F_0(0) = -0.876, \quad (3.90)$$

yielding the adimensional poles

$$p_0^2 = (0.4575 \pm 1.0130 i) m^2(0) . \quad (3.91)$$

The functions $m^2(\xi)$ and $F_0(\xi)$ which enforce the gauge-parameter independence of the poles at the given value of $F_0(0)$ can be approximated by the polynomials

$$m^2(\xi) \approx (1 - 0.39997 \xi + 0.064141 \xi^2) m^2(0) \quad (3.92)$$

and

$$F_0(\xi) \approx -0.8759 - 0.01260 \xi + 0.009536 \xi^2 + 0.009012 \xi^3 , \quad (3.93)$$

shown in Figs. 3.14 and 3.15 together with the corresponding optimized curves. These approximations are quite accurate up to and beyond the Feynman gauge ($\xi = 1$).

The phase $\theta(\xi)$ corresponding to $F_0(0) = -0.876$ – highlighted in red in Fig. 3.12 – was found to be

$$\theta(\xi) = 1.262_{-0.22\%}^{+0.22\%} , \quad (3.94)$$

the quoted value being the Landau-gauge phase, $\theta(0) = 1.262$, whereas the maximum and minimum deviations $\Delta\theta(\xi) = \pm 0.22\% \theta(0)$ were found at $\xi \approx 0.9$ and $\xi \approx 0.2$, respectively, with $\max_{\xi \in [0, 1.2]} \{|\Delta\theta(\xi)|\}$ being less than 2.5 parts in 1000. A summary of the optimized results is reported in Tab. 3.3.

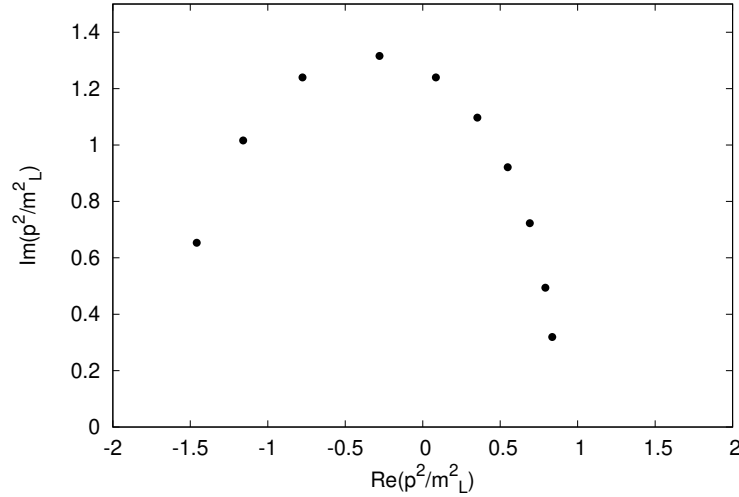


Figure 3.13: Adimensional poles of the transverse gluon propagator as a function of $F_0(0) \in [-2.00, -0.10]$. Left to right: $F_0(0) = -2.00, -1.90, -1.75, -1.50, -1.25, -1.00, -0.75, -0.50, -0.25, -0.10$. For each pole p_0^2 , its complex conjugate $\overline{p_0^2}$ is also a pole of the propagator. $m_L = m(0)$.

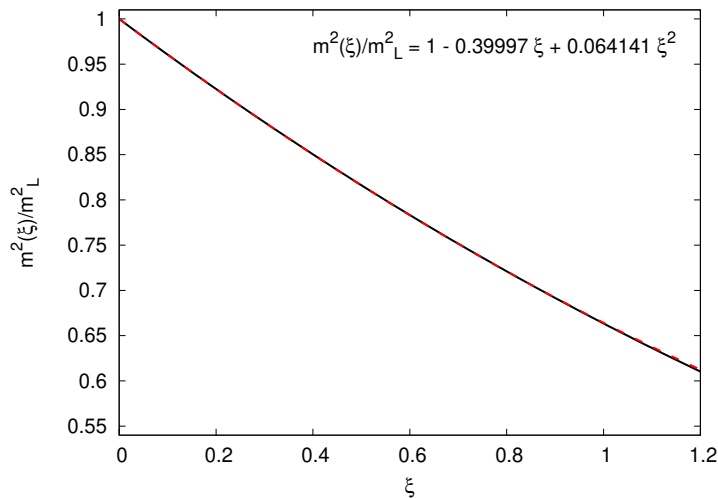


Figure 3.14: Optimal mass parameter $m^2(\xi)$ as a function of ξ computed at $F_0(0) = -0.876$. Dashed red line: polynomial approximation given by Eq. (3.92). $m_L = m(0)$.

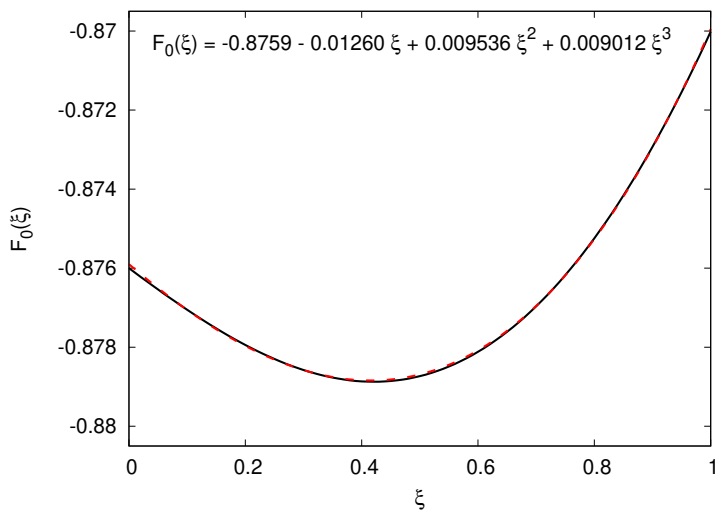


Figure 3.15: Optimal additive normalization constant $F_0(\xi)$ as a function of ξ computed at $F_0(0) = -0.876$. Dashed red line: polynomial approximation given by Eq. (3.93).

$F_0(0) = -0.876$	$\frac{p_0^2}{m^2(0)} = 0.4575 \pm 1.0130 i$	$\frac{p_0}{m(0)} = \pm 0.8857 \pm 0.5718 i$	$\theta = \pm 1.262$
-------------------	--	--	----------------------

Table 3.3: Position and phases of the residues of the gluon poles for $F_0(0) = -0.876$.

It is apparent that the optimization procedure described in this section yields parameters which lie very close to those obtained by fitting the lattice data: the relative difference between the optimized value of $F_0(0)$ and the one provided by the fit is around 1%, whereas the phases of the residues provided by the two approaches are equal up to the third decimal digit. As a result, as we will explicitly see in the next section, the optimized Euclidean Landau-gauge gluon propagator turns out to be undistinguishable from that which is obtained by fitting $F_0(0)$. This gives us confidence that the assumption that $d\theta/d\xi = 0$ yields sensible results regardless of the specific criterion which is chosen to minimize the dependence of $\theta(\xi)$ on the gauge parameter ξ .

3.2.3 The optimized gluon and ghost propagators

Within the Screened Massive Expansion, by enforcing the gauge-parameter independence of the poles and phases of the residues as laid out in the previous sections, the gluon propagator can be computed from first principles in any covariant gauge. The optimized SME propagator,

$$\Delta_E(p_E^2, \xi) = \frac{Z_\Delta(\xi)}{p_E^2 [F(s/a(\xi)) + \xi F_\xi(s/a(\xi)) + F_0(\xi)]}, \quad (3.95)$$

where $s = p_E^2/m^2(0)$ and $a(\xi) = m^2(\xi)/m^2(0)$, is expressed in terms of the known functions $a(\xi)$ and $F_0(\xi)$ – approximated by Eqs. (3.92) and (3.93) in Sec. 3.2.2 –, of a multiplicative renormalization constant $Z_\Delta(\xi)$ and of the Landau-gauge gluon mass parameter $m^2(0)$.

Since pure Yang-Mills theory is scale free, the value of the gluon mass parameter $m^2(0)$ cannot be predicted from first principles, and must instead be fixed by a comparison with the experiments¹³. In this respect, its status is similar to that of the QCD scale Λ_{QCD} of ordinary perturbation theory (Sec. 1.2.3): it is $m^2(0)$ that sets the energy units of the approximation. The value of $Z_\Delta(\xi)$, on the other hand, is determined by the normalization conditions which are chosen for the propagator.

In what follows we will compare our optimized results with the lattice data. Unfortunately, most of the lattice calculations of the QCD propagators are carried out in the Landau gauge, due to numerical difficulties which arise on the lattice when trying to enforce the gauge-fixing conditions for $\xi \neq 0$. Therefore, we shall limit ourselves with making our main comparisons with the Landau-gauge lattice data, using Ref. [BBC⁺15] as the only available benchmark for the gluon propagator in covariant gauges $\xi \neq 0$.

In Fig. 3.16 the Landau-gauge Euclidean transverse gluon propagators computed in the SME are shown together with the lattice data of [DOS16]. The solid black curve is the full fit already presented in Sec. 3.1.4 (see Tab. 3.2 for the fit parameters). The dashed green curve, on the other hand, is obtained by first fixing $F_0 = -0.876$, as determined via the optimization procedure discussed in Secs. 3.2.1 and 3.2.2, and then fitting the gluon mass parameter $m^2(0)$ and the multiplicative renormalization constant $Z_\Delta(0)$. The outcome of the fit is reported in Tab. 3.4.

As we can see from the figure, the optimized and the fully-fitted propagators cannot be distinguished to the naked eye. The value of the gluon mass parameter obtained for the optimized curve, $m = 0.6557$ GeV, is equal to the one obtained via the full fit ($m = 0.6541$ GeV) to within less than 1%; the same holds true for the multiplicative constants Z_Δ . This happens because, as we noted in the last section, the optimized and the fitted Landau-gauge additive renormalization constants F_0 are extremely close to each other. In

¹³Or with the lattice data, given that pure Yang-Mills theory is not realized in the physical world.

Tab. 3.5 we report the dimensionful position of the gluon poles, computed from Tab. 3.3 by making use of the fitted value of $m^2(0)$ at $F_0(0) = -0.876$.

The precision with which the optimized propagator reproduces the infrared lattice data substantiates the hypothesis that an accurate description of the low-energy dynamics of the gluon can be obtained from first principles by enforcing the gauge-parameter independence of the poles and of the phases of the residues.

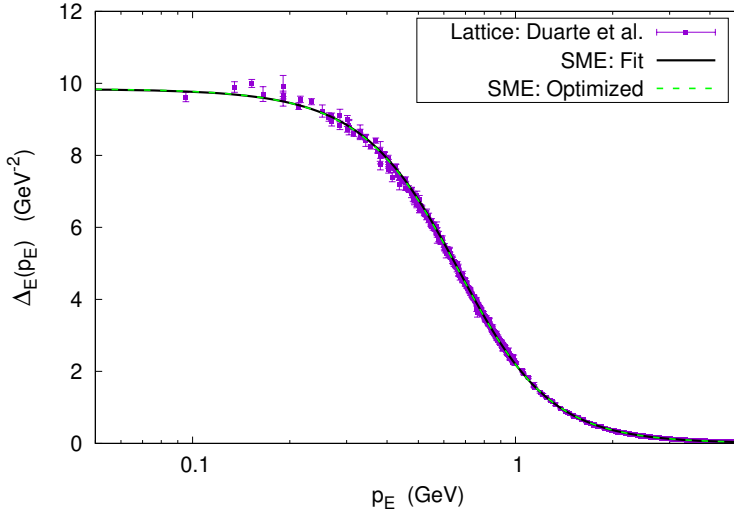


Figure 3.16: Euclidean transverse gluon propagator in the Landau gauge ($\xi = 0$). Solid black curve: SME with F_0 fitted from the lattice data (Tab. 3.2). Dashed green curve: SME with F_0 optimized by gauge invariance ($F_0 = -0.876$, Tab. 3.4). Squares: lattice data from [DOS16].

F_0	m (GeV)	Z_Δ
-0.876	0.6557	2.6481

Table 3.4: Parameters obtained by fitting the lattice data of [DOS16] for the Landau-gauge Euclidean transverse gluon propagator in the range 0-4 GeV at fixed $F_0 = -0.876$.

$F_0^L = -0.876$	$p_0^2 = (0.1969 \pm 0.4359 i) \text{ GeV}^2$	$p_0 = (\pm 0.5810 \pm 0.3751 i) \text{ GeV}$
------------------	---	---

Table 3.5: Dimensionful position of the gluon poles for $F_0(0) = -0.876$ and $m(0) = 0.6557$ GeV. The latter is obtained by fitting the optimized gluon propagator to the lattice data of Ref. [DOS16].

For future reference, we mention that in the Landau gauge the gluon propagator is well approximated by multiplying the principal part $\Delta_E^{(\text{PP})}(p_E^2)$ of the optimized propagator by a constant ≈ 1 . $\Delta_E^{(\text{PP})}(p_E^2, \xi)$ itself, in a general covariant gauge, is defined as

$$\Delta_E^{(\text{PP})}(p_E^2, \xi) = \frac{R(\xi)}{p_E^2 + p_0^2} + \frac{\overline{R(\xi)}}{p_E^2 + p_0^2}. \quad (3.96)$$

In the Landau gauge, with $Z_\Delta = 2.6481$ obtained by the fit, $|R|$ is found to be equal to

$$|R| = 0.947 Z_\Delta = 2.508. \quad (3.97)$$

The principal part $\Delta_E^{(\text{PP})}(p_E^2)$ of the propagator (solid red curve) is displayed together with the Landau-gauge optimized propagator (dashed green curve) in Fig. 3.17. As is clear from the figure, $\Delta_E^{(\text{PP})}(p_E^2)$ makes up for the majority of the optimized propagator $\Delta_E(p_E^2)$. Moreover, when normalized by a factor of 0.945 (solid blue curve), the principal part provides a quite accurate approximation of the full optimized propagator up to momenta ≈ 4 GeV.

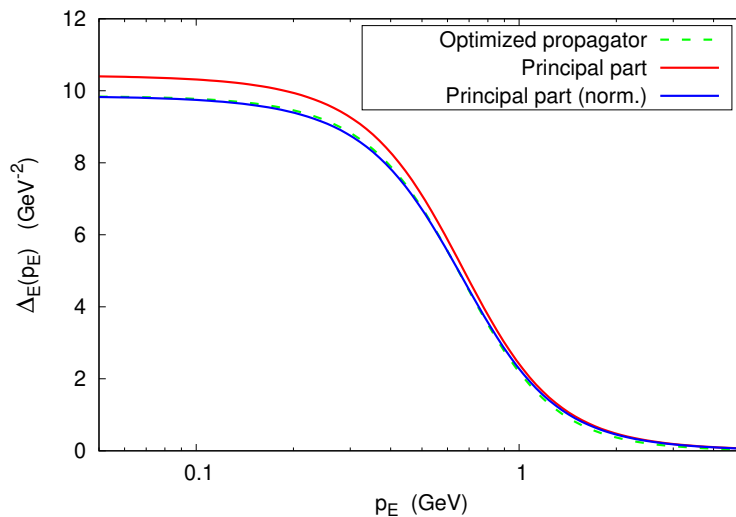


Figure 3.17: Euclidean transverse gluon propagator in the Landau gauge ($\xi = 0$). Dashed green curve: optimized propagator, with parameters given by Tab. 3.4. Solid red curve: principal part of the optimized propagator, with poles and residues given by Tabs. 3.3 and 3.5, $|R| = 0.947 Z_\Delta$. Solid blue curve: principal part of the optimized propagator, multiplied by a factor of 0.945. $m = 0.6557$ GeV.

Outside of the Landau gauge, the optimized gluon propagator behaves as displayed in Fig. 3.18, where the lattice data for $\xi = 0, 0.5$ were extracted from Ref. [BBC⁺15]. In order to compare the propagator with the data, the former was renormalized in the MOM scheme,

$$\Delta_E(\mu^2, \xi) = \frac{1}{\mu^2} \quad (3.98)$$

at $\mu = 4.317$ GeV, as reported in [BBC⁺15]. The mass parameter $m(0) = 0.6557$ GeV fitted from the lattice data of [DOS16] was used to obtain the curves shown in the figure.

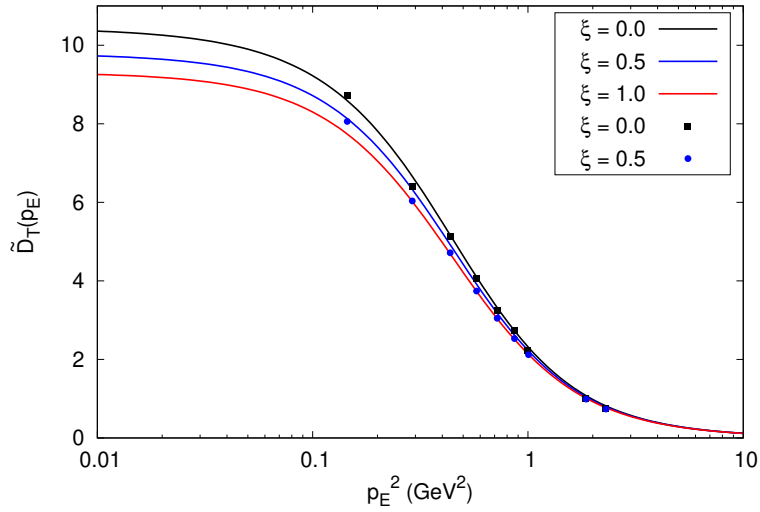


Figure 3.18: Optimized SME Euclidean transverse gluon propagator computed in different gauges, renormalized at $\mu = 4.317$ GeV. Lattice data from [BBC⁺15]. $m(0) = 0.6557$ GeV.

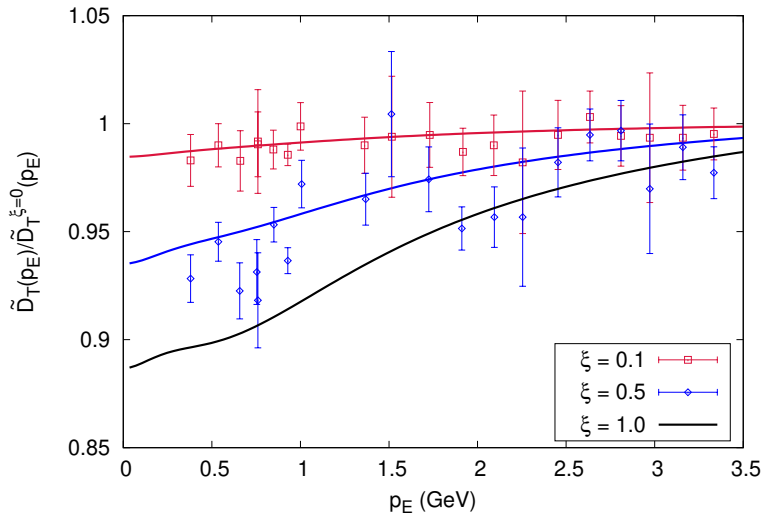


Figure 3.19: Ratio between the optimized SME Euclidean gluon propagators computed in a general covariant gauge and in the Landau gauge ($\xi = 0$), renormalized at $\mu = 4.317$ GeV. Lattice data from [BBC⁺15].

As the gauge increases, the lattice propagator remains massive and slightly decreases in value at fixed momentum. The optimized SME propagator reproduces this behavior, showing a good qualitative agreement with the lattice. When the ratios between the $\xi \neq 0$ propagators and their Landau-gauge counterpart are compared (Fig. 3.19), no definite conclusion can be reached regarding the quantitative agreement between the analytical predictions and the lattice results due to the errors which affect the lattice data.

In the introduction to Sec. 3.2, we anticipated that the ghost additive renormalization constant G_0 that appears in the expression

$$\mathcal{G}(p^2) = \frac{iZ_G}{p^2 (G(s) - \xi \log(s)/12 + G_0)} \quad (3.99)$$

for the SME ghost propagator can be determined from the knowledge of the gluon constant F_0 by making use of principles of minimal sensitivity. This is possible because F_0 and G_0 are not actually fully independent parameters, being defined as

$$\begin{aligned} F_0 &= \frac{1}{\alpha} + f_0 , \\ G_0 &= \frac{1}{\alpha} + g_0 \end{aligned} \quad (3.100)$$

(see Secs. 3.1.3 and 3.1.4), where f_0 and g_0 are adimensional constants which are fixed once renormalization conditions are imposed on the gluon and ghost propagator, respectively. As long as the renormalization conditions are left arbitrary, as we did in this chapter, the values of F_0 and G_0 can be chosen independent of each other. If, on the other hand, the renormalization conditions are specified, then the knowledge of F_0 , together with that of f_0 and g_0 , are sufficient to compute G_0 .

A straightforward calculation allows us to make the dependence of G_0 and F_0 on the renormalization conditions and on α explicit. From the definition of the one-loop Euclidean gluon and ghost SME propagators $\Delta_E(p_E^2)$ and $\mathcal{G}_E(p_E^2)$, we find that¹⁴

$$G_0 = \frac{1}{\alpha(\mu)} (\mu^2 \mathcal{G}_E(\mu^2))^{-1} - G(\mu^2/m^2) + \frac{\xi}{12} \ln(\mu^2/m^2) , \quad (3.101)$$

$$F_0 = \frac{1}{\alpha(\mu)} (\mu^2 \Delta_E(\mu^2))^{-1} - F(\mu^2/m^2) - \xi F_\xi(\mu^2/m^2) , \quad (3.102)$$

where μ is the renormalization scale for the propagators in a MOM-like renormalization scheme. In particular, since by Eq. (3.102) the coupling is given in terms of the gluon functions as

$$\frac{1}{\alpha(\mu)} = \mu^2 \Delta_E(\mu^2) (F(\mu^2/m^2) + \xi F_\xi(\mu^2/m^2) + F_0) , \quad (3.103)$$

the ghost additive renormalization constant can be computed as

$$G_0 = \frac{\Delta_E(\mu^2)}{\mathcal{G}_E(\mu^2)} (F(\mu^2/m^2) + \xi F_\xi(\mu^2/m^2) + F_0) - G(\mu^2/m^2) + \frac{\xi}{12} \ln(\mu^2/m^2) . \quad (3.104)$$

In the above expression, the parameters $m^2 = m^2(\xi)$ and $F_0 = F_0(\xi)$ are known thanks to the optimization procedure presented in the previous sections. Therefore, the only unknowns are the gluon and the ghost propagators $\Delta_E(\mu^2)$ and $\mathcal{G}_E(\mu^2)$ at the scale μ , and the scale μ itself. These are determined by the renormalization conditions.

In Refs. [Sir19a, Sir19b], the propagators were defined in the so-called screened MOM (SMOM) scheme, by which¹⁵

$$\Delta_E(\mu^2; \mu^2) = \frac{1}{\mu^2 + m^2} , \quad \mathcal{G}_E(\mu^2; \mu^2) = \frac{1}{\mu^2} . \quad (3.105)$$

¹⁴For simplicity, in the following expressions we omit the explicit dependence of G_0 , F_0 , m^2 and the propagators on the gauge parameter ξ .

¹⁵The renormalization conditions reported in Eq. (3.105) are the same as those of the Curci-Ferrari's IRS scheme – Sec. 2.4.1 –, the only difference being the independence of the gluon mass parameter m^2 from the renormalization scale.

In the SMOM scheme, the ghost constant G_0 is explicitly given by

$$G_0 = \left(1 + \frac{m^2}{\mu^2}\right)^{-1} \left(F(\mu^2/m^2) + \xi F_\xi(\mu^2/m^2) + F_0\right) - G(\mu^2/m^2) + \frac{\xi}{12} \ln(\mu^2/m^2) . \quad (3.106)$$

The optimal renormalization scale μ was then determined by requiring that G_0 be scale independent,

$$\frac{\partial G_0}{\partial \mu} = 0 . \quad (3.107)$$

Such a requirement is made necessary by the observation, made in [Sir19a], that a μ -dependent G_0 would spoil the multiplicative renormalizability of the theory if F_0 is taken to be scale independent, as is implied by the optimization procedure of Secs. 3.2.1 and 3.2.2. The principle of minimal sensitivity on the scale μ applied to G_0 provides us with a single optimal value of G_0 . In the Landau gauge, this was found to be equal to

$$G_0 = 0.1452 , \quad (3.108)$$

corresponding to $\mu = \mu^* = 1.004 m(0)$ in Eq. (3.107). Like for the gluon, the additive renormalization constant of the optimized ghost propagator is equal to the corresponding fitted value ($G_0 = 0.1464$, Tab. 3.6) to within less than 1%.

m (GeV)	G_0	Z_G
0.6557	0.1452	1.0959

Table 3.6: Parameter Z_G obtained by fitting the lattice data of [DOS16] for the Landau-gauge Euclidean ghost propagator in the range 0-2 GeV at fixed $m = 0.6557$ GeV and $G_0 = 0.1452$.

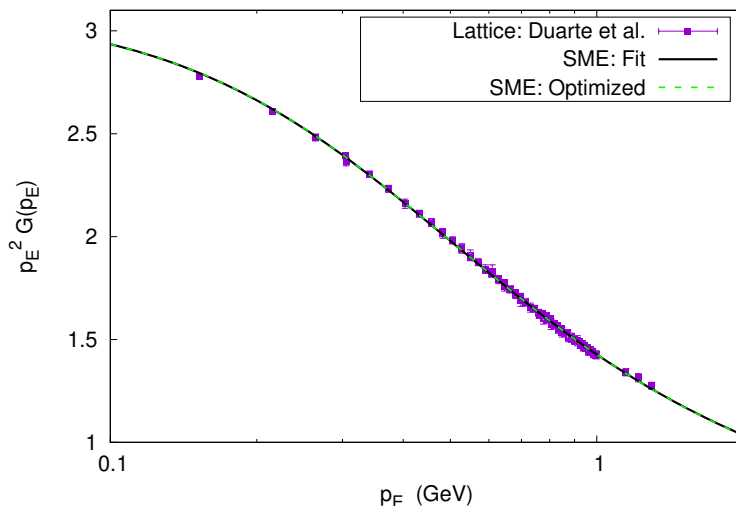


Figure 3.20: Euclidean ghost dressing function in the Landau gauge ($\xi = 0$). Solid black curve: SME with G_0 fitted from the lattice data (Tab. 3.1). Dashed green curve: SME with G_0 optimized by gauge invariance and minimal sensitivity on the renormalization scale ($G_0 = 0.1452$, Tab. 3.6). Squares: lattice data from [DOS16]. $m = 0.6557$ GeV.

In Fig. 3.20 we show the Landau-gauge Euclidean ghost dressing functions computed in the SME together with the lattice data of [DOS16]. The solid black curve is the fully-fitted dressing function already presented in Sec. 3.1.3 (parameters in Tab. 3.1). The dashed green curve, on the other hand, was obtained by fitting the multiplicative renormalization constant Z_G alone, as reported in Tab. 3.6, using $m = 0.6557$ GeV and $G_0 = 0.1452$.

As a consequence of the constants G_0 obtained by the two approaches being very close to each other, the optimized Landau-gauge ghost dressing function quantitatively matches the infrared lattice data just as well as its fully-fitted counterpart. This result validates the optimization procedure laid out for the ghost propagator, based on principles of gauge invariance and of minimal sensitivity. A thorough discussion of the gauge dependence of the optimized ghost propagator can be found in [Sir19b] together with a comparison with the lattice data of [CDM⁺18].

In the present section we have described optimization procedures that enable us to compute the gluon and the ghost propagators in the framework of the Screened Massive Expansion from first principles, using the gluon mass parameter $m^2(0)$ and two multiplicative renormalization constants – one for each propagator – as the only external inputs for the calculations. We have shown that enforcing the gauge-parameter independence of the poles and of the phases of the residues of the gluon propagator is sufficient to reduce the number of free parameters in the expressions, fixing the value of the gluon additive renormalization constant $F_0(\xi)$ and of the adimensional ratio $m^2(\xi)/m^2(0)$ in any gauge. Starting from the optimized F_0 , we were able to determine an optimal value for the ghost additive renormalization constant G_0 by minimal sensitivity, which in turn provided us with an optimized expression for the ghost propagator. When compared with the lattice data in the Landau gauge, the optimized gluon and ghost propagators were found to accurately reproduce the infrared dynamics of pure Yang-Mills theory.

In order to test the validity of the Screened Massive Expansion over the full dynamical range of momenta, encompassing both the IR and the UV regimes, Renormalization Group methods (Sec. 1.2.3) need to be employed. The Renormalization Group analysis of the Screened Massive Expansion is the subject of the next section. Studying the dependence of the strong coupling constant α_s and of the propagators on the renormalization scale will allow us to address the topic of the breakdown of perturbation theory in the low-energy limit of QCD.

3.3 Renormalization Group analysis of the Screened Massive Expansion in the Landau gauge

As discussed in Sec. 1.2.3, the presence of large logs in the perturbative series of the Green functions of a quantum field theory spoils the validity of the fixed-scale approximations at energies much different from the renormalization scale. The Screened Massive Expansion is not immune from this issue, as is clearly illustrated by the fact that, in Secs. 3.1.3, 3.1.4 and 3.2.3, we were able to compare the SME results with the lattice data only up to momenta of 2 GeV (for the ghost dressing function) or 4 GeV (for the gluon propagator).

While the renormalization scale is not explicitly present in the expressions for the SME propagators, we note that – either by fitting the lattice data or by optimization – our determination of the free parameters of the expansion was essentially made at low energies, effectively giving them the status of infrared parameters. Even the optimization of F_0 and of G_0 was more or less implicitly carried out in the low-energy regime: F_0 was determined by enforcing the gauge-parameter independence of the gluon poles, whose position is found

at a scale set by the gluon mass parameter $m^2(0)$, whereas G_0 was fixed by minimizing its value with respect to a renormalization scale μ , yielding $\mu = \mu^* = 1.004 m(0)$ in the Landau gauge. From an analytical perspective, the SME propagators contain logarithms of the form $\ln(-p^2/m^2)$ ¹⁶, implying that, as far as the large logs are concerned, the SME is affected by the same problems as ordinary perturbation theory when the momenta are not of the order of the gluon mass parameter m^2 .

In this section, we wish to extend the validity of the SME propagators to scales larger than the gluon mass parameter. Achieving this goal requires us to make use of Renormalization Group methods (Sec. 1.2.3), by which the coupling constant and the propagators are treated as functions of the renormalization scale. In order to perform the RG analysis of the SME, we will need to go back to the expressions (3.31) and (3.51) for the ghost and gluon propagators, in which the coupling constant appears explicitly. Moreover, we will need to fix appropriate renormalization conditions for the propagators, instead of leaving them arbitrary as we did up to this point. The analysis will be carried out in the Landau gauge, where the calculations are especially simple.

By integrating the RG equations, we will obtain expressions that – at least in principle – remain valid over a wide range of momenta. In particular, we will see that the strong running coupling $\alpha_s(\mu^2)$ computed in the Screened Massive Expansion does not develop Landau poles, provided that the value of the coupling $\alpha_s(\mu_0^2)$ at the initial renormalization scale μ_0 is sufficiently small. This is a crucial feature of the SME: on the one hand, it confirms that the massive shift that defines the expansion yields a self-consistent perturbative series; on the other hand, it proves that the infrared Landau pole that affects the running coupling of ordinary pQCD is just an artifact of the choice of a massless expansion point.

The one-loop RG-improved ghost and gluon propagators will be shown to be in good agreement with the lattice data from momenta of the order of 10 GeV down to $p \approx m$. Below this threshold, the coupling becomes quite too large for the one-loop approximation to provide sufficiently accurate results: in the deep infrared regime, the fixed-scale results of Sec. 3.2.3 still represent our best estimate for the behavior of the propagators. The overlap between the RG-improved and the fixed-scale propagators at momenta $p \approx m$ will be exploited in Sec. 3.3.3 to compute an optimal value of the coupling constant $\alpha_s(\mu_0^2)$ at the initial renormalization scale μ_0 as a function of the gluon mass parameter m^2 . This will again leave us with expressions whose only free parameter is m^2 , playing the same role as the QCD scale Λ_{QCD} in ordinary perturbation theory.

3.3.1 MOM-Taylor-scheme renormalization of the Screened Massive Expansion

In Sec. 3.1 we saw that, in the Landau gauge ($\xi = 0$), the one-loop Euclidean transverse gluon and ghost propagators $\Delta(p^2)$ and $\mathcal{G}(p^2)$ computed in the Screened Massive Expansion can be expressed as¹⁷

$$\Delta(p^2) = \frac{1}{p^2 [1 + \alpha (F(s) + f_0)]}, \quad \mathcal{G}(p^2) = \frac{1}{p^2 [1 + \alpha (G(s) + g_0)]}, \quad (3.109)$$

where $s = p^2/m^2$, α is a rescaled coupling constant,

$$\alpha = \frac{3N\alpha_s}{4\pi} = \frac{3Ng^2}{16\pi^2}, \quad (3.110)$$

¹⁶And others such as $\ln(\sqrt{-p^2/m^2 + 4} \pm \sqrt{-p^2/m^2})$ and $\ln(-p^2/m^2 + 1)$.

¹⁷For conciseness of notation, in the rest of this chapter we will drop the subscript E from the quantities defined in Euclidean space. Thus the p^2 in Eq. (3.109) is actually a Euclidean momentum squared.

the functions $G(s)$ and $F(s)$ were defined in Eqs. (3.29) and (3.46), and f_0 and g_0 are additive renormalization constants. The latter are fixed as soon as the renormalization conditions for the propagators are chosen. In [CS20], the RG analysis of the Screened Massive Expansion was carried out in two renormalization schemes: the MOM scheme, described in Secs. 1.2.2 and 1.2.3, and the SMOM scheme, defined in Sec. 3.2.3. During the rest of this chapter, we will focus only on the former.

In the MOM scheme, the gluon and ghost propagators are renormalized by fixing their value at a given renormalization scale μ so that

$$\Delta(\mu^2) = \mathcal{G}(\mu^2) = \frac{1}{\mu^2} . \quad (3.111)$$

By looking at Eq. (3.109), we see that, to one loop, these renormalization conditions are equivalent to choosing

$$f_0 = -F(\mu^2/m^2) , \quad g_0 = -G(\mu^2/m^2) . \quad (3.112)$$

Going back to the explicit one-loop expressions for the ghost and gluon field renormalization factors Z_c and Z_A in terms of the constants g_0 and f_0 – Eqs. (3.30) and (3.50) –,

$$Z_c = 1 + \frac{\alpha}{4} \left[\left(1 - \frac{\xi}{3}\right) \left(\frac{2}{\epsilon} - \ln \frac{m^2}{\bar{\mu}^2}\right) + \frac{8}{3} \right] + \alpha g_0 , \quad (3.113)$$

$$Z_A = 1 + \frac{\alpha}{3} \left(\frac{13}{6} - \frac{\xi}{2} \right) \left(\frac{2}{\epsilon} - \ln \frac{m^2}{\bar{\mu}^2} \right) + \alpha(f_0 - \mathcal{C}) , \quad (3.114)$$

where $\bar{\mu} = \sqrt{4\pi} \mu_{\text{d.r.}} e^{-\gamma_E/2}$, $\mu_{\text{d.r.}}$ being the scale introduced by dimensional regularization, Eq. (3.112) yields the following MOM gluon and ghost field renormalization constants:

$$Z_A = 1 + \frac{\alpha}{3} \left(\frac{13}{6} - \frac{\xi}{2} \right) \left(\frac{2}{\epsilon} - \ln \frac{m^2}{\bar{\mu}^2} \right) - \alpha(F(\mu^2/m^2) + \mathcal{C}) , \quad (3.115)$$

$$Z_c = 1 + \frac{\alpha}{4} \left[\left(1 - \frac{\xi}{3}\right) \left(\frac{2}{\epsilon} - \ln \frac{m^2}{\bar{\mu}^2}\right) + \frac{8}{3} \right] - \alpha G(\mu^2/m^2) . \quad (3.116)$$

The gluon and ghost anomalous dimensions γ_A and γ_c , defined as (see Sec. 1.2.2)

$$\gamma_A = \frac{\mu}{Z_A} \frac{dZ_A}{d\mu} , \quad \gamma_c = \frac{\mu}{Z_c} \frac{dZ_c}{d\mu} , \quad (3.117)$$

can be explicitly computed in the MOM scheme thanks to Eqs. (3.115) and (3.116). To lowest order in the coupling constant, they read

$$\gamma_A = -2\alpha \frac{\mu^2}{m^2} F'(\mu^2/m^2) , \quad \gamma_c = -2\alpha \frac{\mu^2}{m^2} G'(\mu^2/m^2) , \quad (3.118)$$

where

$$F'(s) = \frac{dF}{ds}(s) , \quad G'(s) = \frac{dG}{ds}(s) . \quad (3.119)$$

Observe that in Eqs. (3.115) and (3.116), the terms which depend on the renormalization scale μ only implicitly through the coupling constant α do not contribute to the MOM anomalous dimensions to $O(\alpha_s)$ since the derivative of α with respect to μ , given by the beta function,

$$\mu \frac{d\alpha}{d\mu} = \mu \frac{d}{d\mu} \left(\frac{3Ng^2}{16\pi^2} \right) = 2 \frac{\alpha}{g} \beta_g \quad \left(\mu \frac{dg}{d\mu} = \beta_g \right) , \quad (3.120)$$

is higher-order: being β_g of order g^3 , $\mu d\alpha/d\mu$ is of order α_s^2 . Similarly, if the gluon mass parameter were taken to depend on the renormalization scale, then $\mu dm^2/d\mu$ would be at least of order α_s , so that the product $\alpha \mu dm^2/d\mu$ would be at least $O(\alpha_s^2)$ and would not contribute to the one-loop anomalous dimensions.

In what follows, we will assume that the gluon mass parameter m^2 is independent from the renormalization scale. This assumption is motivated by an in-depth order-by-order analysis of the RG equations for the Screened Massive Expansion in the MOM scheme, which shows that, to one-loop, the derivative $\mu dm^2/d\mu$ drops out of the equations just like it does from the anomalous dimensions, implying that the μ -dependence of the gluon mass parameter is arbitrary to $O(\alpha_s)$ [CS20]. The simplest solutions to the MOM RG equations thus have m^2 being independent from μ .

With Z_A and Z_c defined in the MOM scheme, the renormalization of the SME is completed by specifying the renormalization conditions for the coupling constant. In the Landau gauge, the latter is conveniently defined in the so-called Taylor scheme, which we have already encountered in Chpt. 2. Recalling that the renormalized coupling g is defined as

$$g = Z_g^{-1} g_B, \quad (3.121)$$

where g_B is the bare coupling constant and Z_g is the coupling renormalization factor, a theorem by Taylor [Tay71] shows that, in the Landau gauge, the *diverging* terms¹⁸ of the renormalization factors Z_A , Z_c , and Z_g satisfy the relation

$$\left(Z_g Z_A^{1/2} Z_c \right)_{\text{div.}} = 1. \quad (3.122)$$

The choice

$$Z_g = Z_A^{-1/2} Z_c^{-1}, \quad (3.123)$$

which extends the Taylor relation (3.122) to the full renormalization factors, is thus consistent with the divergences of the theory, and its adoption yields a renormalized coupling constant known as the Taylor coupling.

In the Taylor scheme, the beta function β_g takes on an especially simple form. Since by Eq. (3.121)

$$\beta_g = \mu \frac{dg}{d\mu} = -\frac{\mu}{Z_g} \frac{dZ_g}{d\mu}, \quad (3.124)$$

because of the Taylor condition – Eq. (3.123) – we find that

$$\beta_g = \frac{g}{2} (\gamma_A + 2\gamma_c). \quad (3.125)$$

Thus the knowledge of the gluon and ghost anomalous dimensions is sufficient to compute the beta function associated to the Taylor coupling.

In the context of the Screened Massive Expansion, we can define a beta function β_α associated to the rescaled coupling α ¹⁹:

$$\beta_\alpha = \frac{d\alpha}{d \ln \mu^2}. \quad (3.126)$$

Using Eq. (3.120), it is easy to verify that

$$\beta_\alpha = \frac{\alpha}{g} \beta_g. \quad (3.127)$$

¹⁸That is, the terms which would make up the renormalization factors in the MS scheme.

¹⁹Note the μ^2 in β_α .

In particular, in the MOM-Taylor scheme, we find that

$$\beta_\alpha = \frac{\alpha}{2}(\gamma_A + 2\gamma_c) = -\alpha^2 \frac{\mu^2}{m^2} H'(\mu^2/m^2), \quad (3.128)$$

where the function $H(s)$ is defined as

$$H(s) = F(s) + 2G(s) \quad (3.129)$$

and $H'(s) = dH(s)/ds$.

As the next step in our RG analysis of the SME, in the following section we will analytically solve the RG equation for the running coupling constant and numerically integrate the RG-improved propagators defined in the MOM-Taylor scheme.

3.3.2 The SME strong running coupling and RG-improved propagators

To one loop, the Renormalization Group equation for the SME coupling constant α reads

$$\mu^2 \frac{d\alpha}{d\mu^2} = \beta_\alpha = -\alpha^2 \frac{\mu^2}{m^2} H'(\mu^2/m^2). \quad (3.130)$$

Since m^2 does not depend on μ , the latter can be rewritten in terms of the adimensional variable s as

$$\frac{d\alpha}{d \ln s} = -\alpha^2 H'(s). \quad (3.131)$$

The solution of Eq. (3.131) is easily found to be

$$\alpha(s) = \frac{\alpha(s_0)}{1 + \alpha(s_0) [H(s) - H(s_0)]}, \quad (3.132)$$

where $s_0 = \mu_0^2/m^2$ is the adimensionalized initial renormalization scale and $\alpha(s_0)$ is the rescaled coupling constant defined at the same scale.

The one-loop MOM-Taylor strong running coupling $\alpha_s(\mu^2)$ is obtained from the last equation using $\alpha = 3N\alpha_s/4\pi$. Explicitly,

$$\alpha_s(\mu^2) = \frac{\alpha_s(\mu_0^2)}{1 + \frac{3N\alpha_s(\mu_0^2)}{4\pi} [H(\mu^2/m^2) - H(\mu_0^2/m^2)]}. \quad (3.133)$$

In the high-energy limit $\mu^2, \mu_0^2 \gg m^2$ ($s \gg 1$), by Eqs. (3.34) and (3.54),

$$F(s) \rightarrow \frac{13}{18} \ln s + \frac{17}{18}, \quad G(s) \rightarrow \frac{1}{4} \ln s + \frac{1}{3}, \quad (3.134)$$

the function $H(s)$ and the difference $H(\mu^2/m^2) - H(\mu_0^2/m^2)$ that appears in the denominator of $\alpha_s(\mu^2)$ approach

$$H(s) \rightarrow \frac{11}{9} \ln s + \frac{29}{18}, \quad H(\mu^2/m^2) - H(\mu_0^2/m^2) \rightarrow \frac{11}{9} \ln(\mu^2/\mu_0^2). \quad (3.135)$$

In particular, in this limit the gluon mass parameter disappears from $\alpha_s(\mu^2)$, while the strong running coupling itself reduces to

$$\alpha_s(\mu^2) \rightarrow \frac{\alpha_s(\mu_0^2)}{1 + \frac{11N}{3} \frac{\alpha_s(\mu_0^2)}{4\pi} \ln(\mu^2/\mu_0^2)}. \quad (3.136)$$

This is the result found in ordinary perturbation theory, Eq. (1.159), with $n_f = 0$ in the beta function coefficient β_0 . In the low-energy limit, on the other hand, again by Eqs. (3.34) and (3.54),

$$F(s) \rightarrow \frac{5}{8s}, \quad G(s) \rightarrow \frac{5}{24} \quad \Longrightarrow \quad H(s) \rightarrow \frac{5}{8s}. \quad (3.137)$$

Therefore, as $\mu^2 \rightarrow 0$,

$$\alpha_s(\mu^2) \rightarrow \frac{32\pi}{15N} \frac{\mu^2}{m^2} \rightarrow 0 : \quad (3.138)$$

the running coupling vanishes like μ^2 , as predicted by the lattice calculations – see Sec. 2.1.2. This is not accidental: the lattice coupling, as well as ours, is defined in the Taylor scheme, starting from the behavior of the MOM gluon and ghost propagators. It will become clear by the end of this section that the vanishing of the MOM-Taylor coupling at zero momentum is the consequence of the gluon propagator becoming massive and of the gluon dressing function remaining finite at $p = 0$. To one loop, the speed at which $\alpha_s(\mu^2)$ approaches zero does not depend on the initial conditions of the RG flow (i.e. on $\alpha_s(\mu_0^2)$ and μ_0^2), but only on the value of the gluon mass parameter m^2 .

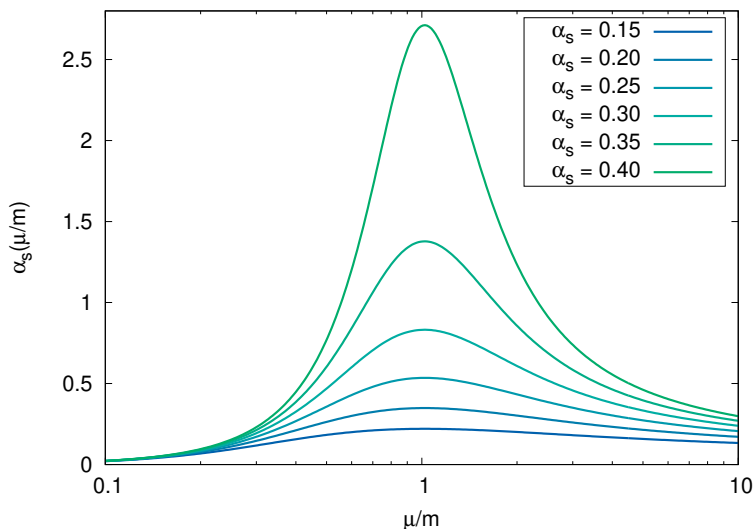


Figure 3.21: One-loop MOM-Taylor SME running coupling $\alpha_s(\mu^2)$ as a function of the adimensional scale μ/m for different initial values of the coupling $\alpha_s(\mu_0^2)$ at the scale $\mu_0/m = 6.098$. With $m = 0.656$ GeV, this corresponds to $\mu_0 = 4$ GeV.

The one-loop MOM-Taylor SME running coupling $\alpha_s(\mu^2)$ is shown in Fig. 3.21 for $N = 3$ as a function of $\sqrt{s} = \mu/m$ for different initial values of the coupling constant $\alpha_s(\mu_0^2)$. The adimensional initial renormalization scale μ_0/m was chosen equal to 6.098 so that, with our previous determination of the gluon mass parameter ($m = 0.656$ GeV), $\mu_0 = 4$ GeV.

As we can see, for sufficiently small initial values of the coupling constant, the strong running coupling $\alpha_s(\mu^2)$ computed in the SME has no Landau poles. Instead, it first increases in value as μ decreases, then hits a maximum at a fixed scale $\mu_* = 1.022 m$, and finally it decreases to zero as $\mu \rightarrow 0$. That the position of the maximum is independent

from the value of the initial coupling $\alpha_s(\mu_0^2)$ is a consequence of the one-loop beta function having a zero at the renormalization scale μ_* such that

$$H'(\mu_*^2/m^2) = 0 . \quad (3.139)$$

The solution of this equation, $\mu_* = 1.022 m$, can be obtained numerically and is clearly independent from $\alpha_s(\mu_0^2)$.

For $\alpha_s(\mu_0) \geq 0.469$, on the other hand, the running coupling develops an infrared Landau pole. To see this, suppose that $\alpha_s(\mu^2)$ becomes infinite at the scale μ_{pole}^2 . This can only happen if

$$1 + \frac{3N\alpha_s(\mu_0^2)}{4\pi} [H(\mu_{\text{pole}}^2/m^2) - H(\mu_0^2/m^2)] = 0 , \quad (3.140)$$

implying that the initial value of the coupling is related to μ_{pole}^2 via the equation

$$\alpha_s(\mu_0^2) = \frac{4\pi}{3N[H(\mu_0^2/m^2) - H(\mu_{\text{pole}}^2/m^2)]} . \quad (3.141)$$

Since $\mu_* = 1.022 m$ is a minimum for $H(\mu^2/m^2)$, we have $H(\mu^2/m^2) \geq H(\mu_*^2/m^2)$ for any value of the renormalization scale μ . It follows that

$$\alpha_s(\mu_0^2) \geq \frac{4\pi}{3N[H(\mu_0^2/m^2) - H(\mu_*^2/m^2)]} = \alpha_s^{(\text{thr.})}(\mu_0^2) = 0.469 \quad (3.142)$$

at $N = 3$ and $\mu_0 = 6.098 m$. We remark that the threshold value $\alpha_s^{(\text{thr.})}(\mu_0)$ defined by the last equation depends on the initial renormalization scale μ_0 , as well as on the number of colors N .

Recall from Sec. 1.2.3 that the RG-improved gluon and ghost propagators renormalized at the scale $\mu_0 - \Delta(p^2; \mu_0^2)$ and $\mathcal{G}(p^2; \mu_0^2)$, respectively, can be expressed in terms of their anomalous dimensions γ_A and γ_c as²⁰

$$\Delta(p^2; \mu_0^2) = e^{\int_{\mu_0}^p \frac{d\mu}{\mu} \gamma_A(\mu)} \Delta(p^2; p^2) , \quad (3.143)$$

$$\mathcal{G}(p^2; \mu_0^2) = e^{\int_{\mu_0}^p \frac{d\mu}{\mu} \gamma_c(\mu)} \mathcal{G}(p^2; p^2) . \quad (3.144)$$

In the MOM scheme, the values $\Delta(p^2; p^2)$ and $\mathcal{G}(p^2; p^2)$ of the propagators at a momentum equal to their renormalization scale are given by the renormalization conditions themselves, Eq. (3.111), which we can rewrite as

$$\Delta(p^2; p^2) = \mathcal{G}(p^2; p^2) = \frac{1}{p^2} . \quad (3.145)$$

By making use of the explicit expressions for the one-loop MOM gamma functions, Eq. (3.118), we then find that the RG-improved one-loop SME propagators read

$$\Delta(p^2; \mu_0^2) = \frac{1}{p^2} \exp\left(-\int_{\mu_0^2/m^2}^{p^2/m^2} ds \alpha(s) F'(s)\right) , \quad (3.146)$$

$$\mathcal{G}(p^2; \mu_0^2) = \frac{1}{p^2} \exp\left(-\int_{\mu_0^2/m^2}^{p^2/m^2} ds \alpha(s) G'(s)\right) . \quad (3.147)$$

²⁰The derivation of Eq. (3.144) is identical in all respects to the one carried out in Sec. 1.2.3 to obtain Eq. (3.143), so we will not repeat it in this section.

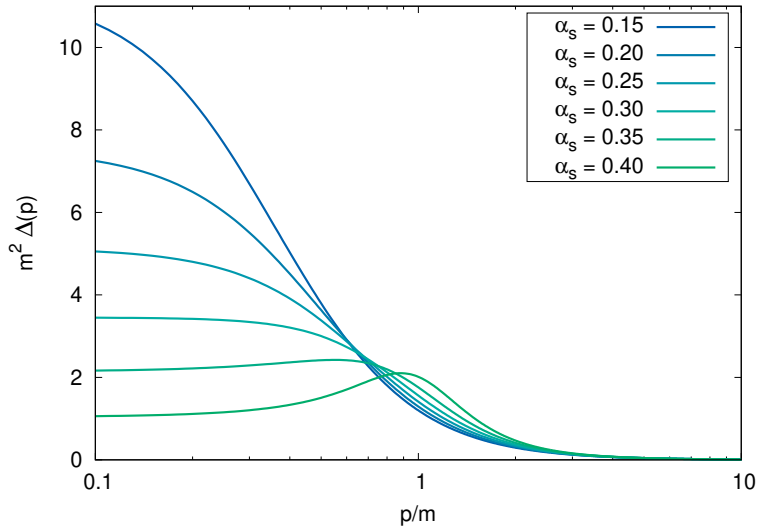


Figure 3.22: One-loop Landau-gauge RG-improved Euclidean transverse gluon propagator computed in the MOM-Taylor scheme as a function of the adimensional momentum p/m for different initial values of the coupling $\alpha_s(\mu_0^2)$ at the scale $\mu_0/m = 6.098$. Adimensionalized by m^2 .

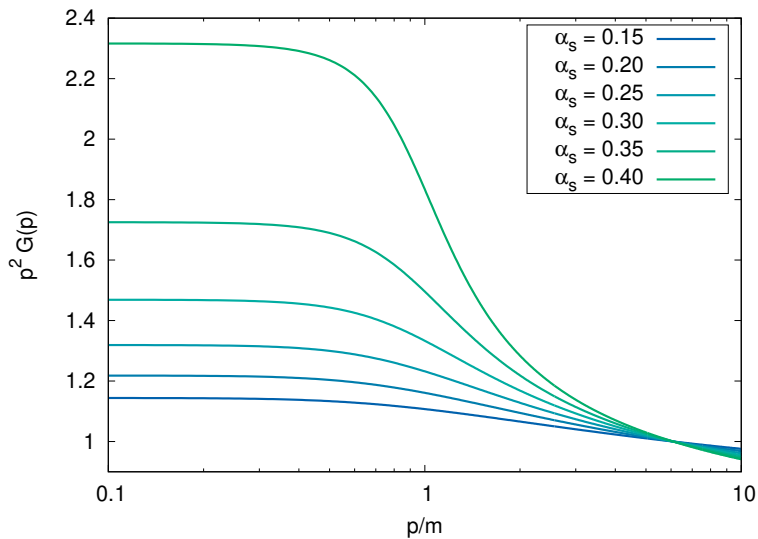


Figure 3.23: One-loop Landau-gauge RG-improved Euclidean ghost dressing function computed in the MOM-Taylor scheme as a function of the adimensional momentum p/m for different initial values of the coupling $\alpha_s(\mu_0^2)$ at the scale $\mu_0/m = 6.098$.

The integrals in Eqs. (3.146) and (3.147) cannot be evaluated analytically. In order to compute the RG-improved propagators, one thus has to resort to numerical integration. Nonetheless, as shown in [CS20], the asymptotic limits of $\Delta(p^2; \mu_0^2)$ and $\mathcal{G}(p^2; \mu_0^2)$ can still be put in closed form by making use of the $s \rightarrow 0$ and $s \rightarrow \infty$ expressions for $F(s)$, $G(s)$

and $\alpha(s)$. One then finds that in the UV, provided that $\mu_0^2 \gg m^2$ as well as $p^2 \gg m^2$,

$$\Delta(p^2; \mu_0^2) \rightarrow \frac{1}{p^2} \left[\frac{\alpha_s(p^2)}{\alpha_s(\mu_0^2)} \right]^{\frac{13}{22}}, \quad \mathcal{G}(p^2; \mu_0^2) \rightarrow \frac{1}{p^2} \left[\frac{\alpha_s(p^2)}{\alpha_s(\mu_0^2)} \right]^{\frac{9}{44}}, \quad (3.148)$$

which is just the ordinary pQCD result for $n_f = 0$, while in the deep IR

$$\Delta(p^2; \mu_0^2) \rightarrow \frac{\kappa}{m^2}, \quad \mathcal{G}(p^2; \mu_0^2) \rightarrow \frac{\kappa'}{p^2}, \quad (3.149)$$

where κ and κ' are constants. By Eq. (3.149) we see that, at vanishing momenta, the RG-improved SME gluon and ghost propagators are massive and massless, respectively, just like their fixed-scale counterparts.

In Figs. 3.22 and 3.23 we show the RG-improved gluon propagator and ghost dressing function computed for different values of the initial coupling constant $\alpha_s(\mu_0^2) < \alpha_s^{\text{(thr.)}}(\mu_0^2)$, again at the initial scale $\mu_0 = 6.098 m$. Observe that, in the figures, both $\Delta(p^2; \mu_0^2)$ and the momenta are adimensionalized by appropriate factors of the gluon mass parameter m . The propagators clearly display the asymptotic behavior we just described. Notably, the gluon propagator attains a maximum for any value of the initial coupling²¹, whereas the ghost dressing function quickly saturates to a constant at momenta of the order of the gluon mass parameter.

For future reference, we make an observation on the relation between the Taylor coupling and the RG-improved propagators. Going back to Eqs. (3.143) and (3.144), it is interesting to compute the product between the gluon propagator and the square of the ghost propagator. A simple calculation shows that

$$\begin{aligned} \Delta(p^2; \mu_0^2) [\mathcal{G}(p^2; \mu_0^2)]^2 &= e^{\int_{\mu_0}^p \frac{d\mu}{\mu} [\gamma_A(\mu) + 2\gamma_c(\mu)]} \Delta(p^2; p^2) [\mathcal{G}(p^2; p^2)]^2 = \\ &= e^{2 \int_{\mu_0}^p \frac{d\mu}{\mu} \frac{\beta_\alpha}{\alpha}} \Delta(p^2; p^2) [\mathcal{G}(p^2; p^2)]^2 = \\ &= e^{\int_{\mu_0}^p \frac{d\mu}{\alpha} \frac{d\alpha}{d\mu}} \Delta(p^2; p^2) [\mathcal{G}(p^2; p^2)]^2 = \\ &= \frac{\alpha(p^2/m^2)}{\alpha(\mu_0^2/m^2)} \Delta(p^2; p^2) [\mathcal{G}(p^2; p^2)]^2, \end{aligned} \quad (3.150)$$

where we have used the Taylor condition in the form $\beta_\alpha = \frac{\alpha}{2}(\gamma_A + 2\gamma_c)$. It follows that the Taylor coupling can be expressed in terms of the propagators as

$$\alpha_s(\mu^2) = \alpha_s(\mu_0^2) \left[\frac{\Delta(\mu^2; \mu_0^2)}{\Delta(\mu^2; \mu^2)} \right] \left[\frac{\mathcal{G}(\mu^2; \mu_0^2)}{\mathcal{G}(\mu^2; \mu^2)} \right]^2. \quad (3.151)$$

In particular, when $\Delta(p^2)$ and $\mathcal{G}(p^2)$ are renormalized in the MOM scheme, the latter reads

$$\alpha_s(\mu^2) = \alpha_s(\mu_0^2) [\mu^2 \Delta(\mu^2; \mu_0^2)] [\mu^2 \mathcal{G}(\mu^2; \mu_0^2)]^2. \quad (3.152)$$

An explicit example of this relation is given by the UV limit of the SME propagators (equivalently, by the results of ordinary perturbation theory) reported in Eq. (3.148). From Eq. (3.152), it is clear that, in the MOM scheme, the finiteness of $\Delta(p^2)$ and $p^2 \mathcal{G}(p^2)$ in the limit $p^2 \rightarrow 0$ always implies that the Taylor coupling vanishes at zero momentum.

²¹Though this is less clear from the figure for lower values of $\alpha_s(\mu_0^2)$, the existence of a maximum for every initial value of the coupling can be proved analytically, see [CS20].

In this section we have explored the analytical properties of the MOM-Taylor scheme SME strong running coupling and presented results regarding the corresponding RG-improved gluon and ghost propagators. The absence of Landau poles from the SME running coupling $\alpha_s(\mu^2)$ for sufficiently small initial values of the coupling constant is an essential check on the validity of the method. Indeed, if the running coupling computed in the SME had IR Landau poles regardless of the initial conditions of the RG flow (as it happens in ordinary pQCD), then the results obtained in Secs. 3.1 and 3.2 would bear no connection to the well-established UV behavior of the theory, having been obtained at a scale where the theory would essentially be undefined. On the contrary, the finiteness of $\alpha_s(\mu^2)$ confirms both that the Screened Massive Expansion is self-consistent as a computational method, and that the dynamics of QCD can in principle be studied over an unlimited range of momenta by making use of the Renormalization Group.

We observe that, in the Screened Massive Expansion, the finiteness of the running coupling is made possible by the presence of a non-perturbative mass scale – namely, the gluon mass parameter – in the equations. To one loop, it is the vanishing of the adimensional function $H'(s)$ in the MOM-scheme beta function – see Eq. (3.130) – that allows $\alpha_s(\mu^2)$ to attain a maximum at a fixed renormalization scale $\mu = \mu_*$, instead of diverging like in ordinary pQCD. In the absence of the gluon mass parameter, or in scale-independent renormalization schemes, $sH'(s)$ would be replaced by a constant in β_α , forcing the latter to be negative at every renormalization scale, as is the case in pQCD. Instead, around $\mu = \mu_* = 1.022 m$, the running of the coupling slows down, stops and then changes sign as the renormalization scale decreases.

Of course, the fact that $\alpha_s(\mu^2)$ diverges for large values of $\alpha_s(\mu_0^2)$ calls for further investigations on the behavior of the RG-improved propagators. In particular, we need to make sure that the exact propagators, as given for instance by the lattice data, can be reproduced by making use of values of $\alpha_s(\mu_0^2)$ smaller than the threshold at which the Landau pole appears, $\alpha_s^{(\text{thr.})}(\mu_0^2) = 0.469$ at $\mu_0/m = 6.098$. In addition to this, the RG-improved SME propagators depend on two free parameters, $\alpha_s(\mu_0^2)$ and m^2 , at variance with their ordinary pQCD analogues – which clearly only depend on the initial value of the coupling constant. Thus we find ourself in the same situation in which we were at the end of Sec. 3.1, with the propagators needing optimization in order for predictions to be made from first principles. The determination of an optimal value of $\alpha_s(\mu_0^2)$ is the subject of the next section.

3.3.3 Intermediate-energy matching with the fixed-scale optimized results and comparison with the lattice data

While in principle the validity of the RG-improved results presented in the last section extends to arbitrary energy scales, in practice the one-loop approximation by which they were obtained is accurate only provided that the value of the running coupling is sufficiently small. By Fig. 3.21 we see that, depending on the value of the initial coupling, the maximum $\alpha_s(\mu = 1.022 m)$ can become quite large for the perturbative standards. Therefore, we may expect the one-loop RG-improved propagators to deviate from the exact results at the corresponding momenta $p \approx m$, when integrated starting from the UV region.

The accuracy of the one-loop approximation can be tested by making use of the optimized fixed-scale (OFS) expressions derived in Sec. 3.2. Since these are valid up to scales of the order of the gluon mass parameter, we expect the RG-improved and OFS results to overlap at least in the intermediate-energy region where $p \approx m$. Such an overlap, of course, will occur only for those values of the initial coupling $\alpha_s(\mu_0^2)$ which yield a good approximation of the exact propagators. Matching the high-energy RG-improved results

to their low-energy fixed-scale counterpart thus provides us with a way to fix an optimal value of $\alpha_s(\mu_0^2)$ from first principles.

In [CS20], the intermediate-energy matching of the RG-improved and optimized fixed-scale results was carried out by comparing the respective running couplings as functions of the renormalization scale. In the context of the OFS approach, a Taylor coupling $\alpha_s^{(\text{OFS})}(\mu^2)$ can be defined by making use of Eqs. (3.151) and (3.152)²². Assuming that the fixed-scale propagators are renormalized in the MOM scheme, Eq. (3.152) can be rewritten as

$$\alpha_s^{(\text{OFS})}(\mu^2) = \kappa [F(\mu^2/m^2) + F_0]^{-1} [G(\mu^2/m^2) + G_0]^{-2}, \quad (3.153)$$

where F_0 and G_0 take on the values obtained by optimization, whereas κ is a constant that absorbs both $\alpha_s^{(\text{OFS})}(\mu_0^2)$ and the multiplicative renormalization constants Z_Δ and Z_G contained in the OFS gluon and ghost propagators. Since $\alpha_s^{(\text{OFS})}(\mu_0^2)$ is undefined in the fixed-scale approach²³, in the above expression κ is a free parameter.

The normalization of $\alpha_s^{(\text{OFS})}(\mu^2)$ – i.e., the value of κ – can be fixed by requiring that the former be equal to its RG counterpart $\alpha_s(\mu^2)$ at an intermediate-energy renormalization scale μ_1 , yielding

$$\alpha_s^{(\text{OFS})}(\mu^2) = \alpha_s(\mu_1^2) \left[\frac{F(\mu_1^2/m^2) + F_0}{F(\mu^2/m^2) + F_0} \right] \left[\frac{G(\mu_1^2/m^2) + G_0}{G(\mu^2/m^2) + G_0} \right]^2. \quad (3.154)$$

In [CS20], the scale μ_1 was chosen equal to $1.372m$, corresponding to 0.9 GeV for $m = 0.656$ GeV. We note that, if the running couplings $\alpha_s^{(\text{OFS})}(\mu^2)$ and $\alpha_s(\mu^2)$ do match at intermediate energies, then the specific choice of the scale μ_1 is irrelevant to the normalization of $\alpha_s^{(\text{OFS})}(\mu^2)$, as long as $\mu_1 \approx m$.

In Fig. 3.24 we compare the OFS strong running coupling $\alpha_s^{(\text{OFS})}(\mu^2)$ – Eq. (3.154) – and its RG counterpart $\alpha_s(\mu^2)$ for different values of the initial RG coupling constant $\alpha_s(\mu_0^2)$. $\alpha_s^{(\text{OFS})}(\mu^2)$ clearly shows the same behavior as $\alpha_s(\mu^2)$. Nonetheless, despite having chosen κ in such a way that the two functions coincide at $\mu = \mu_1$, the two running couplings are far from being equal for arbitrary values of $\alpha_s(\mu_0^2)$; this is true in the low- and high-energy regimes, as well as at intermediate energies. There exists, however, an interval of values, centered around $\alpha_s(\mu_0^2) \approx 0.39$, for which the OFS and RG running couplings overlap at renormalization scales $\mu \approx \mu_1$.

In [CS20] it was found that the relative difference between the two couplings is less than 1% over the widest possible interval of momenta – ranging from $\mu \approx 1.1m$ to $\mu \approx 2m$ – when $\alpha_s(\mu_0^2)$ is chosen equal to 0.391. The running couplings corresponding to such a value are displayed in Fig. 3.25. For $\alpha_s(\mu_0^2) = 0.391$, the maximum of $\alpha_s(\mu^2)$ is found to be $\alpha_s(\mu_*^2) \approx 2.34$, suggesting – as previously anticipated – that the one-loop RG-improved propagators may diverge from the exact results for $p \lesssim m$.

With $\alpha_s(\mu_0^2)$ determined by the intermediate-scale matching with the OFS results, the gluon mass parameter m^2 is left as the only free parameter of the RG-improved propagators. Observe that the value of m^2 sets not only the energy scale of the propagators, but also that of the initial renormalization scale μ_0 and of the matching scale μ_1 .

²²We remark that Eq. (3.151) can be derived from general principles of renormalizability which do not require the propagators to be RG improved, see [CS20]. For this reason, it can also be employed in the context of non-improved approaches, like the fixed-scale approximation of Secs. 3.1 and 3.2.

²³Recall that the fixed-scale expressions of Secs. 3.1 and 3.2 do not explicitly contain the coupling constant.

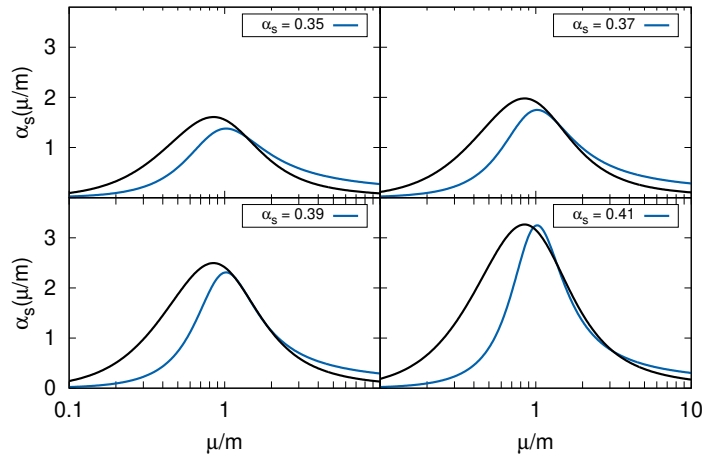


Figure 3.24: $N = 3$ optimized fixed-scale (black) and RG (blue) strong running couplings as a function of the adimensional renormalization scale μ/m for different values of the initial RG coupling $\alpha_s(\mu_0^2)$ ($\mu_0 = 6.098 m$). The matching scale is set to $\mu_1 = 1.372 m$.

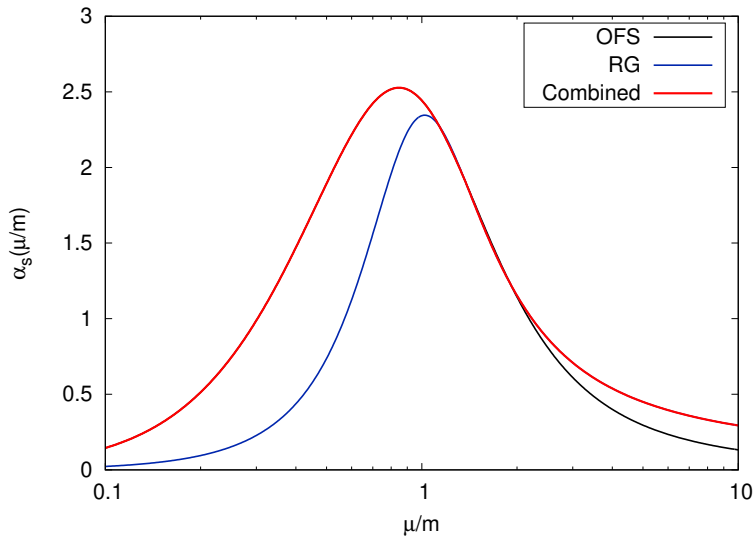


Figure 3.25: $N = 3$ optimized fixed-scale (black) and RG (blue) strong running couplings as a function of the adimensional renormalization scale μ/m for $\alpha_s(\mu_0^2) = 0.391$ ($\mu_0 = 6.098 m$). Matching scale set to $\mu_1 = 1.372 m$. The red curve is obtained by combining the low-energy OFS coupling and the high-energy RG coupling.

In Figs. 3.26, 3.27 and 3.28 we display the Euclidean transverse gluon propagator and dressing function computed by different methods within the Screened Massive Expansion, together with the lattice data of [DOS16]. For obtaining each of the curves, the gluon mass parameter was set to $m = 0.656$ GeV. As a result, as previously reported, the initial

renormalization scale is equal to $\mu_0 = 4$ GeV, while the matching scale is $\mu_1 = 0.9$ GeV. We remark that the lattice data of [DOS16] were originally renormalized at 4 GeV, explaining our choice of μ_0 .

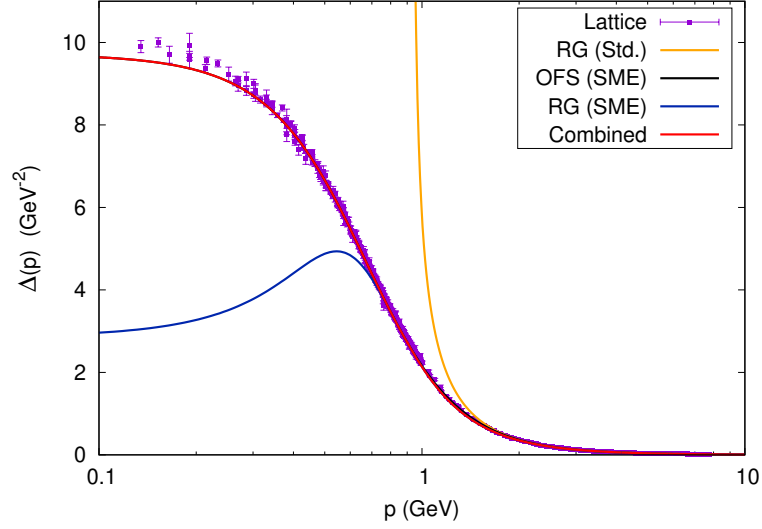


Figure 3.26: Landau-gauge Euclidean transverse gluon propagator renormalized at the scale $\mu_0 = 4$ GeV. Black curve: optimized fixed-scale SME renormalized by matching at $\mu_1 = 0.9$ GeV. Blue curve: RG-improved SME. Red curve: combined OFS and RG-improved SME matched at μ_1 . Orange curve: ordinary pQCD. Squares: lattice data of [DOS16]. $m = 0.656$ GeV, $\alpha_s(\mu_0) = 0.391$.

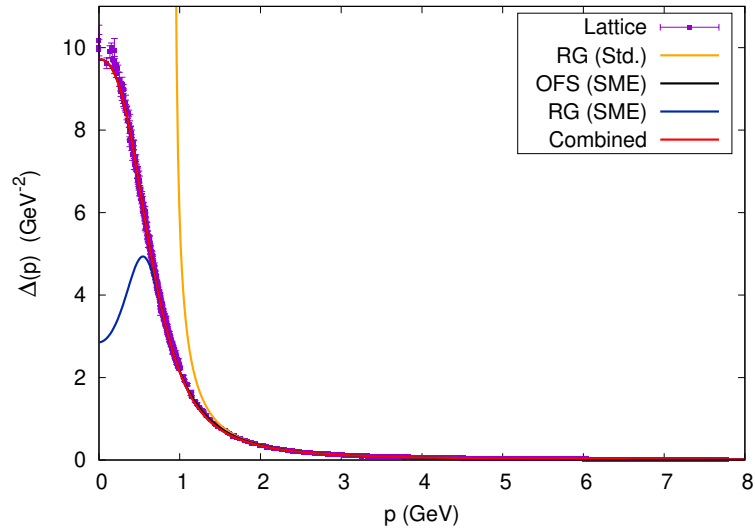


Figure 3.27: Landau-gauge Euclidean transverse gluon propagator renormalized at the scale $\mu_0 = 4$ GeV with the lattice data of [DOS16]. Linear x axis. Curves as in Fig. 3.26.

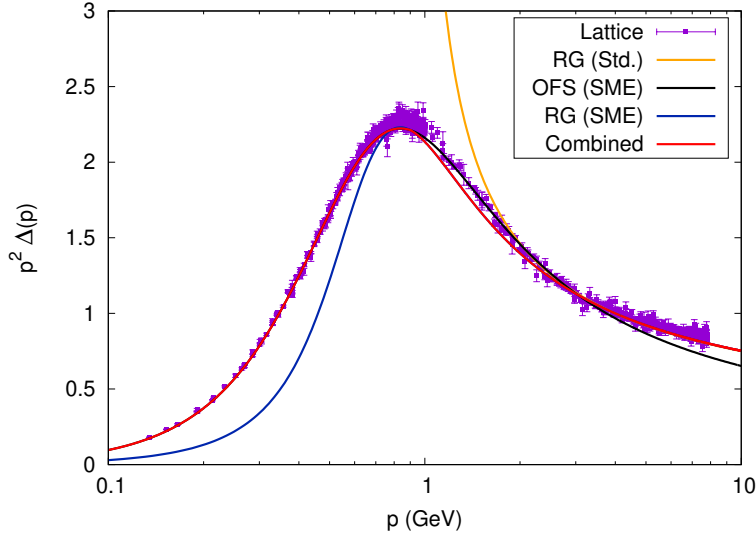


Figure 3.28: Landau-gauge Euclidean transverse gluon dressing function renormalized at the scale $\mu_0 = 4$ GeV with the lattice data of [DOS16]. Curves as in Fig. 3.26.

The optimized fixed-scale propagator and dressing function are shown in black in the figures. At variance with the previous sections, in Figs. 3.26, 3.27 and 3.28 these are normalized by matching their value with that of their RG analogues at $p = \mu_1$, rather than by fitting the multiplicative renormalization constant Z_Δ .

The RG-improved gluon propagator and dressing function computed for the optimal value $\alpha_s(\mu_0^2) = 0.391$, on the other hand, are shown in blue. As expected, the propagator/dressing function deviates from the lattice data at $p \approx m$: for smaller values of the momentum, the OFS results (black curve, hidden behind the red curve in the IR, see ahead) still yield a better approximation of the lattice data. In particular, compared to the exact results, the RG-improved propagator appears strongly suppressed at low energies. This behavior is often observed in one-loop gluon propagators computed by massive perturbative methods²⁴; the two-loop results obtained within the Curci-Ferrari model [GPRT19] suggest that taking into account the higher-order corrections to the propagator will enhance its IR limit.

At high energies, especially for $p > 3$ -4 GeV, the RG-improved results (hidden below the red curve in the figures, see ahead) generally show a better agreement with the lattice data in comparison to their OFS counterpart. Despite the former falling somewhat below the data in the range ≈ 1 -3 GeV, the RG-improved propagator still reproduces the lattice UV tail quite accurately up to $p \approx 8$ GeV. At such large scales, the SME results are indistinguishable from those computed by ordinary perturbation theory, displayed in orange in the figures²⁵. The red curves in Figs. 3.26, 3.27 and 3.28 are obtained by combining the low-energy OFS gluon propagator with its high-energy RG-improved counterpart at the matching scale $\mu_1 = 0.9$ GeV²⁶. The combined propagator/dressing function pro-

²⁴The Dynamical Model of Chapter 5 explicitly shares this feature. As for the IRS Curci-Ferrari one-loop propagator reported in [GPRT19], the latter either matches the IR lattice data and misses the UV tail, or it reproduces well the UV tail and displays a suppressed IR limit when rescaled – see Note 12, Sec. 2.4.2.

²⁵For integrating the ordinary pQCD propagator, the value $\alpha_s(\mu_0^2) = 0.391$ was used.

²⁶In particular, the combined propagator is superimposed to the OFS propagator (black curve) in the

vides the best overall approximation of the lattice data over the whole momentum range $p \in [0, 8]$ GeV.

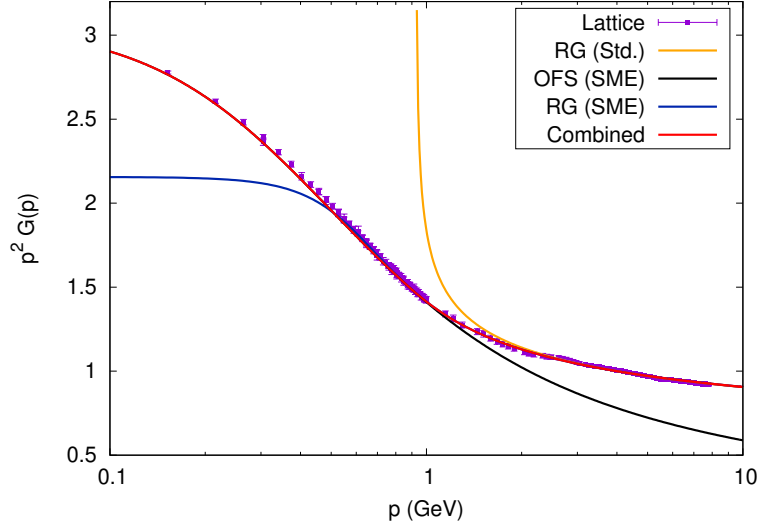


Figure 3.29: Landau-gauge Euclidean ghost dressing function renormalized at the scale $\mu_0 = 4$ GeV with the lattice data of [DOS16]. Curves as in Fig. 3.26.

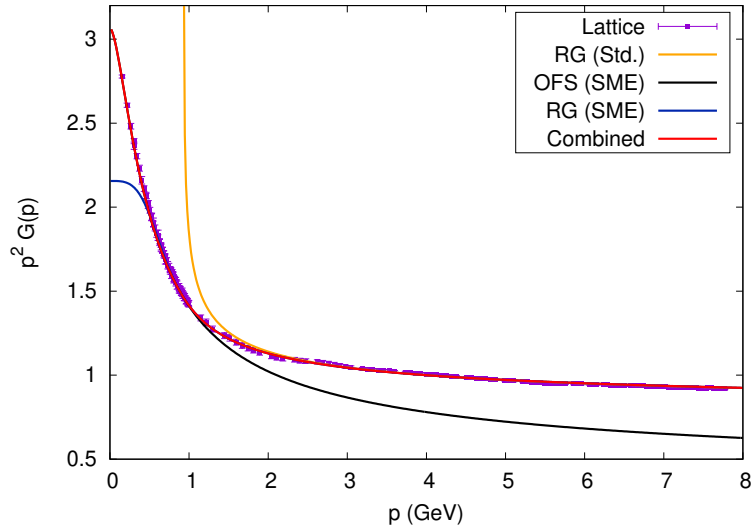


Figure 3.30: Landau-gauge Euclidean ghost dressing function renormalized at the scale $\mu_0 = 4$ GeV with the lattice data of [DOS16]. Linear x axis. Curves as in Fig. 3.26.

In Figs. 3.29 and 3.30 we show the Landau-gauge Euclidean ghost dressing function with the same color coding and parameters m^2 , $\alpha_s(\mu_0^2)$, μ_0 and μ_1 as in the previous figures. The improvement brought about in the UV by the Renormalization Group is

IR, and to the RG-improved propagator (blue curve) in the UV.

remarkable. While the OFS dressing function fails to reproduce the lattice data already at momenta $p \approx 2$ GeV, its RG-improved counterpart is in excellent agreement with them up to $p \approx 8$ GeV. At low momenta $p \lesssim m$, on the other hand, the RG-improved dressing function saturates too quickly, and the OFS results provide a better approximation, just like in the gluon sector.

As reported before, the propagators shown in Figs. 3.26 to 3.30 use the gluon mass parameter m^2 as their only free parameter, the initial coupling constant $\alpha_s(\mu_0^2)$ at $\mu_0 = 4$ GeV and normalization of the optimized fixed-scale results having been obtained by matching the OFS and RG running coupling at $\mu_1 = 0.9$ GeV. For m^2 , we chose the value fitted in Sec. 3.2 – namely, $m = 0.656$ GeV – starting from the lattice gluon propagator and the optimized-fixed scale expressions.

An alternative determination of m^2 can be obtained by making use of the combined low-energy OFS and high-energy RG-improved propagators as follows. First, the RG-improved propagators renormalized at the scale μ_0 are defined as functions of $\alpha_s(\mu_0^2)$ and m^2 , with the dimensionful value of μ_0 set to 4 GeV following the lattice data of [DOS16]. Then $\alpha_s(\mu_0^2)$ is expressed as a function of the gluon mass parameter by making use of the running of the strong coupling, with the initial renormalization scale set to $\mu = 6.098 m$, where we know by optimization that $\alpha_s(\mu^2) = \alpha_s^{\text{opt.}} = 0.391$. Explicitly,

$$\alpha_s(\mu_0^2) = \frac{\alpha_s^{\text{opt.}}}{1 + \frac{3N\alpha_s^{\text{opt.}}}{4\pi} [H(\mu_0^2/m^2) - H(6.098^2)]} . \quad (3.155)$$

Since $\alpha_s(\mu_0^2)$ is completely determined by the value of m^2 , the same will hold true for the RG-improved propagators. Finally, the latter are combined with the OFS propagators at the matching scale $p = \mu_1 = 1.372 m$, retaining the RG-improved propagators for $p \geq \mu_1$ and the OFS propagators for $p \leq \mu_1$. The resulting combined propagators are functions of the gluon mass parameter alone. In particular, the value of m^2 can be determined by fitting the combined gluon propagator with the lattice data of [DOS16] over the widest possible range of momenta.

The outcome of the fit is shown in Fig. 3.31. It was found that the value that best fits the lattice data of [DOS16] is $m = 0.651$ GeV, very close to our previous determination (also shown in the figure). The difference between the $m = 0.651$ GeV and $m = 0.656$ GeV combined propagators is minimal, being visible only in the deep IR, where the former is closer to the lattice data when compared to the latter. Analogous plots for the ghost dressing function can be found in [CS20]; in the ghost sector, the $m = 0.651$ GeV and $m = 0.656$ GeV dressing functions are indistinguishable to the naked eye.

In this section we have discussed the optimization of the RG-improved propagators computed in the Screened Massive Expansion. While formally the RG-improved propagators depend both on the value of the coupling constant $\alpha_s(\mu_0^2)$ at the initial renormalization scale μ_0 and on the gluon mass parameter m^2 , the requirement that the former match with their optimized fixed-scale counterpart at intermediate energy scales ($p \approx m$) allowed us to determine the value of $\alpha_s(\mu_0^2)$ as a function of m^2 . The resulting propagators show a good agreement with the lattice data for $p \gtrsim m$ up to 8 GeV, but deviate from the exact results at low energies. This is due to the fact that, in the IR, the SME running coupling computed in the MOM-Taylor scheme attains a maximum $\alpha_s^{\text{max}} \approx 2.34$ which is quite large for the perturbative standards, thus preventing the one-loop approximation from fully capturing the low-energy behavior of the propagators.

For $p \lesssim m$, the optimized fixed-scale results of Sec. 3.2 still provide the best description of the lattice data. When the low-energy OFS propagators are combined with their

high-energy RG-improved counterpart at the matching scale $\mu_1 = 1.372 m$, the resulting combined functions succeed in reproducing the lattice data over the whole momentum range $p \in [0, 8]$ GeV. By making use of these, one is able to obtain an alternative determination of the gluon mass parameter, $m = 0.651$ GeV, which is very close to the value found in Sec. 3.2 by fitting the OFS gluon propagator ($m = 0.656$ GeV).

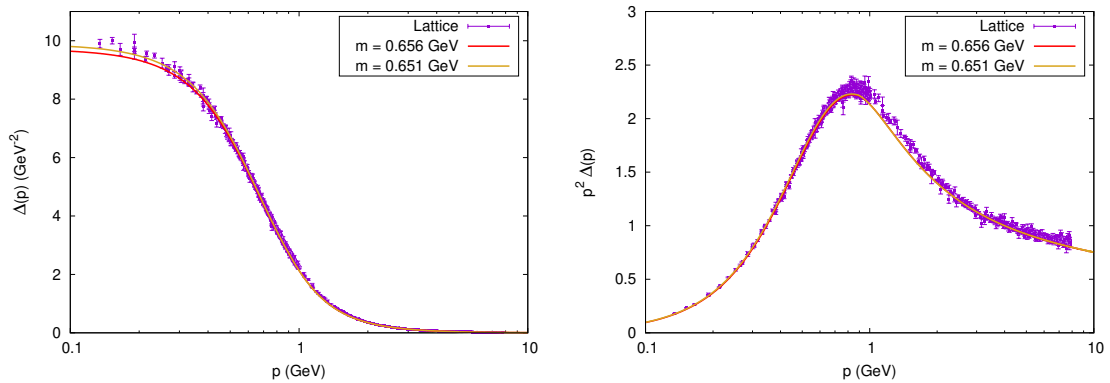


Figure 3.31: Landau-gauge RG-improved Euclidean transverse gluon propagator (left) and dressing function (right) renormalized at the scale $\mu_0 = 4$ GeV, obtained by combining the low-energy OFS results with the high-energy RG-improved results. Lattice data from [DOS16].

3.4 Conclusions

The results presented in this chapter show that the Screened Massive Expansion is capable of describing the dynamics of the gluons and ghosts from first principles over a wide range of momenta. After optimization, the gluon mass parameter m^2 is left as the only free parameter of the expansion both at low energies, where the optimized fixed-scale propagators of Sec. 3.2 provide the best approximation of the lattice data, and at high energies, where the RG-improved propagators derived in Sec. 3.3.3 manage to reproduce the lattice UV tails up to $p \approx 8$ GeV.

The absence of Landau poles from the SME running coupling, made possible by the explicit scale dependence of the beta function, confirms that the method is self-consistent and well-defined in the infrared. Moreover, it proves that the diverging of the ordinary pQCD coupling at low energies is just an artifact of the expansion, ultimately due to the failure of pQCD in accounting for the dynamical generation of an IR gluon mass.

The precision with which the Screened Massive Expansion is able to reproduce the lattice results already to one loop seems to indicate that most of the non-perturbative effects which shape the IR dynamics of the gauge sector of QCD can be incorporated in a perturbative series that treats the transverse gluons as massive at tree level.

4

Applications of the Screened Massive Expansion

As an application of the Screened Massive Expansion presented in Chpt. 3, in this chapter we summarize the main findings of [CS18], [CRBS21] and [SC21] regarding the thermal behavior of the gluons in pure Yang-Mills theory and the dynamical generation of a mass for the quarks in full QCD. In Sec. 4.1 we will extend the GEP analysis of Sec. 3.1.1 to finite temperature [CS18] and study the gluon propagator and its poles as functions of the temperature [SC21]. In Sec. 4.2 we will make use of the techniques presented in the last chapter to show that a shift of the quark action similar to the one employed in the gluon sector is able to account for dynamical mass generation in the quark sector, as is expected in full QCD as a consequence of chiral symmetry breaking [CRBS21].

Refs. [CS18], [CRBS21] and [SC21] are attached as an insert to this thesis, to be found in Appendix C.

4.1 The Screened Massive Expansion at finite temperature

The Screened Massive Expansion can be extended to finite temperatures $T > 0$ by making use of the formalism of thermal field theory (TFT). In the framework of TFT [KG06], the partition function and the quantum fields are defined in Euclidean space, with the imaginary-time variable $\tau = it$ taken to lie in the interval $\tau \in [0, \beta]$. The dimensionful quantity $\beta = 1/T$ – that is, the inverse temperature of the system – tends to infinity as $T \rightarrow 0$; thanks to the boundary conditions imposed on the finite-temperature fields, the results of ordinary zero-temperature quantum field theory are recovered in such a limit.

The set-up of the Screened Massive Expansion at $T > 0$ is discussed in depth in [CS18] and [SC21]. The shift of the expansion point of the perturbative series that defines the SME is replicated in the framework of TFT to obtain expressions that depend on the gluon mass parameter m^2 as well as on the temperature. Since m^2 is a mass scale whose value depends on the problem at hand, in the context of the SME the former can itself be taken to be a function of the temperature, $m^2 = m^2(T)$.

4.1.1 The Gaussian Effective Potential at finite temperature and the deconfinement phase transition

In Sec. 3.1.1 we argued that treating the gluons as massive at tree level is expected to provide a better approximation of the low-energy dynamics of QCD compared to ordinary massless perturbation theory because such a choice minimizes the Gaussian Effective Potential of pure Yang-Mills theory. The GEP analysis carried out in Sec. 3.1.1 can be

repeated at finite temperature in order to check that this remains true for $T > 0$ [CS18]. At non-zero temperatures, the GEP can be interpreted as a first-order approximation of the temperature-dependent free energy density $\mathcal{F}(T)$ of the theory [CS18]. Therefore, in what follows, we will denote the former by $\mathcal{F}_G(T, m)$.

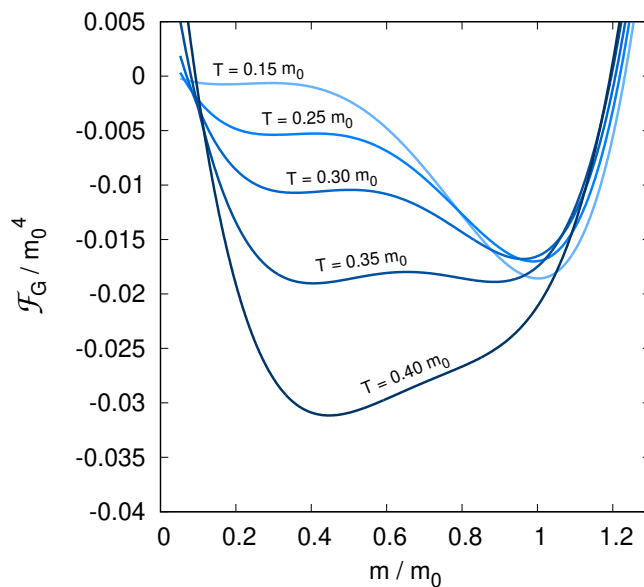


Figure 4.1: Gaussian Effective Potential of pure Yang-Mills theory as a function of the gluon mass parameter for different values of the temperature. All dimensional quantities are adimensionalized by factors of $m_0 = m(T = 0)$.

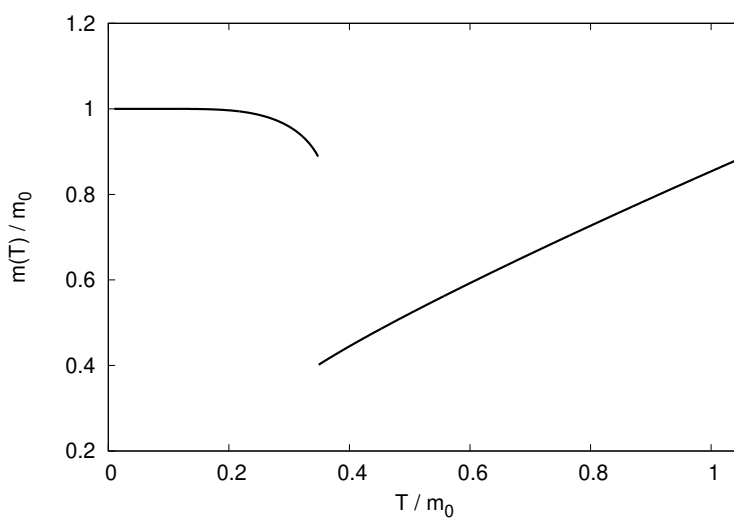


Figure 4.2: Global minimum of the Gaussian Effective Potential of pure Yang-Mills theory as a function of the temperature. The discontinuity is found at $T = T_c \approx 0.35 m_0$.

The Gaussian Effective Potential $\mathcal{F}_G(T, m)$ of Yang-Mills theory is displayed in Fig. 4.1 as a function of the gluon mass parameter m for different values of the temperature. In the figure, all the quantities are adimensionalized by the value of m which minimizes the GEP at zero temperature, $m_0 = m(T = 0)$.

We recall from Sec. 3.1.1 that for $T = 0$ the GEP has a global minimum at $m = m_0 \neq 0$ and a local minimum at $m = 0$. As we can see from Fig. 4.1, as the temperature increases, the position of the $m = 0$ minimum shifts towards larger values of the mass and the corresponding value of the GEP grows more negative, until the two minima align at $T = T_c \approx 0.35 m_0$. For $T > T_c$, the lower-mass minimum becomes the global minimum of the GEP, and its position starts to increase roughly linearly with the temperature.

The position of the global minimum of the GEP is shown in Fig. 4.2 as a function of temperature. At low temperatures, the value of m which minimizes the GEP, denoted by $m(T)$, remains roughly equal to its $T = 0$ value until it starts to decrease at $T \approx 0.2 m_0$. After hitting the critical temperature T_c , the high-temperature behavior of $m(T)$ becomes similar to that of the thermal masses computed for the massless particles in the framework of TFT [KG06], $m(T) \propto T$. For this reason, we may interpret $T = T_c$ as the temperature at which the gluon ceases to be massive and starts to behave as a massless particle.

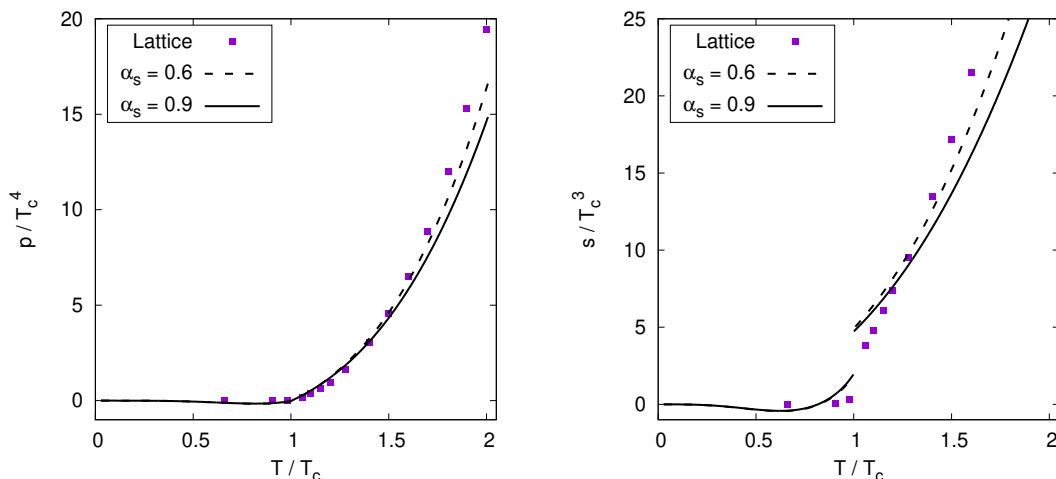


Figure 4.3: Pressure (left) and entropy density (right) as functions of temperature computed in the GEP approximation, together with the lattice data of [GP17]. Adimensionalized by the critical temperature T_c . For a discussion on the value of the coupling constant α_s see [CS18].

What are the consequences of the discontinuity found in $m(T)$ by the minimization of the GEP? In Fig. 4.3 we display the pressure p and entropy density s computed in the GEP approximation,

$$p = -[\mathcal{F}_G(T, m(T)) - \mathcal{F}_G(0, m_0)] , \quad s = -\frac{d}{dT} \mathcal{F}_G(T, m(T)) . \quad (4.1)$$

While the pressure is a continuous function of the temperature, the entropy density has a discontinuity at $T = T_c$; this indicates that the system undergoes a first-order phase transition. Such a transition is well-known to occur in pure Yang-Mills theory: it is the

deconfinement phase transition, by which the gluons¹ cease to be confined in color-singlet bound states and start behaving as free particles. Once again, we see that the existence of a link between the IR-massiveness of the gluon and the phenomenon of confinement is suggested by the results of the SME. With $m \approx 0.66$ GeV, T_c would be predicted to be around 230 MeV, not too far from the critical temperature found by lattice methods for pure Yang-Mills theory, $T_c \approx 270$ MeV [SOBC14]. In passing, we note that the pressure and entropy density computed in the GEP approximation, when adimensionalized by the critical temperature T_c , are in fair agreement with the lattice data of [GP17].

The GEP analysis of pure Yang-Mills theory at $T \geq 0$ confirms that, below the critical temperature T_c , the Screened Massive Expansion is still expected to provide a better approximation of the infrared dynamics of the gauge sector compared to ordinary perturbation theory. At larger temperatures, on the other hand, the T -dependent gluon mass parameter can be understood to play essentially the same role as the ordinary thermal mass of massless particles, so that more specialized approaches such as the Hard Thermal Loop resummation [BP92] might yield better results.

4.1.2 The Landau-gauge gluon propagator and its poles at finite temperature

In thermal field theory, the restriction of the imaginary time variable to the interval $[0, 1/T]$ causes the breaking of the symmetry group $SO(4)$ of 4-dimensional Euclidean spacetime down to $SO(3)$ – that is, the group of ordinary spatial rotations. From a physical point of view, this is equivalent to the adoption of a reference frame with respect to which the state variables and the state functions of the thermodynamical system, such as the temperature and energy, are to be defined.

As a consequence of the breaking of $SO(4)$ symmetry, at finite temperature the gluon propagator $\Delta_{\mu\nu}^{ab}$ cannot be expressed anymore in terms of just two scalar functions – namely, its 4-dimensionally transverse and longitudinal components –, but is instead determined by *three* scalar components. Indeed, it can be shown [KG06] that, in Fourier space, the most general expression for $\Delta_{\mu\nu}^{ab}$ at $T \geq 0$ is given by²

$$\Delta_{\mu\nu}^{ab}(p, T) = \left(\Delta_T(p, T) \mathcal{P}_{\mu\nu}^T(p) + \Delta_L(p, T) \mathcal{P}_{\mu\nu}^L(p) + \frac{\xi}{p^2} \ell_{\mu\nu}(p) \right) \delta^{ab}, \quad (4.2)$$

where $\mathcal{P}_{\mu\nu}^T(p)$ and $\mathcal{P}_{\mu\nu}^L(p)$ are *3-dimensionally* transverse and longitudinal projectors,

$$\mathcal{P}_{\mu\nu}^T(p) = (1 - \delta_{\mu 4})(1 - \delta_{\nu 4}) \left(\delta_{\mu\nu} - \frac{p_\mu p_\nu}{|\vec{p}|^2} \right), \quad \mathcal{P}_{\mu\nu}^L(p) = t_{\mu\nu}(p) - \mathcal{P}_{\mu\nu}^T(p), \quad (4.3)$$

the fourth direction being that of the imaginary time variable, $x^4 = \tau = it = ix^0$, and $\Delta_{T,L}(p, T)$ are the 3-dimensionally transverse and longitudinal components of the gluon propagator. Because of $SO(3)$ symmetry, the functions $\Delta_{T,L}$ do not depend on the direction of the three-dimensional vector \vec{p} , but only on its modulus $|\vec{p}|$,

$$\Delta_{T,L}(p, T) = \Delta_{T,L}(p^4, |\vec{p}|, T). \quad (4.4)$$

That the 4-dimensionally longitudinal component of $\Delta_{\mu\nu}^{ab}(p, T)$, ξ/p^2 , is equal to its $T = 0$ limit can be proved by exploiting the BRST invariance of the Faddeev-Popov Lagrangian,

¹And, in full QCD, the quarks, although strictly speaking in this case there is no phase transition, but rather a crossover [AEF⁺06, BBC⁺12, BBD⁺14].

²We remark that, in Euclidean space, the 4-dimensional transverse and longitudinal projectors are defined, respectively, as $t_{\mu\nu}(p) = \delta_{\mu\nu} - p_\mu p_\nu / p^2$ and $\ell_{\mu\nu}(p) = p_\mu p_\nu / p^2$.

which still holds at finite temperature. During the rest of this section, we will use the terms transverse and longitudinal in the 3-dimensional sense, unless otherwise specified.

Observe that, in order for SO(4) symmetry and the ordinary result to be recovered at zero temperature, we must have

$$\Delta_T(p, T = 0) = \Delta_L(p, T = 0) = \Delta(p) \quad (4.5)$$

for the transverse and longitudinal propagators, where $\Delta(p)$ is the Euclidean (4-dimensionally transverse) propagator studied in Chpt. 3. A similar relation can be shown to hold [KG06] when the spatial momentum \vec{p} vanishes at $p^4 \neq 0$:

$$\Delta_T(p^4, |\vec{p}| = 0, T) = \Delta_L(p^4, |\vec{p}| = 0, T) \quad (p^4 \neq 0) . \quad (4.6)$$

Eq. (4.6) is easily understood to be a consequence of the fact that, at zero momentum, $\vec{p} = \vec{0}$, there is no spatial direction with respect to which the transverse and longitudinal components of the propagator $\Delta_{T,L}(p, T)$ can be distinguished.

Since the interval $[0, 1/T]$ is bounded, the Fourier variable p^4 corresponding to the imaginary time $x^4 = \tau$ is a discrete variable. Due to the boundary conditions of the thermal problem, which require the gluon field to be periodic in τ [KG06], p^4 takes on the values

$$p^4 = \omega_n = 2\pi nT \quad (n \in \mathbb{N}) . \quad (4.7)$$

The ω_n 's are known as *Matsubara frequencies*.

In [SC21], the Landau-gauge transverse and longitudinal components of the gluon propagator were computed to one loop at finite temperature in the Screened Massive Expansion, yielding

$$\Delta_{T,L}(p, T) = \frac{Z_{T,L}(T)}{p^2[F(s(T)) + F_0^{T,L}(T) + \pi_{T,L}(p, m(T), T)]} . \quad (4.8)$$

In the above equation, $s(T) = p^2/m^2(T)$ is the adimensionalized Euclidean momentum, the gluon mass parameter $m^2 = m^2(T)$ is taken to be a function of the temperature, $F(s)$ is the function already reported in Sec. 3.1.4, $Z_{T,L}(T)$ and $F_0^{T,L}(T)$ are, respectively, multiplicative and additive temperature-dependent renormalization constants, and the functions $\pi_{T,L}(p, m, T)$, defined so that

$$\pi_{T,L}(p, m, T = 0) = 0 , \quad (4.9)$$

contain the one-loop thermal corrections to the components of the propagator. The explicit form of $\pi_T(p, m, T)$ and $\pi_L(p, m, T)$ is reported in [SC21] in terms of one-dimensional integrals which cannot be evaluated analytically.

The finite-temperature SME gluon propagator was then compared to the Landau-gauge lattice data of [SOBC14] at zero Matsubara frequency ($n = 0$). While the standard definition of the Screened Massive Expansion makes use of a single gluon mass parameter m^2 to rearrange the QCD perturbative series, in [SC21] it was found that for $T > 0$, and especially at high temperatures, it is not possible to reproduce the behavior of both the components of the gluon propagator by a single T -dependent value of m^2 in Eq. 4.8. This is not totally unexpected, for the following reason. First of all, observe that the gluon mass term which is added and subtracted from the Faddeev-Popov action,

$$\delta S = \frac{1}{2} \int \frac{d^4 p}{(2\pi)^4} A_\mu^a(-p) m^2 t^{\mu\nu}(p) A_\nu^a(p) , \quad (4.10)$$

is 4-dimensionally transverse, and therefore does not take into account possible differences in the behavior of the 3-dimensionally transverse and longitudinal masses that can only arise at finite temperature. Second, the GEP analysis of the last section already showed that, at high temperatures, the minimum of the GEP is found at a linearly rising mass $m(T) \propto T$, which, as we noticed, resembles the thermal mass of a massless particle. For the vector bosons, it is well-known that the thermal masses associated to the transverse and the longitudinal components of the propagators *do* have a different dependence on the temperature [BP92]. Therefore, if the picture painted by the GEP analysis is qualitatively accurate, then the δS in Eq. (4.10) indeed will not be able to accurately reproduce the exact results at sufficiently high temperatures.

Nonetheless, the Screened Massive Expansion was still found to be able to provide a good semi-quantitative description of the gluon propagator at $T > 0$, so long as the mass parameters in $\Delta_T(p, T)$ and $\Delta_L(p, T)$ are tuned separately as functions of the temperature. Of course, since using two different mass parameters is not allowed in the standard SME formalism, the results described in what follows are to be interpreted as estimates, rather than as first-principles calculations.

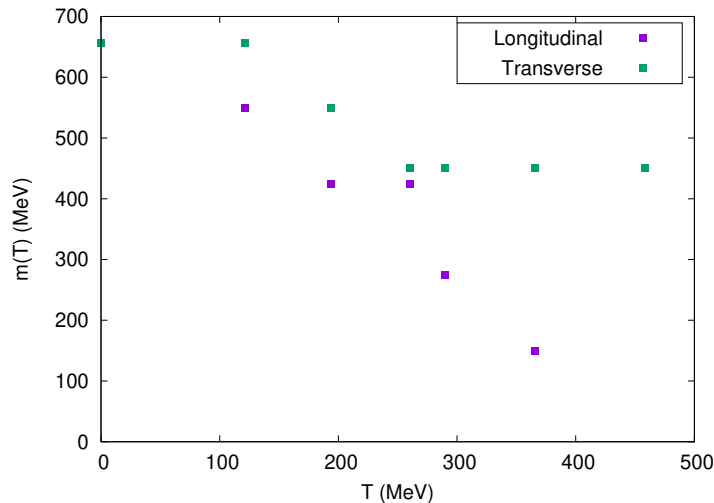


Figure 4.4: Values of the gluon mass parameter which best fit the lattice data of [SOBC14] for the transverse and the longitudinal components of the Landau-gauge Euclidean gluon propagator at zero Matsubara frequency, as a function of temperature.

The values of the gluon mass parameter m^2 which yield the best fit with the transverse and the longitudinal components of the lattice gluon propagator of [SOBC14] at zero Matsubara frequency ($n = 0$) are shown in Fig. 4.4 as functions of the temperature. As we can see, while at low temperatures the transverse and the longitudinal mass remain sufficiently close to each other, as soon as the temperature approaches $T_c \approx 270$ MeV their behavior starts to diverge radically. In particular, at high temperatures, the transverse gluon mass parameter is essentially constant, whereas the longitudinal one decreases with the temperature. We reiterate that, having been obtained by a non-standard procedure, the fitted values of the parameters should be regarded as effective values whose sole purpose is to reproduce the components of the propagator.

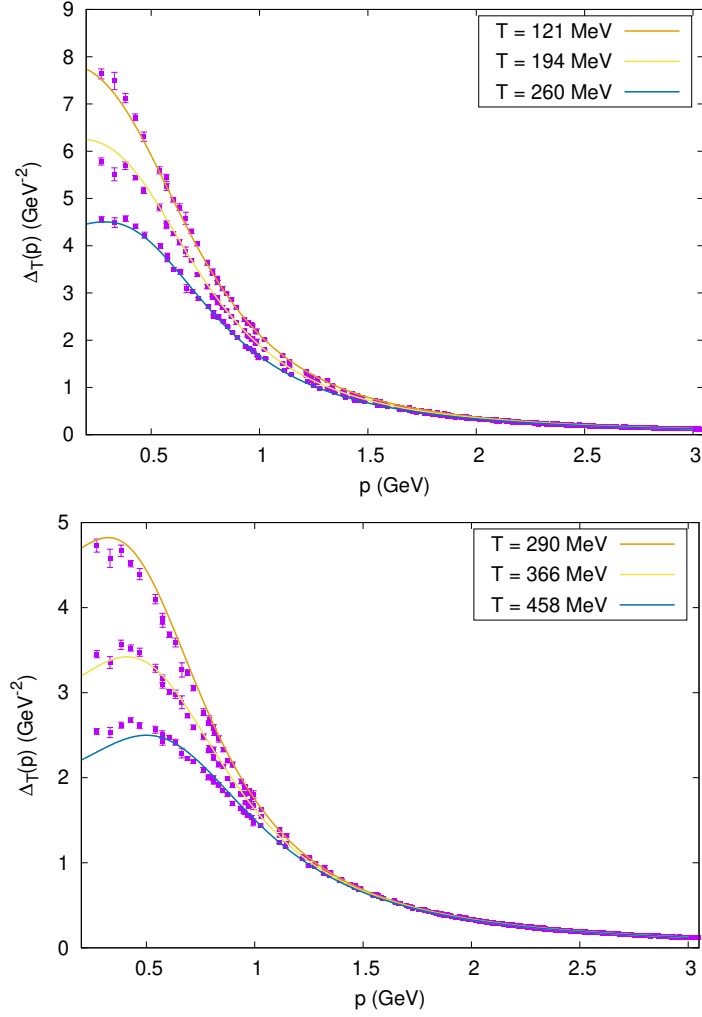


Figure 4.5: Transverse component of the Landau-gauge Euclidean gluon propagator at zero Matsubara frequency ($n = 0$) as a function of the modulus $|\vec{p}|$ of the 3-dimensional momentum, for $T < T_c$ (top) and $T > T_c$ (bottom). Multiplicatively renormalized at $\mu_0 = 4$ GeV. Lattice data from [SOBC14].

In Fig. 4.5 we display the transverse component of the Landau-gauge Euclidean gluon propagator at zero Matsubara frequency ($n = 0$) as a function of the modulus $|\vec{p}|$ of the 3-dimensional momentum for different values of the temperature. By tuning the gluon mass parameter as in Fig. 4.4, we see that the SME expression is able to give a good quantitative description of the transverse propagator over the whole momentum range $[0, 3]$ GeV and for all the tested values of the temperature. When multiplicatively normalized at $\mu_0 = 4$ GeV as in the figure, $\Delta_T(p, T)$ monotonically decreases with the temperature at every fixed momentum $|\vec{p}| \leq 3$ GeV. We remark that, in order to obtain the curves in Fig. 4.5, as well as those in the figures that follow, the values of the additive constants $F_0^{T,L}(T)$ contained in Eq. (4.8) were also fitted at each temperature from the lattice data.

In Fig. 4.6 we display the longitudinal component of the Landau-gauge Euclidean gluon propagator at zero Matsubara frequency ($n = 0$) as a function of the modulus $|\vec{p}|$ of the

3-dimensional momentum. At variance with the transverse propagator, the longitudinal one – when renormalized at $\mu_0 = 4$ GeV and at fixed momentum $|\vec{p}|$ – is a non-monotonic function of the temperature. Specifically, $\Delta_L(p, T)$ first increases with the temperature, then attains a maximum at $T = T_c$, and finally it decreases at high temperatures just like its transverse counterpart. The critical temperature T_c can indeed be defined as the point at which the longitudinal propagator changes its behavior. Interestingly, the change in behavior of $\Delta_L(p, T)$ at some fixed temperature is built into the SME propagator itself, as opposed to being an effect of our choice of free parameters [SC21].

As we can see, at low momenta and already for $T < T_c$, the SME longitudinal expression fails to reproduce the lattice data for all but the lowest value of temperature, $T = 121$ MeV, the deviation from the lattice being larger around T_c . On the other hand, the agreement with the data is satisfactory for $|\vec{p}| \gtrsim 0.5$ GeV.

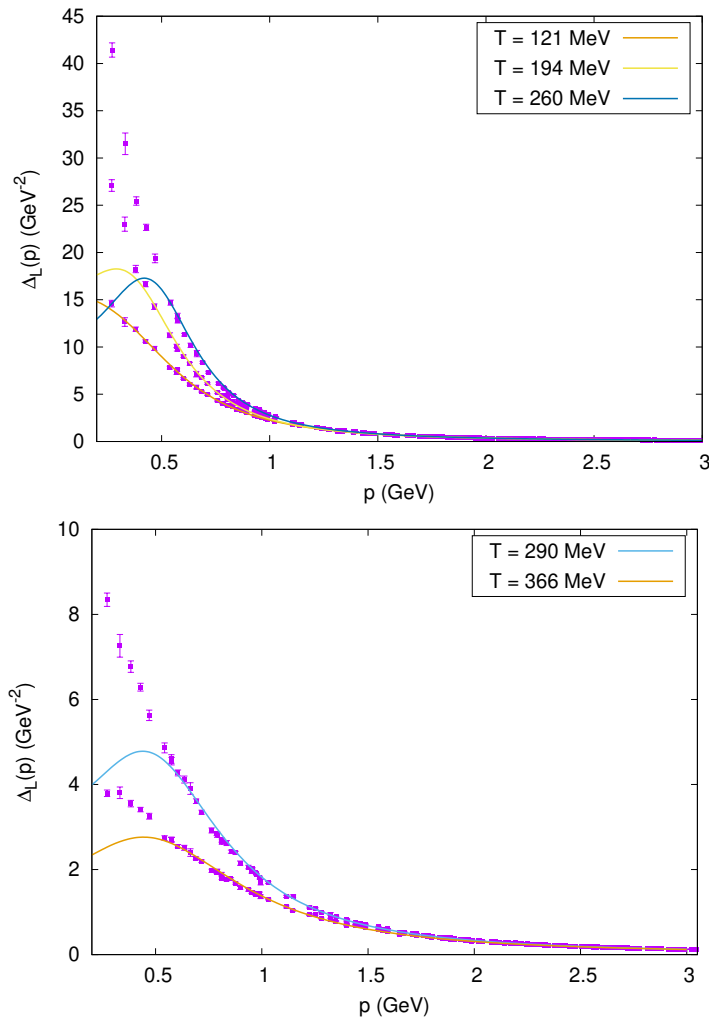


Figure 4.6: Longitudinal component of the Landau-gauge Euclidean gluon propagator at zero Matsubara frequency ($n = 0$) as a function of the modulus $|\vec{p}|$ of the 3-dimensional momentum, for $T < T_c$ (top) and $T > T_c$ (bottom). Multiplicatively renormalized at $\mu_0 = 4$ GeV. Lattice data from [SOBC14].

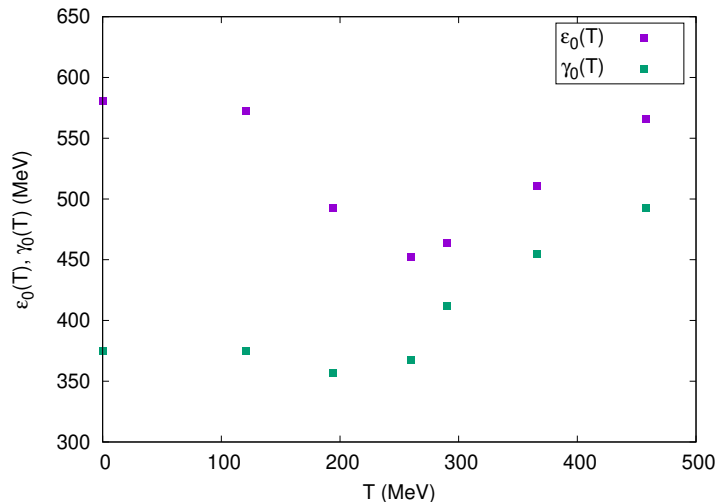


Figure 4.7: Real ($\varepsilon_0(T)$) and imaginary part ($\gamma_0(T)$) of the gluon pole at vanishing spatial momentum $\vec{p} = 0$ as functions of the temperature, obtained from the transverse component of the Landau-gauge gluon propagator.

Since the transverse component of the SME gluon propagator was found to be in good quantitative agreement with the lattice data down to vanishingly small spatial momenta, the results we just presented can be exploited to compute the position of the pole of the gluon propagator at $\vec{p} = 0$ – that is, the pole mass of the gluon – as a function of the temperature³. Recall that, for $\vec{p} = 0$ and $p^4 \neq 0$, the two components of the gluon propagator coincide. Therefore, assuming that the determination of the gluon mass parameter $m(T)$ carried out by fitting the transverse propagator (Fig. 4.4) remains valid at non-zero Matsubara frequencies, what follows can in principle be interpreted to hold for both the components of the propagator.

By extending the imaginary-time component p^4 of the Euclidean momentum from the set of Matsubara frequencies $p^4 \in 2\pi T \mathbb{N}$ to the whole complex plane $p^4 \in \mathbb{C}$, the equation $\Delta_T^{-1}(p^4, \vec{p} = \vec{0}, T) = 0$ can be solved for $p^4 = -i(\varepsilon_0(T) - i\gamma_0(T))$ at $m = m(T)$ – the latter having been obtained by fitting the transverse data – to yield the temperature-dependent mass $\varepsilon_0(T)$ and the zero-momentum damping factor $\gamma_0(T)$ of the gluon quasi-particles [SC21]. The solutions are shown in Fig. 4.7. At $T = 0$, the gluon poles are found at the position already reported in Sec. 3.2.3, namely

$$\varepsilon_0(T = 0) = \pm 0.5810 \text{ GeV}, \quad \gamma_0(T = 0) = \pm 0.3751 \text{ GeV} . \quad (4.11)$$

As the temperature increases, the mass $\varepsilon_0(T)$ first decreases to about 450 MeV at $T = T_c$, and then starts to increase again, linearly with the temperature, for $T > T_c$. A similar pattern is followed by the damping rate, with some uncertainty on the temperature at which $\gamma_0(T)$ becomes an increasing function of the temperature⁴ after having reached its minimum value of about 350 MeV. The linear increase of the pole mass and zero-momentum

³A similar calculation was carried out in [Sir17c] under the assumption that the gluon mass parameter and additive renormalization constants can be approximated by their zero-temperature value at $T \neq 0$.

⁴ $\gamma_0(T)$ apparently starts to increase at a temperature $T < T_c$, rather than at $T = T_c$. However, this is most probably caused by the uncertainty that affects the underlying parameters, which is about ± 50 MeV for the mass parameter.

damping rate found at high temperatures is typical of massless particles [KG06]. An estimate of the full dispersion relations – that is, of the gluon energy $\varepsilon_{|\vec{p}|}(T)$ and damping rate $\gamma_{|\vec{p}|}(T)$ as a function of the spatial momentum $|\vec{p}|$ – at finite temperature can be found in [SC21].

The results presented in this section paint the picture of gluon quasi-particles which behave as massive below the critical temperature, and then become massless above $T = T_c$, where $\varepsilon_0(T)$ and $\gamma_0(T)$ can be interpreted, respectively, as a thermal mass and a thermal zero-momentum damping rate. Since $T_c \approx 270$ MeV is the temperature at which the deconfinement phase transition occurs, we see that the SME predicts a strong correlation between dynamical mass generation and confinement in the gauge sector.

As for the accuracy of the Screened Massive Expansion at finite temperature, we saw that tuning the gluon mass parameter separately for the transverse and longitudinal components of the gluon propagator is able to provide an effective description of the dynamics of the gluons which is in good agreement with the lattice data at large spatial momenta, while being insufficient at small momenta as far as the longitudinal component is concerned. A proposal for an extension of the SME that would take into account the different behavior of the longitudinal and transverse gluon mass was advanced in [SC21].

4.2 The Screened Massive Expansion of full QCD

4.2.1 Dynamical mass generation in the quark sector

It is a well-known fact that, due to the strong interactions, at low energies the quarks acquire a mass which for the lightest flavors is much larger than the quark mass parameter present in the Lagrangian. Such a phenomenon can be interpreted as a remnant of the violation of chiral symmetry that occurs in the limit in which the quarks are massless. In what follows, we give a brief introduction to this topic.

As we saw in Sec. 2.2.2, the non-vanishing of the quark condensate $\langle \bar{\psi}\psi \rangle$ triggers the dynamical generation of a mass for the massless quarks. $\langle \bar{\psi}\psi \rangle$ is a gauge-invariant quantity which, in the presence of chiral symmetry, would be forbidden to have a non-zero value. Indeed, if chiral transformations⁵,

$$\psi \rightarrow e^{i\alpha\gamma^5} \psi, \quad \bar{\psi} \rightarrow \bar{\psi} e^{i\alpha\gamma^5} \quad (\alpha \in \mathbb{R}), \quad (4.12)$$

were a symmetry of the vacuum, then the VEV of the quark operator $\bar{\psi}\psi$, which is not invariant under such transformations since

$$\bar{\psi}\psi = \psi_L^\dagger \psi_R + \psi_R^\dagger \psi_L \rightarrow \bar{\psi} e^{2i\alpha\gamma^5} \psi = e^{2i\alpha} \psi_L^\dagger \psi_R + e^{-2i\alpha} \psi_R^\dagger \psi_L, \quad (4.13)$$

would necessarily vanish. On the other hand, the fact that $\langle \bar{\psi}\psi \rangle \neq 0$ signals the violation of chiral symmetry.

Symmetry under chiral transformations, which in the limit of massless quarks leave the classical quark Lagrangian invariant given that, for every quark flavor,

$$e^{i\alpha\gamma^5} \gamma^\mu e^{i\alpha\gamma^5} = \gamma^\mu e^{-i\alpha\gamma^5} e^{i\alpha\gamma^5} = \gamma^\mu \quad \Longrightarrow \quad \bar{\psi} e^{i\alpha\gamma^5} i\not{D} e^{i\alpha\gamma^5} \psi = \bar{\psi} i\not{D} \psi, \quad (4.14)$$

can be violated for a multitude of reasons. First of all, it may happen that the symmetry is *anomalous*, in the sense that it cannot be realized at the level of the quantum theory. The

⁵We recall that the fifth gamma matrix γ^5 is defined as $\gamma^5 = i\gamma^0\gamma^1\gamma^2\gamma^3$ and has vanishing anticommutation relations with the other gamma matrices, $\{\gamma^\mu, \gamma^5\} = 0$. Also, $\gamma^5 = \mathcal{P}_R - \mathcal{P}_L$, where $\mathcal{P}_{L,R}$ are the projectors onto the left- and right-handed components of the Dirac field.

most renowned example of an anomalous chiral symmetry is the U(1) axial symmetry of full QCD, under which the up (u), down (d) and strange (s) quark fields – taken to be massless – transform as

$$u \rightarrow e^{i\alpha\gamma^5} u, \quad d \rightarrow e^{i\alpha\gamma^5} d, \quad s \rightarrow e^{i\alpha\gamma^5} s. \quad (4.15)$$

The divergence of the corresponding current,

$$j_5^\mu = \bar{u}\gamma^\mu\gamma^5 u + \bar{d}\gamma^\mu\gamma^5 d + \bar{s}\gamma^\mu\gamma^5 s, \quad (4.16)$$

instead of vanishing as would be suggested by the classical field equations, acquires a term which is quadratic in the gluon field-strength tensor,

$$\partial_\mu j_5^\mu = \frac{3N\alpha_s}{8\pi} \epsilon^{\mu\nu\sigma\tau} F_{\mu\nu}^a F_{\sigma\tau}^a, \quad (4.17)$$

implying that the symmetry is violated at the quantum level.

Second, it may happen that, while being a symmetry of the quantum theory, the vacuum state of the latter is not invariant under the chiral transformation. As a consequence, the symmetry is spontaneously broken in the vacuum. An example of a spontaneously broken chiral symmetry is the SU(n_f) axial symmetry – with n_f the number of quarks –, which in the case $n_f = 3$ acts on the up, down and quark fields as

$$\begin{pmatrix} u \\ d \\ s \end{pmatrix} \rightarrow e^{i\alpha^A T_A \gamma^5} \begin{pmatrix} u \\ d \\ s \end{pmatrix}, \quad (4.18)$$

where the T_A 's ($A = 1, \dots, 8$) are Gell-Mann matrices which generate the flavor SU(3) transformations. The currents associated to this symmetry,

$$j_{5A}^\mu = \bar{Q}\gamma^\mu T_A Q, \quad Q = \begin{pmatrix} u \\ d \\ s \end{pmatrix}, \quad (4.19)$$

are indeed conserved, $\partial_\mu j_A^\mu = 0$; nonetheless, the vacuum state of QCD is not invariant under such transformations, resulting in chiral symmetry breaking (CSB) and in the existence of massless pseudo-scalar Goldstone bosons, namely – in the limit of massless quarks – the pions, kaons and lightest eta mesons.

Finally, chiral symmetry can be explicitly broken by the presence of quark mass terms $\bar{\psi}M\psi$ in the Lagrangian, which, as we saw earlier, are not invariant under chiral transformations. This is what happens in real-world QCD, where the pions, kaons and lightest eta mesons, instead of being massless as a consequence of CSB, possess masses that range from 135 MeV to 548 MeV.

Despite chiral symmetry not being an exact symmetry of full QCD, the mechanisms at play in chiral symmetry violation (either through anomalies or through chiral symmetry breaking) still cause an enhancement of the quark masses in the infrared. For the light quarks, this enhancement makes up for the majority of the mass with which they propagate at zero momentum; for instance, quarks with a Lagrangian mass of a few MeV turn out to propagate with masses ≈ 300 -400 MeV in the $p \rightarrow 0$ limit. Such a phenomenon cannot be described in the framework of ordinary perturbation theory for two main reasons. First of all, the radiative pQCD corrections which contribute to the dressing of the quark masses are far too small to increase the values of the latter by orders of magnitude at energy scales in which the strong running coupling is well behaved. Second of all, the breakdown of ordinary perturbation theory in the infrared prevents us from computing the momentum-dependent quark masses at low energies, where their enhancement occurs.

The main objective of the following sections is to discuss how a shift of the quark Lagrangian similar to the one performed in Chpt. 3 in the gluon sector of pure Yang-Mills theory can be exploited in full QCD to describe the phenomenon of dynamical mass generation in the quark sector, with a focus on the light quarks.

4.2.2 The massive shift of the quark Lagrangian

Recall that the quark Lagrangian \mathcal{L}_q that appears in the Faddeev-Popov action of full QCD can be expressed in terms of the bare fields, coupling and quark mass as

$$\mathcal{L}_q = \bar{\psi}_B(i\cancel{\partial} - M_B + g_B \gamma^\mu A_{B\mu}^a T_a)\psi_B . \quad (4.20)$$

Given that, in what follows, we will not get into the specifics of renormalization – which is discussed at length in [CRBS21] –, we can assume that all the quantities in the above equation are renormalized and finite. In particular, we will denote the Lagrangian quark mass with a subscript R and call it the *renormalized mass*, in order to distinguish it from the mass developed by the quark in the infrared regime, whose scale is set by a parameter M which we will refer to as the *chiral mass*. The expression from which we will start for our study of the quark sector is then

$$\mathcal{L}_q = \bar{\psi}(i\cancel{\partial} - M_R + g \gamma^\mu A_\mu^a T_a)\psi . \quad (4.21)$$

In the previous section, we noted that the infrared enhancement of the light quark's mass caused by chiral symmetry violation cannot be described in ordinary perturbation theory, since the latter is unable to modify the value of any parameter by orders of magnitude via the radiative corrections. From a mathematical perspective, this translates to the fact that the scale M of the infrared quark mass cannot be computed from the light quark's renormalized mass M_R by truncating the ordinary perturbative series to any finite order in the coupling constant. Therefore, when setting up perturbation theory in the quark sector, we find ourselves in a similar situation to that which occurs in the gluon sector.

If the aim of the perturbative expansion is to describe the low-energy dynamics of the light quarks, we should expect that a more accurate approximation of the exact results would be obtained by expanding around the infrared quark mass M , rather than around the renormalized value M_R . This can be achieved by splitting the quark Lagrangian \mathcal{L}_q as

$$\mathcal{L}_q = \mathcal{L}_{q,0} + \mathcal{L}_{q,\text{int}} \quad (4.22)$$

with

$$\mathcal{L}_{q,0} = \bar{\psi}(i\cancel{\partial} - M)\psi , \quad \mathcal{L}_{q,\text{int}} = \bar{\psi}(g\cancel{A}^a T_a + M - M_R)\psi , \quad (4.23)$$

and by using $\mathcal{L}_{q,0}$ as the order zero of the perturbative series and $\mathcal{L}_{q,\text{int}}$ as the interaction Lagrangian. Note that the split does not modify the quark Lagrangian \mathcal{L}_q as a whole. It is understood that the expansion point for the gluon propagator must be chosen massive as in Chpt. 3 in order to capture the correct infrared behavior of the gluons in addition to that of the quarks.

As a consequence of the split in Eq. (4.22), the zero-order quark propagator $S_M(p)$ reads

$$S_M(p) = \frac{i}{\cancel{p} - M} , \quad (4.24)$$

with the chiral mass M replacing the renormalized mass M_R . Furthermore, two new quark two-point vertices arise in the interaction action:

$$S_{q,\text{int}} = -i \int d^4x \bar{\psi}(ig\cancel{A}^a T_a + \delta\Gamma_{q,1} + \delta\Gamma_{q,2})\psi , \quad (4.25)$$

where

$$\delta\Gamma_{q,1} = iM, \quad \delta\Gamma_{q,2} = -iM_R. \quad (4.26)$$

The latter essentially play the same role as the gluon mass counterterm, and will thus be referred to as the quark mass counterterms.

$$\begin{aligned} \Sigma = & \text{---} \times_1 \text{---} + \text{---} \times_2 \text{---} + \text{---} \text{---} \text{---} \text{---} + \\ & (1a) \quad (1b) \quad (2a) \\ & + \text{---} \text{---} \text{---} \text{---} \times_1 \text{---} + \text{---} \text{---} \text{---} \text{---} \times_2 \text{---} + \text{---} \text{---} \text{---} \text{---} \times \text{---} \text{---} + \dots \\ & (2b) \quad (2c) \quad (2d) \end{aligned}$$

Figure 4.8: Diagrams for the one-loop SME quark self-energy

The dressed quark propagator $S(p)$ computed via Eq. (4.22) can be expressed in terms of the quark self-energy $\Sigma(p)$ as

$$S(p) = \frac{i}{\not{p} - M - \Sigma(p)}. \quad (4.27)$$

The quark mass counterterms in Eq. (4.26) contribute to $\Sigma(p)$ already at tree level via the diagrams (1a) and (1b) displayed in Fig. 4.8; it is easy to see that the quark self-energy $\Sigma(p)$ can be put in the form

$$\Sigma(p) = -M + M_R + \Sigma^{(\text{loop})}(p), \quad (4.28)$$

where the first two terms are provided by $\delta\Gamma_{q,1/2}$, whereas $\Sigma^{(\text{loop})}(p)$ is the contribution coming from the loops of the expansion. Since

$$S(p) = \frac{i}{\not{p} - M_R - \Sigma^{(\text{loop})}(p)}, \quad (4.29)$$

it is clear that, in the framework of the Screened Massive Expansion, the infrared enhancement of the quark mass, if any, will originate non-trivially from the loops, and not from the tree-level chiral mass present in Eq. (4.27), just like in the gluon sector the gluon mass is generated by the loops and not by the tree-level gluon mass term m^2 .

By defining functions $A(p^2)$ and $B(p^2)$ such that

$$\begin{aligned} A(p^2) &= 1 - \Sigma_V(p^2), \\ B(p^2) &= M_R + \Sigma_S(p^2), \end{aligned} \quad (4.30)$$

where $\Sigma_V(p^2)$ and $\Sigma_S(p^2)$ are, respectively, the vector and the scalar component of $\Sigma^{(\text{loop})}(p)$,

$$\Sigma^{(\text{loop})}(p) = \not{p} \Sigma_V(p^2) + \Sigma_S(p^2), \quad (4.31)$$

the dressed quark propagator $S(p)$ can be put in the form

$$S(p) = \frac{iZ(p^2)}{\not{p} - \mathcal{M}(p^2)}, \quad (4.32)$$

where the functions $Z(p^2)$ and $\mathcal{M}(p^2)$, given by

$$Z(p^2) = \frac{1}{A(p^2)}, \quad \mathcal{M}(p^2) = \frac{B(p^2)}{A(p^2)}, \quad (4.33)$$

are known respectively as the quark Z -function and mass function. By comparing Eq. (4.32) with the general form of the zero-order quark propagator, we see that $\mathcal{M}(p^2)$ plays the role of the momentum-dependent mass of the quark. In particular, $\mathcal{M}(p^2)$ determines the position of the poles of the quark propagator, given that

$$\frac{1}{\not{p} - \mathcal{M}(p^2)} = \frac{\not{p} + \mathcal{M}(p^2)}{p^2 - \mathcal{M}^2(p^2)} = \infty \quad \iff \quad p^2 = \mathcal{M}^2(p^2). \quad (4.34)$$

In the zero-momentum limit, the quark mass function approaches the value

$$\mathcal{M}(0) = \frac{M_R + \Sigma_S(0)}{1 - \Sigma_V(0)}. \quad (4.35)$$

Therefore, if the components of the quark self-energy do not vanish at $p = 0$, $\Sigma_V(0), \Sigma_S(0) \neq 0$, the zero-momentum mass of the quark will be different from its renormalized mass, $\mathcal{M}(0) \neq M_R$. As we will see, this indeed turns out to be the case. In the framework of the Screened Massive Expansion, the energy scale for the difference between $\mathcal{M}(0)$ and M_R will be set by M , and not by M_R , since as a consequence of the shift of the quark action it is the chiral mass M that runs into the quark loops. By this mechanism, the infrared enhancement of the quark mass is made possible in the SME.

To end this section, we observe that – at variance with ordinary pQCD – the relation $\mathcal{M}(0) \neq M_R$ also holds within the SME in the chiral limit ($M_R = 0$). In particular, the SME quark propagator can acquire a mass even when no mass term is present in the Lagrangian, as discussed in Secs. 2.2.2 and 4.2.1. The chiral limit of the Screened Massive Expansion was investigated in [Sir16a], where the first results for full QCD were presented⁶.

4.2.3 The quark propagator in the Landau gauge

To compute the SME quark propagator, we follow the prescriptions laid down in Sec. 3.1.2 regarding the number of mass counterterms to retain at a given order in perturbation theory. In Secs. 3.1.3 and 3.1.4 the ghost and gluon propagator were expanded to one loop and three vertices; in the quark sector we will do the same, working within the truncation scheme that in [CRBS21] was termed the vertex-wise scheme. Additionally, we will present some results obtained in the so-called complex-conjugate scheme, to be illustrated later on. A third truncation scheme – termed the minimalistic scheme – was investigated in [CRBS21] and will not be reported in what follows. The results presented in this section were obtained in the Landau gauge.

The diagrams with at most one loop and at most three vertices which contribute to the SME quark self-energy are displayed in Fig. 4.8. In the figure, the crosses denoted with 1 and 2 are the quark mass counterterms $\delta\Gamma_{q,1}$ and $\delta\Gamma_{q,2}$, whereas the unlabeled cross is the gluon mass counterterm $\delta\Gamma_{\mu\nu}^{ab}$ – Eq. (3.11). As we saw in Sec. 3.1, diagrams with one gluon mass counterterm can be computed from the corresponding uncrossed diagrams by differentiating the latter with respect to the gluon mass parameter. Similarly, since

⁶We should mention that [Sir16a] made use of lattice data for the quark mass function whose large errors – customary in the context of unquenched calculations in the chiral limit – only allowed for a qualitative comparison with the results of the SME.

$$\frac{i}{\not{p} - M}(i\lambda)\frac{i}{\not{p} - M} = -\lambda \frac{\partial}{\partial M} \frac{i}{\not{p} - M}, \quad (4.36)$$

where $\lambda = M, -M_R$, diagrams with one quark mass counterterm can be computed from the uncrossed diagrams by differentiating them with respect to the quark chiral mass M . In particular, we find that

$$\begin{aligned} \Sigma^{(2b)}(p) &= -M \frac{\partial}{\partial M} \Sigma^{(2a)}(p), \\ \Sigma^{(2c)}(p) &= M_R \frac{\partial}{\partial M} \Sigma^{(2a)}(p), \\ \Sigma^{(2d)}(p) &= -m^2 \frac{\partial}{\partial m^2} \Sigma^{(2a)}(p), \end{aligned} \quad (4.37)$$

where $\Sigma^{(2a,2b,2c,2d)}(p)$ denote the contributions to $\Sigma(p)$ due to diagrams (2a) to (2d).

Diagram (2a) contains a mass divergence proportional to the quark chiral mass M which has no counterpart in ordinary perturbation theory – the mass divergences of the latter being proportional to M_R . Diagram (2b) cancels such a divergence by a mechanism analogous to the one discussed in Sec. 3.1.4 when addressing the gluon mass divergences. On the other hand, diagram (2c) contains the ordinary mass divergence $\propto M_R$, which only contributes to the renormalization of M_R itself⁷. Finally, diagram (2d) is convergent. Since in the Landau gauge none of the one-loop diagrams contain vector divergences – that is, divergences proportional to the Dirac matrix \not{p} –, the sum (2a+2b+2c+2d) only contains a divergence proportional to M_R , which is eliminated by renormalizing M_R .

As for the finite parts of diagrams (2b) and (2c), since

$$\Sigma^{(2b)}(p) + \Sigma^{(2c)}(p) = -(M - M_R) \frac{\partial}{\partial M} \Sigma^{(2a)}(p), \quad (4.38)$$

we see that for the light quarks – $M_R \ll M$ – we have $|\Sigma^{(2c)}(p)| \ll |\Sigma^{(2b)}(p)|$. Therefore, in what follows we will neglect⁸ the finite part of $\Sigma^{(2c)}(p)$ [CRBS21].

An explicit calculation carried out in Euclidean space yields⁹

$$\Sigma_V(p^2) = \frac{\alpha_s}{3\pi} \sigma_V(p^2), \quad \Sigma_S(p^2) = \frac{\alpha_s}{\pi} \sigma_S(p^2), \quad (4.39)$$

for the vector and the scalar component of the quark self-energy, where the functions $\sigma_V(p^2)$ and $\sigma_S(p^2)$ are reported in [CRBS21]. In terms of these, the Euclidean quark Z - and mass function can be expressed as

$$Z(p^2) = \frac{1}{Z_\psi - \frac{\alpha_s}{3\pi} \sigma_V(p^2)}, \quad \mathcal{M}(p^2) = \frac{M_R + \frac{\alpha_s}{\pi} \sigma_S(p^2)}{Z_\psi - \frac{\alpha_s}{3\pi} \sigma_V(p^2)}, \quad (4.40)$$

where for completeness in the above equations we have reinstated the quark field renormalization factor Z_ψ . We remark that, because of the absence of vector divergences in the Landau-gauge one-loop quark self-energy, Z_ψ is a finite quantity. By defining constants

$$h_0 = \frac{3\pi}{\alpha_s} Z_\psi, \quad k_0 = \frac{\pi}{\alpha_s} M_R, \quad Z_S = \frac{3\pi}{\alpha_s}, \quad (4.41)$$

$Z(p^2)$ and $\mathcal{M}(p^2)$ can be put in the form

$$Z(p^2) = \frac{Z_S}{h_0 - \sigma_V(p^2)}, \quad \mathcal{M}(p^2) = \frac{3[k_0 + \sigma_S(p^2)]}{h_0 - \sigma_V(p^2)}. \quad (4.42)$$

⁷More details on this can be found in [CRBS21].

⁸We checked that this does not substantially affect the results.

⁹In what follows we omit the subscripts E from quantities defined in Euclidean space.

The constant Z_S can be fixed by renormalizing $Z(p^2)$ in the MOM scheme,

$$Z(\mu^2) = 1 \quad (4.43)$$

at the initial renormalization scale μ .

M_{lat} (MeV)	M (MeV)	h_0	k_0 (MeV)
18	268.0	2.656	-16.9
18*	197.6	2.051	6.8
36	228.7	2.418	11.5
54	221.4	2.577	40.0
72	238.4	2.977	70.1
90	249.0	3.207	102.5

Table 4.1: Parameters obtained by fitting the lattice data of [KBL⁺05] for the Landau-gauge Euclidean quark mass function. The asterisked row was obtained by fixing $k_0 = 6.8$ and fitting the remaining parameters (see the text for details). $m = 0.6557$ GeV.

M_{lat} (MeV)	α_s	M_R (MeV)	P_0 (MeV)
18	2.605	-14.0	$\pm 387.4 \pm 180.9i$
18*	3.128	6.8	$\pm 349.2 \pm 193.1i$
36	2.788	10.2	$\pm 371.7 \pm 185.4i$
54	2.663	33.9	$\pm 375.2 \pm 177.2i$
72	2.393	53.4	$\pm 392.9 \pm 167.6i$
90	2.261	73.8	$\pm 410.8 \pm 170.2i$

Table 4.2: Coupling constant, renormalized mass and quark poles corresponding to the parameters in Tab. 4.1.

In [CRBS21], the Landau-gauge Euclidean quark propagator computed in the Screened Massive Expansion was compared with the quenched lattice data of [KBL⁺05] for quarks with masses M_{lat} ranging from 18 MeV to 271 MeV¹⁰. In what follows, we report our results up to $M_{\text{lat}} = 90$ MeV, for which the condition $M_R \ll M$ is better fulfilled. The constants h_0 and k_0 that appear in Eq. (4.42) were fitted from the data for the quark mass function $\mathcal{M}(p^2)$ together with the chiral mass M for each separate value of M_{lat} . As for the value of the gluon mass parameter m^2 , we used $m = 0.6557$ GeV, like in Sec. 3.2. Albeit having been determined in pure Yang-Mills theory, this value is appropriate for comparisons with

¹⁰Roughly speaking, M_{lat} is the mass that appears at tree level in the bare lattice quark propagator. See [KBL⁺05] for more details.

quenched lattice data, since the latter do not take into account the corrections to the gluon propagator due to the interactions with the quarks [CRBS21].

The outcome of the fit is reported in Tab. 4.1. One may notice that the value of the constant k_0 obtained by fitting the $M_{\text{lat}} = 18$ MeV dataset (first row) is negative, in contradiction with the definition given in Eq. (4.41), which for $M_R, \alpha_s \geq 0$ would necessarily require $k_0 \geq 0$. This issue was investigated in depth in [CRBS21], where it was noted that at high energies the $M_{\text{lat}} = 18$ MeV data of [KBL⁺05] are plagued by large oscillations – presumably caused by discretization errors – which make it very difficult to unambiguously extract a value of k_0 from the lattice results. As an alternative, in Tab. 4.1 we record a second determination of the $M_{\text{lat}} = 18$ MeV parameters (second row, asterisked), which was obtained by fixing $k_0 = 6.8$ MeV¹¹, a value which – modulo oscillations – is still able to reproduce the lattice data with good precision.

In Tab. 4.2, we report the values of the coupling constant α_s and of the renormalized mass M_R and the position of the poles of the quark propagator corresponding to the parameters in Tab. 4.1. By Eqs. (4.40), (4.41) and (4.42), α_s and M_R can be computed from h_0 and k_0 via

$$\alpha_s = 3\pi[h_0 - \sigma_V(\mu^2)]^{-1}, \quad M_R = \frac{3k_0}{h_0}, \quad (4.44)$$

where the renormalization scale μ was fixed to 4 GeV. As discussed in [CRBS21], one should be careful when interpreting α_s with the actual value of the coupling constant at the scale μ , mainly because the former is defined starting from the (renormalization of the) function $Z(p^2)$, which to one loop – as we will see in a moment – is not well-behaved in the SME. The position of the quark poles is found by first solving the equation

$$p^2 + \mathcal{M}^2(p^2) = 0 \quad (4.45)$$

in the complexified Euclidean space, and then converting the solutions to Minkowski space.

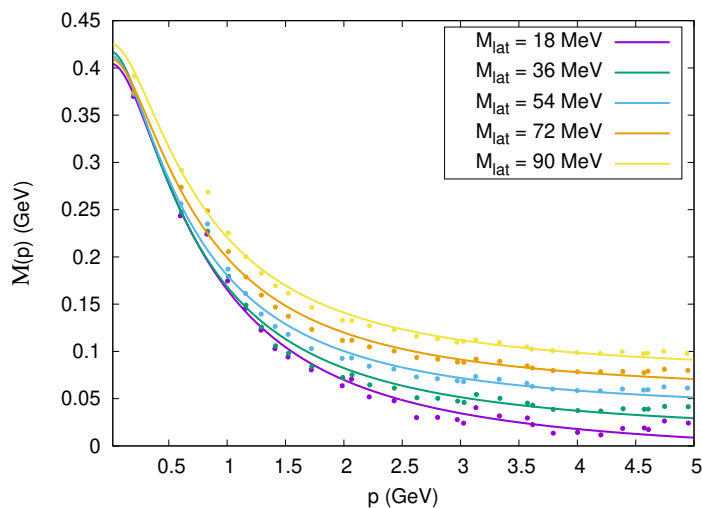


Figure 4.9: Euclidean quark mass function in the Landau gauge ($\xi = 0$) for different values of the quark mass. Colored curves: SME with h_0 , k_0 and M fitted from the lattice data (Tab. 4.1). Dots: lattice data from [KBL⁺05]. $m = 0.6557$ GeV.

¹¹More details can be found in [CRBS21] for the reasoning that leads to this (non-unique) choice.

In Fig. 4.9 we display the SME quark mass functions $\mathcal{M}(p^2)$ computed by making use of the parameters in Tab. 4.1, together with the lattice data of [KBL⁺05]. As we can see, at zero momentum the quarks develop a mass $\mathcal{M}(0) \approx 400$ MeV which is much larger than the UV limit of $\mathcal{M}(p^2)$. While this infrared enhancement could not have been described within ordinary perturbation theory, the Screened Massive Expansion succeeds in reproducing the correct behavior of the mass function, thanks to the latter being dependent on two mass scales: a renormalized mass M_R , whose value is relevant to the UV regime, and a “chiral” mass M , which sets the scale for $\mathcal{M}(0)$. In doing so, it uses values of the coupling which are not too far from that of the SME running coupling at its maximum (Sec. 3.3). Notably, the value of the zero-momentum mass is nearly the same for all quarks with lattice masses up to 90 MeV, confirming that in the deep infrared the origin of the quark masses is almost entirely accounted for by chiral symmetry violation. On the other hand, M_R increases monotonically with M_{lat} and is of the same order as the value of $\mathcal{M}(p^2)$ evaluated at high energies. As for the chiral mass M , we find that its value also increases with M_{lat} , indicating that M should be interpreted as a mass scale appropriate to the quark under examination, despite it yielding a value of $\mathcal{M}(0)$ which is independent from M_{lat} .

The quark poles calculated from the fitted mass functions are complex-conjugated (see Tab. 4.2), like in the gluon sector. This can be regarded both as evidence for quark confinement and as a hint that the quarks may be confined by a similar underlying mechanism to that which is at play for the gluons. The real and the imaginary part of the quark poles for $M_{\text{lat}} \leq 90$ MeV are found in the range [349, 411] MeV and [170, 193] MeV, respectively, with the former increasing with M_{lat} and the latter slightly decreasing. In particular, we see that the energy scale for the poles is set by the chiral mass, rather than by M_R .

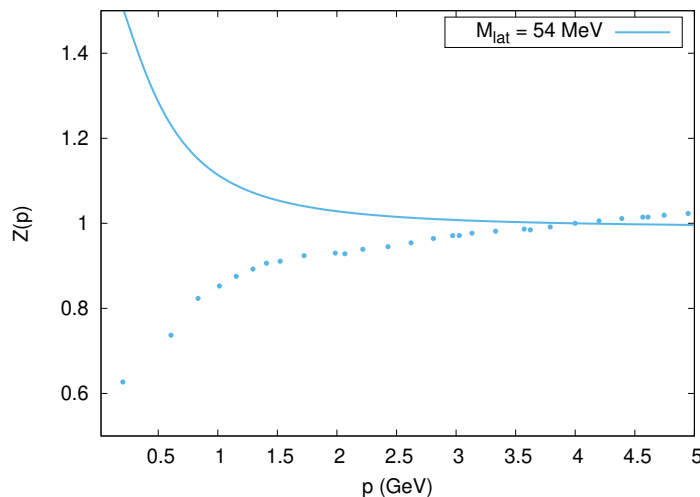


Figure 4.10: Euclidean quark Z -function in the Landau gauge ($\xi = 0$) for $M_{\text{lat}} = 54$ MeV. Blue curve: SME with h_0 , k_0 and M fitted from the lattice data (Tab. 4.1). Dots: lattice data from [KBL⁺05]. $m = 0.6557$ GeV.

In Fig. 4.10 we show the SME quark Z -function computed by the parameters in Tab. 4.1 for the single value $M_{\text{lat}} = 54$ MeV, again with the lattice data of [KBL⁺05]; as the results obtained for the other quark masses are similar to those in the figure, we will not display them in what follows. Clearly, the Screened Massive Expansion is not able to reproduce the correct behavior of $Z(p^2)$ to one loop, yielding a function which decreases with momentum,

instead of increasing as is found on the lattice. This is most probably due to the fact that – as first argued by [PTW14] – the one-loop corrections to the vector component of the Landau-gauge quark self-energy are unusually small, even vanishing at $m^2 = 0$, so that the two-loop corrections must necessarily be taken into account. And indeed, in the framework of the Curci-Ferrari model, it was shown [BGPR21] that the behavior of the Z -function can be fixed by going to two loops. Within the Screened Massive Expansion, similar knowledge is gained by computing the quark propagator in an alternative truncation scheme which in [CRBS21] was termed the complex-conjugate (CC) scheme.

In the CC scheme, the one-loop quark self-energy is calculated by replacing the zero-order gluon propagator with the principal part of the dressed propagator in the internal gluon lines of the Feynman diagrams,

$$\Delta_m(p^2) = \frac{1}{p^2 + m^2} \rightarrow \frac{1}{2\text{Re}\{R\}} \left[\frac{R}{p^2 + p_0^2} + \frac{\bar{R}}{p^2 + \bar{p}_0^2} \right], \quad (4.46)$$

where p_0^2, \bar{p}_0^2, R and \bar{R} are, respectively, the poles and the residues of the optimized gluon propagator of Sec. 3.2.3, and the normalization of the principal part is chosen so that the latter equals $1/p^2$ at high energies. As we saw in Sec. 3.2.3, the principal part of the gluon propagator yields a good approximation of the full propagator provided that the former is multiplied by a constant. Since in the self-energy the zero-order gluon propagator always appears multiplied by the coupling constant α_s , changing the normalization of the gluon propagator amounts to a redefinition of the coupling. Therefore, the replacement defined by Eq. (4.46) allows us to compute the quark propagator in an approximation which takes into account the radiative corrections to the gluon propagator. While not being equivalent to a full two-loop calculation, the truncation provided by the CC scheme still implicitly includes contributions from the higher orders in the gluon perturbative series.

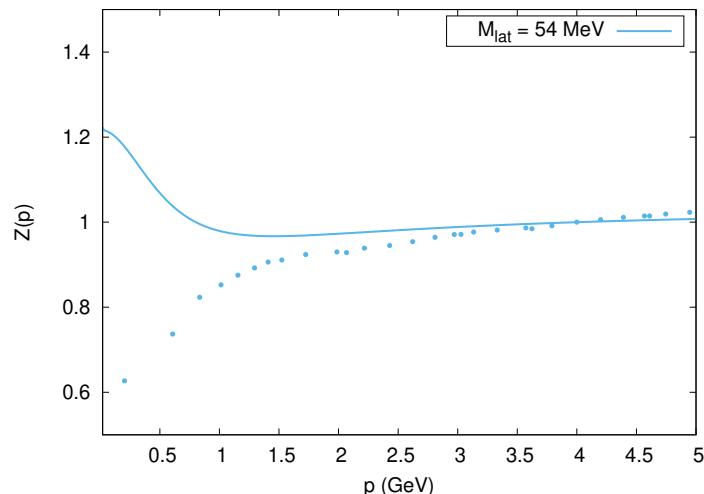


Figure 4.11: Euclidean quark Z -function in the Landau gauge ($\xi = 0$) for $M_{\text{lat}} = 54$ MeV. Blue curve: CC-scheme SME with h_0, k_0 and M fitted from the lattice data. Dots: lattice data from [KBL⁺05].

The SME Z -function computed in the CC scheme is shown in Fig. 4.11, again for $M_{\text{lat}} = 54$ MeV. As we can see, the higher-order corrections to the gluon propagator change

the high-energy behavior of $Z(p^2)$, turning it into an increasing function of momentum – as it should be. Nonetheless, the quantitative agreement with the lattice data is still not good in the UV; moreover, at low energies, the CC-scheme Z -function still shows the incorrect behavior, indicating that a full two-loop calculation is required in order for the SME to be able to reproduce the lattice data. Further details on the CC scheme can be found in [CRBS21].

4.2.4 Conclusions

Despite not being as theoretically developed as in the gluon sector, lacking optimization procedures which would allow us to compute the parameters that appear in the quark propagator from first principles, the Screened Massive Expansion of full QCD still provides us with an accurate picture of dynamical mass generation in the quark sector. By shifting the expansion point for the quark perturbative series, the SME is able to incorporate a parameter M – the chiral mass – into the expressions, that acts as the energy scale for the mass $\mathcal{M}(0)$ with which the quarks propagate at zero momentum.

In the framework of the Screened Massive Expansion, the infrared enhancement of the quark masses originates from the radiative corrections to the propagator, as expected for a truly dynamical phenomenon. The Euclidean mass functions $\mathcal{M}(p^2)$ computed for the light quarks are found to be in good agreement with the quenched lattice data over a wide range of (lattice) masses, displaying saturation at $\mathcal{M}(0) \approx 400$ MeV and a UV tail dominated by the value of the renormalized mass M_R . As a result of $\mathcal{M}(0)$ being much larger than M_R for the light quarks, the latter have poles which, instead of being real and of the order of the renormalized mass, are complex-conjugate and of the order of $\mathcal{M}(0)$, giving evidence for quark confinement. These conclusions are expected to apply also to the chiral limit ($M_R = 0$), although only preliminary results are available at present [Sir16b].

Due to the smallness of the $O(g^2)$ corrections to the Landau-gauge self-energy, the standard one-loop truncation of the Screened Massive Expansion is inadequate for the calculation of the Landau-gauge quark Z -function. An alternative truncation of the quark propagator that takes into account the higher-order corrections to the gluon propagator can be shown to fix the high-energy qualitative behavior of $Z(p^2)$, although neither the quantitative agreement with the lattice data, nor the low-energy limit of the Z -function substantially improved by employing such a method.

5

The Dynamical Model

While the Screened Massive Expansion presented in Chpts. 3 and 4 is able to account for dynamical mass generation in the gluon sector from first principles, the actual mechanism that triggers such a phenomenon is far from made clear by its formalism. Indeed, the shift that defines the SME – motivated by the GEP favoring a massive gluon vacuum over the massless one of ordinary perturbation theory – incorporates the gluon mass into the equations of QCD without explaining where the mass term in the Lagrangian originates from in the first place. A second drawback of the Screened Massive Expansion is the absence of a rigorous prescription for the truncation of its perturbative series at a given loop order. In Sec. 3.1.2, the minimum number of mass counterterms to include in the Feynman diagrams was fixed by the necessary requirement that the resulting Green functions be renormalizable. Their maximum number, on the other hand, was decided on principles of minimality which – albeit certainly meaningful – are perhaps not as strong as one would like.

The main objective of this chapter is to present a second perturbative framework for the computation of the Green functions of QCD at low energies, termed the Dynamical Model (DM). The Dynamical Model addresses both of the aforementioned issues moving from the hypothesis that a gauge-invariant, quadratic gluon condensate $\langle(A^h)^2\rangle$ may be the root cause of DMG in the gauge sector. By making use of local composite operator (LCO) methods, it demonstrates that a mass term for the gluons is generated in the QCD Lagrangian as a consequence of the non-vanishing VEV of $(A^h)^2$. The resulting Landau-gauge perturbative series has features that place it half way in between the Curci-Ferrari Model and the Screened Massive Expansion: with the former it has in common the explicit form of the one-loop gluon polarization and ghost self-energy, whereas with the latter it shares the fact that the gluon mass is generated beyond the tree level, from the loops of the expansion. At variance with the SME, the Dynamical Model can be formulated in such a way that the number of diagrams in the expansion is finite at fixed order in the coupling constant g^2 .

The idea that DMG might be realized via gluon condensation is not at all new; as we saw in the Introduction, the gluon mass has often been studied in the literature in terms of the dimension-4 condensate $\langle F^2 \rangle$ [Cor82, DL89, JA90, Lav91, LW96]. The possibility that a dimension-2 condensate of the form $\langle A^2 \rangle$ [CNZ99, BLYL⁺01, GSZ01, GZ01] may contribute to mass generation (see Sec. 2.2.2), on the other hand, was explored only more recently, the main reason for this being that, since A^2 is not a gauge-invariant operator, the non-vanishing of its VEV could be interpreted as an indication that gauge symmetry is broken in the vacuum. Nonetheless, it was soon realized [CDG⁺05, CDF⁺15] that a suitable generalization of the Landau-gauge operator A^2 could yield a gauge-invariant and BRST-invariant condensate with the right dimensions for playing the role of a gluon mass

parameter m^2 . Such a generalization was achieved by defining a gauge-invariant gluon field, customarily denoted by A^h in the literature, which reduces to the ordinary gluon field A in the Landau gauge.

The field A^h as a tool to systematically investigate the infrared behavior of pure Yang-Mills theory was first introduced in the context of the Gribov-Zwanziger model [CDF⁺15, CDF⁺16a, CDF⁺16b, CDP⁺17, CFPS17, CDG⁺18, MPPS19, DFP⁺19] with the objective of extending the framework of Gribov and Zwanziger to arbitrary covariant gauges while complying with BRST symmetry. The study of A^h and its quadratic condensate in ordinary pure Yang-Mills theory – that is, neglecting the issue of the Gribov copies –, on the other hand, was undertaken in [CFG⁺16, CvEP⁺18] and more recently in [DM20], where the first preliminary expressions for the Landau-gauge gluon and the ghost propagators in the presence of a non-vanishing $\langle(A^h)^2\rangle$ condensate were derived¹.

In the present chapter we take up where [DM20] left off and discuss the generation of the infrared gluon mass within the framework of the Dynamical Model. As we will see, the inclusion of the $\langle(A^h)^2\rangle$ condensate in the action of pure Yang-Mills theory causes the gluons to propagate as massive at tree level. The resulting Feynman diagrams contain internal gluon lines whose mass parameter $m^2 \propto \langle(A^h)^2\rangle$ sets the scale for the non-vanishing of the gluon polarization at zero momentum, yielding a propagator which – as we will explicitly show in the Landau gauge – saturates to a finite non-zero constant at $p = 0$. In other words, a dynamical mass is generated for the gluons in the deep infrared within the Dynamical Model. The condensate $\langle(A^h)^2\rangle$ itself – and m^2 with it – can be computed from first principles by solving a gap equation derived from a suitably defined effective potential.

Our results will be shown to be in good agreement with the lattice data of [DOS16] over a wide range of momenta, once improved by Renormalization Group methods. The latter will also allow us to study the behavior of the Taylor running coupling computed in the Landau gauge, which in the Dynamical Model turns out to be free of Landau poles. The relevance of such a feature was already discussed in the framework of the Screened Massive Expansion, and does not need to be restated here.

This chapter is organized as follows. In Sec. 5.1 we will define the field A^h , derive an effective potential for its quadratic condensate and solve the corresponding gap equation. In the process of doing so, we will show that, on the shell of the gap equation, the Faddeev-Popov action S_{FP} is dynamically equivalent to a second action I whose explicit expression will be reported in Sec. 5.1.3. The action I defines the Dynamical Model, which is the subject of Sec. 5.2. In the latter, we will compute the Landau-gauge gluon and ghost propagators, perform their Renormalization Group improvement and compare our results with the lattice data of [DOS16]. Finally, in Sec. 5.3 we present our conclusions.

Most of the material presented in Sec. 5.1 and in Secs. 5.2.1-5.2.2 is a review of the theory already developed in [CFG⁺16, CvEP⁺18, DM20]. The main contribution of this thesis to the research on the Dynamical Model is the formulation of a new renormalization scheme – the Dynamically Infrared-Safe (DIS) scheme, Sec. 5.2.3 – in which the Landau-gauge propagators are well behaved and are found to reproduce well the lattice data (Sec. 5.2.4). The results of Secs. 5.2.3 and 5.2.4 are part of ongoing work in collaboration with D. Dudal, *et al.*

¹See also [DvERV22] for an application of the method to the study of the deconfinement phase transition.

5.1 The BRST-invariant quadratic gluon condensate

5.1.1 A note on the conventions

For the rest of this chapter, we will slightly change our formalism in order to conform to the conventions used in [CFG⁺16, CvEP⁺18, DM20]. In the latter, like in Sec. 2.4, all of the calculations are carried out in Euclidean space, where the Faddeev-Popov action S_{FP} can be expressed as

$$S_{\text{FP}} = \int d^4x \left(\frac{1}{4} F_{\mu\nu}^a F^{a\mu\nu} + \frac{\alpha}{2} B^a B^a + iB^a \partial^\mu A_\mu^a + \bar{c}^a \partial^\mu D_\mu c^a \right), \quad (5.1)$$

with the Nakanishi-Lautrup field B^a replaced by iB^a and the ghost field c^a replaced by $-c^a$. Because of these replacements, the BRST transformations under which S_{FP} is invariant are given by

$$sA_\mu^a = -D_\mu c^a, \quad sc^a = \frac{g}{2} f^{abc} c^b c^c, \quad s\bar{c}^a = iB^a, \quad sB^a = 0. \quad (5.2)$$

In Eq. (5.1) the symbol α is used in place of ξ ² to denote the gauge parameter.

As for A^U – that is, the field which is obtained by applying a gauge transformation U to the gauge field A –, we will adopt the definition

$$A_\mu^U = U^\dagger \left(A_\mu + \frac{i}{g} \partial_\mu \right) U \quad (5.3)$$

instead of one in which U and U^\dagger are interchanged. With this convention, the consecutive application of two gauge transformations U_1 and U_2 reads

$$(A^{U_1})^{U_2} = A^{(U_1 U_2)}. \quad (5.4)$$

5.1.2 The field A^h and its quadratic condensate

Consider the functional $f_A[U]$ defined as [CDG⁺05]

$$f_A[U] = \text{Tr} \left\{ \int d^4x A^U \cdot A^U \right\}, \quad (5.5)$$

where the dot product denotes a contraction of the spacetime indices of the A^U 's and the trace is taken over the product of the $\text{SU}(N)$ generators. A straightforward calculation [CDG⁺05] shows that $f_A[U]$ is minimized by the transformation $U = h[A]$ which enforces the divergence equation

$$\partial^\mu A_\mu^{h[A]} = 0. \quad (5.6)$$

The resulting field $A^{h[A]}$, which for simplicity will also be denoted by A^h in what follows, has the important property of being gauge invariant. This is a consequence of the identity

$$h[A^U] = U^\dagger h[A], \quad (5.7)$$

which can be derived from Eqs. (5.4) and (5.6) by observing that

$$\partial^\mu A_\mu^{h[A]} = 0 \quad \iff \quad \partial^\mu [(A_\mu^U)^{U^\dagger h[A]}] = 0, \quad (5.8)$$

²The symbol ξ will be reused for a new dynamical field, which will be defined in the next section.

and implies the transformation law

$$A^{h[A]} \rightarrow (A^U)^{h[A^U]} = A^{h[A]} . \quad (5.9)$$

While the general solution of Eq. (5.6) is not known in closed form, an explicit perturbative expression for A^h can still be obtained by defining a set of A -dependent fields $\xi^a[A]$ such that, with $\xi = \xi^a T_a$,

$$h[A] = e^{ig\xi[A]} . \quad (5.10)$$

By plugging the latter into Eq. (5.6) and solving the equation order by order in g , one finds that [CDG⁺05]

$$\xi[A] = \frac{\partial \cdot A}{\partial^2} + i \frac{g}{\partial^2} \left[\partial \cdot A, \frac{\partial \cdot A}{\partial^2} \right] + i \frac{g}{\partial^2} \left[A_\mu, \partial^\mu \frac{\partial \cdot A}{\partial^2} \right] + \frac{i}{2} \frac{g}{\partial^2} \left[\frac{\partial \cdot A}{\partial^2}, \partial \cdot A \right] + \dots ; \quad (5.11)$$

it follows that the field A^h can be expressed as

$$A_\mu^h = \left(\delta_{\mu\nu} - \frac{\partial_\mu \partial_\nu}{\partial^2} \right) \phi^\nu[A] , \quad (5.12)$$

where the vector field $\phi_\mu[A]$ is given by

$$\phi_\mu[A] = A_\mu - ig \left[\frac{\partial \cdot A}{\partial^2}, A_\mu \right] + \frac{ig}{2} \left[\frac{\partial \cdot A}{\partial^2}, \partial_\mu \frac{\partial \cdot A}{\partial^2} \right] + \dots . \quad (5.13)$$

Eqs. (5.12) and (5.13) explicitly exhibit A^h as a divergenceless version of the gauge field A , the difference $A^h - A$ being a non-local functional of the divergence $\partial \cdot A$. It is clear from the above expressions that A^h and A perturbatively coincide in the Landau gauge ($\alpha = 0$, $\partial \cdot A = 0$): if $\partial \cdot A = 0$, then

$$\phi_\mu = A_\mu \quad \Longrightarrow \quad A_\mu^h = A_\mu . \quad (5.14)$$

In the quantum context, the gauge invariance of A^h translates into an invariance under BRST symmetry. Since $(A^h)^2 = (A^h)^a \cdot (A^h)^a$ is clearly also BRST invariant, its vacuum expectation value $\langle (A^h)^2 \rangle$ is not constrained to vanish in the covariant gauges under the assumption that BRST symmetry is not broken in the vacuum. In particular, it makes sense to ask whether such a condensate indeed exists and – if it does – what the consequences of its existence are on the vacuum structure of QCD.

The VEV of the quadratic operator $(A^h)^2$ can be studied by making use of the local composite operator (LCO) formalism [Ver95, VKVAV01, DVS03]. Within the latter, a current J is coupled to the operator $(A^h)^2$ by introducing two extra terms in the Faddeev-Popov action,

$$S_{\text{FP}} \rightarrow S^{(1)}[J] , \quad (5.15)$$

where

$$S^{(1)}[J] = S_{\text{FP}} + \int d^4x \left(\frac{J}{2} (A^h)^2 - \frac{\zeta}{2} J^2 \right) . \quad (5.16)$$

In the above equation, the term quadratic in the current is introduced in order to ensure the renormalizability of the partition function $Z[J]$ [VKVAV01], which, in Euclidean space, reads

$$Z[J] = e^{-W[J]} = \int \mathcal{D}\mathcal{F} e^{-S^{(1)}[J]} \quad (\mathcal{D}\mathcal{F} = \mathcal{D}A \mathcal{D}\bar{c} \mathcal{D}c \mathcal{D}B) . \quad (5.17)$$

$Z[J]$ can be differentiated with respect to the current J to yield

$$\frac{\delta W}{\delta J}[J] = \frac{1}{2} \left\langle (A^h)^2 \right\rangle_J - \zeta J = \sigma[J] ; \quad (5.18)$$

when evaluated at $J = 0$, the last expression is equal to the BRST-invariant condensate $\sigma[J = 0] = \frac{1}{2} \left\langle (A^h)^2 \right\rangle_{J=0}$.

An effective action $\Gamma[\sigma]$ for the condensate can be defined starting from $W[J]$. As in Sec. 1.1.3, $\Gamma[\sigma]$ is obtained by first inverting the functional $\sigma[J]$ to a $J[\sigma]$, which we will simply denote by J_σ ,

$$\frac{\delta W}{\delta J}[J_\sigma] = \frac{1}{2} \left\langle (A^h)^2 \right\rangle_{J_\sigma} - \zeta J_\sigma = \sigma , \quad (5.19)$$

and then by computing the Legendre transform of $W[J]$,

$$\Gamma[\sigma] = W[J_\sigma] - \int d^4x J_\sigma \sigma . \quad (5.20)$$

The on-shell value of the BRST-invariant condensate is then obtained by differentiating $\Gamma[\sigma]$ with respect to σ ,

$$\frac{\delta \Gamma}{\delta \sigma}[\sigma] = -J_\sigma , \quad (5.21)$$

and setting the derivative to zero:

$$\frac{\delta \Gamma}{\delta \sigma}[\sigma] = 0 \quad \Longleftrightarrow \quad \sigma = \frac{1}{2} \left\langle (A^h)^2 \right\rangle_{J=0} . \quad (5.22)$$

The calculation of the effective action will be carried out explicitly in the next section.

5.1.3 Calculation of the condensate's effective action

In order to compute the effective action $\Gamma[\sigma]$ – Eq. (5.20) – in a general covariant gauge, we first need to address two unusual properties of the action $S^{(1)}$ that appears in Eq. (5.17). These are the non-locality of the operator A^h and the quadratic dependence of $S^{(1)}$ on both the current J and the field A^h . Let us start from the first one.

As we saw in the last section, A^h can be computed as a power series in the coupling g whose zero-order term is the transverse projection A^T of the field A ,

$$A_\mu^T = \left(\delta_{\mu\nu} - \frac{\partial_\mu \partial_\nu}{\partial^2} \right) A^\nu , \quad (5.23)$$

and the remaining terms only depend on the divergence $\partial \cdot A$ of the gauge field. The presence of the operator $(\partial^2)^{-1}$ both in the higher-order terms and in A^T makes the series that defines A^h highly non-local.

If we wish to localize the operator A^h , then a new dynamical field ξ can be introduced in the FP action in such a way that A^h will be expressed as a polynomial of infinite degree in ξ . This can be done as follows [CvEP⁺18]. First we insert a unity

$$1 = \int \mathcal{D}F \delta(F) \quad (5.24)$$

in the partition function $Z[J]$. Then we redefine F to be a functional of a $SU(N)$ algebra field $\xi = \xi^a T_a$, chosen so that $A^{h(\xi)}$ – with $h(\xi) = e^{ig\xi}$ – is divergenceless. In other words, we set

$$F = F[\xi] = \partial^\mu A_\mu^{h(\xi)} \quad (5.25)$$

and change variables of integration in Eq. (5.24) from F to ξ ,

$$1 = \int \mathcal{D}\xi \det\left(\frac{\delta F}{\delta \xi}\right) \delta(\partial^\mu A_\mu^{h(\xi)}) . \quad (5.26)$$

Under the sign of integral, $A^{h(\xi)}$ is clearly equal to the gauge-invariant field A^h defined in the previous section. In particular, the A^h which appears in the source term of $S^{(1)}$ can be replaced by $A^{h(\xi)}$ without spoiling the physical content of the partition function. In what follows, we will denote $h(\xi)$ simply by h , it being understood that the latter is ξ -dependent and equal to $e^{ig\xi}$.

With regard to the determinant and delta in Eq. (5.26), these can be rewritten as a functional integral over new dynamical fields τ^a and $\eta^a, \bar{\eta}^a$,

$$\begin{aligned} \det\left(\frac{\delta F}{\delta \xi}\right) \delta(\partial^\mu A_\mu^{h(\xi)}) &= \det\left(-\partial^\mu D_\mu(A^h)\Lambda(\xi)\right) \delta(\partial^\mu A_\mu^{h(\xi)}) = \\ &= \mathcal{N} \int \mathcal{D}\tau \mathcal{D}\bar{\eta} \mathcal{D}\eta e^{-\Delta S_1} \det(\Lambda(\xi)) . \end{aligned} \quad (5.27)$$

In the above equation, \mathcal{N} is an irrelevant constant, the action term ΔS_1 reads

$$\Delta S_1 = \int d^4x \left(\tau^a \partial^\mu A_\mu^{h,a} + \bar{\eta}^a \partial^\mu D_\mu(A^h) \eta^a \right) , \quad (5.28)$$

where $D_\mu(A^h)$ is the covariant derivative associated to the field A^h ,

$$D_\mu^{ab}(A^h) = \delta^{ab} \partial_\mu - g f^{abc} (A_\mu^h)^c , \quad (5.29)$$

and $\Lambda(\xi)$ is defined as

$$\Lambda_{ab}(\xi) = \frac{2i}{g} \text{Tr} \left\{ t_a \frac{\partial h^\dagger}{\partial \xi^b} h \right\} . \quad (5.30)$$

The determinant $\det(\Lambda(\xi))$ makes its first appearance in this thesis, having been neglected in [CFG⁺16, CvEP⁺18, DM20]³. In Appendix B, we show that it decouples from the rest of the integral as long as the partition function is defined in dimensional regularization and the calculations are carried out perturbatively. Since we will be working under these hypotheses, the determinant will be dropped in what follows.

With the modifications we just discussed, the partition function $Z[J]$ reads

$$Z[J] = \int \mathcal{D}\mathcal{F} e^{-S^{(2)}[J]} , \quad (5.31)$$

where the integration measure $\mathcal{D}\mathcal{F}$ is given by

$$\mathcal{D}\mathcal{F} = \mathcal{D}A \mathcal{D}\bar{c} \mathcal{D}c \mathcal{D}B \mathcal{D}\xi \mathcal{D}\tau \mathcal{D}\bar{\eta} \mathcal{D}\eta \quad (5.32)$$

and in the action $S^{(2)}$,

$$S^{(2)} = S^{(1)} + \Delta S_1 , \quad (5.33)$$

A^h is to be expanded perturbatively,

$$A_\mu^h = A_\mu - \partial_\mu \xi + ig[A_\mu, \xi] + \dots . \quad (5.34)$$

³[CFG⁺16] also neglected the ghost term in Eq. (5.28), which was introduced in [CvEP⁺18].

Crucially, $S^{(2)}$ is invariant under an extended BRST symmetry which acts on the new fields as [CvEP⁺18]

$$s\tau^a = s\bar{\eta}^a = s\eta^a = 0, \quad sh = -igc^a T_a h. \quad (5.35)$$

The latter translates into a corresponding transformation for the field ξ , which to lowest order reads

$$s\xi^a = -c^a + \frac{g}{2} f_{bc}^a c^b \xi^c + O(g^2). \quad (5.36)$$

This extended BRST transformation, easily seen to be nilpotent since $s^2 h = 0$, was exploited in [CvEP⁺18] to prove the renormalizability of the theory defined by the action $S^{(2)}$.

The effective action $\Gamma[F]$ associated to the elementary fields \mathcal{F} is usually computed by shifting the latter as $\mathcal{F} \rightarrow F + \delta\mathcal{F}$, so as to factorize an exponential of the form $\exp(-\int JF)$ from the partition function. In terms of the functional $W[J]$, such an exponential translates into the integral $-\int JF$ that appears in the definition of $\Gamma[F]$. In our partition function, Eq. (5.31), the shift cannot be performed in terms of the elementary fields due to the fact that the condensate A^h not only appears quadratically in the source term, but is also a complicated function of both the gauge field A and the algebra field ξ . In order to overcome this obstacle, a new dynamical field σ can be introduced in the action in such a way that its Green functions coincide with those of the condensate [VKVAV01]. In the process of doing so, we will also get rid of the action term $\propto J^2$, which could potentially obstruct the calculation of the effective action.

Consider what happens if we insert a unity of the form

$$1 = \mathcal{N} \int \mathcal{D}\sigma e^{-\Delta S_2} \quad (5.37)$$

in the partition function $Z[J]$, where the action term ΔS_2 is given by

$$\Delta S_2 = \frac{1}{2\zeta} \int d^4x \left(\sigma - \frac{1}{2} (A^h)^2 + \zeta J \right)^2. \quad (5.38)$$

If we define a new action $S^{(3)}$ as

$$S^{(3)} = S^{(2)} + \Delta S_2, \quad (5.39)$$

then it is easy to see, by shifting $\sigma \rightarrow \sigma + \frac{1}{2} (A^h)^2 - \zeta J$ in the partition function, that

$$\langle \sigma \rangle_J \Big|_{S^{(3)}} = \sigma[J] \Big|_{S^{(2)}}, \quad (5.40)$$

where the left-hand-side average is computed with respect to the action $S^{(3)}$, whereas $\sigma[J]$ is the condensate given by Eq. (5.18) – computed with respect to $S^{(2)}$. Since for any value of the current J the VEV of the dynamical field σ is equal to the BRST-invariant condensate, the latter can be studied by making use of the modified partition function

$$Z[J] = \int \mathcal{D}\mathcal{F} e^{-S^{(3)}[J]}, \quad (5.41)$$

where the action $S^{(3)}$ explicitly reads [VKVAV01]

$$S^{(3)} = S_{\text{FP}} + \Delta S_1 + \int d^4x \left\{ J\sigma + \frac{1}{2\zeta} \sigma^2 - \frac{1}{2\zeta} \sigma (A^h)^2 + \frac{1}{8\zeta} [(A^h)^2]^2 \right\}. \quad (5.42)$$

As we can see, both the quadratic coupling of A^h to J and the quadratic current term $\propto J^2$ have disappeared from the new action. Instead, $S^{(3)}$ is linear in J , which is itself linearly coupled to the field σ .

Thanks to these features, the effective action can be computed by shifting $\sigma \rightarrow \Sigma + \delta\sigma$, where Σ is the value of the condensate and $\delta\sigma$ quantifies the fluctuations of the new field around its VEV. Explicitly,

$$Z[J] = e^{-W[J]} = e^{-\int d^4x J\Sigma} \int \mathcal{D}\mathcal{F} e^{-S^{(4)}}, \quad (5.43)$$

where the measure of integration $\mathcal{D}\mathcal{F}$ is given by

$$\mathcal{D}\mathcal{F} = \mathcal{D}A \mathcal{D}\bar{c} \mathcal{D}c \mathcal{D}B \mathcal{D}\xi \mathcal{D}\tau \mathcal{D}\bar{\eta} \mathcal{D}\eta \mathcal{D}\delta\sigma \quad (5.44)$$

and the action $S^{(4)}$ reads

$$S^{(4)} = S_{\text{FP}} + \Delta S_1 + \int d^4x \left\{ J\delta\sigma + \frac{1}{2\zeta} (\Sigma + \delta\sigma)^2 - \frac{1}{2\zeta} (\Sigma + \delta\sigma)(A^h)^2 + \frac{1}{8\zeta} [(A^h)^2]^2 \right\}. \quad (5.45)$$

After renaming $\Sigma \rightarrow \sigma$, from Eq. (5.43) we obtain the following expression for the effective action $\Gamma[\sigma]$:

$$\Gamma[\sigma] = W[J_\sigma] - \int d^4x J_\sigma \sigma = \frac{1}{2\zeta} \int d^4x \sigma^2 - \ln \int_{\langle \delta\sigma \rangle = 0} \mathcal{D}\mathcal{F} e^{-I}, \quad (5.46)$$

where the action I is given by [DM20]

$$I = S_{\text{FP}} + \int d^4x \left(\tau^a \partial^\mu A_\mu^{h,a} + \bar{\eta}^a \partial^\mu D_\mu(A^h) \eta^a \right) + \int d^4x \left\{ \frac{1}{2\zeta} (\delta\sigma)^2 - \frac{1}{2\zeta} (\sigma + \delta\sigma)(A^h)^2 + \frac{1}{8\zeta} [(A^h)^2]^2 \right\} \quad (5.47)$$

and the linear terms $\propto \sigma\delta\sigma$ and $\propto J\delta\sigma$ have been replaced in Eq. (5.45) by the requirement that the VEV $\langle \delta\sigma \rangle$ be equal to zero, so that σ is the true value of the condensate.

Let us analyze the action I . First of all, we see that – with $s\delta\sigma = 0$ and by Eq. (5.35) – I is BRST invariant. Second, we see that in I the fluctuation field $\delta\sigma$ has a quadratic term which we can interpret as the kinetic term for a perturbative expansion of $\Gamma[\sigma]$. The corresponding zero-order propagator $D_{(\delta\sigma)}(p^2)$ reads

$$D_{(\delta\sigma)}(p^2) = \zeta. \quad (5.48)$$

Third, the field $\delta\sigma$ is coupled to the BRST-invariant gauge field A^h via a cubic interaction $\propto \delta\sigma(A^h)^2$. Moreover, as a result of our manipulations, a new interaction quartic in A^h arises. Both of these terms are proportional to ζ^{-1} , which can thus be regarded as a small parameter for the set-up of perturbation theory⁴. We should remark that these interaction terms actually incorporate an infinite number of vertices that couple the gauge field A to the fluctuation field $\delta\sigma$, to the algebra field ξ and to itself, given that A^h must be expanded in powers of $g\xi$. Finally, a quadratic term in A^h is present in I , proportional to the VEV σ . Just like the cubic and quartic interactions, this term needs to be expanded in powers of g . To lowest order,

$$-\frac{\sigma}{2\zeta} (A^h)^2 = -\frac{\sigma}{2\zeta} (A - \partial\xi)^2 + O(g/\zeta). \quad (5.49)$$

⁴Later on we will see that, by employing a procedure known as the reduction of couplings, ζ^{-1} can be taken to be proportional to g^2 to lowest order in perturbation theory, thus confirming this statement.

We then see that the quadratic interaction yields a mass term for the gluon field,

$$\delta\mathcal{L} = \frac{m^2}{2} A^2, \quad (5.50)$$

where the gluon mass parameter m^2 is given by⁵

$$m^2 = -\frac{\sigma}{\zeta}. \quad (5.51)$$

As long as σ is computed on-shell – that is, as long as σ solves the effective action equation $\delta\Gamma/\delta\sigma = 0$ –, the Green functions of pure Yang-Mills theory can be evaluated by making use of the action I instead of S_{FP} . This holds true due to the fact that setting the derivative of the effective action to zero is equivalent to computing the action at vanishing external current, so that S_{FP} is recovered in the partition function⁶. In particular, if the effective action equation yields a non-zero value for σ , then a formulation of pure Yang-Mills theory that uses I as its defining action will treat the gluons as massive at tree level from first principles, without changing the content of the FP action. The experience gained thanks to the Curci-Ferrari model and to the Screened Massive Expansion tells us that this should be sufficient to lead to dynamical mass generation in the gluon sector. We will come back to this subject in Sec. 5.2.

Having laid out the technique for calculating the effective action associated to the BRST-invariant condensate, we can now proceed to derive an explicit expression for the effective potential $V(\sigma)$, defined as

$$V(\sigma) = \Gamma[\sigma]/\mathcal{V}_4, \quad (5.52)$$

where \mathcal{V}_4 is the 4-dimensional Euclidean volume and $\Gamma[\sigma]$ is evaluated at constant σ . Since σ is BRST invariant, the effective potential can be computed in the Landau gauge ($\alpha = 0$) without any loss of generality.

As we saw in the last section, in the Landau gauge the fields A^h and A coincide. In particular, for $\alpha = 0$ it is not necessary to localize the field A^h , so that the steps that led to the introduction of the fields τ and $\eta, \bar{\eta}$ can be skipped; moreover, h can be everywhere set to $\mathbb{1}$. In other words, in the Landau gauge we can use the action

$$I_L = S_{\text{FP}}|_{\alpha=0} + \int d^4x \left\{ \frac{1}{2\zeta} (\delta\sigma)^2 - \frac{1}{2\zeta} (\sigma + \delta\sigma) A^2 + \frac{1}{8\zeta} (A^2)^2 \right\}. \quad (5.53)$$

By Eq. (5.46), the effective potential will then be given by

$$V(\sigma) = \frac{1}{2\zeta} \sigma^2 - \frac{1}{\mathcal{V}_4} \ln \int \mathcal{D}\mathcal{F} e^{-I_L}, \quad (5.54)$$

where

$$\mathcal{D}\mathcal{F} = \mathcal{D}A \mathcal{D}\bar{c} \mathcal{D}c \mathcal{D}B \mathcal{D}\delta\sigma. \quad (5.55)$$

To lowest order in perturbation theory, the path integral in Eq. (5.54) is equal to the product of the determinants of the fields' zero-order propagators⁷. All of these propagators

⁵Observe that $\sigma = \frac{1}{2} \langle (A^h)^2 \rangle$ does not necessarily imply $\sigma > 0$, since the VEV needs to be renormalized and its value can become negative in the process. The renormalization of the condensate will be discussed in Sec. 5.2.1.

⁶We remark that the modifications of the action which were performed in the present section – being the result of insertions of unities in $Z[J]$ – do not change neither the partition function, nor the physical content of the theory.

⁷Raised to the power of 1/2 for the bosonic fields or to the power of -1 for the fermionic fields.

are independent from σ , except for that of the gauge field – Δ_σ in the following equations –, which will thus yield the only non-constant contribution to $V(\sigma)$. Explicitly, to one loop, modulo σ -independent terms,

$$V(\sigma) = \frac{1}{2\zeta} \sigma^2 - \frac{1}{\mathcal{V}_4} \ln[\det(\Delta_\sigma)^{1/2}] , \quad (5.56)$$

where, in momentum space,

$$(\Delta_\sigma)_{\mu\nu}^{ab}(q) = \frac{1}{q^2 - \sigma/\zeta} t_{\mu\nu}(p) \delta^{ab} . \quad (5.57)$$

It follows that

$$V(\sigma) = \frac{\mu^\epsilon}{2\zeta} \sigma^2 + \frac{(d-1)N_A}{2} \mu^\epsilon \int \frac{d^d q}{(2\pi)^d} \ln \left(q^2 - \mu^\epsilon \frac{\sigma}{\zeta} \right) , \quad (5.58)$$

where $N_A = N^2 - 1$ is the dimension of the gauge group $SU(N)$ and we have generalized to $d = 4 - \epsilon$ dimensions with an eye to the renormalization of $V(\sigma)$. In the above equation, μ is the scale introduced by dimensional regularization. The evaluation of the logarithmic integral yields the following regularized expression for the effective potential [VKVAV01, DM20]:

$$V(\sigma) = \frac{\mu^\epsilon}{2\zeta} \sigma^2 - \frac{3N_A}{64\pi^2\zeta^2} \sigma^2 \left[\frac{2}{\epsilon} + \ln \left(-\frac{\bar{\mu}^2}{\mu^\epsilon \sigma/\zeta} \right) + \frac{5}{6} \right] , \quad (5.59)$$

where $\bar{\mu} = \sqrt{4\pi} e^{-\gamma_E/2} \mu$. It is clear from Eq. (5.59) where the need to introduce a new constant ζ comes from. Since the second term of the equation contains a divergence, we need a tunable – and, more specifically, a renormalizable – parameter in the first term in order to be able to absorb it. This is done by interpreting ζ as a bare parameter, $\zeta \rightarrow \zeta_B$, which is multiplicatively renormalized to a finite constant⁸,

$$\zeta_B = \mu^{-\epsilon} Z_\zeta \zeta . \quad (5.60)$$

With these modifications, the effective potential reads [VKVAV01, DM20]

$$V(\sigma) = \frac{\mu^{2\epsilon}}{2\zeta} (1 - \delta Z_\zeta) \sigma^2 - \frac{3N_A}{64\pi^2\zeta^2} \mu^{2\epsilon} \sigma^2 \left[\frac{2}{\epsilon} + \ln \left(-\frac{\bar{\mu}^2}{\mu^\epsilon \sigma/\zeta} \right) + \frac{5}{6} \right] , \quad (5.61)$$

where $\delta Z_\zeta = Z_\zeta - 1$ and Z_ζ does not appear in the second term since the latter can be interpreted as a higher-order term. Setting

$$\delta Z_\zeta = -\frac{3N_A}{32\pi^2\zeta} \frac{2}{\epsilon} \quad (5.62)$$

provides us with the effective potential renormalized in the $\overline{\text{MS}}$ scheme,

$$V(\sigma) = \frac{\mu^{2\epsilon}}{2\zeta} \sigma^2 - \frac{3N_A}{64\pi^2\zeta^2} \mu^{2\epsilon} \sigma^2 \left[\ln \left(-\frac{\bar{\mu}^2}{\mu^\epsilon \sigma/\zeta} \right) + \frac{5}{6} \right] . \quad (5.63)$$

In the next section we will rephrase $V(\sigma)$ in terms of the gluon mass parameter m^2 and show that its minimization leads to a non vanishing value of m^2 .

⁸We should mention that here we are not renormalizing the parameters in a systematic way. In Sec. 5.2.1, we will give a slightly different definition of the renormalization factor Z_ζ , which also takes into account the renormalization of the condensate $\langle (A^b)^2 \rangle$.

5.1.4 Dynamical mass generation: the gap equation

Tracing back our steps to the definition of the gluon mass parameter, we see that in $d = 4 - \epsilon$ dimensions m^2 can be expressed in terms of the renormalized parameter ζ as

$$m^2 = -\frac{\mu^\epsilon \sigma}{\zeta}, \quad (5.64)$$

where the factor of μ^ϵ ensures that the right-hand side has the correct dimensions in the $\epsilon \rightarrow 0$ limit. A renormalized effective potential $V(m^2)$ for the gluon mass parameter can then be derived from Eq. (5.63), yielding [VKVAV01, DM20]

$$V(m^2) = \zeta \frac{m^4}{2} - \frac{3N_A}{64\pi^2} m^4 \left(\ln \frac{\bar{\mu}^2}{m^2} + \frac{5}{6} \right). \quad (5.65)$$

Both of the above equations have an explicit dependence on ζ . Since the latter has no counterpart in the ordinary formulation of Yang-Mills theory, before trying to compute the on-shell value of the gluon mass parameter from the minimization of the effective potential we should find a way to fix its value from first principles.

To this extent, we observe that the fundamental quantities of Yang-Mills theory should not explicitly depend on ζ , since the latter disappears from the equations in the limit of zero source J . The most obvious way to fix ζ would then be to require that the effective potential does not depend on it – that is, to enforce the equation $dV/d\zeta = 0$. Unfortunately, to the current order in perturbation theory, such a constraint does not yield meaningful results. In fact, not only does the vanishing of the derivative $dV/d\zeta$ give us no clue on the value of ζ , but it also yields $m^2 = 0$, which is easily seen not to be a minimum of the effective potential: while $V(m^2 = 0) = 0$, there exist values of m^2 for which $V(m^2)$ is negative.

As an alternative, we could require that ζ be a function of the coupling constant g^2 alone – so that ζ may be regarded as a quantity whose value is fixed order by order in perturbation theory by the interactions themselves [Ver95, VKVAV01, DM20]. In other words, we may seek an expansion of ζ in the form

$$\zeta(g^2) = \frac{1}{g^2} \sum_n \zeta_n g^{2n}, \quad (5.66)$$

where the reason for having divided by g^2 in the above equation will become clear in a moment. If we want Eq. (5.66) to be valid at all scales, then we should also require that the running of ζ be controlled by that of g^2 – which in particular will lead to the constants ζ_n being scale-independent. These assumptions are at the core of the so-called Zimmermann reduction of couplings programme [Zim85, HMTZ19], which was proved to yield accurate results when applied in the context of the Gross-Neveu model [VSV97]. In [VKVAV01, Gra03], it was found that, in the $\overline{\text{MS}}$ scheme, the reduction yields

$$\zeta(g^2) = \frac{N_A}{g^2 N} \frac{9}{13} + \frac{161}{52} \frac{N_A}{16\pi^2} + \dots \quad (5.67)$$

Thus, to lowest order, ζ can be taken to be proportional to g^{-2} , with the first non-zero coefficients in Eq. (5.66) given by

$$\zeta_0 = \frac{9N_A}{13N}, \quad \zeta_1 = \frac{161N_A}{52 \cdot 16\pi^2}. \quad (5.68)$$

As a consequence of ζ being expressed as a power series in g^2 , the mass parameter m^2 defined by Eq. (5.64) contains higher-order terms in the coupling constant [VKVAV01, DM20],

$$m^2 = -\frac{\mu^\epsilon \sigma}{(\zeta_0/g^2 + \zeta_1) + O(g^2)} = m_0^2 \left(1 - \frac{\zeta_1}{\zeta_0} g^2 + O(g^4) \right), \quad (5.69)$$

where

$$m_0^2 = -\frac{\mu^\epsilon g^2 \sigma}{\zeta_0}. \quad (5.70)$$

Since our calculation of the effective potential $V(m^2)$ stops at one loop, we must be careful to separate the contributions coming from the different orders in g^2 . An explicit calculation shows that, when expressed in terms of m_0^2 , the effective potential reads [VKVAV01, DM20]

$$V(m_0^2) = \frac{9}{13} \frac{N_A}{N} \frac{m_0^4}{2g^2} - \frac{3N_A}{64\pi^2} m_0^4 \left(\ln \frac{\bar{\mu}^2}{m_0^2} + \frac{113}{39} \right) + O(g^2), \quad (5.71)$$

where the higher-order terms come both from the $O(g^4)$ corrections to ζ and m^2 and from the interaction terms in the Landau-gauge action I_L that defines the partition function. In Sec. 5.2 we will see that, to lowest order in the coupling, only m_0^2 enters the expression of the gluon propagator computed in the presence of a non-vanishing condensate. For this reason, in what follows we will focus on the above expression for the effective potential, which allows us to compute the value of the mass parameter m_0^2 in terms of g^2 and of the renormalization scale $\bar{\mu}$.

The first derivative of $V(m_0^2)$ with respect to m_0^2 reads

$$V'(m_0^2) = \frac{9}{13} \frac{N_A}{N} \frac{m_0^2}{g^2} - \frac{3N_A}{32\pi^2} m_0^2 \left(\ln \frac{\bar{\mu}^2}{m_0^2} + \frac{187}{78} \right). \quad (5.72)$$

Equating the latter to zero yields the so-called *gap equation*, which provides us with the on-shell value of the gluon mass parameter m_0^2 [DM20]:

$$m_0^2 = \frac{13Ng^2}{3 \cdot 32\pi^2} m_0^2 \left(\ln \frac{\bar{\mu}^2}{m_0^2} + \frac{187}{78} \right). \quad (5.73)$$

The gap equation has two solutions. The first of these, $m_0^2 = 0$, corresponds to a vanishing potential,

$$V(m_0^2 = 0) = 0. \quad (5.74)$$

The second solution,

$$m_0^2 = \bar{\mu}^2 \exp \left(\frac{187}{78} - \frac{3 \cdot 32\pi^2}{13Ng^2} \right), \quad (5.75)$$

on the other hand, corresponds to a negative value of $V(m_0^2)$,

$$V(m_0^2) = -\frac{3N_A m_0^4}{128\pi^2} < 0. \quad (5.76)$$

Clearly, Eq. (5.75) yields the global minimum of the effective potential.

The fact that the minimum of $V(m_0^2)$ lies at a non-zero value of m_0^2 has far-reaching consequences. First of all, it proves that the gluon condensate $\langle (A^h)^2 \rangle$ does not vanish in pure Yang-Mills theory. We remark that, albeit having been derived in the Landau gauge, this result holds in every covariant gauge thanks to the BRST invariance of the operator A^h

and of its square. Second of all, as a consequence of $\langle (A^h)^2 \rangle \neq 0$, it shows that a mass term for the gluons is generated in every covariant gauge via the inclusion of the BRST-invariant condensate in the Faddeev-Popov Lagrangian. In the previous sections, this was achieved by consecutive transformations of the action S_{FP} – performed in such a way as to leave the contents of the theory unchanged – which resulted in an action I with respect to which the gluons propagate at tree level like massive particles. As we know by now, treating the gluons as massive at order zero in perturbation theory is expected to yield a dressed gluon propagator whose transverse component remains finite in the deep infrared. If this turns out to be the case also for the propagator computed by using the action I , then our findings will provide a strong indication that the occurrence of dynamical mass generation in the gluon sector may be triggered by the BRST-invariant condensate $\langle (A^h)^2 \rangle$. In the next section we will test our hypothesis by computing the DM propagators in the Landau gauge.

5.2 Dynamical Model: the propagators in the Landau gauge

Having seen how the BRST-invariant condensate $\langle (A^h)^2 \rangle$ can be included in the formalism of QCD, we are now in a position to give a precise definition of the Dynamical Model. The Dynamical Model (DM) is the reformulation of pure Yang-Mills theory that uses the action I – Eq. (5.47) – in place of the Faddeev-Popov action S_{FP} to study the dynamics of the SU(N) gauge theories in a general covariant gauge. The equivalence between the Dynamical Model and the ordinary formulation of pure Yang-Mills theory was proved to hold in Sec. 5.1 provided that the gluon mass parameter m^2 – equivalently, the gluon condensate – is computed on shell – that is, on the solutions of the gap equation $V'(m^2) = 0$.

In the present section, the dressed gluon and ghost propagators will be computed in the Landau gauge within the framework of the Dynamical Model both at fixed scale and by making use of the Renormalization Group. As we will see, in the limit of vanishing momenta the DM gluon propagator saturates to a finite constant. The latter will be shown to be proportional to the inverse of the gluon mass parameter m^2 , implying that – as far as the Landau gauge is concerned – dynamical mass generation in the gluon sector can be accounted for by the non-vanishing of the BRST-invariant condensate $\langle (A^h)^2 \rangle$.

As the first step in our derivation of the propagators, we will start by discussing the renormalization of the Dynamical Model and by presenting its Feynman rules.

5.2.1 Renormalization and Feynman rules

In Sec. 5.1.2, the source term for the BRST-invariant condensate $\langle (A^h)^2 \rangle$ was introduced disregarding the issue of renormalization. Since keeping track of the renormalization factors will be essential in what follows, let us take a step back and show how the parameters and fields of the Dynamical Model are to be renormalized.

When coupling the condensate to the external current J , two things need to be kept in mind. First of all, the BRST-invariant gauge field A^h needs to be renormalized by making use of an appropriate renormalization factor Z_{A^h} . Second of all, even after having renormalized A^h , the VEV $\langle (A^h)^a(x) \cdot (A^h)^a(x) \rangle$ is still divergent due to the fact that, as a product of operators evaluated at the same spacetime point, the operator $(A^h)^2$ is singular. This issue can be overcome by interpreting the partition function $Z[J]$ to be a functional of a renormalized current J – that is, by introducing a renormalization factor Z_J for the current as well.

Starting from Z_{A^h} and Z_J , one can define two mutually independent renormalization factors Z_2 and Z_ζ via the equations [VKVAV01]

$$J_B A_B^h \cdot A_B^h = (Z_J Z_{A^h}) J A^h \cdot A^h = Z_2 J A^h \cdot A^h , \quad (5.77)$$

$$\zeta_B J_B^2 = Z_\zeta \zeta \mu^{-\epsilon} J^2 . \quad (5.78)$$

Note that, at variance with Sec. 5.1.3, the Z_ζ in Eq. (5.78) does not renormalize the parameter ζ alone, but it also includes the renormalization of the current J . We will come back to this point at the end of the present section. Z_2 and Z_ζ are the renormalization factors that appear in the source term ΔS for the BRST-invariant potential. Explicitly,

$$\Delta S = \int d^4x \left(\frac{Z_2}{2} J A^h \cdot A^h - \mu^{-\epsilon} \frac{Z_\zeta \zeta}{2} J^2 \right) . \quad (5.79)$$

Differentiating the partition function $Z[J]$ with respect to J while using Eq. (5.79) now yields the condensate $\sigma[J]$ in the form

$$\sigma[J] = \frac{\delta W}{\delta J}[J] = \frac{Z_2}{2} \langle A^h \cdot A^h \rangle_J - Z_\zeta \zeta \mu^{-\epsilon} J , \quad (5.80)$$

where the fields A^h and J are to be interpreted as renormalized quantities. In the above equation, the factors Z_2 and Z_ζ are needed to remove the divergences that arise from the product $A^h(x) \cdot A^h(x)$ and its VEV.

The fields ξ , τ , η and $\bar{\eta}$ that were introduced in Sec. 5.1.3 with the purpose of localizing the operator A^h also need to be renormalized. Since the main focus of what follows is computing the propagators in the Landau gauge – within which, as discussed earlier, the localization step can be skipped –, we will go no further in discussing this topic. A complete treatment of the renormalization of the action I in a general covariant gauge can be found in [CvEP⁺18].

In the Landau gauge ($\alpha = 0$) the DM action $I_L = I|_{\alpha=0}$ amended by taking Z_2 and Z_ζ into account can be explicitly computed to be

$$I_L = S_{\text{FP}}|_{\alpha=0} + \int d^d x \left\{ \frac{\mu^\epsilon}{2Z_\zeta \zeta} (\delta\sigma)^2 - \frac{\mu^\epsilon Z_2}{2Z_\zeta \zeta} (\sigma + \delta\sigma) A^2 + \frac{\mu^\epsilon Z_2^2}{8Z_\zeta \zeta} (A^2)^2 \right\} . \quad (5.81)$$

By rewriting the mass term as

$$-\frac{\mu^\epsilon Z_2}{2Z_\zeta \zeta} \sigma A^2 = -\frac{\mu^\epsilon}{2\zeta} \sigma A^2 - \left(\frac{Z_2}{Z_\zeta} - 1 \right) \frac{\mu^\epsilon}{2\zeta} \sigma A^2 , \quad (5.82)$$

a renormalized gluon mass parameter can be still defined in terms of the finite quantities σ and ζ as

$$m^2 = -\frac{\mu^\epsilon \sigma}{\zeta} , \quad (5.83)$$

so that the zero-order Euclidean gluon propagator $\Delta_{m\mu\nu}^{ab}(p)$ reads

$$\Delta_{m\mu\nu}^{ab}(p) = \frac{\delta^{ab} t_{\mu\nu}(p)}{p^2 + m^2} . \quad (5.84)$$

The second term in Eq. (5.82), on the other hand, provides a renormalization counterterm for the gluon mass operator: to lowest order,

$$\Delta \mathcal{L}_{\text{c.t.}} = (\delta Z_2 - \delta Z_\zeta) \frac{m^2}{2} A^2 \quad (\delta Z_{2,\zeta} = Z_{2,\zeta} - 1) . \quad (5.85)$$

As for the other terms in I_L , we see that – as before – the zero-order propagator $D_{(\delta\sigma)}(p^2)$ of the fluctuation field $\delta\sigma$ can be expressed as

$$D_{(\delta\sigma)}(p^2) = \zeta \mu^{-\epsilon} . \quad (5.86)$$

Additionally, the analytical expressions for the cubic $\delta\sigma A^2$ and quartic $(A^2)^2$ vertices, $\delta\Gamma_{\mu\nu}^{ab}$ ⁹ and $\delta\Gamma_{\mu\nu\rho\sigma}^{abcd}$, respectively, are seen to be given by [DM20]

$$\delta\Gamma_{\mu\nu}^{ab} = \frac{\mu^\epsilon}{\zeta} \delta^{ab} \delta_{\mu\nu} \quad (5.87)$$

and

$$\delta\Gamma_{\mu\nu\rho\sigma}^{abcd} = -\frac{\mu^\epsilon}{\zeta} \left(\delta^{ab} \delta^{cd} \delta_{\mu\nu} \delta_{\rho\sigma} + \delta^{ac} \delta^{bd} \delta_{\mu\rho} \delta_{\nu\sigma} + \delta^{ad} \delta^{bc} \delta_{\mu\sigma} \delta_{\nu\rho} \right) . \quad (5.88)$$

The renormalization factors Z_2 and Z_ζ contribute to these vertices and to the quadratic $\delta\sigma$ operator via appropriate renormalization counterterms, to be added to $\mathcal{L}_{\text{c.t.}}$. Finally, the remaining Feynman rules of the Dynamical Model are identical to those of ordinary pure Yang-Mills theory, and include the renormalization counterterms Z_A and Z_g for the gluon field and for the coupling constant.

To end this section, we point out that the condensate's effective potential $V(\sigma)$, computed to one loop while taking into account the appropriate renormalization factors, is given by

$$V(\sigma) = \frac{\mu^{2\epsilon}}{2Z_\zeta\zeta} \sigma^2 + \frac{(d-1)N_A}{2} \mu^\epsilon \int \frac{d^d q}{(2\pi)^d} \ln \left(q^2 - \mu^\epsilon \frac{\sigma}{\zeta} \right) , \quad (5.89)$$

where now Z_ζ is the renormalization factor defined by Eq. (5.78). Thus, while in Sec. 5.1.3 Z_ζ was referred to ζ alone, we see that the renormalized expression of the potential does not change even when the correct renormalization factors are included. From $V(\sigma)$ we can derive a renormalized potential $V(m^2)$ for the mass parameter m^2 ,

$$V(m^2) = \frac{\zeta m^4}{2Z_\zeta} + \frac{(d-1)N_A}{2} \mu^\epsilon \int \frac{d^d q}{(2\pi)^d} \ln (q^2 + m^2) \quad (5.90)$$

whose first derivative $V'(m^2)$,

$$V'(m^2) = \frac{\zeta m^2}{Z_\zeta} + \frac{(d-1)N_A}{2} \mu^\epsilon \int \frac{d^d q}{(2\pi)^d} \frac{1}{q^2 + m^2} , \quad (5.91)$$

once set to zero, provides us with the renormalized gap equation.

5.2.2 The gluon and ghost propagators

Let us proceed to the calculation of the gluon and of the ghost propagators within the Dynamical Model. The Landau-gauge (inverse) gluon propagator computed in the framework of the DM can be expressed as [DM20]

$$[\Delta^{-1}(p)]_{\mu\nu}^{ab} = \delta^{ab} \left[Z_A p^2 t_{\mu\nu}(p) + (1 + \delta Z_2 - \delta Z_\zeta) m^2 \delta_{\mu\nu} + \Pi_{\mu\nu}(p) \right] . \quad (5.92)$$

In the above equation, Z_A is the gluon field strength renormalization factor, the renormalization constants δZ_2 and δZ_ζ arise from the renormalization of the gluon mass operator

⁹Not to be confused with the gluon mass counterterm of Chpts. 3 and 4.

$m^2 A^2$, and $\Pi_{\mu\nu}(p)$ – modulo color structure – is the Landau-gauge gluon polarization. An explicit calculation shows that, to one loop,

$$\begin{aligned} \Pi_{\mu\nu}(p) = & \Pi_{\mu\nu}^{(\text{CF})}(p) - \frac{4 \cdot 2}{2!} \left(\frac{\mu^\epsilon}{2\zeta} \right)^2 \frac{\zeta}{\mu^\epsilon} \int \frac{d^d q}{(2\pi)^d} \Delta_{m\mu\nu}(q) + \\ & + \frac{4 \cdot 3}{4!} \frac{\mu^\epsilon}{\zeta} \left[\delta_{\mu\nu} N_A \int \frac{d^d q}{(2\pi)^d} \delta^{\sigma\tau} \Delta_{m\sigma\tau}(q) + 2 \int \frac{d^d q}{(2\pi)^d} \Delta_{m\mu\nu}(q) \right]. \end{aligned} \quad (5.93)$$

Here $\Pi^{(\text{CF})}(p)$ – given by diagrams (1), (2a) and (3a) in Fig. 3.7 – is the gluon polarization computed in pure Yang-Mills theory by replacing the ordinary Landau-gauge massless zero-order gluon propagator by a massive one; as such, it is equal to the polarization computed within the Curci-Ferrari model – hence the label CF. On the other hand, the second and third terms in Eq. (5.93) arise, respectively, from the interaction of the gluon field with the fluctuation field $\delta\sigma$ and from the self-interaction mediated by the new quartic $(A^2)^2$ vertex. The corresponding diagrams are depicted in Fig. 5.1.



Figure 5.1: Diagrams that contribute to the DM one-loop gluon polarization, arising from the new cubic and quartic vertices in the action I_L . The wiggly line represents the fluctuation field $\delta\sigma$'s propagator.

It is easy to see that, in Eq. (5.93), the second term inside the brackets cancels the second term in the first line. Therefore, the DM gluon polarization simplifies to

$$\Pi_{\mu\nu}(p) = \Pi_{\mu\nu}^{(\text{CF})}(p) + \frac{(d-1)N_A}{2} \frac{\mu^\epsilon}{\zeta} \delta_{\mu\nu} \int \frac{d^d q}{(2\pi)^d} \frac{1}{q^2 + m^2}. \quad (5.94)$$

By plugging Eq. (5.94) into Eq. (5.92) and observing that, to lowest order, the tree-level mass term in the latter can be rewritten as

$$(1 + \delta Z_2 - \delta Z_\zeta) m^2 = \delta Z_2 m^2 + Z_\zeta^{-1} m^2, \quad (5.95)$$

we find that the DM gluon propagator can be put in the form [DM20]

$$\begin{aligned} \Delta_{\mu\nu}^{-1}(p) = & Z_A p^2 t_{\mu\nu}(p) + \delta Z_2 m^2 \delta_{\mu\nu} + \Pi_{\mu\nu}^{(\text{CF})}(p) + \\ & + \delta_{\mu\nu} \left(Z_\zeta^{-1} m^2 + \frac{(d-1)N_A}{2} \frac{\mu^\epsilon}{\zeta} \int \frac{d^d q}{(2\pi)^d} \frac{1}{q^2 + m^2} \right). \end{aligned} \quad (5.96)$$

By comparing the last expression with Eq. (5.91), we see that the terms in brackets are none other than the first derivative $V'(m^2)$ of the gluon mass parameter's effective potential, divided by ζ . In particular, if m^2 solves the gap equation – $V'(m^2) = 0$ –, then these terms vanish and we are left with

$$\Delta(p^2) = \frac{1}{Z_A p^2 + \delta Z_2 m^2 + \Pi_T^{(\text{CF})}(p^2)} \quad (5.97)$$

for the transverse component $\Delta(p^2)$ of the gluon propagator, where $\Pi_T^{(\text{CF})}(p^2)$ is the transverse component of the Curci-Ferrari polarization. Since the equivalence between the Dynamical Model and ordinary pure Yang-Mills theory only holds on the solutions of $V'(m^2) = 0$, we can take Eq. (5.97) as our final expression for $\Delta(p^2)$.

Interestingly, the constant ζ disappears from the DM gluon propagator once the latter is computed on the shell of the gap equation. This could have been foreseen, given that such a parameter was not present in the Faddeev-Popov action in the first place. Nonetheless, an implicit dependence of the propagator on ζ still survives via the solutions of $V'(m^2) = 0$. Within the reductions of coupling programme, this dependence on ζ is traded with a dependence on the coupling constant g^2 in a perturbative fashion – see Sec. 5.1.4. In particular, since both δZ_2 and $\Pi_T^{(\text{CF})}(p^2)$ are already first-order in g^2 , the mass parameter in Eq. (5.97) can be identified with the lowest-order m_0^2 defined in Sec. 5.1.4 – namely

$$m_0^2 = -\frac{\mu^\epsilon g^2 Z_2 \langle A^2 \rangle}{2\zeta_0} \quad \left(\zeta_0 = \frac{9N_A}{13N} \right). \quad (5.98)$$

In what follows, we will not distinguish between m^2 and m_0^2 , denoting by m^2 the value provided by the last equation.

A second observation we wish to make is that, again when enforcing $V'(m^2) = 0$, the tree-level mass term m^2 is removed from $\Delta(p^2)$. This is akin to what happens in the Screened Massive Expansion after the single-cross diagram – Fig. 3.6 – is added to the polarization; similar cancellations can be shown to occur at every order in perturbation theory [DM20]. At variance with the SME, however, a renormalization counterterm of the form $\delta Z_2 m^2$ is still left in $\Delta(p^2)$. Such a feature is not accidental: the Curci-Ferrari polarization, in fact, contains a mass divergence (proportional to m^2) which needs to be absorbed into δZ_2 in order to obtain a finite result. Let us see explicitly how this works.

The one-loop Curci-Ferrari polarization was first computed in [TW10]. Its transverse component reads

$$\begin{aligned} \Pi_T^{(\text{CF})}(p^2) = & -\frac{\lambda m^2}{6} \left(13s - \frac{9}{2} \right) \left(\frac{2}{\epsilon} + \ln \frac{\bar{\mu}^2}{m^2} \right) + \\ & -\frac{\lambda m^2}{24s^2} \left[\frac{242}{3} s^3 - 126s^2 + 2s + (s^2 - 2)s^3 \ln s + \right. \\ & \quad \left. - 2(s+1)^3 (s^2 - 10s + 1) \ln(s+1) + \right. \\ & \quad \left. - s^{3/2} (s+4)^{3/2} (s^2 - 20s + 12) \ln \left(\frac{\sqrt{s+4} - \sqrt{s}}{\sqrt{s+4} + \sqrt{s}} \right) \right], \end{aligned} \quad (5.99)$$

where $s = p^2/m^2$, $\bar{\mu} = \sqrt{4\pi} e^{\gamma_E/2} \mu$ is the scale introduced by dimensional regularization and λ is a normalized coupling constant defined as

$$\lambda = \frac{N\alpha_s}{4\pi}. \quad (5.100)$$

The divergent part of $\Pi_T^{(\text{CF})}(p^2)$ is given by

$$[\Pi_T^{(\text{CF})}(p^2)]_{\text{div.}} = -\lambda \left(\frac{13}{6} p^2 - \frac{3}{4} m^2 \right) \frac{2}{\epsilon} \quad (5.101)$$

and contains two terms. The first one, proportional to p^2 , is absorbed by the usual gluon field renormalization factor $Z_A = 1 + \delta Z_A$. The second one, proportional to m^2 , can

only be removed from the propagator if a corresponding counterterm is available. In the framework of the Dynamical Model, this counterterm is precisely δZ_2 . In particular, from Eq. (5.101), we see that δZ_A and δZ_2 must be chosen according to

$$\delta Z_A = \frac{13\lambda}{6} \frac{2}{\epsilon} + \text{fin.} , \quad \delta Z_2 = -\frac{3\lambda}{4} \frac{2}{\epsilon} + \text{fin.} , \quad (5.102)$$

where the finite terms depend on the renormalization scheme in which the propagator is defined. Note that δZ_A contains the ordinary gluon field divergence – see e.g. Sec. 3.1.4. This happens because, just like the SME and the Curci-Ferrari model, the Dynamical Model as well does not modify the UV limit of pure Yang-Mills theory.

Once renormalized, the Landau-gauge DM gluon propagator reads

$$\Delta(p) = \frac{1}{p^2 + \Pi_{T,R}^{(\text{CF})}(p^2)} , \quad (5.103)$$

where $\Pi_{T,R}^{(\text{CF})}(p^2)$ is the renormalized transverse Curci-Ferrari polarization. In the limit of vanishing momentum $p^2 \rightarrow 0$, since

$$\Pi_T^{(\text{CF})}(p^2) \rightarrow \frac{3\lambda m^2}{4} \left(\frac{2}{\epsilon} + \frac{5}{6} + \ln \frac{\bar{\mu}^2}{m^2} \right) \neq 0 , \quad (5.104)$$

the gluon propagator remains finite – and is thus massive – unless the finite terms of the renormalization constant δZ_2 are chosen to exactly eliminate the finite terms in $\Pi_{T,R}^{(\text{CF})}(p^2)$. Of course, this will need to be avoided.

We now turn to the ghost sector. In the framework of the Dynamical Model, the ghost propagator can be expressed as

$$\mathcal{G}(p^2) = \frac{1}{Z_c p^2 + \Sigma(p^2)} , \quad (5.105)$$

where Z_c is the ghost field renormalization constant and $\Sigma(p^2)$ is the ghost self-energy. To one loop, since the corrections coming from the cubic $\delta\sigma A^2$ and quartic $(A^2)^2$ vertices are higher-order, the Landau-gauge ghost self-energy diagrams are the same as those of ordinary Yang-Mills theory¹⁰, albeit with massive zero-order propagators in their internal gluon lines. In other words, the DM ghost self-energy is equal to its Curci-Ferrari counterpart $\Sigma^{(\text{CF})}(p^2)$ [DM20],

$$\Sigma(p^2) = \Sigma^{(\text{CF})}(p^2) . \quad (5.106)$$

Like the gluon polarization, the one-loop Curci-Ferrari ghost self-energy was also first computed in [TW10], yielding

$$\Sigma^{(\text{CF})}(p^2) = -\frac{3\lambda}{4} p^2 \left(\frac{2}{\epsilon} + \ln \frac{\bar{\mu}^2}{m^2} \right) + \frac{\lambda}{4} p^2 \left[\frac{(s+1)^3}{s^2} \ln(1+s) - s \ln s - \frac{1}{s} - 5 \right] . \quad (5.107)$$

Since the divergent part of $\Sigma^{(\text{CF})}(p^2)$ reads

$$[\Sigma^{(\text{CF})}(p^2)]_{\text{div.}} = -\frac{3\lambda}{4} p^2 \frac{2}{\epsilon} , \quad (5.108)$$

¹⁰Namely, the diagram on the left in Fig. (3.4).

we see that the ghost field renormalization constant must be chosen according to

$$\delta Z_c = \frac{3\lambda}{4} \frac{2}{\epsilon} + \text{fin.} . \quad (5.109)$$

Again, the latter is equal to the ordinary divergence of pure Yang-Mills theory – see e.g. Sec. 3.1.3.

In the limit of vanishing momenta $p^2 \rightarrow 0$, the Landau-gauge ghost self-energy goes to zero like p^2 . Explicitly,

$$\Sigma^{(\text{CF})}(p^2) \rightarrow -\frac{3\lambda p^2}{4} \left(\frac{2}{\epsilon} + \frac{5}{6} + \ln \frac{\bar{\mu}^2}{m^2} \right) . \quad (5.110)$$

It follows from Eq. (5.105) that the ghost propagator grows to infinity as $p^2 \rightarrow 0$, confirming that within the Landau-gauge Dynamical Model the ghosts remain massless.

5.2.3 RG improvement of the Dynamical Model in the Dynamically Infrared-Safe scheme

In order to extend the validity of the Dynamical Model propagators to the widest possible range of momenta, the fixed-scale results described in the previous section can be improved by making use of Renormalization Group methods. In what follows, the propagators, the gluon mass parameter m^2 and the coupling λ will be defined in the so-called Dynamically Infrared-Safe (DIS) scheme, which is presented for the first time in this thesis. The DIS scheme is just the MOM-Taylor scheme discussed in the context of the Screened Massive Expansion (Sec. 3.3.1), with an additional renormalization condition for the gluon mass parameter – that is, for the renormalization factor Z_2 .

Within the DIS scheme, the propagators are defined in the MOM scheme: denoting by $\Delta(p^2; \mu^2)$ and $\mathcal{G}(p^2; \mu^2)$, respectively, the gluon and ghost propagators renormalized at the scale μ , we set

$$\Delta(\mu^2; \mu^2) = \frac{1}{\mu^2} , \quad \mathcal{G}(\mu^2; \mu^2) = \frac{1}{\mu^2} . \quad (5.111)$$

From Eqs. (5.97) and (5.105), it follows that in the DIS scheme the one-loop Landau-gauge DM field renormalization factors Z_A and Z_c are given by

$$Z_A = 1 - \delta Z_2 \frac{m^2}{\mu^2} - \frac{\Pi_T^{(\text{CF})}(p^2 = \mu^2)}{\mu^2} , \quad Z_c = 1 - \frac{\Sigma^{(\text{CF})}(p^2 = \mu^2)}{\mu^2} , \quad (5.112)$$

where δZ_2 in the first of the above equations still needs to be fixed by appropriate renormalization conditions. The strong coupling, on the other hand, is defined in the Taylor scheme – that is, by choosing the coupling renormalization factor Z_g so that

$$Z_g Z_A^{1/2} Z_c = 1 . \quad (5.113)$$

As we saw in Sec. 3.3.1, this is equivalent to having the beta function β_g be equal to

$$\beta_g = \frac{g}{2} (\gamma_A + 2\gamma_c) , \quad (5.114)$$

where γ_A and γ_c are the gluon and ghost anomalous dimensions. A beta function β_λ for the normalized coupling $\lambda = Ng^2/16\pi^2$ can be introduced as well, yielding

$$\beta_\lambda = \mu \frac{d\lambda}{d\mu} = \lambda (\gamma_A + 2\gamma_c) . \quad (5.115)$$

With Z_A , Z_c and Z_g defined in the MOM-Taylor scheme, the only counterterm that remains to be fixed to complete the renormalization of the Landau-gauge Dynamical Model is Z_2 . The latter, as we saw in the previous section, determines the renormalization of the gluon mass term in the propagator $\Delta(p^2)$. Moreover, it enters the renormalization of the gluon mass parameter m^2 directly. In order to see this, recall that – to lowest order in $g^2 - m^2$ can be expressed in terms of the BRST-invariant condensate as

$$m^2 = -\frac{g^2 \mu^\epsilon}{2\zeta_0} Z_2 \langle A^2 \rangle . \quad (5.116)$$

Substituting the coupling and the gluon field with their bare counterparts, we find that

$$m^2 = -\frac{g^2 \mu^\epsilon}{2\zeta_0} Z_2 \langle A^2 \rangle = -\frac{g_B^2 \mu^\epsilon}{2\zeta_0} \frac{Z_2}{Z_g^2 Z_A} \langle A_B^2 \rangle . \quad (5.117)$$

In particular, again to lowest order, the renormalization factor of m^2 is given by $Z_2/Z_g^2 Z_A$. If the coupling is defined in the Taylor scheme, then such a factor can be rewritten as

$$\frac{Z_2}{Z_g^2 Z_A} = \frac{Z_2 Z_c^2}{Z_g^2 Z_A Z_c^2} = Z_2 Z_c^2 . \quad (5.118)$$

By introducing a gamma function γ_{m^2} for the mass, such that

$$\mu \frac{dm^2}{d\mu} = \gamma_{m^2} m^2 , \quad (5.119)$$

we see that in the Taylor scheme

$$\gamma_{m^2} = \gamma_2 + 2\gamma_c , \quad (5.120)$$

where γ_2 is the gamma function associated to the factor Z_2 ,

$$\gamma_2 = \frac{\mu}{Z_2} \frac{dZ_2}{d\mu} . \quad (5.121)$$

In order to fix Z_2 , we first notice that, by Eqs. (5.102) and (5.109),

$$(Z_2 Z_c)_{\text{div.}} = 1 . \quad (5.122)$$

This relation was proved to hold to any perturbative order in [DVS03]. Therefore, we could choose to set $Z_2 = Z_c^{-1}$, extending the equality in Eq. (5.122) from the divergent terms to the full renormalization factors. However, this choice turns out to be disastrous when the MOM scheme is used for the propagators. To see this, observe that, by Eq. (5.112), $Z_2 = Z_c^{-1}$ would yield

$$\delta Z_2 = -\delta Z_c = \frac{\Sigma^{(\text{CF})}(p^2 = \mu^2)}{\mu^2} . \quad (5.123)$$

By expanding $\Sigma^{(\text{CF})}(\mu^2)$ around $\mu^2 = 0$ – Eq. (5.110) –, we find that $\delta Z_2 = -\delta Z_c$ would then imply the following asymptotic limit for the product $\delta Z_2 m^2$ that appears in the gluon propagator:

$$\delta Z_2 m^2 \rightarrow -\frac{3\lambda m^2}{4} \left(\frac{2}{\epsilon} + \frac{5}{6} + \ln \frac{\bar{\mu}^2}{m^2} \right) , \quad (5.124)$$

By Eq. (5.104), the latter is equal to $-\Pi_T^{(\text{CF})}(0)$. In other words, in the limit of vanishing renormalization scales, δZ_2 would kill the finite terms of the zero-momentum gluon

polarization, which is precisely what we wanted to avoid in the context of the fixed-scale expansion.

The asymptotic behavior described by Eq. (5.124) leads to a massless RG-improved gluon propagator, just like it does at fixed scale. To solve this issue, we can impose a slightly different renormalization condition on δZ_2 : instead of setting $\delta Z_2 = -\delta Z_c$, we define the former as

$$\delta Z_2 = -\delta Z_c + \frac{5\lambda}{8} . \quad (5.125)$$

The constant $5\lambda/8$, when multiplied by m^2 , prevents the corresponding finite term in Eq. (5.124) from entering δZ_2 , so that $\Pi^{(\text{CF})}(0)$ is not renormalized to zero and the gluon propagator remains massive¹¹.

Eq. (5.125) – together with the MOM condition for the propagator and the Taylor condition for the coupling – completes the definition of the Dynamically Infrared-Safe scheme. We note that, since the derivative of λ with respect to μ is $O(\lambda^2)$, Eq. (5.125) implies that, to lowest order,

$$\gamma_2 = -\gamma_c . \quad (5.126)$$

In particular, by Eq. (5.120), the gluon mass parameter's DIS anomalous dimension γ_{m^2} reads

$$\gamma_{m^2} = \gamma_c . \quad (5.127)$$

Thus, in the DIS scheme, the RG flow is determined by the beta and gamma functions

$$\beta_\lambda = \lambda(\gamma_A + 2\gamma_c) , \quad \gamma_{m^2} = \gamma_c , \quad (5.128)$$

where, to one loop,

$$\gamma_A = -\mu \frac{d}{d\mu} \left(\frac{\Pi_T^{(\text{CF})}(p^2 = \mu^2)}{\mu^2} + \frac{m^2 \Sigma^{(\text{CF})}(p^2 = \mu^2)}{\mu^2} + \frac{5\lambda m^2}{8\mu^2} \right) , \quad (5.129)$$

$$\gamma_c = -\mu \frac{d}{d\mu} \left(\frac{\Sigma^{(\text{CF})}(p^2 = \mu^2)}{\mu^2} \right) . \quad (5.130)$$

An explicit calculation yields

$$\gamma_A \rightarrow -\frac{13\lambda}{3} , \quad \gamma_c \rightarrow -\frac{3\lambda}{2} \quad (\mu^2 \rightarrow \infty) \quad (5.131)$$

for the high-energy limit of the gluon and ghost anomalous dimensions. The latter are just the ordinary pQCD gamma functions: in the UV regime, the RG-improved gluon and ghost propagators will have the standard pQCD behavior. As for the running coupling and gluon mass parameter, we find that

$$\beta_\lambda \rightarrow -\frac{22\lambda^2}{3} , \quad \gamma_{m^2} \rightarrow -\frac{3\lambda}{2} \quad (\mu^2 \rightarrow \infty) , \quad (5.132)$$

the first of which, again, is just the ordinary pQCD beta function, whereas the second yields a running $m^2(\mu^2)$ which at large renormalization scales behaves as

$$m^2(\mu^2) \sim [\lambda(\mu^2)]^{\frac{9}{44}} \sim [\ln \mu^2]^{-\frac{9}{44}} , \quad (5.133)$$

¹¹We remark that the massiveness of the RG-improved gluon propagator does not depend on the specific coefficient of the constant term in Eq. (5.125), as long as it is chosen different from zero. The factor of $5/8$ is the most natural choice, given that an opposite term is present in the low-energy expansion of δZ_c .

thus decreasing as a negative rational power of the logarithm at high energies.

To end this section, we derive some useful expressions for the RG-improved gluon and ghost propagators¹². Let us start from the latter. Recall that the MOM-scheme RG-improved ghost propagator $\mathcal{G}(p^2; \mu_0^2)$ renormalized at the scale μ_0 can be expressed in terms of the gluon anomalous dimension γ_c as

$$\mathcal{G}(p^2; \mu_0^2) = \frac{1}{p^2} \exp\left(\int_{\mu_0}^p \frac{d\mu}{\mu} \gamma_c\right). \quad (5.134)$$

Since in the DIS scheme $\gamma_c = \gamma_{m^2}$, the above equation can be rewritten as

$$\begin{aligned} \mathcal{G}(p^2; \mu_0^2) &= \frac{1}{p^2} \exp\left(\int_{\mu_0}^p \frac{d\mu}{\mu} \gamma_c\right) = \frac{1}{p^2} \exp\left(\int_{\mu_0}^p \frac{d\mu}{\mu} \gamma_{m^2}\right) = \\ &= \frac{1}{p^2} \exp\left(\int_{\mu_0}^p \frac{d\mu}{m^2} \frac{dm^2}{d\mu}\right) = \frac{1}{p^2} \frac{m^2(p^2)}{m^2(\mu_0^2)}. \end{aligned} \quad (5.135)$$

We thus see that in the DIS scheme the RG-improved ghost propagator is equal to the running gluon mass parameter $m^2(p^2)$ divided by p^2 , normalized by the value of m^2 at the renormalization scale μ_0 . Similarly, since by Eq. (5.128) the gluon anomalous dimension γ_A can be expressed as

$$\gamma_A = \frac{\beta_\lambda}{\lambda} - 2\gamma_{m^2}, \quad (5.136)$$

the RG-improved DIS gluon propagator $\Delta(p^2; \mu_0^2)$ renormalized at the scale μ_0 can be put in the form

$$\begin{aligned} \Delta(p^2; \mu_0^2) &= \frac{1}{p^2} \exp\left(\int_{\mu_0}^p \frac{d\mu}{\mu} \gamma_A\right) = \frac{1}{p^2} \exp\left(\int_{\mu_0}^p \frac{d\mu}{\mu} \left[\frac{\beta_\lambda}{\lambda} - 2\gamma_{m^2}\right]\right) \\ &= \frac{1}{p^2} \exp\left(\int_{\mu_0}^p d\mu \left[\frac{1}{\lambda} \frac{d\lambda}{d\mu} - \frac{2}{m^2} \frac{dm^2}{d\mu}\right]\right) = \\ &= \frac{1}{p^2} \frac{\lambda(p^2)}{\lambda(\mu_0^2)} \frac{m^4(\mu_0^2)}{m^4(p^2)}. \end{aligned} \quad (5.137)$$

Eqs. (5.135) and (5.137) allow us to study the infrared behavior of the RG-improved propagators analytically. Indeed, assuming that, as $p^2 \rightarrow 0$, the running mass parameter $m^2(p^2)$ saturates to a non-zero constant while the running coupling $\lambda(p^2)$ goes to zero like p^2 , the last equations tell us that $\Delta(p^2; \mu_0^2)$ also saturates to a non-zero constant, whereas $\mathcal{G}(p^2; \mu_0^2)$ diverges like $1/p^2$. The validity of these assumptions can be proved by solving the DIS RG equations for λ and m^2 in the low-energy limit,

$$\mu \frac{d\lambda}{d\mu} \propto \frac{m^2 \lambda^2}{\mu^2}, \quad \mu \frac{dm^2}{d\mu} \propto \lambda \mu^2, \quad (5.138)$$

which follow from the asymptotic behavior

$$\gamma_A \propto \frac{m^2 \lambda}{\mu^2}, \quad \gamma_c \propto \frac{\mu^2 \lambda}{m^2} \quad (\mu^2 \rightarrow 0). \quad (5.139)$$

We thus conclude that in the deep infrared the RG-improved DIS propagators have the expected limits. In the next section, we will put our results to the test by comparing them with the lattice data.

¹²These can be shown to hold also in renormalization schemes which slightly differ from the DIS scheme – see e.g. [DM20].

5.2.4 Comparison with the lattice data

As we saw at the end of the previous section, the RG-improved Landau-gauge DM gluon and ghost propagators renormalized at the scale μ_0 in the DIS scheme can be expressed as

$$\Delta(p^2; \mu_0^2) = \frac{1}{p^2} \frac{\lambda(p^2) m^4(\mu_0^2)}{\lambda(\mu_0^2) m^4(p^2)}, \quad \mathcal{G}(p^2; \mu_0^2) = \frac{1}{p^2} \frac{m^2(p^2)}{m^2(\mu_0^2)}, \quad (5.140)$$

where $\lambda(p^2) = N\alpha_s(p^2)/4\pi$ is the running coupling and $m^2(p^2)$ is the running gluon mass parameter. The latter can be computed by numerically integrating the Renormalization Group equations

$$\mu \frac{d\lambda}{d\mu} = \beta_\lambda, \quad \mu \frac{dm^2}{d\mu} = \gamma_{m^2} m^2, \quad (5.141)$$

with the beta and gamma functions β_λ and γ_{m^2} provided by Eqs. (5.128) and (5.129), starting from initial values $\lambda(\mu_0^2)$ and $m^2(\mu_0^2)$ at the renormalization scale μ_0^2 .

Within the Dynamical Model, λ and m^2 are not independent parameters. On the contrary, they are related to one another via the gap equation $V'(m^2) = 0$. Since the effective potential $V(m^2)$ is RG invariant by definition, the order in which one solves the gap equation and the RG equations is irrelevant, as long as the choice of the renormalization scheme is consistent between the two.

In Sec. 5.1.4, the gap equation was renormalized in the $\overline{\text{MS}}$ scheme and evaluated at fixed scale. To be consistent with the RG improvement of the propagators, in what follows we will instead use the RG-improved version of the potential – namely,

$$V(m^2) = \frac{9}{13} \frac{N_A}{N} \frac{m^4(\mu)}{2g^2(\mu)} \left(1 + \beta_0 \frac{g^2(\mu)}{16\pi^2} \ln \frac{m^2(\mu)}{\mu^2} \right)^{1+\gamma_0/\beta_0}, \quad (5.142)$$

where

$$\beta_0 = \frac{11N}{3}, \quad \gamma_0 = -\frac{3N}{2} \quad (5.143)$$

are the one-loop coefficients of the $\overline{\text{MS}}$ beta function β_g and gamma function γ_{m^2} . Eq. (5.142) can be obtained by resumming $V(m^2)$ to leading log within the $\overline{\text{MS}}$ scheme, as explained in [Kas92].

To find the DIS solutions of $V'(m^2) = 0$ starting from Eq. (5.142), one has to convert the coupling and mass parameter from one scheme to the other. This can be done by making use of the equations

$$m_{\text{DIS}}^2 = \frac{Z_{m^2, \overline{\text{MS}}}}{Z_{m^2, \text{DIS}}} m_{\overline{\text{MS}}}^2, \quad \lambda_{\text{DIS}} = \frac{Z_{g, \overline{\text{MS}}}^2}{Z_{g, \text{DIS}}^2} \lambda_{\overline{\text{MS}}}, \quad (5.144)$$

where $Z_{m^2, \text{DIS}}$ and $Z_{g, \text{DIS}}$ (resp. $Z_{m^2, \overline{\text{MS}}}$ and $Z_{g, \overline{\text{MS}}}$) are the mass and coupling renormalization factors evaluated in the DIS (resp. $\overline{\text{MS}}$) scheme. Explicitly, to one loop, these read

$$m_{\text{DIS}}^2 = \left[1 + \frac{5\lambda}{8} + (\delta Z_{c, \text{DIS}} - \delta Z_{c, \overline{\text{MS}}}) \right] m_{\overline{\text{MS}}}^2, \quad (5.145)$$

$$\lambda_{\text{DIS}} = \left[1 + (\delta Z_{A, \text{DIS}} - \delta Z_{A, \overline{\text{MS}}}) + 2(\delta Z_{c, \text{DIS}} - \delta Z_{c, \overline{\text{MS}}}) \right] \lambda_{\overline{\text{MS}}}. \quad (5.146)$$

The solutions of the RG-improved gap equation are displayed in Fig. 5.2 both in the DIS scheme and in the $\overline{\text{MS}}$ scheme.

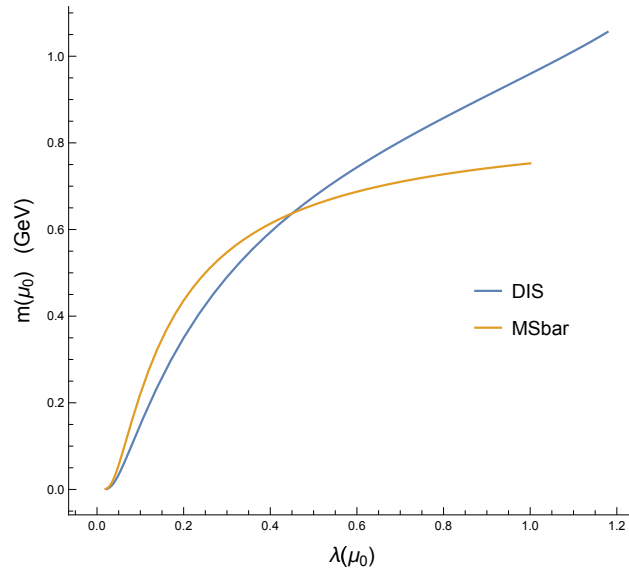


Figure 5.2: Solutions of the RG-improved gap equation at the renormalization scale $\mu_0 = 1$ GeV. Blue curve: DIS scheme. Orange curve: $\overline{\text{MS}}$ scheme.

In what follows, the one-loop RG-improved Landau-gauge DM propagators $\Delta(p^2; \mu_0^2)$ and $\mathcal{G}(p^2; \mu_0^2)$ will be compared with the lattice data of [DOS16]. The only free parameter of the comparison will be the value of the DIS coupling $\lambda(\mu_0^2)$ at the initial renormalization scale μ_0 – taken to be equal to 1 GeV¹³ –, the value of the DIS gluon mass parameter $m^2(\mu_0^2)$ being calculated from the gap equation as a function of $\lambda(\mu_0^2)$.

In order to fix $\lambda(\mu_0^2)$, a combined fit of the gluon and ghost dressing functions – $p^2\Delta(p^2; \mu_0^2)$ and $p^2\mathcal{G}(p^2; \mu_0^2)$, respectively – was performed, with equal weights for both the functions. The fit yielded $\lambda(\mu_0^2) = 0.473$, corresponding to $\alpha_s(\mu_0^2) = 1.981$ and to $m(\mu_0^2) = 0.655$ GeV by the DIS gap equation (Fig. 5.2).

The RG-improved one-loop Landau-gauge DM gluon propagator and dressing function are displayed, respectively, in Figs. 5.3 and 5.4, together with the lattice data of [DOS16]. As we can see, the DIS functions show a very good agreement with the lattice over a wide range of momenta, extending from $p \approx 0.5$ GeV up to $p \approx 8$ GeV. In the infrared, as anticipated in the previous section, the gluon propagator saturates to a finite non-zero value, confirming that within the framework of the Landau-gauge Dynamical Model the gluon develops a mass. Nonetheless, the one loop approximation in which the propagator is computed is not able to reproduce the lattice results at energies lower than ≈ 0.5 GeV. As discussed in Sec. 3.3.3 and reported likewise for the Screened Massive Expansion, this issue is common to massive perturbative truncations of Yang-Mills theory improved by the Renormalization Group, and is expected to be solved by going to higher order in perturbation theory [GPRT19, CS20].

¹³Since the lattice data of [DOS16] were originally renormalized at 4 GeV, a rescaling of the data was necessary to renormalize them at 1 GeV.

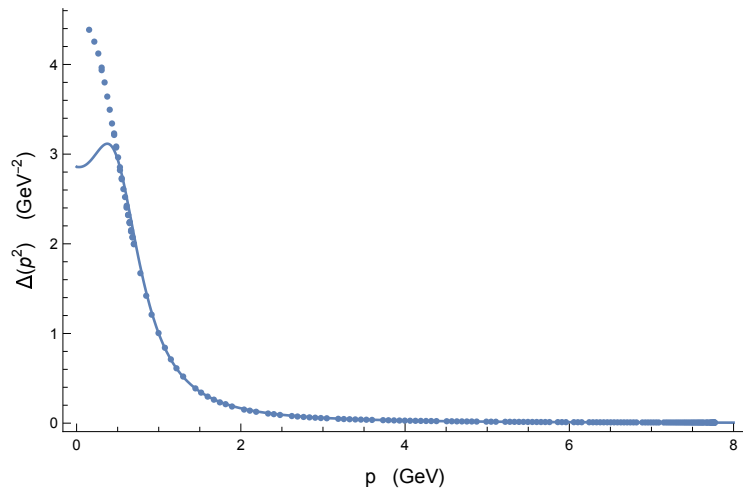


Figure 5.3: Euclidean transverse gluon propagator in the Landau gauge ($\alpha = 0$) renormalized at the scale $\mu_0 = 1$ GeV. Solid curve: one-loop RG-improved DM in the DIS scheme with the gluon mass parameter obtained from the gap equation; $\lambda(\mu_0^2) = 0.473$, $m(\mu_0^2) = 0.655$ GeV. Dots: lattice data from [DOS16].

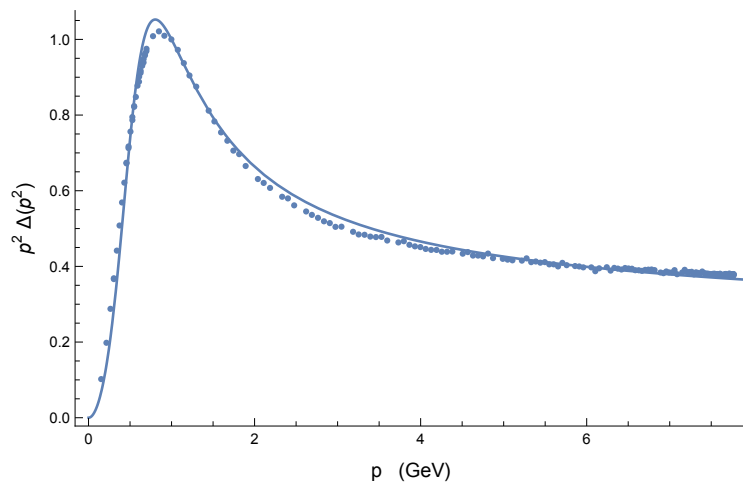


Figure 5.4: Euclidean gluon dressing function in the Landau gauge ($\alpha = 0$) renormalized at the scale $\mu_0 = 1$ GeV. As in Fig. 5.3.

In Fig. 5.5 we display the RG-improved one-loop Landau-gauge DM ghost dressing function. At variance with the gluon sector, the agreement between the DIS function and the lattice deteriorates below $p \approx 1$ GeV. Nonetheless, the match between the two is very good at larger momenta – up to $p \approx 8$ GeV. In the limit of vanishing momenta, the dressing function $p^2\mathcal{G}(p^2; \mu_0^2)$ saturates to a constant, implying that $\mathcal{G}(p^2; \mu_0^2)$ grows to infinity like $1/p^2$. In other words, the RG-improved ghost propagator is massless, as expected.

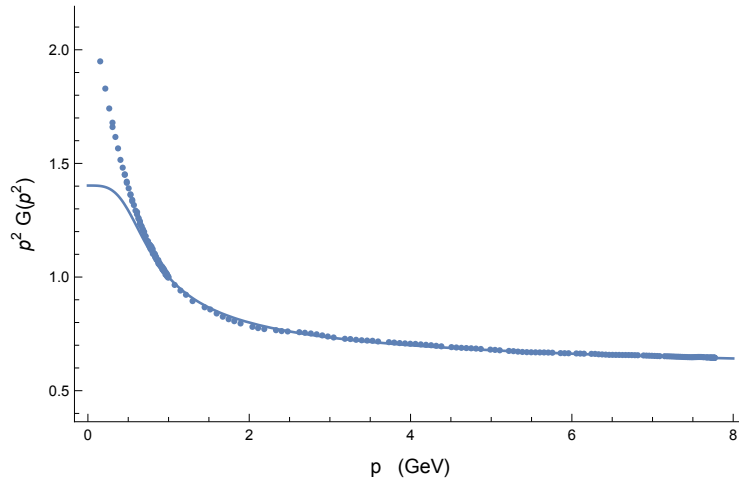


Figure 5.5: Euclidean ghost dressing function in the Landau gauge ($\alpha = 0$) renormalized at the scale $\mu_0 = 1$ GeV. As in Fig. 5.3.

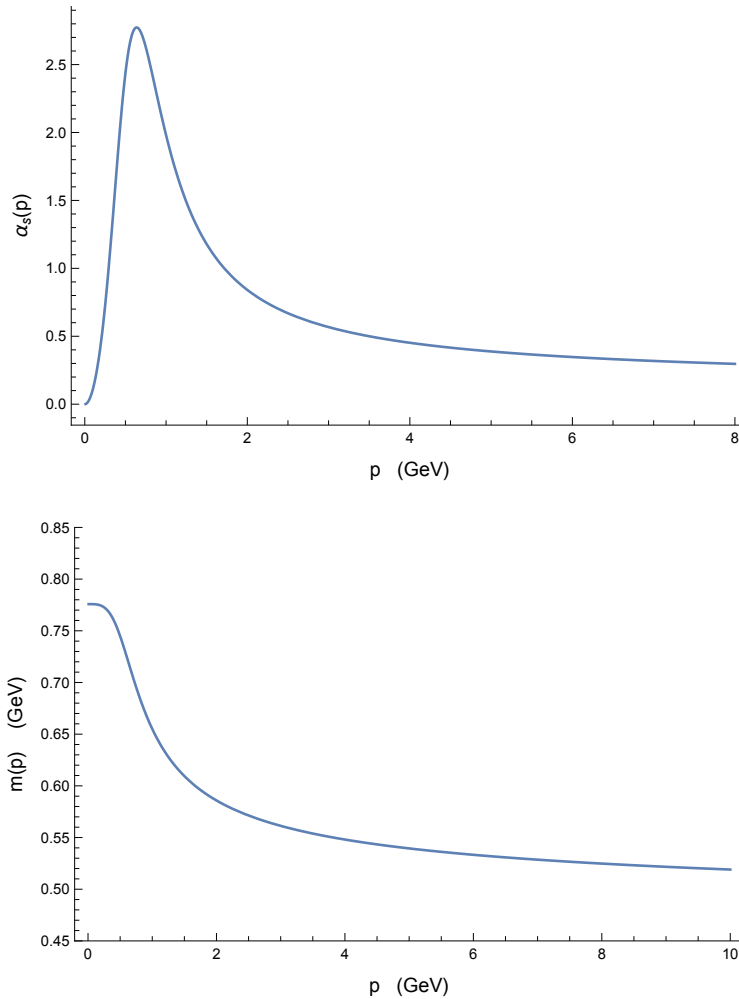


Figure 5.6: DM running coupling (top) and gluon mass parameter (bottom) for the initial values $\lambda(\mu_0^2) = 0.473$ and $m(\mu_0^2) = 0.655$ GeV at $\mu_0 = 1$ GeV.

In Fig. 5.6 we show the DIS running coupling $\alpha_s(p^2) = \frac{4\pi}{3}\lambda(p^2)$ and gluon mass parameter $m(p^2)$ obtained by integrating the RG equations with initial values $\lambda(\mu_0^2) = 0.473$ and $m(\mu_0^2) = 0.655$ GeV at $\mu_0 = 1$ GeV. Given that, within the DIS scheme, the coupling and propagators are defined, respectively, in the Taylor scheme and in the MOM scheme, the relation

$$\alpha_s(p^2) = \alpha_s(\mu_0^2) [p^2\Delta(p^2; \mu_0^2)][p^2\mathcal{G}(p^2; \mu_0^2)]^2 \quad (5.147)$$

still holds between $\alpha_s(p^2)$ and $\Delta(p^2; \mu_0^2)$ and $\mathcal{G}(p^2; \mu_0^2)$, as can be easily seen from Eq. (5.140). In particular, since the gluon propagator and the ghost dressing function saturate to a non-zero constant as $p^2 \rightarrow 0$, $\alpha_s(p^2)$ tends to zero like p^2 in the deep infrared. At intermediate energies, the running coupling first increases with the momentum – attaining a maximum at $p \approx 0.64$ GeV, where $\alpha_s \approx 2.77$ – and then decreases again, showing the same behavior as the MOM-Taylor SME running coupling. In the UV, since the high-energy limit of the theory is not modified by the introduction of the condensate, $\alpha_s(p^2)$ reduces to the ordinary one-loop pQCD running coupling.

The running gluon mass parameter $m^2(p^2)$ is a decreasing function of momentum. For the fitted initial coupling $\lambda(\mu_0^2) = 0.473$, its saturation value at $p = 0$ is found to be $m(0) \approx 0.78$ GeV. At high energies, $m^2(p^2)$ was already shown to have the behavior

$$m^2(p^2) \sim \lambda^{\frac{9}{44}}(p^2) \propto [\ln(p^2)]^{-\frac{9}{44}}. \quad (5.148)$$

5.3 Conclusions

In this chapter we showed that the non-vanishing of the BRST-invariant condensate $\sigma = \frac{1}{2}\langle(A^h)^2\rangle$ in pure Yang-Mills theory can be proved in any covariant gauge by minimizing an effective potential $V(\sigma)$ derived by coupling the condensate to an external current J in the Faddeev-Popov action S_{FP} . Subsequent manipulations of S_{FP} , performed with the double objective of localizing the field A^h and of linearizing the source terms, led us to an action I which, when computed on the shell of the gap equation $V'(\sigma) = 0$, is dynamically equivalent to the Faddeev-Popov action. I defines the reformulation of pure Yang-Mills theory which we referred to as the Dynamical Model.

In the framework of the Dynamical Model, the gluons propagate as massive at tree level due to a mass term $\propto (A^h)^2$ which appears in the action as a result of the non-vanishing of the condensate. The corresponding gluon mass parameter m^2 was found to be equal to $-\sigma/\zeta$, where ζ is a free parameter introduced in the formalism in order to renormalize the effective potential. By resorting to a procedure known as the reduction of couplings, the parameter ζ was expressed as a power series in the coupling constant g^2 ; given that, to lowest order, ζ was found to be proportional to the inverse coupling g^{-2} , the mass parameter m^2 turned out to be proportional to $\langle g^2(A^h)^2 \rangle$ plus higher-order corrections, which were tracked up to next-to-leading order as required for solving the gap equation.

In a general covariant gauge, the DM action contains a number of new fields. These are the field $\delta\sigma$ – which quantifies the fluctuations of the operator $\frac{1}{2}(A^h)^2$ around its vacuum expectation value – and the fields τ^a and η^a , $\bar{\eta}^a$ – which enforce the divergencelessness of the field A^h . τ^a and η^a , $\bar{\eta}^a$ can be neglected in the Landau gauge, where – at least perturbatively – A^h coincides with the ordinary gluon field A , and as such already has zero divergence. As a result, the Landau-gauge DM action I_L takes on a considerably simpler form, in which the $(A^h)^2$ operator (and the corresponding condensate) is replaced by the ordinary quadratic gluon operator A^2 and the only new field is the fluctuation field $\delta\sigma$.

Following [DM20], the one-loop DM gluon and ghost propagators were computed in the Landau gauge by making use of the action I_L . The latter contains two new interaction

terms – namely, a cubic interaction $\delta\sigma A^2$ and a quartic interaction $(A^2)^2$ – which are proportional to ζ^{-1} . On the shell of the gap equation, the inclusion of the corresponding diagrams was shown to have the sole effect of removing the tree-level gluon mass term m^2 from the dressed gluon propagator, while leaving behind a counterterm δZ_2 required to renormalize the gluon polarization. Because of this, the one-loop Landau-gauge DM gluon and ghost propagators are the same as those computed within the Curci-Ferrari model, with the notable exception of the aforementioned lack of a tree-level mass term in the gluon propagator.

The Renormalization Group improvement of the DM propagators was performed in a renormalization scheme termed the Dynamically Infrared-Safe (DIS) scheme. In the DIS scheme, the propagators and coupling are defined, respectively, in the MOM and in the Taylor scheme, while the renormalization counterterm δZ_2 is chosen in such a way as to preserve the massiveness of the RG-improved gluon propagator at zero momentum. To one loop, the Landau-gauge DIS propagators can be expressed in terms of the running coupling $\lambda(p^2) = \frac{N}{4\pi}\alpha_s(p^2)$ and running gluon mass parameter $m^2(p^2)$ alone. The former were compared to the lattice results of [DOS16] and were found to be in very good agreement with the data over a wide range of momenta, extending from $p \approx 0.5$ GeV up to $p \approx 8$ GeV. Below $p \approx 0.5$ GeV, the one-loop approximation is insufficient to reproduce the exact results; the agreement with the data is nonetheless expected to improve by going to higher order in perturbation theory.

The DIS running coupling was shown to have the behavior typical of Taylor couplings computed by massive perturbative methods: instead of developing an infrared Landau pole as in ordinary perturbation theory, it hits a maximum at $p \approx m$ and then decreases to zero like p^2 as $p \rightarrow 0$; in the UV, it reduces to the running coupling of ordinary pQCD. The running gluon mass parameter, on the other hand, strictly decreases with the momentum, reaching a saturation value $m(0) \approx 0.78$ GeV and vanishing at high energies like a rational power of $\ln p^2$.

The Dynamical Model has the advantage of being a renormalizable framework within which – by procedures such as the reduction of couplings – the Green functions can be computed order-by-order in perturbation theory in terms of the strong coupling constant alone. This is made possible by the fact that the value of the condensate, and thus of the gluon mass parameter, can be computed by solving a gap equation which is itself built into the definition of the theory.

In the infrared, the Landau-gauge Dynamical Model reproduces the expected, non-perturbative behavior of pure Yang-Mills theory not only qualitatively – by the saturation of the gluon propagator at zero momentum – but also quantitatively, as demonstrated by a comparison with the lattice data. In the UV, where the effects of the gluon condensate are negligible, it reduces to ordinary perturbation theory.

The results presented in this chapter indicate that the non-vanishing of the BRST-invariant gluon condensate $\langle (A^h)^2 \rangle$ is a good candidate for explaining the mechanism by which dynamical mass generation occurs in the gluon sector of pure Yang-Mills theory.

6

Conclusions and outlook

The breakdown of ordinary perturbation theory in the infrared regime of Quantum Chromodynamics, together with the occurrence of dynamical mass generation in the gluon sector, make it necessary to devise new analytical methods for studying the low-energy behavior of the strong interactions. In this thesis, two such methods – the Screened Massive Expansion and the Dynamical Model – have been presented within the framework of pure Yang-Mills theory, with applications of the former to full QCD.

The Screened Massive Expansion (SME) is a perturbative formulation of Quantum Chromodynamics that treats the transverse gluons as massive at tree level by performing a shift of the expansion point of the Faddeev-Popov gauge-fixed action. The shift is achieved by adding a mass term for the transverse gluons in the kinetic part of the FP Lagrangian and subtracting it back from its interaction part, so that the total action is left unchanged. As a result of the shift, the gluons propagate with a massive propagator at order zero in the perturbative series; moreover, a new interaction vertex – quadratic in the gluon fields – arises in the Feynman rules of perturbation theory.

The presence of a gluon mass in the loops of the SME prevents the latter from developing infrared divergences and makes it possible for the gluon polarization not to vanish in the zero-momentum limit. Due to a cancellation which occurs between the tree-level mass inherited from the zero-order propagator and an opposite term contained in the polarization, the low-energy behavior of the transverse (dressed) gluon propagator is entirely determined by the interactions. At variance with ordinary pQCD, the one-loop SME gluon propagator is found to saturate to a finite constant – and thus to develop a mass – at zero momentum, in agreement with the predictions of the lattice calculations. The ghost propagator, on the other hand, diverges in the infrared, thus remaining massless as expected. Both the propagators – when evaluated in Euclidean space and at fixed scale – accurately reproduce the Landau-gauge pure Yang-Mills lattice data up to momenta of ≈ 4 GeV for the gluon, and of ≈ 2 GeV for the ghost.

By making use of optimization procedures based on principles of gauge invariance and of minimal sensitivity, the pure Yang-Mills fixed-scale SME propagators evaluated in a general covariant gauge can be made to depend – modulo multiplicative renormalization – on the Landau-gauge value of the gluon mass parameter m^2 alone. In the gluon sector, this is accomplished by enforcing the gauge-parameter independence of the position of the (complex-conjugate) poles of the propagator – as required by the Nielsen identities – and by assuming that the phases of the residues at the poles are independent from the gauge parameter as well. The optimized propagators are found to be indistinguishable from those obtained from a full fit of the lattice data.

The domain of validity of the SME propagators can be extended to arbitrarily large

momenta by resorting to Renormalization Group (RG) methods. Within such a framework, the Taylor-scheme SME running coupling is free of Landau poles provided that the value of the coupling at the initial renormalization scale is not too large. At intermediate energies, the RG-improved and the optimized fixed-scale results can be made to match by choosing a suitable value of the initial coupling, leaving yet again m^2 as the only free parameter of the expansion. The corresponding propagators are found to be in good agreement with the lattice calculations over a wide range of momenta, extending from ≈ 0.7 GeV up to ≈ 8 GeV. At low energies, the one-loop approximation is unable to capture the behavior of the lattice data. The discrepancy between the two is expected to be mitigated by going to higher order in perturbation theory.

The Screened Massive Expansion can be extended to finite temperatures $T \neq 0$ in order to study the thermal behavior of QCD. Within pure Yang-Mills theory, a one-loop evaluation of the (spatially) transverse and longitudinal gluon propagators is able to reproduce the lattice results only if the temperature dependence of the SME parameters is tuned separately for the two components. Doing so provides an effective description of the propagators at zero Matsubara frequency which is quite accurate in the transverse sector, but less so in the longitudinal one – especially at low momenta and at high temperatures. The temperature dependence of the zero-(spatial-)momentum gluon poles – that is, of the mass and damping factor of the gluon quasi-particles – can be estimated by making use of the results obtained in the transverse sector. Both of them are found to decrease with T below the critical temperature $T_c \approx 270$ MeV corresponding to the deconfinement phase transition, and to increase roughly linearly with T – as is expected for massless particles – for $T > T_c$. Overall, we assess that at high temperatures the SME may be suboptimal as a perturbative method when compared to more refined approaches such as the Hard Thermal Loop resummation.

Within the quark sector of full QCD, a shift analogous to the one performed in the gluon sector can be used to study the infrared enhancing of the quark mass brought by the violation of chiral symmetry. The Landau-gauge Euclidean quark mass functions computed to one loop in the SME are found to be in very good agreement with the unquenched lattice results for light quarks of masses ≤ 90 MeV, displaying saturation values of about ≈ 400 MeV which are much larger than the quarks' renormalized masses. The one-loop SME quark Z -function, on the other hand, shows a decreasing behavior which conflicts with the lattice results. This might be a consequence of the unusually small one-loop corrections to the vector part of the Landau-gauge quark self-energy, which make it necessary to at least include the two-loop diagrams in the calculations. Evidence that the behavior of the Z -function can be fixed by going to higher order in perturbation theory can be provided within the framework of the SME by replacing the internal gluon lines of the one-loop self-energy diagrams with (the principal-part approximation of) the full dressed gluon propagator, thus taking into account the higher-order corrections to the latter. Doing so provides a Z -function which correctly increases with momentum at high energies, despite still showing the wrong behavior at low energies.

The Dynamical Model (DM) explores the possibility that the dynamical generation of an infrared mass for the gluons might be triggered by a non-vanishing condensate of dimension 2 of the form $\langle (A^h)^2 \rangle$, where A^h is a gauge- and BRST-invariant non-local version of the gluon field A . The former can be defined as the field obtained by applying a gauge transformation to A in such a way as to make the latter divergenceless. When expanded in powers of the coupling constant, A^h is found to be perturbatively equal to the transverse component of the gluon field, plus an infinite number of higher-order

terms which depend non-locally on the divergence $\partial \cdot A$.

The non-vanishing of the VEV $\langle (A^h)^2 \rangle$ within pure Yang-Mills theory can be studied by making use of Local Composite Operator methods. After coupling the operator $(A^h)^2$ to an external current in the Faddeev-Popov action, successive transformations of the partition function lead to a BRST-invariant action I in which the condensate $\langle (A^h)^2 \rangle$ appears multiplied by the operator $(A^h)^2$ itself – thus yielding a mass term for the gluons. An effective potential can then be derived which is found to have a minimum for a non-zero value of the condensate, showing that $\langle (A^h)^2 \rangle \neq 0$ in any covariant gauge.

When evaluated on the solutions of the gap equation – that is, at vanishing first derivative of the effective potential –, the action I is dynamically equivalent to the Faddeev-Popov action. The Green functions of pure Yang-Mills theory can thus be computed in any covariant gauge within the Dynamical Model, by making use of the action I . The DM incorporates the non-perturbative corrections brought by the condensate via a gluon mass parameter $m^2 \propto -\langle (A^h)^2 \rangle$ and via a number of new vertices which also involve new bosonic and fermionic auxiliary fields. The derivation of the DM gluon and ghost propagators is the simplest in the Landau gauge, where $A^h = A$ and most of the auxiliary fields decouple. An explicit calculation shows that the one-loop Landau-gauge DM gluon polarization is equal to its Curci-Ferrari counterpart modulo new terms which cancel the tree-level gluon mass as soon as the gap equation is enforced. Similarly, the one-loop ghost self-energy is equal to the one computed within the Curci-Ferrari model. When renormalized in the Dynamically Infrared-Safe (DIS) scheme, the Euclidean RG-improved DM propagators are found to be in very good agreement with the Landau-gauge lattice data down to momenta ≈ 0.5 GeV. Thanks to the gap equation, this is achieved by making use of the strong coupling constant at the initial renormalization scale as the only free parameter of the expansion. The corresponding DIS running coupling is free of Landau poles, but still quite too large at intermediate energies for a one-loop approximation to be accurate down to vanishing scales; indeed, the approximation fails to reproduce the lattice data at momenta smaller than ≈ 0.5 GeV. The running gluon mass parameter is found to saturate to a finite constant in the zero momentum limit, and to vanish like a negative rational power of the logarithm at high energies.

The Screened Massive Expansion and the Dynamical Model paint a picture of the infrared regime of Quantum Chromodynamics which agrees with the Landau-gauge lattice calculations both qualitatively – displaying dynamical mass generation in the gluon sector and a massless ghost propagator – and quantitatively, within the limits of a one-loop approximation. The advantage they provide over other frameworks for studying the strong interactions at low energy is that of being first-principles, fully analytic methods, whose predictions can be improved systematically by evaluating the higher-order contributions to the QCD perturbative series. The way in which such predictions are made from first principles differs between the two frameworks. In the SME, the spurious free parameters of the expansion are fixed by requirements of gauge invariance and minimal sensitivity, which in the context of the Renormalization Group can then be exploited to express the strong running coupling as a function of the gluon mass parameter. In contrast, the Dynamical Model achieves the same goal – although practically in the opposite sense, expressing the mass parameter in terms of the coupling – thanks to a gap equation which is built into its very definition.

Both the SME and the DM use the ordinary Faddeev-Popov action as the starting point for the set-up of a modified perturbative expansion of QCD. This has three important consequences on the overall structure of the resulting frameworks. First of all, BRST invariance is retained as a symmetry: in the SME, this is true at the exact level, given that the total FP

action is not changed at all; in the DM, on the other hand, BRST invariance is achieved by a natural (nilpotent) extension of the standard BRST transformations to the new fields that appear in the action I . Second of all, the tree-level mass term which appears in the zero-order gluon propagators is removed from the corresponding dressed propagator: in the SME this happens thanks to an opposite gluon mass counterterm in the polarization, whereas in the DM the cancellation occurs as soon as the gap equation is enforced. In particular, in both cases the massiveness of the propagator can be specifically traced back to the loops of the expansion. Finally, none of the two frameworks addresses the issue of the Gribov copies. As we argued in the Introduction, this can be justified on the account that the effects of the Gribov copies on the dynamics of the theory are expected to be less strong if the gluons acquire a mass.

Whereas the perturbative series of the SME contains an infinite number of crossed diagrams at each order in the coupling – so that a criterion for its truncation has to be chosen explicitly by moving first and foremost from renormalizability requirements –, the opposite applies to the Dynamical Model. In practical terms, this means on the one hand that the SME and the DM radiative corrections turn out to be different when computed to fixed order in perturbation theory, and on the other hand that the gluon mass parameters m^2 defined within the two frameworks cannot be directly identified with one another. This last aspect is confirmed by the fact that the mass parameter of the SME is found not to run with the renormalization scale at one loop – at variance with its DM counterpart, whose running is determined by that of the strong coupling constant and of the BRST-invariant condensate. Thus, while in the Dynamical Model the gluon mass parameter is interpreted in terms of the latter by its very definition, within the SME m^2 must be simply regarded as a dimensionful scale introduced in the formalism with the objective of providing the transverse gluons with a mass. Despite these differences, the results obtained at one loop within the two frameworks remain overall quite similar, and yield a value of $m \approx 0.65$ GeV (at 1 GeV, as far as the DM is concerned) when the energy units of the theory are fixed by a comparison with the lattice data.

The achievements of the SME and of the DM in the two-point sector of pure Yang-Mills theory make the two approaches worthy of further research. As far as the Dynamical Model is concerned, work is already in progress to evaluate the propagators in an arbitrary covariant gauge so as to test whether the model is able to predict dynamical mass generation for the gluons beyond the Landau gauge. This is widely expected on the basis of the massiveness of the corresponding zero-order propagator, but needs to be confirmed by explicit calculations carried out in the context of specific renormalization schemes. Once in possession of the relevant analytic expressions, we will also be able to investigate whether the poles of the propagator are complex-conjugate and gauge-parameter independent, and to test the hypothesis – advanced within the SME – that the phases of its residues as well do not depend on the gauge.

In the framework of the Screened Massive Expansion, the gauge invariance of the gluon phases can in principle be used to make a determination of the gluon free parameters also within full QCD. Preliminary results suggest that this will be trickier to achieve than in pure Yang-Mills theory due to the larger number of parameters, which encompasses the chiral mass – that is, the mass parameter that sets the scale for the quark mass function at low energies –, as well as the quark's renormalized mass and various renormalization constants. The latter might be fixed – or at least put in relation to one another – by enforcing the gauge invariance of the quark poles, which again holds because of the Nielsen identities. One-loop expressions for the SME quark propagator in an arbitrary covariant gauge have already been derived with the objective of undertaking these analyses.

In the long run, it would be interesting to extend the Dynamical Model to full QCD and to use both the SME and the DM to evaluate higher-point Green functions such as the 3-gluon, the ghost-gluon and the quark-gluon interactions vertices. Moreover, the calculations could be pushed to two loops in order to test whether the deep IR behavior of the RG-improved propagators and the overall behavior of the quark Z -function improve as expected when the higher-order corrections are included in the perturbative series. Our hope is that the results presented in this thesis and by previous works will generate further interest in the research on perturbative methods for probing the non-perturbative regime of Quantum Chromodynamics.

Appendices

Appendix A

Canonical quantization of the Faddeev-Popov action

In Secs. 1.1.2 and 1.1.4 we saw that in the presence of the Nakanishi-Lautrup field B^a the Faddeev-Popov Lagrangian \mathcal{L}_{FP} can be expressed as

$$\begin{aligned} \mathcal{L}_{\text{FP}} = & -\frac{1}{2} \partial_\mu A_\nu^a (\partial^\mu A^{a\nu} - \partial^\nu A^{a\mu}) - g f_{bc}^a \partial_\mu A_\nu^a A^{b\mu} A^{c\nu} + \\ & -\frac{1}{4} g^2 f_{bc}^a f_{de}^a A_\mu^b A_\nu^c A^{d\mu} A^{e\nu} + \frac{\xi}{2} B^a B^a - \partial^\mu B^a A_\mu^a + \\ & + \bar{\psi} (i\gamma^\mu \partial_\mu - M) \psi + g \bar{\psi} \gamma^\mu T_a \psi A_\mu^a + \\ & + \partial^\mu \bar{c}^a \partial_\mu c^a + g f_{bc}^a \partial^\mu \bar{c}^a A_\mu^b c^c . \end{aligned} \quad (\text{A.1})$$

Just like any Lagrangian, \mathcal{L}_{FP} can be quantized by making use of the canonical formalism.

Within the canonical formalism, one associates conjugate momenta Π to the time-derivatives of the fields F using the formula

$$\Pi = \frac{\partial_R \mathcal{L}}{\partial \dot{F}} \quad (\text{A.2})$$

and then computes the Hamiltonian density \mathcal{H} by performing a Legendre transform of the Lagrangian \mathcal{L} ,

$$\mathcal{H}(F, \Pi) = \Pi \dot{F}(F, \Pi) - \mathcal{L}(F, \dot{F}(F, \Pi)) , \quad (\text{A.3})$$

where the functions $\dot{F}(F, \Pi)$ are obtained by inverting Eq. (A.2). As quantum operators, the fields and their conjugate momenta are endowed with canonical (equal-time) anti/commutation relations of the form

$$[F(\vec{x}, t), \Pi(\vec{y}, t)]_{\mp} = i \delta(\vec{x} - \vec{y}) , \quad (\text{A.4})$$

where the upper (resp. lower) sign holds for bosonic (resp. fermionic) fields. The Heisenberg equations for the fields and their conjugate momenta are then obtained by taking the commutators of the former with the Hamiltonian operator $H = \int d^3x \mathcal{H}$,

$$\dot{F} = i[H, F] , \quad \dot{\Pi} = i[H, \Pi] . \quad (\text{A.5})$$

By applying these definitions to \mathcal{L}_{FP} , we find that the momenta $\Pi^{a\mu}$, Π_B^a , Π_c^a , $\Pi_{\bar{c}}^a$, Π_ψ conjugate to the fields A_μ^a , B^a , c^a , \bar{c}^a and ψ , respectively, are given by

$$\Pi^{a\mu} = F^{a\mu 0} , \quad \Pi_B^a = -A_0^a , \quad \Pi_c^a = \partial_0 \bar{c}^a , \quad \Pi_{\bar{c}}^a = -D_0 c^a , \quad \Pi_\psi = i\psi^\dagger . \quad (\text{A.6})$$

We see that, formally, $\Pi^{a0} = 0$. The term $\Pi^{a0}\dot{A}_0^a$ will thus vanish in Eq. (A.3). Moreover, $\Pi_B^a = -A_0^a$. It follows that in the canonical formalism A_0^a must not be treated as a field variable, but rather as the momentum conjugate to the field B^a (modulo sign). From Eqs. (A.4) and (A.6) we can read out the following non-vanishing anti/commutation relations for the fields:

$$\begin{aligned} [A_i^a(\vec{x}, t), F^{bj0}(\vec{y}, t)] &= i\delta^{ab}\delta_i^j\delta(\vec{x} - \vec{y}) , & [A_0^a(\vec{x}, t), B^b(\vec{y}, t)] &= i\delta^{ab}\delta(\vec{x} - \vec{y}) , \\ \{c^a(\vec{x}, t), \partial_0\bar{c}^b(\vec{y}, t)\} &= i\delta^{ab}\delta(\vec{x} - \vec{y}) , & \{\bar{c}^a(\vec{x}, t), D_0c^b(\vec{y}, t)\} &= -i\delta^{ab}\delta(\vec{x} - \vec{y}) , \\ \{\psi(\vec{x}, t), \psi^\dagger(\vec{y}, t)\} &= \delta(\vec{x} - \vec{y}) \mathbb{1} . \end{aligned} \quad (\text{A.7})$$

In order to derive the Faddeev-Popov Hamiltonian, we first note that, by Eq. (A.6), the time derivatives of the fields A_i^a , c^a and \bar{c}^a can be expressed in terms of the fields themselves and of their conjugate momenta as

$$\dot{A}_i^a = -\Pi_i^a + \partial_i A_0^a + gf_{bc}^a A_i^b A_0^c , \quad \dot{c}^a = -\Pi_c^a - gf_{bc}^a A_0^b c^c , \quad \dot{\bar{c}}^a = \Pi_c^a . \quad (\text{A.8})$$

Despite the lack of analogous relations for the time derivatives of the fields ψ and B^a , the linearity of \mathcal{L}_{FP} in $\dot{\psi}$ and \dot{B}^a , together with the result $\Pi_\psi = i\psi^\dagger$, $\Pi_B^a = -A_0^a$, allow us to compute \mathcal{H} from Eq. (A.8) alone. An explicit calculation that uses

$$\mathcal{H} = \Pi^{ai}\dot{A}_i^a + \Pi_B^a\dot{B}^a + \Pi_c^a\dot{c}^a + \Pi_{\bar{c}}^a\dot{\bar{c}}^a + \Pi_\psi\dot{\psi} - \mathcal{L}_{\text{FP}} \quad (\text{A.9})$$

as its starting point yields

$$\begin{aligned} \mathcal{H} &= -\frac{1}{2}\Pi^{ai}\Pi_i^a + \Pi^{ai}(\partial_i A_0^a + gf_{bc}^a A_i^b A_0^c) + \frac{1}{4}F_{ij}^a F^{aij} - \frac{\xi}{2}B^a B^a + \partial^i B^a A_i^a + \\ &+ i\Pi_\psi\gamma^0(i\gamma^i D_i + g\gamma^0 T^a A_0^a - M)\psi - \Pi_c^a(\Pi_{\bar{c}}^a + gf_{bc}^a A_0^b c^c) - \partial^i \bar{c}^a D_i c^a . \end{aligned} \quad (\text{A.10})$$

It can be checked that the Heisenberg equations for A_i^a , c^a and \bar{c}^a coincide with Eqs. (A.8), whereas the other Heisenberg equations can be rearranged so as to be formally identical to the field equations obtained by minimizing the Faddeev-Popov action $S_{\text{FP}} = \int d^4x \mathcal{L}_{\text{FP}}$.

Appendix B

Perturbative decoupling of the determinant $\det(\Lambda(\xi))$ within dimensional regularization in the Dynamical Model

In order to localize the BRST-invariant gluon field A^h , in Sec. 5.1.3 we introduced a unity of the form

$$1 = \mathcal{N} \int \mathcal{D}\xi \mathcal{D}\tau \mathcal{D}\bar{\eta} \mathcal{D}\eta e^{-\Delta S_1} \det(\Lambda(\xi)) \quad (\text{B.1})$$

in the partition function of the Dynamical Model. In this Appendix we show that the determinant $\det(\Lambda(\xi))$ does not perturbatively contribute to the n -point Green functions of the theory, as long as it is defined in dimensional regularization. As a consequence, when doing calculations in perturbation theory using dimensional regularization, the determinant can be suppressed by setting $\det(\Lambda(\xi)) = 1$.

In order to prove our statement, we first rewrite the determinant in terms of a functional integral over a new pair of ghost fields $(\lambda, \bar{\lambda})$,

$$\det(\Lambda(\xi)) = \int \mathcal{D}\bar{\lambda} \mathcal{D}\lambda \exp \left\{ - \int d^d x \bar{\lambda}^a \Lambda_{ab}(\xi) \lambda^b \right\} . \quad (\text{B.2})$$

Since perturbatively

$$\Lambda_{ab}(\xi) = \delta_{ab} - \frac{g}{2} f_{abc} \xi^c + \frac{g^2}{3!} f_{ace} f_{edb} \xi^c \xi^d + \dots , \quad (\text{B.3})$$

we may re-express Eq. (B.2) as

$$\det(\Lambda(\xi)) = \int \mathcal{D}\bar{\lambda} \mathcal{D}\lambda e^{-(I_0 + I_1)} , \quad (\text{B.4})$$

where the action terms I_0 and I_1 read

$$I_0 = \int d^d x \bar{\lambda}^a \lambda^a , \quad I_1 = \int d^d x \bar{\lambda}^a \Omega_{ab}(\xi) \lambda^b , \quad (\text{B.5})$$

and $\Omega_{ab}(\xi)$ is given by

$$\Omega_{ab}(\xi) = \Lambda_{ab}(\xi) - \delta_{ab} . \quad (\text{B.6})$$

The action term I_1 contains the interactions between $(\lambda, \bar{\lambda})$ and ξ . The latter are quadratic in the ghost fields, with their ξ dependence encoded in the function $\Omega_{ab}(\xi)$. I_0 , on the other hand, contains the zero-order ghost propagator, which is easily seen to be $Q^{ab}(p) = \delta^{ab}$ in momentum space, or $Q^{ab}(x) = \delta^{ab}\delta(x)$ in coordinate space.

Consider the vacuum expectation value $\langle \mathcal{O} \rangle$ of an operator \mathcal{O} which does not depend on the newly-introduced fields $(\lambda, \bar{\lambda})$. This can be computed as

$$\langle \mathcal{O} \rangle = \frac{\langle \mathcal{O} e^{-I_1} \rangle_0}{\langle e^{-I_1} \rangle_0} = \langle \mathcal{O} e^{-I_1} \rangle_{0, \text{conn.}} = \sum_{n=0}^{+\infty} \frac{(-1)^n}{n!} \langle \mathcal{O} I_1^n \rangle_{0, \text{conn.}} , \quad (\text{B.7})$$

where the subscript 0 denotes that the average is to be taken with respect to the action I_0 plus any other $(\lambda, \bar{\lambda})$ -independent term originally present in the full action of the theory. In d dimensions, $\langle \mathcal{O} I_1^n \rangle_{0, \text{conn.}}$ explicitly reads

$$\begin{aligned} \langle \mathcal{O} I_1^n \rangle_{0, \text{conn.}} &= \int \prod_{i=1}^n d^d x_i \left\langle \mathcal{O} \prod_{j=1}^n \Omega_{a_j b_j}(\xi(x_j)) \right\rangle_{00, \text{conn.}} \times \\ &\times \left\langle \bar{\lambda}^{a_1}(x_1) \lambda^{b_1}(x_1) \cdots \bar{\lambda}^{a_n}(x_n) \lambda^{b_n}(x_n) \right\rangle_{\text{gh.}, \text{conn.}} , \end{aligned} \quad (\text{B.8})$$

where the subscript 00 denotes that the first average is to be taken with respect to the original action of the theory, whereas the subscript ‘‘gh.’’ denotes that the second average is to be taken with respect to the zero-order ghost action I_0 . Diagrammatically, for each $n \geq 1$, the ghost average receives contributions from a single ghost loop, depicted in Fig. B.1. In coordinate space, suppressing the color structure, the diagram reads

$$(-1)(n-1)! \delta(x_1 - x_2) \cdots \delta(x_{n-1} - x_n) \delta(x_n - x_1) , \quad (\text{B.9})$$

or, equivalently,

$$(-1)(n-1)! \delta(0) \int d^d x \prod_{i=1}^n \delta(x_i - x) , \quad (\text{B.10})$$

where $\delta(0)$ is a Dirac delta in coordinate space,

$$\delta(0) = \int \frac{d^d q}{(2\pi)^d} 1 . \quad (\text{B.11})$$

Therefore, for $n \geq 1$,

$$\langle \mathcal{O} I_1^n \rangle_{0, \text{conn.}} = (-1)(n-1)! \delta(0) \int d^d x \langle \mathcal{O} \text{Tr} \{ \Omega^n(\xi(x)) \} \rangle_{00, \text{conn.}} , \quad (\text{B.12})$$

where $\Omega^n(\xi)$ is the matrix product of n factors of $\Omega(\xi)$ and the trace is taken over the color indices.

In dimensional regularization, the integral in Eq. (B.11) vanishes (see e.g. [Col84]). It follows that $\langle \mathcal{O} I_1^n \rangle_{0, \text{conn.}} = 0$ for every $n \geq 1$, so that, going back to Eq. (B.7),

$$\langle \mathcal{O} \rangle = \langle \mathcal{O} \rangle_0 = \langle \mathcal{O} \rangle_{00} , \quad (\text{B.13})$$

where to obtain $\langle \mathcal{O} \rangle_{00}$ we have integrated out the free ghost action I_0 from $\langle \mathcal{O} \rangle_0$. What Eq. (B.13) means is that the perturbative corrections to the vacuum expectation value $\langle \mathcal{O} \rangle$ due to the determinant $\det(\Lambda(\xi))$ vanish in dimensional regularization. Therefore, the vacuum expectation value of any operator \mathcal{O} in the full theory can be computed by setting $\det(\Lambda(\xi)) = 1$ in its dimensionally regularized partition function.

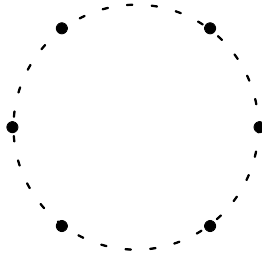


Figure B.1: Loop contributing to the ghost average in Eq. (B.8) (example for $n = 6$). The dashed line is the $(\lambda, \bar{\lambda})$ zero-order propagator.

One may have noticed that our proof – besides dimensional regularization – relies exclusively on the fact that $\Lambda(\xi)$ is equal to the unit matrix to lowest order in perturbation theory. The question arises, then, whether the proof is general enough to apply to the determinant of any such matrix. The answer is that, in general, it does not. Indeed, setting $\delta(0) = 0$ in dimensional regularization is allowed if and only if the calculations can be carried out without spoiling the symmetries of the theory.

While Lorentz invariance is clearly preserved by the action in Eq. (B.2), showing that the latter does not violate the BRST invariance of the full action of the theory requires us to extend the symmetry to the ghost fields λ and $\bar{\lambda}$. Indeed, a straightforward calculation starting from Eq. (5.35) and from the definition of $\Lambda_{ab}(\xi)$ in Eq. (5.30) yields

$$s\Lambda_{ab}(\xi) = \Lambda_{ac}(\xi) \Psi_b^c(c, \xi) , \quad (\text{B.14})$$

where

$$\Psi_b^a(c, \xi) = -\frac{\partial(s\xi^a)}{\partial\xi^b} , \quad (\text{B.15})$$

so that the new ghosts must have non-vanishing BRST transformations if the action in Eq. (B.2) is to be invariant. Since the BRST transformation does not act on the anti-ghost index of $\Lambda_{ab}(\xi)$, it is reasonable to define

$$s\lambda^a = -\Psi_b^a(c, \xi) \lambda^b , \quad s\bar{\lambda}^a = 0 , \quad (\text{B.16})$$

where $s\lambda^a$ is chosen so that $s(\Lambda\lambda) = 0$. The action in Eq. (B.2) – and the full action of the theory together with it – is invariant with respect to this extended BRST transformation. The nilpotency of the extended BRST operator is easily proved by observing that $s^2\Lambda_{ab}(\xi) = 0$ – which holds thanks to the nilpotency of s on the fields ξ and c – implies that

$$0 = s^2\Lambda_{ab} = \Lambda_{ac} \left(\Psi_d^c \Psi_b^d + s\Psi_b^c \right) , \quad (\text{B.17})$$

that is, $s\Psi = -\Psi^2$. When plugged into Eq. (B.16), this relation ensures that $s^2\lambda^a = s^2\bar{\lambda}^a = 0$.

Appendix C

Published papers

Variational study of mass generation and deconfinement in Yang-Mills theory

Giorgio Comitini and Fabio Siringo

*Dipartimento di Fisica e Astronomia dell'Università di Catania,
INFN Sezione di Catania, Via S.Sofia 64, I-95123 Catania, Italy*



(Received 19 August 2017; published 20 March 2018)

A very simple variational approach to pure $SU(N)$ Yang-Mills theory is proposed, based on the Gaussian effective potential in a linear covariant gauge. The method provides an analytical variational argument for mass generation. The method can be improved order by order by a perturbative massive expansion around the optimal trial vacuum. At finite temperature, a weak first-order transition is found (at $T_c \approx 250$ MeV for $N = 3$) where the mass scale drops discontinuously. Above the transition the optimal mass increases linearly as expected for deconfined bosons. The equation of state is found in good agreement with the lattice data.

DOI: [10.1103/PhysRevD.97.056013](https://doi.org/10.1103/PhysRevD.97.056013)

I. INTRODUCTION

In the last decades the dynamics of QCD has been under intensive theoretical study, aimed at understanding the properties of matter under the extreme conditions reached by heavy-ion collisions. Our understanding of the phase diagram has further motivated the study of pure $SU(N)$ Yang-Mills theory in the IR and at finite temperature, neglecting quarks as a first approximation. However, despite the important progresses made, we still miss an analytical description of $SU(N)$ theory from first principles, because of the breaking down of standard perturbation theory below the QCD scale.

The numerical simulation of the theory on a lattice has provided many important insights into the gluon dynamics. Among them, the dynamical generation of a gluon mass in the dressed propagator in the Landau gauge [1–8] and the occurrence of a phase transition with the gluons that become deconfined above the critical temperature [9–11]. However, since the numerical simulations can only provide data in the Euclidean space, no direct information can be gained in the Minkowski space where the dynamical properties of the gluon are defined. For instance, no direct proof of confinement can be obtained on the lattice and even the definition of mass can only be regarded as an energy scale without any clear dynamical meaning.

Continuous methods have been developed such as functional renormalization group [12–15], truncation of Dyson-Schwinger equations [16–23] and Hamiltonian

approaches [24,25]. They usually require the numerical solution of integral equations and there is no simple way to extract analytical results from the data.

On the other hand, effective models have been studied analytically, but they are not from first principles and are usually based on some modified quantization procedure [26–29] or different Lagrangians. For instance, adding a gluon mass to the Lagrangian is enough for extending the validity of perturbation theory down to the deep IR, yielding a very good overall picture of Yang-Mills theory at one loop [30–32]. In the context of background field methods the added gluon mass has provided a good description of the phase diagram at finite temperature, enforcing the idea that most of the nonperturbative effects can be embedded in the gluon-mass parameter [33–36]. While those models are important for understanding the physics of gluons, there is a growing interest in the study of analytical approaches to the exact $SU(N)$ theory.

In this paper, we discuss a very simple variational approach to $SU(N)$ theory, based on the Gaussian effective potential (GEP) in a linear covariant gauge. We do not modify the original Lagrangian of the theory but optimize the perturbative expansion by a variational argument, yielding a calculational analytical method that already provides very important predictions at the lowest orders of the approximation. Among the main results achieved by the present study we mention: (i) a variational argument for mass generation; (ii) the prediction of a first-order deconfinement transition at $T_c \approx 250$ MeV for $N = 3$; (iii) the formal definition of a perturbative expansion around the optimized vacuum, allowing for an order-by-order improvement of the approximation.

The original approach of Ref. [37] is here improved and extended to finite temperature, yielding analytical results up to a one-dimensional numerical integration that is

Published by the American Physical Society under the terms of the Creative Commons Attribution 4.0 International license. Further distribution of this work must maintain attribution to the author(s) and the published article's title, journal citation, and DOI. Funded by SCOAP³.

required for the thermal functions. The perturbative expansion around the vacuum turns out to be the massive expansion developed in Refs. [38–41] which was found in excellent agreement with the lattice data [42]. Thus, the present study enforces the validity of that expansion and provides a variational argument for its derivation. Moreover, while by itself the massive expansion cannot give a genuine proof of mass generation, the variational nature of the GEP can be used as a tool for demonstrating that a massless gaussian vacuum of Yang-Mills theory is unstable against the vacuum of massive gluons [37].

The expansion has been extended to finite temperature in Ref. [41] allowing for a direct calculation of the gluon damping rate in the IR and providing a direct proof of confinement. While in that study the zeroth order mass parameter was kept fixed, at finite temperature the GEP provides the free energy and allows us to determine the trial mass parameter variationally, as a function of temperature. The optimal mass scale is found discontinuous at the deconfinement transition, leading to an enhancement of the mass decrease that was already found in Ref. [41], in agreement with the observed behavior of the Debye mass in lattice simulations [10].

The GEP is the energy density of a trial Gaussian vacuum functional that is centered at a given average value of the field. The width of the functional is given by the mass of the trial free theory and is determined variationally at each value of the average field, yielding an effective potential that has been studied by several authors, mainly in the context of spontaneous symmetry breaking and scalar theories [43–64]. While the GEP is a genuine variational method [46,47], several extensions to higher orders have been proposed [56–59]. The idea of an expansion around the optimized vacuum of the GEP is not new [65] but has not been developed further. Expanding around the optimized massive vacuum of the GEP, the unconventional massive expansion of Refs. [38–40] is recovered in a natural way [37]. Thus, the phenomenological success of the expansion might be due to the variational choice of a zeroth order vacuum which incorporates most of the nonperturbative effects, leaving a residual interaction term that can be treated by perturbation theory.

One of the important merits of the GEP is its paradox of being a pure variational method disguised as a perturbative calculation, making use of the standard graphs of perturbation theory. Moreover, in the present context, the calculation is highly simplified by the assumption that the average of the gauge field is zero at the minimum of the potential. In other words, we only need the effective potential at its minimum where it is a function $V(m)$ of the trial mass parameter m . However, at variance with perturbation theory, the issue of renormalization is less standardized in a variational method and the regularization of the diverging integrals becomes a central aspect of the calculation.

The paper is organized as follows: in Sec. II the general formalism is discussed in the simple case of a scalar theory where standard well known results are recovered by the method; in Sec. III the delicate issue of regularization of the diverging integrals and renormalization of the GEP is addressed; in Sec. IV the GEP for pure $SU(N)$ Yang-Mills theory is studied at $T = 0$, providing a simple variational argument for mass generation; in Sec. V the GEP is extended to finite temperature and the phase transition is discussed; a general discussion and a summary of the results follow in Sec. VI.

II. GEP AND MASS GENERATION IN THE SCALAR THEORY

In order to illustrate the method, in this section we revise the formalism for the simple case of a self-interacting scalar theory [46] where the effective potential is well known and is given by three vacuum graphs as shown in Fig. 1. The renormalization scheme will be discussed in the next section. Most of the arguments developed here are quite general and will be used in the rest of the paper.

Let us consider the Lagrangian

$$\mathcal{L} = \frac{1}{2}\phi(-\partial^2 - m_B^2)\phi - \frac{\lambda}{4!}\phi^4 \quad (1)$$

where m_B is a bare mass. We can split the total Lagrangian as $\mathcal{L} = \mathcal{L}_0 + \mathcal{L}_{\text{int}}$ where the trial quadratic part is

$$\mathcal{L}_0 = \frac{1}{2}\phi(-\partial^2 - m^2)\phi \quad (2)$$

and describes a free scalar particle with a trial mass $m \neq m_B$. The new interaction follows as

$$\mathcal{L}_{\text{int}} = -\frac{\lambda}{4!}\phi^4 - \frac{1}{2}(m_B^2 - m^2)\phi^2 \quad (3)$$

so that the total Lagrangian is left unchanged. If we neglect the interaction, then a free Hamiltonian \mathcal{H}_0 is derived from \mathcal{L}_0 and its ground state $|m\rangle$ satisfies

$$\mathcal{H}_0|m\rangle = E_0(m)|m\rangle \quad (4)$$

and depends on the trial mass m . Restoring the interaction \mathcal{L}_{int} , the full Hamiltonian reads $\mathcal{H} = \mathcal{H}_0 + \mathcal{H}_{\text{int}}$ and by

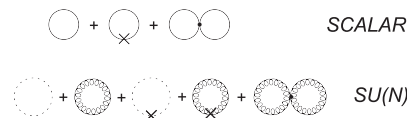


FIG. 1. Vacuum graphs contributing to the GEP for the scalar theory (first row) and pure $SU(N)$ Yang-Mills theory (second row).

standard perturbation theory, the first-order energy of the ground state reads

$$E_1(m) = E_0(m) + \langle m | \mathcal{H}_{\text{int}} | m \rangle = \langle m | \mathcal{H} | m \rangle \quad (5)$$

and is equivalent to the first-order effective potential $V_1(m)$ evaluated by perturbation theory in the covariant formalism with the interaction \mathcal{L}_{int} . Thus, the stationary condition

$$\frac{\partial V_1(m)}{\partial m} = \frac{\partial E_1(m)}{\partial m} = 0 \quad (6)$$

gives the best value of m that minimizes the vacuum energy of the ground state $|m\rangle$.

While being a pure variational method, the first-order effective potential $V_1(m) = E_1(m)$ can be evaluated by the sum of all the vacuum graphs up to first order (the three loop graphs in Fig. 1). The resulting optimized effective potential is the GEP. Usually, the effective potential is evaluated for any value of the average $\varphi = \langle \phi \rangle$ and the best m also depends on that average. If the symmetry is not broken, then the minimum of the effective potential is at $\varphi = 0$ where $V_1(m)$ is a function of the trial mass, to be fixed by the stationary condition Eq. (6). We assume that the gauge symmetry is not broken in Yang-Mills theory so that $V_1(m)$ at $\varphi = 0$ is the effective potential we are interested in.

The variational nature of the method ensures that the true vacuum energy is smaller than the minimum of $V_1(m)$. At the minimum, $|m\rangle$ provides an approximation for the vacuum and is given by the vacuum of a free massive scalar particle with mass equal to the optimized mass parameter $m \neq m_B$. Of course, the optimal state $|m\rangle$ is just a first approximation and the actual vacuum is much richer. However, we expect that a perturbative expansion around that approximate vacuum would be the best choice for the Lagrangian \mathcal{L} , prompting towards an expansion with an interaction \mathcal{L}_{int} and a free part \mathcal{L}_0 that depend on m and can be optimized by a clever choice of the parameter m . Different strategies have been proposed for the optimization, ranging from the stationary condition of the GEP, Eq. (6), to Stevenson's principle of minimal sensitivity [66]. A method based on the minimal variance has been recently proposed for QCD and other gauge theories [57,67–71]. In all those approaches, the underlying idea is that an optimal choice of m could minimize the effect of higher orders in the expansion. Since the total Lagrangian does not depend on m , the physical observables are expected to be stationary at the optimal m , thus suggesting the use of stationary conditions for determining the free parameter. As a matter of fact, if all graphs were summed up exactly, then the dependence on m would cancel in the final result, so that the strength of that dependence measures the weight of the neglected graphs at any order.

Leaving aside the problem of the best choice of m , we observe that at $\varphi = 0$ the calculation of the first-order effective potential $V_1(m)$ is quite straightforward and follows from the first-order expansion of the effective action $\Gamma(\varphi)$

$$e^{i\Gamma(\varphi)} = \int_{1PI} \mathcal{D}_\phi e^{iS_0(\phi+\varphi)+iS_{\text{int}}(\phi+\varphi)} \quad (7)$$

where the functional integral is the sum of all one-particle irreducible (1PI) graphs and $S = S_0 + S_{\text{int}}$ is the action. The effective potential then follows as $V(m) = -\Gamma(0)/\mathcal{V}_4$ where \mathcal{V}_4 is a total space-time volume. The sum of graphs up to first order gives the first-order effective potential $V_1(m)$ which is the GEP when optimized by Eq. (6).

At finite temperature, the effective potential is replaced by a density of free energy $\mathcal{F}(T, m)$ according to

$$e^{-\beta[\mathcal{V}_3\mathcal{F}(T, m)]} = \int \mathcal{D}_\phi e^{(S_0+S_{\text{int}})} \quad (8)$$

where the action $S = S_0 + S_{\text{int}}$ is the integral over imaginary time τ

$$S = \int_0^\beta d\tau \int d^3x \mathcal{L}, \quad (9)$$

$\beta = 1/T$ and \mathcal{V}_3 is a total three-dimensional space volume. The perturbative expansion of the free energy follows by the same connected graphs contributing to the effective potential, with loop integrals replaced by a sum over discrete frequencies and a three-dimensional integration. In the limit $T \rightarrow 0$ the effective potential is recovered as $V(m) = \mathcal{F}(0, m)$ and each thermal graph gives the corresponding vacuum term. Because of the one to one correspondence of the graphs we can easily switch from the thermal to the vacuum formalism when required. Moreover, at finite temperature, the GEP maintains its genuine variational nature. In the Hamiltonian formalism, the variational argument that follows Eq. (5) can be generalized by Bogolubov's inequality

$$\mathcal{F} \leq \mathcal{F}_0 + \frac{1}{\mathcal{V}_3} \frac{\text{Tr}[\mathcal{H}_{\text{int}} \exp(-\beta\mathcal{H}_0)]}{\text{Tr}[\exp(-\beta\mathcal{H}_0)]} = \mathcal{F}_1 \quad (10)$$

while in the Lagrangian formalism the same result is found by Jensen-Feynman inequality

$$\mathcal{F} \leq \mathcal{F}_0 - \frac{1}{\beta\mathcal{V}_3} \frac{\int \mathcal{D}_\phi S_{\text{int}} e^S}{\int \mathcal{D}_\phi e^S} = \mathcal{F}_1 \quad (11)$$

where \mathcal{F}_0 is the free energy obtained by the trial Lagrangian \mathcal{L}_0 while \mathcal{F}_1 is the first order approximation which becomes the GEP when optimized. The two inequalities tell us that the expansion must be truncated at first order for a genuine variational approximation. Here and in

the next two sections, when not specified, we will deal with the effective potential and with the renormalization of the vacuum graphs at zero temperature. The thermal corrections are finite and do not require any further renormalization.

Since we are interested in the massless Yang-Mills theory, we set $m_B = 0$ in the interaction Eq. (3) and study a massless scalar theory as a toy model for the problem of mass generation. The vertices of the theory can be read from \mathcal{L}_{int} in Eq. (3) where we set $m_B = 0$ and are used in Fig. 1 in the vacuum graphs. The usual four-point vertex $-\lambda$ is accompanied by the counterterm $\delta\Gamma = m^2$ that is denoted by a cross in the graphs. This counterterm must be regarded as part of the interaction so that the expansion is not loopwise and we find one-loop and two-loop graphs summed together in the first-order effective potential. That is where the nonperturbative nature of the method emerges since the expansion is not in powers of λ but of the whole interaction \mathcal{L}_{int} . The zeroth order (massive) propagator Δ_m follows from \mathcal{L}_0

$$\Delta_m(p) = \frac{1}{p^2 - m^2} \quad (12)$$

and is shown as a straight line in the vacuum graphs.

The tree term is the classical potential and vanishes in the limit $\varphi \rightarrow 0$. The first one-loop graph in Fig. 1 gives the standard one-loop effective potential, containing some effects of quantum fluctuations. It must be added to the second one-loop graph in Fig. 1, the crossed graph containing one insertion of the counterterm.

It is instructive to see that the exact sum of all one-loop graphs with n insertions of the counterterm gives the standard vacuum energy of a massless particle. In other words, if we sum all the crossed one-loop graphs the dependence on m disappears and we are left with the standard one-loop effective potential of Coleman and Weinberg [72] $V_{1L}^0 = -\Gamma_{1L}^0/\mathcal{V}_4$ where Γ_{1L}^0 is the standard one-loop effective action at $\varphi = 0$

$$e^{i\Gamma_{1L}^0} = \int \mathcal{D}\phi e^{i \int \frac{1}{2}\phi(-\partial^2)\phi d^4x} \sim [\text{Det}(\Delta_0^{-1})]^{-\frac{1}{2}} \quad (13)$$

and $\Delta_0^{-1} = p^2$ is the free-particle propagator of a massless scalar particle. Up to an additive constant, not depending on m , Eq. (13) can be written as

$$V_{1L}^0 = \frac{-i}{2\mathcal{V}_4} \text{Tr} \log(\Delta_m^{-1} + m^2) \quad (14)$$

then expanding the log we obtain a *massive expansion*

$$V_{1L}^0 = \frac{-i}{2\mathcal{V}_4} \text{Tr} \left\{ \log(\Delta_m^{-1}) - \sum_{n=1}^{\infty} \frac{(-m^2\Delta_m)^n}{n} \right\} \quad (15)$$

that is shown pictorially in Fig. 2 as a sum of crossed one-loop vacuum graphs. While the sum cannot depend on m , if

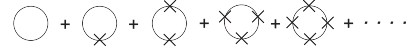


FIG. 2. Pictorial display of the right hand side of Eq. (15).

we truncate the expansion at any finite order we obtain a function of the mass parameter. As a test of consistency, one can easily check that, once renormalized as described below, the sum of all the crossed one-loop vacuum graphs in Fig. 2 gives zero exactly.

The calculation of the GEP requires the sum of only the first two terms of Eq. (15), the two one-loop graphs in Fig. 1. We cannot add higher-order terms without spoiling the variational method since the average value of the Hamiltonian in the trial state $|m\rangle$ is $E_1(m) = V_1(m)$, according to Eq. (5). Using the identity

$$\Delta_m = -\frac{\partial}{\partial m^2} \log(\Delta_m^{-1}) \quad (16)$$

the sum of one-loop graphs in Fig. 1 can be written as

$$V_{1L}(m) = \left(1 - m^2 \frac{\partial}{\partial m^2}\right) K(m) = K(m) - \frac{1}{2} m^2 J(m) \quad (17)$$

where $K(m)$ and $J(m)$ are defined as

$$\begin{aligned} K(m) &= \frac{-i}{2\mathcal{V}_4} \text{Tr} \log(\Delta_m^{-1}) \\ J(m) &= \frac{i}{\mathcal{V}_4} \text{Tr} \Delta_m \end{aligned} \quad (18)$$

and because of Eq. (16), satisfy the identity

$$\frac{\partial K(m)}{\partial m^2} = \frac{1}{2} J(m). \quad (19)$$

At $T = 0$ they can be written as explicit diverging integrals

$$\begin{aligned} K(m) &= \frac{1}{2i} \int \frac{d^4 p}{(2\pi)^4} \log(-p^2 + m^2) \\ J(m) &= -i \int \frac{d^4 p}{(2\pi)^4} \frac{1}{-p^2 + m^2} \end{aligned} \quad (20)$$

to be regularized in some renormalization scheme. At finite temperature Eq. (19) still holds, but the integrals acquire a finite additive thermal part.

We recognize $K(m)$ as the standard one-loop effective potential of Coleman and Weinberg for a massive scalar particle in the limit $\varphi \rightarrow 0$. This term contains the quantum fluctuations at one-loop. The second term in Eq. (17) is a correction coming from the counterterm and arises because the exact Lagrangian was massless.

The calculation of the GEP also requires the two-loop graph in Fig. 1 which is first-order in λ . It can be recovered from the crossed one-loop graph by just substituting the vertex $-m^2$ with the seagull one-loop self energy Σ_{1L} that reads [57]

$$\Sigma_{1L} = \frac{\lambda}{2} J(m) \quad (21)$$

and adding a $1/2$ symmetry factor. The resulting two-loop term is

$$V_{2L}(m) = \frac{\lambda}{8} [J(m)]^2. \quad (22)$$

The GEP follows as the sum $V_{1L} + V_{2L}$

$$V_G(m) = K(m) - \frac{1}{2} m^2 J(m) + \frac{\lambda}{8} [J(m)]^2. \quad (23)$$

At this stage we have just recovered the GEP in the limit $\varphi \rightarrow 0$ and Eq. (23) agrees with the well known GEP in that limit [46,56,57,59,60].

More precisely, V_G is the GEP when m is optimized by the stationary condition Eq. (6) that reads

$$\frac{\partial V_G(m)}{\partial m^2} = \frac{1}{2} \left(\frac{\partial J(m)}{\partial m^2} \right) \left[\frac{\lambda J(m)}{2} - m^2 \right] = 0 \quad (24)$$

yielding the usual gap equation of the GEP

$$m^2 = \frac{\lambda J(m)}{2}. \quad (25)$$

From a mere formal point of view, if Eq. (25) has a nonzero solution, the GEP predicts the existence of a mass for the massless scalar theory. That is of special interest because for $m_B = 0$ the Lagrangian in Eq. (1) has no energy scale, just like Yang-Mills theory and QCD in the chiral limit. Thus, it can be regarded as a toy model for the more general problem of mass generation and chiral symmetry breaking.

III. RENORMALIZATION OF THE GEP

The scalar theory has been studied by many authors in the past, using different regulators, ranging from the insertion of a cut-off to dimensional regularization and, of course, to lattice regularization. The resulting physical theories are not always equivalent and the problem of triviality is still not totally solved. The issue is quite subtle and has to do with the physical meaning that we give to the theory in a four dimensional space. The regularization of the GEP has also been addressed by many methods [44,46,60–64]. The most intuitive way of regularizing the integrals is by inserting a large but finite cutoff Λ which provides the physical units of the theory, as in lattice calculations where the finite lattice spacing a cuts the

energies larger than $\Lambda \sim 1/a$. In the Euclidean space, the integral J reads

$$J(m) = \int_0^{\Lambda^2} \frac{p^2 dp^2}{16\pi^2} \left[\frac{1}{p^2 + m^2} \right] > 0 \quad (26)$$

and is a finite positive-definite function of the mass parameter. The gap equation, Eq. (25), has a well defined solution at $m^2 = m_0^2 = c_\lambda \lambda \Lambda^2 / (32\pi^2)$ where c_λ is a coefficient of order unity, with $0 < c_\lambda < 1$ and $c_\lambda \approx 1$ in the limit $\lambda \rightarrow 0$. Since the derivative

$$\frac{\partial J(m)}{\partial m^2} < 0 \quad (27)$$

is negative for any value of m^2 , the derivative of the effective potential in Eq. (24) changes sign at $m = m_0$ and becomes positive for $m > m_0$. Thus, the GEP has an absolute minimum at m_0 and the simple cutoff regularization predicts a mass. The existence of a minimum at $m = m_0 > 0$ makes sense when compared with the data of lattice simulations that predict the existence of a finite mass in the limit $m_B^2 \rightarrow 0^+$ of the unbroken-symmetry theory [73]. However, that mass is not a dynamical mass and arises from the quadratic divergence of J because no special symmetry protects the theory. That is not a desirable feature in a toy model for Yang-Mills theory since Becchi-Rouet-Stora-Tyutin (BRST) invariance, which is not broken on the lattice, forbids the appearance of diverging mass terms. In that context, dimensional regularization is the first choice since it leaves BRST unbroken and is the simplest and usual way to cancel the quadratic divergence.

Having set $d = 4 - \epsilon$, in the limit $\epsilon \rightarrow 0$ the integral J is redefined as $J\mu^\epsilon$ where μ is an arbitrary scale of the order of m and expanding in powers of ϵ

$$J(m) = -\frac{m^2}{16\pi^2} \left[\frac{2}{\epsilon} + \log \frac{\bar{\mu}^2}{m^2} + 1 + \mathcal{O}(\epsilon) \right] \quad (28)$$

where $\bar{\mu} = (2\sqrt{\pi}\mu) \exp(-\gamma/2)$. Integrating Eq. (19) and neglecting an integration constant (that does not depend on m)

$$K(m) = -\frac{m^4}{64\pi^2} \left[\frac{2}{\epsilon} + \log \frac{\bar{\mu}^2}{m^2} + \frac{3}{2} + \mathcal{O}(\epsilon) \right]. \quad (29)$$

In the usual approach of Coleman and Weinberg [72], the divergences are absorbed by the (infinite) integration constants that are traded as finite and physical renormalized parameters. Following that approach, we could hide the poles in the definition of an energy scale Λ_ϵ such that

$$\log \Lambda_\epsilon^2 = \log \bar{\mu}^2 + \frac{2}{\epsilon} + 1 \quad (30)$$

and write the integrals K, J as simply as

$$\begin{aligned} J(m) &= \frac{m^2}{16\pi^2} \log \frac{m^2}{\Lambda_\epsilon^2} \\ K(m) &= \frac{m^4}{64\pi^2} \left[\log \frac{m^2}{\Lambda_\epsilon^2} - \frac{1}{2} \right]. \end{aligned} \quad (31)$$

If Λ_ϵ were traded as a finite unknown energy scale, then the regularized expressions of J and K would be finite.

Let us investigate the limits of Eq. (31) when the definition of Λ_ϵ , Eq. (30), is taken literally, in the attempt to give it a physical meaning. While ϵ might even be a complex variable and the physical meaning of the poles is quite obscure in general, Eq. (30) only makes sense if we assume that ϵ is real, at least. Moreover, the expansion can only be trusted if $|\epsilon \log(\bar{\mu}^2/m^2)| \ll 1$ which is equivalent to say that

$$\log \frac{\Lambda_\epsilon^2}{m^2} \approx \frac{2}{\epsilon} \rightarrow \pm\infty \quad (32)$$

yielding $m \ll \Lambda_\epsilon$ if $\epsilon > 0$ and $m \gg \Lambda_\epsilon$ if $\epsilon < 0$. Thus, if we literally assume to work in a $(4 \mp |\epsilon|)$ -dimensional space-time, Eq. (31) holds asymptotically for a very small or a very large mass compared to Λ_ϵ . The energy scale Λ_ϵ can be regarded as a very large UV cutoff or a very small IR cutoff, according to the sign of ϵ . In both cases, we must face the non-intuitive result that the regularized J and its derivative change sign according to the value of m : for $m \ll \Lambda_\epsilon$ the integral J is negative while for $m \gg \Lambda_\epsilon$ the derivative of J becomes positive, which is at odds with the intuitive result obtained by a simple cutoff in Eqs. (26), (27). Actually, we must recognize that dimensional regularization is not neutral but its way to make sense of divergences is part of the physical interpretation of a field theory, with scaleless integrals that vanish exactly and a less marked difference between UV and IR divergences. Moreover, the use of dimensional regularization is controversial in the scalar theory and different physical theories seem to arise when the limit $d \rightarrow 4$ is taken from above ($d > 4$) or below ($d < 4$), as first pointed out by Stevenson [62] in 1987. While it is still not obvious if any of them describes the lattice-regulated scalar theory, they could be very relevant for our toy model of Yang-Mills theory. After reviewing them briefly, we will show how a dimensional regularization scheme can be set up for the variational effective potential of Yang-Mills theory.

A. The autonomous theory ($d < 4$)

The autonomous renormalization of scalar theory [46,61] can be easily recovered by dimensional regularization for $d < 4$ [62,64]. It shows spontaneous symmetry breaking and asymptotic freedom but cannot be connected, perturbatively, to the usual low energy phenomenology that

emerges by perturbation theory and $1/N$ expansion [62,63].

The search for a minimum of the GEP yields the coupled equations [61,64]

$$\begin{aligned} m_0^2 &= \frac{1}{3} \lambda \varphi_0^2 \\ m_0^2 &= -\frac{\lambda}{2} J(m_0) \end{aligned} \quad (33)$$

where φ_0 is the optimal average value of the scalar field that would eventually break the symmetry if a solution exists. In that case, the other stationary point at $\varphi = 0$ is a maximum where Eq. (25) holds. If the symmetry is broken Eq. (25) is replaced by the second of Eq. (33), which has the opposite sign and has a physical solution if $\epsilon \rightarrow 0^+$ ($d < 4$). In fact, using the first of Eq. (31), the new gap equation reads

$$\frac{1}{\alpha} = \log \frac{\Lambda_\epsilon}{m_0} \quad (34)$$

where $\alpha = \lambda/(16\pi^2)$ is a bare effective coupling and $\Lambda_\epsilon \rightarrow \infty$ in the limit $\epsilon \rightarrow 0^+$ so that $\alpha \rightarrow 0^+$ is positive. The solution m_0 of the gap equation can be regarded as a physical scale which breaks the symmetry according to the first of Eq. (33). Assuming that m_0 takes some fixed phenomenological value, the large scale Λ_ϵ can be eliminated as

$$\Lambda_\epsilon = m_0 e^{1/\alpha} \quad (35)$$

so that the theory shows asymptotic freedom. Inserting the explicit expressions of J and K in the effective potential, the GEP at its minimum is [61,64]

$$V_G = -\frac{m_0^4}{128\pi^2} < 0 \quad (36)$$

and Λ_ϵ can be sent to infinity ($\epsilon \rightarrow 0^+$) yielding a finite energy density, spontaneous symmetry breaking and a finite physical mass m_0 .

At variance with perturbation theory, in principle, the variational method does not require the use of a renormalized coupling. However, it is useful to parametrize the gap equation in terms of a finite running coupling α_μ which can be defined according to [60,64]

$$\frac{1}{\alpha} = \frac{1}{\alpha_\mu} + \log \frac{\Lambda_\epsilon}{\mu} > 0 \quad (37)$$

where μ is any finite scale. The gap equation, Eq. (34), is written as a finite renormalized gap equation

$$\frac{1}{\alpha_\mu} = \log \frac{\mu}{m_0} \quad (38)$$

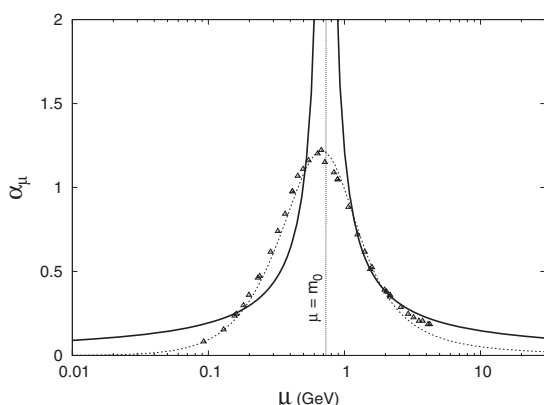


FIG. 3. The running coupling α_μ of Eq. (43) is shown for $m_0 = 0.73$ GeV (solid line), together with the lattice data of Ref. [4] for the strong coupling α_s of Yang-Mills theory in the Taylor scheme. The exponent ν is arbitrarily fixed by matching the data at $\mu = 2$ GeV. The dotted line is the analytical result of Ref. [39], obtained by a one-loop expansion around the Gaussian massive vacuum at $m = m_0 = 0.73$ GeV.

where m_0 is assumed to be the physical RG invariant mass. As a toy model of Yang-Mills theory, we assume that $\alpha_\mu > 0$, so that μ must be larger than m_0 and the running of α_μ takes place in the UV sector, limited from below by the Landau pole at $\mu = m_0$. The beta function is negative and the running coupling shows asymptotic freedom. A plot of the coupling α_μ is shown (up to a factor) as a solid line on the right side of Fig. 3. The breaking of symmetry and the existence of a mass scale seem to reverse the usual trivial behavior of the scalar theory. The autonomous behavior is separated from the usual weak coupling limit which is observed below the Landau pole. However, we must mention that Eq. (38) is just a possible reparametrization of Eq. (34); it is not necessary, since the effective potential is anyway RG invariant at its minimum; and besides, the parametrization is not unique. It has some features that make it a good candidate as a physical renormalized coupling at the scale μ : in fact, reversing Eq. (37) it can be written in the perturbative weak coupling limit as $\alpha_\mu = \alpha[1 + \mathcal{O}(\alpha)]$ and $\alpha_\mu \rightarrow \alpha$ in the UV limit $\mu \rightarrow \Lambda_\epsilon$. But, it is not obvious how α_μ is related to the four-point function at the scale μ . Moreover, the parametrization is not unique: the existence of a RG invariant energy scale m_0 allows us to define a generic scale

$$\Lambda'_\epsilon = m_0 \left(\frac{\Lambda_\epsilon}{m_0} \right)^\nu \quad (39)$$

and a different running coupling α'_μ according to

$$\frac{1}{\alpha} = \frac{1}{\alpha'_\mu} + \frac{1}{\nu} \log \frac{\Lambda'_\epsilon}{\mu} \quad (40)$$

yielding by Eq. (34) the finite equation

$$\frac{1}{\alpha'_\mu} = \frac{1}{\nu} \log \frac{\mu}{m_0}. \quad (41)$$

Thus, the coefficient of the beta function is somehow arbitrary and we do not expect that any serious prediction can be made without an explicit calculation of the four-point function. Quite interesting, the exponent ν can be taken negative, inverting the sign of the beta function. However, assuming that $\alpha'_\mu > 0$, we obtain $\mu < m_0$ if $\nu < 0$. The negative beta function would be defined below the Landau pole, and the new parametrization would describe the IR sector of the theory showing the same behavior that is predicted by perturbation theory and $1/N$ expansion: an increasing running coupling and triviality. For a negative ν , a plot of α'_μ is shown as a solid line on the left side of Fig. 3. We observe that if $\nu < 0$ then $\Lambda'_\epsilon \rightarrow 0$ in the limit $\epsilon \rightarrow 0^+$ when $\Lambda_\epsilon \rightarrow \infty$. Let us consider the special case $\nu = -1$ and call $\delta_\epsilon = \Lambda'_\epsilon$ in order to make clear that it is an infinitesimal IR scale, $\delta_\epsilon \rightarrow 0$. Eq. (34) can be written as

$$\frac{1}{\alpha} = \log \frac{m_0}{\delta_\epsilon} \quad (42)$$

which has the same identical content as before, but in terms of the IR vanishing scale $\delta_\epsilon = m_0 \exp(-1/\alpha)$. Thus the same theory now looks trivial. It is important to see that different parametrizations for $\nu = \pm 1$, predicting opposite beta functions, refer to different ranges of μ , separated by the Landau pole. Thus the respective weak coupling limits cannot be connected by perturbation theory, yielding a double-valued beta which is legitimate when the running coupling is not a monotone function. In fact, joining together the outcome of Eq. (41) for $\pm\nu$ we obtain

$$\frac{1}{\alpha'_\mu} = \left| \frac{1}{\nu} \log \frac{\mu}{m_0} \right| \quad (43)$$

which holds for any $\mu \neq m_0$, as shown in Fig. 3 where $|\nu|$ is arbitrarily chosen to match the strong coupling α_s at $\mu = 2$ GeV.

B. The precarious theory ($d > 4$)

Despite its name, the precarious renormalization of scalar theory [46] predicts the same phenomenology of perturbation theory and $1/N$ expansion [63]. Its handling by a cutoff is problematic since it seems to be unstable until the cut-off is sent to infinite. It emerges in a natural and straightforward way by dimensional regularization in $d > 4$, as first shown by Stevenson [62].

In the limit $\epsilon \rightarrow 0^-$, the energy scale Λ_ϵ goes to zero according to Eq. (30). Let us call it δ_ϵ in order to make clear that $\delta_\epsilon = \Lambda_\epsilon \rightarrow 0$. In the same limit, the coupled equations

for the minimum of the GEP, Eq. (33), have no solution because the bare coupling α would become negative in Eq. (34). There is no spontaneous symmetry breaking and the minimum of the effective potential is at $\varphi = 0$. At that point, having ruled out the breaking of symmetry, Eq. (25) holds and can be written as

$$\frac{1}{\alpha} = \log \frac{m_0}{\delta_\epsilon} \quad (44)$$

which has the opposite sign of Eq. (34). In the limit $\delta_\epsilon \rightarrow 0$ the bare coupling α is positive and an acceptable solution m_0 exists. As before, we assume that m_0 is a RG invariant physical mass which is generated dynamically in the massless theory. Thus, the small energy scale δ_ϵ can be eliminated as $\delta_\epsilon = m_0 \exp(-1/\alpha)$ in the effective potential. We observe that Eq. (44) is identical to Eq. (42), and the theory appears as trivial.

At its minimum $\varphi = 0$, the effective potential is given by Eq. (23) and inserting the regularized expressions of the integrals J , K , as given by Eq. (31) with $\Lambda_\epsilon = \delta_\epsilon \rightarrow 0$, we can write it as

$$V_G(m) = \frac{m^4}{128\pi^2} \left[\alpha \left(\log \frac{m^2}{\delta_\epsilon^2} \right)^2 - 2 \log \frac{m^2}{\delta_\epsilon^2} - 1 \right] \quad (45)$$

which obviously makes sense only if $m \gg \delta_\epsilon$. Eliminating δ_ϵ by Eq. (44) the renormalized GEP reads

$$V_G(m) = \frac{m^4}{128\pi^2} \left[\alpha \left(\log \frac{m^2}{m_0^2} \right)^2 + 2 \log \frac{m^2}{m_0^2} - 1 \right] \quad (46)$$

and is shown in Fig. 4. The only physical point is the absolute minimum at $m^2 = m_0^2$ where the effective potential does not depend on the bare coupling α and takes the value

$$V_G(m_0) = -\frac{m_0^4}{128\pi^2} < 0. \quad (47)$$

Then we can safely send $\epsilon \rightarrow 0$. We obtain the same identical vacuum energy that was found in Eq. (36) by the autonomous renormalization in $d < 4$, but here the mass m_0 is generated without any symmetry breaking.

We observe that the stationary point m_0 is the physical mass that emerges as the pole of the self-consistent propagator. Actually, up to first order, the self-energy is the sum of the tree-level counterterm $-m^2$ and the seagull graph Σ_{1L} in Eq. (21), so that the self-consistency condition $m = m_0$ is equivalent to the vanishing of the first-order self energy [57]

$$\Sigma_1 = -m^2 + \frac{\lambda}{2} J(m) = 0 \quad (48)$$

which is just the stationary condition Eq. (25) satisfied by m_0 .

As discussed for $d < 4$, we do not need to introduce any running coupling in the variational calculation, because the effective potential is finite in units of m_0 . However, it might be useful to reparametrize the gap equation by a finite running coupling α_μ which can be defined as before [62]

$$\frac{1}{\alpha} = \frac{1}{\alpha_\mu} + \log \frac{\mu}{\delta_\epsilon} > 0 \quad (49)$$

where μ is an arbitrary energy scale. The gap equation, Eq. (44), is then written as a finite renormalized gap equation

$$\frac{1}{\alpha_\mu} = \log \frac{m_0}{\mu} \quad (50)$$

where m_0 is the physical RG invariant mass. Since we assume that $\alpha_\mu > 0$, here μ must be smaller than m_0 and the running of α_μ takes place in the IR sector, below the Landau pole at $\mu = m_0$. While we could deduce, naively, that the theory is trivial and the beta function is positive, again we must recognize that the parametrization is not unique and the running of α_μ is limited in the IR sector. In fact, Eq. (50) is identical to Eq. (41) for $\nu = -1$ and the present theory gives the same running predicted by the autonomous theory in the IR sector. Again, the existence of the RG invariant mass m_0 allows us to define a new energy scale

$$\Lambda'_\epsilon = m_0 \left(\frac{\delta_\epsilon}{m_0} \right)^\nu \quad (51)$$

and a different running coupling α'_μ according to

$$\frac{1}{\alpha} = \frac{1}{\alpha'_\mu} + \frac{1}{\nu} \log \frac{\mu}{\Lambda'_\epsilon} \quad (52)$$

yielding by Eq. (44) the finite equation

$$\frac{1}{\alpha'_\mu} = \frac{1}{\nu} \log \frac{m_0}{\mu}. \quad (53)$$

Joining together the outcome of Eq. (53) for $\pm\nu$ we obtain the same identical result of Eq. (43) which holds for any $\mu \neq m_0$ and is shown as a solid line in Fig. 3. We conclude that, up to an unknown factor ν , the beta function might have the same behavior in both renormalization schemes.

C. A toy model for Yang-Mills theory

When regularized dimensionally, two different renormalized theories seem to emerge in the limit $d \rightarrow 4$. However, for many aspects, the two renormalized theories appear as two sides of the same coin. Both theories share a dynamical mass generation, the same vacuum energy density, a Landau pole at $\mu = m_0$ and can be parametrized by the same running coupling which is not monotone, showing asymptotic freedom in the UV and a trivial Gaussian fixed point in the IR.

In both cases the Landau pole that emerges in the reparametrization has no effect on the effective potential which is RG invariant and is valid at any energy scale. Actually, at variance with perturbation theory, the variational method does not even require the use of a running coupling. However, the existence of the pole says that the two weak-coupling limits cannot be connected by perturbation theory which must break down at the scale $\mu \approx m_0$. In fact, by general arguments, perturbation theory predicts that the beta function must be unique at the lowest orders of approximation and cannot depend on the special regularization scheme. But, if the running coupling is not a monotone function, a double valued beta function is found, taking different (opposite) values in different sectors that cannot be connected by perturbation theory. That scenario is only compatible with the existence of a RG invariant phenomenological energy scale where perturbation theory breaks down.

If we look at the strong coupling α_s of Yang-Mills theory in the Taylor scheme, a non-monotonic behavior is found in the Landau gauge on the lattice [4], assuming that the ghost-gluon vertex is regular and a running coupling can be defined from the product of the dressing functions of two-point correlators. Some lattice data of Ref. [4] are shown in Fig. 3 together with the analytical prediction of Ref. [39], obtained by a one-loop massive expansion around the zeroth-order Gaussian propagator $(-p^2 + m_0^2)^{-1}$ with $m_0 = 0.73$ GeV.

The energy $\mu \approx 0.7$ GeV, where the coupling reaches its maximum, is the phenomenological scale where perturbation theory breaks down. Somehow, the running coupling α_μ of Eq. (43) can be seen as a zeroth-order Gaussian approximation for the strong coupling $\alpha_s(\mu)$ of Yang-Mills theory. Actually, that is no coincidence since a gauge invariant effective potential will be derived in the next section for Yang-Mills theory, which is exactly the same GEP of Eq. (46) and Fig. 4, apart from a normalization

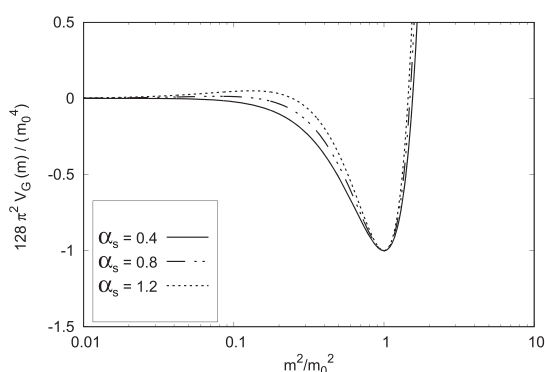


FIG. 4. The renormalized GEP of Eq. (46) is shown in units of m_0 for different values of the strong coupling α_s , having set $\alpha = \frac{9N}{8\pi}\alpha_s$.

factor and the precise definition of the effective coupling α . Thus, irrespective of the agreement with the lattice-regulated scalar theory, the dimensional-regulated GEP of scalar theory is a useful toy model for pure Yang-Mills theory.

The two scalar theories only differ because of the breaking of symmetry which appears for $d < 4$; while, for $d > 4$, a dynamical mass generation occurs without any symmetry breaking. Since gauge symmetry is not broken in Yang-Mills theory, we expect that the correct phenomenology can only be reproduced if we adopt the second scheme and regularize the theory keeping $d > 4$.

IV. GEP AND MASS GENERATION IN SU(N) THEORY

The Lagrangian of pure SU(N) Yang-Mills theory can be written as

$$\mathcal{L} = \mathcal{L}_{\text{YM}} + \mathcal{L}_{\text{fix}} + \mathcal{L}_{\text{FP}} \quad (54)$$

where \mathcal{L}_{YM} is the Yang-Mills term

$$\mathcal{L}_{\text{YM}} = -\frac{1}{2} \text{Tr}(\hat{F}_{\mu\nu} \hat{F}^{\mu\nu}) \quad (55)$$

\mathcal{L}_{fix} is a gauge fixing term and \mathcal{L}_{FP} is the ghost Lagrangian arising from the Faddeev-Popov determinant. In terms of the gauge fields, the tensor operator $\hat{F}_{\mu\nu}$ is

$$\hat{F}_{\mu\nu} = \partial_\mu \hat{A}_\nu - \partial_\nu \hat{A}_\mu - ig[\hat{A}_\mu, \hat{A}_\nu] \quad (56)$$

where

$$\hat{A}^\mu = \sum_a \hat{T}_a A_a^\mu \quad (57)$$

and the generators of SU(N) satisfy the algebra

$$[\hat{T}_a, \hat{T}_b] = if_{abc} \hat{T}_c \quad (58)$$

with the structure constants normalized according to

$$f_{abc} f_{dbc} = N\delta_{ad}. \quad (59)$$

If a generic linear covariant gauge-fixing term is chosen

$$\mathcal{L}_{\text{fix}} = -\frac{1}{\xi} \text{Tr}[(\partial_\mu \hat{A}^\mu)(\partial_\nu \hat{A}^\nu)], \quad (60)$$

where $\xi > 0$ is an arbitrary positive number, the total action can be written as $\mathcal{S}_{\text{tot}} = \mathcal{S}_0 + \mathcal{S}_I$ where the free-particle term is

$$\begin{aligned} \mathcal{S}_0 &= \frac{1}{2} \int A_{a\mu}(x) \delta_{ab} \Delta_0^{-1\mu\nu}(x, y) A_{b\nu}(y) d^d x d^d y \\ &+ \int \omega_a^*(x) \delta_{ab} \mathcal{G}_0^{-1}(x, y) \omega_b(y) d^d x d^d y \end{aligned} \quad (61)$$

and the interaction is

$$\mathcal{S}_I = \int d^d x [\mathcal{L}_{3g} + \mathcal{L}_{4g} + \mathcal{L}_{gh}] \quad (62)$$

with the usual local interaction terms that read

$$\begin{aligned} \mathcal{L}_{3g} &= -gf_{abc}(\partial_\mu A_{a\nu}) A_b^\mu A_c^\nu \\ \mathcal{L}_{4g} &= -\frac{1}{4} g^2 f_{abc} f_{ade} A_{b\mu} A_{c\nu} A_d^\mu A_e^\nu \\ \mathcal{L}_{gh} &= -gf_{abc}(\partial_\mu \omega_a^*) \omega_b A_c^\mu. \end{aligned} \quad (63)$$

In Eq. (61), Δ_0 and \mathcal{G}_0 are the standard free-particle propagators for gluons and ghosts and their Fourier transforms are

$$\begin{aligned} \Delta_0^{\mu\nu}(p) &= \Delta_0(p) [t^{\mu\nu}(p) + \xi \ell^{\mu\nu}(p)] \\ \Delta_0(p) &= \frac{1}{-p^2}, \quad \mathcal{G}_0(p) = \frac{1}{p^2}. \end{aligned} \quad (64)$$

Here the transverse and longitudinal projectors are defined as

$$t_{\mu\nu}(p) = g_{\mu\nu} - \frac{p_\mu p_\nu}{p^2}; \quad \ell_{\mu\nu}(p) = \frac{p_\mu p_\nu}{p^2} \quad (65)$$

where $g_{\mu\nu}$ is the metric tensor.

As discussed in Refs. [39,40], an unconventional massive expansion can be introduced by adding and subtracting mass terms $\delta\mathcal{S}_i$ in the total action, just like we did for the scalar theory in Eqs. (2), (3). The method can be generalized by redefining the free and interacting parts of the action

$$\begin{aligned} \mathcal{S}_0 &\rightarrow \mathcal{S}_0 - \sum_i \delta\mathcal{S}_i \\ \mathcal{S}_I &\rightarrow \mathcal{S}_I + \sum_i \delta\mathcal{S}_i. \end{aligned} \quad (66)$$

For the gluon we can take

$$\delta\mathcal{S}_g = \frac{1}{2} \int A_{a\mu}(x) \delta_{ab} \delta\Gamma^{\mu\nu}(x, y) A_{b\nu}(y) d^d x d^d y \quad (67)$$

where the vertex function $\delta\Gamma^{\mu\nu}$ is given by a shift of the inverse propagator

$$\delta\Gamma^{\mu\nu}(x, y) = [\Delta_0^{-1\mu\nu}(x, y) - \Delta_m^{-1\mu\nu}(x, y)] \quad (68)$$

and $\Delta_m^{\mu\nu}$ is the massive free-particle propagator

$$\begin{aligned} \Delta_m^{-1\mu\nu}(p) &= \Delta_m^T(p)^{-1} t^{\mu\nu}(p) + \Delta_m^L(p)^{-1} \ell^{\mu\nu}(p) \\ \Delta_m^T(p) &= \frac{1}{-p^2 + m^2}, \quad \Delta_m^L(p) = \frac{\xi}{-p^2 + m_L^2} \end{aligned} \quad (69)$$

As a general variational ansatz, the two masses m and m_L can be different.

In principle, we would also have the freedom to insert a mass shift $\delta\mathcal{S}_{gh}$ for the ghost

$$\delta\mathcal{S}_{gh} = \int \omega_a^*(x) \delta_{ab} \delta\Gamma(x, y) \omega_b(y) d^d x d^d y \quad (70)$$

together with its counterterm $\delta\Gamma$

$$\delta\Gamma(x, y) = [\mathcal{G}_0^{-1}(x, y) - \mathcal{G}_M^{-1}(x, y)] \quad (71)$$

where \mathcal{G}_M would be a massive ghost propagator

$$\mathcal{G}_M = \frac{1}{p^2 - M^2}. \quad (72)$$

One could wonder if the inclusion of a mass parameter in the trial ghost propagator could shift the pole of the ghost at one-loop, yielding a phenomenological mass which would be at odds with the lattice data for the dressed ghost propagator. However, in the massive expansion of the propagators [39,40] the counterterm cancels the shift at tree level and any real mass term can only arise from loops. That is the reason why no mass would arise for the photon in QED by the same method. It can be easily shown [71] that the ghost self energy is of order $\mathcal{O}(p^2)$ and vanishes when the external momentum $p \rightarrow 0$, so that the dressed ghost propagator still has a pole at $p^2 = 0$. That is an other way to see that the gluon mass arises from gluon loops in the expansion and is not a mere shift by a mass parameter.

The case of a finite ghost trial-mass $M > 0$ has been explored in Ref. [74] and found to be sub-optimal when compared with the standard choice of a massless ghost. Then, we will assume $M = 0$ in the present variational study. It must be mentioned that, if the ghost mass M were regarded as an independent variational parameter, then its stationary point would be at $M = 0$ because there are no ghost-gluon vertices in the first order effective potential. Actually, the ghost contribution would be maximal at that stationary point, because of the wrong sign of ghost statistics. However, as discussed in the next section, in the more general context of the finite temperature formalism, a maximal ghost energy minimizes the eventual weakening of Jensen-Feynman inequality that might occur in non-Abelian theories. While that weakening cannot be avoided entirely, we will suggest a rigorous way to control the error on the variational bound. Let us take aside the

problem for a while and assume that the GEP can be trusted as a variational method.

Since we have not changed the total action at all, we know that the sum of all graphs contributing to the longitudinal gluon polarization must give zero, because of gauge invariance. Thus, the exact longitudinal part of the gluon propagator must be equal to the free longitudinal propagator $\Delta_0^L(p) = \xi/(-p^2)$. While, in principle, m_L could be used as a variational parameter, we expect that the best result is achieved if the trial Δ_m^L is taken to be equal to the exact Δ_0^L by setting $m_L = 0$ in Eq. (69).

Having set $M = m_L = 0$, the variational ansatz becomes the same that was used in the massive expansion of Refs. [39,40,42] where no ghost and longitudinal masses were inserted. Only the pole of the transverse free-particle propagator is shifted and compensated by inserting a transverse counterterm

$$\delta\Gamma^{\mu\nu}(p) = -m^2 t^{\mu\nu}(p) \quad (73)$$

among the vertices of the interaction, while the gauge-dependent longitudinal part of the gluon propagator is left unchanged and equal to the exact result. As shown in Ref. [42], that massive expansion is in very good agreement with the data of lattice simulations. Moreover, that choice of counterterms has the merit of providing a fully gauge invariant GEP at $T = 0$, as shown below.

The calculation of the GEP follows the same steps as for the scalar theory. The GEP is obtained as the first-order effective potential in the covariant formalism, including the counterterms among the interaction vertices and in the limit of a vanishing background field, i.e., assuming that $\langle A_{a\mu} \rangle = 0$ since gauge symmetry is not broken in the vacuum. The effective action reads

$$e^{i\Gamma(a)} = \int_{1PI} \mathcal{D}_{A,\omega} e^{iS_0(a+A,\omega) + iS_m(a+A,\omega)} \quad (74)$$

and the effective potential follows as $V = -\Gamma(0)/\mathcal{V}_4$ and is the sum of all connected 1PI vacuum graphs. The first order graphs contributing to the GEP are shown in the second row of Fig. 1.

The zeroth order gluon and ghost loops in Fig. 1 give

$$V_0 = \frac{i}{2\mathcal{V}_4} \log \text{Det} \Delta_m^{\mu\nu} - \frac{i}{\mathcal{V}_4} \log \text{Det} \mathcal{G}_0. \quad (75)$$

The determinant of $\Delta_m^{\mu\nu}$ can be split as the product of determinants in the orthogonal Lorentz subspaces, $\text{Det} \Delta_m^{\mu\nu} = \text{Det}[\Delta_m^T t^{\mu\nu}] \text{Det}[\Delta_0^L \ell^{\mu\nu}]$, yielding

$$V_0 = \frac{i(d-1)}{2\mathcal{V}_4} \text{Tr} \log \Delta_m^T + \frac{i}{2\mathcal{V}_4} \text{Tr} \log \Delta_0^L - \frac{i}{\mathcal{V}_4} \text{Tr} \log \mathcal{G}_0. \quad (76)$$

where $d = 4$ in a four dimensional space-time.

The constant gauge dependent (infinite) term $\text{Tr} \log \xi$ is canceled by an equal factor in the normalization of the Faddeev-Popov functional, so that using $\Delta_0^L/\xi = -\mathcal{G}_0$, one-half of the ghost cancels the longitudinal term yielding

$$V_0(m) = N_A [(d-1)K(m) - K(0)] \quad (77)$$

where $N_A = N^2 - 1$.

The crossed one-loop graphs in Fig. 1 are obtained by one insertion of the counterterms. Since there are no ghost and longitudinal counterterms, there is only one crossed loop for the transverse gluon. The identity Eq. (16) changes its sign for Δ_m^T and inserting the counterterm of Eq. (73) the sum of all one-loop graphs (zeroth and first order) can be written as

$$V_{1L}(m) = \left(1 - m^2 \frac{\partial}{\partial m^2}\right) V_0(m) \quad (78)$$

which reads

$$\frac{V_{1L}(m)}{N_A} = (d-1) \left[K(m) - \frac{1}{2} m^2 J(m) \right] - K(0). \quad (79)$$

The functions $K(m)$ and $J(m)$ were defined in Eq. (20) and their explicit regularized expression were given in Eq. (31). The formal result of Eq. (79) is gauge invariant and also valid at finite temperature, since Eq. (16) still holds when the integrals K, J acquire a thermal part.

The first-order effective potential also includes the two-loop gluon graph in Fig. 1. For $m_L = 0$ each loop of the longitudinal propagator contributes a factor $\xi J(0)$ which is zero by dimensional regularization, so that the two-loop term is also gauge invariant at $T = 0$. The same identical expression would be obtained in Landau gauge ($\xi = 0$) if $m_L > 0$. The calculation is formally different in the finite temperature formalism and will be studied in the next section. Here, we examine the vacuum part that contributes to the GEP at $T = 0$ and is relevant for discussing the issue of mass generation. Inserting the seagull one-loop graph [71]

$$\Pi_{1L} = -\frac{(d-1)^2 N g^2}{d} J(m) \quad (80)$$

the two-loop term reads

$$V_{2L}(m) = \frac{N_A N g^2 (d-1)^3}{4d} [J(m)]^2. \quad (81)$$

Setting $d = 4$ and adding the one-loop term of Eq. (79), in terms of the new effective coupling α

$$\alpha = \frac{9N g^2}{32\pi^2} = \frac{9N}{8\pi} \alpha_s, \quad \alpha_s = \frac{g^2}{4\pi} \quad (82)$$

a gauge invariant GEP is found that can be written as

$$\frac{V_G(m)}{3N_A} = K(m) - \frac{m^2}{2} J(m) + 2\pi^2 \alpha [J(m)]^2 \quad (83)$$

having dropped the constant $K(0)$ which is zero at $T = 0$. That is the same identical result obtained in Eq. (23) for the scalar theory, provided that the effective coupling α is replaced by $\lambda/(16\pi^2)$. Thus, using the same dimensional regularization scheme of Sec. III and keeping $d > 4$, the renormalized GEP of Eq. (46) is recovered in units of the optimal gluon-mass parameter m_0 . Inserting the correct normalization factor, the GEP reads

$$\frac{V_G(m)}{3N_A} = \frac{m^4}{128\pi^2} \left[\alpha \left(\log \frac{m^2}{m_0^2} \right)^2 + 2 \log \frac{m^2}{m_0^2} - 1 \right] \quad (84)$$

and was shown in Fig. 4. That figure shows the existence of two competing stationary points for the vacuum: an unstable stationary point at $m = 0$ and a stable minimum at $m = m_0$.

The existence of a stable massive vacuum is a remarkable nonperturbative prediction of the present variational method and can be regarded as an argument for mass generation in pure Yang-Mills theory. We are tempted to identify the unstable stationary point at $m = 0$ with the massless scaling solution of Schwinger-Dyson equations. That solution is not found in lattice simulations.

In the next section, we will show that the two stationary points acquire a very different behavior at finite temperature. The massless vacuum at $m = 0$ develops a thermal mass that increases with temperature like for a standard massless boson, while the minimum at $m = m_0$ shows a decrease of the mass until a weak first order transition occurs before the merging of the minima.

As shown in Fig. 4, when written in physical units of m_0 , the renormalized GEP is not very sensitive to the actual value of the strong coupling α_s , especially at the stationary points that might be identified as physical configurations. Thus everything seems to be settled by the physical scale m_0 , while the coupling α_s must be regarded as a bare coupling at the scale Λ_ϵ according to our renormalization scheme discussed in Sec. III. Its actual value should be almost irrelevant and will be fixed by the principle of minimal sensitivity [66] as the stationary point of the critical temperature.

Since there is no scale in the original Lagrangian, the actual value of the mass m_0 cannot be predicted by the theory and must come from the phenomenology. The massive expansion of Refs. [39,40] arises as the natural expansion around the best trial massive vacuum at $m = m_0$. By that expansion, at one loop, the gluon propagator was found in perfect agreement with the data of lattice simulations [42] in the Landau gauge. The inverse dressing function, which is basically given by the gluon self-energy,

is determined without any free parameter and is not monotone, with a pronounced minimum that allows us to fix the energy scale with good accuracy. As shown in Fig. 3, the one-loop analytical expression for the running coupling reproduces the lattice data very well. Sharing the same units of the lattice data in the Landau gauge, the scale $m_0 = 0.73$ GeV is extracted for $N = 3$ [39,42]. We will use that scale in the next sections.

V. THE GEP AT FINITE TEMPERATURE AND DECONFINEMENT

At finite temperature, supposing that Jensen-Feynman inequality Eq. (11) holds, the first-order free energy is bounded below by the exact free energy $\mathcal{F}(T)$ that can be expressed as

$$e^{-\beta[V_3, \mathcal{F}(T)]} = \mathcal{Z} = \int \mathcal{D}_{A,\omega} e^{(S_0 + S_{\text{int}})} \quad (85)$$

where the thermal action is the integral over imaginary time defined in Eq. (9). If we split the action as in the previous section, inserting the mass term Eq. (67) in the free part and the counterterm Eq. (73) among the vertices, the free energy in Eq. (85) is expanded by the same formal massive expansion as before. The first-order approximation $\mathcal{F}_1(T, m)$ depends on the mass parameter m and is given by the same graphs in the second row of Fig. 1. When optimized it gives the GEP, while the optimal value of m that minimizes $\mathcal{F}_1(T, m)$ provides the best trial mass parameter $m(T)$ at finite temperature, so that $m(0) = m_0$.

In non-Abelian theories, the GEP might be bounded below by an approximate free energy rather than the exact free energy. Actually, the existence of ghosts in the covariant formalism and the appearance of states with negative norm in the Hamiltonian formalism might limit the use of Jensen-Feynman inequality Eq. (11) and Bogolubov's inequality Eq. (10), respectively, unless we have some physical evidence about the safe cancellation of the unphysical degrees of freedom in the averages. However, we can show that a weaker form of Jensen-Feynman inequality still holds for the GEP.

The partition function in Eq. (85) can be written as

$$\mathcal{Z} = \int \mathcal{D}_{A,\omega} e^{S'} \text{Det} \mathcal{M}_{\text{FP}}(A) \quad (86)$$

where $\mathcal{M}_{\text{FP}}(A)$ is the Faddeev-Popov matrix, which is linear in the field A_a^μ , and S' is the original total action without any ghost term, obtained by setting $\omega_a = 0$ in the sum $S_0 + S_{\text{int}}$. We can also define zeroth order free energy \mathcal{F}'_0 and partition function \mathcal{Z}'_0 without ghost terms as

$$e^{-\beta[V_3, \mathcal{F}'_0]} = \mathcal{Z}'_0 = \int \mathcal{D}_A e^{S'_0} \quad (87)$$

where S'_0 is the quadratic part of S' , including the gluon-mass term. The exact free energy $\mathcal{F}_{\text{exact}}$ follows as

$$\mathcal{F}_{\text{exact}} = \mathcal{F}'_0 - T \log \langle e^{S'_{\text{int}}} \text{Det} \mathcal{M}_{\text{FP}}(A) \rangle_0 \quad (88)$$

where $S'_{\text{int}} = S' - S'_0$ and the average over A''_a is defined according to

$$\langle \dots \rangle_0 = \frac{1}{Z'_0} \int \mathcal{D}_A e^{S'_0}(\dots). \quad (89)$$

In Eq. (88), we can use Jensen inequality in the pure bosonic average of the convex exponential function and write

$$\mathcal{F}_{\text{exact}} \leq \mathcal{F}'_1 + \mathcal{F}^{gh} \quad (90)$$

where

$$\mathcal{F}'_1 = \mathcal{F}'_0 - T \langle S'_{\text{int}} \rangle_0 \quad (91)$$

is the sum of all first-order gluon graphs in the second row of Fig. 1 and gives the gluon contribution to the first-order free energy, while \mathcal{F}^{gh} is a ghost free-energy given by

$$\mathcal{F}^{gh} = -T \langle \log \text{Det} \mathcal{M}_{\text{FP}}(A) \rangle_0 \quad (92)$$

which is different from the sum of all first-order ghost graphs \mathcal{F}^{gh}_1 contributing to the GEP in Fig. 1. If the ghost term \mathcal{F}^{gh} were known exactly, then its sum with the gluon first-order term \mathcal{F}'_1 would provide through Eq. (90) a pure variational approximation, bounded below by the exact free energy.

We can loop expand \mathcal{F}^{gh} by inserting the explicit form of the matrix \mathcal{M}_{FP} . In any linear covariant gauge

$$\mathcal{M}_{\text{FP}}(A) = \mathcal{G}_M^{-1} + \delta \mathcal{M}(A) \quad (93)$$

where the massive ghost propagator was defined in Eq. (72) and takes account of a generic shift of the pole, while $\delta \mathcal{M}(A)$ is the sum of the ghost vertex of \mathcal{L}_{gh} in Eq. (63) (proportional to the gauge field A''_a) and the ghost counter-term $\delta \Gamma$ of Eq. (71). Expanding the log we obtain

$$\begin{aligned} \beta \mathcal{F}^{gh} &= \text{Tr} \log \mathcal{G}_M - \text{Tr}(\mathcal{G}_M \delta \Gamma) \\ &+ \frac{1}{2} \langle \text{Tr}[\mathcal{G}_M \delta \mathcal{M}(A) \mathcal{G}_M \delta \mathcal{M}(A)] \rangle_0 + \dots \end{aligned} \quad (94)$$

which is a sum of vacuum ghost graphs with insertions of the standard vertices. The first two terms of the expansion are just the first-order ghost graphs in Fig. 1 and give the ghost term \mathcal{F}^{gh}_1 contributing to the GEP. The third term is the two-loop graph

$$\mathcal{F}^{gh}_{2L} \sim \alpha \int \mathcal{G}_M \Delta_m \mathcal{G}_M \quad (95)$$

which might be added to the first-order terms for improving the approximation, as discussed by previous work in the Lagrangian and Hamiltonian formalism [24,58]. We observe that, while the bound in Eq. (90) is exact, any arbitrary truncation of the expansion would invalidate it. Thus, there is no way to tell if adding the two-loop term would give a better result compared with the simple GEP where only the first-order terms are retained. Denoting by $\delta \mathcal{F}$ the difference between the exact ghost term and the first-order terms retained in the GEP

$$\delta \mathcal{F} = \mathcal{F}^{gh} - \mathcal{F}^{gh}_1 \quad (96)$$

We can write the exact bound in Eq. (90) as

$$\mathcal{F}_{\text{GEP}} = \mathcal{F}'_1 + \mathcal{F}^{gh}_1 \geq \mathcal{F}_{\text{exact}} - \delta \mathcal{F}. \quad (97)$$

The GEP might actually fall below the exact free energy, but we can minimize the problem by *maximizing* the ghost term \mathcal{F}^{gh}_1 in the GEP, as suggested by Eq. (96). In fact, it can be easily shown that $\delta \mathcal{F} \geq 0$ and \mathcal{F}^{gh}_1 is bounded above by the exact ghost term \mathcal{F}^{gh} . By use of Jensen inequality in the average of the log in Eq. (92)

$$\begin{aligned} \mathcal{F}^{gh} &\geq -T [\text{Tr} \log \langle \mathcal{M}_{\text{FP}}(A) \rangle_0] \\ &= T [\text{Tr} \log \mathcal{G}_0] = \mathcal{F}^{gh}_1|_{M=0} \end{aligned} \quad (98)$$

and since \mathcal{F}^{gh}_1 is maximal at its stationary point $M = 0$, that point is also the safest choice that maximizes the ghost term without reaching the exact value \mathcal{F}^{gh} . Having shown that $\delta \mathcal{F}$ is positive, we could estimate its value by an explicit evaluation of the two-loop term in Eq. (95) in order to keep the approximation under control. We must mention that the GEP might be closer to the exact free energy than expected by the mathematical bound of Eq. (97) since $\delta \mathcal{F}$ is just the maximal error that we have been able to establish in the worst case. In fact, by a comparison with the data of lattice simulations, we will show that at finite temperature the GEP does very well, better than expected by the present analysis.

At finite temperature, the explicit calculation of the GEP follows by the graphs of Fig. 1. The sum of one-loop graphs is still given by Eq. (79) where the integrals K, J in Eq. (18) now include a sum over discrete frequencies and their explicit expressions in Eq. (20) are replaced by

$$\begin{aligned} K(T, m) &= \frac{1}{2} T \sum_n \int \frac{d^3 \mathbf{p}}{(2\pi)^3} \log(\mathbf{p}^2 + \omega_n^2 + m^2) \\ J(T, m) &= T \sum_n \int \frac{d^3 \mathbf{p}}{(2\pi)^3} \frac{1}{\mathbf{p}^2 + \omega_n^2 + m^2} \end{aligned} \quad (99)$$

having used in Eq. (18) the massive free propagator

$$\Delta_m(\omega_n, \mathbf{p}) = \frac{1}{\mathbf{p}^2 + \omega_n^2 + m^2} \quad (100)$$

in the Euclidean space where $p^\mu = (\omega_n, \mathbf{p})$ and $\omega_n = 2\pi nT$. In the limit $T \rightarrow 0$ the vacuum integrals in Eq. (20) are recovered as $J(m) = J(0, m)$ and $K(m) = K(0, m)$. We denote them by $J_V(m)$ and $K_V(m)$, respectively. They contain the diverging part of the integrals and can be regularized as discussed in the previous sections. Their explicit expression is given by Eq. (31). The thermal parts are finite but depend on T . We denote them by $J_T(T, m)$ and $K_T(T, m)$, respectively. Omitting the arguments for brevity, they can be written by an explicit calculation as

$$\begin{aligned} K_T &= K - K_V = -\frac{1}{6\pi^2} \int_0^\infty \frac{n(\epsilon_{k,m})}{\epsilon_{k,m}} k^4 dk \\ J_T &= J - J_V = \frac{1}{2\pi^2} \int_0^\infty \frac{n(\epsilon_{k,m})}{\epsilon_{k,m}} k^2 dk \end{aligned} \quad (101)$$

where $\epsilon_{k,m} = \sqrt{k^2 + m^2}$ and $n(\epsilon) = [\exp(\beta\epsilon) - 1]^{-1}$ is the Bose distribution.

The first-order free energy $\mathcal{F}_1(T, m)$ can be written as the sum of one-loop and two-loop terms

$$\mathcal{F}_1(T, m) = \mathcal{F}_{1L}(T, m) + \mathcal{F}_{2L}(T, m). \quad (102)$$

The sum of one-loop graphs is obtained by just setting $d = 4$ in Eq. (79)

$$\mathcal{F}_{1L}(T, m) = 3N_A \left[K(T, m) - \frac{1}{2} m^2 J(T, m) \right] - N_A K(T, 0). \quad (103)$$

The second term $\mathcal{F}_{2L}(T, m)$ is the two-loop graph in the second row of Fig. 1. Because of the breaking of Lorentz invariance at finite T , its expression gets formally different than the vacuum term in Eq. (81) and also becomes gauge dependent. In order to make contact with previous analytical and numerical work in the Landau gauge we set $\xi = 0$, which is the most common choice for the study of the correlators, so that the scale $m_0 = 0.73$ GeV will be used. In fact, that scale was extracted by matching the predictions of the massive expansion with the data of numerical simulations in the Landau gauge [39,42]. Assessing the whole gauge dependence of the GEP at finite temperature is not an easy task, as the scale m_0 should be also changed by matching the gauge-dependent correlators in a different gauge.

Following the same steps of the previous sections, in the Landau gauge, the seagull graph of the gluon self energy can be written as [71]

$$\Pi_{ab}^{\mu\nu} = -\delta_{ab} N g^2 T \sum_n \int \frac{d^3 \mathbf{p}}{(2\pi)^3} [2\delta^{\mu\nu} \Delta_m + p^\mu p^\nu \Delta_0 \Delta_m] \quad (104)$$

where $\Delta_m = \Delta_m(p)$ is the Euclidean propagator in Eq. (100). Integrating the single terms, it can be written as

$$\Pi_{ab}^{\mu\nu} = -\delta_{ab} N g^2 [2\delta^{\mu\nu} J + I^{\mu\nu}] \quad (105)$$

where

$$I^{\mu\nu} = T \sum_n \int \frac{d^3 \mathbf{p}}{(2\pi)^3} p^\mu p^\nu \Delta_m(p) \Delta_0(p). \quad (106)$$

The trace of $I^{\mu\nu}$ is $I^{\mu\mu} = J$, so that at $T = 0$, by Lorentz invariance, the self energy of Eq. (80) is recovered for $d = 4$. At finite temperature, $I^{\mu\nu}$ is still diagonal but $I^{00} \neq I^{ii}$. By rotational invariance, using the trace again, we can write

$$I^{11} = I^{22} = I^{33} = \frac{1}{3} (J - I^{00}) \quad (107)$$

which holds separately for the thermal and vacuum parts. While the vacuum part is just $I_V^{00} = I_V^{ii} = J_V/4$, the thermal part can be obtained by an explicit integration as

$$I_T^{00} = \frac{1}{m^2} (h_m - h_0) \quad (108)$$

where h_m is the integral

$$h_m = \frac{1}{2\pi^2} \int_0^\infty \epsilon_{k,m} n(\epsilon_{k,m}) k^2 dk \quad (109)$$

that can be evaluated exactly for $m = 0$ yielding

$$h_0 = -3K_T(T, 0) = \frac{\pi^2 T^4}{30}. \quad (110)$$

Closing the second loop with the transverse gluon propagator ($\xi = 0$) and inserting the symmetry factor 1/4

$$\mathcal{F}_{2L} = -\frac{1}{4} \Pi_{ab}^{\mu\nu} T \sum_n \int \frac{d^3 \mathbf{p}}{(2\pi)^3} \Delta_m(p) t_{\mu\nu}(p) \delta_{ab}. \quad (111)$$

Then, using Eq. (105), the two-loop term reads

$$\mathcal{F}_{2L} = \frac{N_A N g^2}{4} (7J^2 - I^{\mu\nu} I^{\mu\nu}) \quad (112)$$

and its inclusion in Eq. (102) together with Eq. (103) gives the first-order free energy in closed form. When optimized, it provides the GEP at finite temperature. With some abuse

of language we can denote the first-order free energy by $\mathcal{F}_G(T, m)$ and call it the GEP.

It is useful to separate the thermal and vacuum parts of the GEP. If we do that and use the explicit regularized expressions Eq. (31) for the vacuum parts J_V, K_V , the total first-order free energy of Eqs. (102), (103), (112) can be easily shown to become

$$\mathcal{F}_G(T, m) = \mathcal{F}_G(0, m) + \Delta\mathcal{F}_G(T, m) \quad (113)$$

where the vacuum part $\mathcal{F}_G(0, m) = V_G(m)$ is just the GEP at $T = 0$, given by Eq. (84) when expressed in terms of m_0 . The thermal part $\Delta\mathcal{F}_G(T, m)$ vanishes at $T = 0$ and can be written as

$$\frac{\Delta\mathcal{F}_G(T, m)}{3N_A} = K_T + \frac{\pi^2}{270} T^4 + \frac{\alpha m^2}{4} J_T \log \frac{m^2}{m_0^2} + 2\pi^2 \alpha \left[J_T^2 - \left(\frac{2}{3} \right)^4 \left(\frac{J_T}{4} - I_T^{00} \right)^2 \right]. \quad (114)$$

The GEP is shown in Fig. 5 for different values of the temperature and in Fig. 6 for several values of the coupling α_s . As already discussed in the previous sections, the GEP is not very sensitive to the coupling, especially in the physical ranges around the minima and for $T < 2T_c \approx 0.5$ GeV.

While the physical value of the GEP was not sensitive at all to a change of α_s at $T = 0$, other observables, at finite temperature, might depend on α_s because the variational method is not an exact calculation. In lattice simulations, the bare coupling and the cutoff are finite, since the lattice spacing cannot be set to zero. However, a stationary regime is reached where the physical predictions seem to be not sensitive to the actual value of the bare coupling. In the present calculation, because of the approximations, we fail to reach an exactly stationary regime for all the thermal

observables. Albeit small, a residual sensitivity to the bare α_s is found, posing the problem of the choice of the coupling. We argue that, for any finite value of coupling and cutoff, the outcome of the variational calculation is more reliable and closer to the lattice data if the physical observables are less sensitive to the arbitrary value of the bare coupling. Thus, the best agreement with the data of lattice simulations is expected in the range $0.6 < \alpha_s < 1.2$ where a real plateau is observed, rather than in the limit $\alpha_s \rightarrow 0$ where a slightly larger sensitivity is found. For that reason, even if α_s should be sent to zero in the limit $\epsilon \rightarrow 0$, we prefer to keep α_s fixed at the optimal value $\alpha_s = 0.9$ in the following discussion and in the comparison with the lattice data. We checked that any other choice does not introduce important changes in the results.

At finite temperature, we observe that the minima of the GEP have a very different behavior. The absolute minimum at $m = m_0$ is almost frozen when $T \ll m_0$, as expected for a massive confined gluon. When the temperature increases the minimum moves backwards, so that the optimal mass parameter $m(T)$ is a decreasing function of the temperature, in fair agreement with the decrease of mass that is observed on the lattice below T_c [10]. The unstable minimum, at $m = 0$ in Fig. 4, moves forward when $T > 0$ and its mass value increases almost linearly like the thermal mass of a massless boson. It gets deeper with increasing temperature. Thus the GEP seems to show the competition between a confined boson with a dynamical mass and a free boson with a thermal mass. As shown in Fig. 5, at a critical temperature $T_c \approx 0.35 m_0$ the minima reach the same free energy before they can merge, so that a weak first-order phase transition is predicted with a discontinuous drop of the optimal mass parameter $m(T)$ that is displayed in Fig. 7. The free energy at the minima is shown in Fig. 8 across the transition. Below the transition point, the upper curve is the

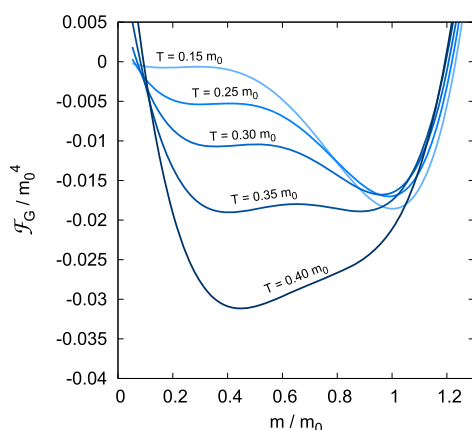


FIG. 5. The renormalized GEP of Eqs. (113), (114) is shown in units of m_0 for $\alpha_s = 0.9$ and different values of the temperature.

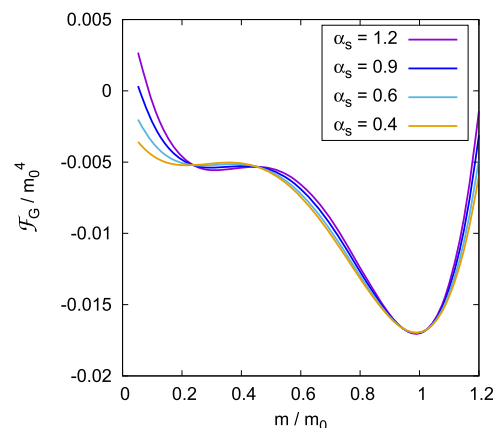


FIG. 6. The renormalized GEP of Eqs. (113), (114) is shown in units of m_0 for $T/m_0 = 0.25$ and different values of the strong coupling α_s .

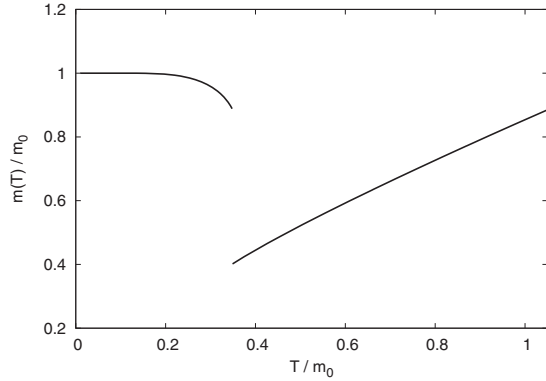


FIG. 7. The optimal mass parameter $m(T)$ which minimizes the GEP is shown as a function of temperature for $\alpha_s = 0.9$.

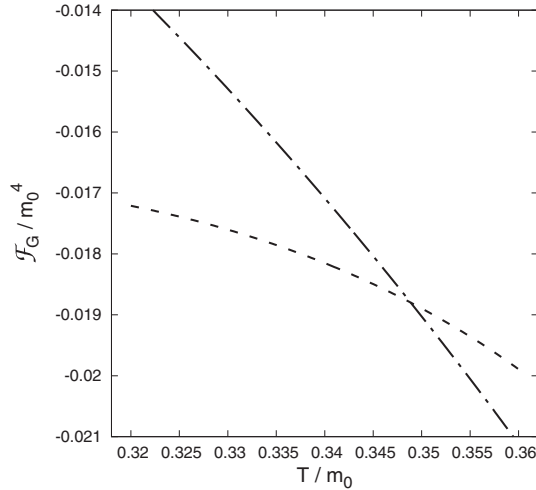


FIG. 8. The Free energy at the minima of the GEP across the transition for $\alpha_s = 0.9$. Below the transition point, the upper curve (dot-dashed) is the GEP at the unstable thermal mass while the lower curve (dashed) is the GEP at the stable dynamical mass. The order reverses above the transition point.

GEP at the unstable thermal mass, while the lower curve is the GEP at the stable dynamical mass. Above the transition point they reverse. At any temperature, the physical free energy is the lower curve $\mathcal{F}_G(T, m(T))$.

The slight effect of a change of α_s on the critical temperature is less than $\pm 1\%$ in Fig. 9, where it is shown at a very enlarged scale. Apart the effect of the scale, the critical temperature is basically unchanged for a large range of α_s , including the phenomenological interval $0.4 < \alpha_s < 1.2$ which would be ranged by a running coupling in the

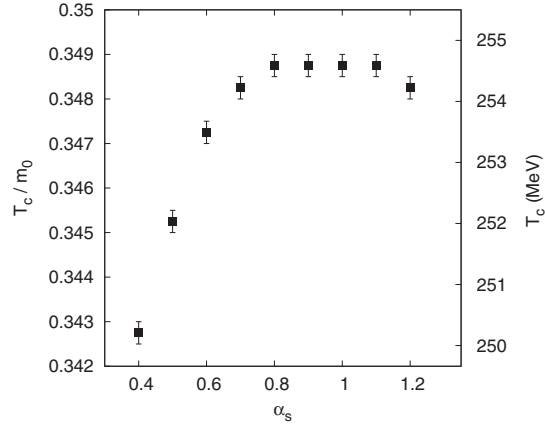


FIG. 9. The critical temperature is shown at a very enlarged scale, as a function of the coupling α_s . The minor effect of its change is less than $\pm 1\%$. Error bars are the numerical error in the calculation. The right hand scale is obtained by taking $m_0 = 0.73$ GeV.

IR. The plateau has a stationary point at $\alpha_s \approx 0.9$ where $T_c = 0.349 m_0$. We take that as the best prediction of the GEP according to the principle of minimal sensitivity [66].

Using the scale $m_0 = 0.73$ GeV that arises for $N = 3$ from the massive expansion at one-loop [37–42], we predict $T_c = 255$ MeV, which is very close to the value $T_c = 270$ MeV that is found on the lattice [10].

It is important to mention that if the bare coupling were sent to zero in the limit $\epsilon \rightarrow 0$, the resulting qualitative picture would remain basically unchanged. In the limit $\alpha_s \rightarrow 0$, the deconfinement transition still takes place, is weakly first order and with a critical temperature $T_c \approx 0.32 m_0$ not too far from that found on the plateau. The only relevant difference is in the behavior of the unstable minimum, whose position does not change with the temperature and remains fixed at $m = 0$ for every value of T , even if it gets deeper and eventually becomes the stable minimum above T_c . Thus, in the limit $\alpha_s \rightarrow 0$, the optimal mass parameter is $m \approx m_0$ for $T < T_c$, and $m = 0$ for $T > T_c$. In the same limit, the critical temperature can be estimated by observing that the gluon thermal term is exponentially suppressed at $m \approx m_0$ and cancels the opposite ghost term, so that the minimum of $\mathcal{F}_G(T, m)$ is basically frozen at the vacuum value $\mathcal{F}_G(T, m) \approx V_G(m_0) = -3N_A m_0^4 / (128\pi^2)$ if $T \ll m_0$. On the other hand, setting $\alpha = 0$ in Eq. (114), the unstable minimum at $m = 0$ is given by $\mathcal{F}_G(T, 0) = -3N_A \pi^2 T^4 / 135$, so that a first order phase transition occurs at $T_c \approx (\frac{135}{128})^{1/4} \frac{m_0}{\pi} = 0.32 m_0$ where the optimal mass parameter drops to zero.

The equation of state can be studied by introducing pressure and entropy density according to

$$\begin{aligned}
p &= -[\mathcal{F}_G(T, m(T)) - \mathcal{F}_G(0, m_0)] \\
s &= -\frac{\partial}{\partial T} \mathcal{F}_G(T, m(T)).
\end{aligned}
\tag{115}$$

The reader might have noticed in Fig. 5 that below T_c the minimum at $m = m_0$ moves slightly upwards. That behaviour gives an unphysical negative entropy for a limited range of temperatures, as reported by other massive approximations at one-loop [33,35] and by other variational methods [75]. That minor shortcoming might be expected since the contribution of the massless ghost is enhanced when $T \ll m$ compared to the massive gluon. The problem becomes more evident if we look at the ratio p/T^4 in the limit $T \rightarrow 0$. That ratio should be exponentially suppressed and dominated by the lightest glueball mass, in agreement with the data of lattice simulations [76–78]. By inspection of Eq. (114), we observe that while the thermal functions K_T, J_T, I_T^{00} are exponentially suppressed, the second term on the right hand side contributes with the fourth power of T , originating from the massless ghost loop in Eq. (110) which, besides, is taken with the opposite sign. When all other terms are suppressed, the ghost loop dominates the leading behavior yielding a finite nonzero ratio in the limit $T \rightarrow 0$

$$\frac{p}{T^4} \rightarrow -\frac{N_A \pi^2}{90}
\tag{116}$$

and a negative entropy in the same limit. That seems to be a shortcoming of the Landau gauge, since the same identical finite values were found in Refs. [34,35] in that gauge. The same authors find smaller finite values and a positive entropy in the Landau-De Witt gauge by a two-loop calculation. As discussed in Ref. [75], one would be tempted to cancel the unphysical term by hand, but that term gives an important contribution above the transition where it cancels unphysical gluon terms.

On the other hand, the mismatch can only be observed below T_c where the exact free-energy is almost constant and the pressure is basically zero, so that even a very small (positive) deviation can give an increasing free-energy and a decreasing pressure. Actually, the effect can be hardly seen in Fig. 10 where the pressure of Eq. (115) is shown together with the recent lattice data of Ref. [76] which are consistent with previous existing data [77,78]. We observe that the figure is not a fit and that there are no free parameters in the calculation. Moreover, in units of T_c the pressure in Fig. 10 does not even depend on the energy scale m_0 . Thus, it is remarkable that the data points fall so close to the prediction of the calculation, at least for $T < 2T_c$. As shown in the figure, the GEP provides a pressure that seems to be bounded above by the data points, as expected if the GEP were bounded below by the exact free energy, suggesting that the error in the ghost free-energy $\delta\mathcal{F}$ might be very small in Eq. (97). For comparison,

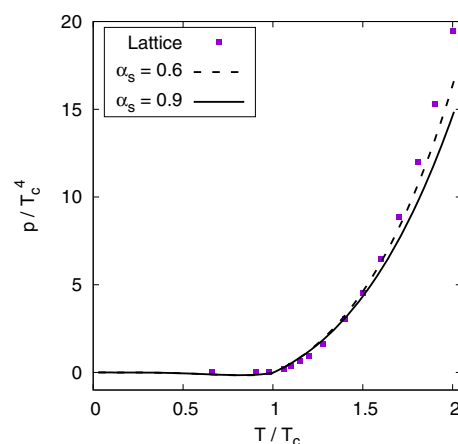


FIG. 10. Equation of state. The pressure is evaluated by Eq. (115) and shown in units of T_c for the optimal coupling $\alpha_s = 0.9$ (solid line) and for $\alpha_s = 0.6$ (broken line). The squares are the lattice data of Ref. [76].

in Fig. 10 the pressure is also shown for a coupling $\alpha_s = 0.6$, smaller than the optimal value $\alpha_s = 0.9$. While the predictions are not sensitive to the choice of the coupling at low temperature, above $1.5 T_c$ the pressure acquires a slight dependence on it and the agreement with the data improves by decreasing α_s .

The problem of a negative entropy becomes more evident in Fig. 11 where the entropy density of Eq. (115) is shown together with the lattice data of Ref. [76]. The small jump of the entropy density at $T = T_c$ is $\Delta s/T_c^3 = 2.7$ yielding a

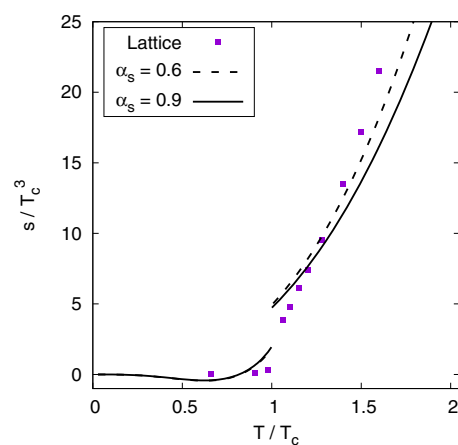


FIG. 11. Equation of state. The entropy density is evaluated by Eq. (115) and shown in units of T_c for the optimal coupling $\alpha_s = 0.9$ (solid line) and for $\alpha_s = 0.6$ (broken line). The squares are the lattice data of Ref. [76].

latent heat $\Delta H_0 = 2.7 T_c^4$ which is larger than the values 1.3–1.5 found in lattice simulations [76–78]. However, we expect that the overall picture of dynamical mass generation, deconfinement transition and equation of state might improve greatly by adding higher-order terms of the expansion in the free energy, as it is the case for the dressed propagator which gets on top of the lattice data when the one-loop terms are added to the zeroth-order massive propagator $\Delta_m = 1/(p^2 + m_0^2)$ [39,40,42].

VI. DISCUSSION

The self-consistency gap equation of the GEP, Eq. (25) has attracted a lot of attention in the past [19,20,45] as a basic physical tool for explaining the dynamical mass generation of Yang-Mills theories. The main difficulty of handling the gap equation has always been the regularization of the diverging integral $J(m)$ and its physical meaning. Here, we have shown that, by dimensional regularization in $d > 4$, the GEP provides a reasonable account of the general features of Yang-Mills theory. The existence of a deep minimum at $m = m_0 \neq 0$ can be regarded as a variational argument for dynamical mass generation in the original scale-less theory.

In order to enforce our confidence on the genuine physical nature of the minimum, we explored the model at finite temperature. The emerging scenario for the equation of state and the deconfinement transition is in very good agreement with the data of lattice simulations, leaving no doubt about the physical interpretation of the minima in the GEP.

Moreover, the method provides a perturbative tool for improving the results order by order. The expansion around the optimal vacuum of the GEP turns out to be the massive expansion developed in Refs. [38–40] which provides accurate and analytical expressions for the propagators at one-loop already. Once the nonperturbative effects are embedded in the optimal variational mass, the residual interaction can be described by perturbation theory yielding a powerful analytical tool for QCD in the IR.

Thus, we argue that the present variational estimate of the thermodynamical potentials might be improved by inclusion of higher order terms. Second order extensions of the GEP have been discussed by several authors [56–59]. In general, they do not retain the genuine variational property of the GEP but different optimization strategies have been proposed ranging from the principle of minimal sensitivity [66] to the method of minimal variance [68–71]. Explicit massive two-loop thermal graphs have been evaluated in Ref. [35]. Here, we limited the calculation at the first order, just because we preferred to maintain the genuine variational nature of the method unspoiled, as much as Jensen-Feynman inequality allows in presence of ghost fields. Nevertheless, the pure GEP provides a remarkably good picture of the deconfinement transition. From first principles, without any fit parameter, the simple first-order calculation predicts a weak first order transition at $T_c \approx 250$ MeV for $N = 3$, with a pressure which is very close to the data points of lattice simulations. We must mention that the method fails to predict a continuous transition for $N = 2$. That could be the consequence of a known issue for the GEP which usually predicts a weak first-order transition even when the transition is second-order, e.g. for the scalar theory [46,56]. In that case, a continuous transition is restored by inclusion of second order terms [56]. Moreover, the GEP is known [43,63] to predict the correct $N \rightarrow \infty$ limit of $1/N$ expansions, so that its reliability increases when N is large.

Finally, even if the present variational study is limited to the low temperature range $T < m_0$, where no resummation of hard thermal loops is required because of the finite mass in the loops, the effects of a finite mass become negligible for large energies and $T \gg m_0$ and the standard results of perturbation theory would be recovered by the massive expansion in that limit.

ACKNOWLEDGMENTS

We thank V. Branchina, M. Consoli and U. Reinosa for helpful discussions and feedback on the manuscript.

-
- [1] A. G. Duarte, O. Oliveira, and P. J. Silva, *Phys. Rev. D* **94**, 014502 (2016).
 - [2] A. Cucchieri and T. Mendes, *Phys. Rev. D* **78**, 094503 (2008).
 - [3] A. Cucchieri and T. Mendes, *Phys. Rev. Lett.* **100**, 241601 (2008).
 - [4] I. L. Bogolubsky, E. M. Ilgenfritz, M. Muller-Preussker, and A. Sternbeck, *Phys. Lett. B* **676**, 69 (2009).
 - [5] D. Dudal, O. Oliveira, and N. Vandersickel, *Phys. Rev. D* **81**, 074505 (2010).
 - [6] A. Ayala, A. Bashir, D. Binosi, M. Cristoforetti, and J. Rodríguez-Quintero, *Phys. Rev. D* **86**, 074512 (2012).
 - [7] O. Oliveira and P. J. Silva, *Phys. Rev. D* **86**, 114513 (2012).
 - [8] G. Burgio, M. Quandt, H. Reinhardt, and H. Vogt, *Phys. Rev. D* **92**, 034518 (2015).
 - [9] B. Lucini, M. Teper, and U. Wenger, *J. High Energy Phys.* **01** (2004) 061.
 - [10] P. J. Silva, O. Oliveira, P. Bicudo, and N. Cardoso, *Phys. Rev. D* **89**, 074503 (2014).

- [11] R. Aouane, V. Bornyakov, E.-M. Ilgenfritz, V. Mitrjushkin, M. Müller-Preussker, and A. Sternbeck, *Phys. Rev. D* **85**, 034501 (2012).
- [12] F. Marhauser and J. M. Pawłowski, [arXiv:0812.1144](https://arxiv.org/abs/0812.1144).
- [13] J. Braun, H. Gies, and J. M. Pawłowski, *Phys. Lett. B* **684**, 262 (2010).
- [14] J. Braun, A. Eichhorn, H. Gies, and J. M. Pawłowski, *Eur. Phys. J. C* **70**, 689 (2010).
- [15] L. Fister and J. M. Pawłowski, *Phys. Rev. D* **88**, 045010 (2013).
- [16] D. Epple, H. Reinhardt, and W. Schleifenbaum, *Phys. Rev. D* **75**, 045011 (2007).
- [17] R. Alkofer, C. S. Fischer, and F. J. Llanes-Estrada, *Mod. Phys. Lett. A* **23**, 1105 (2008).
- [18] C. S. Fischer, *Phys. Rev. Lett.* **103**, 052003 (2009).
- [19] A. C. Aguilar, D. Binosi, and J. Papavassiliou, *Phys. Rev. D* **78**, 025010 (2008).
- [20] A. C. Aguilar and J. Papavassiliou, *Phys. Rev. D* **81**, 034003 (2010).
- [21] A. C. Aguilar, D. Binosi, and J. Papavassiliou, *Phys. Rev. D* **89**, 085032 (2014).
- [22] A. C. Aguilar, D. Binosi, D. Ibanez, and J. Papavassiliou, *Phys. Rev. D* **90**, 065027 (2014).
- [23] A. C. Aguilar, D. Binosi, and J. Papavassiliou, *Phys. Rev. D* **91**, 085014 (2015).
- [24] H. Reinhardt and C. Feuchter, *Phys. Rev. D* **71**, 105002 (2005).
- [25] H. Reinhardt and J. Hefner, *Phys. Lett. B* **718**, 672 (2012); *Phys. Rev. D* **88**, 045024 (2013).
- [26] D. Zwanziger, *Nucl. Phys.* **B323**, 513 (1989).
- [27] D. Dudal, J. A. Gracey, S. P. Sorella, N. Vandersickel, and H. Verschelde, *Phys. Rev. D* **78**, 065047 (2008).
- [28] D. Dudal, S. P. Sorella, N. Vandersickel, and H. Verschelde, *Phys. Rev. D* **77**, 071501 (2008).
- [29] D. Dudal, S. P. Sorella, and N. Vandersickel, *Phys. Rev. D* **84**, 065039 (2011).
- [30] M. Tissier and N. Wschebor, *Phys. Rev. D* **82**, 101701(R) (2010).
- [31] M. Tissier and N. Wschebor, *Phys. Rev. D* **84**, 045018 (2011).
- [32] U. Reinosa, J. Serreau, M. Tissier, and N. Wschebor, *Phys. Rev. D* **89**, 105016 (2014).
- [33] U. Reinosa, J. Serreau, M. Tissier, and N. Wschebor, *Phys. Lett. B* **742**, 61 (2015).
- [34] U. Reinosa, J. Serreau, M. Tissier, and N. Wschebor, *Phys. Rev. D* **91**, 045035 (2015).
- [35] U. Reinosa, J. Serreau, and M. Tissier, *Phys. Rev. D* **92**, 025021 (2015).
- [36] U. Reinosa, J. Serreau, M. Tissier, and N. Wschebor, *Phys. Rev. D* **93**, 105002 (2016).
- [37] F. Siringo, in *Correlations in Condensed Matter under Extreme Conditions*, edited by G. G. N. Angilella and A. La Magna (Springer International Publishing AG, New York, 2017); [arXiv:1701.00286](https://arxiv.org/abs/1701.00286).
- [38] F. Siringo, [arXiv:1509.05891](https://arxiv.org/abs/1509.05891).
- [39] F. Siringo, *Nucl. Phys.* **B907**, 572 (2016).
- [40] F. Siringo, *Phys. Rev. D* **94**, 114036 (2016).
- [41] F. Siringo, *Phys. Rev. D* **96**, 114020 (2017).
- [42] F. Siringo, *Eur. Phys. J. Web Conf.* **137**, 13016 (2017).
- [43] R. Ibañez-Meier, I. Stancu, and P. M. Stevenson, *Z. Phys. C* **70**, 307 (1996).
- [44] J. M. Cornwall, R. Jackiw, and E. Tomboulis, *Phys. Rev. D* **10**, 2428 (1974).
- [45] J. M. Cornwall, *Phys. Rev. D* **26**, 1453 (1982).
- [46] P. M. Stevenson, *Phys. Rev. D* **32**, 1389 (1985).
- [47] P. M. Stevenson, G. A. Hajj, and J. F. Reed, *Phys. Rev. D* **34**, 3117 (1986).
- [48] F. Siringo, *Phys. Rev. D* **62**, 116009 (2000).
- [49] F. Siringo, *Europhys. Lett.* **59**, 820 (2002).
- [50] F. Siringo and L. Marotta, *Int. J. Mod. Phys. A* **25**, 5865 (2010).
- [51] F. Siringo and L. Marotta, *Phys. Rev. D* **78**, 016003 (2008).
- [52] F. Siringo and L. Marotta, *Phys. Rev. D* **74**, 115001 (2006).
- [53] M. Camarda, G. G. N. Angilella, R. Pucci, and F. Siringo, *Eur. Phys. J. B* **33**, 273 (2003).
- [54] L. Marotta, M. Camarda, G. G. N. Angilella, and F. Siringo, *Phys. Rev. B* **73**, 104517 (2006).
- [55] L. Marotta and F. Siringo, *Mod. Phys. Lett. B* **26**, 1250130 (2012).
- [56] I. Stancu and P. M. Stevenson, *Phys. Rev. D* **42**, 2710 (1990).
- [57] F. Siringo, *Phys. Rev. D* **88**, 056020 (2013).
- [58] F. Siringo, *Phys. Rev. D* **86**, 076016 (2012).
- [59] I. Stancu, *Phys. Rev. D* **43**, 1283 (1991).
- [60] U. Reinosa and Z. Szep, *Phys. Rev. D* **83**, 125026 (2011).
- [61] M. Consoli and A. Ciancetto, *Nucl. Phys.* **B254**, 653 (1985).
- [62] P. M. Stevenson, *Z. Phys. C* **35**, 467 (1987).
- [63] P. M. Stevenson, B. Alles, and R. Tarrach, *Phys. Rev. D* **35**, 2407 (1987).
- [64] V. Branchina, P. Castorina, M. Consoli, and D. Zappalà, *Phys. Rev. D* **42**, 3587 (1990).
- [65] P. Cea and L. Tedesco, *Phys. Rev. D* **55**, 4967 (1997).
- [66] P. M. Stevenson, *Phys. Rev. D* **23**, 2916 (1981).
- [67] F. Siringo and L. Marotta, *Eur. Phys. J. C* **44**, 293 (2005).
- [68] F. Siringo, *Mod. Phys. Lett. A* **29**, 1450026 (2014).
- [69] F. Siringo, *Phys. Rev. D* **89**, 025005 (2014).
- [70] F. Siringo, *Phys. Rev. D* **90**, 094021 (2014).
- [71] F. Siringo, *Phys. Rev. D* **92**, 074034 (2015).
- [72] S. Coleman and E. Weinberg, *Phys. Rev. D* **7**, 1888 (1973).
- [73] K. Huang, E. Manoussakis, and J. Polonyi, *Phys. Rev. D* **35**, 3187 (1987).
- [74] G. Comitini, Thesis for the degree in Physics, University of Catania, 2017, [arXiv:1803.02335](https://arxiv.org/abs/1803.02335).
- [75] M. Quandt and H. Reinhardt, *Phys. Rev. D* **96**, 054029 (2017).
- [76] L. Giusti and M. Pepe, *Phys. Lett. B* **769**, 385 (2017).
- [77] Sz. Borsanyi, G. Endrodi, Z. Fodor, S. D. Katz, and K. K. Szabo, *J. High Energy Phys.* **07** (2012) 056.
- [78] G. Boyd, J. Engels, F. Karsch, E. Laermann, C. Legeland, M. Luetgemeier, and B. Petersson, *Nucl. Phys.* **B469**, 419 (1996).

Gluon propagator in linear covariant R_ξ gauges

Fabio Siringo and Giorgio Comitini

*Dipartimento di Fisica e Astronomia dell'Università di Catania,
INFN Sezione di Catania, Via S.Sofia 64, I-95123 Catania, Italy*

(Received 25 June 2018; published 23 August 2018)

Explicit analytical expressions are derived for the gluon propagator in a generic linear covariant R_ξ gauge, by a screened massive expansion for the exact Faddeev-Popov Lagrangian of pure Yang-Mills theory. At one-loop, if the gauge invariance of the pole structure is enforced, the gluon dressing function is entirely and uniquely determined, without any free parameter or external input. The gluon propagator is found finite in the IR for any ξ , with a slight decrease of its limit value when going from the Landau gauge ($\xi = 0$) toward the Feynman gauge ($\xi = 1$). An excellent agreement is found with the lattice in the range $0 < \xi < 0.5$ where the data are available.

DOI: [10.1103/PhysRevD.98.034023](https://doi.org/10.1103/PhysRevD.98.034023)**I. INTRODUCTION**

Almost all the visible mass in the universe arises from dynamical mass generation, a mechanism that converts chiral current quarks into constituent quarks, each carrying one third of the proton mass. The mechanism can be understood as the effect of low-energy gluon clouds dressing the current quark, so that the study of the gluon propagator in the IR becomes of paramount importance for a full comprehension of the mass generation [1–7]. Unfortunately, even in the pure gauge sector, perturbation theory breaks down in the IR and the results of lattice simulations [5,8–18] are regarded as the only benchmark for the continuum approaches [19–38] that have been developed. Among them, a purely analytical method has been proposed in the last years [39–41], which is based on a change of the expansion point of ordinary perturbation theory and provides explicit and very accurate expressions for the gluon propagator in the Landau gauge [42]. The method relies on a screened massive expansion, with massive propagators in the internal gluon lines of Feynman graphs, and is derived from the exact Faddeev-Popov Lagrangian of pure Yang-Mills theory, from first principles, without adding any phenomenological parameter. The expansion can be seen to emerge from the Gaussian effective potential [43,44] which provides a simple argument for the dynamical mass generation of the gluon and has been also studied at finite temperature [44,45].

In this paper, the massive expansion is extended to the more general case of a linear covariant R_ξ gauge and explicit analytical expressions are provided for the gluon propagator at any generic value of the gauge-fixing parameter ξ , yielding new insight into the gauge dependence of the propagator, that cannot be extracted by any other method.

Exploring the gauge dependence of the gluon propagator is in itself important in order to individuate the properties that are gauge invariant and might be directly related to physical observables. Despite that, the covariant R_ξ gauge, which is under control at the perturbative level, is basically unexplored in the IR because of convergence problems in lattice calculations [46–48]. Quite recently, a lattice simulation has been extended up to $\xi = 0.5$ [49], predicting a saturation of the propagator deep in the IR, with very small deviations from the results in the Landau gauge, but in strong disagreement with some recent predictions of a continuum study [25]. On the other hand, the lattice data seem to be in qualitative agreement with the picture emerging by Nielsen identities in Ref. [22]. Out of the Euclidean space, no information has been reported so far about the analytic properties in R_ξ gauge.

On general grounds, because of Nielsen identities [50], we know that the poles and the residues of the gluon propagator, i.e., the principal part, must be gauge parameter independent [51–53]. While no information on the existence and properties of the poles can be extracted from lattice calculations in the Euclidean space, the massive expansion provides explicit analytical expressions that can be continued to the complex plane [41]. Some attempts at reconstructing the spectral functions from the lattice data have been reported [54,55] and are in qualitative agreement with the predictions of the expansion [41].

At one-loop, by the massive expansion, a pair of complex conjugated poles were found in the Landau gauge

Published by the American Physical Society under the terms of the Creative Commons Attribution 4.0 International license. Further distribution of this work must maintain attribution to the author(s) and the published article's title, journal citation, and DOI. Funded by SCOAP³.

[45], as also predicted by different phenomenological models [56–58], again in strong disagreement with other continuum studies [59] based on the truncation of an infinite set of Dyson-Schwinger equations. While the genuine nature of the poles was already shown by studying their behavior at finite temperature [45], their explicit gauge invariance would provide further evidence that they are not artifact of the expansion. Strictly speaking, by changing the expansion point, the Becchi-Rouet-Stora-Tyutin (BRST) symmetry of the quadratic part of the Lagrangian is broken in the expansion and we should not expect that the pole structure might be exactly gauge invariant at any finite order. However, since the total Lagrangian is not modified, the gauge parameter independence must be recovered if the expansion provides a very good approximation of the exact propagator. Thus the gauge parameter independence of the pole structure would give a quantitative estimate of the accuracy in the complex plane, where no comparison with the lattice can be made.

By the same argument, the massive expansion can be optimized by enforcing the gauge parameter independence of the whole pole structure, yielding a fully self-contained calculation from first principles, without any adjustable parameter or external input. Moreover, once optimized in the complex plane, the result is found in excellent agreement with the lattice data in the Euclidean space, not only in the Landau gauge, but for the whole range, up to $\xi = 0.5$, that has been explored in the lattice so far [49]. No dramatic difference is found for larger values of ξ and even in the Feynman gauge the gluon propagator is finite in the IR, with a slight suppression of its saturation value compared to the Landau gauge. Being gauge parameter independent, the principal part of the propagator might be directly related to physical observables like glueball masses, as recently discussed by a quite general method [58].

The paper is organized as follows: in Sec. II the massive expansion of Refs. [39,40] is extended to a generic R_ξ gauge; in Sec. III the expansion is optimized by requiring that the pole structure is gauge parameter independent as demanded by Nielsen identities; in Sec. IV the optimized gluon propagator is shown for a wide range of the gauge parameter ξ , including the Feynman gauge ($\xi = 1$), and is compared with the available lattice data; Section V contains a brief discussion of the main results. Explicit analytical expressions for the propagator in R_ξ gauge are derived in Appendix with many details on the calculation of the graphs.

II. THE MASSIVE EXPANSION IN R_ξ GAUGE

The massive expansion has been first developed in Refs. [39,40] and related to the Gaussian effective potential in Refs. [43,44]. It is based on a change of the expansion point of ordinary perturbation theory for the exact gauge-fixed Faddeev-Popov Lagrangian of pure Yang-Mills $SU(N)$ theory. The Lagrangian can be written as

$$\mathcal{L} = \mathcal{L}_{\text{YM}} + \mathcal{L}_{\text{fix}} + \mathcal{L}_{\text{FP}} \quad (1)$$

where \mathcal{L}_{YM} is the Yang-Mills term

$$\mathcal{L}_{\text{YM}} = -\frac{1}{2} \text{Tr}(\hat{F}_{\mu\nu} \hat{F}^{\mu\nu}), \quad (2)$$

the tensor operator $\hat{F}_{\mu\nu}$ is

$$\hat{F}_{\mu\nu} = \partial_\mu \hat{A}_\nu - \partial_\nu \hat{A}_\mu - ig[\hat{A}_\mu, \hat{A}_\nu], \quad (3)$$

\mathcal{L}_{FP} is the ghost term arising from the Faddeev-Popov determinant and \mathcal{L}_{fix} is the covariant gauge-fixing term

$$\mathcal{L}_{\text{fix}} = -\frac{1}{\xi} \text{Tr}[(\partial_\mu \hat{A}^\mu)(\partial_\nu \hat{A}^\nu)]. \quad (4)$$

The gauge field operators are

$$\hat{A}^\mu = \sum_a \hat{X}_a A_a^\mu \quad (5)$$

where the generators of $SU(N)$ satisfy the algebra

$$[\hat{X}_a, \hat{X}_b] = if_{abc} \hat{X}_c, \quad f_{abc} f_{dbc} = N \delta_{ad}. \quad (6)$$

In the standard perturbation theory, the total action is split as $S_{\text{tot}} = S_0 + S_I$ where the quadratic part can be written as

$$S_0 = \frac{1}{2} \int A_{a\mu}(x) \delta_{ab} \Delta_0^{-1\mu\nu}(x, y) A_{b\nu}(y) d^4x d^4y \\ + \int \omega_a^*(x) \delta_{ab} \mathcal{G}_0^{-1}(x, y) \omega_b(y) d^4x d^4y \quad (7)$$

and the interaction is

$$S_I = \int d^d x [\mathcal{L}_{gh} + \mathcal{L}_3 + \mathcal{L}_4]. \quad (8)$$

with the three local interaction terms that read

$$\mathcal{L}_3 = -gf_{abc} (\partial_\mu A_{a\nu}) A_b^\mu A_c^\nu \\ \mathcal{L}_4 = -\frac{1}{4} g^2 f_{abc} f_{ade} A_{b\mu} A_{c\nu} A_d^\mu A_e^\nu \\ \mathcal{L}_{gh} = -gf_{abc} (\partial_\mu \omega_a^*) \omega_b A_c^\mu. \quad (9)$$

In Eq. (7), Δ_0 and \mathcal{G}_0 are the standard free-particle propagators for gluons and ghosts and their Fourier transforms are

$$\Delta_0^{\mu\nu}(p) = \Delta_0(p) [t^{\mu\nu}(p) + \xi \ell^{\mu\nu}(p)] \\ \Delta_0(p) = \frac{1}{-p^2}, \quad \mathcal{G}_0(p) = \frac{1}{p^2}. \quad (10)$$

having used the transverse and longitudinal projectors

$$t_{\mu\nu}(p) = \eta_{\mu\nu} - \frac{p_\mu p_\nu}{p^2}; \quad \ell_{\mu\nu}(p) = \frac{p_\mu p_\nu}{p^2} \quad (11)$$

where $\eta_{\mu\nu}$ is the metric tensor.

The massive expansion is obtained by adding a transverse mass term to the quadratic part of the action and subtracting it again from the interaction, leaving the total action unchanged.

In some detail, we add and subtract the action term

$$\delta S = \frac{1}{2} \int A_{a\mu}(x) \delta_{ab} \delta\Gamma^{\mu\nu}(x, y) A_{b\nu}(y) d^4x d^4y \quad (12)$$

where the vertex function $\delta\Gamma$ is a shift of the inverse propagator

$$\delta\Gamma^{\mu\nu}(x, y) = [\Delta_m^{-1\mu\nu}(x, y) - \Delta_0^{-1\mu\nu}(x, y)] \quad (13)$$

and $\Delta_m^{\mu\nu}$ is a new massive free-particle propagator

$$\Delta_m^{-1\mu\nu}(p) = (-p^2 + m^2)t^{\mu\nu}(p) + \frac{-p^2}{\xi}\ell^{\mu\nu}(p). \quad (14)$$

Adding that term is equivalent to substituting the new massive propagator $\Delta_m^{\mu\nu}$ for the old massless one $\Delta_0^{\mu\nu}$ in the quadratic part.

In order to leave the total action unaffected by the change, we must add the same term in the interaction, providing a new interaction vertex $\delta\Gamma$. Dropping all color indices in the diagonal matrices and inserting Eqs. (10) and (14) in Eq. (13) the vertex is just the transverse mass shift of the quadratic part

$$\delta\Gamma^{\mu\nu}(p) = m^2 t^{\mu\nu}(p) \quad (15)$$

and must be added to the standard set of vertices in Eq. (9).

The proper gluon polarization Π and ghost self energy Σ can be evaluated, order by order, by perturbation theory. In all Feynman graphs the internal gluon lines are replaced by the massive free-particle propagator $\Delta_m^{\mu\nu}$ and all insertions are considered of the (transverse) mass counterterm $\delta\Gamma^{\mu\nu}$ which plays the role of a new two-point vertex. It is shown as a cross in Fig. 1 where some two-point self-energy graphs are displayed. We will refer to the graphs with a cross as *crossed* graphs.

Since the total gauge-fixed FP Lagrangian is not modified and because of gauge invariance, the longitudinal polarization is known exactly and is zero, so that the total polarization is transverse

$$\Pi^{\mu\nu}(p) = \Pi(p)t^{\mu\nu}(p) \quad (16)$$

and the (exact) dressed propagators read

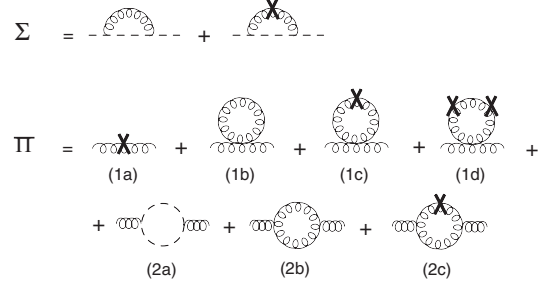


FIG. 1. Two-point self-energy graphs with no more than three vertices and no more than one loop.

$$\begin{aligned} \Delta_{\mu\nu}(p) &= \Delta(p)t_{\mu\nu}(p) + \Delta^L(p)\ell^{\mu\nu}(p) \\ \mathcal{G}^{-1}(p) &= p^2 - \Sigma(p) \end{aligned} \quad (17)$$

where the transverse and longitudinal parts are

$$\begin{aligned} \Delta^{-1}(p) &= -p^2 + m^2 - \Pi(p) \\ \Delta^L(p) &= \frac{\xi}{-p^2}. \end{aligned} \quad (18)$$

At tree level, the polarization is just given by the counterterm $\delta\Gamma$ of Eq. (15), so that the tree-term $\Pi_{\text{tree}} = m^2$ just cancels the mass in the dressed propagator Δ of Eq. (18), giving back the standard free-particle propagator of Eq. (10).

Finally, summing up the loops and switching to Euclidean space, the transverse dressed propagator can be written as

$$\Delta(p) = [p^2 - \Pi_{\text{loops}}(p)]^{-1} \quad (19)$$

where $\Pi_{\text{loops}}(p)$ is given by the transverse part of all the loop graphs for the (proper) polarization.

At one-loop, as discussed in Refs. [39,40], we sum all the graphs with no more than three vertices and no more than one loop, which are displayed in Fig. 1. In Appendix, explicit analytical expressions are given for all the polarization graphs of the figure.

The diverging integrals are made finite by dimensional regularization and can be evaluated in the Euclidean space, by setting $d = 4 - \epsilon$. An important feature of the massive expansion is that the crossed graphs cancel all the spurious diverging mass terms exactly, so that no mass renormalization is required. That is a very welcome feature since there is no bare mass in the original Lagrangian. At one-loop, as shown in Appendix, in the $\overline{\text{MS}}$ scheme, the diverging part of the proper transverse polarization can be written as

$$\Pi^\epsilon(p) = \frac{Ng^2}{(4\pi)^2} \left(\frac{2}{\epsilon} + \log \frac{\mu^2}{m^2} \right) p^2 \left(\frac{13}{6} - \frac{\xi}{2} \right) \quad (20)$$

which is the same identical result of standard perturbation theory [60] and ensures that we obtain the correct leading

behavior in the UV where the mass insertions are negligible, as shown in Eq. (A49).

As usual the diverging part can be canceled by wave function renormalization, by subtraction at an arbitrary point. Of course, a finite term $\sim \text{const} \times p^2$ arises from the subtraction and cannot be determined in any way. It also depends on the regularization scheme and on the arbitrary scale μ , so that its actual value remains somehow arbitrary. It basically is the only free parameter of the approximation, as discussed later. For an observable particle, the constant would be fixed on mass shell, by requiring that the pole of the propagator is at the physical mass with a residue equal to 1. The confinement of the gluon has been related to the existence of complex conjugated poles [45], so that if, on the one hand, there is nothing like an observable gluon mass, on the other hand, the analytic properties at the poles and their gauge parameter independence will be shown to be enough for determining the propagator entirely and uniquely.

The finite part of the one-loop proper polarization, as resulting from the sum of all the graphs in Fig. 1, reads

$$\Pi^f(p) = -\frac{3Ng^2}{(4\pi)^2} p^2 [F(s) + \xi F_\xi(s) + C] \quad (21)$$

where $s = p^2/m^2$ is the Euclidean momentum. The functions $F(s)$ and $F_\xi(s)$ are adimensional and do not depend on any parameter. Their explicit expressions are derived in Appendix by a detailed calculation of the integrals and the final result is reported in Eqs. (A41), (A44). The constant C arises from the subtraction of the diverging part by wave function renormalization. For a generic subtraction point $p = \mu$, the one-loop transverse propagator follows from Eq. (19)

$$\Delta(p) = \frac{Z_\mu}{p^2 + \frac{3Ng^2}{(4\pi)^2} p^2 [F(s) + \xi F_\xi(s) - F(\frac{\mu^2}{m^2}) - \xi F_\xi(\frac{\mu^2}{m^2})]} \quad (22)$$

where Z_μ is the arbitrary finite renormalization constant $Z_\mu = \mu^2 \Delta(\mu)$. Finally, the propagator can be written as

$$\Delta(p) = \frac{Z}{p^2 [F(s) + \xi F_\xi(s) + F_0]} \quad (23)$$

where the coupling and all other constants are absorbed by a finite renormalization factor Z and the new constant F_0 which depend on the subtraction point μ according to

$$Z = \frac{(4\pi)^2 Z_\mu}{3Ng^2} \quad (24)$$

$$F_0 = \frac{(4\pi)^2}{3Ng^2} - F(\mu^2/m^2) - \xi F_\xi(\mu^2/m^2).$$

Eq. (23) provides an explicit analytical expression for the one-loop gluon propagator. It contains three parameters: m ,

TABLE I. Parameters of Eq. (23) optimized by the $SU(3)$ data of Ref. [18] (in the range 0–4 GeV) and Ref. [12] (0–2 GeV), and by the $SU(2)$ data of Refs. [9,10] (0–2 GeV).

Data set	N	F_0	m (GeV)	Z
Duarte <i>et al.</i> [18]	$SU(3)$	-0.887	0.654	2.631
Bogolubsky <i>et al.</i> [12]	$SU(3)$	-1.035	0.733	3.360
Cucchieri, Mendes [9,10]	$SU(2)$	-0.743	0.859	1.737

Z and F_0 . However, the finite renormalization factor Z is irrelevant, while m is the unique energy scale. Since the exact Lagrangian does not contain any energy scale, m cannot be determined by the theory: the mass parameter m determines the overall energy scale and can only be fixed by comparison with some physical observable. That is not a limitation of the approximation but is a standard feature of Yang-Mills theory. Moreover, being just a scale parameter, the mass m is not a physical or dynamical mass and is not even required to be gauge invariant. We will use the energy scale of the lattice and fix m by comparison with the data of simulations in the Landau gauge. Thus, the only free parameter in Eq. (23) is the constant F_0 which is related to the arbitrary ratio μ/m . Since the result does depend on F_0 , the expansion must be optimized by a criterion for determining the best F_0 , yielding a special case of optimized perturbation theory by variation of the renormalization scheme, a method that has been proven to be very effective for the convergence of the expansion [61].

Assuming that the expansion converges more quickly for an optimal value of F_0 , the one-loop result might be very close to the exact result for a special choice of the constant. That is shown to be the case in Refs. [39–42] where an excellent agreement with the lattice is found in the Landau gauge. Unfortunately, the available data are not fully consistent and a best fit yields slightly different values of F_0 and m for different data sets, as shown in Table I. The deviations might be related to a slightly different choice of units as recently discussed in Ref. [62]. We can extract a global average $F_0 \approx -0.9 \pm 0.1$. Of course, the actual value of the constant F_0 depends on the details of the definition of the functions $F(s)$, $F_\xi(s)$ which are evaluated up to an (omitted) arbitrary additive constant in Appendix. In this paper, all the values of F_0 refer to the definition given by Eqs. (A41), (A44) for those functions.

In the Landau gauge, the best agreement is found for the data set of Ref. [18], with a best fit parameter $F_0 = -0.887$ and a mass scale $m = 0.654$ GeV, evaluated in the range $0 < p < 4$ GeV. The resulting gluon propagator is shown in Fig. 2 together with the lattice data.

III. OPTIMIZATION FROM FIRST PRINCIPLES

If the expansion is optimized in the Euclidean space, by a direct comparison with the lattice data, any control of the approximation is lost in Minkowski space and one might

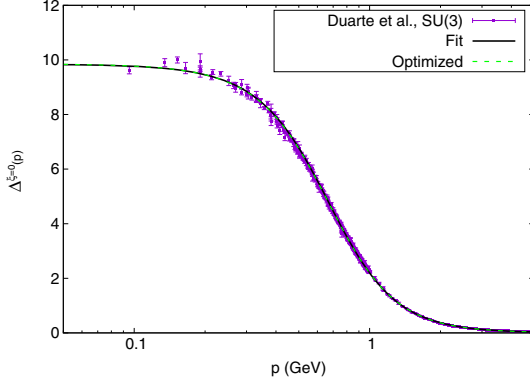


FIG. 2. The one-loop transverse gluon propagator $\Delta(p)$ of Eq. (23) is shown for the best fit parameters $F_0 = -0.887$, $m = 0.654$ GeV in the Landau gauge $\xi = 0$ (solid line), together with the lattice data of Ref. [18]. The broken line is the same propagator obtained by Eq. (23) with the optimized parameters $F_0 = -0.876$, $m = 0.656$ GeV determined by the gauge parameter independence of the pole structure in Sec. III.

wonder how robust the optimal choice would be when continued to the complex plane. Moreover, a self-contained optimization strategy, which does not require any external input, would be essential for exploring new aspects that are out of the reach of lattice calculations. In this section, we show that the expansion can be optimized from first principles in the complex plane by enforcing some general exact analytic properties that arise from the BRST invariance of the gauge-fixed Lagrangian.

The Nielsen identities [50] are exact equations connecting the gauge parameter dependence of some correlation functions with other Green functions. Their proof follows from the BRST invariance of the Faddeev-Popov Lagrangian, Eq. (1), which has not been modified by our change of the expansion point. They have been used as a tool for establishing general invariance properties of the pole structure in QCD [52] and in other Yang-Mills theories [57].

Following the detailed derivation of Ref. [52], the exact transverse projection of the gluon propagator $\Delta(p)$ must satisfy the Nielsen identity

$$\frac{\partial}{\partial \xi} \frac{1}{\Delta(p)} = G^T(p) \left[\frac{1}{\Delta(p)} \right]^2 \quad (25)$$

where, omitting the diagonal color indices, $G^T(p)$ is the transverse component

$$G^T(p) = \frac{t_{\mu\nu}(p)}{3} G_{aa}^{\mu\nu}(-p, p, 0) \quad (26)$$

of the Green function $G_{ab}^{\mu\nu}(-p, p, 0)$ which is defined as

$$\begin{aligned} G_{ab}^{\mu\nu}(-p, p, 0) &= \int d^4x d^4y e^{ip \cdot (x-y)} \langle 0 | T [D^\mu \omega_a(y) A_b^\nu(x) \omega_c^*(0) B_c(0)] | 0 \rangle \end{aligned} \quad (27)$$

in terms of the Nakanishi-Lautrup auxiliary field B_a and of the covariant derivative of the ghost field $D^\mu \omega_a$. If the gluon propagator has a pole in the complex plane at $p^2 = p_0^2(\xi)$, then the inverse propagator has a zero and we can write the identities

$$\frac{1}{\Delta(p_0(\xi))} = 0; \quad \frac{d}{d\xi} \frac{1}{\Delta(p_0(\xi))} = 0. \quad (28)$$

Then, the vanishing of the right-hand side of Eq. (25) at $p = p_0(\xi)$ says that the partial derivative is also zero and the pole p_0 must be gauge parameter independent

$$\frac{d}{d\xi} p_0(\xi) = 0. \quad (29)$$

By the same argument, the residues at the poles are also gauge parameter independent [53]. In fact, if we differentiate Eq. (25) with respect to p^2

$$\begin{aligned} \frac{\partial}{\partial \xi} \left[\frac{d}{dp^2} \frac{1}{\Delta(p)} \right] &= \left[\frac{d}{dp^2} G^T(p) \right] \left[\frac{1}{\Delta(p)} \right]^2 \\ &+ 2G^T(p) \frac{1}{\Delta(p)} \left[\frac{d}{dp^2} \frac{1}{\Delta(p)} \right], \end{aligned} \quad (30)$$

the right-hand side vanishes at $p = p_0$ because of Eq. (28), so that the residue R , defined as

$$R = \lim_{p \rightarrow p_0} \Delta(p) (p^2 - p_0^2) = \lim_{p \rightarrow p_0} \left[\frac{d}{dp^2} \frac{1}{\Delta(p)} \right]^{-1}, \quad (31)$$

satisfies the exact equation

$$\frac{\partial}{\partial \xi} R = 0. \quad (32)$$

We conclude that, for the gauge-fixed Yang-Mills Lagrangian, the principal part Δ^P of the exact gluon propagator

$$\Delta^P(p) = \frac{R}{p^2 - p_0^2} + \frac{R^*}{p^2 - p_0^{*2}} \quad (33)$$

must be gauge parameter independent. The argument fails if $G^T(p)$ has a pole in $p = p_0$, which is usually not the case.

In the quadratic part of the Lagrangian, the BRST symmetry is broken by the mass term that has been added and has been subtracted again from the interaction. Thus, while the total Lagrangian is BRST invariant, the symmetry

is broken at any finite order of the massive expansion. For that reason, we do not expect that the one-loop propagator might satisfy the Nielsen identity exactly. However, the closer we reach to the exact result, the better is expected to be the agreement with the exact identities. Thus, we can exploit the dependence on the parameters F_0, m in Eq. (23) and optimize the expansion by requiring that the pole structure of the propagator is gauge parameter independent. That is equivalent to an optimal choice of the subtraction point μ/m , which is usually fixed on mass shell for an observable particle. Without any observable gluon mass at hand, the invariance of the poles and residues turns out to be enough for determining the one-loop gluon propagator entirely and for any choice of the gauge parameter.

For a generic choice of the gauge parameter ξ , the optimal parameters can be regarded as functions $F_0(\xi), m(\xi)$, to be determined by the requirement that the pole and the residue do not depend on ξ . Of course, the finite renormalization factor Z remains arbitrary and has no physical relevance. Let us denote by $\Psi(z, \xi, F_0, m)$ the inverse dressing function in Eq. (23)

$$\Psi(z, \xi, F_0, m) = F(-z^2/m^2) + \xi F_\xi(-z^2/m^2) + F_0 \quad (34)$$

which is an analytic function of the complex variable $z = x + iy$. On the imaginary axis, for $x = 0$, $p_E^2 = -z^2 = y^2$ is the Euclidean momentum. On the real axis, for $y = 0$, we recover the Minkowskian momentum $p_M^2 = z^2 = x^2$. Thus, the variable z is the analytic continuation of the physical momentum p_M . The pole $z_0^2 = -p_0^2$ is a zero of the inverse dressing function Ψ and must satisfy the equation $\Psi(z_0, \xi, F_0, m) = 0$. The gauge parameter independence of the pole requires that

$$\Psi(z_0, \xi_1, F_0(\xi_1), m(\xi_1)) = \Psi(z_0, \xi_2, F_0(\xi_2), m(\xi_2)) \quad (35)$$

yielding a set of two coupled real equations for the real and imaginary parts. The equations can be solved for $F_0(\xi_2)$ and $m(\xi_2)$ from a given initial value $F_0(\xi_1), m(\xi_1)$. Taking the Landau gauge as the initial point $\xi_1 = 0$ and fixing a scale $m_0 = m(0)$ as energy units, the functions $F_0(\xi)$ and $m(\xi)$ are determined for any value of the gauge parameter ξ from the initial value $F_0(0)$ which remains the only free parameter. Thus, we can encode the gauge parameter independence of the pole in the optimized propagator and evaluate it for any value of the parameter ξ . The functions $F_0(\xi), m^2(\xi)$ are shown in Figs. 3 and 4 for different choices of the initial value $F_0(0)$ in the Landau gauge.

In the range $-2 < F_0(0) < 0$, the gluon propagator of Eq. (23) has a single pair of complex conjugated poles, while other values of $F_0(0)$, out of that range, seem to be unphysical. For $F_0(0) < -2$ the expression in Eq. (23) has poles in the Euclidean space and changes sign at the poles, on the positive s axis. Moreover, according to Eq. (24), the

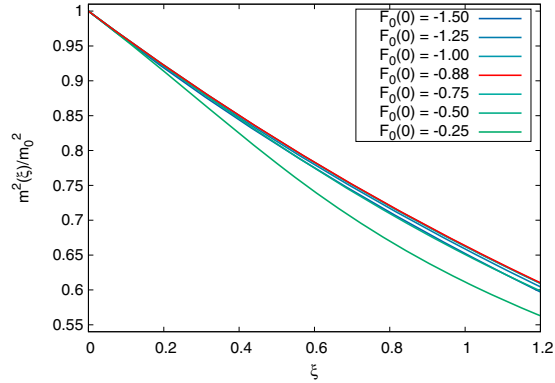


FIG. 3. The mass parameter ratio $m^2(\xi)/m_0^2$ as a function of the gauge parameter ξ for different initial values of $F_0(0)$. The red line is obtained for the optimal value $F_0(0) = -0.876$.

coupling g^2 would become negative in that range because the minimal value of $F(s)$ is ≈ 2 . For $F_0(0) > 0$ the coupling g^2 becomes very small in Eq. (24) for any μ and the pole topology becomes very different. As discussed in the previous section, in the Landau gauge, the best agreement with the lattice is found for $F_0 \approx -0.9$ which is at the center of the physical allowed range.

It is remarkable that, close to the best fit value $F_0(0) \approx -0.9$, the contour lines $\text{Re}\Psi = 0, \text{Im}\Psi = 0$, at the crossing point z_0 (the pole), are basically not rotated by any change of ξ . That can be seen in Fig. 5 where the contour lines are displayed for $\xi = 0$ and $\xi = 1$ and are shown to be approximately tangent at the intersection point. In other words, when the initial value $F_0(0)$ approaches the best fit value $F_0(0) \approx -0.9$, the conformal map $z_1 \rightarrow z_2$, defined by

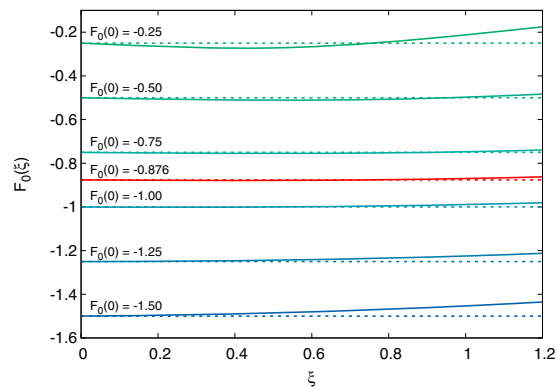


FIG. 4. The parameter $F_0(\xi)$ as a function of the gauge parameter ξ for different initial values of $F_0(0)$. The red line is obtained for the optimal value $F_0(0) = -0.876$.

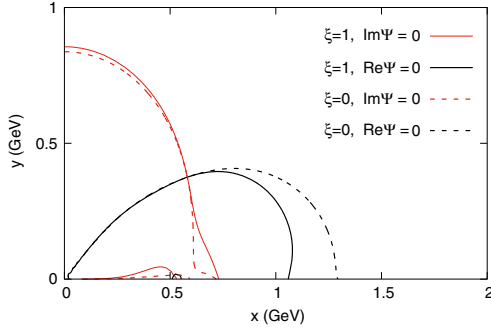


FIG. 5. Contour plots of $\text{Re}\Psi = 0$, $\text{Im}\Psi = 0$ in the complex plane $z = x + iy$ for $\xi = 1$ (solid lines) and $\xi = 0$ (dashed lines), with $F_0(0) = -0.876$ and $m_0 = 0.656$ GeV (see Table II). The curves are approximately tangent (i.e., $\theta \approx 0$) at the intersection point z_0 (the pole) whenever $F_0 \approx -0.9$.

$$\Psi(z_1, \xi_1, F_0(\xi_1), m(\xi_1)) = \Psi(z_2, \xi_2, F_0(\xi_2), m(\xi_2)) \quad (36)$$

becomes a local identity at the fixed point (the pole $z_0^2 = -p_0^2$). Denoting by θ the rotation angle of the contour lines in the map and setting $\xi_1 = 0$, $\xi_2 = \xi$, we can write

$$\theta(\xi) = \text{Arg} \left\{ \frac{\frac{d}{dz} \Psi(z, 0, F_0(0), m(0))}{\frac{d}{dz} \Psi(z, \xi, F_0(\xi), m(\xi))} \right\}_{z=z_0} \quad (37)$$

and because of Eq. (31), the angle θ gives the phase change of the residue R which can be written, as a function of ξ ,

$$R(\xi) = R(0)e^{i\theta(\xi)} \quad (38)$$

since the modulus $|R|$ can always be made invariant by an appropriate choice of the real renormalization constant $Z(\xi)$. Explicit analytical expressions for the derivative of Ψ are reported in Eqs. (A50), (A53) of Appendix.

We observe that the angle θ is not exactly zero, so that in general, the Nielsen identity Eq. (25) and its consequences Eqs. (29), (32) cannot be all satisfied. However, as shown in Figs. 5 and 6, the angle θ becomes very small, for a wide range of ξ , if the initial constant $F_0(0)$ is close to the value $F_0 \approx -0.9$ which already described the lattice data very well in the Euclidean space. In other words, the optimal propagator in the Euclidean space is also the one that best satisfies the Nielsen identity in the complex plane, giving us confidence in the general accuracy of the approximation. We must mention that averaging over Gribov copies might break BRST invariance in the lattice. However, we are assuming that the Nielsen identities are not seriously affected in lattice calculations.

Reversing the argument, the expansion can be optimized in a self-contained way, by first principles and without any external input, by assuming that the best choice for the

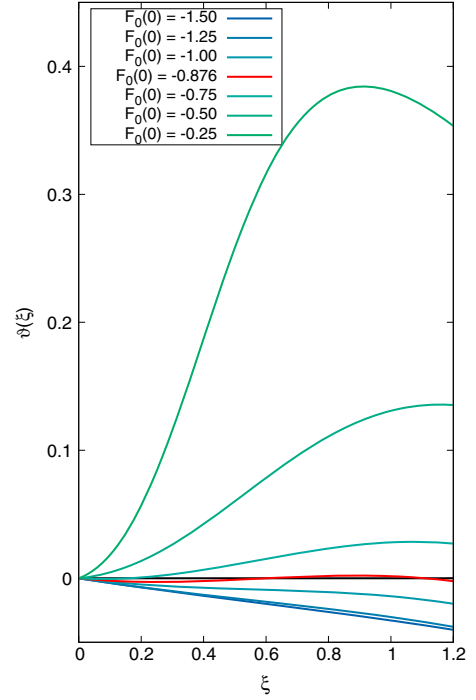


FIG. 6. The phase change θ of the residue is shown as a function of ξ for different initial values of $F_0(0)$. The red line is obtained for the optimal value $F_0(0) = -0.876$.

initial constant $F_0(0)$ is the one that makes the angle θ smaller in a wider range of ξ . Even if there are no technical reasons for limiting the value of the gauge parameter, we expect that perturbation theory would be more effective when ξ is small and the expansion might be out of control for very large $\xi \gg 1$. Prudentially, the present study is limited to the range $\xi < 1.2$, including the Feynman gauge.

The minimal phase deviation is observed for the initial value $F_0(0) = -0.876$. As shown in Fig. 6, for that choice, the phase θ fluctuates around zero in the whole range $0 < \xi < 1.2$, with very small deviations which are less than 0.003. Nevertheless, no fine tuning is required since θ is very small around $F_0(0) \approx -0.9$ and any slight change of $F_0(0)$ can be compensated by an appropriate choice of Z and m . In fact, as shown in Fig. 2, when the present new set of first-principle optimal parameters are inserted in Eq. (23), the propagator is indistinguishable from the previous one that was obtained by a best fit of the lattice data. Actually, the optimal initial value $F_0(0)$ not only minimizes the phase deviation $\theta(\xi)$, but also makes $m^2(\xi)$ stationary and maximal for any fixed ξ , as shown in Fig. 3 where the optimal curve is plotted as a red line. That is a geometric consequence of the pole being the tangency point in Fig. 5. Moreover, the optimal function $F_0(\xi)$ is the

FABIO SIRINGO and GIORGIO COMITINI

PHYS. REV. D **98**, 034023 (2018)

TABLE II. Set of optimal parameters, obtained by enforcing the gauge parameter independence of the pole structure in the range $0 < \xi < 1.2$. The energy scale m_0 and the finite renormalization constant $Z(0)$ are determined by the data of Ref. [18] which are shown in Fig. 2.

OPTIMIZATION BY GAUGE INVARIANCE
$F_0(0) = -0.876$, $m_0 = m(0) = 0.656$ GeV, $Z(0) = 2.684$ $ \theta(\xi) < 2.76 \times 10^{-3}$, $0 < \xi < 1.2$
$F_0(\xi) \approx -0.8759 - 0.01260\xi + 0.009536\xi^2 + 0.009012\xi^3$ $m^2(\xi)/m_0^2 \approx 1 - 0.39997\xi + 0.064141\xi^2$
$z_0/m_0 = 0.8857 + 0.5718i$, $t_R = \text{Im}R(0)/\text{Re}R(0) = 3.132$ $M = 0.581$ GeV, $\gamma = 0.375$ GeV (invariant pole)

most gauge parameter invariant curve in Fig. 4 (shown as a red line).

The optimal parameters are summarized in Table II together with very accurate polynomial interpolation formula for the optimal functions $F_0(\xi)$, $m^2(\xi)$. Extracting the energy scale $m_0 = m(0) = 0.656$ GeV from the lattice data of Ref. [18] in the Landau gauge, the invariant pole is found at $x_0 = M = 0.581$ GeV and $y_0 = \gamma = 0.375$ GeV, which might be regarded as the physical mass and the damping rate of the quasigluon, respectively, as discussed in Ref. [45].

IV. THE PROPAGATOR AT $\xi \neq 0$

In the Euclidean space, the gluon propagator can be evaluated analytically by Eq. (23), for any value of the gauge parameter ξ , inserting the optimal parameters of Table II which enforce the gauge parameter independence of the pole structure in the complex plane. In order to compare with the available lattice data of Ref. [49], the finite renormalization constant Z is fixed by the same momentum subtraction scheme of that work, i.e., requiring that $\mu^2\Delta(\mu) = 1$ for any ξ and taking the same renormalization point $\mu = 4.317$ GeV. That is equivalent to taking the constant Z in Eq. (23) to be $Z = \Psi(i\mu, \xi, F_0, m)$.

The gluon propagator is shown in Fig. 7, for several values of the gauge parameter ξ , together with some data points extracted from Ref. [49]. The agreement with the data is very good in the limited range $\xi < 0.5$ where they are available. For $\xi \neq 0$, the propagator is slightly suppressed in the IR compared with the Landau gauge. We must mention that previous continuum studies, based on the truncation of an infinite set of exact Dyson-Schwinger equations, reached contrasting and ambiguous results. While a strong dependence on the gauge parameter was predicted in Ref. [25], with large deviations from the Landau gauge, a qualitative agreement with the lattice was reported in Ref. [22] by the aid of exact Nielsen identities which seem to play a key role. The gauge dependence was found small but no quantitative prediction

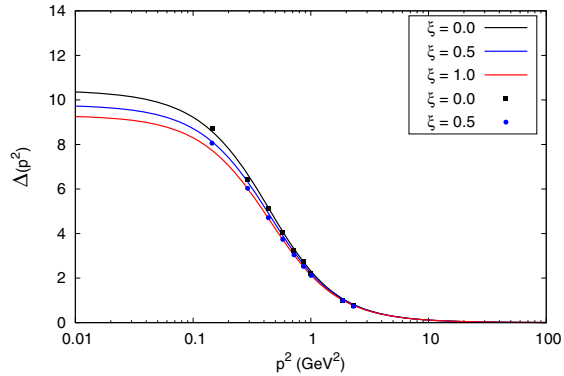


FIG. 7. The gluon propagator of Eq. (23) is evaluated as a function of the Euclidean momentum p^2 with the first-principle optimized parameters of Table II, for $\xi = 0, 0.5, 1$ and renormalized at $\mu = 4.317$ GeV. The points are the lattice data of Ref. [49].

could be made and even the sign of the change was not defined by that method.

As shown in Fig. 7, up to and beyond the Feynman gauge ($\xi = 1$), no dramatic change occurs and the suppression of the propagator increases very smoothly with the increasing of ξ . The change can best be seen by evaluating the ratio between $\Delta(p)$ at $\xi \neq 0$ and at $\xi = 0$, as shown in Fig. 8 together with the lattice data of Ref. [49]. Even if the lattice calculation is plagued by large statistical errors, with scattered data and large error bars, the optimized propagator seems to be in quantitative agreement with the data and reproduces the correct trend predicted by the lattice. We stress that the curves are not a fit of the data and the agreement is reached from first principles without any adjustable parameter.

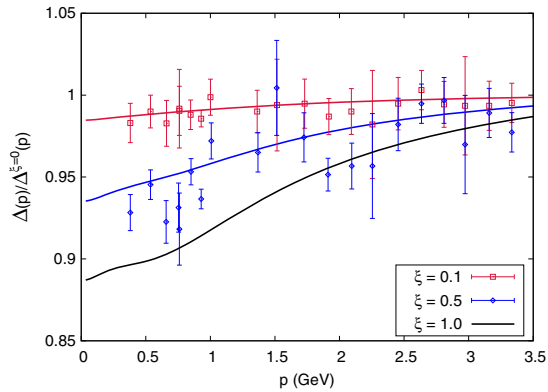


FIG. 8. The ratio $\Delta(p)/\Delta^{\xi=0}(p)$ as a function of the Euclidean momentum p with the first-principle optimized parameters of Table II, for $\xi = 0.1, 0.5$, and 1 . The bars are the lattice data of Ref. [49].

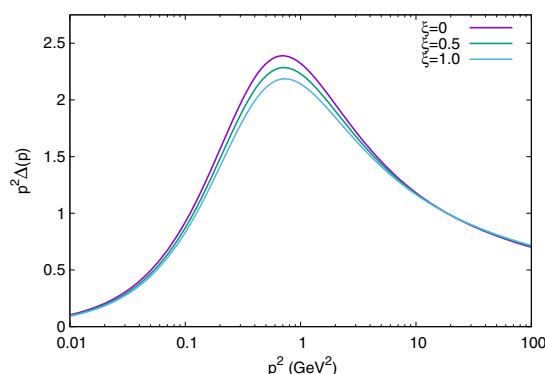


FIG. 9. The dressing function $p^2\Delta(p)$ as a function of the Euclidean momentum p^2 for the same parameters of Fig. 7.

The dressing function is shown in Fig. 9. As predicted by the lattice [49], the maximum is basically fixed at the same energy for any ξ . We argue that the Nielsen identity gives the correct scale factor $m(\xi)/m(0)$ that keeps the maximum fixed, at variance and in strong contrast with the continuum calculation of Ref. [25] which might miss that important constraint.

In the studied range of ξ , the whole principal part of the propagator in Eq. (33) is basically invariant up to a finite renormalization factor. The pole p_0 is fixed at the value of Table II, while the phase of the residue is $\text{Arg}R(\xi) = 1.262 + \theta(\xi)$ where $|\theta(\xi)| < 2.75 \times 10^{-3}$, yielding the ratio $t_R = \text{Im}R(\xi)/\text{Re}R(\xi) = 3.132 \pm 0.03$. This ratio is important for determining the explicit parameters of the rational part Eq. (33) which has been derived at tree level by other phenomenological models like the refined Gribov-Zwanziger model [56–58]. Being gauge parameter independent, the parameters of the rational part might be directly related to physical observables or condensates [63,64] and a recent general method has been proposed for extracting information on the glueball masses [58]. Using the notation of Ref. [64], the principal part of the propagator, Eq. (33), can be written as

$$\Delta^P(p) = Z_{\text{GZ}} \frac{p^2 + M_1^2}{p^4 + M_2^2 p^2 + M_3^4} \quad (39)$$

where

$$\begin{aligned} Z_{\text{GZ}} &= 2\text{Re}R \\ M_1^2 &= M^2 - \gamma^2 + 2M\gamma t_R = 1.562 \text{ GeV}^2 \\ M_2^2 &= 2(M^2 - \gamma^2) = 0.394 \text{ GeV}^2 \\ M_3^4 &= (M^2 + \gamma^2)^2 = 0.229 \text{ GeV}^4 \end{aligned} \quad (40)$$

having made use of the optimized parameters of Table II. Below 1 GeV, the masses M_i seem to be compatible with

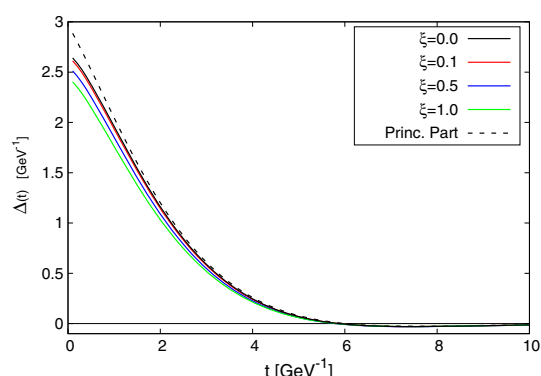


FIG. 10. The Schwinger function is shown, as a function of the Euclidean time t , for different values of the gauge parameter. The broken line is the analytical result of Eq. (42) which is obtained by the principal part of the gluon propagator.

the statistical analysis of Ref. [64], even if the simple rational part Δ^P was used in that work for a fit of the lattice data, ignoring the corrections which are included in the present optimized one-loop propagator. In fact, the corrections are gauge dependent and very small below 1 GeV, as already shown in the Landau gauge by a direct evaluation of the spectral function [41,65].

The Schwinger function $\Delta(t)$ can be evaluated by a numerical integration, as a function of the Euclidean time t , according to its definition

$$\Delta(t) = \int_{-\infty}^{+\infty} \frac{d^4 p_A}{2\pi} e^{i p_A t} \Delta(\vec{p} = 0, p_A) \quad (41)$$

and is shown in Fig. 10 for different values of the gauge parameter. In the Landau gauge, the Schwinger function is found in qualitative agreement with the result of Ref. [66], with a positivity violation that occurs above the point $t = t_0 \approx 5.8 \text{ GeV}^{-1}$ where the function crosses the zero and becomes negative. The scale t_0 is roughly the size of a hadron and in Ref. [66] it was conjectured to be a physical gauge-invariant scale at which gluon screening occurs. Actually, as shown in Fig. 10, the crossing point t_0 is found to be almost gauge parameter independent. Moreover, the large t behavior seems to be dominated by the singularities and the whole Schwinger function is very well approximated by inserting in Eq. (41) the simple principal part $\Delta^P(p)$ of Eq. (33), which is gauge parameter independent, yielding the analytical result

$$\Delta^P(t) = \left[\frac{|R|}{\sqrt{M^2 + \gamma^2}} \right] e^{-Mt} \cos \left(\gamma t - \theta + \arctan \frac{\gamma}{M} \right) \quad (42)$$

which is shown in Fig. 10 as a broken line.

We cannot end this section without a brief discussion of the spectral function, which has attracted great interest [54,55] even if its physical content is quite unclear in presence of complex poles and confinement. In fact, the usual Källén-Lehmann representation must be replaced by the more general integral representation [65]

$$\begin{aligned} \text{Re}\Delta(p^2) &= \Delta^P(p^2) + \text{P.V.} \int_0^{+\infty} \frac{\rho(\mu^2)}{p^2 - \mu^2} d\mu^2 \\ \rho(p^2) &= -\frac{1}{\pi} \text{Im}\Delta(p^2 + i\epsilon) \end{aligned} \quad (43)$$

where the spectral function $\rho(p^2)$ is gauge dependent and does not contain any information on the gauge parameter independent principal part Δ^P which must be added to the integral for reproducing the whole propagator. Moreover, $\rho(p^2)$ is even not positive defined for a confined particle. In the Landau gauge, the spectral function was evaluated by the massive expansion in Ref. [41] and the dispersion relation of Eq. (43) was checked in Ref. [65] by a numerical integration. The integral provides the difference between the principal part and the whole propagator, so that the difference can be large only if the total weight which comes from the integration of $\rho(p^2)$ is large. Moreover, $\rho(p^2)$ changes sign and the contributions arising from different signs can partially cancel.

The one-loop spectral density can be easily evaluated by the explicit expression of the propagator, Eq. (23), using the optimal parameters of Table II, and is shown in Fig. 11 for different values of the gauge parameter ξ . It has some gauge dependent features, like a cusp at the two-particle threshold $p = 2m(\xi)$ and a finite spike at $p \approx m(\xi)$. In the Landau gauge, the spike is just a smooth maximum but is enhanced for $\xi > 0.08$ by the appearance of a gauge dependent pole near the real axis, at $x \approx m(\xi)$. Some details of the finite peak on the real axis are shown in Fig. 12. Apart from the peak, the spectral density is very small and even the peak

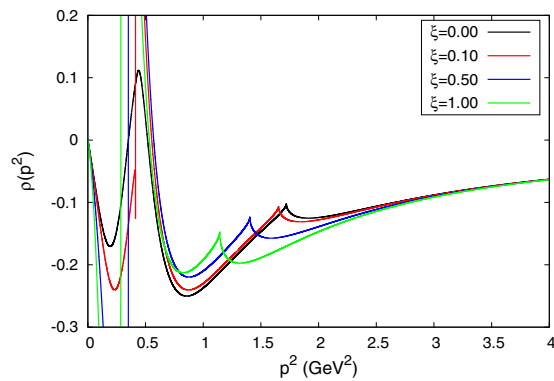


FIG. 11. The one-loop spectral density $\rho(p^2)$ is shown for different values of the gauge parameter.

area gives a small contribution to the integral in Eq. (43) because of the change of sign that occurs just at the peak, in agreement with a confinement scenario. While the peak resembles the spike which was observed in Ref. [59], its physical nature is unclear and is certainly related to the nature of the new gauge dependent pole which might be an artifact of the one-loop approximation.

From a technical point of view, the new pole arises because of the logarithmic divergence of the real part of $F_\xi(-z^2/m^2)$ at the branch point $x = m$ on the real axis. The divergence occurs because of the bad IR behavior of the crossed gluon loop, Π_{2c} in Fig. 1, in the limit $p \rightarrow im$, since the denominator in Eq. (A19) becomes

$$k^2[(k+p)^2 + m^2]^{n+1} \rightarrow k^2[k^2 + 2k \cdot p]^{n+1} \sim k^{n+3} \quad (44)$$

if there are n insertions of the counterterm in the transverse gluon line. Thus the integral diverges in the IR and the divergence becomes worse and worse at higher orders, requiring some resummation which might cancel the divergence in the exact result. For $n = 1$ the divergence appears as a branch point at $s = -1$ for the logarithmic term $\log(1+s)$ of $F_\xi(s)$ in Eq. (A44). Near the branch point, for $x \approx m$ and any finite $\xi \neq 0$, the real part of the inverse dressing function $\Psi(z)$, Eq. (34), can be written as

$$\text{Re}\Psi(z) \approx \text{Re}\Psi_{\text{reg}}(z) + \xi A(m) \log|z - m| \quad (45)$$

where Ψ_{reg} is the regular part and the prefactor $A(z)$ of the log is a rational function which is real on the real axis, with $A(m) = -2/3$. Then, taking $z = m + re^{i\phi}$, the contour line $\text{Re}\Psi = 0$ is given by

$$r \approx \exp\left(-\frac{\text{Re}\Psi_{\text{reg}}(m)}{\xi A(m)}\right) = e^{-C/\xi} \quad (46)$$

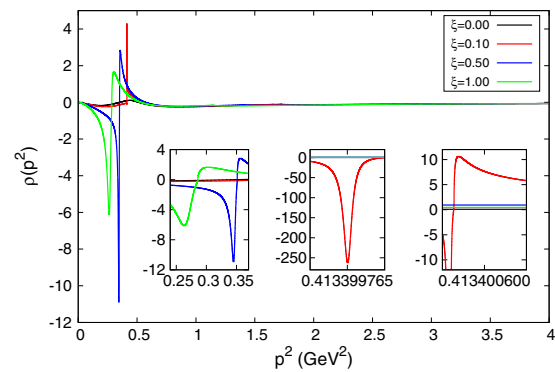


FIG. 12. The same curves of Fig. 11 on a different scale. The peaks of $\rho(p^2)$ are shown in the inserts on a very enlarged scale. The rightmost inserts both have a width of 2×10^{-7} GeV².

which is a very small circle centered at $x = m$ on the real axis, with an exponentially small radius in the limit $\xi \rightarrow 0$ if $C > 0$. In the Feynman gauge, $\xi = 1$, the contour line is just visible in Fig. 5 as a small black semi-circle centered at $x = m(1) = 0.53$ GeV on the real axis. It gets hardly visible for $\xi < 0.5$.

At the same branch point, the imaginary part of $F_\xi(s)$ has a large discontinuous step yielding a change of the whole imaginary part

$$\delta(\text{Im}\Psi) \approx \xi\pi A(m) = -2.1 \cdot \xi \quad (47)$$

which is quite larger than $\text{Im}\Psi_{\text{reg}}(m) \approx 0.17$ and gives rise to a sharp change of sign at $x = m(\xi)$, even when ξ is small, provided that $\xi > 0.08$. On the complex plane, the discontinuous step is smeared out and the imaginary part $\text{Im}\Psi$ changes sign on a contour line $\text{Im}\Psi = 0$ which originates from the branch point $x = m(\xi)$, just at the center of the circle $\text{Re}\Psi = 0$. The resulting contour line $\text{Im}\Psi = 0$ is visible in Fig. 5 as a solid red line ending at the center of the black semicircle. The crossing point of the two contour lines is the new pole that appears for $\xi > 0.08$. On the other hand, if $\xi < 0.08$, the imaginary part $\text{Im}\Psi$ changes sign below $x = m(\xi)$, out of the circle, the contour lines do not cross and the extra pole disappears when approaching the Landau gauge.

By the previous analysis we conclude that the narrow peak of the spectral function must have a very small width, roughly given by the distance of the pole from the real axis $r \approx \exp(-C/\xi)$, getting smaller and smaller when $\xi \ll 1$, as shown in Fig. 12. Moreover, $\text{Im}\Psi$ and $\rho(p^2)$ change sign across the peak and the overall effect of the peak on the integral, in Eq. (43), is expected to be negligible.

It is likely that the sharp peak of the spectral function and the gauge dependent pole get smoothed in the exact propagator since the Nielsen identity, Eq. (25) would forbid the existence of a pole which depends on the gauge parameter ξ , unless the Green function $G^T(p)$ in Eq. (26) has a pole at the same point. Having traced the source of the pole and found it related to the logarithmic divergence of the crossed graphs at $p^2 = -m^2$, we cannot exclude that the same divergence might occur in the ghost sector and in other Green functions. Thus, in principle, we cannot rule out that the pole might be genuine, even if probably related to unphysical degrees of freedom of the ghost sector.

V. DISCUSSION

There is a growing consensus that QCD and Yang-Mills theory are self-contained theories that dynamically generate their own infrared cutoff. The numerical simulations on the lattice have shown that the exact theory generates a dynamical mass which screens the gluon interaction in the IR. Therefore, any continuum first-principle study should reproduce the same results without the aid of any adjustable parameter, except for the overall energy scale

that must come from the phenomenology. It could be argued that, because of Gribov ambiguity, in R_ξ gauge the Faddeev-Popov Lagrangian is just an approximation of the full theory. The approximation works very well in the usual perturbative approach but could be out of control in the IR because of nonperturbative effects. A phenomenological parameter has been introduced by several authors for locating the Gribov horizon, yielding an interaction-induced mass scale which screens the theory in the IR [56–58,67–72]. However, even averaging over Gribov copies, a dynamical mass is generated in the theory, as shown by the gauge-fixed lattice calculations in the Landau gauge. A recent analysis [73] has made clear that the dynamical mass would be as effective as the Gribov parameter for screening the theory and that its dynamical appearance alone would eliminate the problem of Gribov copies and complete the definition of the theory.

The same argument holds for the massive expansion which is a screened expansion from the beginning and can be safely used in the IR. Having changed the expansion point, the gauge-fixed theory can be studied by plain perturbation theory and the agreement with the lattice data shows that, when the expansion is optimized, higher order graphs are very small and negligible. Thus, ignoring the Gribov ambiguity does not seem to be a problem as far as perturbation theory works well. Again, it is a consequence of the dynamical mass that screens the theory, yielding a self-contained perturbative description from first principles.

It is not surprising that, without using any adjustable parameter and without modifying the original gauge-fixed Lagrangian, the massive expansion predicts the same pole structure which was found by the refined Gribov-Zwanziger model [56–58]. The two approaches are very different but they study the same identical physical system, so that if both are valid approximations they must reach the same conclusions. Moreover, our analysis supports the physical relevance of the principal part: having established its gauge parameter independence [53], we argue that the simple rational part $\Delta^P(p)$ might play an important role in the phenomenology, more than the (small) gauge dependent spectral density. The conclusions of the present work would be enforced by a comparison with position-space lattice data, because of their sensitivity to the analytical structure of the propagator. Unfortunately, at the moment, for a generic covariant gauge, no such data are available.

An apparent drawback of the massive expansion is that the BRST invariant action is arbitrarily splitted in two parts that are not BRST invariant. The Nielsen identities cannot be satisfied exactly at any finite order of the expansion. However, because of the spurious dependence of the approximation on the subtraction point μ/m , the expansion can be optimized by enforcing the gauge parameter invariance of the pole structure. Thus, the extension to R_ξ gauge, not only gives new information on the gluon propagator in a generic gauge, but also provides a unique

way to fix the optimal expansion even in the Landau gauge. The good agreement with the available lattice data, which is reached without any fit of adjustable parameters, increases our confidence in the general validity of the method as a first-principle benchmark for more phenomenological models.

ACKNOWLEDGMENTS

We are in debt to David Dudal for suggesting the proof of gauge parameter independence of the residues. We also thank Orlando Oliveira for sharing with us the lattice data of Ref. [18].

APPENDIX: ONE-LOOP GRAPHS

In this Appendix, explicit analytical expressions are derived for the one-loop polarization graphs of Fig. 1. The graphs are evaluated using the free-particle (gauge-dependent) propagator of Eq. (14) and inserting the transverse counterterm of Eq. (15) as a new two-point vertex which is shown as a cross in the figure. We refer to the graphs with one insertion of the counterterm as crossed graphs.

1. Graphs Π_{1b} , Π_{1c} , and Π_{1d} (tadpoles)

In the Euclidean space, the constant tadpole Π_{1b} can be written as

$$\Pi_{1b} = -\frac{Ng^2(d-1)^2}{d} \int \frac{d^d k}{(2\pi)^d} \frac{1}{k^2 + m^2} \quad (\text{A1})$$

having dropped the longitudinal loop which is scaleless and vanishes in dimensional regularization. Setting $d = 4 - \epsilon$, in the $\overline{\text{MS}}$ scheme,

$$\Pi_{1b} = \frac{3(3Ng^2)}{4(4\pi)^2} m^2 \left(\frac{2}{\epsilon} + \log \frac{\mu^2}{m^2} + C \right) \quad (\text{A2})$$

where C is a constant which depends on the regularization scheme.

The crossed graphs do not contain any longitudinal gluon line since the counterterm $\delta\Gamma$ is transverse in Eq. (15). The graph Π_{1c} can be written as a derivative

$$\Pi_{1c} = -m^2 \frac{\partial \Pi_{1b}}{\partial m^2} = -\frac{3(3Ng^2)}{4(4\pi)^2} m^2 \left(\frac{2}{\epsilon} + \log \frac{\mu^2}{m^2} + C - 1 \right). \quad (\text{A3})$$

As expected, the diverging terms cancel in the sum $\Pi_{1b} + \Pi_{1c}$. The double-crossed tadpole Π_{1d} is finite and including its symmetry factor it reads

$$\Pi_{1d} = \frac{1}{2} m^4 \frac{\partial^2 \Pi_{1b}}{\partial (m^2)^2} = -\frac{3(3Ng^2)}{8(4\pi)^2} m^2 \quad (\text{A4})$$

so that the sum of the constant graphs is

$$\Pi_{1b} + \Pi_{1c} + \Pi_{1d} = \frac{3(3Ng^2)}{8(4\pi)^2} m^2. \quad (\text{A5})$$

2. Ghost loop Π_{2a}

The ghost loop Π_{2a} is a standard graph and does not depend on ξ . In the Euclidean space it is given by the integral [32]

$$\Pi_{2a}(p) = -\frac{Ng^2}{(d-1)} \int \frac{d^d k}{(2\pi)^d} \frac{k_\perp^2}{k^2(p+k)^2}. \quad (\text{A6})$$

The integral is straightforward and setting $d = 4 - \epsilon$ the diverging part is

$$\Pi_{2a}^\epsilon(p) = \frac{(3Ng^2)}{(4\pi)^2} \frac{p^2}{36} \left(\frac{2}{\epsilon} + \log \frac{\mu^2}{m^2} \right) \quad (\text{A7})$$

while the finite part reads

$$\Pi_{2a}^f(p) = \frac{(3Ng^2)}{(4\pi)^2} \frac{m^2}{36} (C_0 s - s \log s) \quad (\text{A8})$$

where $s = p^2/m^2$ and the constant C_0 depends on the regularization scheme.

3. Gluon loop Π_{2b}

The gluon loop Π_{2b} can be written as

$$\Pi_{2b}(p) = \Pi_{2b}^0(p) + \xi \Pi_{2b}^\xi(p) + \xi^2 \Pi_{2b}^{\xi\xi}(p) \quad (\text{A9})$$

where $\Pi_{2b}^0(p)$ is the graph in the Landau gauge, $\xi = 0$. In the Euclidean space, setting $d = 4$, it reads [32]

$$\Pi_{2b}^0(p) = \frac{Ng^2}{6} \int \frac{d^4 k}{(2\pi)^4} \frac{k_\perp^2 \mathcal{F}^0(k, p)}{(k^2 + m^2)[(k+p)^2 + m^2]} \quad (\text{A10})$$

where $k_\perp^2 = [k^2 - (k \cdot p)^2/p^2]$ and the kernel \mathcal{F}^0 can be derived by the explicit expressions of Ref. [32]

$$\mathcal{F}^0(k, p) = \frac{10(k^2 + p^2) + (k+p)^2}{k^2} + \frac{p^4 + 10p^2k^2 + k^4}{(k+p)^2}. \quad (\text{A11})$$

It is useful to decompose it as

$$\frac{\mathcal{F}^0(k, p)}{12} = \frac{k^2 + p^2}{k^2} + \frac{p^2}{(k+p)^2} - \frac{p^2 k_\perp^2}{3(k+p)^2 k^2} \quad (\text{A12})$$

and using the identity

$$\frac{1}{q^2(q^2 + m^2)} = \frac{1}{m^2} \left[\frac{1}{q^2} - \frac{1}{q^2 + m^2} \right] \quad (\text{A13})$$

the graph can be split as

$$\Pi_{2b}^0(p) = 2Ng^2[I_A(p) + 2I_B(p) + I_C(p)] \quad (\text{A14})$$

where

$$\begin{aligned} I_A(p) &= \int \frac{d^4k}{(2\pi)^4} \frac{k_\perp^2 (1 - \frac{2p^2}{m^2} - \frac{p^2 k_\perp^2}{3m^4})}{(k^2 + m^2)[(k+p)^2 + m^2]} \\ I_B(p) &= \frac{p^2}{m^2} \int \frac{d^4k}{(2\pi)^4} \frac{k_\perp^2 (1 + \frac{k_\perp^2}{3m^2})}{k^2[(k+p)^2 + m^2]} \\ I_C(p) &= -\frac{p^2}{3m^4} \int \frac{d^4k}{(2\pi)^4} \frac{k_\perp^4}{k^2(k+p)^2}. \end{aligned} \quad (\text{A15})$$

The integrals can be evaluated analytically [40,67,68] by dimensional regularization for $d = 4 - \epsilon$, yielding a diverging part

$$\Pi_{2b}^{0\epsilon}(p) = -\frac{3Ng^2}{(4\pi)^2} \left(m^2 - \frac{25}{36} p^2 \right) \left(\frac{2}{\epsilon} + \log \frac{\mu^2}{m^2} \right) \quad (\text{A16})$$

and a finite part

$$\begin{aligned} \Pi_{2b}^{0f} &= \frac{3Ng^2 m^2}{(4\pi)^2 72} \left[\frac{2}{s} + C_1 + C_2 s + s^3 \log s \right. \\ &\quad \left. - sL_A(s) - sL_B(s) \right] \end{aligned} \quad (\text{A17})$$

where C_1, C_2 are constants which depend on the regularization scheme, $s = p^2/m^2$ and L_A, L_B are the logarithmic functions

$$\begin{aligned} L_A(s) &= (s^2 - 20s + 12) \left(\frac{4+s}{s} \right)^{3/2} \log \left(\frac{\sqrt{4+s} - \sqrt{s}}{\sqrt{4+s} + \sqrt{s}} \right) \\ L_B(s) &= \frac{2(1+s)^3}{s^3} (s^2 - 10s + 1) \log(1+s). \end{aligned} \quad (\text{A18})$$

The other terms, Π_{2b}^ξ and $\Pi_{2b}^{\xi\xi}$, arise by substituting one and two transverse lines, respectively, with the longitudinal ones. By the general scheme of Ref. [32], for $d = 4$, they follow as

$$\begin{aligned} \Pi_{2b}^\xi(p) &= \frac{Ng^2}{6} \int \frac{d^4k}{(2\pi)^4} \frac{\mathcal{F}^{0\xi}(k,p)}{(k^2 + m^2)(k+p)^2} \\ &\quad + \frac{Ng^2}{6} \int \frac{d^4k}{(2\pi)^4} \frac{\mathcal{F}^{\xi 0}(k,p)}{k^2[(k+p)^2 + m^2]} \end{aligned} \quad (\text{A19})$$

$$\Pi_{2b}^{\xi\xi}(p) = \frac{Ng^2}{6} \int \frac{d^4k}{(2\pi)^4} \frac{\mathcal{F}^{\xi\xi}(k,p)}{k^2(k+p)^2} \quad (\text{A20})$$

where

$$\begin{aligned} \mathcal{F}^{0\xi}(k,p) &= \frac{(3k^2 - k_\perp^2)(k^2 - p^2)^2}{k^2(k+p)^2} \\ &= 3(k+p)^2 - \frac{(10p^2 + k^2)k_\perp^2}{(k+p)^2} \\ &\quad - \frac{p^4 k_\perp^2}{k^2(k+p)^2} - 12(p \cdot k), \\ \mathcal{F}^{\xi 0}(k,p) &= 3k^2 + 12p^2 + 12(k \cdot p) - k_\perp^2 \\ &\quad - k_\perp^2 \left[\frac{11p^2 + 2(k \cdot p)}{k^2} + \frac{p^4}{(k+p)^2 k^2} \right], \\ \mathcal{F}^{\xi\xi}(k,p) &= \frac{p^4 k_\perp^2}{k^2(k+p)^2}. \end{aligned} \quad (\text{A21})$$

The quadratic term is trivial since the integral $\Pi_{2b}^{\xi\xi}$ is scaleless and by a dimensional argument $\Pi_{2b}^{\xi\xi}(p) = \text{const} \times p^2$. The constant can be absorbed by a finite wave function renormalization and the term can be ignored.

The two integrals in Eq. (A19) must be the same, as can be easily seen by substituting $k \rightarrow (-k-p)$ in Eq. (A21). Taking twice the explicit expression of $\mathcal{F}^{\xi 0}$, the integral can be written as

$$\Pi_{2b}^\xi(p) = Ng^2[I_A^\xi(p) + I_B^\xi(p) + I_C^\xi(p) + I_D^\xi(p)] \quad (\text{A22})$$

where

$$\begin{aligned} I_A^\xi(p) &= \int \frac{d^4k}{(2\pi)^4} \frac{1}{[(k+p)^2 + m^2]} \\ I_B^\xi(p) &= \frac{1}{3} \int \frac{d^4k}{(2\pi)^4} \frac{12p^2 + 12(k \cdot p) - k_\perp^2}{k^2[(k+p)^2 + m^2]} \\ I_C^\xi(p) &= -\frac{p^4}{3m^2} \int \frac{d^4k}{(2\pi)^4} \frac{k_\perp^2}{(k^2)^2(k+p)^2} \\ I_D^\xi(p) &= \frac{1}{3} \int \frac{d^4k}{(2\pi)^4} \frac{k_\perp^2 \left[\frac{p^4}{m^2} - 11p^2 - 2(k \cdot p) \right]}{(k^2)^2[(k+p)^2 + m^2]} \end{aligned} \quad (\text{A23})$$

By dimensional regularization, taking $d = 4 - \epsilon$, the integrals can be evaluated analytically in the $\overline{\text{MS}}$ scheme. The first integral is the same occurring in Eq. (A2)

$$I_A^\xi(p) = -\frac{m^2}{(4\pi)^2} \left(\frac{2}{\epsilon} + \log \frac{\mu^2}{m^2} + C_A \right) \quad (\text{A24})$$

The other integrals are

$$\begin{aligned} I_B^\xi(p) &= \frac{2m^2}{(4\pi)^2} \left\{ \left(\frac{2}{\epsilon} + \log \frac{\mu^2}{m^2} \right) \left(\frac{25}{24}s + \frac{1}{8} \right) + C_B s + C_B' \right. \\ &\quad \left. + \frac{24s(1-s^2) - (1+s)^3}{24s^2} \log(1+s) + \frac{1}{24s} \right\} \end{aligned} \quad (\text{A25})$$

$$I_C^\xi(p) = -\frac{m^2 s^2}{4(4\pi)^2} \left\{ \left(\frac{2}{\epsilon} + \log \frac{\mu^2}{m^2} + C_C \right) - \log s \right\} \quad (\text{A26})$$

$$I_D^\xi(p) = \frac{m^2 s^2}{4(4\pi)^2} \left\{ \left(\frac{2}{\epsilon} + \log \frac{\mu^2}{m^2} + C_C \right) + \frac{(1-s^2)}{s^2} \log(1+s) \right\} \\ + \frac{m^2}{12(4\pi)^2} \left\{ -31s \left(\frac{2}{\epsilon} + \log \frac{\mu^2}{m^2} + C_D \right) + C'_D \right. \\ \left. + \frac{(1+s)(31s^2 - 31s + 4)}{s^2} \log(1+s) - \frac{4}{s} \right\} \quad (\text{A27})$$

where all constants C_X , C'_X depend on the regularization scheme. In Eq. (A27), the first two lines arise from the p^4 term of $I_D^\xi(p)$ and the diverging term cancels the corresponding divergence of $I_C^\xi(p)$ in Eq. (A26).

Adding up the different integrals we obtain a diverging part

$$\Pi_{2b}^{\xi\epsilon}(p) = -\frac{Ng^2}{4(4\pi)^2} (3m^2 + 2p^2) \left(\frac{2}{\epsilon} + \log \frac{\mu^2}{m^2} \right) \quad (\text{A28})$$

and a finite part

$$\Pi_{2b}^{\xi f} = \frac{Ng^2}{(4\pi)^2} \frac{m^2}{4} \left[\frac{(1+s)(1-s)^3}{s^2} \log(1+s) + s^2 \log s - \frac{1}{s} \right] \quad (\text{A29})$$

where we have omitted the irrelevant constants.

Finally, the gluon loop has the following structure

$$\Pi_{2b} = \left[\Pi_{2b}^{0\epsilon} + \xi \Pi_{2b}^{\xi\epsilon} \right] + \left[\Pi_{2b}^{0f} + \xi \Pi_{2b}^{\xi f} \right]. \quad (\text{A30})$$

4. Standard one-loop graphs

The standard one-loop result of perturbation theory does not contain any contribution from the crossed graphs. In a generic linear covariant gauge, the standard one-loop polarization $\Pi_1(p)$ is obtained as the sum

$$\Pi_1(p) = \Pi_{1b} + \Pi_{2a}(p) + \Pi_{2b}(p) \quad (\text{A31})$$

and summing up the explicit expressions reported above, we find a diverging part

$$\Pi_1^\xi(p) = \frac{Ng^2}{(4\pi)^2} \left(\frac{2}{\epsilon} + \log \frac{\mu^2}{m^2} \right) \left[p^2 \left(\frac{13}{6} - \frac{\xi}{2} \right) - \frac{3}{4} m^2 (1 + \xi) \right] \quad (\text{A32})$$

and a finite part

$$\Pi_1^f(p) = -\frac{Ng^2}{4!(4\pi)^2} p^2 \left\{ C_p + \frac{1}{s} [C_m + f(s) + \xi f'_\xi(s)] \right\} \quad (\text{A33})$$

where

$$f(s) = s[L_A(s) + L_B(s) + (2-s^2) \log s - 2s^{-2}] \\ f'_\xi(s) = 6 \left[s^{-1} - s^2 \log s - \frac{(1+s)(1-s)^3}{s^2} \log(1+s) \right]. \quad (\text{A34})$$

In the limit $m \rightarrow 0$ the diverging part in Eq. (A32) agrees with the well known result of perturbation theory [60]. In the limit $\xi \rightarrow 0$ the finite part in Eq. (A33) gives the known result in the Landau gauge [67,68]. The constants C_m and C_p are arbitrary since they depend on the regularization scheme and on the arbitrary energy scale μ in Eq. (A32). In the standard perturbation theory, they are the finite parts resulting from the cancellation of the divergences by mass and wave function renormalization, respectively. In pure Yang-Mills theory, there is no mass term in the original Lagrangian and no mass renormalization for the cancellation. However, all constant mass terms cancel exactly by inclusion of the crossed graphs.

5. Total polarization (including the crossed graphs)

All crossed graphs, containing one insertion of the transverse mass counterterm, can be added to the total one-loop polarization by a simple derivative, as discussed above, for the tadpole. The sum of all graphs in Fig. 1 follows as

$$\Pi_{\text{tot}}(p) = \left(1 - m^2 \frac{\partial}{\partial m^2} \right) \Pi_1(p) + \Pi_{1d}. \quad (\text{A35})$$

Using the identity

$$\left(1 - m^2 \frac{\partial}{\partial m^2} \right) = \left(1 + s \frac{\partial}{\partial s} \right) \quad (\text{A36})$$

and adding up the terms, we obtain a total diverging part

$$\Pi_{\text{tot}}^\epsilon(p) = \frac{Ng^2}{(4\pi)^2} \left(\frac{2}{\epsilon} + \log \frac{\mu^2}{m^2} \right) p^2 \left(\frac{13}{6} - \frac{\xi}{2} \right) \quad (\text{A37})$$

and a total finite part

$$\Pi_{\text{tot}}^f(p) = -3 \frac{Ng^2}{(4\pi)^2} p^2 \left\{ \frac{1}{s} \left(\frac{5}{8} + \frac{\xi}{4} \right) \right. \\ \left. + \frac{1}{3 \cdot 4!} [f'(s) + \xi f'_\xi(s)] + \text{const} \right\} \quad (\text{A38})$$

where $f'(s)$ and $f'_\xi(s)$ are the derivatives of the functions $f(s)$ and $f_\xi(s)$, respectively.

Finally, inserting the polarization in Eq. (19) and canceling the divergence by the usual wave function renormalization, the renormalized dressed propagator reads

$$\Delta(p) = \frac{Z}{p^2[F(s) + \xi F_\xi(s) + F_0]} \quad (\text{A39})$$

where Z is an arbitrary finite renormalization factor, F_0 is a finite additive constant and the adimensional functions F, F_ξ do not depend on any parameter and are defined as

$$\begin{aligned} F(s) &= \frac{5}{8s} + \frac{1}{3 \cdot 4!} f'(s) \\ F_\xi(s) &= \frac{1}{4s} + \frac{1}{3 \cdot 4!} f'_\xi(s). \end{aligned} \quad (\text{A40})$$

Their explicit expressions follow by the simple derivative of Eq. (A34). The function $F(x)$ was first derived in Refs. [39,40] and it reads

$$F(x) = \frac{5}{8x} + \frac{1}{72} [L_a + L_b + L_c + R_a + R_b + R_c] \quad (\text{A41})$$

where the logarithmic functions L_x are

$$\begin{aligned} L_a(x) &= \frac{3x^3 - 34x^2 - 28x - 24}{x} \\ &\quad \times \sqrt{\frac{4+x}{x}} \log\left(\frac{\sqrt{4+x} - \sqrt{x}}{\sqrt{4+x} + \sqrt{x}}\right) \\ L_b(x) &= \frac{2(1+x)^2}{x^3} (3x^3 - 20x^2 + 11x - 2) \log(1+x) \\ L_c(x) &= (2 - 3x^2) \log(x) \end{aligned} \quad (\text{A42})$$

and the rational parts R_x are

$$\begin{aligned} R_a(x) &= -\frac{4+x}{x} (x^2 - 20x + 12) \\ R_b(x) &= \frac{2(1+x)^2}{x^2} (x^2 - 10x + 1) \\ R_c(x) &= \frac{2}{x^2} + 2 - x^2. \end{aligned} \quad (\text{A43})$$

The explicit expression of $F_\xi(x)$ is

$$\begin{aligned} F_\xi(x) &= \frac{1}{4x} - \frac{1}{12} \left[2x \log x - \frac{2(1-x)(1-x^3)}{x^3} \log(1+x) \right. \\ &\quad \left. + \frac{3x^2 - 3x + 2}{x^2} \right] \end{aligned} \quad (\text{A44})$$

and has the leading behavior in the limit $x \rightarrow 0$

$$F_\xi(x) = \frac{1}{4x} - \frac{1}{9} - \frac{x}{6} \log x + \mathcal{O}(x). \quad (\text{A45})$$

In the same IR limit, the transverse propagator is finite

$$\Delta(0) = \frac{Z}{M_\xi^2} \quad (\text{A46})$$

and the mass parameter M_ξ^2 is defined as

$$M_\xi^2 = \frac{5m^2}{8} \left(1 + \frac{2}{5} \xi \right). \quad (\text{A47})$$

In the limit $x \rightarrow \infty$, the asymptotic UV behavior is

$$\begin{aligned} F_\xi(x) &\sim -\frac{1}{6} \log x \\ F(x) &\sim \frac{13}{18} \log x \end{aligned} \quad (\text{A48})$$

and by Eqs. (A38), (A39), the standard one-loop behavior is recovered in the UV for the total polarization and the dressed propagator

$$\begin{aligned} \Pi_{\text{tot}}^f(p) &\sim -\frac{Ng^2}{(4\pi)^2} p^2 \left(\frac{13}{6} - \frac{\xi}{2} \right) \log \frac{p^2}{\mu^2} \\ \frac{Z}{\Delta(p)} &\sim p^2 \left(\frac{13}{6} - \frac{\xi}{2} \right) \log \frac{p^2}{\mu^2}. \end{aligned} \quad (\text{A49})$$

The discussion on gauge invariance requires the derivatives of the functions $F(x)$ and $F_\xi(x)$. The derivative of $F(x)$ reads

$$F'(x) = -\frac{5}{8x^2} + \frac{1}{72} [L'_a + L'_b + L'_c + R(x)] \quad (\text{A50})$$

where the logarithmic functions L'_x , for $x = a, b, c$, are

$$\begin{aligned} L'_a(x) &= \frac{6x^4 - 16x^3 - 68x^2 + 80x + 144}{x^2(x+4)} \\ &\quad \times \sqrt{\frac{4+x}{x}} \log\left(\frac{\sqrt{4+x} - \sqrt{x}}{\sqrt{4+x} + \sqrt{x}}\right) \\ L'_b(x) &= \frac{4(1+x)}{x^4} (3x^4 - 10x^3 + 10x^2 - 10x + 3) \log(1+x) \\ L'_c(x) &= -6x \log x \end{aligned} \quad (\text{A51})$$

and $R(x)$ is the sum of all the rational terms coming out from the derivatives

$$R(x) = \frac{12}{x} + \frac{106}{x^2} - \frac{12}{x^3}. \quad (\text{A52})$$

The derivative of $F_\xi(x)$ reads

$$\begin{aligned} F'_\xi(x) &= \frac{x^4 + 2x - 3}{6x^4} \log(1+x) - \frac{1}{6} \log x \\ &\quad + \frac{(1-x)(1-x^3)}{6x^3(1+x)} + \frac{1}{3x^3} - \frac{1}{2x^2} - \frac{1}{6}. \end{aligned} \quad (\text{A53})$$

- [1] J. M. Cornwall, *Phys. Rev. D* **26**, 1453 (1982).
 [2] C. W. Bernard, *Nucl. Phys.* **B219**, 341 (1983).
 [3] J. F. Donoghue, *Phys. Rev. D* **29**, 2559 (1984).
 [4] O. Philipsen, *Nucl. Phys.* **B628**, 167 (2002).
 [5] O. Oliveira and P. Bicudo, *J. Phys. G* **38**, 045003 (2011).
 [6] A. C. Aguilar and A. A. Natale, *J. High Energy Phys.* **08** (2004) 057.
 [7] D. Binosi, L. Chang, J. Papavassiliou, and C. D. Roberts, *Phys. Lett. B* **742**, 183 (2015).
 [8] A. Cucchieri and T. Mendes, *Proc. Sci.*, LAT2007 (2007) 297.
 [9] A. Cucchieri and T. Mendes, *Phys. Rev. D* **78**, 094503 (2008).
 [10] A. Cucchieri and T. Mendes, *Phys. Rev. Lett.* **100**, 241601 (2008).
 [11] A. Cucchieri and T. Mendes, *Proc. Sci.*, QCD-TNT09 (2009) 026.
 [12] I. L. Bogolubsky, E. M. Ilgenfritz, M. Muller-Preussker, and A. Sternbeck, *Phys. Lett. B* **676**, 69 (2009).
 [13] O. Oliveira and P. J. Silva, *Proc. Sci.*, LAT2009 (2009) 226.
 [14] D. Dudal, O. Oliveira, and N. Vandersickel, *Phys. Rev. D* **81**, 074505 (2010).
 [15] A. Ayala, A. Bashir, D. Binosi, M. Cristoforetti, and J. Rodriguez-Quintero, *Phys. Rev. D* **86**, 074512 (2012).
 [16] O. Oliveira and P. J. Silva, *Phys. Rev. D* **86**, 114513 (2012).
 [17] G. Burgio, M. Quandt, H. Reinhardt, and H. Vogt, *Phys. Rev. D* **92**, 034518 (2015).
 [18] A. G. Duarte, O. Oliveira, and P. J. Silva, *Phys. Rev. D* **94**, 014502 (2016).
 [19] A. C. Aguilar, D. Binosi, and J. Papavassiliou, *Phys. Rev. D* **78**, 025010 (2008).
 [20] A. C. Aguilar and J. Papavassiliou, *Phys. Rev. D* **81**, 034003 (2010).
 [21] A. C. Aguilar, D. Binosi, and J. Papavassiliou, *Phys. Rev. D* **89**, 085032 (2014).
 [22] A. C. Aguilar, D. Binosi, and J. Papavassiliou, *Phys. Rev. D* **91**, 085014 (2015).
 [23] C. S. Fischer, A. Maas, and J. M. Pawłowski, *Ann. Phys. (Amsterdam)* **324**, 2408 (2009).
 [24] A. L. Blum, M. Q. Huber, M. Mitter, and L. von Smekal, *Phys. Rev. D* **89**, 061703 (2014).
 [25] M. Q. Huber, *Phys. Rev. D* **91**, 085018 (2015).
 [26] A. K. Cyrol, M. Q. Huber, and L. von Smekal, *Eur. Phys. J. C* **75**, 102 (2015).
 [27] F. Marhauser and J. M. Pawłowski, [arXiv:0812.1144](https://arxiv.org/abs/0812.1144).
 [28] J. Braun, H. Gies, and J. M. Pawłowski, *Phys. Lett. B* **684**, 262 (2010).
 [29] J. Braun, A. Eichhorn, H. Gies, and J. M. Pawłowski, *Eur. Phys. J. C* **70**, 689 (2010).
 [30] L. Fister and J. M. Pawłowski, *Phys. Rev. D* **88**, 045010 (2013).
 [31] F. Siringo, *Phys. Rev. D* **90**, 094021 (2014).
 [32] F. Siringo, *Phys. Rev. D* **92**, 074034 (2015).
 [33] P. Watson and H. Reinhardt, *Phys. Rev. D* **82**, 125010 (2010).
 [34] P. Watson and H. Reinhardt, *Phys. Rev. D* **85**, 025014 (2012).
 [35] E. Rojas, J. de Melo, B. El-Bennich, O. Oliveira, and T. Frederico, *J. High Energy Phys.* **10** (2013) 193.
 [36] C. Feuchter and H. Reinhardt, *Phys. Rev. D* **70**, 105021 (2004).
 [37] H. Reinhardt and C. Feuchter, *Phys. Rev. D* **71**, 105002 (2005).
 [38] M. Quandt, H. Reinhardt, and J. Heffner, *Phys. Rev. D* **89**, 065037 (2014).
 [39] F. Siringo, [arXiv:1509.05891](https://arxiv.org/abs/1509.05891).
 [40] F. Siringo, *Nucl. Phys.* **B907**, 572 (2016).
 [41] F. Siringo, *Phys. Rev. D* **94**, 114036 (2016).
 [42] F. Siringo, *EPJ Web Conf.* **137**, 13016 (2017).
 [43] F. Siringo, in *Correlations in Condensed Matter under Extreme Conditions*, edited by G. G. N. Angilella and A. La Magna (Springer International Publishing AG, New York, 2017); F. Siringo, [arXiv:1701.00286](https://arxiv.org/abs/1701.00286).
 [44] G. Comitini and F. Siringo, *Phys. Rev. D* **97**, 056013 (2018).
 [45] F. Siringo, *Phys. Rev. D* **96**, 114020 (2017).
 [46] A. Cucchieri, T. Mendes, and E. M. Santos, *Phys. Rev. Lett.* **103**, 141602 (2009).
 [47] A. Cucchieri, T. Mendes, and E. M. S. Santos, *Proc. Sci.*, QCD-TNT09 (2009) 009.
 [48] A. Cucchieri, T. Mendes, G. M. Nakamura, and E. M. Santos, *Proc. Sci.*, FACESQCD2010 (2010) 026.
 [49] P. Bicudo, D. Binosi, N. Cardoso, O. Oliveira, and P. J. Silva, *Phys. Rev. D* **92**, 114514 (2015).
 [50] N. K. Nielsen, *Nucl. Phys.* **B97**, 527 (1975); **B101**, 173 (1975).
 [51] R. Kobes, G. Kunstatter, and A. Rebhan, *Phys. Rev. Lett.* **64**, 2992 (1990).
 [52] J. C. Breckenridge, M. J. Lavelle, and T. G. Steele, *Z. Phys. C* **65**, 155 (1995).
 [53] A proof of gauge parameter independence of the residues was suggested by D. Dudal (private communication).
 [54] D. Dudal, O. Oliveira, and P. J. Silva, *Phys. Rev. D* **89**, 014010 (2014).
 [55] A. K. Cyrol, J. M. Pawłowski, A. Rothkopf, and N. Wink, [arXiv:1804.00945](https://arxiv.org/abs/1804.00945).
 [56] D. Dudal, J. A. Gracey, S. P. Sorella, N. Vandersickel, and H. Verschelde, *Phys. Rev. D* **78**, 065047 (2008).
 [57] M. A. L. Capri, D. Dudal, A. D. Pereira, D. Fiorentini, M. S. Guimaraes, B. W. Mintz, L. F. Palhares, and S. P. Sorella, *Phys. Rev. D* **95**, 045011 (2017).
 [58] D. Dudal, M. S. Guimaraes, and S. P. Sorella, *Phys. Rev. Lett.* **106**, 062003 (2011).
 [59] S. Strauss, C. S. Fischer, and C. Kellermann, *Phys. Rev. Lett.* **109**, 252001 (2012).
 [60] M. E. Peskin and D. V. Schroeder, *An Introduction To Quantum Field Theory* (CRC Press, Boca Raton, 1996).
 [61] P. M. Stevenson, *Nucl. Phys.* **B868**, 38 (2013); **B910**, 469 (2016).
 [62] Ph. Boucaud, F. De Soto, J. Rodriguez-Quintero, and S. Zafeiropoulos, *Phys. Rev. D* **96**, 098501 (2017).
 [63] D. Dudal, O. Oliveira, and N. Vandersickel, *Phys. Rev. D* **81**, 074505 (2010).
 [64] D. Dudal, O. Oliveira, and P. J. Silva, [arXiv:1803.02281](https://arxiv.org/abs/1803.02281).
 [65] F. Siringo, *EPJ Web Conf.* **137**, 13017 (2017).
 [66] R. Alkofer, W. Detmold, C. S. Fischer, and P. Maris, *Phys. Rev. D* **70**, 014014 (2004).
 [67] M. Tissier and N. Wschebor, *Phys. Rev. D* **82**, 101701(R) (2010).

-
- [68] M. Tissier and N. Wschebor, *Phys. Rev. D* **84**, 045018 (2011).
- [69] M. Pelaez, M. Tissier, and N. Wschebor, *Phys. Rev. D* **90**, 065031 (2014).
- [70] U. Reinosa, J. Serreau, M. Tissier, and N. Wschebor, *Phys. Rev. D* **89**, 105016 (2014).
- [71] U. Reinosa, J. Serreau, M. Tissier, and N. Wschebor, *Phys. Rev. D* **96**, 014005 (2017).
- [72] M. Pelaez, U. Reinosa, J. Serreau, M. Tissier, and N. Wschebor, *Phys. Rev. D* **96**, 114011 (2017).
- [73] F. Gao, S.-X. Qin, C.D. Roberts, and J. Rodriguez-Quintero, *Phys. Rev. D* **97**, 034010 (2018).

One-loop RG improvement of the screened massive expansion in the Landau gauge

Giorgio Comitini^{*} and Fabio Siringo[†]

*Dipartimento di Fisica e Astronomia dell'Università di Catania, INFN Sezione di Catania,
Via S. Sofia 64, I-95123 Catania, Italy*

 (Received 9 July 2020; accepted 19 October 2020; published 5 November 2020)

The RG improvement of the screened massive expansion is studied at one loop in two renormalization schemes, the momentum subtraction (MOM) scheme and the screened momentum subtraction scheme. The respective Taylor-scheme running couplings are shown not to develop a Landau pole, provided that the initial value of the coupling is sufficiently small. The improved ghost and gluon propagators are found to behave as expected, displaying dynamical mass generation for the gluons and the standard UV limit of ordinary perturbation theory. In the MOM scheme, when optimized by matching with the fixed-coupling framework, the approach proves to be a powerful method for obtaining propagators, which are in excellent agreement with the lattice data already at one loop. After optimization, the gluon mass parameter is left as the only free parameter of the theory and is shown to play the same role of the ordinary perturbative QCD scale Λ_{QCD} .

DOI: [10.1103/PhysRevD.102.094002](https://doi.org/10.1103/PhysRevD.102.094002)

I. INTRODUCTION

Being able to describe the nonperturbative regime of QCD is of paramount importance for understanding the low-energy phenomenology of hadrons, for predicting the observed hadron-mass spectrum and for addressing many unsolved problems like confinement, chiral symmetry breaking, and dynamical mass generation [1–7]. Indeed, almost all of the observed mass in the Universe seems to be generated by such mechanisms. Unfortunately, since perturbation theory (PT) breaks down in the infrared of QCD and in the pure-gauge Yang–Mills (YM) theory, to date a complete analytical treatment of the nonperturbative low-energy regime is still missing. In the last decades a considerable amount of knowledge has been provided by numerical methods based on lattice calculations [7–18] and numerical integration of integral equations in the continuum [19–43]. The breakdown of PT and the lack of an alternative analytical approach from first principles has also motivated the study of phenomenological models, mainly based on *ad hoc* modified Lagrangians [44–50].

In the last years, a purely analytical approach to the exact gauge-fixed Lagrangian of QCD has been developed

[51–59] based on a mere change of the expansion point of ordinary PT, showing that the breakdown of the theory may not be due to the perturbative method itself, but rather a consequence of a bad choice of its zero-order Lagrangian—namely that of a massless free-particle theory—which is good enough only in the UV because of asymptotic freedom. In the IR, because of mass generation, a *massive* free-particle theory could constitute the best expansion point, leading to a screened perturbative expansion which does not break down at any energy scale and is under control if the coupling is moderately small (as it turns out to be). Then, quite paradoxically, the *nonperturbative* regime of QCD and YM theory may be accessible by plain PT. Furthermore, in the IR and as far as the two-point functions are concerned, the higher-order terms of the perturbative series were shown to be minimized by an optimal choice of the renormalization scheme [55,58,59], yielding a very predictive analytical tool and one-loop results that are in excellent agreement with the available lattice data for YM theory. A remarkable feature of this *optimized* expansion is that the method is genuinely from first principles and does not require any external input apart from fixing the energy units.

The screened massive expansion shares with ordinary PT the problem of large logs that limit the validity of the optimized expansion to a low energy range, up to about 2 GeV [59]. In this paper we show how the problem can be solved by the renormalization group (RG), yielding an improved screened expansion whose validity can be virtually extended to any energy scale. Our findings corroborate the idea that QCD is a complete theory valid

^{*}giorgio.comitini@dfa.unict.it
[†]fabio.siringo@ct.infn.it

Published by the American Physical Society under the terms of the Creative Commons Attribution 4.0 International license. Further distribution of this work must maintain attribution to the author(s) and the published article's title, journal citation, and DOI. Funded by SCOAP³.

at all energies. In what follows, the RG-improved screened expansion is studied at one loop for the pure-gauge YM theory in two different renormalization schemes and is shown to be under control down to arbitrarily small scales, even if higher-order terms become important in the IR, where the one-loop RG-improved results get worse than the optimized fixed-coupling expressions. Eventually, a matching between the two expansions provides a good agreement with the lattice data at all energies.

It is remarkable that, at one loop, the RG equation for the coupling can be integrated exactly in the different schemes providing analytical expressions for the running coupling, which merge with the universal one-loop result in the UV. In the IR, due to the nonperturbative scale set by the gluon mass, the coupling is scheme dependent and finite if the flow starts from a moderate value in the UV, smaller than a threshold value. Above that threshold the running coupling develops an IR Landau pole.

This paper is organized as follows. In Sec. II the optimized screened expansion is reviewed for pure YM theory and its general renormalization and RG improvement are discussed. In Sec. III the RG-improved expansion is studied in the momentum-subtraction (MOM) scheme and in its screened version, which we term screened MOM (SMOM). In Sec. IV the results of the previous sections are compared with the predictions of the optimized fixed-scale expansion and with the available lattice data. A matching between the two expansions provides a predictive theory, which is in good agreement with the lattice data at all energy scales. Finally, in Sec. V the main results are summarized and discussed.

II. THE SCREENED MASSIVE EXPANSION AND ITS RENORMALIZATION IN THE LANDAU GAUGE

The screened massive expansion for the gauge-fixed and renormalized YM Lagrangian was first developed in Refs. [51,52], extended to finite temperature in Refs. [56,57], and to the full QCD in Ref. [54]. The extension to a generic covariant gauge [55,58] has already demonstrated the predictive power of the method when the expansion is optimized by the constraints of the Becchi-Rouet-Stora-Tyutin (BRST) symmetry satisfied by the Faddeev-Popov Lagrangian. The renormalization of the screened expansion in the Landau gauge was discussed in Ref. [59], where different renormalization schemes were considered and analytical expressions were reported for the beta function.

The screened expansion is obtained by a shift of the expansion point of PT, performed *after* having renormalized the fields and the coupling, as discussed in Ref. [59]. Following Refs. [52,55], the shift is enforced by simply adding a transverse mass term to the quadratic part of the action and subtracting it again from the interaction so that

the total action is left unchanged. The action term, which is added and subtracted, is given by

$$\delta S = \frac{1}{2} \int A_{a\mu}(x) \delta_{ab} \delta\Gamma^{\mu\nu}(x,y) A_{b\nu}(y) d^4x d^4y, \quad (1)$$

where the vertex function $\delta\Gamma$ is a shift of the inverse propagator,

$$\delta\Gamma^{\mu\nu}(x,y) = [\Delta_m^{-1\mu\nu}(x,y) - \Delta_0^{-1\mu\nu}(x,y)], \quad (2)$$

and $\Delta_m^{\mu\nu}$ is a massive free-particle propagator,

$$\Delta_m^{-1\mu\nu}(p) = (-p^2 + m^2)t^{\mu\nu}(p) + \frac{-p^2}{\xi} \ell^{\mu\nu}(p), \quad (3)$$

with the transverse and longitudinal projectors defined according to

$$t_{\mu\nu}(p) = g_{\mu\nu} - \frac{p_\mu p_\nu}{p^2}, \quad \ell_{\mu\nu}(p) = \frac{p_\mu p_\nu}{p^2}. \quad (4)$$

Adding the term δS is equivalent to substituting the new massive propagator $\Delta_m^{\mu\nu}$ for the old massless one $\Delta_0^{\mu\nu}$ in the quadratic part of the action. The shift itself is motivated *a posteriori* by the former being much closer to the exact propagator in the IR than the latter and *a priori* by a Gaussian effective potential (GEP) analysis of pure YM theory [57].

In order to leave the total action unchanged, the opposite term $-\delta S$ is added in the interaction, providing a new two-point interaction vertex $\delta\Gamma$. Dropping all color indices in the diagonal matrices and inserting Eq. (3) into Eq. (2), the vertex is just the transverse mass shift of the quadratic part,

$$\delta\Gamma^{\mu\nu}(p) = m^2 t^{\mu\nu}(p). \quad (5)$$

The new vertex does not contain any renormalization constant and is part of the interaction even if it does not explicitly depend on the coupling. Thus the expansion itself must be regarded as a δ -expansion, rather than a loop expansion, since different powers of the coupling coexist at each order in powers of the total interaction.

The self-energies and the propagators are evaluated, order by order, by PT with a modified set of Feynman rules by which the gluon lines are associated to massive free-particle propagators $\Delta_m^{\mu\nu}$ and the new two-point vertex $\delta\Gamma^{\mu\nu}$ is included in the graphs. Since the total gauge-fixed Faddeev-Popov Lagrangian is not modified, and because of gauge invariance, the exact gluon longitudinal polarization is known to vanish. The exact gluon polarization can thus be written as

$$\Pi^{\mu\nu}(p) = \Pi(p^2) t^{\mu\nu}(p). \quad (6)$$

It follows that in the Landau gauge, $\xi = 0$, the exact gluon propagator is transverse,

$$\Delta_{\mu\nu}(p) = \Delta(p^2)t_{\mu\nu}(p), \quad (7)$$

and defined by the single scalar function $\Delta(p^2)$. In the Euclidean formalism and Landau gauge, the dressed gluon and ghost propagators of the screened expansion can be expressed as

$$\begin{aligned} \Delta^{-1}(p^2) &= p^2 + m^2 - \Pi(p^2), \\ \mathcal{G}^{-1}(p^2) &= -p^2 - \Sigma(p^2), \end{aligned} \quad (8)$$

where the proper gluon polarization $\Pi(p^2)$ and ghost self-energy $\Sigma(p^2)$ are the sum of all one-particle-irreducible (1PI) graphs in the screened expansion, including the mass and renormalization counterterms.

It is important to keep in mind that, since the total Lagrangian is not modified, the exact renormalization constants satisfy the Slavnov–Taylor identities. Nonetheless, the added mass term breaks the BRST symmetry of the quadratic part and of the interaction when these are taken apart. Therefore, some of the constraints arising from BRST symmetry are not satisfied exactly at any finite order of the screened expansion. While the soft breaking has no effect on the UV behavior or on the diverging parts of the renormalization constants, some spurious diverging mass terms do appear in the expansion at some stage. However, as discussed in Refs. [51,52,54,55], the insertions of the new vertex $\delta\Gamma$, Eq. (5), cancel the spurious divergences exactly, without the need of any mass renormalization counterterm, as a consequence of the unbroken BRST symmetry of the whole action. This aspect makes the screened expansion very different from effective models where a bare mass term is added to the Lagrangian from the beginning. In the screened massive expansion, the gluon mass parameter is an arbitrary and finite quantity which is added and subtracted again in the renormalized action and, as such, it can be taken to be an RG invariant.

As shown, for instance, in Ref. [52], the exact self-energies of the screened expansion can be written as

$$\begin{aligned} \Pi(p^2) &= m^2 - p^2\delta Z_A + \Pi_{\text{loop}}(p^2), \\ \Sigma(p^2) &= p^2\delta Z_c + \Sigma_{\text{loop}}(p^2), \end{aligned} \quad (9)$$

where the tree-level contribution m^2 comes from the new two-point vertex $\delta\Gamma$ in Eq. (5), while the tree-level terms $-p^2\delta Z_A$, $p^2\delta Z_c$ arise from the respective field-strength renormalization counterterms. Observe that the vertex mass term in Eq. (9) exactly cancels the zero-order gluon propagator's mass in Eq. (8): in the screened expansion, the gluon's mass is not a mere artifact of the choice of a massive tree-level propagator, but rather it is dynamically generated by the loops' contribution to the self-energy

(more precisely, it comes from the gluon loops [51,52,55]). Indeed, the screened expansion of QED would not predict the existence of a mass for the photons, which are not self-interacting.

The proper functions $\Pi_{\text{loop}}(p^2)$, $\Sigma_{\text{loop}}(p^2)$ are given by the sum of all 1PI graphs containing loops. The diverging parts of δZ_A , δZ_c cancel the UV divergences of Π_{loop} and Σ_{loop} , respectively. Since these divergences do not depend on mass scales, they are exactly the same as in the standard PT so that in the $\overline{\text{MS}}$ scheme Z_A and Z_c have their standard expressions, as manifest in the explicit one-loop calculation [51,52,59]. The finite parts of δZ_A , δZ_c , on the other hand, are arbitrary and depend on the renormalization scheme. Indeed, the self-energies themselves each contain an arbitrary term of the form $\mathcal{C}p^2$, where \mathcal{C} is a constant whose value depends on the regularization method.

To one loop, the explicit expressions for the loop self-energies, as computed from the diagrams in Fig. 1, can be written as

$$\begin{aligned} \Pi_{\text{loop}}(p^2) &= \alpha p^2 \left\{ \frac{13}{18} \left(\frac{2}{\epsilon} + \ln \frac{\bar{\mu}^2}{m^2} \right) - F(s) - \mathcal{C} \right\}, \\ \Sigma_{\text{loop}}(p^2) &= -\alpha p^2 \left\{ \frac{1}{4} \left(\frac{2}{\epsilon} + \ln \frac{\bar{\mu}^2}{m^2} \right) - G(s) - \mathcal{C}' \right\}, \end{aligned} \quad (10)$$

where

$$\alpha = \frac{3N\alpha_s}{4\pi} = \frac{3Ng^2}{16\pi^2}, \quad (11)$$

\mathcal{C} and \mathcal{C}' are constants and $F(s)$, $G(s)$ are dimensionless functions of the ratio $s = p^2/m^2$, whose explicit expressions were derived in Refs. [51,52] and are reported in the Appendix. For further details on the screened expansion we refer to [55,58,59], where explicit analytical expressions for the propagators are reported to third order in the δ -expansion and to one loop, also in an arbitrary covariant gauge.

While the exact observables must be RG-invariant and cannot depend on the renormalization scale, the

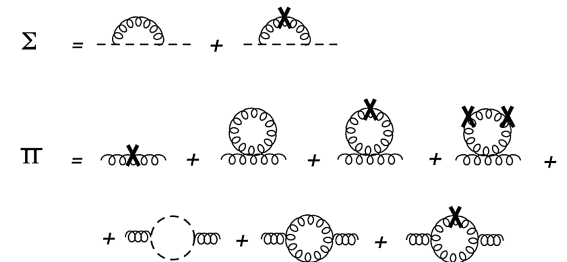


FIG. 1. Diagrams that contribute to the ghost self-energy and gluon polarization to third order in the δ -expansion and one loop. The crosses denote the insertions of the vertex $\delta\Gamma$.

approximate one-loop expressions do depend on the scale and on the scheme. Moreover, some exact consequences of BRST symmetry, like the Nielsen identities [60–62], might not be satisfied at any finite order of the screened expansion. An optimal choice of the finite parts of the renormalization constants provides propagators, which are closer to the exact RG-invariant result, and can be determined by the principle of minimal sensitivity [63]. The resulting optimized PT is known as renormalization-scheme optimized PT [64] and turns out to be quite effective.

For an observable particle, the finite parts are usually fixed on mass shell. For instance, the Nielsen identities are satisfied at any finite order of PT for electrons and quarks when the self-energy is renormalized on shell [62]. For the gluons, without an observable mass at hand, the argument can be reversed. The scheme can be defined by imposing that the Nielsen identities are satisfied, i.e., by requiring that the poles and residues of the propagator be gauge-parameter independent. While this condition is not generally satisfied at one loop, in Refs. [55,59] we showed that there exists an optimal choice of the renormalization constants which makes the pole structure gauge invariant. For this special choice, the higher-order terms turn out to be minimal and negligible in the IR so that the optimized one-loop analytical expressions provide an excellent agreement with the available low-energy lattice data when the energy scale is fixed by setting $m = 0.656$ GeV. The resulting optimized expansion is very predictive and gives valuable quantitative information on the analytical properties in Minkowski space even for different covariant gauges, which are not accessible by lattice calculations.

Unfortunately, being based on an optimal choice of the renormalization scale, the optimized expansion is not reliable for $p/m \gtrsim 3$ (corresponding to $p \gtrsim 2$ GeV for $m = 0.656$ GeV) because of the large logs. For instance, in Eq. (10), the ghost self-energy contains a leading term $G(s) \approx \ln(s)/4$ which spoils the multiplicative renormalizability of the propagator for a finite change of scale, unless the shift $\mu' - \mu \ll m$. This problem is usually solved by integrating the RG flow, yielding an improved version of the perturbative expansion.

The evaluation of the RG-improved gluon and ghost propagators requires the knowledge of the respective anomalous dimensions and of the beta function. In a momentum-subtraction-like renormalization scheme defined by the values of the propagators and coupling at the scale μ , the calculation of the anomalous dimensions and beta function from the explicit expressions of the self-energies in Eqs. (10) is straightforward. At $p^2 = \mu^2$, using Eqs. (8) and (9), we can write

$$\begin{aligned} \mu^{-2}\Delta^{-1}(\mu^2) &= 1 + \delta Z_A - \mu^{-2}\Pi_{\text{loop}}(\mu^2), \\ -\mu^{-2}\mathcal{G}^{-1}(\mu^2) &= 1 + \delta Z_c + \mu^{-2}\Sigma_{\text{loop}}(\mu^2), \end{aligned} \quad (12)$$

so that

$$\begin{aligned} Z_A &= \mu^{-2}[\Delta^{-1}(\mu^2) + \Pi_{\text{loop}}(\mu^2)], \\ Z_c &= -\mu^{-2}[\mathcal{G}^{-1}(\mu^2) + \Sigma_{\text{loop}}(\mu^2)]. \end{aligned} \quad (13)$$

The gluon and ghost anomalous dimensions γ_A and γ_c are then defined as

$$\gamma_A = \frac{1}{2} \frac{d \ln Z_A}{d \ln \mu}, \quad \gamma_c = \frac{1}{2} \frac{d \ln Z_c}{d \ln \mu}. \quad (14)$$

As for the renormalized strong coupling constant g , this can be defined as

$$g = g_B \frac{Z_c Z_A^{1/2}}{Z_1^c}, \quad (15)$$

where g_B is the bare coupling, and Z_1^c is the renormalization factor of the ghost-gluon vertex. In the Landau gauge, $\xi = 0$, the divergent part of the ghost-gluon vertex is known to vanish, so that Z_1^c is finite. The simplest renormalization condition for the vertex is, therefore, given by $Z_1^c = 1$. The latter defines the Taylor scheme [65–68], in which

$$g = g_B Z_c Z_A^{1/2}. \quad (16)$$

From the above equation we can immediately derive the beta function:

$$\beta = \mu \frac{dg}{d\mu} = g(2\gamma_c + \gamma_A). \quad (17)$$

Thus in the Taylor scheme the knowledge of γ_A and γ_c is sufficient for computing β .

The RG-improved propagators renormalized at the scale μ_0 are defined in terms of the anomalous dimensions according to

$$\begin{aligned} \Delta(p^2; \mu_0) &= \hat{\Delta}(p^2) \exp\left(\int_{\mu_0^2}^{p^2} \frac{d\mu'^2}{\mu'^2} \gamma_A(\mu'^2)\right), \\ \mathcal{G}(p^2; \mu_0) &= \hat{\mathcal{G}}(p^2) \exp\left(\int_{\mu_0^2}^{p^2} \frac{d\mu'^2}{\mu'^2} \gamma_c(\mu'^2)\right). \end{aligned} \quad (18)$$

Here $\hat{\Delta}(p^2)$ and $\hat{\mathcal{G}}(p^2)$ are scheme-dependent functions that are determined by the renormalization conditions: since for any value of the initial renormalization scale

$$\begin{aligned} \hat{\Delta}(\mu_0^2) &= \Delta(\mu_0^2; \mu_0), \\ \hat{\mathcal{G}}(\mu_0^2) &= \mathcal{G}(\mu_0^2; \mu_0), \end{aligned} \quad (19)$$

the functions $\hat{\Delta}$, $\hat{\mathcal{G}}$ evaluated at p^2 are simply equal to the values of the respective propagators, renormalized at $\mu^2 = p^2$, and evaluated at the same scale.

In the next section we will investigate the behavior of the one-loop RG-improved propagators and running coupling in two renormalization schemes: the ordinary MOM scheme and the SMOM scheme. In the UV, any RG-improvement of the screened expansion must lead to the standard PT RG-improved results since for $p \gg m$ the mass effects become irrelevant. It follows that the improved screened expansion predicts the correct asymptotic UV behavior for the propagators and coupling already at one loop. On the other hand, in the IR, where the one-loop optimized fixed-scale expansion of Refs. [55,59] has already proven successful, the RG-improved results may actually turn out to be quantitatively inaccurate (regardless of the value of m) when truncated to leading order: while the higher-order terms are minimal at the optimal scale, as the scale runs down with the momentum the higher-loop corrections to the anomalous dimensions can become quite large since, in the IR, the running coupling becomes of order unity. Nevertheless, perhaps remarkably, it turns out that already at one loop the improvement of the screened expansion provides a qualitatively accurate picture of the IR behavior of the propagators with a running coupling that does not exhibit a Landau pole. Quantitatively, we expect the accuracy of the approximation to improve by including the higher-order corrections to the anomalous dimensions and beta function.

The screened massive expansion introduces the gluon mass parameter m as a spurious free parameter, whose value cannot be determined from first principles since Yang-Mills theory is scale invariant at the classical level. Of course, the arbitrariness of m results in a loss of predictivity of the method, allowing for infinitely many solutions for the YM n -point functions, namely, one for every pair $(m^2, \alpha_s(\mu_0^2))$. In Sec. III we do not address this issue; instead, we study the behavior of the gluon and ghost two-point functions by expressing every dimensionful quantity in units of m and letting $\alpha_s(\mu_0^2)$ vary. When needed for comparison, we will take $m = 0.656$ GeV as determined, e.g., in Ref. [55], by fitting the fixed-scale gluon propagator to the lattice data of Ref. [18]. Then, in Sec. IV, we will present a method for optimizing the initial value of the coupling $\alpha_s(\mu_0^2)$; the dimensionful value of the renormalization scale μ_0 itself will depend on the mass scale set by m . With $\alpha_s(\mu_0^2)$ fixed by optimization, the redundancy in the choice of free parameters is removed—thus restoring the predictivity of the screened expansion—and m is left as the only free parameter to determine the physics of the theory, playing the same role of Λ_{QCD} in standard perturbation theory as the fundamental energy scale of YM theory.

III. RUNNING COUPLING AND RG-IMPROVED PROPAGATORS

A. MOM scheme

The MOM scheme is defined by the renormalization conditions

$$\begin{aligned}\Delta^{-1}(\mu^2) &= \mu^2, \\ \mathcal{G}^{-1}(\mu^2) &= -\mu^2.\end{aligned}\quad (20)$$

When plugged into Eq. (13), these lead to the following one-loop field strength renormalization counterterms (modulo irrelevant constants):

$$\begin{aligned}\delta Z_A^{(\text{MOM})} &= \alpha \left\{ \frac{13}{18} \left(\frac{2}{\epsilon} + \ln \frac{\bar{\mu}^2}{m^2} \right) - F \left(\frac{\mu^2}{m^2} \right) \right\}, \\ \delta Z_c^{(\text{MOM})} &= \alpha \left\{ \frac{1}{4} \left(\frac{2}{\epsilon} + \ln \frac{\bar{\mu}^2}{m^2} \right) - G \left(\frac{\mu^2}{m^2} \right) \right\}.\end{aligned}\quad (21)$$

In the limit of large renormalization scales ($\mu^2 \gg m^2$, $x \rightarrow \infty$),

$$\begin{aligned}F(x) &\rightarrow \frac{13}{18} \ln x, \\ G(x) &\rightarrow \frac{1}{4} \ln x\end{aligned}\quad (22)$$

(cf. the Appendix), and we recover the leading-order counterterms of ordinary PT. From Eq. (21), the one-loop gluon and ghost field anomalous dimensions in the MOM scheme follow as

$$\begin{aligned}\gamma_A^{(\text{MOM})}(\mu^2) &= -\alpha(\mu^2) \frac{\mu^2}{m^2} F'(\mu^2/m^2), \\ \gamma_c^{(\text{MOM})}(\mu^2) &= -\alpha(\mu^2) \frac{\mu^2}{m^2} G'(\mu^2/m^2).\end{aligned}\quad (23)$$

Due to the presence of the mass scale set by the gluon mass parameter m , the anomalous dimensions $\gamma_A^{(\text{MOM})}$ and $\gamma_c^{(\text{MOM})}$ depend explicitly on the renormalization scale, rather than only implicitly through the running coupling $\alpha(\mu^2)$. This dependence is lost at high renormalization scales, where $F'(x)$ and $G'(x)$ are proportional to x^{-1} [see Eq. (22)] and the anomalous dimensions of ordinary PT are recovered.

To the coupling α we may associate a beta function β_α , defined as

$$\beta_\alpha = \frac{d\alpha}{d \ln \mu^2} = \alpha \frac{\beta}{g}.\quad (24)$$

Using Eq. (17), β_α can be computed in the MOM scheme from the anomalous dimensions $\gamma_A^{(\text{MOM})}$ and $\gamma_c^{(\text{MOM})}$, yielding

$$\beta_\alpha^{(\text{MOM})}(\mu^2) = -\alpha^2 \frac{\mu^2}{m^2} H'(\mu^2/m^2)\quad (25)$$

to one loop. Here the function $H(x)$, shown in Fig. 2, is defined as

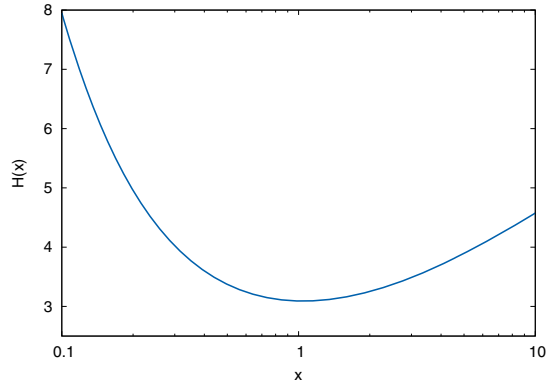


FIG. 2. Function $H(x)$. The minimum $H(x_0) \approx 3.090$ is found at $x_0 \approx 1.044$.

$$H(x) = 2G(x) + F(x), \quad (26)$$

and has limiting behavior [see Eq. (22)]

$$H(x) \rightarrow \frac{11}{9} \ln x \quad (x \rightarrow \infty). \quad (27)$$

From Eq. (25) we see that, along with the anomalous dimensions, the MOM beta function of the screened expansion also has an explicit dependence on the renormalization scale μ . As we will show in a moment, this is a most important feature of the modified perturbation theory, bringing in mass effects which are able to prevent the developing of a Landau pole in the running coupling.

To one loop, the differential equation for the running coupling $\alpha_s^{(\text{MOM})}(\mu^2)$,

$$\frac{d\alpha_s^{(\text{MOM})}}{d \ln s} = -(\alpha_s^{(\text{MOM})})^2 s H'(s), \quad (28)$$

($s = \mu^2/m^2$) can be solved exactly. In terms of α_s , its solution is given by

$$\alpha_s^{(\text{MOM})}(\mu^2) = \frac{\alpha_s^{(\text{MOM})}(\mu_0^2)}{1 + \frac{3N}{4\pi} \alpha_s^{(\text{MOM})}(\mu_0^2) [H(s) - H(s_0)]}, \quad (29)$$

where μ_0 is the initial renormalization scale $s_0 = \mu_0^2/m^2$, and $\alpha_s^{(\text{MOM})}(\mu_0^2)$ is the value of the MOM coupling renormalized at μ_0 (initial condition of the RG flow). This result was already derived directly from Eq. (16) in Refs. [51,52].

In the limit of high initial and final renormalization scales ($s, s_0 \gg 1$), using Eq. (27), it is easy to see that $\alpha_s^{(\text{MOM})}(\mu^2)$ reduces to the standard one-loop running coupling,

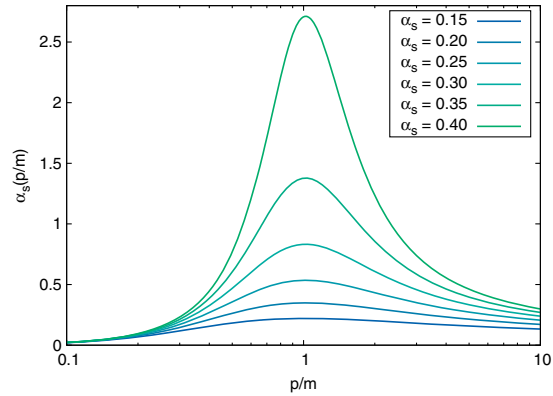


FIG. 3. $N = 3$ one-loop running coupling of the screened expansion in the MOM scheme for different initial values of the coupling at the scale $\mu_0/m = 6.098$. With $m = 0.656$ GeV as in our previous works, this corresponds to $\mu_0 = 4$ GeV. The running coupling develops a Landau pole for $\alpha_s^{(\text{MOM})}(\mu_0^2) \geq 0.469$.

$$\alpha_s^{(\text{MOM})}(\mu^2) \rightarrow \frac{\alpha_s(\mu_0^2)}{1 + \frac{11N}{3} \frac{\alpha_s(\mu_0^2)}{4\pi} \ln(\mu^2/\mu_0^2)}. \quad (30)$$

At intermediate and low momenta, on the other hand, the behavior of $\alpha_s^{(\text{MOM})}(\mu^2)$ radically differs from that of its counterpart in ordinary PT (see Fig. 3). Due to the explicit dependence of $\beta_\alpha^{(\text{MOM})}$ on the renormalization scale, the latter is allowed to vanish already at one loop for a nonzero value of the coupling constant. The vanishing occurs at the fixed renormalization scale μ_* that solves the equation

$$H'(\mu_*^2/m^2) = 0. \quad (31)$$

Numerically, one finds that

$$\mu_* \approx 1.022m \quad (32)$$

or $\mu_* \approx 0.67$ GeV for $m = 0.656$ GeV. Of course, since the beta function vanishes as a function of μ , rather than for some specific value of the coupling, the existence of a zero for $\beta_\alpha^{(\text{MOM})}$ does not result in a fixed point of the RG flow. Instead, it provides a mechanism by which, at scales of the order of the gluon mass parameter, the running of the coupling is allowed to slow down, thus making it possible to prevent the developing of a Landau pole in $\alpha_s^{(\text{MOM})}(\mu^2)$. Indeed, since μ_*^2/m^2 is actually a minimum for $H(s)$,

$$H(s) \geq H(\mu_*^2/m^2) \approx 3.090, \quad (33)$$

Eq. (29) implies that the one-loop MOM running coupling remains finite at all renormalization scales, provided that its

value renormalized at the scale μ_0 is smaller than the scale-dependent threshold value $\alpha_{\text{pole}}^{(\text{MOM})}(\mu_0^2)$ defined by

$$\alpha_{\text{pole}}^{(\text{MOM})}(\mu_0^2) = \frac{1}{H(\mu_0^2/m^2) - H(\mu_*^2/m^2)}. \quad (34)$$

At $\mu_0 = 6.098m$ (corresponding to $\mu_0 = 4$ GeV in physical units), Eq. (34) yields

$$\alpha_{\text{pole}}^{(\text{MOM})}(6.098m) \approx 0.336, \quad (35)$$

or, in terms of $\alpha_s = 4\pi\alpha/3N$,

$$\alpha_{s,\text{pole}}^{(\text{MOM})}(6.098m) \approx 0.469 \quad (36)$$

for $N = 3$. If $\alpha^{(\text{MOM})}(\mu_0^2) \geq \alpha_{\text{pole}}^{(\text{MOM})}(\mu_0^2)$, the denominator of Eq. (29) eventually vanishes and the running still encounters a Landau pole: for $\alpha^{(\text{MOM})}(\mu^2) = \alpha_{\text{pole}}^{(\text{MOM})}(\mu_0^2)$ the pole is found exactly at $\mu = \mu_*$, whereas for larger values of the coupling, it is found at scales between μ_* and μ_0 .

If the initial value of the coupling is smaller than $\alpha_{s,\text{pole}}^{(\text{MOM})}$, as the momentum decreases the one-loop running coupling remains finite and attains a maximum at $\mu = \mu_*$, where the beta function switches from being negative to being positive and $\alpha_s^{(\text{MOM})}(\mu^2)$ starts to decrease. The value of the coupling at the maximum is an increasing and unbounded function of $\alpha_s^{(\text{MOM})}(\mu_0^2)$. At vanishing renormalization scales ($\mu^2 \ll m^2$), due to the limiting behavior

$$H(x) \rightarrow \frac{5}{8x} \quad (x \rightarrow 0) \quad (37)$$

(cf. the Appendix), the running coupling decreases linearly with μ^2 ,

$$\alpha_s^{(\text{MOM})}(\mu^2) \rightarrow \frac{32\pi}{15N} \frac{\mu^2}{m^2}, \quad (38)$$

and tends to zero with a derivative that does not depend on the initial conditions of the RG flow. As we will see, even if the coupling vanishes at $\mu = 0$, the low-energy dynamics of the gluons remains highly nontrivial.

Once the running coupling is known, the RG-improved gluon and ghost propagators can be computed using Eq. (18) by an appropriate choice of the functions $\hat{\Delta}(p^2)$ and $\hat{\mathcal{G}}(p^2)$. In the MOM scheme, in order to fulfill the renormalization conditions given by Eq. (20), one must set

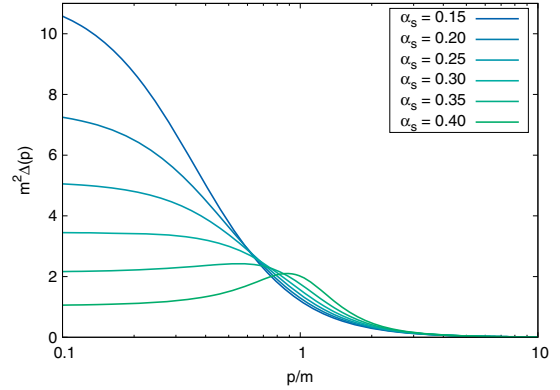


FIG. 4. $N = 3$ one-loop RG-improved gluon propagator in the MOM scheme, renormalized at the scale $\mu_0/m = 6.098$ (corresponding to $\mu_0 = 4$ GeV for $m = 0.656$ GeV), and computed for different initial values of the coupling at the same scale.

$$\begin{aligned} \hat{\Delta}^{(\text{MOM})}(p^2) &= \frac{1}{p^2}, \\ \hat{\mathcal{G}}^{(\text{MOM})}(p^2) &= -\frac{1}{p^2} \end{aligned} \quad (39)$$

(see Eq. (19)). The one-loop RG-improved propagators renormalized at the scale μ_0 then read

$$\begin{aligned} \Delta^{(\text{MOM})}(p^2; \mu_0^2) &= \frac{1}{p^2} \exp\left(-\int_{\mu_0^2/m^2}^{p^2/m^2} ds \alpha^{(\text{MOM})}(s) F'(s)\right), \\ \mathcal{G}^{(\text{MOM})}(p^2; \mu_0^2) &= -\frac{1}{p^2} \exp\left(-\int_{\mu_0^2/m^2}^{p^2/m^2} ds \alpha^{(\text{MOM})}(s) G'(s)\right), \end{aligned} \quad (40)$$

where the running coupling is expressed as a function of the dimensional variable $s = \mu^2/m^2$. The one-loop improved gluon propagator and ghost dressing function renormalized at the scale $\mu_0 = 6.098m$ (corresponding to $\mu_0 = 4$ GeV in physical units) are shown, respectively, in Figs. 4 and 5 for different initial values of the coupling constant below the threshold value $\alpha_{s,\text{pole}}^{(\text{MOM})} \approx 0.47$.

Since in the high momentum limit the MOM anomalous dimensions and running coupling reduce to their standard one-loop perturbative expression, asymptotically¹ the one-loop RG-improved propagators behave as known fractional powers of the running coupling divided by the momentum squared,

¹Provided that the initial renormalization scale μ_0 is much larger than m .

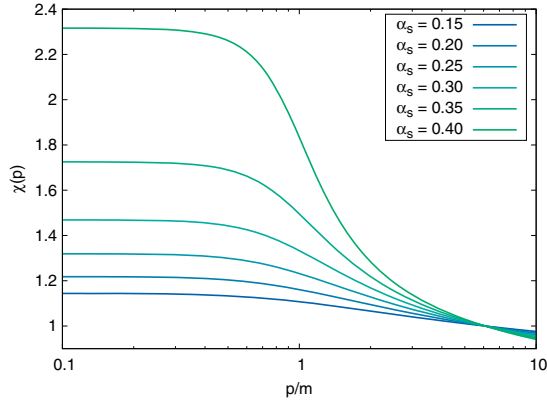


FIG. 5. $N = 3$ one-loop RG-improved ghost dressing function $\chi(p) = -p^2 \mathcal{G}(p)$ in the MOM scheme, renormalized at the scale $\mu_0/m = 6.098$ (corresponding to $\mu_0 = 4$ GeV for $m = 0.656$ GeV), and computed for different initial values of the coupling at the same scale.

$$\begin{aligned} \Delta^{(\text{MOM})}(p^2) &\rightarrow \frac{1}{p^2} \left[\frac{\alpha_s(p^2)}{\alpha_s(\mu_0^2)} \right]^{13/22}, \\ \mathcal{G}^{(\text{MOM})}(p^2) &\rightarrow -\frac{1}{p^2} \left[\frac{\alpha_s(p^2)}{\alpha_s(\mu_0^2)} \right]^{9/44}. \end{aligned} \quad (41)$$

At intermediate and low momenta, if the running coupling does not develop a Landau pole, then the one-loop improved gluon propagator attains a maximum at the momentum p that solves the equation

$$1 + \alpha^{(\text{MOM})}(p^2) \frac{p^2}{m^2} F'(p^2/m^2) = 0. \quad (42)$$

That Eq. (42) always admits a solution follows from the asymptotic behavior

$$\begin{aligned} 1 + \alpha^{(\text{MOM})}(s) s F'(s) &\rightarrow \frac{2}{45} s \ln s \leq 0 \quad (s \rightarrow 0), \\ 1 + \alpha^{(\text{MOM})}(s) s F'(s) &\rightarrow 1 > 0 \quad (s \rightarrow \infty) \end{aligned} \quad (43)$$

(cf. the Appendix). The position of the maximum depends on the initial conditions of the running and shifts from higher to lower momenta as $\alpha_s^{(\text{MOM})}(\mu_0^2)$ is decreased, eventually coming arbitrarily close to $p = 0$. At vanishing small momenta, due to the low energy limits

$$\begin{aligned} \alpha^{(\text{MOM})}(s) F'(s) &\rightarrow -\frac{1}{s}, \\ \alpha^{(\text{MOM})}(s) G'(s) &\rightarrow -\frac{4}{15} s \ln s \end{aligned} \quad (44)$$

(cf. the Appendix), the one-loop improved propagators behave as

$$\begin{aligned} \Delta^{(\text{MOM})}(p^2) &\rightarrow \frac{s e^k}{p^2} = \frac{e^k}{m^2}, \\ \mathcal{G}^{(\text{MOM})}(p^2) &\rightarrow -\frac{e^{k'}}{p^2}, \end{aligned} \quad (45)$$

where k and k' are constants that generally depend on the initial conditions of the running. Since $\Delta^{(\text{MOM})}(p^2)$ remains finite as $p^2 \rightarrow 0$, in the MOM-scheme RG-improved picture the gluons are still predicted to dynamically acquire a mass. The ghosts, on the other hand, remain massless ($\mathcal{G}^{(\text{MOM})}(p^2) \rightarrow \infty$ as $p^2 \rightarrow 0$).

The most notable feature of the one-loop RG-improved screened expansion in the MOM scheme is the absence of a Landau pole in its running coupling for sufficiently small initial values of $\alpha_s^{(\text{MOM})}(\mu_0^2)$, a necessary condition for the consistency of a perturbation theory which aims to be valid at all energy scales. As we saw, instead of growing to infinity at a finite momentum, the one-loop MOM coupling interpolates between the standard high-energy logarithmic behavior and a decreasing low-energy behavior ($\alpha_s^{(\text{MOM})}(p^2) \sim p^2$ as $p^2 \rightarrow 0$) by attaining a maximum at the fixed scale $\mu_* \approx 1.022m$. Depending on the initial conditions of the RG flow, the value of the coupling at the maximum can become quite large for the perturbative standards. As a consequence, the higher orders of the perturbative expansion might become significant at scales comparable to that of the gluon mass parameter.

Since our one-loop, low-energy results evolve from a region of generally large couplings, we should expect these to give, at best, a good qualitative approximation of the exact, nonperturbative behavior of Yang–Mills theory for any given value of the pair $(m^2, \alpha_s(\mu_0^2))$. In the absence of estimates for the higher-order corrections to the propagators, the extent to which the approximation is good can be established only *a posteriori*, by a comparison with non-perturbative results such as those obtained on the lattice. This aspect will be investigated in Sec. IV, where we will also propose a method for fixing the value of the spurious free parameter (either the gluon mass parameter m or the value of the coupling at some fixed renormalization scale) of the RG-improved screened expansion.

B. SMOM scheme

The SMOM scheme [59] is defined by the renormalization conditions

$$\begin{aligned} \Delta^{-1}(\mu^2) &= \mu^2 + m^2, \\ \mathcal{G}^{-1}(\mu^2) &= -\mu^2. \end{aligned} \quad (46)$$

To one loop, these require the field strength counterterms to be chosen (modulo irrelevant constants) according to

$$\begin{aligned}\delta Z_A^{(\text{SMOM})} &= \frac{m^2}{\mu^2} + \alpha \left\{ \frac{13}{18} \left(\frac{2}{\epsilon} + \ln \frac{\bar{\mu}^2}{m^2} \right) - F \left(\frac{\mu^2}{m^2} \right) \right\}, \\ \delta Z_c^{(\text{SMOM})} &= \alpha \left\{ \frac{1}{4} \left(\frac{2}{\epsilon} + \ln \frac{\bar{\mu}^2}{m^2} \right) - G \left(\frac{\mu^2}{m^2} \right) \right\},\end{aligned}\quad (47)$$

see Eq. (13). Observe that $\delta Z_A^{(\text{SMOM})}$ contains an $O(\alpha_s^0)$ term proportional to the gluon mass parameter m^2 . This happens because in the SMOM scheme the tree-level contribution to the gluon polarization arising from the first single-cross diagram in Fig. 1, $\Pi_{\text{cross}} = m^2$ does not get cancelled by the equal and opposite mass term in the bare massive gluon propagator.

Due to the presence of the $O(\alpha_s^0)$ term in $\delta Z_A^{(\text{SMOM})}$, a naive application of Eq. (14) to the first of Eq. (47) would yield an anomalous dimension that is not finite in the limit $\epsilon \rightarrow 0$. In the SMOM scheme, in order to derive a finite γ_A , one must first subtract the divergences from Eq. (47) and then apply Eq. (14) to the resulting finite field-strength counterterms.² By doing so, one obtains the following one-loop SMOM scheme anomalous dimensions:

$$\begin{aligned}\gamma_A^{(\text{SMOM})} &= -\frac{\mu^2}{\mu^2 + m^2} \left\{ \frac{m^2}{\mu^2} + \alpha \frac{\mu^2}{m^2} F'(\mu^2/m^2) \right\}, \\ \gamma_c^{(\text{SMOM})} &= -\alpha \frac{\mu^2}{m^2} G'(\mu^2/m^2).\end{aligned}\quad (48)$$

In Ref. [59] the same result was found by direct integration of the RG flow. In the limit of large renormalization scales, using Eq. (22), it is easy to see that $\gamma_A^{(\text{SMOM})}$ and $\gamma_c^{(\text{SMOM})}$ reduce to the one-loop anomalous dimensions of ordinary PT.

The one-loop SMOM beta function can be computed from Eq. (48) and Eq. (17), yielding

$$\begin{aligned}\beta_\alpha^{(\text{SMOM})} &= -\frac{\alpha m^2}{\mu^2 + m^2} - \alpha^2 \frac{\mu^2}{m^2} \left\{ \frac{\mu^2}{\mu^2 + m^2} F'(\mu^2/m^2) \right. \\ &\quad \left. + 2G'(\mu^2/m^2) \right\}.\end{aligned}\quad (49)$$

As in the MOM scheme, $\beta_\alpha^{(\text{SMOM})}$ explicitly depends on the renormalization scale μ and reduces to the ordinary perturbative beta function for $\mu \gg m$. At variance with $\beta_\alpha^{(\text{MOM})}$, it contains an $O(\alpha_s)$ term and a different scale-dependent prefactor for the derivative $F'(s)$.

The differential equation for the one-loop SMOM running coupling reads

²Equivalently, one could derive the anomalous dimensions by a term-by-term matching of coefficients in the Callan–Symanzik equation for the inverse dressed propagators.

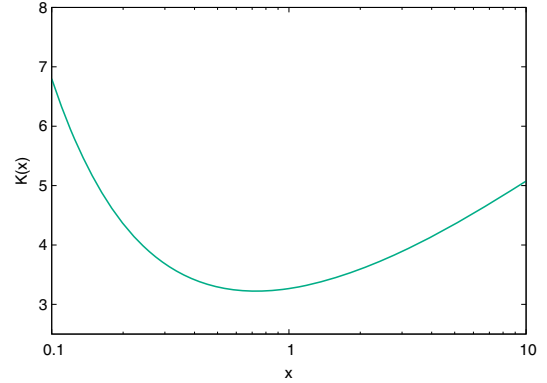


FIG. 6. Function $K(x)$. The minimum $K(x_0) \approx 3.224$ is found at $x_0 \approx 0.726$.

$$\frac{d\alpha^{(\text{SMOM})}}{ds} = -b_{-1}\alpha^{(\text{SMOM})} - b_0(\alpha^{(\text{SMOM})})^2, \quad (50)$$

where $s = \mu^2/m^2$ and

$$\begin{aligned}b_{-1}(s) &= \frac{1}{s(s+1)}, \\ b_0(s) &= \left\{ \frac{s}{s+1} F'(s) + 2G'(s) \right\}.\end{aligned}\quad (51)$$

Equation (50) can be integrated exactly, yielding

$$\begin{aligned}\alpha^{(\text{SMOM})}(s) &= \frac{\alpha^{(\text{SMOM})}(s_0) e^{-\int_{s_0}^s ds' b_{-1}(s')}}{1 + \alpha^{(\text{SMOM})}(s_0) \int_{s_0}^s ds' b_0(s') e^{-\int_{s_0}^{s'} ds'' b_{-1}(s'')}},\end{aligned}\quad (52)$$

where $s_0 = \mu_0^2/m^2$ is the initial renormalization scale. With $b_{-1}(s)$ and $b_0(s)$ as in Eq. (51), we find

$$\begin{aligned}\exp\left(-\int_{s_0}^s ds' b_{-1}(s')\right) &= \frac{s+1}{s} \frac{s_0}{s_0+1}, \\ \int_{s_0}^s ds' b_0(s') e^{-\int_{s_0}^{s'} ds'' b_{-1}(s'')} &= \frac{s_0}{s_0+1} [K(s) - K(s_0)],\end{aligned}\quad (53)$$

where the function $K(x)$, shown in Fig. 6, is defined as³

³ $\text{Li}_2(z)$ is the dilogarithm, $\text{Li}_2(z) = \sum_{n=1}^{+\infty} \frac{z^n}{n^2}$.

$$\begin{aligned}
K(x) &= \int dx \left\{ H'(x) + \frac{2}{x} G'(x) \right\} \\
&= H(x) - \frac{1}{3} \left\{ \text{Li}_2(-x) + \frac{1}{2} \ln^2 x \right. \\
&\quad \left. + \frac{x^3 + 1}{3x^3} \ln(1+x) - \frac{1}{3} \ln x - \frac{1}{3x^2} + \frac{1}{6x} \right\} \quad (54)
\end{aligned}$$

and differs from the $H(x)$ of the MOM scheme by the integral of $2G'(x)/x$, which was evaluated analytically in Eq. (54).

Using Eq. (53), the one-loop SMOM running coupling, Eq. (52), can be brought to the final form

$$\begin{aligned}
\alpha^{(\text{SMOM})}(\mu^2) &= \frac{\mu^2 + m^2}{\mu^2} \\
&\times \frac{\frac{\mu_0^2}{\mu_0^2 + m^2} \alpha^{(\text{SMOM})}(\mu_0^2)}{1 + \frac{\mu_0^2}{\mu_0^2 + m^2} \alpha^{(\text{SMOM})}(\mu_0^2) [K(s) - K(s_0)]}. \quad (55)
\end{aligned}$$

At large renormalization scales, as long as the initial scale μ_0 is much larger than m and because of the high energy limit

$$K(x) \rightarrow \frac{11}{9} \ln x \quad (x \rightarrow \infty) \quad (56)$$

(cf. the Appendix), the one-loop SMOM running coupling reduces to the standard perturbative coupling, Eq. (30). At intermediate and low momenta, on the other hand, its behavior is entirely different from that of both the ordinary PT and MOM-scheme couplings (see Fig. 7).

At scales of the order of the gluon mass parameter, as in the MOM scheme, the μ -dependence of the SMOM beta function is responsible for a slowing down of the running of the coupling. Indeed, due to the inequality

$$K(s) \geq K(\mu_*^2/m^2) \approx 3.224, \quad (57)$$

where μ_*^2/m^2 is the position of the minimum of $K(s)$,

$$\mu_*' \approx 0.852m, \quad (58)$$

$\alpha^{(\text{SMOM})}(\mu^2)$ does not develop a Landau pole so long as $\alpha^{(\text{SMOM})}(\mu_0^2)$ is smaller than the scale-dependent threshold value

$$\alpha_{\text{pole}}^{(\text{SMOM})}(\mu_0^2) = \frac{\mu_0^2 + m^2}{\mu_0^2} \frac{1}{K(\mu_0^2/m^2) - K(\mu_*^2/m^2)}. \quad (59)$$

At $\mu_0 = 6.098m$ (corresponding to $\mu = 4$ GeV in physical units), Eq. (59) reads

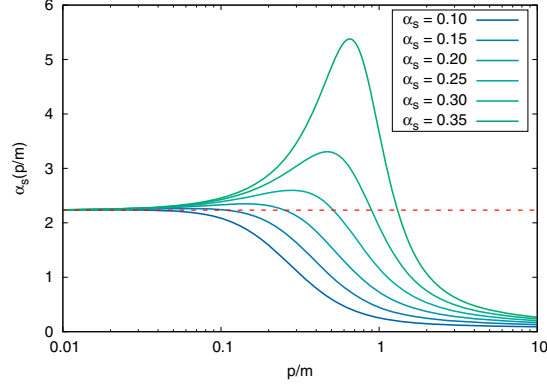


FIG. 7. $N = 3$ one-loop running coupling of the screened expansion in the SMOM scheme for different initial values of the coupling at the scale $\mu_0/m = 6.098$. With $m = 0.656$ GeV, this corresponds to $\mu_0 = 4$ GeV. The running coupling develops a Landau pole for $\alpha_s^{(\text{SMOM})}(\mu_0^2) \geq 0.425$. The dashed red line displays the limiting value $\alpha_s^{(\text{SMOM})}(0) \approx 2.234$.

$$\alpha_{\text{pole}}^{(\text{SMOM})}(6.098m) \approx 0.304, \quad (60)$$

or, in terms of $\alpha_s = 4\pi\alpha/3N$, for $N = 3$,

$$\alpha_{s,\text{pole}}^{(\text{SMOM})}(6.098m) \approx 0.425. \quad (61)$$

If $\alpha^{(\text{SMOM})}(\mu_0^2) < \alpha_{\text{pole}}^{(\text{SMOM})}(\mu_0^2)$, the running coupling attains a maximum at the renormalization scale that solves the equation

$$\beta_\alpha^{(\text{SMOM})} = 0 \Leftrightarrow 1 + \alpha^{(\text{SMOM})}(s)s^2 K'(s) = 0. \quad (62)$$

That Eq. (62) always admits a solution follows from the asymptotic limits

$$\begin{aligned}
1 + \alpha^{(\text{SMOM})}(s)s^2 K'(s) &\rightarrow -\frac{4s}{15} \ln^2 s < 0 \quad (s \rightarrow 0), \\
1 + \alpha^{(\text{SMOM})}(s)s^2 K'(s) &\rightarrow \frac{s}{\ln s} > 0 \quad (s \rightarrow \infty) \quad (63)
\end{aligned}$$

(cf. the Appendix). At variance with the MOM scheme and due to the prefactor $(\mu^2 + m^2)/\mu^2$ in Eq. (55), the position of the maximum of the one-loop SMOM running coupling is not fixed. Instead, it depends on the initial conditions of the RG flow and shifts towards lower renormalization scales as $\alpha^{(\text{SMOM})}(\mu_0^2)$ is decreased. In the limit of very small $\alpha^{(\text{SMOM})}(\mu_0^2)$'s, an expansion of the solutions of Eq. (62) around $s = 0$ yields

$$\ln^2 s - 6 \frac{1 + m^2/\mu_0^2}{\alpha^{(\text{SMOM})}(\mu_0^2)} = 0. \quad (64)$$

Therefore, in the limit of vanishingly small initial couplings, the maximum of $\alpha^{(\text{SMOM})}(\mu^2)$ is attained at the scale

$$\mu = m \exp\left(-\sqrt{\frac{3}{2}} \frac{1 + m^2/\mu_0^2}{\alpha^{(\text{SMOM})}(\mu_0^2)}\right). \quad (65)$$

Being its position exponentially suppressed, for small enough initial values of the coupling, the maximum is essentially indistinguishable from the $\mu \rightarrow 0$ limit of $\alpha^{(\text{SMOM})}(\mu^2)$. The latter reads

$$\alpha^{(\text{SMOM})}(\mu^2) \rightarrow \frac{8}{5} \left\{ 1 + \frac{4}{15} \frac{\mu^2}{m^2} \ln^2(\mu^2/m^2) \right\} \quad (\mu \rightarrow 0), \quad (66)$$

so that the one-loop SMOM coupling saturates to a finite value, given in terms of α_s by

$$\alpha_s^{(\text{SMOM})}(0) = \frac{32\pi}{15N} \approx 2.234 \quad (67)$$

for $N = 3$.

The one-loop SMOM RG-improved propagators are readily derived from Eqs. (18), (19), and (46). With

$$\begin{aligned} \hat{\Delta}^{(\text{SMOM})}(p^2) &= \frac{1}{p^2 + m^2}, \\ \hat{\mathcal{G}}^{(\text{SMOM})}(p^2) &= -\frac{1}{p^2}, \end{aligned} \quad (68)$$

we find that, when renormalized at the scale μ_0 ,

$$\begin{aligned} \Delta^{(\text{SMOM})}(p^2; \mu_0^2) &= \frac{1}{p^2 + m^2} \exp\left(-\int_{\mu_0^2/m^2}^{p^2/m^2} ds \frac{1}{s+1}\right) \\ &\quad \times \left\{ \frac{1}{s} + \alpha^{(\text{SMOM})}(s) s F'(s) \right\}, \\ \mathcal{G}^{(\text{SMOM})}(p^2; \mu_0^2) &= -\frac{1}{p^2} \exp\left(-\int_{\mu_0^2/m^2}^{p^2/m^2} ds \alpha^{(\text{SMOM})}(s) G'(s)\right). \end{aligned} \quad (69)$$

Equivalently, the first of Eq. (69) can be expressed as

$$\begin{aligned} \Delta^{(\text{SMOM})}(p^2; \mu_0^2) &= \frac{1}{p^2 \mu_0^2 + m^2} \exp\left(-\int_{\mu_0^2/m^2}^{p^2/m^2} ds \frac{s}{s+1} \alpha^{(\text{SMOM})}(s) F'(s)\right). \end{aligned} \quad (70)$$

The improved gluon propagator and ghost dressing function renormalized at the scale $\mu_0 = 6.098m$

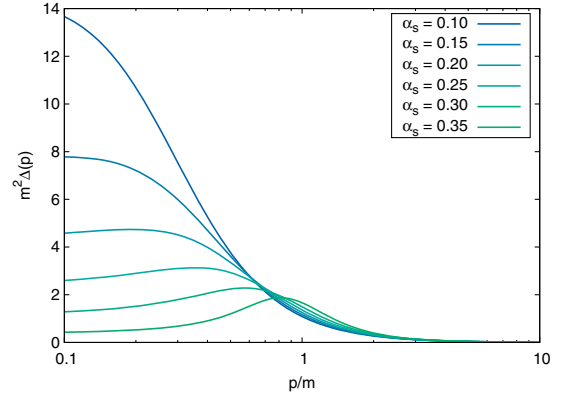


FIG. 8. $N = 3$ one-loop RG-improved gluon propagator in the SMOM scheme, renormalized at the scale $\mu_0/m = 6.098$ (corresponding to $\mu_0 = 4$ GeV for $m = 0.656$ GeV), and computed for different initial values of the coupling at the same scale.

(corresponding to $\mu_0 = 4$ GeV in physical units) are shown in Figs. 8 and 9, respectively, for different initial values of the coupling constant below the threshold value $\alpha_{s,\text{pole}}^{(\text{SMOM})} \approx 0.43$. In the high momentum limit both the SMOM anomalous dimensions and running coupling reduce to the respective standard one-loop expressions. Therefore, Eq. (41) is also verified in the SMOM scheme for $p, \mu_0 \gg m$. At intermediate and low momenta, the general behavior of the SMOM propagators parallels that of the MOM scheme. In particular, provided that the SMOM running coupling does not develop a Landau pole, the gluon propagator attains a maximum at the momentum $p = \sqrt{s}m$ that solves the equation

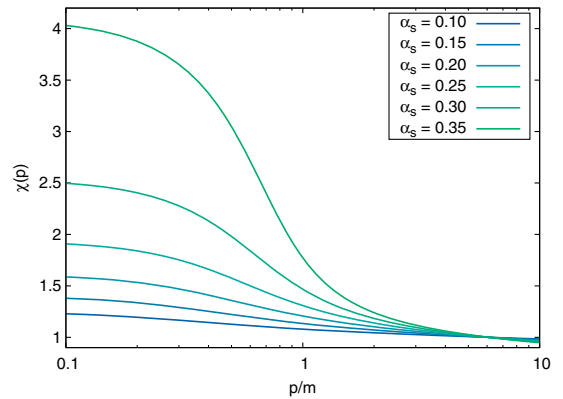


FIG. 9. $N = 3$ one-loop RG-improved ghost dressing function $\chi(p) = -p^2 \mathcal{G}(p)$ in the SMOM scheme, renormalized at the scale $\mu_0/m = 6.098$ (corresponding to $\mu_0 = 4$ GeV for $m = 0.656$ GeV), and computed for different initial values of the coupling at the same scale.

$$1 + \frac{s^2}{s+1} \alpha^{(\text{SMOM})}(s) F'(s) = 0. \quad (71)$$

Equation (71) always admits a solution since

$$1 + \frac{s^2}{s+1} \alpha^{(\text{SMOM})}(s) F'(s) \rightarrow -\frac{4}{15} s \ln^2 s \leq 0 \quad (s \rightarrow 0),$$

$$1 + \frac{s^2}{s+1} \alpha^{(\text{SMOM})}(s) F'(s) \rightarrow 1 > 0 \quad (s \rightarrow \infty) \quad (72)$$

(cf. the Appendix). As in the MOM scheme, the position of the maximum depends on the initial conditions of the RG flow and shifts to lower momenta as $\alpha^{(\text{SMOM})}(\mu_0^2)$ is decreased. In the limit of vanishing momenta, since for $s \rightarrow 0$

$$\frac{s}{s+1} \alpha^{(\text{SMOM})}(s) F'(s) \rightarrow -\frac{1}{s},$$

$$\alpha^{(\text{SMOM})}(s) G'(s) \rightarrow -\frac{4}{15} \ln s \quad (73)$$

(cf. the Appendix), the one-loop improved propagators again have the same behavior as in the MOM scheme, Eq. (45). In particular, while the ghosts remain massless, the gluons acquire a mass.

In the SMOM scheme, the one-loop running coupling has a distinctive behavior: as we saw, after attaining a maximum at an intermediate scale, at low momenta it saturates to a finite value which does not depend on the initial conditions of the RG flow, namely $\alpha_s^{(\text{SMOM})}(0) \approx 2.23$ (for $N = 3$). As a consequence, regardless of the initial conditions, in the whole range $\mu \lesssim m$ the values of the one-loop SMOM running coupling become quite large for the perturbative standards. We should then expect the higher orders of the perturbative series to become non-negligible at scales lower than m . The situation is somewhat worse than in the MOM scheme: in the latter, the one-loop running coupling at any fixed scale is an increasing function of $\alpha_s^{(\text{MOM})}(\mu_0^2)$, so that, at least in principle, for sufficiently small initial values of the coupling the one-loop results can still provide a good approximation to the exact propagators if the gluon mass parameter m is chosen appropriately. In the SMOM scheme, on the other hand, it is the fixed value of the zero-momentum coupling that dominates over the low-energy behavior of $\alpha_s^{(\text{SMOM})}(\mu^2)$. In particular, we should expect the perturbative series to converge more slowly in the SMOM scheme, rather than in the MOM scheme.

C. Comparison between the MOM and the SMOM schemes

As shown in Secs. III A and III B, both the MOM and the SMOM one-loop running coupling and RG-improved propagators have the ordinary perturbative UV limit. In the

IR, the behavior of the propagators is in mutual qualitative agreement, while that of the running couplings shows significant differences. In order to make a quantitative comparison between the predictions of the two schemes, what we need to do is find a correspondence between the values of their renormalized couplings.

The qualitative difference between the MOM and the SMOM one-loop running couplings ultimately originates in the prefactor $(\mu^2 + m^2)/\mu^2$ in Eq. (55). Indeed, if we define a function $\tilde{\alpha}^{(\text{SMOM})}(\mu^2)$ such that

$$\alpha^{(\text{SMOM})}(\mu^2) = \frac{\mu^2 + m^2}{\mu^2} \tilde{\alpha}^{(\text{SMOM})}(\mu^2), \quad (74)$$

then

$$\tilde{\alpha}^{(\text{SMOM})}(\mu^2) = \frac{\tilde{\alpha}^{(\text{SMOM})}(\mu_0^2)}{1 + \tilde{\alpha}^{(\text{SMOM})}(\mu_0^2)[K(s) - K(s_0)]} \quad (75)$$

is formally identical to the MOM running coupling, Eq. (29), with the substitution $H(s) \rightarrow K(s)$. As shown in Fig. 10, the functions $H(s)$ and $K(s)$ themselves have the same qualitative behavior.

The factor $(\mu^2 + m^2)/\mu^2$ in Eq. (74) is a by-product of the $O(\alpha_s^0)$ term in the SMOM gluon anomalous dimension, Eq. (48), which results in the SMOM beta function $\beta_\alpha^{(\text{SMOM})}$ containing an $O(\alpha_s)$ term. This is made explicit by computing the beta function analogue associated to $\tilde{\alpha}^{(\text{SMOM})}(\mu^2)$: to one loop

$$\beta_\alpha^{(\text{SMOM})} = \frac{d\tilde{\alpha}^{(\text{SMOM})}}{d \ln \mu^2} = -(\tilde{\alpha}^{(\text{SMOM})})^2 \frac{\mu^2}{m^2} K' \left(\frac{\mu^2}{m^2} \right). \quad (76)$$

The latter contains no $O(\alpha_s^0)$ terms and has the same form of the MOM beta function, Eq. (25), again with the substitution $H(s) \rightarrow K(s)$. At the level of the

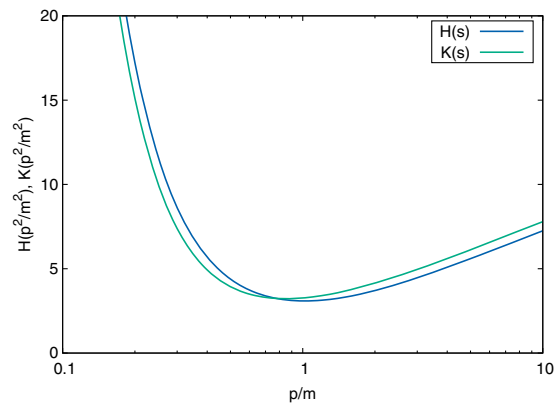


FIG. 10. $H(s)$ and $K(s)$ as functions of the ratio p/m .

renormalization conditions that define the two schemes, the appearance of the factor of $(\mu^2 + m^2)/\mu^2$ can be understood as follows. From Eq. (16) we know that in the Taylor scheme

$$\frac{\alpha^{(\text{SMOM})}(\mu^2)}{\alpha^{(\text{MOM})}(\mu^2)} = \frac{Z_A^{(\text{SMOM})}(\mu^2)(Z_c^{(\text{SMOM})}(\mu^2))^2}{Z_A^{(\text{MOM})}(\mu^2)(Z_c^{(\text{MOM})}(\mu^2))^2}. \quad (77)$$

Now, while $Z_c^{(\text{SMOM})}$, $Z_A^{(\text{MOM})}$, and $Z_c^{(\text{MOM})}$ are all equal to 1 to $O(\alpha_s^0)$,

$$Z_A^{(\text{SMOM})}(\mu^2) = 1 + \frac{m^2}{\mu^2} + O(\alpha_s). \quad (78)$$

Therefore,

$$\frac{\alpha^{(\text{SMOM})}(\mu^2)}{\alpha^{(\text{MOM})}(\mu^2)} = \frac{\mu^2 + m^2}{\mu^2} + O(\alpha_s). \quad (79)$$

In the next section we will show that the relation $\alpha^{(\text{SMOM})}(\mu^2) = (\mu^2 + m^2)/\mu^2 \times \alpha^{(\text{MOM})}(\mu^2)$ is indeed exact, although not necessarily satisfied at any finite order in perturbation theory.

In conclusion, we find that the conversion factor between $\alpha^{(\text{SMOM})}$ and $\alpha^{(\text{MOM})}$ is precisely $(\mu^2 + m^2)/\mu^2$: in order to compare the two schemes, to one loop we need to choose values of the couplings such that $\alpha^{(\text{MOM})}(\mu_0^2) = \tilde{\alpha}^{(\text{SMOM})}(\mu_0^2)$. At $\mu_0 = 6.098m$ (corresponding to 4 GeV in physical units), this translates into

$$\alpha^{(\text{SMOM})}(\mu_0^2) \approx 1.027\alpha^{(\text{MOM})}(\mu_0^2). \quad (80)$$

For our first comparison, in Fig. 11 we show the one-loop MOM and SMOM running couplings for two different values of α_s at the initial renormalization scale $\mu_0 = 6.098m$. The SMOM coupling is plotted in terms of $\tilde{\alpha}_s^{(\text{SMOM})}$, as per Eq. (79). As discussed above, $\alpha^{(\text{MOM})}(\mu^2)$ and $\tilde{\alpha}_s^{(\text{SMOM})}(\mu^2)$ have the same qualitative behavior: they both attain a maximum at a fixed scale of the order of m and tend to zero at vanishing renormalization scales. The position of the maximum of $\tilde{\alpha}_s^{(\text{SMOM})}(\mu^2)$, however, lies below that of the MOM running coupling; moreover, in the whole range $p \lesssim m$ the values of $\tilde{\alpha}_s^{(\text{SMOM})}(\mu^2)$ are generally larger than those of $\alpha_s^{(\text{MOM})}(\mu^2)$. Since $(\mu^2 + m^2)/\mu^2 > 1$, we find that in the IR $\alpha_s^{(\text{SMOM})}(\mu^2) > \alpha_s^{(\text{MOM})}(\mu^2)$, enforcing the idea that the SMOM perturbative series may converge more slowly than that of the MOM scheme.

In Figs. 12 and 13 we compare the one-loop improved gluon propagators and ghost dressing functions renormalized at the scale $\mu_0 = 6.098m$ (corresponding to $\mu_0 = 4$ GeV in physical units) in the two schemes with the correspondence between the renormalized couplings as discussed above. As we can see, at low momenta the propagators agree only qualitatively: at scales less than $\approx m$ the MOM gluon propagator is enhanced with respect to the SMOM propagator, while the ghost dressing function shows the opposite behavior. The relative difference between the propagators increases with the value of the coupling at μ_0 and decreases as a function of momentum (indeed, we know that the propagators have the same, standard perturbative UV behavior in both the renormalization schemes). In the IR and for large values of the

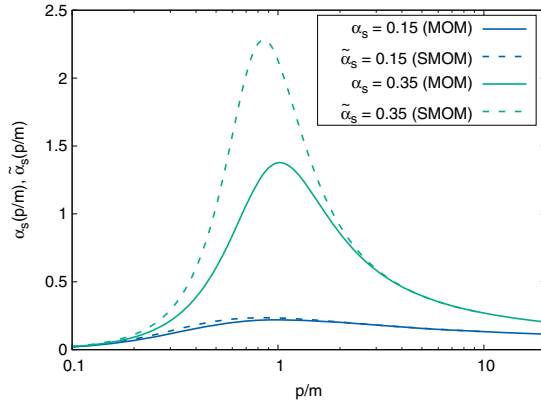


FIG. 11. Comparison between the $N = 3$ MOM and SMOM one-loop running couplings renormalized at the scale $\mu_0/m = 6.098$ (corresponding to $\mu_0 = 4$ GeV for $m = 0.656$ GeV). For $N = 3$, the MOM running coupling develops a Landau pole at $\alpha_s^{(\text{MOM})}(\mu_0^2) \approx 0.469$, while the SMOM running coupling develops it at $\tilde{\alpha}_s^{(\text{SMOM})}(\mu_0^2) \approx 0.413$. See the text for the details of the comparison.

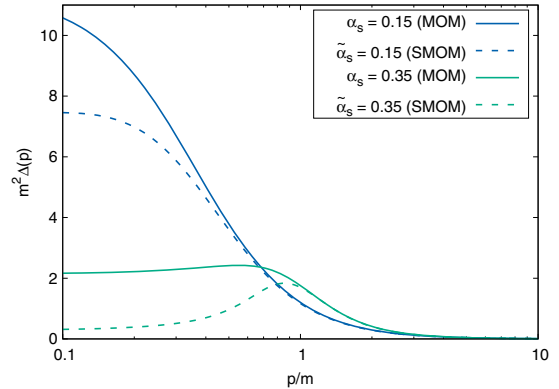


FIG. 12. $N = 3$ one-loop RG-improved gluon propagator in the SMOM scheme, renormalized at the scale $\mu_0/m = 6.098$ (corresponding to $\mu_0 = 4$ GeV for $m = 0.656$ GeV), and computed for different initial values of the coupling at the same scale.

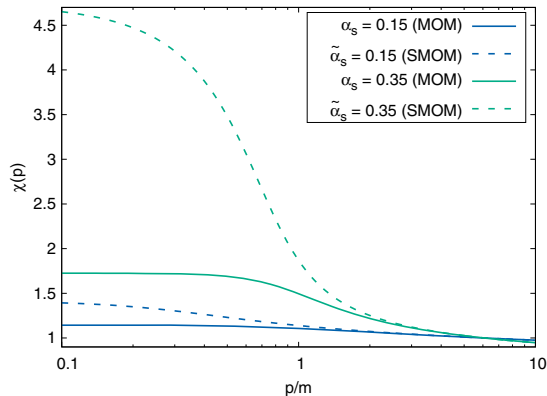


FIG. 13. $N = 3$ one-loop RG-improved ghost dressing function $\chi(p) = -p^2 \mathcal{G}(p)$ in the SMOM scheme, renormalized at the scale $\mu_0/m = 6.098$ (corresponding to $\mu_0 = 4$ GeV for $m = 0.656$ GeV), and computed for different initial values of the coupling at the same scale.

renormalized couplings the difference between the two schemes can become quite large.

IV. OPTIMIZED RG IMPROVEMENT AND COMPARISON WITH THE LATTICE DATA

By removing the Landau pole from the running of the coupling constant, the RG-improved screened massive expansion provides us with a consistent analytical framework for computing quantities at all scales in pure Yang-Mills theory, albeit at the cost of introducing a new free parameter, namely the gluon mass parameter m . Already at one loop, the RG-improved gluon and ghost propagators derived in such a framework display the correct qualitative behavior (as found, for example, on the lattice), being able to encode both the IR phenomenon of dynamical mass generation for the gluons and the correct UV asymptotic limits of standard perturbation theory.

Nevertheless, as discussed in Sec. III, the one-loop RG-improved results are not expected to be quantitatively reliable below scales of the order of the gluon mass parameter m , the reason being that the one-loop running coupling of the screened expansion either attains a maximum at $\mu \sim m$ (in the MOM scheme) or saturates to a finite value at scales $\mu \lesssim m$ (in the SMOM scheme), becoming too large to justify the truncation of the perturbative series to first order in the coupling. In the IR, it is the one-loop fixed-scale optimized screened expansion of Refs. [55,59] that proves successful in reproducing the lattice data for the propagators: in Ref. [55,59] it was shown that the renormalization scheme in which the pole structure of the gluon propagator is gauge invariant also yields propagators for which the terms of $O(\alpha_s^2)$ and higher are negligible at low energies. The fixed-scale expansion is predictive in that its

only free parameter is the energy scale of the theory, which enters the equations through the gluon mass parameter m itself. We then find ourselves in possession of two distinct computational frameworks, one of which (the fixed-scale expansion) works well in the IR, while the other (the RG-improved expansion) works well in the UV. In the respective domains of applicability, both of them yield satisfactory approximations (at this stage at least qualitatively, as far as the RG-improved one is concerned) already at one loop.

A natural question to ask is whether the predictions of the two frameworks agree over some intermediate range of momenta. In general, this may depend on which values are chosen for the free parameters of the theory. Indeed, we reiterate that whereas the results of the fixed-scale expansion are completely determined once the energy scale is set by the gluon mass parameter m (see Ref. [55]), those of the RG-improved expansion also depend on the value of the strong coupling constant at the initial renormalization scale, $\alpha_s(\mu_0^2)$.

Actually, the fact that in the RG-improved formalism the mass parameter m and the renormalized coupling $\alpha_s(\mu_0^2)$ can be chosen independently of one another is a major weakness of the method: already in standard perturbation theory, once the energy scale is set by the Yang-Mills analogue of Λ_{QCD} —which we denote by Λ_{YM} —the value of the coupling is fixed at all renormalization scales by the equation

$$\alpha_s(\mu^2) = \frac{12\pi}{11N \ln(\mu^2/\Lambda_{\text{YM}}^2)} \quad (81)$$

(valid to one loop); in the fixed-scale framework the redundancy of free parameters is dealt with by optimization; in the formulation of the RG-improved screened PT presented in Sec. III, no such constraint exists, resulting in a loss of predictivity of the method.

The condition that the propagators and/or the running coupling computed in the fixed-scale and RG-improved frameworks match at intermediate energies can, however, be exploited as a criterion for fixing the value of $\alpha_s(\mu_0^2)$: if the matching singled out a value of the coupling $\alpha_s(\mu_0^2)$ for which the predictions of the two frameworks are in better agreement, then the gluon mass parameter m —by setting the scale for the dimensionful value of μ_0 —would play the same role as the Λ_{YM} of ordinary perturbation theory. In particular, given some value of m , the value of $\alpha_s(\mu^2)$ at any renormalization scale would be completely determined, just as it happens in standard perturbation theory once Λ_{YM} is fixed. In turn, the redundancy in the free parameters of the RG-improved framework would be removed and the predictivity of the method would be restored.

In Sec. IVA we will show that, at least in the MOM scheme, an optimal value of $\alpha_s(\mu_0^2)$ for the matching of the fixed-scale and the RG-improved results at intermediate

scales indeed exists. The predictions that follow, with the low energy behavior dictated by the fixed-scale expansion, are collected under the name of optimized RG-improved screened PT and turn out to reproduce the lattice data quite well in the whole available range of momenta, given an appropriate choice of the energy units (cf. Sec. IV B, where our results are compared with the data of Ref. [18]).

A. Intermediate-scale matching of the fixed-scale and RG-improved results

In order to determine which value of $\alpha_s(\mu_0^2)$, if any, results in the best agreement between the IR fixed-scale and the UV RG-improved predictions, we may investigate the intermediate energy behavior either of the propagators or of the strong running coupling. In what follows we choose to work with the latter, the reason being that in the Taylor scheme the running coupling contains immediate information about both the gluon and the ghost propagators: from Eq. (16) one finds that

$$\alpha_s(p^2) = \alpha_s(\mu_0^2) \frac{Z_A(p^2)Z_c^2(p^2)}{Z_A(\mu_0^2)Z_c^2(\mu_0^2)}, \quad (82)$$

where the renormalization factors $Z_A(\mu^2)$ and $Z_c(\mu^2)$ can be obtained from the propagators through the relations

$$Z_A(\mu^2) = \frac{J_B(q^2)}{J(q^2; \mu^2)}, \quad Z_c(\mu^2) = \frac{\chi_B(q^2)}{\chi(q^2; \mu^2)}, \quad (83)$$

with $J(q^2; \mu^2)$ and $\chi(q^2; \mu^2)$ the gluon and ghost dressing functions renormalized at the scale μ^2 ,

$$\begin{aligned} J(q^2; \mu^2) &= q^2 \Delta(q^2; \mu^2), \\ \chi(q^2; \mu^2) &= -q^2 \mathcal{G}(q^2; \mu^2), \end{aligned} \quad (84)$$

and $J_B(q^2)$ and $\chi_B(q^2)$ their bare counterparts,

$$\begin{aligned} J_B(q^2) &= q^2 \Delta_B(q^2), \\ \chi_B(q^2) &= -q^2 \mathcal{G}_B(q^2). \end{aligned} \quad (85)$$

Plugging Eqs. (83) into Eq. (82) after setting $q^2 = p^2$ yields the following expression for the Taylor-scheme running coupling in terms of the *renormalized* gluon and ghost dressing functions:

$$\alpha_s(p^2) = \alpha_s(\mu_0^2) \frac{J(p^2; \mu_0^2) \chi^2(p^2; \mu_0^2)}{J(p^2; p^2) \chi^2(p^2; p^2)}. \quad (86)$$

In the above equation, which can be explicitly checked for the MOM and SMOM schemes of Sec. III, the functions $J(p^2; p^2)$ and $\chi(p^2; p^2)$ define the renormalization of the propagators. For instance, in the MOM scheme

$$J^{(\text{MOM})}(p^2; p^2) = \chi^{(\text{MOM})}(p^2; p^2) = 1, \quad (87)$$

whereas in the SMOM scheme

$$\begin{aligned} J^{(\text{SMOM})}(p^2; p^2) &= \frac{p^2}{p^2 + m^2}, \\ \chi^{(\text{SMOM})}(p^2; p^2) &= 1. \end{aligned} \quad (88)$$

Apart from these functions, Eq. (86) shows that in the Taylor scheme the running coupling is proportional to a product of the gluon and ghost dressing functions, so that a comparison between the couplings of different frameworks also yields a comparison between the propagators.

Incidentally, Eq. (83) can be used to prove that Eq. (79) is exact: taking the ratio between the field-strength renormalization factors defined in the SMOM and in the MOM scheme and setting $q^2 = \mu^2$, we find

$$\frac{Z_A^{(\text{SMOM})}(\mu^2)}{Z_A^{(\text{MOM})}(\mu^2)} = \frac{\mu^2 + m^2}{\mu^2}, \quad \frac{Z_c^{(\text{SMOM})}(\mu^2)}{Z_c^{(\text{MOM})}(\mu^2)} = 1. \quad (89)$$

Once these ratios are plugged back into Eq. (77), the relation $\alpha^{(\text{SMOM})}(\mu^2) = (\mu^2 + m^2)/\mu^2 \times \alpha^{(\text{MOM})}(\mu^2)$ is recovered, with no higher-order contributions.

The Taylor scheme is also suitable for defining a running coupling in the context of the fixed-scale perturbation theory.⁴ Indeed, if we renormalize the fixed-scale propagators in a MOM-like fashion by requiring that $J(p^2; p^2)$ and $\chi(p^2; p^2)$ be momentum independent, then we can define a fixed-scale (FS) scheme Taylor running coupling as

$$\alpha_s^{(\text{FS})}(p^2) = \kappa J^{(\text{FS})}(p^2) \chi^{(\text{FS})}(p^2)^2, \quad (90)$$

where at one loop, absorbing the multiplicative renormalization constants of the dressing functions into the adimensional constant κ ,

$$\begin{aligned} J^{(\text{FS})}(p^2) &= \frac{1}{F(p^2/m^2) + F_0}, \\ \chi^{(\text{FS})}(p^2) &= \frac{1}{G(p^2/m^2) + G_0} \end{aligned} \quad (91)$$

(cf. Sec. II and the Appendix). Of course, Eqs. (90) and (91) do not fix the overall normalization of $\alpha_s^{(\text{FS})}(p^2)$, which at this stage remains undefined. The constant κ will be determined in what follows by the matching condition.

⁴In the formalism of Refs. [51–58] (see also the Appendix) the gluon and ghost propagators are expressed in an essentially coupling-independent way, so that an explicit definition of what $\alpha_s(p^2)$ is in the fixed-scale framework is still required. See also Ref. [59] for a different definition of the coupling in the SMOM scheme.

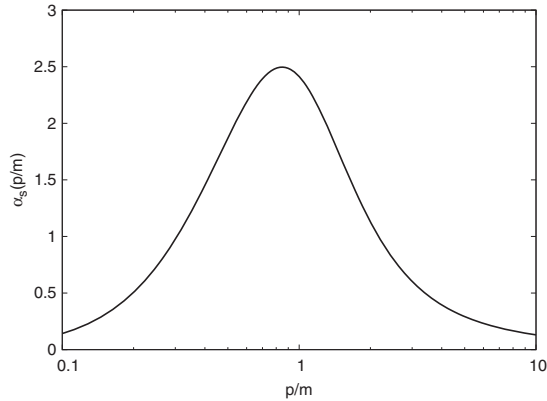


FIG. 14. One-loop running coupling of the screened expansion in the FS scheme. The normalization of the curve is arbitrary.

The unnormalized one-loop FS running coupling is shown in Fig. 14. Its qualitative behavior is that of the MOM-scheme running coupling (cf. Fig. 3), as one would expect from having chosen momentum-independent $J(p^2; p^2)$ and $\chi(p^2; p^2)$. Accordingly, the comparison between $\alpha_s^{(\text{FS})}(p^2)$ and the SMOM running coupling will be carried out using $\tilde{\alpha}_s^{(\text{SMOM})}(p^2)$ rather than $\alpha_s^{(\text{SMOM})}(p^2)$ (cf. the discussion in Sec. III C).

With $\alpha_s^{(\text{FS})}(p^2)$ as in Eq. (90) and $\alpha_s^{(\text{MOM})}(p^2)$ and $\tilde{\alpha}_s^{(\text{SMOM})}(p^2)$ as in Eqs. (29) and (75), we must now identify a range of momenta over which the running couplings of the FS and RG-improved frameworks may be expected to agree. To one loop, the latter becomes unreliable below $\mu \sim m$, corresponding to $\mu \approx 0.7$ GeV in physical units; the matching window, therefore, should lie somewhat above this value. Likewise, the upper limit of the matching interval should be set by the scale at which the one-loop results derived in the FS framework are likely to break down; this should happen at scales larger than m but of the same order of m .

As for the normalization of the FS running coupling, under the hypothesis that at intermediate momenta the latter agrees with $\alpha_s^{(\text{RG})}(p^2)$ —where this is taken to be either $\alpha_s^{(\text{MOM})}(p^2)$ or $\tilde{\alpha}_s^{(\text{SMOM})}(p^2)$, depending on the scheme we are interested in—we may require $\alpha_s^{(\text{FS})}(p^2)$ to be equal to the RG-improved coupling at some fixed renormalization scale $p = \mu_1$ belonging to the momentum range that we have just identified,

$$\alpha_s^{(\text{FS})}(\mu_1^2) = \alpha_s^{(\text{RG})}(\mu_1^2). \quad (92)$$

This amounts to setting

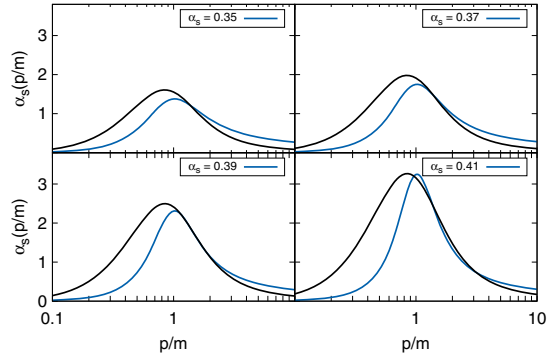


FIG. 15. $N = 3$ intermediate-energy matching between the FS running coupling (black curves) and the MOM running coupling (blue curves) for different values of the MOM coupling renormalized at the scale $\mu_0/m = 6.098$ (corresponding to $\mu_0 = 4$ GeV in physical units). The matching scale (see the text for details) is set to $\mu_1/m = 1.372$ (corresponding to $\mu_1 = 0.9$ GeV).

$$\kappa = \frac{\alpha_s^{(\text{RG})}(\mu_1^2)}{J^{(\text{FS})}(\mu_1^2)\chi^{(\text{FS})}(\mu_1^2)^2} \quad (93)$$

in Eq. (90). Of course, the actual value of the so-defined constant κ will depend not only on the matching scale μ_1 , but also—through $\alpha_s^{(\text{RG})}(\mu_1^2)$ —on the initial value $\alpha_s^{(\text{RG})}(\mu_0^2)$ of the RG coupling.

In Figs. 15 and 16 we show a comparison of the normalized FS running coupling and, respectively, the MOM-scheme and SMOM-scheme running couplings, for $N = 3$ and different initial values of $\alpha_s^{(\text{RG})}(p^2)$ renormalized at the scale $\mu_0 = 6.098m$ (corresponding to 4 GeV in physical units). For these plots the matching scale μ_1 was

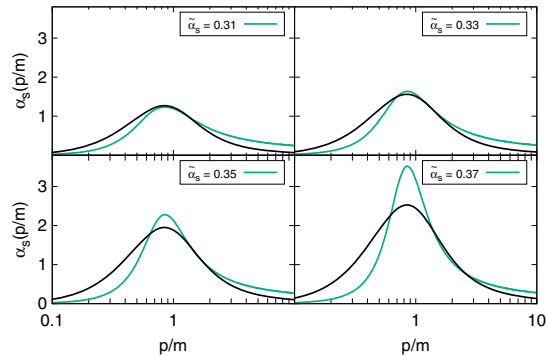


FIG. 16. $N = 3$ intermediate-energy matching between the FS running coupling (black curves) and the SMOM running coupling (green curves) for different values of the MOM coupling renormalized at the scale $\mu_0/m = 6.098$ (corresponding to $\mu_0 = 4$ GeV in physical units). The matching scale (see the text for details) is set to $\mu_1/m = 1.372$ (corresponding to $\mu_1 = 0.9$ GeV).

chosen equal to $1.372m$ (corresponding to 0.9 GeV). Clearly, despite the $\alpha_s^{(\text{RG})}(\mu_0^2)$ -dependent matching condition contained in Eq. (93), the running couplings computed in the two frameworks do not agree at intermediate momenta for arbitrary values of $\alpha_s^{(\text{RG})}(\mu_0^2)$. In the MOM scheme, the choice $\alpha_s^{(\text{MOM})}(\mu_0^2) \approx 0.39$ leads to the overlap of the running couplings at scales between $p \approx m$ and $p \approx 2m$. In the SMOM scheme, on the other hand, no single choice of $\tilde{\alpha}_s^{(\text{SMOM})}(\mu_0^2)$ results in the running couplings to agree over a comparably wide momentum interval.⁵ Why this is so can be understood in the light of the considerations made at the end of Sec. III B: at scales of order m and at one loop, the SMOM scheme is expected to be less reliable than the MOM scheme; therefore, under the assumption that the one-loop predictions of the FS framework are nearly exact up to $p \sim m$, the better agreement of $\alpha_s^{(\text{FS})}(p^2)$ with $\alpha_s^{(\text{MOM})}(p^2)$, rather than with $\tilde{\alpha}_s^{(\text{SMOM})}(p^2)$, could have been anticipated. In what follows we will push no farther the comparison between the FS and the SMOM-scheme RG-improved frameworks, limiting ourselves to present our results for the MOM scheme.

In order to single out an optimal value of $\alpha_s^{(\text{MOM})}(\mu_0^2)$ for the matching, we will adopt the following criterion. Denoting with $\varepsilon(p^2)$ the momentum-dependent relative difference between the MOM running coupling and the FS running coupling [the latter normalized as in Eq. (93)],

$$\varepsilon(p^2) = \frac{\alpha_s^{(\text{MOM})}(p^2) - \alpha_s^{(\text{FS})}(p^2)}{\alpha_s^{(\text{FS})}(p^2)}, \quad (94)$$

we say that $\alpha_s^{(\text{MOM})}(\mu_0^2)$ is optimal for the matching if it results in a MOM running coupling for which $|\varepsilon(p^2)| \leq 1\%$ over the widest possible range of momenta in the previously identified matching interval. The matching scale μ_1 itself—Eq. (92)—is fixed according to the same criterion.

In Fig. 17 we show the relative difference $\varepsilon(p^2)$ computed for the optimal value $\alpha_s^{(\text{MOM})}(\mu_0^2) = 0.391$ ($\mu_0 = 6.098m$, i.e., 4 GeV in physical units) obtained for $N = 3$ at the matching scale $\mu_1 = 1.372m$ (0.9 GeV) by the criterion detailed above. The range over which $|\varepsilon(p^2)| \leq 1\%$ has width $\Delta p \approx 0.9m$ (0.6 GeV) and extends from $p \approx 1.1m$ to $p \approx 2m$. In Fig. 18 the corresponding running couplings are displayed. The combined red curve, which we denote by $\alpha_s^{(\text{opt})}(p^2)$, is obtained by gluing the low-energy portion of the FS coupling to the high-energy portion of the MOM coupling at $p = \mu_1$. Note that

⁵We checked that tuning the matching scale μ_1 between $\approx m$ and $\approx 2.5m$ does not improve this behavior: in no case were we able to obtain an overlap between the FS and the SMOM running coupling over a wider range of momenta without entering a regime in which the SMOM coupling develops a Landau pole.

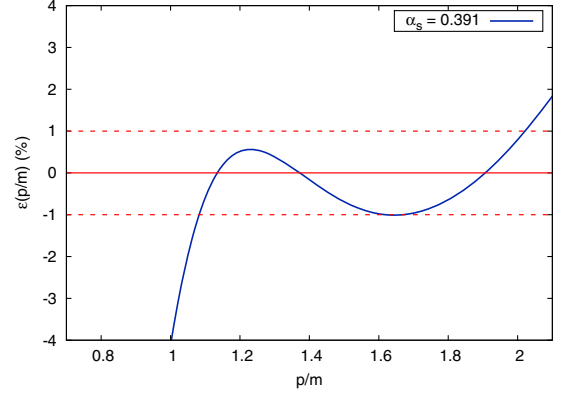


FIG. 17. Relative difference between the $N = 3$ MOM running coupling and the FS running coupling for the optimal value $\alpha_s^{(\text{MOM})}(\mu_0^2) = 0.391$. The initial renormalization scale is $\mu_0/m = 6.098$ (corresponding to $\mu_0 = 4$ GeV in physical units), while the matching scale is $\mu_1/m = 1.372$ (corresponding to $\mu_1 = 0.9$ GeV).

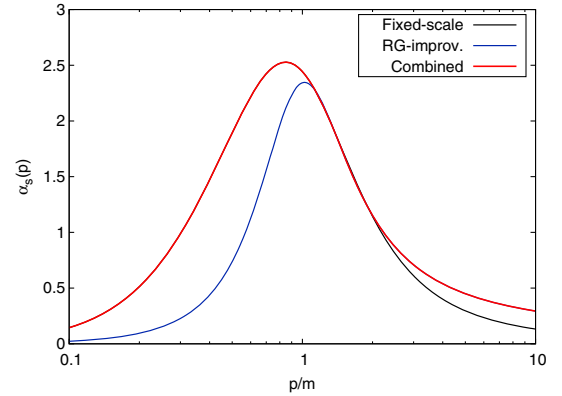


FIG. 18. Intermediate-energy matching between the FS running coupling (black curve) and the $N = 3$ MOM running coupling (blue curve) for the optimal value $\alpha_s^{(\text{MOM})}(\mu_0^2) = 0.391$ ($\mu_0 = 6.098m$, corresponding to 4 GeV in physical units). The matching scale is $\mu_1 = 1.372m$ (0.9 GeV) and the FS coupling is normalized by $\kappa = 1.200$. The red curve is obtained by combining the low-energy FS coupling and the high-energy MOM coupling.

$\alpha_s^{(\text{opt})}(p^2)$ attains a maximum at $p = p_{\text{max}} \approx 0.847m$ (corresponding to 0.556 GeV in physical units),

$$\begin{aligned} p_{\text{max}} &\approx 0.847m, \\ \alpha_s^{(\text{opt})}(p_{\text{max}}^2) &\approx 2.527. \end{aligned} \quad (95)$$

In Sec. IV B the combined predictions of the FS and MOM-scheme RG-improved frameworks will be compared with the lattice data for $N = 3$.

B. Comparison with the lattice data

Having found that the optimal value of $\alpha_s^{(\text{MOM})}(\mu_0^2)$ for the matching of the $N = 3$ one-loop RG-improved MOM scheme to the one-loop FS framework is 0.391 (with $\mu_0 = 6.098m$ as the renormalization scale and $\mu_1 = 1.372m$ as the matching scale), we now proceed to compare our combined results with the lattice data of Ref. [18]. We reiterate that once the RG-improved expansion is optimized by fixing $\alpha_s^{(\text{MOM})}(\mu_0^2)$ —with μ_0 expressed in units of m —the gluon mass parameter is left to stand as the only free parameter of the theory. Being a mass scale, m plays the same role as Λ_{YM} in standard perturbation theory, entering the MOM running coupling through the ratio p^2/m^2 in the denominator of

$$\alpha_s^{(\text{MOM})}(p^2) = \frac{4\pi}{9[H(p^2/m^2) - \bar{H}]} \quad (N = 3), \quad (96)$$

which is just Eq. (29) with \bar{H} defined as

$$\bar{H} = H(\mu_0^2/m^2) - \frac{4\pi}{9[\alpha_s^{(\text{MOM})}(\mu_0^2)]_{\text{optim}}} \approx 2.4926 \quad (97)$$

(having been obtained by optimization, \bar{H} must be regarded as a constant; it does not depend either on m nor on μ_0). As a consequence, m must be inferred from experiments or, in our case, from the lattice data. Since up until this point the conversion from adimensional to physical units has been made by taking $m = 0.656$ GeV (as in our previous works, see e.g., Ref. [55]), in what follows we will present our results both for the aforementioned value of the mass parameter and for the value that is obtained from a fit of the combined propagators to lattice data. We remark that fitting m to the lattice data only serves the purpose of fixing the energy scale of the combined results, in order to be able to compare them with the former. When all the dimensionful quantities of the theory are expressed in units of m , unlike the results of Sec. III—which still depended on a spurious free parameter—the combined propagators are uniquely determined.

In Figs. 19 and 20 the $N = 3$ gluon propagator and ghost dressing function renormalized at the scale $\mu_0 = 4$ GeV are shown as functions of momentum. The energy scale for the analytical results is set by the gluon mass parameter m , preliminarily taken to be equal to 0.656 GeV. In the figures, the red curves are obtained by combining the high-energy predictions of the RG-improved MOM scheme at $\alpha_s^{(\text{MOM})}(\mu_0^2) = 0.391$ (displayed as blue curves) with the low-energy ones of the FS framework (displayed as black curves), the latter normalized so as to match the former at

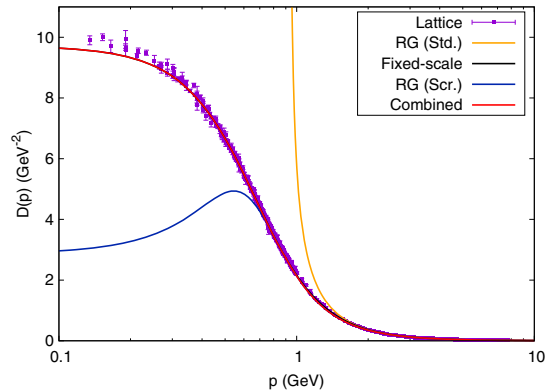


FIG. 19. $N = 3$ gluon propagator renormalized at the scale $\mu_0 = 4$ GeV. The lattice data are taken from Ref. [18]. The one-loop predictions of the MOM-scheme RG-improved and FS frameworks, computed for $\alpha_s^{(\text{MOM})}(\mu_0^2) = 0.391$ and $m = 0.656$ GeV, are reported in blue and in black, respectively. The red curve is obtained by their matching at $\mu_1 = 0.9$ GeV. The orange curve is the standard perturbative one-loop RG-improved result. See the text for details.

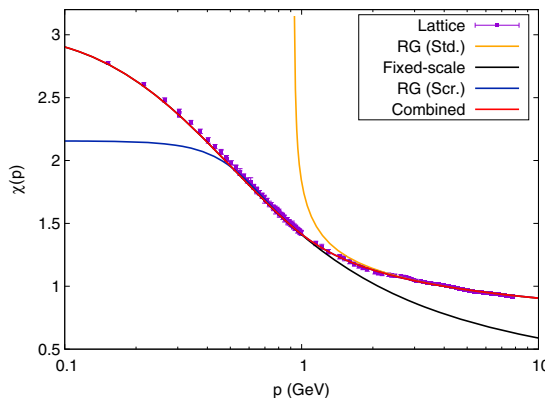


FIG. 20. $N = 3$ ghost dressing function renormalized at the scale $\mu_0 = 4$ GeV. The lattice data are taken from Ref. [18]. The one-loop predictions of the MOM-scheme RG-improved and FS frameworks, computed for $\alpha_s^{(\text{MOM})}(\mu_0^2) = 0.391$ and $m = 0.656$ GeV, are reported in blue and in black, respectively. The red curve is obtained by their matching at $\mu_1 = 0.9$ GeV. The orange curve is the standard perturbative one-loop RG-improved result. See the text for details.

$p = \mu_1 = 0.9$ GeV. For comparison, the standard perturbative one-loop results for $\alpha_s(\mu_0^2) = 0.391$ (corresponding to $\Lambda_{\text{YM}} = 0.928$ GeV) are also displayed in the figures as orange curves. In Fig. 21 we show the $N = 3$ gluon dressing functions associated to the propagators of Fig. 19.

As we can see, already at one loop and for $m = 0.656$ GeV, the combined results manage to reproduce

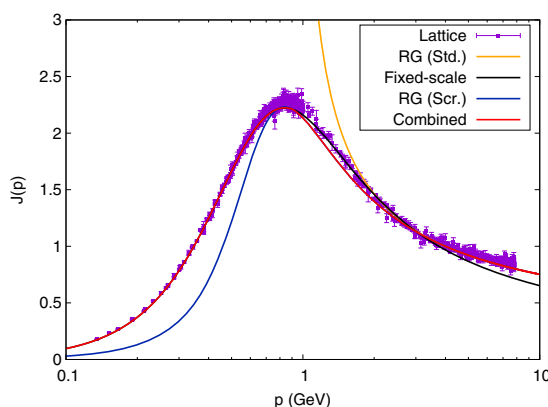


FIG. 21. $N = 3$ gluon dressing function renormalized at the scale $\mu_0 = 4$ GeV. The lattice data are taken from Ref. [18]. The one-loop predictions of the MOM-scheme RG-improved and FS frameworks, computed for $\alpha_s^{(\text{MOM})}(\mu_0^2) = 0.391$ and $m = 0.656$ GeV, are reported in blue and in black, respectively. The red curve is obtained by their matching at $\mu_1 = 0.9$ GeV. The orange curve is the standard perturbative one-loop RG-improved result. See the text for details.

quite well the lattice data over the whole available range of momenta (approximately 0.1 GeV to 8 GeV), especially for what concerns the ghost dressing function. At scales larger than $p \approx 3$ GeV, the RG-improved screened-PT propagators are indistinguishable from their standard-PT analogues and constitute a considerable improvement over the FS screened results, which are unable to reproduce the lattice propagators for $p > 1-3$ GeV. At lower intermediate scales, as the momentum p approaches Λ_{YM} , the mass effects of screened PT kick in and the screened propagators deviate from the standard perturbative behavior, avoiding the Landau pole and following the lattice data. Below $p \approx m$, as was to be expected, the higher-order terms of the RG-improved expansion become non-negligible, and the one-loop improved MOM-scheme calculations no longer provide a good approximation to the exact results. A good approximation is nonetheless provided by the combined results, which in this regime follow the predictions of the FS framework.

The agreement improves further if the value of m is determined by fitting the combined gluon propagator to the lattice data. In Figs. 22 and 23 we show the combined gluon propagator and ghost dressing function, respectively, computed for the fitted value of the gluon mass parameter, namely $m = 0.651$ GeV (the curves computed for $m = 0.656$ GeV are also displayed in the figures for comparison). Clearly, the ever so slight decrease in the value of the mass parameter is sufficient to enhance the gluon propagator at low momenta, bringing it onto the lattice data without spoiling either its intermediate- and high-energy behavior, or that of the ghost dressing function.

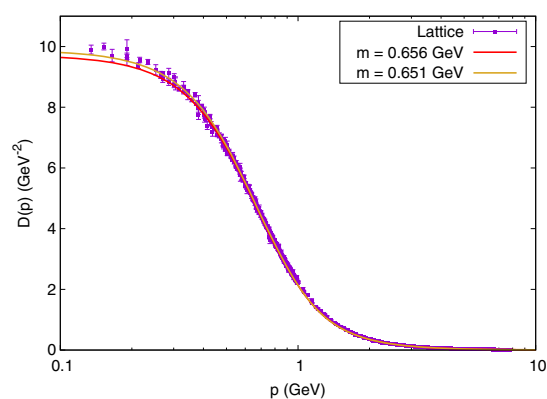


FIG. 22. $N = 3$ gluon propagator renormalized at the scale $\mu_0 = 4$ GeV with the lattice data of Ref. [18]. The one-loop predictions of the combined MOM-scheme RG-improved/FS frameworks, computed for $m = 0.656$ GeV and $m = 0.651$ GeV, are reported in red and gold, respectively. See the text for details.

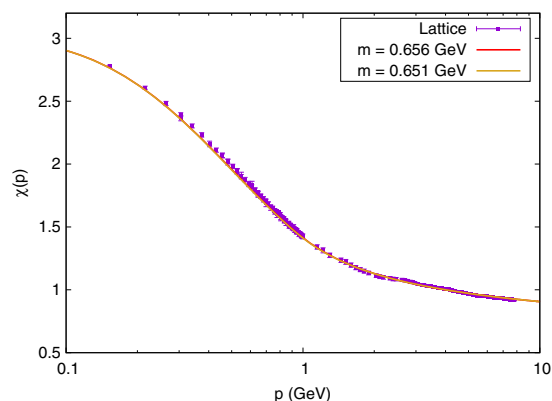


FIG. 23. $N = 3$ ghost dressing function renormalized at the scale $\mu_0 = 4$ GeV with the lattice data of Ref. [18]. The one-loop predictions of the combined MOM-scheme RG-improved/FS frameworks, computed for $m = 0.656$ GeV and $m = 0.651$ GeV, are reported in red and gold, respectively. See the text for details.

We should remark that, for these last plots, in changing the value of m the previously reported values of μ_1 and μ_0 in physical units have also changed. The matching scale $\mu_1 = 1.372m$ for combining the fixed-scale results with the MOM-scheme RG-improved ones is now equal to 0.89 GeV (instead of 0.9 GeV for $m = 0.656$ GeV), whereas the scale $\mu_0 = 6.098m$, interpreted as the scale at which, by optimization, $\alpha_s^{(\text{MOM})} = 0.391$, now equals 3.97 GeV (instead of 4 GeV). As for the renormalization scale of the propagators—previously denoted also with μ_0 and rigorously defined by Eqs. (20)—in order to compare our results with the lattice data we had to set it back to

4 GeV, rather than keeping it equal to the new value 3.97 GeV. Indeed, observe that the scale at which the propagators are defined and the one at which the initial value of the running coupling is defined do not need to coincide, as long as the initial value of the coupling is chosen so as to follow the RG flow. If we want to know the value of the coupling constant at 4 GeV for $m = 0.651$ GeV, then we can compute it directly from Eq. (96) using physical units: we find

$$\alpha_s^{(\text{MOM})}(4 \text{ GeV}) = 0.389 \quad (m = 0.651 \text{ GeV}). \quad (98)$$

Of course, the difference between 0.391 and 0.389, 3.97 GeV and 4 GeV, 0.89 GeV and 0.90 GeV, etc., is minimal; we may expect larger approximation errors to influence the numerical outcome of our analysis. Nonetheless, these calculations make explicit the role of the gluon mass parameter as the (only) mass scale of the theory, following the optimization of the screened massive expansion.

V. DISCUSSION

The dynamical generation of an infrared mass for the gluons raises questions as to whether the standard expansion point of QCD perturbation theory—namely, a massless vacuum for the gauge sector—is an appropriate choice for describing the low-energy behavior of the theory. That in the IR a massive expansion point for the gluons may improve the QCD perturbative series is corroborated by a GEP variational analysis of pure Yang–Mills theory: by minimizing the vacuum energy of the latter, a massive zero-order gluon propagator was shown [57] to bring us closer to the exact, nonperturbative vacuum of the gauge sector. The resulting perturbation theory—defined by a simple shift of the kinetic and interaction Lagrangian—was termed screened massive expansion and studied in Refs. [51–59].

In its fixed-coupling, fixed-scale formulation, the screened massive expansion proved successful in accurately reproducing the infrared lattice data for the propagators of pure Yang–Mills theory already at one loop [51,52,55]. Moreover, it was proven capable of describing the phenomenon of dynamical mass generation for the gluons in a nontrivial manner: whereas the zero-order gluon propagator is massive by the definition of the method itself, the tree-level mass terms, which appear in the dressed propagator, cancel out so that the saturation of the gluon propagator at zero momentum turns out to be an actual effect of the loops, i.e., of the strong interactions between the gluons. Nonetheless—strictly speaking—the screened expansion alone cannot be used to prove that the gluons acquire a mass in the infrared. Albeit it being a nontrivial prediction of the method for any nonzero value of the gluon mass parameter m , when the latter is set to zero the ordinary perturbative series of YM theory is recovered so that no mass generation occurs. In the context of the screened expansion, that $m \neq 0$ should lead to more reliable results

in the IR can only be inferred from the aforementioned GEP analysis.

Following the optimization of the screened expansion by principles of gauge invariance [55,59], the gluon mass parameter m is left as the only free parameter of the theory, playing the same role as the QCD/YM scale Λ_{YM} of the standard perturbative expansion, with respect to which all the dimensionful values—including the proper gluon’s mass—are to be measured. One could still wonder how a mass parameter, which is added and subtracted again in the Lagrangian, can have a physical role at all in the dynamics of the theory. From a variational point of view, since the optimal value of m yields the best expansion around a Gaussian massive vacuum [57], the mass parameter itself must be regarded as the best Gaussian approximation for the dynamically generated mass of the full theory. Such a mass is then subject to quantum corrections, which ultimately determine the value of the proper gluon’s mass.

At energies larger than about 2 GeV, the fixed-scale one-loop approximation breaks down due to the presence of large logarithms. This can be dealt with by resorting to ordinary RG methods, i.e., by defining a scheme-dependent running coupling constant and integrating the RG flow for the propagators. A second, most important, reason to study the RG flow of the screened expansion is to address the issues related to the strong interactions’ IR Landau pole. From both a theoretical and a practical point of view, the negativity of the coefficients of the standard QCD beta function (at least to five loops [69] and for a sufficiently small number of quarks), paired with the absence of mass scales in the Lagrangian (other than the quark masses), results in a strong running coupling which, in mass-independent renormalization schemes, diverges in the infrared, thus making ordinary perturbation theory inconsistent at energies of the order of the QCD scale. In order for the screened expansion to be meaningful in the IR, the Landau pole must be shown to disappear from the running coupling constant when the former is used to compute the latter.

In the previous sections, the RG improvement of the screened massive expansion was studied at one loop in two renormalization schemes, namely, the MOM and the SMOM schemes, with the running coupling $\alpha_s(p^2)$ defined in the Taylor scheme ($Z_i^T = 1$). In both schemes, the existence of a nonperturbative mass scale set by the gluon mass parameter m causes the beta function to explicitly depend on the renormalization scale, thus providing a mechanism by which the running of the coupling is allowed to slow down in the infrared. The most notable feature of the RG-improved screened expansion in the MOM and SMOM schemes is indeed the absence of Landau poles in their running couplings (at one loop and for sufficiently small initial values of the coupling), a necessary condition for the consistency of any perturbative approach which aims to be valid at all scales. Instead of diverging, the one-loop MOM running coupling $\alpha_s^{(\text{MOM})}(p^2)$ attains a

maximum at the fixed scale $\mu_* \approx 1.022m$ and then decreases to zero as $p^2 \rightarrow 0$. The one-loop SMOM running coupling $\alpha_s^{(\text{SMOM})}(p^2)$, on the other hand, attains a maximum at a scale that depends on the initial value of the coupling and then saturates to the finite nonzero value $\alpha_s^{(\text{SMOM})}(0) = 32\pi/15N \approx 2.234$ for $N = 3$. Both $\alpha_s^{(\text{MOM})}(p^2)$ and $\alpha_s^{(\text{SMOM})}(p^2)$ have the ordinary perturbative (one-loop) limit in the UV, where the mass effects due to the gluon mass become negligible.

Since in both the renormalization schemes the one-loop running coupling becomes quite large at scales of the order of m , the one-loop predictions of the RG-improved framework are expected to become quantitatively unreliable at low energies. In particular, for comparable initial values of the coupling, the one-loop SMOM running coupling is always larger than the one-loop MOM running coupling in the IR (a feature which is mostly, but not exclusively, due to the saturation of the former at low momenta), so that the perturbative series is expected to converge more slowly in the SMOM scheme than in the MOM scheme.

The MOM and SMOM RG-improved gluon and ghost propagators were computed at one loop, for different initial values of the coupling constant, by numerically integrating the respective anomalous dimensions. We found that the improved propagators have the expected qualitative behavior—as determined, for instance, by the lattice calculations—showing mass generation for the gluons, no mass generation for the ghosts, and the logarithm-to-rational-power UV tails of ordinary perturbation theory.

Under the hypothesis that the one-loop RG-improved results are sufficiently accurate down to $p \approx m$, the initial value of the coupling $\alpha_s(\mu_0^2)$ —one of the two free parameters of the RG-improved screened framework, together with the gluon mass parameter—can be fixed by requiring the improved predictions to match those of the fixed-scale expansion at intermediate energies. The matching was found to work better in the MOM scheme, where the optimal choice $\alpha_s^{(\text{MOM})}(\mu_0^2) = 0.391$ at $\mu_0 = 6.098m$ yields a running coupling, which agrees to less than 1% with its FS analogue over a momentum range of width $\Delta p \approx m$.

The optimization of the value of $\alpha_s(\mu_0^2)$, where the initial renormalization scale μ_0 itself is expressed in units of m , leaves the gluon mass parameter as the only free parameter of the RG-improved framework. This is, of course, highly desirable since (modulo the renormalization conditions) pure Yang–Mills theory has only one free parameter, namely, the coupling or the QCD/YM scale Λ_{YM} . In the optimized framework, m uniquely determines the value of the running coupling at any given renormalization scale and, more generally, it sets the scale for the dimensionful values of the theory. In this sense, optimization enables us to truly regard the gluon mass parameter as the screened-expansion analogue of Λ_{YM} .

The predictions obtained by combining the low-energy results ($p < 1.372m$) for the propagators in the FS screened expansion with the high-energy ones ($p > 1.372m$) of the optimized MOM-scheme RG-improved screened expansion were compared with the lattice data of Ref. [18] and found to be in excellent agreement if the value $m = 0.651$ GeV (obtained by a fit of the data themselves) is used.

The intermediate-scale matching between the FS and RG-improved MOM frameworks proves to be a powerful method for quantitatively predicting the behavior of the gluon and ghost propagators, over a wide range of momenta and from first principles, already at one loop. This reinforces the idea that the full dynamics of YM theory and, perhaps, of full QCD, may be accessible by plain—albeit optimized—PT, by a mere change of the expansion point of the perturbative series, allowing for massive transverse gluons at tree level.

At present, whether the optimized implementations of the screened massive expansion yield a good approximation of the exact results beyond the two-point sector remains an open issue. In this respect, it would be interesting to make use of the present formalism to study the behavior of the ghost-gluon and three-gluon vertices, which have already been computed—for specific kinematic configurations of the external momenta—e.g., on the lattice [70–73] and by the numerical integration of Schwinger–Dyson equations [28,74,75]. Encouraging signs that the screened expansion may work in the three-point sector come from the asymptotic analysis of the fixed-scale-framework gluon propagator $\Delta(p^2)$ in the deep IR, where (cf. Eqs. (A6) and (A9) in the Appendix)

$$Z_\Delta \Delta^{-1}(p^2) \rightarrow \frac{5m^2}{8} + \frac{13}{18} p^2 \ln(p^2/m^2) + O(p^2). \quad (99)$$

Here Z_Δ is a multiplicative renormalization constant, and the logarithmic term comes from the massless ghost loop in the gluon polarization tensor. By the Slavnov–Taylor identities, such a logarithm is inherited by the form factor of the three-gluon vertex [76–78] and is responsible for its characteristic “zero crossing”, i.e., its becoming negative at low energies, a feature which has been confirmed by multiple studies. Thus the behavior of the propagators computed in the screened expansion appears to be consistent with what we know—both analytically and numerically—about the three-point functions. An explicit computation of the latter will help to clarify the extent to which the screened massive expansion is able to describe the full dynamics of pure Yang–Mills theory and QCD.

ACKNOWLEDGMENTS

This research was supported in part by “Piano per la Ricerca di Ateneo 2017/2020—Linea di intervento 2” of the University of Catania.

APPENDIX: FIXED-SCALE SCREENED PT AND THE FUNCTIONS $H(x)$ AND $K(x)$

In Euclidean space, the renormalized one-loop gluon polarization $\Pi_{\text{loop}}^{(R)}$ and ghost self-energy $\Sigma_{\text{loop}}^{(R)}$ computed in the framework of the massive screened expansion are given by [51,52]

$$\begin{aligned}\Pi_{\text{loop}}^{(R)}(p^2) &= -\alpha p^2(F(s) + C), \\ \Sigma_{\text{loop}}^{(R)}(p^2) &= \alpha p^2(G(s) + C'),\end{aligned}\quad (\text{A1})$$

where $s = p^2/m^2$ (m being the gluon mass parameter),

$$\alpha = \frac{3N\alpha_s}{4\pi} = \frac{3Ng^2}{16\pi^2}, \quad (\text{A2})$$

and C and C' are renormalization-scheme-dependent constants. The adimensional functions F and G [51,52] are defined as

$$\begin{aligned}F(x) &= \frac{5}{8x} + \frac{1}{72}[L_a(x) + L_b(x) + L_c(x) + R(x)], \\ G(x) &= \frac{1}{12}[L_g(x) + R_{gh}(x)],\end{aligned}\quad (\text{A3})$$

where the logarithmic functions L_i are

$$\begin{aligned}L_a(x) &= \frac{3x^3 - 34x^2 - 28x - 24}{x} \\ &\quad \times \sqrt{\frac{4+x}{x}} \ln\left(\frac{\sqrt{4+x} - \sqrt{x}}{\sqrt{4+x} + \sqrt{x}}\right), \\ L_b(x) &= \frac{2(1+x)^2}{x^3}(3x^3 - 20x^2 + 11x - 2) \ln(1+x), \\ L_c(x) &= (2 - 3x^2) \ln x, \\ L_g(x) &= \frac{(1+x)^2(2x-1)}{x^2} \ln(1+x) - 2x \ln x,\end{aligned}\quad (\text{A4})$$

and the rational parts R_i are

$$\begin{aligned}R(x) &= \frac{4}{x^2} - \frac{64}{x} + 34, \\ R_{gh}(x) &= \frac{1}{x} + 2.\end{aligned}\quad (\text{A5})$$

The fixed-scale one-loop gluon and ghost propagators computed in the screened expansion can be expressed as

$$\begin{aligned}\Delta(p^2) &= \frac{Z_\Delta}{p^2[F(p^2/m^2) + F_0]}, \\ \mathcal{G}(p^2) &= -\frac{Z_G}{p^2[G(p^2/m^2) + G_0]},\end{aligned}\quad (\text{A6})$$

where Z_Δ and Z_G are multiplicative renormalization factors and F_0 and G_0 are additive renormalization constants. In Refs. [55,59], the latter were optimized by requirements of gauge invariance and minimal sensitivity, and their optimal value was found to be

$$F_0 = -0.876, \quad G_0 = 0.145. \quad (\text{A7})$$

As for the functions F and G , in the limit $x \rightarrow \infty$, we find

$$\begin{aligned}F(x) &\rightarrow \frac{13}{18} \ln x + \frac{17}{18} + \frac{5}{8x} + O(x^{-2}), \\ G(x) &\rightarrow \frac{1}{4} \ln x + \frac{1}{3} + \frac{1}{4x} + O(x^{-2}).\end{aligned}\quad (\text{A8})$$

On the other hand, for $x \rightarrow 0$,⁶

$$\begin{aligned}F(x) &\rightarrow \frac{5}{8x} + \frac{1}{36} \ln x + \frac{257}{216} + \frac{389}{1080}x + O(x^2), \\ G(x) &\rightarrow \frac{5}{24} - \frac{1}{6}x \ln x + \frac{2}{9}x + O(x^2).\end{aligned}\quad (\text{A9})$$

The function $H(x)$, whose derivative is proportional to the beta function of the MOM running coupling, is defined as

$$H(x) = 2G(x) + F(x). \quad (\text{A10})$$

For $x \rightarrow \infty$ we have

$$H(x) \rightarrow \frac{11}{9} \ln x + \frac{29}{18} + \frac{9}{8x} + O(x^{-2}), \quad (\text{A11})$$

whereas for $x \rightarrow 0$

$$H(x) \rightarrow \frac{5}{8x} + \frac{1}{36} \ln x + \frac{347}{216} - \frac{1}{3}x \ln x + \frac{869}{1080}x + O(x^2). \quad (\text{A12})$$

The one-loop MOM running coupling $\alpha_s^{(\text{MOM})}(p^2)$ has the following asymptotic behavior:

$$\alpha_s^{(\text{MOM})}(p^2) \rightarrow \frac{32\pi}{15N} \frac{p^2}{m^2} \left(1 - \frac{2}{45} \frac{p^2}{m^2} \ln \frac{p^2}{m^2}\right) \quad (\text{A13})$$

as $p \rightarrow 0$ and

$$\alpha_s^{(\text{MOM})}(p^2) \rightarrow \frac{12\pi}{11N \ln(p^2/m^2)} \quad (\text{A14})$$

as $p \rightarrow \infty$.

⁶Here we correct an error in Ref. [59], where the coefficients of x in the expansion of $L_a(x)$, $L_b(x)$, and $F(x)$ around $x = 0$ (Eqs. (A7) and (A8) of Ref. [59]) were reported incorrectly.

The expressions for the SMOM scheme beta function and running coupling involve the function $K(x)$, defined as

$$\begin{aligned} K(x) &= \int dx \left\{ H'(x) + \frac{2}{x} G'(x) \right\} \\ &= H(x) - \frac{1}{3} \left\{ \text{Li}_2(-x) + \frac{1}{2} \ln^2 x \right. \\ &\quad \left. + \frac{x^3 + 1}{3x^3} \ln(1+x) - \frac{1}{3} \ln x - \frac{1}{3x^2} + \frac{1}{6x} \right\}, \end{aligned} \quad (\text{A15})$$

where $\text{Li}_2(z)$ is the dilogarithm $\text{Li}_2(z) = \sum_{n=1}^{+\infty} \frac{z^n}{n^2}$. In the limit $x \rightarrow \infty$ we find

$$K(x) \rightarrow \frac{11}{9} \ln x + \frac{\pi^2 + 29}{18} + \frac{5}{8x} + O(x^{-2}), \quad (\text{A16})$$

whereas in the limit $x \rightarrow 0$

$$\begin{aligned} K(x) &\rightarrow \frac{5}{8x} - \frac{1}{6} \ln^2 x + \frac{5}{36} \ln x + \frac{113}{72} + \\ &\quad - \frac{1}{3} x \ln x + \frac{1139}{1080} x + O(x^2). \end{aligned} \quad (\text{A17})$$

The asymptotic limits of the one-loop SMOM running coupling $\alpha_s^{(\text{SMOM})}(p^2)$ are computed to be

$$\alpha_s^{(\text{SMOM})}(p^2) \rightarrow \frac{32\pi}{15N} \left(1 + \frac{4}{15} \frac{p^2}{m^2} \ln^2 \frac{p^2}{m^2} \right) \quad (\text{A18})$$

as $p \rightarrow 0$ and

$$\alpha_s^{(\text{SMOM})}(p^2) \rightarrow \frac{12\pi}{11N \ln(p^2/m^2)} \quad (\text{A19})$$

as $p \rightarrow \infty$.

-
- [1] J. M. Cornwall, *Phys. Rev. D* **26**, 1453 (1982).
[2] C. W. Bernard, *Nucl. Phys.* **B219**, 341 (1983).
[3] J. F. Donoghue, *Phys. Rev. D* **29**, 2559 (1984).
[4] O. Philipsen, *Nucl. Phys.* **B628**, 167 (2002).
[5] A. C. Aguilar and A. A. Natale, *J. High Energy Phys.* **08** (2004) 057.
[6] D. Binosi, L. Chang, J. Papavassiliou, and C. D. Roberts, *Phys. Lett. B* **742**, 183 (2015).
[7] O. Oliveira and P. Bicudo, *J. Phys. G* **38**, 045003 (2011).
[8] A. Cucchieri and T. Mendes, *Proc. Sci.*, LAT2007 (2007) 297.
[9] A. Cucchieri and T. Mendes, *Phys. Rev. D* **78**, 094503 (2008).
[10] A. Cucchieri and T. Mendes, *Phys. Rev. Lett.* **100**, 241601 (2008).
[11] A. Cucchieri and T. Mendes, *Proc. Sci.*, QCD-TNT09 (2009) 026.
[12] I. L. Bogolubsky, E. M. Ilgenfritz, M. Muller-Preussker, and A. Sternbeck, *Phys. Lett. B* **676**, 69 (2009).
[13] O. Oliveira and P. Silva, *Proc. Sci.*, LAT2009 (2009) 226.
[14] D. Dudal, O. Oliveira, and N. Vandersickel, *Phys. Rev. D* **81**, 074505 (2010).
[15] A. Ayala, A. Bashir, D. Binosi, M. Cristoforetti, and J. Rodríguez-Quintero, *Phys. Rev. D* **86**, 074512 (2012).
[16] O. Oliveira and P. J. Silva, *Phys. Rev. D* **86**, 114513 (2012).
[17] G. Burgio, M. Quandt, H. Reinhardt, and H. Vogt, *Phys. Rev. D* **92**, 034518 (2015).
[18] A. G. Duarte, O. Oliveira, and P. J. Silva, *Phys. Rev. D* **94**, 014502 (2016).
[19] P. Boucaud, J. P. Leroy, A. Le Yaouanc, J. Micheli, O. Pène, and J. Rodríguez-Quintero, *J. High Energy Phys.* **06** (2008) 012.
[20] P. Boucaud, J. P. Leroy, A. Le Yaouanc, J. Micheli, O. Pène, and J. Rodríguez-Quintero, *J. High Energy Phys.* **06** (2008) 099.
[21] A. C. Aguilar, D. Binosi, and J. Papavassiliou, *Phys. Rev. D* **78**, 025010 (2008).
[22] A. C. Aguilar and J. Papavassiliou, *Phys. Rev. D* **81**, 034003 (2010).
[23] J. Rodríguez-Quintero, *J. High Energy Phys.* **01** (2011) 105.
[24] D. Dudal, O. Oliveira, and J. Rodríguez-Quintero, *Phys. Rev. D* **86**, 105005 (2012).
[25] A. C. Aguilar, D. Binosi, and J. Papavassiliou, *Phys. Rev. D* **89**, 085032 (2014).
[26] A. C. Aguilar, D. Binosi, and J. Papavassiliou, *Phys. Rev. D* **91**, 085014 (2015).
[27] C. S. Fischer, A. Maas, and J. M. Pawłowski, *Ann. Phys. (Amsterdam)* **324**, 2408 (2009).
[28] A. L. Blum, M. Q. Huber, M. Mitter, and L. von Smekal, *Phys. Rev. D* **89**, 061703(R) (2014).
[29] M. Q. Huber, *Phys. Rev. D* **91**, 085018 (2015).
[30] A. K. Cyrol, M. Q. Huber, and L. von Smekal, *Eur. Phys. J. C* **75**, 102 (2015).
[31] F. Marhauser and J. M. Pawłowski, *arXiv:0812.1144*.
[32] J. Braun, H. Gies, and J. M. Pawłowski, *Phys. Lett. B* **684**, 262 (2010).
[33] J. Braun, A. Eichhorn, H. Gies, and J. M. Pawłowski, *Eur. Phys. J. C* **70**, 689 (2010).
[34] L. Fister and J. M. Pawłowski, *Phys. Rev. D* **88**, 045010 (2013).
[35] F. Siringo, *Phys. Rev. D* **90**, 094021 (2014).
[36] F. Siringo, *Phys. Rev. D* **92**, 074034 (2015).
[37] F. Siringo, *Phys. Rev. D* **88**, 056020 (2013).
[38] P. Watson and H. Reinhardt, *Phys. Rev. D* **82**, 125010 (2010).

GIORGIO COMITINI and FABIO SIRINGO

PHYS. REV. D **102**, 094002 (2020)

- [39] P. Watson and H. Reinhardt, *Phys. Rev. D* **85**, 025014 (2012).
- [40] E. Rojas, J. de Melo, B. El-Bennich, O. Oliveira, and T. Frederico, *J. High Energy Phys.* **10** (2013) 193.
- [41] C. Feuchter and H. Reinhardt, *Phys. Rev. D* **70**, 105021 (2004).
- [42] H. Reinhardt and C. Feuchter, *Phys. Rev. D* **71**, 105002 (2005).
- [43] M. Quandt, H. Reinhardt, and J. Heffner, *Phys. Rev. D* **89**, 065037 (2014).
- [44] D. Zwanziger, *Nucl. Phys.* **B323**, 513 (1989).
- [45] D. Dudal, J. A. Gracey, S. P. Sorella, N. Vandersickel, and H. Verschelde, *Phys. Rev. D* **78**, 065047 (2008).
- [46] D. Dudal, S. P. Sorella, N. Vandersickel, and H. Verschelde, *Phys. Rev. D* **77**, 071501(R) (2008).
- [47] D. Dudal, S. P. Sorella, and N. Vandersickel, *Phys. Rev. D* **84**, 065039 (2011).
- [48] M. Tissier and N. Wschebor, *Phys. Rev. D* **82**, 101701(R) (2010).
- [49] M. Tissier and N. Wschebor, *Phys. Rev. D* **84**, 045018 (2011).
- [50] U. Reinosa, J. Serreau, M. Tissier, and N. Wschebor, *Phys. Rev. D* **89**, 105016 (2014).
- [51] F. Siringo, arXiv:1509.05891.
- [52] F. Siringo, *Nucl. Phys.* **B907**, 572 (2016).
- [53] F. Siringo, *EPJ Web Conf.* **137**, 13016 (2017).
- [54] F. Siringo, *Phys. Rev. D* **94**, 114036 (2016).
- [55] F. Siringo and G. Comitini, *Phys. Rev. D* **98**, 034023 (2018).
- [56] F. Siringo, *Phys. Rev. D* **96**, 114020 (2017).
- [57] G. Comitini and F. Siringo, *Phys. Rev. D* **97**, 056013 (2018).
- [58] F. Siringo, *Phys. Rev. D* **99**, 094024 (2019).
- [59] F. Siringo, *Phys. Rev. D* **100**, 074014 (2019).
- [60] N. K. Nielsen, *Nucl. Phys.* **B97**, 527 (1975); **B101**, 173 (1975).
- [61] R. Kobes, G. Kunstatter, and A. Rebhan, *Phys. Rev. Lett.* **64**, 2992 (1990).
- [62] J. C. Breckenridge, M. J. Lavelle, and T. G. Steele, *Z. Phys. C* **65**, 155 (1995).
- [63] P. M. Stevenson, *Phys. Rev. D* **23**, 2916 (1981).
- [64] P. M. Stevenson, *Nucl. Phys.* **B868**, 38 (2013); **B910**, 469 (2016).
- [65] J. C. Taylor, *Nucl. Phys.* **B33**, 436 (1971).
- [66] L. von Smekal, A. Hauck, and R. Alkofer, *Phys. Rev. Lett.* **79**, 3591 (1997).
- [67] A. Sternbeck, E. M. Ilgenfritz, M. Muller-Preussker, L. von Smekal, A. Williams, and K. Maltman, *Proc. Sci., LAT2007* (2007) 256.
- [68] P. Boucaud, F. De Soto, J. P. Leroy, A. Le Yaouanc, J. Micheli, O. Pène, and J. Rodríguez-Quintero, *Phys. Rev. D* **79**, 014508 (2009).
- [69] P. A. Baikov, K. G. Chetyrkin, and J. H. Kühn, *Phys. Rev. Lett.* **118**, 082002 (2017).
- [70] A. Cucchieri, A. Maas, and T. Mendes, *Phys. Rev. D* **74**, 014503 (2006).
- [71] A. Cucchieri, A. Maas, and T. Mendes, *Phys. Rev. D* **77**, 094510 (2008).
- [72] A. Athenodorou, D. Binosi, P. Boucaud, F. De Soto, J. Papavassiliou, J. Rodríguez-Quintero, and S. Zafeiropoulos, *Phys. Lett. B* **761**, 444 (2016).
- [73] A. G. Duarte, O. Oliveira, and P. J. Silva, *Phys. Rev. D* **94**, 074502 (2016).
- [74] G. Eichmann, R. Williams, R. Alkofer, and M. Vujanovic, *Phys. Rev. D* **89**, 105014 (2014).
- [75] R. Williams, C. S. Fischer, and W. Heupel, *Phys. Rev. D* **93**, 034026 (2016).
- [76] A. C. Aguilar, D. Binosi, D. Ibañez, and J. Papavassiliou, *Phys. Rev. D* **89**, 085008 (2014).
- [77] A. C. Aguilar, M. N. Ferreira, C. T. Figueiredo, and J. Papavassiliou, *Phys. Rev. D* **99**, 094010 (2019).
- [78] A. C. Aguilar, F. De Soto, M. N. Ferreira, J. Papavassiliou, J. Rodríguez-Quintero, and S. Zafeiropoulos, *Eur. Phys. J. C* **80**, 154 (2020).

Thermal extension of the screened massive expansion in the Landau gaugeFabio Siringo* and Giorgio Comitini[†]*Dipartimento di Fisica e Astronomia E. Majorana dell'Università di Catania, INFN Sezione di Catania, Via S. Sofia 64, I-95123 Catania, Italy* (Received 20 January 2021; accepted 25 March 2021; published 19 April 2021)

The massive screened expansion for pure SU(3) Yang-Mills theory is extended to finite temperature in the Landau gauge. All thermal integrals are evaluated analytically up to an external one-dimensional integration, yielding explicit integral representations of analytic functions that can be continued to the whole complex plane. The gluon propagator is first explored in the Euclidean space by making use of parameters obtained from first principles, which were already found to accurately reproduce the lattice data at zero temperature. Within such a scheme, the agreement with the lattice at $T \neq 0$ turns out to be only qualitative. The description improves provided that the parameters are tuned in a temperature-dependent way by a fit to the data, carried out separately for each component of the propagator; in particular, the transverse component closely follows the lattice data, while the agreement of the longitudinal component with the data is poor at small momenta and moderately high temperatures. The dispersion relations of the quasi-gluon are then extracted from the pole trajectory in the complex plane using the fitted parameters. A crossover is found for the mass, suppressed by temperature like an order parameter in the confined phase, while increasing like an ordinary thermal mass in the deconfined phase.

DOI: [10.1103/PhysRevD.103.074014](https://doi.org/10.1103/PhysRevD.103.074014)**I. INTRODUCTION**

In the last decades, considerable efforts have been devoted to the study of the complex behavior of quarks and gluons under the extreme conditions which are reached in heavy-ion collisions. In principle, the dynamical and thermal properties of a quark-gluon plasma should descend from the relatively simple Lagrangian of the SU(3) gauge theory which describes QCD. However, things are not so easy because the standard perturbative approach breaks down in the strong-coupling IR limit and is also plagued by further resummation problems at any finite temperature. As a matter of fact, we still miss a full theoretical treatment of the problem.

Even the pure gauge theory, without quarks, is not fully understood, despite its relevance for describing the quark-gluon plasma. Many important advances have been made by the numerical simulation of the pure Yang-Mills (YM) Lagrangian on a lattice, providing insights into the gluon dynamics and the phase diagram. Among them, the confirmation of a dynamically generated gluon mass [1–8], as

predicted by Cornwall in 1982 [9], and the occurrence of a phase transition, with the gluons that become confining below a critical temperature [10–12].

It would be a desirable progress if the dynamical and transport parameters, like masses, widths, dispersion relations, transport coefficients, etc., which are currently regarded as phenomenological parameters [13–16], could be directly evaluated from first principles. That program might be accomplished in part if the elementary correlators and their analytic properties were known in the Minkowski space. Unfortunately, all lattice calculations and most numerical works provide information in the Euclidean space and the analytic continuation is a difficult ill-defined problem for the numerical data [17].

In the last years, a very predictive analytical method has been developed [18–21] by a mere change of the expansion point of ordinary perturbation theory (PT) for the exact gauge-fixed Becchi-Rouet-Stora-Tyutin (BRST) invariant YM Lagrangian, yielding a screened massive expansion which is safe in the IR while recovering the correct results of ordinary PT in the UV. At one-loop and zero temperature, the screened expansion provides analytical results which are in excellent agreement with the lattice and can be easily continued to Minkowski space [21–25]. Thus the method provides a way to extract dynamical details like masses and damping rates from first principles.

In this paper, the formalism is extended to a finite temperature $T \neq 0$, with the aim to provide a complementary tool for the study of the gluon plasma from first

*fabio.siringo@ct.infn.it

†giorgio.comitini@dfa.unict.it

Published by the American Physical Society under the terms of the Creative Commons Attribution 4.0 International license. Further distribution of this work must maintain attribution to the author(s) and the published article's title, journal citation, and DOI. Funded by SCOAP³.

principles. As briefly discussed in Refs. [26,27], the screened expansion can be extended to finite temperature, providing a quasiparticle picture for the gluon which is damped, with a very short finite lifetime, and canceled from the asymptotic states. Here, we give a full account of the details of the calculation and report a comprehensive set of results for the gluon sector, including propagators, analytic properties, poles, masses, widths and dispersion relations. We discuss different optimization strategies and, by a comparison with the available lattice data, we explore how robust the screened expansion is when it is extended to finite temperature.

While the existence of a screening mass mitigates the effects of the hard thermal loops, several problems arise at a finite temperature, ranging from the temperature dependence of the optimal mass scale, to the analytic continuation of the numerical integrals. Actually, even if a formal extension to finite temperature is straightforward and based on standard thermal Feynman graphs, the ambition to extract analytical results requires a quite tedious and lengthy analytical calculation of the integrals and, even so, a final one-dimensional numerical integration cannot be avoided. Nonetheless, the resulting numerical integrals are shown to define analytic functions which can be evaluated in the complex plane. Then, the poles of the gluon propagator and the resulting dispersion relations can be easily extracted numerically.

Overall, despite the expected difficulties, the one-loop screened expansion seems to be reliable at low temperature, with correct predictions which become less quantitative at high temperature, especially for the longitudinal sector, when compared with the lattice data.

At $T = 0$, the one-loop approximation is quite sensitive to the renormalization scheme and to the subtraction point, but it can be shown to be basically *tangent* to the exact result, which is approached for a special choice of the ratio between the gluon mass parameter m and the renormalization scale μ . Here, m is just a mass parameter which defines the shift of the expansion point [18,19,24,25], not to be confused with the physical mass of the gluon. It seems that, for that special ratio μ/m , the higher order terms become negligible, yielding very accurate analytical expressions for the propagators. While that special ratio is scheme dependent, it can be determined from first principles by monitoring some identities which must be fulfilled by the exact propagators, like the Nielsen identities, which express the gauge invariance of the poles [21]. We must mention that, once the ratio is optimized in the complex *Minkowski* space, where the poles are defined, the propagators are found in excellent agreement with the lattice data in the *Euclidean* space. Thus, the optimized analytical expression is not just a good interpolation formula, but a very good approximation for the whole analytic function which is defined in the complex plane. Moreover, at the optimal ratio μ/m there is only one energy scale left in the

calculation, say the mass parameter m , so that its actual value becomes irrelevant, since it can be used as energy units and is eventually determined by a comparison with the phenomenology. For instance, sharing the same units of the lattice data, a value $m = 0.656$ GeV was established in previous works [21,24].

At a finite temperature $T \neq 0$, there is a third energy scale and the optimal parameters m , μ become two independent functions of temperature, $m(T)$, $\mu(T)$, since their optimal ratio is expected to depend on T . In principle, one could proceed as for $T = 0$ and fix the optimal ratio by monitoring the gauge-invariance of the poles. However, that would at least require a knowledge of the thermal propagators in a generic covariant gauge, while the present formalism has been developed only in the Landau gauge. Moreover, no lattice data are available for a comparison in a generic gauge and finite T . This is not a theoretical limitation by itself, but leads to a weakening of the control of the accuracy.

That of the gauge invariance of the poles actually is an additional problem one encounters when extending the theory to finite T [28–31]. Even though the poles of the propagator are constrained to be nonperturbatively gauge-independent by, e.g., the Nielsen identities [32], in the thermal formalism different powers of the coupling constant coexist at the same loop order when hard-thermal-loop effects are taken into account, so that consistent resummation schemes are needed in order to obtain truly gauge-invariant results for the poles' position. To first order in the coupling, this can be shown to only affect the imaginary part of the dispersion relations, i.e., the gluon's damping rate. In this work no attempt has been made to implement such resummation schemes or to keep under control the accuracy of the approximation with respect to the issue of gauge invariance. Whereas at low, nonzero temperatures the screening provided by the gluon's mass may somewhat suppress the effects of the required resummed terms, at higher temperatures the latter are expected to become non-negligible, causing our predictions for the gluon damping rate to become less and less reliable as the temperature is increased.

In the Landau gauge, we explored two complementary strategies and checked that the qualitative description which emerges is robust enough and does not depend on the optimization choice. The first, simpler, strategy consists in using the same m and μ parameters that work at $T = 0$. That choice was already made in Ref. [26] (albeit with different values for the parameters) and makes sense at low temperature where we expect that $m(T) \approx m(0)$ and $\mu(T) \approx \mu(0)$. With this choice, we find the correct qualitative behavior without any adjustment of parameters. In particular, the longitudinal propagator shows a non-monotonic behavior with a crossover at $T/m(0) \approx 0.15$. However, the agreement with the lattice data is not quantitative, and the predicted transition temperature is

too small ($T \approx 100$ MeV), thus indicating that we are already outside the safe low-temperature range. Nonetheless, the disagreement can be absorbed in part by a temperature-dependent optimization of the expansion.

Thus, as a second strategy, we relax the constraints of m and μ being equal to their $T = 0$ values and regard $m(T)$ and $\mu(T)$ as independent unknown functions. Reversing the argument that led to their optimization at $T = 0$, we tune the unknown functions in the Euclidean space by looking for the best agreement with the lattice data. Then, *assuming* that the higher-order terms are smaller when the agreement is better, the optimized propagators are continued to Minkowski space where the pole location gives information on the dispersion relations of the quasi-gluons at finite temperature. We anticipate that, from a strictly quantitative point of view, the agreement with the lattice is not comparable with the excellent result which was reached at $T = 0$. Moreover, while the transverse propagator is generally well described, the longitudinal projection becomes very poor deep in the IR for moderately high temperatures. Since most of the deviation occurs below 500–700 MeV, we expect that the predictions for the pole position at high momenta might not be affected too much. We stress that there are no data available in the Minkowski space for a comparison, thus evidencing the power of the method for exploring the analytic properties of the propagators.

Irrespective of the optimization criterion, we confirm the finding of Ref. [26] and the quasi-gluon scenario which was described by Stingl [33], with a gluon which has a very short finite lifetime and can only exist as a short-lived intermediate state at the origin of a gluon-jet event.

This paper is organized as follows. In Sec. II we review the setup and main features of the screened massive expansion and its extension to finite temperatures. In Sec. III we present our results for the Landau gauge gluon propagator at $T \neq 0$ and vanishing Matsubara frequency, $\omega = 0$. In Sec. IV we derive the dispersion relations for the quasi-gluons at finite temperatures. In Sec. V we discuss our results and present our conclusions. In the Appendix we explicitly compute the gluon polarization and ghost self-energy at finite temperatures using the screened massive expansion.

II. THE SCREENED EXPANSION AND ITS EXTENSION TO FINITE TEMPERATURE

In a linear covariant ξ -gauge, the gauge-fixed BRST invariant Lagrangian of pure Yang-Mills SU(N) theory is

$$\mathcal{L} = \mathcal{L}_{\text{YM}} + \mathcal{L}_{\text{fix}} + \mathcal{L}_{\text{FP}}, \quad (1)$$

where

$$\begin{aligned} \mathcal{L}_{\text{YM}} &= -\frac{1}{2} \text{Tr}(\hat{F}_{\mu\nu} \hat{F}^{\mu\nu}), \\ \mathcal{L}_{\text{fix}} &= -\frac{1}{\xi} \text{Tr}[(\partial_\mu \hat{A}^\mu)(\partial_\nu \hat{A}^\nu)], \end{aligned} \quad (2)$$

and \mathcal{L}_{FP} is the ghost term arising from the Faddeev-Popov (FP) determinant. The tensor operator is defined as

$$\hat{F}_{\mu\nu} = \partial_\mu \hat{A}_\nu - \partial_\nu \hat{A}_\mu - ig[\hat{A}_\mu, \hat{A}_\nu], \quad (3)$$

where the gauge field operators satisfy the SU(N) algebra

$$\begin{aligned} \hat{A}^\mu &= \sum_a \hat{X}_a A_a^\mu, \\ [\hat{X}_a, \hat{X}_b] &= if_{abc} \hat{X}_c, \quad f_{abc} f_{abc} = N\delta_{ad}. \end{aligned} \quad (4)$$

In the standard PT formalism, the total action is split as $S_{\text{tot}} = S_0 + S_I$, where the quadratic part can be written as

$$\begin{aligned} S_0 &= \frac{1}{2} \int A_{a\mu}(x) \delta_{ab} \Delta_0^{-1\mu\nu}(x, y) A_{b\nu}(y) d^4x d^4y \\ &+ \int c_a^*(x) \delta_{ab} \mathcal{G}_0^{-1}(x, y) c_b(y) d^4x d^4y, \end{aligned} \quad (5)$$

while the interaction contains three vertices

$$\begin{aligned} S_I &= \int d^4x [\mathcal{L}_{3g} + \mathcal{L}_3 + \mathcal{L}_4], \quad (6) \\ \mathcal{L}_{3g} &= -gf_{abc} (\partial_\mu A_{a\nu}) A_b^\mu A_c^\nu, \\ \mathcal{L}_{4g} &= -\frac{1}{4} g^2 f_{abc} f_{ade} A_{b\mu} A_{c\nu} A_d^\mu A_e^\nu, \\ \mathcal{L}_{ccg} &= -gf_{abc} (\partial_\mu c_a^*) c_b A_c^\mu. \end{aligned} \quad (7)$$

In Eq. (5), the standard free-particle propagators for gluons and ghosts, Δ_0 and \mathcal{G}_0 respectively, are defined by their Fourier transforms

$$\begin{aligned} \Delta_0^{\mu\nu}(p) &= \Delta_0(p) [t^{\mu\nu}(p) + \xi \ell^{\mu\nu}(p)], \\ \Delta_0(p) &= \frac{1}{-p^2}, \quad \mathcal{G}_0(p) = \frac{1}{p^2}, \end{aligned} \quad (8)$$

where the transverse and longitudinal projectors are used

$$t_{\mu\nu}(p) = g_{\mu\nu} - \frac{p_\mu p_\nu}{p^2}, \quad \ell_{\mu\nu}(p) = \frac{p_\mu p_\nu}{p^2}. \quad (9)$$

Later, we will take the limit $\xi \rightarrow 0$ and use the Landau gauge which is a renormalization group (RG) fixed point and is the most studied gauge on the lattice. In the above equations, the fields and the coupling must be regarded as renormalized objects and the inclusion of the usual set of counterterms is understood in the total Lagrangian.

The massive screened version of PT was developed in Refs. [18–20]. At $T = 0$ and in a generic covariant gauge, the method is very accurate and predictive if the expansion is optimized by the constraints of BRST symmetry [21,24,25]. The expansion arises by a mere change of the expansion point of ordinary PT. Following Refs. [19,21], the new *massive* expansion is recovered by just adding a transverse mass term to the quadratic part of the action and subtracting it again from the interaction, leaving the total action unchanged. In more detail, we add and subtract the action term

$$\delta S = \frac{1}{2} \int A_{a\mu}(x) \delta_{ab} \delta \Gamma^{\mu\nu}(x, y) A_{b\nu}(y) d^4x d^4y, \quad (10)$$

where the vertex function $\delta \Gamma$ is a shift of the inverse propagator,

$$\delta \Gamma^{\mu\nu}(x, y) = [\Delta_m^{-1\mu\nu}(x, y) - \Delta_0^{-1\mu\nu}(x, y)], \quad (11)$$

and $\Delta_m^{\mu\nu}$ is a new *massive* free-particle propagator,

$$\Delta_m^{-1\mu\nu}(p) = (-p^2 + m^2) t^{\mu\nu}(p) + \frac{-p^2}{\xi} \ell^{\mu\nu}(p). \quad (12)$$

Adding that term is equivalent to substituting the new massive propagator $\Delta_m^{\mu\nu}$ for the old massless one $\Delta_0^{\mu\nu}$ in the quadratic part. Thus, the new expansion point is a massive free-particle propagator for the gluon, which is much closer to the exact propagator in the IR. The mass-shift parameter m is irrelevant in the UV, but acts as a natural cutoff which screens the theory in the IR.

Of course, in order to leave the total action unaffected by the change, the same term is subtracted from the interaction, providing a new interaction vertex $-\delta \Gamma$, a two-point vertex which can be regarded as a new counterterm. Dropping all color indices in the diagonal matrices and inserting Eqs. (8) and (12) in Eq. (11), the vertex is just the transverse mass shift of the quadratic part,

$$-\delta \Gamma^{\mu\nu}(p) = -m^2 t^{\mu\nu}(p), \quad (13)$$

and must be added to the standard set of vertices arising from Eq. (7). The new vertex is now part of the interaction, even if it does not depend on the coupling. Thus, the expansion has the nature of a δ -expansion, since different powers of the coupling coexist at each order in powers of the total interaction.

The proper gluon polarization and ghost self energy can be evaluated, order by order, by the modified PT. In all Feynman graphs, any internal gluon line is a massive free-particle propagator $\Delta_m^{\mu\nu}$ and the new insertions of the (transverse) two-point vertex $\delta \Gamma^{\mu\nu}$ are denoted by a cross, as shown in Fig. 1. For further details we refer to Refs. [18,19,21].

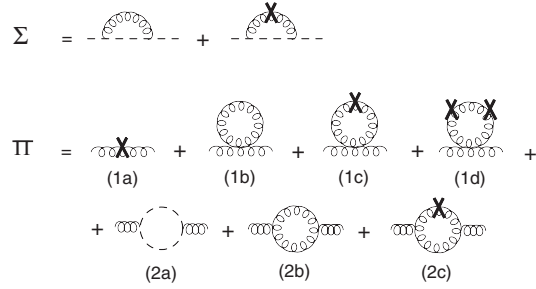


FIG. 1. Two-point graphs with no more than three vertices and no more than one loop. The cross is the transverse mass counterterm of Eq. (13) and is regarded as a two-point vertex. In the Appendix, a detailed description of the calculation at finite T is given for all the polarization graphs in the figure.

Since the total gauge-fixed FP Lagrangian is not modified and because of BRST invariance, the longitudinal polarization is known exactly and is zero. At $T = 0$, the exact polarization and the dressed gluon propagator are defined by a single function,

$$\Pi^{\mu\nu}(p) = \Pi(p) t^{\mu\nu}(p), \quad (14)$$

so that, in the Landau gauge, the exact gluon propagator is transverse,

$$\Delta_{\mu\nu}(p) = \Delta(p) t_{\mu\nu}(p), \quad (15)$$

and defined by the scalar function $\Delta(p)$. This feature is lost at any finite temperature $T > 0$, since Lorentz invariance is broken, and two scalar functions are required instead. In that perspective, it is convenient to maintain the Lorentz structure explicit and to switch to the Euclidean formalism. Then, denoting with p^2 the Euclidean squared momentum, the exact (dressed) gluon and ghost propagators can be written as

$$\begin{aligned} \Delta^{-1}_{\mu\nu}(p) &= (p^2 + m^2) t_{\mu\nu}(p) + \frac{p^2}{\xi} \ell_{\mu\nu}(p) - \Pi_{\mu\nu}(p), \\ \mathcal{G}^{-1}(p) &= -p^2 - \Sigma(p), \end{aligned} \quad (16)$$

where $t_{\mu\nu}$ and $\ell_{\mu\nu}$ are the Euclidean projectors of Eq. (A5). The proper gluon polarization $\Pi_{\mu\nu}$ and the ghost self-energy Σ are the sum of all one-particle-irreducible (1PI) graphs in the screened expansion, including all counterterms. In Fig. 1, the two-point 1PI graphs are shown up to one-loop and third order in the delta expansion. In the exact self-energies, we can single out the tree-level terms and write

$$\begin{aligned}\Pi_{\mu\nu}(p) &= m^2 t_{\mu\nu}(p) - p^2 t_{\mu\nu}(p) \delta Z_A + \Pi_{\mu\nu}^{\text{loop}}(p), \\ \Sigma(p) &= p^2 \delta Z_c + \Sigma^{\text{loop}}(p),\end{aligned}\quad (17)$$

where the first term $m^2 t_{\mu\nu}(p)$ is the tree graph (1a) in Fig. 1 and arises from the insertion of the new two-point vertex $-\delta\Gamma_{\mu\nu}$ of Eq. (13). We observe that this first tree term cancels the mass shift of the gluon propagator in Eq. (16). Indeed, the physical mass of the gluon arises from the loops and is not merely given by the mass-shift parameter m^2 . The other tree-level terms, $-p^2 t_{\mu\nu} \delta Z_A$, $p^2 \delta Z_c$, are not shown in Fig. 1 and are the usual field-strength renormalization counterterms. Their UV diverging parts are not affected by the mass parameter and are the same of standard PT [18,19]. The proper functions, $\Pi_{\mu\nu}^{\text{loop}}$, Σ^{loop} , are given by the sum of all 1PI graphs containing loops. The finite parts of δZ_A , δZ_c are arbitrary and depend on the scheme and on the renormalization scale μ [24,25]. The diverging parts of δZ_A , δZ_c cancel the UV divergences of the functions $\Pi_{\mu\nu}^{\text{loop}}/p^2$ and Σ^{loop}/p^2 which become finite dimensionless functions of the variable p_μ/m . They are defined up to a constant which depends on the dimensionless renormalization scale parameter $t = \mu^2/m^2$. Thus, at $T = 0$, there are two energy scales in the calculation, m and μ . For instance, in a momentum subtraction scheme (MOM) and in the Landau gauge, the one-loop dressed propagators can be written as

$$\begin{aligned}\Delta(p)^{-1} &= p^2 - Ng^2[\Pi^{(1)}(p) - \Pi^{(1)}(\mu)], \\ \mathcal{G}(p)^{-1} &= -p^2 - Ng^2[\Sigma^{(1)}(p) - \Sigma^{(1)}(\mu)],\end{aligned}\quad (18)$$

having made explicit the dependence on N and g^2 as factors in the one-loop functions $\Pi^{(1)}$, $\Sigma^{(1)}$, according to the notation of Appendix A, where all details of the calculation are reported. In Eq. (18), an explicit choice has been made for the finite parts of the renormalization constants δZ_A , δZ_c . Of course, that choice depends on the scheme and on the renormalization scale μ . A more general way to get rid of all the scheme-dependent parameters, including the renormalized coupling g^2 , was discussed in previous papers on the screened expansion [18,19,21,24], where two dimensionless one-loop functions were defined (see Appendix B.1 for their explicit expressions),

$$\begin{aligned}\pi_1(p^2/m^2) &= -\left(\frac{16\pi^2}{3}\right) \frac{\Pi^{(1)}(p)}{p^2}, \\ \sigma_1(p^2/m^2) &= \left(\frac{16\pi^2}{3}\right) \frac{\Sigma^{(1)}(p)}{p^2},\end{aligned}\quad (19)$$

so that the one-loop propagators in Eq. (18) can be recast as functions of the dimensionless variable $s = p^2/m^2$,

$$\begin{aligned}p^2 \Delta(p) &= \frac{z_\pi}{\pi_1(s) + \pi_0}, \\ p^2 \mathcal{G}(p) &= -\frac{z_\sigma}{\sigma_1(s) + \sigma_0},\end{aligned}\quad (20)$$

where z_π and z_σ are irrelevant normalization constants while all the scheme-dependent parameters are embedded in the two constants π_0 and σ_0 . With some abuse of language, we will refer to them as *renormalization* constants. Equation (20) is quite general since it does not require any specific renormalization scheme to be defined. Of course, our ignorance about those constants reflects a well-known weakness of the one-loop approximation which depends on the details of the renormalization scheme and on the actual value of the renormalization scale μ . In this sense, we still have two scales, m and μ , and the arbitrary choice of their ratio $t = \mu^2/m^2$ somehow determines the actual value of the renormalization constants π_0 and σ_0 .

A nice feature of the one-loop result is its apparent *tangency* to the exact result which is approached for special values of the renormalization constants. Those values are equivalent to a choice of the best renormalization scale μ , where the approximation is more effective. It is just an example of the optimized perturbation theory by variation of the renormalization scheme [34,35]. There might be a special scale μ where the expansion converges more quickly and the higher order terms are minimal. Thus, from first principles, we could determine the optimal constants by monitoring some identities which must be satisfied by the exact propagators. For instance, in Ref. [21], the Nielsen identities [36,37] were used, which are a direct consequence of BRST symmetry. From the identities, one can prove the gauge-parameter-independence of the poles and residues of the exact gluon propagator [21]. Then, we might expect that the renormalization constants are optimal when the poles have a minimal sensitivity to the gauge parameter. It is remarkable that the optimized one-loop propagators turn out to be in excellent agreement with the lattice data in the IR. Notably, while the comparison with the data requires an analytic continuation to the Euclidean space, the poles are found in the complex plane. Thus, the one-loop propagators in Eq. (20) are not just one of the many interpolation formulas for the data, but they provide a very accurate analytic function in the whole complex plane. The existence of complex poles is one of the most important predictions of the screened expansion. While a thermal mass and a finite damping rate are expected by PT at high temperature, the existence of finite intrinsic values at $T = 0$ can be regarded as a proof of confinement as first discussed by Stingl [33]. The quasi-gluon has a finite lifetime and can only exist as a short-lived intermediate state. However, at finite temperature, the quasi-gluons play an important role for determining the thermal properties of the hot plasma. Thus, a finite temperature extension of the screened expansion is required

for a full study of the dispersion relations which emerge from the pole location.

At a finite temperature $T > 0$, Eqs. (16) and (17) are still valid, but the one-loop graphs in Fig. 1 acquire a finite thermal part which must be added to the vacuum (diverging) contribution at $T = 0$. The thermal parts are finite and no further renormalization is required. We only have to add the thermal parts to the self-energies in Eq. (17).

We write the Euclidean four-vector as $p^\mu = (\mathbf{p}, \omega)$ where $\omega = p_4 = -ip_0$, while the Lorentz four-vector was (p_0, \mathbf{p}) . In the finite-temperature formalism, $\omega = \omega_n = 2\pi nT$ and the Euclidean integral is replaced by a sum over n and by a three-dimensional integration,

$$\int \frac{d^4 p}{(2\pi)^4} \rightarrow T \sum_n \int \frac{d^3 \mathbf{p}}{(2\pi)^3}, \quad (21)$$

Since Lorentz invariance is obviously broken, we introduce a transverse projector $P_{\mu\nu}^T$, orthogonal to the fourth Euclidean direction, and its longitudinal complement $P_{\mu\nu}^L$, as defined in Eq. (A4), so that the gluon polarization and propagator in Eqs. (16) and (17) can be written in the Landau gauge, $\xi = 0$, as

$$\begin{aligned} \Pi_{\mu\nu}(p, T) &= \Pi_L(p, T)P_{\mu\nu}^L(p) + \Pi_T(p, T)P_{\mu\nu}^T(p), \\ \Delta_{\mu\nu}(p, T) &= \Delta_L(p, T)P_{\mu\nu}^L(p) + \Delta_T(p, T)P_{\mu\nu}^T(p), \end{aligned} \quad (22)$$

where the projected one-loop dressed functions are

$$\begin{aligned} \Delta_T(p, T)^{-1} &= p^2 + p^2 \delta Z_A - Ng^2 \Pi_T^{(1)}(p, T), \\ \Delta_L(p, T)^{-1} &= p^2 + p^2 \delta Z_A - Ng^2 \Pi_L^{(1)}(p, T). \end{aligned} \quad (23)$$

and $\Pi_{L,T}^{(1)}$ are the one-loop projected polarizations, evaluated by projection of the one-loop graphs in Fig 1, omitting the tree graphs. As discussed in Appendix B, each graph contributing to $\Pi_{L,T}^{(1)}$ can be split as

$$\Pi_{L,T}^{(1)}(p, T) = [\Pi_{L,T}^{(1)}]_{Th} + [\Pi_{L,T}^{(1)}]_V, \quad (24)$$

where the vacuum part $[\Pi_{L,T}^{(1)}]_V = \Pi_{L,T}^{(1)}(p, 0)$ is the same graph evaluated at $T = 0$ and does not depend on T , while the thermal part, $[\Pi_{L,T}^{(1)}]_{Th}$, vanishes at $T = 0$. Thus, we can generalize Eqs. (19) and (20) and define dimensionless functions

$$\begin{aligned} [\pi_{L,T}(p, T)]_V &= -\left(\frac{16\pi^2}{3}\right) \frac{[\Pi_{L,T}^{(1)}(p, T)]_V}{p^2} = \pi_1(s), \\ [\pi_{L,T}(p, T)]_{Th} &= -\left(\frac{16\pi^2}{3}\right) \frac{[\Pi_{L,T}^{(1)}(p, T)]_{Th}}{p^2}, \end{aligned} \quad (25)$$

so that the projections of the one-loop propagator can be recast as

$$p^2 \Delta_{L,T}(p, T) = \frac{z_\pi}{\pi_1(s) + \pi_0 + [\pi_{L,T}(p, T)]_{Th}}. \quad (26)$$

In this form Eq. (26) is quite general since it does not require any specific renormalization scheme to be defined. All the scheme-dependent parameters are embedded in the *renormalization* constant π_0 .

It is not obvious that the same scale μ and constant π_0 which were optimal at $T = 0$ are still optimal at finite T . Indeed, they might depend on T and even take a different value for the different projections. Moreover, the mass parameter m , which was the only energy scale left after optimization at $T = 0$, might take a value $m(T)$ which depends on T . Thus we have three energy scales: the optimal $\mu(T)$, the mass parameter $m(T)$ and T itself. In other words, according to Eq. (26), at any T and in units of $m(0)$ we have two free parameters, the ratio $m(T)/m(0)$ and the optimal renormalization constant $\pi_0(T)$. Having the role of variational parameters, to be optimized, their best values might be different for the two projections.

While at $T = 0$ the optimal constant π_0 was determined from first principles [21], by requiring a minimal sensitivity of the poles to any change of the gauge parameter, here we have the less ambitious aim of exploring if a set of optimal parameters does exist such that the screened expansion is able to describe the lattice data with reasonable accuracy. Thus, we work in the Landau gauge and, for each value of $T > 0$, we fix the parameters by a fit of the available lattice data in the Euclidean space.

At low temperature, as we said, we also explored the alternative of maintaining the parameters fixed at their optimal value for $T = 0$, in order to give a general description at finite T from first principles, without any input from the lattice and from the known phenomenology. Of course, this approach can only be reliable if T is very low and the thermal effects are small. However, even extrapolating at higher temperatures, the qualitative predictions turn out to be in agreement with the data. Thus, the screened expansion is able to capture the main features of gluon thermodynamics at finite temperature. This is a very important aspect, since our final aim will be to extract some dynamical properties of the quasi-gluons, like the dispersion relations, which cannot be measured on the lattice. Moreover, even qualitative properties, like the existence of complex poles, are of central interest for understanding the behavior of the gluon plasma at high temperature and its phase transition.

In order to fulfill that program, once optimized by one of the two alternatives discussed above, the gluon propagator must be continued to the complex plane. This is a straightforward step if the one-loop graphs are expressed as analytic functions of the Euclidean momentum. A very detailed but tedious analytical evaluation of the integrals is reported in the Appendix. Most of the integrals were

encountered in a study of the Curci-Ferrari model [38]. We basically use the same method for decomposing the integrals. However, in the screened expansion there are also some different graphs, namely the crossed graphs in Fig. 1, with one insertion of the mass counterterm. Their explicit expressions are obtained by a derivative in the Appendix.

Unfortunately, at finite T , not all the multidimensional integrals can be evaluated analytically and an external one-dimensional numerical integration cannot be avoided for almost all the one-loop graphs. Thus, as shown in the Appendix, all the graphs can be written as analytic functions which are defined by integral representations. The remaining integration can be carried out numerically for any complex value of the external momentum, provided that no singularity is encountered along the integration path. Actually, in general, the analytic continuation of integral functions is not trivial. As discussed in Ref. [39], we must check that the external integration on the real axis does not cross any singular point of the logarithmic functions. Otherwise, a modified path must be chosen before the analytic continuation can be undertaken. As shown in Ref. [26], by inspection of the explicit expressions, the existence of singular points on the integration path can be ruled out in the present case. For instance, denoting with $\Omega = p_0$ and $p^\mu = (\Omega, \mathbf{p})$ the external momentum in Minkowski space, the analytic continuation of the thermal integral $I^{\alpha\beta}(y, -i\Omega)$ is defined by the integral representation of Eq. (B30), where y is the external three vector modulus, $y = |\mathbf{p}|$. We can continue the external energy Ω to the complex plane if there are no singular points on the positive real axis of the integration variable. However, some branch cuts might be present, originating at the singular branch point of the logarithmic function in Eq. (B29) which reads

$$L_\beta(z_\alpha; y, q) = \log \left[\frac{z_\alpha^2 + \epsilon_{y+q,\beta}^2}{z_\alpha^2 + \epsilon_{y-q,\beta}^2} \right], \quad (27)$$

where the complex variable z_α is defined as $z_\alpha = i\Omega \pm i\sqrt{q^2 + \alpha^2}$ and $\epsilon_{y\pm q,\beta}^2 = (y \pm q)^2 + \beta^2$. Here α and β are masses equal to 0 or m and q is the integration variable. Assuming the existence of a branch point at $q = q_0$ on the real axis, the latter must satisfy

$$\pm 2q_0 y = \alpha^2 - \beta^2 - y^2 + \Omega^2 \pm 2\Omega\sqrt{q_0^2 + \alpha^2}, \quad (28)$$

where the \pm signs are independent of each other. Taking a complex energy $\Omega = \text{Re}\Omega + i\text{Im}\Omega$ with $\text{Im}\Omega > 0$, the imaginary part of Eq. (28) gives

$$\text{Re}\Omega = \mp \sqrt{q_0^2 + \alpha^2}, \quad (29)$$

and substituting back in the real part we obtain

$$\epsilon_{y\pm q_0,\beta}^2 + (\text{Im}\Omega)^2 = 0, \quad (30)$$

which is never satisfied unless $\text{Im}\Omega = \beta = 0$. Thus, if Ω is not real, the branch point q_0 cannot be real and the integral over q , on the real axis, defines an analytic function of Ω . The same argument holds for the other thermal integrals in Appendix B. Thus, we can safely continue the numerical integrals from the Euclidean space ($\text{Re}\Omega = 0, \text{Im}\Omega > 0$) to the whole upper half-plane. Moreover, in the large wavelength limit $y \rightarrow 0$, there are no branch points at all because the logarithmic function can be written as $L_\beta(z_\alpha; y, q) \approx \log[1 + \mathcal{O}(y)]$ and the argument of the log does not vanish if y is small enough.

Having ruled out the existence of singularities along the integration path, the poles of the gluon propagator and the dispersion relations can be easily extracted numerically in the complex plane by the integral representation of the thermal integrals which are derived in Appendix B.

III. THE GLUON PROPAGATOR AT FINITE T

The longitudinal and transverse projections of the polarization graphs entering in Eq. (26) are decomposed as the sum of more basic Euclidean integrals in Appendix A, for all the one-loop graphs of Fig. 1. The explicit thermal parts of those integrals are presented in Appendix B by integral representations. For any given value of the external three-momentum $y = \sqrt{\mathbf{p}^2}$ and Euclidean frequency $\omega = p_4 = 2\pi nT$, the one-dimensional integrals are evaluated numerically by a simple integration on the real axis and the result is inserted in Eq. (26). We will first explore the projected propagators for π_0 and m fixed at their zero-temperature values which were determined from first principles in Ref. [21]. Then, we will show how their values can be optimized by a comparison with the available lattice data.

A. Expansion optimized at $T=0$

In the low-temperature limit, we assume that the optimal renormalization constant $\pi_0(T)$ and mass parameter $m(T)$ can be replaced by their zero-temperature values $\pi_0 = -0.876$ and $m(0) = m_0 = 656$ MeV, as determined in Ref. [21] by requiring a minimal sensitivity of the pole structure to the gauge parameter. Strictly speaking, in the Landau gauge, that condition fixes π_0 , while m_0 is the only energy scale left and is fixed in order to match the energy units of the lattice data.

Let us first explore the behavior of the gluon propagators as a function of T in the limit $\omega \rightarrow 0$, where $p^2 = \mathbf{p}^2$, which is the most studied case on the lattice [11,12]. The longitudinal and transverse propagators are shown in units of m_0 in Figs. 2 and 3, respectively. The former were multiplicatively renormalized by requiring that

$$\Delta_{L,T}(p, T)|_{\omega=0, |\mathbf{p}|=\mu_0} = \frac{1}{\mu_0^2} \quad (31)$$

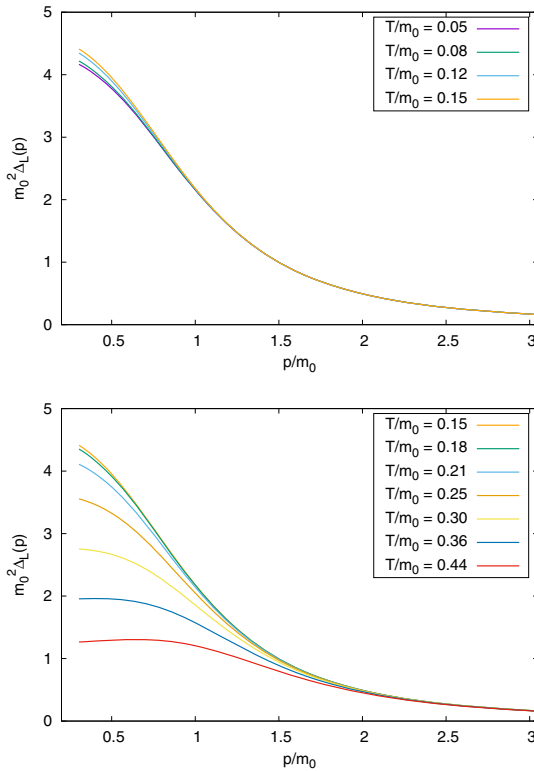


FIG. 2. Longitudinal propagator Δ_L in units of $m_0 = m(0)$ at $\omega = 0$ for the low temperature range $T/m_0 < 0.15$ (top) and the high temperature range $T/m_0 > 0.15$ (bottom). The renormalization constant and the mass parameter are fixed at their optimal $T = 0$ values, $\pi_0(T) = \pi_0(0) = -0.876$ and $m(T) = m_0 = 656$ MeV. All the curves are multiplicatively renormalized at $\mu_0/m_0 = 6.098$ ($\mu_0 = 4$ GeV in physical units).

with $\mu_0/m_0 = 6.098$ (corresponding to $\mu_0 = 4$ GeV for $m_0 = 656$ MeV). We observe that, because of the chosen optimization, in the limit $T \rightarrow 0$ the longitudinal and transverse propagators coincide and reproduce the lattice data extremely well [18,19,21,22,24,25], so that the low-temperature limit can be regarded as exact. For reference, in Table I we report the physical equivalent of the adimensional temperatures T/m_0 used for the plots.

We observe a crossover, in Fig. 2, with the longitudinal propagator which increases in the IR for increasing T below $T_c \approx 0.15 \cdot m_0$, but sharply decreases above T_c . This non-monotonic behavior is a well-known feature which has been reported by several lattice calculations [11,12]. The transverse propagator in Fig. 3, on the other hand, has a monotonic behavior, decreasing for increasing T , again in qualitative agreement with the known predictions of the lattice. Actually, we cannot expect a quantitative agreement at $T \approx T_c$ or larger values, because we are extrapolating the

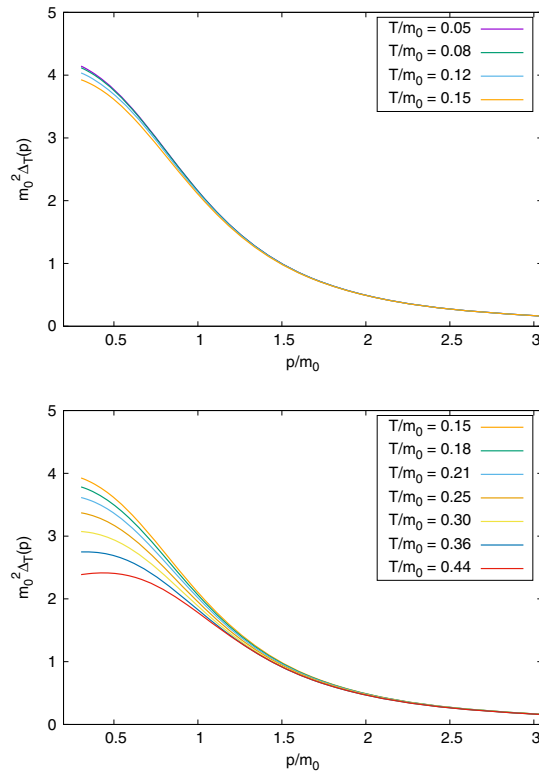


FIG. 3. Transverse propagator Δ_T , with the same notation and parameters of Fig. 2.

optimization condition which was valid at $T = 0$. Thus, the correct qualitative behavior of the propagators at high temperature is an encouraging result. A crude estimate of T_c is found by using the zero-temperature value $m_0 = 656$ MeV for restoring the energy units, yielding at the crossover $T_c \approx 100$ MeV. This value is quite smaller than the known transition temperature $T_c \approx 270$ MeV which is measured on the lattice [10–12]. The difference might well be the consequence of a sub-optimal choice of the renormalization constant, but it could also arise from a change of the mass parameter with temperature or from the more general failure of PT at high temperature. Thus, it becomes

TABLE I. Dimensionful values of the adimensional temperatures T/m_0 plotted in Figs. 2 and 3, given $m_0 = 656$ MeV.

T/m_0	0.05	0.08	0.12	0.15		
T (MeV)	32.80	52.48	78.72	98.40		
T/m_0	0.18	0.21	0.25	0.30	0.36	0.44
T (MeV)	118.08	137.76	164.00	196.80	236.16	288.64

relevant to explore whether a more quantitative agreement might be obtained by a tuning of the free parameters.

B. Optimization by a fit of data at finite T

As the temperature increases, our previous assumption, $m(T) = m(0)$, $\pi_0(T) = \pi_0(0)$, becomes less valid. In what follows, we turn to fixing the optimal value of the parameters at $T \neq 0$ by a fit of the lattice data of Ref. [11]. Since at nonzero temperatures the projections $\Delta_L(p, T)$ and $\Delta_T(p, T)$ have different behaviors with respect to a change in T , we may expect that the optimal values of the parameters will differ depending on which of the two components of the lattice propagator is used for the fit. This is indeed what we found. Of course, since in the subtracted Lagrangian of the present formalism the gluon mass parameter $m^2(T)$ is multiplied by the full four-dimensional transverse projector $t_{\mu\nu}(p)$, choosing different mass parameters/scales for the two components of the propagators is not allowed from first principles. This issue will be addressed at the end of this section.

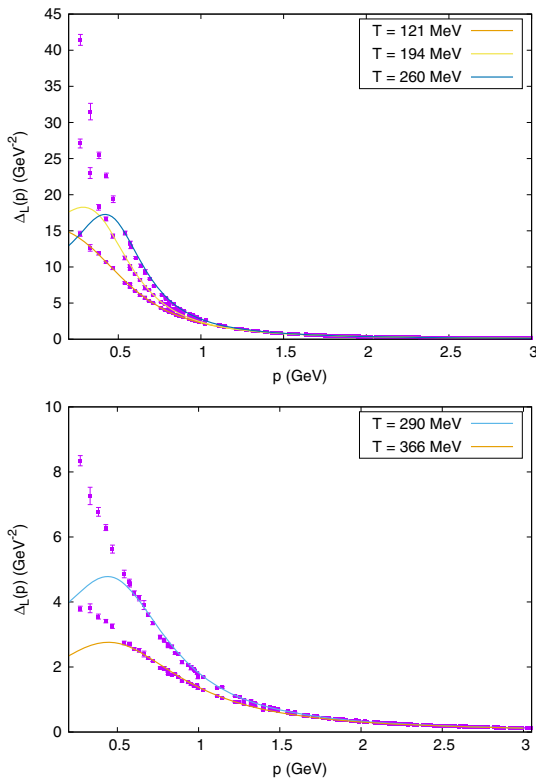


FIG. 4. Longitudinal propagator Δ_L at $\omega = 0$ below (top) and above (bottom) the critical temperature $T_c \approx 270$ MeV. The curves are obtained using the parameters given in Table II. The lattice data were taken from Ref. [11].

In Figs. 4 and 5 we show, respectively, the longitudinal and transverse components of the gluon propagator at $\omega = 0$ (multiplicatively renormalized at $\mu_0 = 4$ GeV), as functions of the three-dimensional momentum $|\mathbf{p}| = \sqrt{\mathbf{p}^2}$, with $m(T)$ and $\pi_0(T)$ as reported in Table II. Such values were obtained by a separate fit of the two components to the lattice data of Ref. [11]; the mass parameters should be understood to have an uncertainty of about ± 50 MeV.

As we can see, once the parameters are tuned to fit the data, the screened expansion is able to reproduce the lattice propagators quite accurately down to momenta of approximately 0.5 GeV. Moreover, the longitudinal propagator still shows the characteristic non-monotonic behavior with respect to a change in the temperature, increasing at fixed momentum below $T = T_c \approx 270$ MeV and decreasing above $T = T_c$.

Below $|\mathbf{p}| \approx 0.5$ GeV, the transverse propagator is still in good agreement with the data, while the longitudinal one shows significant deviations, especially at high temperatures. In particular, from a qualitative standpoint, the

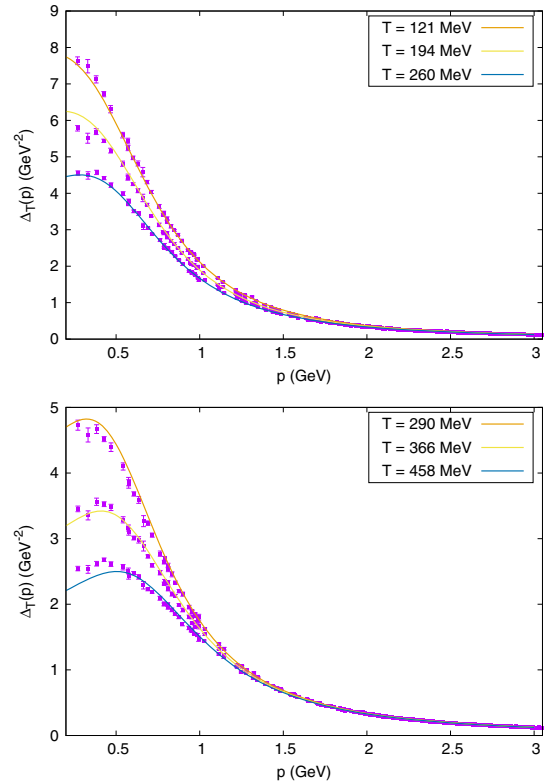


FIG. 5. Transverse propagator Δ_T at $\omega = 0$ below (top) and above (bottom) the critical temperature $T_c \approx 270$ MeV. The curves are obtained using the parameters given in Table II. The lattice data were taken from Ref. [11].

TABLE II. Parameters for the curves in Figs. 4 and 5, obtained by a separate fit of the lattice data for the longitudinal and transverse gluon propagator of Ref. [11].

T (MeV)	$m(T)$ (MeV) (long., trans.)	$\pi_0(T)$ (long., trans.)
121	550, 656	-0.89, -0.84
194	425, 550	-1.10, -0.70
260	425, 450	-1.42, -0.42
290	275, 450	-0.97, -0.48
366	150, 450	-0.60, -0.20
458	//, 450	//, +0.21

longitudinal propagator shows an infrared turnover as a function of momentum which has no counterpart in the lattice data. From a numerical point of view, the difficulty in obtaining a good match with the data is exemplified in Fig. 6, where we display the longitudinal propagator for $T = 458$ MeV and different values of the mass parameter.¹ When tuning the mass parameter $m(T)$, there is a tension between the low- and intermediate-momentum behavior of the propagator: at lower values of m , the propagator is enhanced (suppressed) below (above) $|\mathbf{p}| \approx 1$ GeV, so that achieving a good match at low momenta results in a loss of accuracy at intermediate momenta. This behavior is actually shared by both the components of the propagator and at every $T \neq 0$, albeit being less significant for the transverse component and at low temperatures. In particular, already at $T = 458$ MeV the optimal longitudinal values of the mass parameter and of the renormalization constant strongly depend on the choice of a lower cutoff momentum for the fit to the lattice data; for this reason, we do not report them.

As anticipated earlier, the optimal mass parameters (and renormalization constants) needed to reproduce the lattice data differ for the two components of the propagator. In Fig. 7 we plot the parameters of Table II as functions of the temperature. With the exception of the point $T = 260$ MeV, which is very close to the critical temperature $T_c \approx 270$ MeV, the optimal mass parameter $m(T)$ is a nonincreasing function of the temperature for both the projections. When fitted from the transverse propagator, $m(T)$ shows plateaux both at small and at large temperatures, decreasing from $m(T) = m(0) = 656$ to $m(T) \approx 450$ MeV. As for the longitudinal propagator, except for $T = 260$ MeV, $m(T)$ is approximately linear, with a behavior which is well described by the equation

$$m(T) \approx 656 \text{ MeV} - 1.307T \quad (\text{long}). \quad (32)$$

At $T = 260$ MeV $\approx T_c$, the optimal value of $m(T)$ is nearly equal for both the projections, namely

¹For each value of the mass parameter, the renormalization constant $\pi_0(T)$ was optimized so as to obtain the best fit with the data at large momenta.

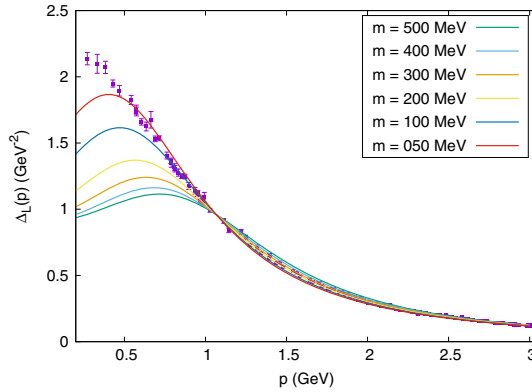


FIG. 6. Longitudinal propagator Δ_L for $\omega = 0$, $T = 458$ MeV and different values of the gluon mass parameter. The lattice data were taken from Ref. [11].

$m(T) = 425\text{--}450$ MeV. As for the renormalization constant, except for the point at $T = 290$ MeV $\approx T_c$, the optimal $\pi_0(T)$ increases with the temperature when fitted from the transverse propagator. When optimized by the longitudinal

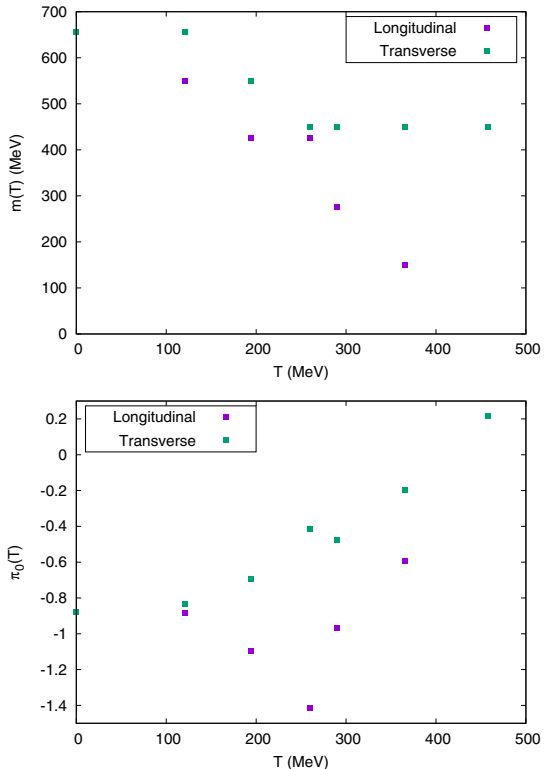


FIG. 7. Mass parameters (top) and renormalization constants (bottom) of Table II, as extracted from the lattice data of Ref. [11].

propagator, on the other hand, it shows a nonmonotonic behavior, decreasing below T_c and increasing again above T_c .

The large differences in the optimal values of $m(T)$ and $\pi_0(T)$ obtained for the two projections make it clear that, in the present formalism, it is not possible to quantitatively recover both the longitudinal and the transverse component of the gluon propagator by a unique choice of parameters. Thus at $T \neq 0$ the screened expansion appears to be suboptimal as a ‘‘variational’’ ansatz. At least in part, this could be expected on the basis of what is known about the high-temperature, low-momentum behavior of the Yang-Mills propagators: at large temperatures and low momenta, the gluons’ thermal mass is best described by a momentum- and direction-dependent hard thermal loop (HTL) term in the Lagrangian, given by [40]

$$\Delta\mathcal{L}_{\text{HTL}} = -\frac{1}{2}m_{el}^2(T)\text{Tr}\left\{F_{\mu\nu}\int\frac{d\Omega}{4\pi}\frac{\hat{y}^\nu\hat{y}^\lambda}{(\hat{y}\cdot D)^2}F_\lambda^\mu\right\}, \quad (33)$$

where $m_{el}^2(T) = g^2NT^2/3$, \hat{y} is a lightlike four-vector and the integration is over the directions of \hat{y} . To first order in the coupling, $\Delta\mathcal{L}_{\text{HTL}}$ generates two different thermal masses for the three-dimensional projections $\Delta_L(p, T)$ and $\Delta_T(p, T)$ of the gluon propagator. By not taking into account this difference, the screened expansion lends itself to a breakdown at large temperatures, which can be partially avoided if the mass parameter and renormalization constant are tuned to separately fit the two projections.

The simplest way of solving this issue in the context of the screened expansion, i.e., without resorting to a HTL resummation, would be to change the expansion point of perturbation theory in such a way that the two three-dimensional projections of the *zero-order* gluon propagator, Δ_m^T and Δ_m^L , have different masses *ab initio*. This can be achieved by redefining the kernel $\delta\Gamma_{\mu\nu}(p; T) = m^2(T)t_{\mu\nu}(p)$ of the shift of the action δS as

$$\delta\Gamma_{\mu\nu}(p; T) \rightarrow m_T^2(T)P_{\mu\nu}^T(p) + m_L^2(T)P_{\mu\nu}^L(p), \quad (34)$$

where $m_T(T)$ and $m_L(T)$ are independent mass-parameter functions for the two projections. With such a prescription, in a general covariant gauge the zero-order Euclidean gluon propagator $\Delta_m^{\mu\nu}(p; T)$ would read

$$\Delta_m(p; T)_{\mu\nu} \rightarrow \Delta_m^T(p; T)P_{\mu\nu}^T(p) + \Delta_m^L(p; T)P_{\mu\nu}^L(p) + \frac{\xi}{p^2}\ell_{\mu\nu}(p), \quad (35)$$

where

$$\Delta_m^{T,L}(p; T) = \frac{1}{p^2 + m_{T,L}^2(T)} \quad (36)$$

are the sought-after zero-order propagators. Setting-up the perturbation theory with independent mass functions for the two projections would give us the freedom to optimize the former separately from first principles, according to the behavior of the respective dressed propagators. Implementing the shift in Eq. (35), however, is a nontrivial task: having different longitudinal and transverse masses running in the loops breaks the Lorentz invariance even of the simplest vacuum integrals and, more generally, requires a complete recalculation of the gluon polarization.

IV. DISPERSION RELATIONS AT FINITE T

Being in possession of analytical expressions (modulo a one-dimensional integration at finite T) for the Euclidean gluon propagator allows us to analytically continue the latter to the whole complex plane so as to study its singularities. As is well known, the location of the poles of the propagator gives us information on the dispersion relations of the gluonic quasiparticles: the energy $\varepsilon_{T,L}(\mathbf{p}, T)$ and damping rate $\gamma_{T,L}(\mathbf{p}, T)$ of the quasiparticles, as functions of the three-dimensional momentum \mathbf{p} and of the temperature T , are obtained by solving the equation

$$\Delta_{T,L}^{-1}(-i\omega_{T,L}(\mathbf{p}, T), \mathbf{p}, T) = 0, \quad (37)$$

where $\omega = \varepsilon - i\gamma$ (modulo a factor of i) extends the real and discrete Matsubara frequencies $\omega_n = 2\pi nT$ to the complex plane and the subscripts T, L refer to the components of the propagator. At nonzero temperatures and momenta, the poles of the two components are expected to be found at different locations, yielding two separate branches of the dispersion relations.

The limit $T \rightarrow 0$ of the dispersion relations was already studied in the framework of the screened massive expansion in Refs. [20–22]. In [21] we found that the zero-temperature gluon propagator (whose longitudinal and transverse three-dimensional components are constrained to be equal by Lorentz symmetry) has two complex-conjugate poles at $-p^2 = m_{\text{pole}}^2, (m_{\text{pole}}^2)^*$, where, setting $m_0 = 656$ MeV by sharing the same units of the lattice,

$$m_R^2 = 0.197 \text{ GeV}^2, \quad m_I^2 = 0.436 \text{ GeV}^2, \quad (38)$$

with $m_{\text{pole}}^2 = m_R^2 + im_I^2$. In terms of $\varepsilon_{\text{vac}}(\mathbf{p}) = \lim_{T \rightarrow 0} \varepsilon_{T,L}(\mathbf{p}, T)$ and $\gamma_{\text{vac}}(\mathbf{p}) = \lim_{T \rightarrow 0} \gamma_{T,L}(\mathbf{p}, T)$ —and singling out one of the poles—, this translates into the dispersion relations

$$\varepsilon_{\text{vac}}(\mathbf{p}) = \left[\frac{1}{2} \sqrt{(\mathbf{p}^2 + m_R^2)^2 + (m_I^2)^2} + \frac{1}{2}(\mathbf{p}^2 + m_R^2) \right]^{1/2},$$

$$\gamma_{\text{vac}}(\mathbf{p}) = \left[\frac{1}{2} \sqrt{(\mathbf{p}^2 + m_R^2)^2 + (m_I^2)^2} - \frac{1}{2}(\mathbf{p}^2 + m_R^2) \right]^{1/2}. \quad (39)$$

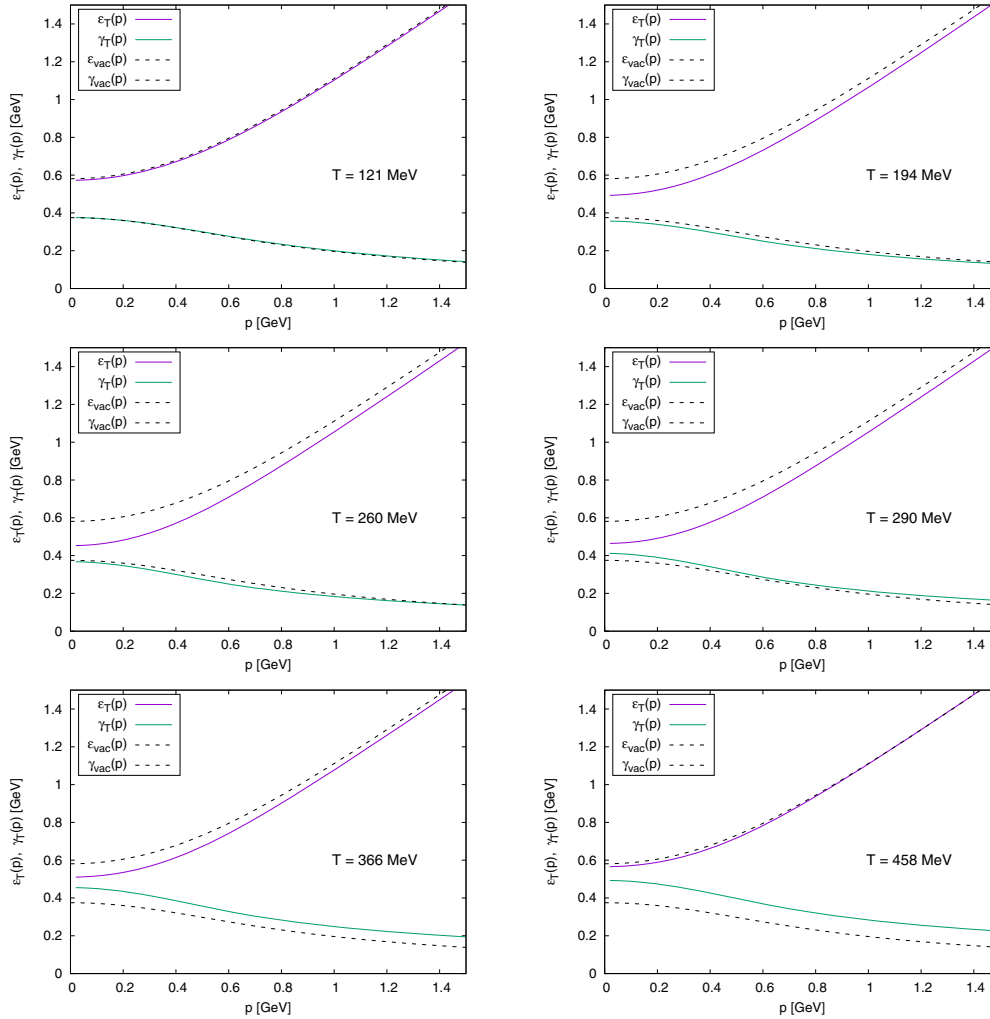


FIG. 8. Transverse dispersion relations for the gluon quasiparticles. The broken lines are the vacuum dispersion relations, common to both projections and given by Eq. (39). The gluon mass parameters $m(T)$ and renormalization constants $\pi_0(T)$ used for the plots are reported in Table II.

Clearly, $m_R^2 = (\epsilon_{\text{vac}}^2 - \gamma_{\text{vac}}^2)|_{\mathbf{p}=0}$ and $m_I^2 = 2\epsilon_{\text{vac}}\gamma_{\text{vac}}|_{\mathbf{p}=0}$, where

$$\epsilon_{\text{vac}}(\mathbf{0}) = 581 \text{ MeV}, \quad \gamma_{\text{vac}}(\mathbf{0}) = 375 \text{ MeV}. \quad (40)$$

At the other end of the spectrum, as $|\mathbf{p}| \rightarrow \infty$, the gluon's vacuum dispersion relations reduce to those of a massless particle, $\epsilon_{\text{vac}}(\mathbf{p}) \rightarrow |\mathbf{p}|$, $\gamma_{\text{vac}}(\mathbf{p}) \rightarrow 0$.

Under the assumption that the optimal masses $m(T)$ and renormalization constants $\pi_0(T)$ reported in the previous section only depend on the temperature, and not on the Matsubara frequency ω_n , the finite- T dispersion relations of the gluon quasiparticles can be easily extracted from the

screened expansion's gluon propagator, making use of said parameters (cf. Table II). We remark that, since at low momenta the longitudinal projection was not found to be in good agreement with the lattice data for any value of the parameters, the longitudinal dispersion relations are expected to be reliable only at sufficiently high momenta (say above $|\mathbf{p}| \approx 0.5\text{--}0.7$ GeV).

In Figs. 8 and 9 we plot the energy $\epsilon_{T,L}(\mathbf{p}, T)$ and the damping rate $\gamma_{T,L}(\mathbf{p}, T)$ of the transverse and longitudinal gluons at fixed T , as functions of the momentum $|\mathbf{p}|$. As we can see, below the critical temperature $T_c \approx 270$ MeV both the transverse energy and the transverse damping rate (Fig. 8) are suppressed with respect to their

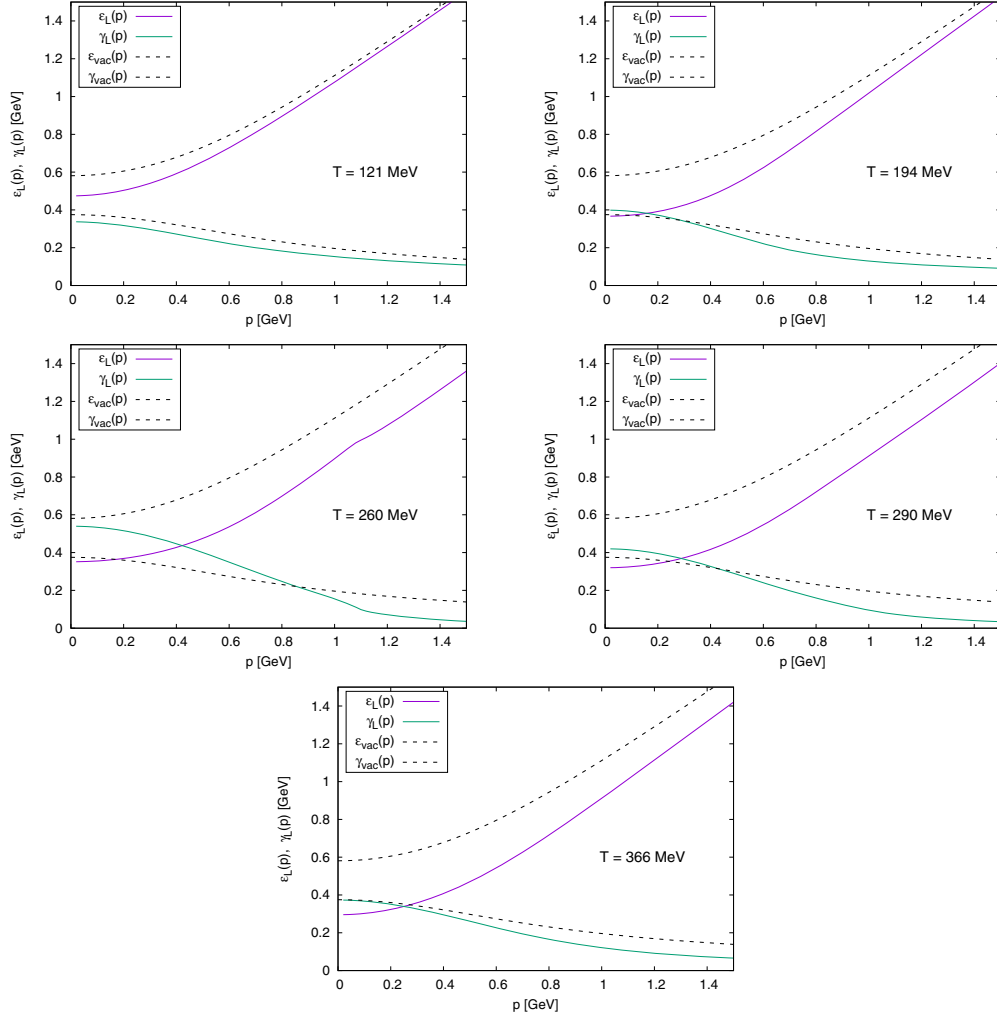


FIG. 9. Longitudinal dispersion relations for the gluon quasiparticles. The broken lines are the vacuum dispersion relations, common to both projections and given by Eq. (39). The gluon mass parameters $m(T)$ and renormalization constants $\pi_0(T)$ used for the plots are reported in Table II. Except for vanishingly small temperatures, these dispersion relations are not expected to be reliable below $|\mathbf{p}| \approx 500\text{--}700$ MeV.

zero-temperature (vacuum) limit, with the effect being more pronounced for ε_T than for γ_T . Above T_c this behavior is reversed; the transverse energy starts to approach again its vacuum limit, while the damping rate grows larger than it. The longitudinal branch (Fig. 9) shows a more significant suppression in both the energy and the damping rate below T_c , with γ_L becoming quite small at high momenta around the critical temperature. At higher temperatures both ε_L and γ_L start to approach back their vacuum limit.²

²Here we are disregarding the low-momentum behavior of the longitudinal dispersion relations due to their lack of reliability, as previously discussed.

In the limit $\mathbf{p} \rightarrow 0$ and for any nonzero ω , the longitudinal and the transverse projection of the gluon propagator are known to collapse to a single temperature-dependent function; as a consequence, the corresponding branches of the dispersion relations share the same zero-momentum limit. The $\mathbf{p} = 0$ poles of the gluon propagator are located at $-i(\varepsilon_0(T) - i\gamma_0(T))$, where

$$\varepsilon_0(T) = \lim_{|\mathbf{p}| \rightarrow 0} \varepsilon_{T,L}(\mathbf{p}, T), \quad \gamma_0(T) = \lim_{|\mathbf{p}| \rightarrow 0} \gamma_{T,L}(\mathbf{p}, T) \quad (41)$$

are, respectively, the mass and the (zero-momentum) damping rate of the gluon quasiparticles. With regards to

such a constraint, the optimized framework of Sec. III B is inconsistent: using different mass parameters for the longitudinal and the transverse projections of the propagator causes the two branches of the dispersion relations to have unequal $\mathbf{p} \rightarrow 0$ limits. All the same, as previously discussed, the low-momentum limit of the longitudinal gluon propagator was found to be quantitatively unreliable at temperatures which are not vanishingly small. It follows that the $\mathbf{p} \rightarrow 0$ limit of the longitudinal dispersion relations cannot be trusted regardless of the inconsistency. Since only the screened expansion's transverse propagator, with the parameters in Table II, was found to reproduce the lattice data at low momenta, in what follows we will make use of the transverse dispersion relations to study the behavior of $\epsilon_0(T)$ and $\gamma_0(T)$. From first principles, it is understood that a good description of the long-wavelength longitudinal gluon excitations must yield the same results.

In Fig. 10 we display the mass and the zero-momentum damping rate of the gluon quasiparticles as functions of the temperature. Across the critical temperature, both of them show a characteristic behavior, decreasing below T_c and increasing again in a linear fashion above T_c . The mass decreases from $\epsilon_0(0) = \epsilon_{\text{vac}}(\mathbf{0}) = 581$ to $\epsilon_0(T_c) \approx 450$ MeV, whereas the zero-momentum damping rate slightly decreases from $\gamma_0(0) = \gamma_{\text{vac}}(\mathbf{0}) = 375$ to about 350 MeV around T_c . The increase in the damping rate actually seems to start somewhat below the critical temperature (see the data point $T = 260$ MeV in Fig. 10); we could not determine whether this is a physically meaningful behavior or an artifact due to uncertainties in the parameters of Table II.

The behavior of the gluon mass in Fig. 10 confirms the picture of a confined gluon—whose mass is dynamically generated through the strong interactions themselves like in the $T \rightarrow 0$ limit—which becomes deconfined above the critical temperature $T_c \approx 270$ MeV. In the deconfined phase, the mass of the gluon is thermal in nature and increases linearly with the temperature. The same qualitative behavior was observed in [26], where the gluon mass and zero-momentum damping rate were studied in the screened expansion at finite T using the same scheme of Sec. III A, i.e., taking temperature-independent values for both the gluon mass parameter m and the renormalization constant π_0 .

V. DISCUSSION

The comparison with the available lattice data showed that, overall, the screened expansion gives a correct qualitative description of the gluon propagator at finite T . The agreement improves if the renormalization constants are tuned at each value of the temperature. At high temperatures and deep in the IR, the failure to reproduce the longitudinal projection might arise from the combined effect of several issues like the need of some HTL resummation, a poor optimization and the inadequacy of

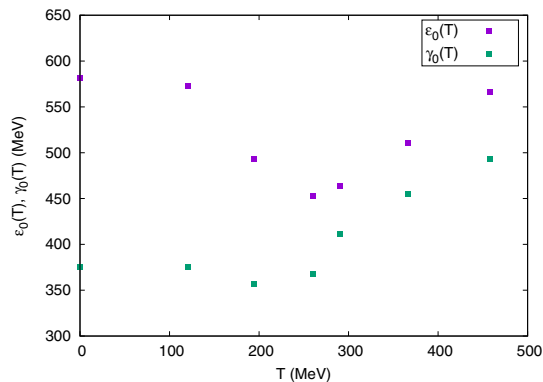


FIG. 10. Mass $\epsilon_0(T)$ and zero-momentum damping rate $\gamma_0(T)$ of the gluon quasiparticles, as functions of the temperature. The parameters used for the plot are reported in Table II under the transverse denomination. See text for further details.

the single-mass splitting of the action at a finite temperature. Indeed, the lattice data seem to suggest that a two-mass scheme should be introduced from the beginning for extending the screened expansion at a finite temperature.

With the exception of an infrared turnover in the longitudinal propagator, which has no counterpart in the lattice data, the qualitative behavior of the propagators seems to be correct and quite robust, irrespective of the optimization scheme. The pole trajectories can be determined in the complex plane, yielding valuable predictions which cannot be extracted from the lattice data in the Euclidean space. We have reported in some detail the dispersion relations of the quasi-gluon for several temperatures across the deconfinement transition.

An important feature which emerges from our study is a crossover at the deconfinement transition. The energy of the quasi-particle is suppressed by temperature in the confined phase. On the other hand, above the critical temperature, the behavior is reversed and the energy increases as a function of temperature. The same effect can be observed for the physical mass, defined as the long-wavelength limit $\epsilon_0(T)$ of the pole's real part, as shown in Fig. 10. In the confined phase, the mass decreases like an order parameter being suppressed by the temperature. This behavior is consistent with that of a dynamical mass which is related to a condensate, the latter being expected to vanish at the transition temperature. However, at finite temperature the quasi-gluon is also expected to acquire a thermal mass which increases linearly, like any other quasiparticle. The two effects might coexist across the transition, yielding a crossover rather than a sharp transition. In the low-temperature limit the dynamical nature of the mass dominates, while above the deconfinement transition the mass becomes a pure thermal mass. Thus, we argue that in the low-temperature phase the mass suppression might be a signature of the dynamical nature

of the gluon mass. On the other hand, as discussed in Ref. [26], the existence of an intrinsic damping rate, which saturates at a finite value at $T = 0$, is a confirmation of the quasi-gluon scenario laid out by Stingl [33]. The massive gluon also has a very short finite lifetime and is canceled from the asymptotic states [26], suggesting that the gluon quasiparticles of the interacting vacuum can only travel the short distance of about a Fermi and can only exist as intermediate states at the origin of a gluon-jet event.

The issue of the gauge invariance of the poles at $T \neq 0$ within the framework of the screened expansion remains, to date, unexplored. One possible development of our study at finite temperature would be to apply the guiding principles and methods of Ref. [21] in order to monitor whether the Nielsen identities can be satisfied in a general covariant gauge, while fixing the values of the free parameters of the formalism from first principles. A thorough analysis of the matter would presumably require the explicit implementation of specific resummation schemes, as is already the case within the framework of ordinary thermal perturbation theory. Nonetheless, the success of the screened expansion in reproducing the lattice data—albeit subject to a fit to the data themselves and with the limitations discussed in the previous sections—leads us to believe that a two-mass shift of the expansion point of the thermal perturbative series may prove to be a robust enough alternative scheme already at one loop. Such a reformulation of the screened expansion requires a full recalculation of both the thermal and vacuum integrals involved in the definition of the propagators, and will be left to future studies.

ACKNOWLEDGMENTS

The authors are in debt to Orlando Oliveira for sharing the lattice data of Ref. [11]. This research was supported in part by “Piano per la Ricerca di Ateneo 2017/2020—Linea di intervento 2” of the University of Catania.

APPENDIX A: ONE-LOOP GRAPHS

1. Notation

The Euclidean four-vector p^μ is defined as

$$p^\mu = (\mathbf{p}, \omega), \quad (\text{A1})$$

where $\omega = p_4 = -ip_0$ and the Lorentz four-vector is (p_0, \mathbf{p}) .

In the finite temperature formalism, $\omega = \omega_n = 2\pi nT$ and the Euclidean integral is replaced by a sum over n and by a three-dimensional integration

$$\int \frac{d^4 p}{(2\pi)^4} \rightarrow \int_p = T \sum_n \int \frac{d^3 \mathbf{p}}{(2\pi)^3}. \quad (\text{A2})$$

The generic (massive) propagator $G_m(p)$ is

$$G_m(p) = \frac{1}{p^2 + m^2} = \frac{1}{\omega_n^2 + \mathbf{p}^2 + m^2}. \quad (\text{A3})$$

At finite temperature, it is useful to introduce the following orthogonal projectors

$$P_{\mu\nu}^T(p) = (1 - \delta_{\mu,4})(1 - \delta_{\nu,4}) \left(\delta_{\mu\nu} - \frac{p_\mu p_\nu}{\mathbf{p}^2} \right),$$

$$P_{\mu\nu}^L(p) = t_{\mu\nu}(p) - P_{\mu\nu}^T(p), \quad (\text{A4})$$

beside the Lorentz projectors

$$t_{\mu\nu}(p) = \delta_{\mu\nu} - \frac{p_\mu p_\nu}{p^2},$$

$$\ell_{\mu\nu}(p) = \frac{p_\mu p_\nu}{p^2}. \quad (\text{A5})$$

The trace of the projectors is

$$P_{\mu\mu}^T = 2, \quad P_{\mu\mu}^L = 1. \quad (\text{A6})$$

The dressed Euclidean propagator of the gluon can be written as $\Delta_{\mu\nu}^{ab}(p) = \delta_{ab} \Delta_{\mu\nu}(p)$ where

$$\Delta_{\mu\nu}^{-1}(p) = G_m(p)^{-1} t_{\mu\nu}(p) - Ng^2 \Pi_{\mu\nu}(p) + \frac{p^2}{\xi} \ell_{\mu\nu}(p) \quad (\text{A7})$$

and the gluon polarization is $\Pi_{\mu\nu}^{ab}(p) = Ng^2 \delta_{ab} \Pi_{\mu\nu}(p)$. Since $\Pi_{\mu\nu}(p)$ is transverse, i.e., $p^\mu \Pi_{\mu\nu}(p) = 0$, in the Landau gauge ($\xi \rightarrow 0$) the dressed propagator is also transverse. We introduce the projected polarizations

$$\Pi_T(p) = \frac{1}{2} P_{\mu\nu}^T(p) \Pi_{\mu\nu}(p),$$

$$\Pi_L(p) = P_{\mu\nu}^L(p) \Pi_{\mu\nu}(p), \quad (\text{A8})$$

so that the total polarization reads

$$\Pi_{\mu\nu}(p) = \Pi_L(p) P_{\mu\nu}^L(p) + \Pi_T(p) P_{\mu\nu}^T(p) \quad (\text{A9})$$

and the dressed propagator can be written as

$$\Delta_{\mu\nu}(p) = \Delta^L(p) P_{\mu\nu}^L(p) + \Delta^T(p) P_{\mu\nu}^T(p)$$

$$+ \frac{\xi}{p^2} \ell_{\mu\nu}(p), \quad (\text{A10})$$

where the projected parts are

$$\Delta_T^{-1}(p) = G_m(p)^{-1} - Ng^2 \Pi_T(p),$$

$$\Delta_L^{-1}(p) = G_m(p)^{-1} - Ng^2 \Pi_L(p). \quad (\text{A11})$$

In the Landau gauge, $\xi \rightarrow 0$, the propagator is transverse and its components are determined by the projected polarizations $\Pi_T(p)$ and $\Pi_L(p)$. The graphs are evaluated in the

Landau gauge, using the (transverse) massive free propagator $[G_m(p)t_{\mu\nu}(p)]$ in the internal gluon lines.

The dressed Euclidean propagator of the ghost can be written as $\mathcal{G}_{ab}(p) = \delta_{ab}\mathcal{G}(p)$, where

$$\mathcal{G}^{-1}(p) = -G_0^{-1}(p) - Ng^2\Sigma(p) \quad (\text{A12})$$

and the ghost self energy is $\Sigma_{ab}(p) = \delta_{ab}\Sigma(p)$. In the graphs, the massless free propagator $-G_0(p)$ is used in the internal ghost lines.

All the uncrossed one-loop graphs can be decoupled by the method of Ref. [38] and written in terms of the set of integrals

$$\begin{aligned} J_\alpha &= \int_k G_\alpha(k), \\ I_{\mu\nu}^{\alpha\beta}(p) &= \int_k G_\alpha(k)G_\beta(p-k)k_\mu k_\nu, \\ I^{\alpha\beta}(p) &= \int_k G_\alpha(k)G_\beta(p-k), \end{aligned} \quad (\text{A13})$$

together with their projections

$$\begin{aligned} I_T^{\alpha\beta}(p) &= \frac{1}{2}P_{\mu\nu}^T(p)I_{\mu\nu}^{\alpha\beta}(p), \\ I_L^{\alpha\beta}(p) &= P_{\mu\nu}^L(p)I_{\mu\nu}^{\alpha\beta}(p), \\ I_{Tp}^{\alpha\beta} &= \frac{1}{2}P_{\mu\nu}^T(p)I_{\mu\nu}^{\alpha\beta}(0), \\ I_{Lp}^{\alpha\beta} &= P_{\mu\nu}^L(p)I_{\mu\nu}^{\alpha\beta}(0). \end{aligned} \quad (\text{A14})$$

Explicit expressions are reported in Appendix B.

By exchanging k_μ and $p_\mu - k_\mu$ in the integrals, it is easy to show that $I^{\alpha\beta}(p) = I^{\beta\alpha}(p)$, while in general $I_{\mu\nu}^{\alpha\beta}(p) \neq I_{\mu\nu}^{\beta\alpha}(p)$. However, since $p^\mu P_{\mu\nu}^{L,T}(p) = 0$,

$$(p^\mu - k^\mu)P_{\mu\nu}^{L,T}(p)(p^\nu - k^\nu) = k^\mu k^\nu P_{\mu\nu}^{L,T}(p) \quad (\text{A15})$$

and the projected integrals turn out to be symmetric, $I_{L,T}^{\alpha\beta} = I_{L,T}^{\beta\alpha}$.

We note that $I_{Lp}^{\alpha\beta}$ and $I_{Tp}^{\alpha\beta}$ might depend on p because of the explicit dependence in the projectors. For instance, let us consider any constant integral

$$I_{\mu\nu} = \int_k k_\mu k_\nu f(k) = \delta_{\mu\nu}I_{\mu\mu}, \quad (\text{A16})$$

which does not depend on the external momentum p . Let us denote by $I_{L,0}$, $I_{T,0}$, the nonzero components that can be written, taking $k_\mu = (\mathbf{k}, \omega_n)$, as

$$\begin{aligned} I_{44} = I_{L,0} &= \int_k \omega_n^2 f(\mathbf{k}, \omega_n), \\ I_{ii} = I_{T,0} &= \frac{1}{3} \int_k \mathbf{k}^2 f(\mathbf{k}, \omega_n), \quad i = 1, 2, 3. \end{aligned} \quad (\text{A17})$$

In fact, the explicit projections $I_{L,p}$, $I_{T,p}$ can be defined and evaluated as in Eqs. (A14):

$$\begin{aligned} I_{T,p} &= \frac{1}{2}P_{\mu\nu}^T(p)I_{\mu\nu} = I_{T,0}, \\ I_{L,p} &= P_{\mu\nu}^L(p)I_{\mu\nu} = (I_{L,0} - I_{T,0})\frac{\mathbf{p}^2}{\mathbf{p}^2 + \omega^2} + I_{T,0}. \end{aligned} \quad (\text{A18})$$

While $I_{T,p} = I_{T,0}$ and does not depend on p , the longitudinal projection depends on p and has the different limits

$$\lim_{\mathbf{p} \rightarrow 0} I_{L,p} = I_{T,0}, \quad \lim_{\omega \rightarrow 0} I_{L,p} = I_{L,0}. \quad (\text{A19})$$

More generally, for the integral $I_{\mu\nu}^{\alpha\beta}(p)$, which has an explicit dependence on p , the projections have the following limits:

$$\begin{aligned} I_{L,0}^{\alpha\beta} &= \lim_{\mathbf{p} \rightarrow 0} \left[\lim_{\omega \rightarrow 0} I_{L,p}^{\alpha\beta}(p) \right], \quad I_{T,0}^{\alpha\beta} = \lim_{\omega \rightarrow 0} \left[\lim_{\mathbf{p} \rightarrow 0} I_{L,p}^{\alpha\beta}(p) \right], \\ I_{T,0}^{\alpha\beta} &= \lim_{\mathbf{p} \rightarrow 0} \left[\lim_{\omega \rightarrow 0} I_{T,p}^{\alpha\beta}(p) \right] = \lim_{\omega \rightarrow 0} \left[\lim_{\mathbf{p} \rightarrow 0} I_T^{\alpha\beta}(p) \right]; \end{aligned} \quad (\text{A20})$$

they are related to the projections of the limit $I_{\mu\nu}^{\alpha\beta}(0)$, as defined in Eqs. (A14),

$$\begin{aligned} I_{T,p}^{\alpha\beta} &= I_{T,0}^{\alpha\beta}, \\ I_{L,p}^{\alpha\beta} &= (I_{L,0}^{\alpha\beta} - I_{T,0}^{\alpha\beta})\frac{\mathbf{p}^2}{\mathbf{p}^2 + \omega^2} + I_{T,0}^{\alpha\beta}, \end{aligned} \quad (\text{A21})$$

where

$$I_{L,0}^{\alpha\beta} = I_{44}^{\alpha\beta}(0), \quad I_{T,0}^{\alpha\beta} = I_{ii}^{\alpha\beta}(0). \quad (\text{A22})$$

The limits in Eq. (A20) agree with the physical requirement that transverse and longitudinal projections must coincide for any ω in the limit $\mathbf{p} \rightarrow 0$, while they are different for any finite \mathbf{p} in the limit $\omega \rightarrow 0$.

Each crossed graph Π^\times , containing one insertion of the mass counterterm, can be obtained by the corresponding uncrossed graph Π by a simple derivative

$$\Pi^\times = -m^2 \frac{\partial}{\partial m^2} \Pi. \quad (\text{A23})$$

Their explicit calculation requires the definition of a new set of integrals $\partial I^{\alpha\beta}$, $\partial I_{L,T}^{\alpha\beta}$, ∂J_m , $\partial^2 J_m$:

$$\begin{aligned}
\partial I^{\alpha\beta}(p) &= \frac{\partial}{\partial \alpha^2} I^{\alpha\beta}(p), \\
\partial I_{L,T}^{\alpha\beta}(p) &= \frac{\partial}{\partial \alpha^2} I_{L,T}^{\alpha\beta}(p), \\
\partial J_m &= \frac{\partial}{\partial m^2} J_m, \\
\partial^2 J_m &= \frac{\partial^2}{(\partial m^2)^2} J_m.
\end{aligned} \tag{A24}$$

We note that the second argument (β) is kept fixed in the derivative, so that $\partial I^{\alpha\beta} \neq \partial I^{\beta\alpha}$. When $\alpha = \beta$ the derivative must be taken twice, so that for instance

$$\frac{\partial}{\partial m^2} I^{mm} = \left[\frac{\partial}{\partial \alpha^2} I^{\alpha\beta} + \frac{\partial}{\partial \beta^2} I^{\alpha\beta} \right]_{\alpha=\beta=m} = 2\partial I^{mm}. \tag{A25}$$

Not all the integrals are independent. For instance, it can be easily shown that

$$\begin{aligned}
I^{\alpha\beta}(0) &= \frac{1}{\beta^2 - \alpha^2} [J_\alpha - J_\beta], \\
\partial J_m &= -I^{mm}(0), \\
\partial I^{\alpha\beta}(0) &= \frac{1}{\beta^2 - \alpha^2} [I^{\alpha\beta}(0) - I^{\alpha\alpha}(0)].
\end{aligned} \tag{A26}$$

It is useful to introduce the integrals $J_m^{L,T}$ which follow by setting $f(k) = G_m(k)$ in Eq. (A17),

$$\begin{aligned}
J_m^L &= \int_k \omega_n^2 G_m(\mathbf{k}, \omega_n), \\
J_m^T &= \frac{1}{3} \int_k \mathbf{k}^2 G_m(\mathbf{k}, \omega_n),
\end{aligned} \tag{A27}$$

so that Eqs. (A26) can be extended to the projected integrals,

$$\begin{aligned}
I_{L,T0}^{\alpha\beta} &= \frac{1}{\beta^2 - \alpha^2} [J_{\alpha}^{L,T} - J_{\beta}^{L,T}], \\
\partial J_m^{L,T} &= -I_{L,T0}^{mm}, \\
\partial I_{L,T0}^{\alpha\beta} &= \frac{1}{\beta^2 - \alpha^2} [I_{L,T0}^{\alpha\beta} - I_{L,T0}^{\alpha\alpha}],
\end{aligned} \tag{A28}$$

and, by Eq. (A21), the projections $I_{L,Tp}^{\alpha\beta}$ can be expressed in terms of the constant integrals $J_m^{L,T}$.

2. Graph 1b—(tadpole)

Setting $d = 4$, Eq. (31) of Ref. [41] reads

$$\Pi_{\mu\nu}^{(1b)}(p) = - \int_k [3\delta_{\mu\nu} - t_{\mu\nu}(k)] G_m(k), \tag{A29}$$

yielding

$$\Pi_{\mu\nu}^{(1b)} = -[2\delta_{\mu\nu} J_m + I_{\mu\nu}^{m0}(0)], \tag{A30}$$

where the integrals J_α , $I_{\mu\nu}^{\alpha\beta}(p)$ were defined in Eqs. (A13) and their explicit expressions are reported in Appendix B. The projected polarization of graph (1b) is

$$\begin{aligned}
\Pi_T^{(1b)}(p) &= -[2J_m + I_{Tp}^{m0}], \\
\Pi_L^{(1b)}(p) &= -[2J_m + I_{Lp}^{m0}].
\end{aligned} \tag{A31}$$

The vacuum contribution can be extracted by evaluating the integrals in the limit $T \rightarrow 0$ where $I_{\mu\nu}^{m0}(0) \rightarrow \frac{1}{4} \delta_{\mu\nu} J_m$ so that

$$\Pi_{\mu\nu}^{(1b)}(T=0) = -\frac{9}{4} \delta_{\mu\nu} J_m \tag{A32}$$

in agreement with the general result of Ref. [19] for $d = 4$.

3. Graph 2b—(gluon loop)

The general explicit expression for the graph (2b) has been reported in Ref. [41], for a generic dimension d and a generic free-particle propagator. In the Landau gauge, the explicit expression for $d = 4$ can be written as (see also Ref. [38])

$$\Pi^{\mu\nu}(p) = \sum_{i=1}^4 \Pi_i^{\mu\nu}(p) \tag{A33}$$

where, denoting $q = p - k$,

$$\begin{aligned}
\Pi_1^{\mu\nu}(p) &= \frac{1}{2} \int_k (q-k)^\mu (q-k)^\nu [t^{\lambda\rho}(q) t_{\rho\lambda}(k)] G_m(k) G_m(q), \\
\Pi_2^{\mu\nu}(p) &= \int_k t^{\mu\nu}(k) [(p+k)_\lambda t^{\lambda\rho}(q) (p+k)_\rho] G_m(k) G_m(q), \\
\Pi_3^{\mu\nu}(p) &= - \int_k [t^{\mu\lambda}(k) (p+q)_\lambda] [t^{\nu\rho}(q) (p+k)_\rho] \\
&\quad \times G_m(k) G_m(q), \\
\Pi_4^{\mu\nu}(p) &= \int_k (q-k)^\mu [t^{\nu\lambda}(k) t_{\lambda\rho}(q) (p+k)^\rho] G_m(k) G_m(q) \\
&\quad + \mu \leftrightarrow \nu.
\end{aligned} \tag{A34}$$

All integrals can be evaluated by the method of Ref. [38] and written in terms of the integrals in Eq. (A13).

In some detail,

$$\Pi_1^{\mu\nu}(p) = \frac{1}{2} \int_k (q-k)^\mu (q-k)^\nu \left[2 + \frac{(k \cdot q)^2}{k^2 q^2} \right] G_m(k) G_m(q), \tag{A35}$$

and making use of the identities

$$\begin{aligned}
2k \cdot q &= (k+q)^2 - k^2 - q^2 = p^2 - G_\alpha(k)^{-1} - G_\beta(q)^{-1} + \alpha^2 + \beta^2, \\
\frac{G_m(k)}{k^2} &= G_0(k)G_m(k) = \frac{1}{m^2}[G_0(k) - G_m(k)], \\
(q-k)_\mu(q-k)_\nu &= 2(q_\mu q_\nu + k_\mu k_\nu) - p_\mu p_\nu
\end{aligned} \tag{A36}$$

we can write

$$\begin{aligned}
\frac{(k \cdot q)^2}{k^2 q^2} G_m(k)G_m(q) &= \frac{1}{4m^4} [(p^2 + 2m^2)^2 G_m(k)G_m(q) + p^4 G_0(k)G_0(q) + \\
&\quad - (p^2 + m^2)^2 (G_0(k)G_m(q) + G_m(k)G_0(q))] + \frac{1}{4} (G_m(k)G_0(k) + G_m(q)G_0(q)),
\end{aligned} \tag{A37}$$

$$\begin{aligned}
\int_k (q-k)_\mu(q-k)_\nu \frac{(k \cdot q)^2}{k^2 q^2} G_m(k)G_m(q) &= \frac{1}{4m^4} [(p^2 + 2m^2)^2 (4I_{\mu\nu}^{mm}(p) - p_\mu p_\nu I^{mm}(p)) + \\
&\quad + p^4 (4I_{\mu\nu}^{00}(p) - p_\mu p_\nu I^{00}(p)) - 2(p^2 + m^2)^2 (2[I_{\mu\nu}^{m0}(p) + I_{\mu\nu}^{0m}(p)] - p_\mu p_\nu I^{m0}(p))] + \\
&\quad + 2I_{\mu\nu}^{m0}(0) + \frac{1}{2} p_\mu p_\nu I^{m0}(0),
\end{aligned} \tag{A38}$$

$$\int_k (q-k)_\mu(q-k)_\nu G_m(k)G_m(q) = 4I_{\mu\nu}^{mm}(p) - p_\mu p_\nu I^{mm}(p) \tag{A39}$$

so that Eq. (A35) reads

$$\begin{aligned}
\Pi_{1\mu\nu}(p) &= \frac{p^4}{2m^4} I_{\mu\nu}^{00}(p) + \left[4 + \frac{(p^2 + 2m^2)^2}{2m^4} \right] I_{\mu\nu}^{mm}(p) - \frac{(p^2 + m^2)^2}{2m^4} (I_{\mu\nu}^{m0}(p) + I_{\mu\nu}^{0m}(p)) + I_{\mu\nu}^{m0}(0) + \\
&\quad - p_\mu p_\nu \left[\frac{p^4}{8m^4} I^{00}(p) + \left(1 + \frac{(p^2 + 2m^2)^2}{8m^4} \right) I^{mm}(p) - \frac{(p^2 + m^2)^2}{4m^4} I^{m0}(p) - \frac{1}{4} I^{m0}(0) \right].
\end{aligned} \tag{A40}$$

The second polarization term in Eq. (A34) reads

$$\begin{aligned}
\Pi_{2\mu\nu}(p) &= 4 \int_k \left[\delta_{\mu\nu} - \frac{k_\mu k_\nu}{k^2} \right] \left(p^2 - \frac{(p \cdot q)^2}{q^2} \right) G_m(k)G_m(q) \\
&= 4 \int_k [\delta_{\mu\nu} p^2 - p^2 k_\mu k_\nu G_0(k) - \delta_{\mu\nu} (p \cdot q)^2 G_0(q) + (p \cdot q)^2 k_\mu k_\nu G_0(k)G_0(q)] G_m(k)G_m(q) \\
&= 4 \left[\delta_{\mu\nu} p^2 I^{mm}(p) - \frac{p^2}{m^2} (I_{\mu\nu}^{0m}(p) - I_{\mu\nu}^{m0}(p)) \right] + \Pi_{2a\mu\nu}(p) + \Pi_{2b\mu\nu}(p),
\end{aligned} \tag{A41}$$

where

$$\begin{aligned}
\Pi_{2a\mu\nu}(p) &= -4\delta_{\mu\nu} \int_k G_m(q)G_m(k)G_0(k)(p \cdot k)^2 = -\frac{4}{m^2} \delta_{\mu\nu} \int_k G_m(q)(G_0(k) - G_m(k))(p \cdot k)^2, \\
\Pi_{2b\mu\nu}(p) &= 4 \int_k G_m(k)G_m(q)G_0(k)G_0(q)(p \cdot q)^2 k_\mu k_\nu.
\end{aligned} \tag{A42}$$

Using the identities

$$\begin{aligned}
2(p \cdot k) &= p^2 + \beta^2 - \alpha^2 + G_\alpha^{-1}(k) - G_\beta^{-1}(q), \\
2(p \cdot k)G_\beta(q)G_\alpha(k) &= (p^2 + \beta^2 - \alpha^2)G_\beta(q)G_\alpha(k) + G_\beta(q) - G_\alpha(k), \\
4(p \cdot k)^2 G_\beta(q)G_\alpha(k) &= (p^2 + \beta^2 - \alpha^2)^2 G_\beta(q)G_\alpha(k) + (p^2 + \beta^2 - \alpha^2)(G_\beta(q) - G_\alpha(k)) + 2(p \cdot k)(G_\beta(q) - G_\alpha(k)),
\end{aligned} \tag{A43}$$

which hold for any pair k, q satisfying $k + q = p$, we obtain for $(\alpha, \beta) = (0, m)$ and for $(\alpha, \beta) = (m, m)$, respectively,

$$\begin{aligned}
4(p \cdot k)^2 G_m(q) G_0(k) &= (p^2 + m^2)^2 G_m(q) G_0(k) + (p^2 + m^2)(G_m(q) - G_0(k)) + 2(p \cdot k)(G_m(q) - G_0(k)), \\
4(p \cdot k)^2 G_m(q) G_m(k) &= p^4 G_m(q) G_m(k) + p^2(G_m(q) - G_m(k)) + 2(p \cdot k)(G_m(q) - G_m(k)),
\end{aligned} \tag{A44}$$

so that the term Π_{2a} can be written as

$$\Pi_{2a\mu\nu} = -\frac{\delta_{\mu\nu}}{m^2} [(p^2 + m^2)^2 I^{0m}(p) - p^4 I^{mm}(p) - m^2(p^2 + m^2) I^{0m}(0)]. \tag{A45}$$

Using the second of Eqs. (A36), the term Π_{2b} can be written as

$$\Pi_{2b\mu\nu}(p) = \frac{4}{m^4} \int_k (p \cdot q)^2 k_\mu k_\nu (G_0(k) G_0(q) - G_0(k) G_m(q) - G_m(k) G_0(q) + G_m(k) G_m(q)), \tag{A46}$$

while reversing k and q in Eq. (A43) we obtain, for α and β that take the values 0 and m ,

$$\begin{aligned}
4(p \cdot q)^2 G_0(k) G_0(q) &= p^4 G_0(k) G_0(q) + 3p^2(G_0(k) - G_0(q)) - 2p \cdot k(G_0(k) - G_0(q)), \\
4(p \cdot q)^2 G_0(k) G_m(q) &= (p^2 - m^2)^2 G_0(k) G_m(q) + (3p^2 - m^2)(G_0(k) - G_m(q)) - 2p \cdot k(G_0(k) - G_m(q)), \\
4(p \cdot q)^2 G_m(k) G_0(q) &= (p^2 + m^2)^2 G_m(k) G_0(q) + (3p^2 + m^2)(G_m(k) - G_0(q)) - 2p \cdot k(G_m(k) - G_0(q)), \\
4(p \cdot q)^2 G_m(k) G_m(q) &= p^4 G_m(k) G_m(q) + 3p^2(G_m(k) - G_m(q)) - 2p \cdot k(G_m(k) - G_m(q)),
\end{aligned} \tag{A47}$$

yielding for Π_{2b}

$$\Pi_{2b\mu\nu}(p) = \frac{1}{m^4} [p^4 (I_{\mu\nu}^{00}(p) + I_{\mu\nu}^{mm}(p)) - (p^2 - m^2)^2 I_{\mu\nu}^{0m}(p) - (p^2 + m^2)^2 I_{\mu\nu}^{m0}(p)] + 2I_{\mu\nu}^{0m}(0) + p_\mu p_\nu I^{0m}(0). \tag{A48}$$

Adding Eqs. (A45) and (A48) in Eq. (A41), the second polarization term in Eq. (A34) is

$$\begin{aligned}
\Pi_{2\mu\nu}(p) &= \delta_{\mu\nu} \left[\frac{p^2}{m^2} (p^2 + 4m^2) I^{mm}(p) - \frac{(p^2 + m^2)^2}{m^2} I^{0m}(p) + (p^2 + m^2) I^{0m}(0) \right] + p_\mu p_\nu I^{0m}(0) + \\
&+ \frac{p^4}{m^4} I_{\mu\nu}^{00}(p) + \frac{p^2}{m^4} (p^2 + 4m^2) I_{\mu\nu}^{mm}(p) - \frac{(p^2 + m^2)^2}{m^4} (I_{\mu\nu}^{m0}(p) + I_{\mu\nu}^{0m}(p)) + 2I_{\mu\nu}^{0m}(0).
\end{aligned} \tag{A49}$$

The third polarization term in Eq. (A34) can be decomposed by observing that

$$[t^{\mu\lambda}(k)(p+q)_\lambda] = 2 \left(p^\mu - \frac{p \cdot k}{k^2} k^\mu \right), \quad [t^{\nu\rho}(q)(p+k)_\rho] = 2 \left(p^\nu - \frac{p \cdot q}{q^2} q^\nu \right), \tag{A50}$$

so that, changing the integration variable from k to q in the $q_\nu p_\mu$ term, Π_3 reads

$$\begin{aligned}
\Pi_{3\mu\nu}(p) &= -4 \int_k \left(p_\mu p_\nu - \frac{p \cdot k}{k^2} (k_\mu p_\nu + k_\nu p_\mu) + \frac{(p \cdot k)(p \cdot q)}{k^2 q^2} k_\mu q_\nu \right) G_m(k) G_m(q) \\
&= -4 p_\mu p_\nu I^{mm}(p) + \Pi_{3a\mu\nu}(p) + \Pi_{3b\mu\nu}(p),
\end{aligned} \tag{A51}$$

where

$$\begin{aligned}
\Pi_{3a\mu\nu}(p) &= 4 \int_k (p \cdot k) (k_\mu p_\nu + k_\nu p_\mu) G_0(k) G_m(k) G_m(q), \\
\Pi_{3b\mu\nu}(p) &= -4 \int_k (p \cdot k) (p \cdot q) k_\mu q_\nu G_0(k) G_0(q) G_m(k) G_m(q).
\end{aligned} \tag{A52}$$

The first integral can be decomposed by using the identity

$$(k^\mu p^\nu + k^\nu p^\mu) = p^\mu p^\nu + k^\mu k^\nu - q^\mu q^\nu \tag{A53}$$

and observing that, by the second of Eqs. (A36) and the second of Eqs. (A43),

$$\begin{aligned} 4(p \cdot k)G_0(k)G_m(k)G_m(q) &= \frac{4(p \cdot k)}{m^2}[G_0(k)G_m(q) - G_m(k)G_m(q)] \\ &= \frac{2}{m^2}[(p^2 + m^2)G_0(k)G_m(q) - p^2G_m(k)G_m(q) - m^2G_0(k)G_m(k)], \end{aligned} \quad (\text{A54})$$

yielding

$$\Pi_{3a\mu\nu}(p) = \frac{2}{m^2}p_\mu p_\nu[(p^2 + m^2)I^{0m}(p) - p^2I^{mm}(p)] + \frac{2}{m^2}(p^2 + m^2)(I_{\mu\nu}^{0m}(p) - I_{\mu\nu}^{m0}(p)). \quad (\text{A55})$$

In the second integral Π_{3b} we can use the identity

$$k_\mu q_\nu = \left[\frac{1}{2}p_\mu p_\nu - k_\mu k_\nu \right] + \frac{1}{2}(k_\mu - q_\mu)p_\nu, \quad (\text{A56})$$

where the last term can be dropped because it is antisymmetric in the exchange of k and q and its contribution to the integral is zero. Taking the second of Eqs. (A43) with $\alpha = \beta = m$ and the same equation with $\alpha = \beta = 0$ and k, q interchanged, their product can be written as

$$\begin{aligned} 4(p \cdot k)(p \cdot q)G_m(k)G_m(q)G_0(k)G_0(q) &= \frac{p^4}{m^4}[G_0(k)G_0(q) + G_m(k)G_m(q)] + \\ &+ \left(1 - \frac{p^4}{m^4}\right)[G_0(k)G_m(q) + G_m(k)G_0(q)] - G_0(q)G_m(q) - G_0(k)G_m(k), \end{aligned} \quad (\text{A57})$$

where the second of Eqs. (A36) has been used for decomposing the products of more than two G functions. Then, the integral can be written

$$\begin{aligned} \Pi_{3b\mu\nu}(p) &= \frac{p^4}{m^4}(I_{\mu\nu}^{00}(p) + I_{\mu\nu}^{mm}(p)) + \left(1 - \frac{p^4}{m^4}\right)(I_{\mu\nu}^{0m}(p) + I_{\mu\nu}^{m0}(p)) + \\ &- p_\mu p_\nu \left[\frac{p^4}{2m^4}(I^{00}(p) + I^{mm}(p)) - \left(\frac{p^4}{m^4} - 1\right)I^{0m}(p) \right] - 2I_{\mu\nu}^{0m}(0). \end{aligned} \quad (\text{A58})$$

Adding Eqs. (A3) and (A58) in Eq. (A51), the third polarization term in Eq. (A34) is

$$\begin{aligned} \Pi_{3\mu\nu}(p) &= \frac{p^4}{m^4}(I_{\mu\nu}^{00}(p) + I_{\mu\nu}^{mm}(p)) + \frac{3m^4 + 2m^2p^2 - p^4}{m^4}I_{\mu\nu}^{0m}(p) - \frac{(p^2 + m^2)^2}{m^4}I_{\mu\nu}^{m0}(p) - 2I_{\mu\nu}^{0m}(0) + \\ &- p_\mu p_\nu \left[\frac{p^4}{2m^4}I^{00}(p) + \frac{p^4 + 4m^2p^2 + 8m^4}{2m^4}I^{mm}(p) - \frac{(p^2 + m^2)^2}{m^4}I^{0m}(p) \right]. \end{aligned} \quad (\text{A59})$$

The last polarization term in Eq. (A34) can be decomposed by observing that

$$[t^{\nu\lambda}(k)t_{\lambda\rho}(q)(p+k)^\rho] = 2\frac{(k \cdot q)}{q^2} \left[\frac{(k \cdot p)}{k^2}k^\nu - p^\nu \right]. \quad (\text{A60})$$

Then, recalling that $q_\mu = p_\mu - k_\mu$, the integral reads

$$\Pi_{4\mu\nu}(p) = 2 \int_k \left[\frac{(k \cdot p)}{k^2}(p_\mu k_\nu - 2k_\mu k_\nu) + (2k_\mu p_\nu - p_\mu p_\nu) \right] (k \cdot q)G_0(q)G_m(k)G_m(q) + \mu \leftrightarrow \nu. \quad (\text{A61})$$

Using the identity

$$p_\mu k_\nu + p_\nu k_\mu = p_\mu p_\nu + k_\mu k_\nu - q_\mu q_\nu \quad (\text{A62})$$

the two pieces can be added together yielding

$$\Pi_{4\mu\nu}(p) = 2 \int_k \left[\frac{(k \cdot p)}{k^2} (p_\mu p_\nu - 3k_\mu k_\nu - q_\mu q_\nu) + 2(k_\mu k_\nu - q_\mu q_\nu) \right] (k \cdot q) G_0(q) G_m(k) G_m(q). \quad (\text{A63})$$

The product of three G functions can be decomposed by the second of Eqs. (A36) and the two arising terms can be written by the first of Eqs. (A36), with $(\alpha, \beta) = (m, 0)$ and $(\alpha, \beta) = (m, m)$, respectively,

$$2(k \cdot q)[G_0(q)G_m(q)]G_m(k) = \frac{p^2 + m^2}{m^2} G_m(k)G_0(q) - \frac{(p^2 + 2m^2)}{m^2} G_m(k)G_m(q) - \frac{1}{m^2} (G_0(q) - G_m(q)). \quad (\text{A64})$$

The integral then reads

$$\Pi_{4\mu\nu}(p) = 2 \frac{p^2 + m^2}{m^2} (I_{\mu\nu}^{m0}(p) - I_{\mu\nu}^{0m}(p)) - 2p_\mu p_\nu I^{0m}(0) + \Pi_{4a\mu\nu}(p), \quad (\text{A65})$$

where

$$\begin{aligned} \Pi_{4a\mu\nu}(p) &= \frac{1}{2} \int_k 2(k \cdot p) G_0(k) (p_\mu p_\nu - 3k_\mu k_\nu - q_\mu q_\nu) \\ &\quad \times \left[\frac{p^2 + m^2}{m^2} G_m(k)G_0(q) - \frac{(p^2 + 2m^2)}{m^2} G_m(k)G_m(q) - \frac{1}{m^2} (G_0(q) - G_m(q)) \right]. \end{aligned} \quad (\text{A66})$$

Using the first of Eqs. (A43) with $\alpha = 0$ and $\beta = m, 0$,

$$2(k \cdot p)G_0(k) = (p^2 + m^2)G_0(k) + 1 - G_m^{-1}(q)G_0(k) = p^2 G_0(k) + 1 - G_0^{-1}(q)G_0(k), \quad (\text{A67})$$

and decoupling the product $G_m(k)G_0(k)$ by the second of Eqs. (A36), the term Π_{4a} can be written as

$$\begin{aligned} \Pi_{4a\mu\nu}(p) &= \frac{1}{2m^2} \int_k (p_\mu p_\nu - 3k_\mu k_\nu - q_\mu q_\nu) \left[\frac{p^4}{m^2} G_0(k)G_0(q) + \frac{p^2(p^2 + 2m^2)}{m^2} G_m(k)G_m(q) + \right. \\ &\quad \left. - \frac{(p^2 + m^2)^2}{m^2} G_0(k)G_m(q) - \frac{p^4 - m^4}{m^2} G_m(k)G_0(q) + m^2(G_0(k)G_m(k) - G_0(q)G_m(q)) \right], \end{aligned} \quad (\text{A68})$$

so that the integral reads

$$\begin{aligned} \Pi_{4a\mu\nu}(p) &= p_\mu p_\nu \left[\frac{p^4}{2m^4} I^{00}(p) + \frac{p^2(p^2 + 2m^2)}{2m^4} I^{mm}(p) - \frac{p^2(p^2 + m^2)}{m^4} I^{m0}(p) + I^{0m}(0) \right] + \\ &\quad - 2 \frac{p^4}{m^4} I_{\mu\nu}^{00}(p) - 2 \frac{p^2(p^2 + 2m^2)}{m^4} I_{\mu\nu}^{mm}(p) + \frac{2p^4 + 3m^2 p^2 + m^4}{m^4} I_{\mu\nu}^{0m}(p) + \frac{2p^4 + m^2 p^2 - m^4}{m^4} I_{\mu\nu}^{m0}(p). \end{aligned} \quad (\text{A69})$$

Inserting the result in Eq. (A65) the fourth polarization term in Eq. (A34) is

$$\begin{aligned} \Pi_{4\mu\nu}(p) &= p_\mu p_\nu \left[\frac{p^4}{2m^4} I^{00}(p) + \frac{p^2(p^2 + 2m^2)}{2m^4} I^{mm}(p) - \frac{p^2(p^2 + m^2)}{m^4} I^{m0}(p) - I^{0m}(0) \right] + \\ &\quad - 2 \frac{p^4}{m^4} I_{\mu\nu}^{00}(p) - 2 \frac{p^2(p^2 + 2m^2)}{m^4} I_{\mu\nu}^{mm}(p) + \frac{2p^4 + 3m^2 p^2 + m^4}{m^4} I_{\mu\nu}^{m0}(p) + \frac{2p^4 + m^2 p^2 - m^4}{m^4} I_{\mu\nu}^{0m}(p). \end{aligned} \quad (\text{A70})$$

Finally, adding up the four polarization terms in Eqs. (A40), (A49), (A59), (A70), the total graph (2b) reads

$$\begin{aligned} \Pi_{\mu\nu}^{(2b)}(p) = & \frac{p^4}{2m^4} I_{\mu\nu}^{00}(p) + \left[4 + \frac{(p^2 + 2m^2)^2}{2m^4} \right] I_{\mu\nu}^{mm}(p) - \frac{(p^2 + m^2)^2}{2m^4} (I_{\mu\nu}^{m0}(p) + I_{\mu\nu}^{0m}(p)) + I_{\mu\nu}^{m0}(0) \\ & + \frac{(p^2 + m^2)}{m^2} (I_{\mu\nu}^{0m}(p) - I_{\mu\nu}^{m0}(p)) + \delta_{\mu\nu} \left[\frac{p^2}{m^2} (p^2 + 4m^2) I^{mm}(p) - \frac{(p^2 + m^2)^2}{m^2} I^{0m}(p) + (p^2 + m^2) I^{0m}(0) \right] + \\ & - p_\mu p_\nu \left[\frac{p^4}{8m^4} I^{00}(p) + \frac{(p^4 + 12m^2 p^2 + 44m^4)}{8m^4} I^{mm}(p) - \frac{(p^2 + m^2)(p^2 + 5m^2)}{4m^4} I^{m0}(p) - \frac{1}{4} I^{m0}(0) \right]. \end{aligned} \quad (\text{A71})$$

The transverse projections of the graph follow by the projected integrals in Eqs. (A14). We observed that by Eq. (A15) the projected integrals turn out to be symmetric, $I_{L,T}^{\alpha\beta} = I_{L,T}^{\beta\alpha}$. Thus, the projection of the graph follows by dropping the longitudinal and the antisymmetric terms, and by replacing the integrals by the projected ones according to

$$\begin{aligned} p_\mu p_\nu & \rightarrow 0, \\ (I_{\mu\nu}^{0m}(p) - I_{\mu\nu}^{m0}(p)) & \rightarrow 0, \\ \delta_{\mu\nu} & \rightarrow 1 \\ I_{\mu\nu}^{\alpha\beta}(p) & \rightarrow I_{L,T}^{\alpha\beta}(p) = I_{L,T}^{\beta\alpha}(p), \\ I_{\mu\nu}^{\alpha\beta}(0) & \rightarrow I_{L,T}^{\alpha\beta} = I_{L,T}^{\beta\alpha}. \end{aligned} \quad (\text{A72})$$

4. Graph 2a—(ghost loop)

In the Landau gauge, setting $d = 4$ and using a free-particle propagator, the general expression of the ghost loop (see e.g., Ref. [41]) reads

$$\Pi_{\mu\nu}^{(2a)}(p) = \int_k (p_\mu - k_\mu) k_\nu G_0(k) G_0(p - k). \quad (\text{A73})$$

By exchanging k^μ and $p^\mu - k^\mu$ the integral shows the symmetry $\Pi_{\mu\nu} = \Pi_{\nu\mu}$ so that, using Eq. (A53), we can replace

$$p_\mu k_\nu \rightarrow \frac{1}{2} (p_\mu k_\nu + k_\mu p_\nu) = \frac{1}{2} (k_\mu k_\nu - q_\mu q_\nu + p_\mu p_\nu). \quad (\text{A74})$$

The first two terms on the right-hand side cancel in the integration yielding

$$\Pi_{\mu\nu}^{(2a)}(p) = \frac{1}{2} p_\mu p_\nu I^{00}(p) - I_{\mu\nu}^{00}(p). \quad (\text{A75})$$

The projected ghost loop is just

$$\Pi_{L,T}^{(2a)}(p) = -I_{L,T}^{00}(p). \quad (\text{A76})$$

5. Total (uncrossed) one-loop polarization

Adding up the uncrossed one-loop graphs (1b), (2b) and (2a), the standard (uncrossed) projected one-loop polarization of Ref. [38] is recovered by the sum of Eqs. (A30), (A71) and (A75):

$$\begin{aligned} \Pi_{L,T}^{1\text{-loop}}(p) = & \left[\frac{p^4}{2m^4} - 1 \right] I_{L,T}^{00}(p) + \left[4 + \frac{(p^2 + 2m^2)^2}{2m^4} \right] I_{L,T}^{mm}(p) - \frac{(p^2 + m^2)^2}{m^4} I_{L,T}^{m0}(p) \\ & + \frac{p^2(p^2 + 4m^2)}{m^2} I^{mm}(p) - \frac{(p^2 + m^2)^2}{m^2} I^{0m}(p) + (p^2 + m^2) I^{0m}(0) - 2J_m. \end{aligned} \quad (\text{A77})$$

6. Ghost self-energy

In this work, the total one-loop ghost self energy is the sum of the standard one-loop graph and the crossed one, which contains the insertion of a mass counterterm,

$$\Sigma^{\text{tot}}(p) = \left(1 - m^2 \frac{\partial}{\partial m^2} \right) \Sigma(p) \quad (\text{A78})$$

where $\Sigma(p)$ is the standard one loop integral [19,41] in the Landau gauge,

$$\Sigma(p) = - \int_k \frac{k^2 p^2 - (k \cdot p)^2}{k^2 (k-p)^2 (k^2 + m^2)} = - \int_k [p^2 G_m(k) G_0(q) - (k \cdot p)^2 G_0(k) G_m(k) G_0(q)]. \quad (\text{A79})$$

Using the last of Eqs. (A43) with $\alpha = m$ and $\beta = 0$, and decoupling the product $G_m(k)G_0(k)$ by the second of Eqs. (A36), we can write

$$4(k \cdot p)^2 G_0(q) G_m(k) G_0(k) = \frac{(p^2 - m^2)^2}{m^2} [G_0(k) G_0(q) - G_m(k) G_0(q)] \\ + (p^2 - m^2) [G_0(k) G_0(q) - G_m(k) G_0(k)] + 2(p \cdot k) [G_0(q) G_0(k) - G_m(k) G_0(k)]. \quad (\text{A80})$$

Then using the second of Eqs. (A43) with $\alpha = \beta = 0$ and dropping the vanishing integrals

$$\int_k [G_0(q) - G_0(k)] = 0, \quad \int_k (p \cdot k) G_m(k) G_0(k) = 0, \quad (\text{A81})$$

the second term of Eq. (A79) reads

$$\int_k (k \cdot p)^2 G_0(k) G_m(k) G_0(q) = - \frac{(p^2 - m^2)^2}{4m^2} \int_k G_m(k) G_0(q) + \frac{p^4}{4m^2} \int_k G_0(k) G_0(q) - \frac{(p^2 - m^2)}{4} \int_k G_m(k) G_0(k) \quad (\text{A82})$$

and the (uncrossed) one-loop self energy can be written as

$$\Sigma(p) = - \frac{(p^2 + m^2)^2}{4m^2} I^{m0}(p) + \frac{p^4}{4m^2} I^{00}(p) + \frac{(p^2 - m^2)}{4m^2} (J_m - J_0), \quad (\text{A83})$$

as derived in Ref. [38] by the same method.

7. Crossed graphs and total polarization

The crossed graphs (1c), (2c), (1d) and the crossed one-loop ghost self energy can be obtained by simple derivatives. The sum of all graphs gives a total one-loop polarization that can be written as

$$\Pi_{L,T}^{\text{tot}}(p) = \Pi_{L,T}^{(a-c)}(p) + \Pi_{L,T}^{(1d)}(p), \quad (\text{A84})$$

where $\Pi_{L,T}^{(a-c)}(p)$ is the sum of graphs (2a), (1b), (2b), (1c), (2c) and can be evaluated as

$$\Pi_{L,T}^{(a-c)}(p) = \left(1 - m^2 \frac{\partial}{\partial m^2}\right) \Pi_{L,T}^{1\text{-loop}}(p). \quad (\text{A85})$$

Here $\Pi_{L,T}^{1\text{-loop}}(p)$ is the projected one-loop polarization of Eq. (A77) and $\Pi_{L,T}^{(1d)}$ is the doubly crossed tadpole, with two counterterm insertions.

The derivative acts on the coefficients of the integrals according to

$$\left(-m^2 \frac{\partial}{\partial m^2}\right) [m^2] = -m^2, \\ \left(-m^2 \frac{\partial}{\partial m^2}\right) \left[\frac{1}{m^2}\right] = \frac{1}{m^2}, \\ \left(-m^2 \frac{\partial}{\partial m^2}\right) \left[\frac{1}{m^4}\right] = \frac{2}{m^4}. \quad (\text{A86})$$

The function $\Pi_{L,T}^{(a-c)}$ then reads

$$\Pi_{L,T}^{(a-c)}(p) = \Pi_{L,T}^{1\text{-loop}}(p) + \left(-m^2 \frac{\partial}{\partial m^2} \Pi_{L,T}^{1\text{-loop}}(p)\right)_I - m^2 (\Pi_{L,T}^{1\text{-loop}}(p))_{I \rightarrow \partial I}, \quad (\text{A87})$$

where the derivative of the coefficients is taken in the second term while the derivative of the integrals is considered in the third term. Using Eqs. (A86) and (A77),

$$\left(-m^2 \frac{\partial}{\partial m^2} \Pi_{L,T}^{1\text{-loop}}(p)\right)_I = \left[\frac{p^4}{m^4}\right] I_{L,T}^{00}(p) + \left[\frac{p^4 + 2m^2 p^2}{m^4}\right] I_{L,T}^{mm}(p) - \left[\frac{2p^4 + 2m^2 p^2}{m^4}\right] I_{L,T}^{m0}(p) \\ + \left[\frac{p^4}{m^2}\right] I^{mm}(p) - \left[\frac{p^4 - m^4}{m^2}\right] I^{0m}(p) - [m^2] I^{0m}(0), \quad (\text{A88})$$

while replacing the integrals I by their derivatives ∂I , Eq. (A77) reads

$$-m^2(\Pi_{L,T}^{1\text{-loop}}(p))_{I \rightarrow \partial I} = - \left[8m^2 + \frac{(p^2 + 2m^2)^2}{m^2} \right] \partial I_{L,T}^{mm}(p) + \frac{(p^2 + m^2)^2}{m^2} \partial I_{L,T}^{m0}(p) - 2p^2(p^2 + 4m^2) \partial I^{mm}(p) \\ + (p^2 + m^2)^2 \partial I^{m0}(p) - m^2(p^2 + m^2) \partial I^{m0}(0) + 2m^2 \partial J_m. \quad (\text{A89})$$

Summing up the contributions of Eqs. (A77), (A88) and (A89) in Eq. (A87) and using Eq. (A26) we obtain

$$\Pi_{L,T}^{(a-c)}(p) = \left[\frac{3p^4}{2m^4} - 1 \right] I_{L,T}^{00}(p) + \left[4 + \frac{3p^4 + 8m^2 p^2 + 4m^4}{2m^4} \right] I_{L,T}^{mm}(p) - \left[\frac{3p^4 + 4m^2 p^2 + m^4}{m^4} \right] I_{L,T}^{m0}(p) \\ + \frac{2p^2(p^2 + 2m^2)}{m^2} I^{mm}(p) - \frac{2p^2(p^2 + m^2)}{m^2} I^{0m}(p) - \left[\frac{2p^2 + 3m^2}{m^2} \right] J_m + \left[\frac{2p^2 + m^2}{m^2} \right] J_0 \\ + - \left[8m^2 + \frac{(p^2 + 2m^2)^2}{m^2} \right] \partial I_{L,T}^{mm}(p) + \frac{(p^2 + m^2)^2}{m^2} \partial I_{L,T}^{m0}(p) - 2p^2(p^2 + 4m^2) \partial I^{mm}(p) \\ + (p^2 + m^2)^2 \partial I^{m0}(p) + (p^2 + 3m^2) \partial J_m. \quad (\text{A90})$$

Finally, the doubly crossed tadpole (1d) in Eq. (A84) can be written as [19,41]

$$\Pi_{L,T}^{(1d)}(p) = \frac{m^4}{2} \frac{\partial^2}{\partial(m^2)^2} \Pi_{L,T}^{(1b)}(p), \quad (\text{A91})$$

and using Eq. (A31)

$$\Pi_{L,T}^{(1d)}(p) = -m^4 \partial^2 J_m - \frac{m^4}{2} \partial^2 I_{L,T}^{m0} p. \quad (\text{A92})$$

By Eqs. (A28) the derivative $\partial^2 I_{L,T}^{m0} p$ can be expressed in terms of the integrals $J_m^{L,T}$ and their derivatives $\partial J_m^{L,T}$, yielding

$$\Pi_{L,T}^{(1d)}(p) = -m^4 \partial^2 J_m + \frac{1}{m^2} (J_{m,p}^{L,T} - J_{0,p}^{L,T}) + \\ - \partial J_{m,p}^{L,T} + \frac{m^2}{2} \partial^2 J_{m,p}^{L,T}, \quad (\text{A93})$$

where

$$\left(-m^2 \frac{\partial}{\partial m^2} \Sigma(p) \right)_I = \frac{(m^4 - p^4)}{4m^2} I^{m0}(p) + \frac{p^4}{4m^2} I^{00}(p) + \frac{p^2}{4m^2} (J_m - J_0). \quad (\text{A97})$$

The total ghost self energy then follows, adding up the contributions of Eqs. (A83), (A97) and (A96) in Eq. (A95)

$$\Sigma^{\text{tot}}(p) = -\frac{p^2(p^2 + m^2)}{2m^2} I^{m0}(p) + \frac{p^4}{2m^2} I^{00}(p) + \frac{(2p^2 - m^2)}{4m^2} (J_m - J_0) + \frac{(p^2 + m^2)^2}{4} \partial I^{m0}(p) - \frac{(p^2 - m^2)}{4} \partial J_m. \quad (\text{A98})$$

$$J_{m,p}^T = J_m^T,$$

$$J_{m,p}^L = (J_m^L - J_m^T) \frac{\mathbf{p}^2}{\mathbf{p}^2 + \omega^2} + J_m^T. \quad (\text{A94})$$

8. Crossed graphs and total ghost self energy

The total ghost self-energy $\Sigma^{\text{tot}}(p)$ can be derived by the same method, as shown in Eq. (A78),

$$\Sigma^{\text{tot}}(p) = \Sigma(p) + \left(-m^2 \frac{\partial}{\partial m^2} \Sigma(p) \right)_I - m^2 [\Sigma(p)]_{I \rightarrow \partial I}, \quad (\text{A95})$$

where the derivative of the coefficients is taken in the second term, while the derivative of the integrals is considered in the third term.

Replacing the integrals I by their derivatives ∂I , Eq. (A83) gives

$$-m^2 [\Sigma(p)]_{I \rightarrow \partial I} = \frac{(p^2 + m^2)^2}{4} \partial I^{m0}(p) - \frac{(p^2 - m^2)}{4} \partial J_m, \quad (\text{A96})$$

while, using Eq. (A86), the derivative of the coefficients in Eq. (A83) gives

APPENDIX B: THERMAL INTEGRALS

By general arguments, the thermal integral $I(T)$ of a function $f(k) = f(\mathbf{k}, k_4)$ can be written as

$$I(T) = \int_k f(k) = T \sum_n \int \frac{d^3 \mathbf{k}}{(2\pi)^3} f(\mathbf{k}, \omega_n) = I_V + I_{Th}(T) \quad (\text{B1})$$

where, setting $k_4 = \omega_n = -ik_0$,

$$I_V = \frac{1}{2\pi i} \int_{-i\infty}^{+i\infty} dk_0 \int \frac{d^3 \mathbf{k}}{(2\pi)^3} f(\mathbf{k}, -ik_0) = \int \frac{d^4 k}{(2\pi)^4} f(k) \quad (\text{B2})$$

is the Euclidean integral at $T = 0$, denoted *vacuum* part $I_V = I(0)$, while the *thermal* part $I_{Th}(T)$ is

$$I_{Th}(T) = - \int \frac{d^3 \mathbf{k}}{(2\pi)^3} \sum_{\text{Resid.}} \left[\frac{2\Re f(\mathbf{k}, ik_0)}{e^{\beta k_0} - 1} \right]_{\text{Re} k_0 > 0} \quad (\text{B3})$$

where the sum is over the residues in the right complex plane of k_0 and the symbol $\Re f$ is defined as

$$\Re f(\mathbf{k}, ik_0) = \frac{f(\mathbf{k}, ik_0) + f(\mathbf{k}, -ik_0)}{2}. \quad (\text{B4})$$

We observe that if $f(k)$ is a complex function, then $\Re f(k)$ is not the true real part $\text{Re} f(k)$. The thermal part vanishes in the limit $T \rightarrow 0$.

Many of the thermal integrals were evaluated in great detail in Ref. [38]. In the next sections we collect the same results and, by the same method, we add the explicit evaluation of all the remaining integrals that are required in the present work.

1. Vacuum integrals

The vacuum parts of all the one-loop graphs were evaluated in Ref. [19]. They can be made finite by wave function renormalization. After subtraction, the sum of all the gluon polarization graphs in Eq. (A84) and of all ghost self-energy graphs in Eq. (A98) give the following vacuum terms at $T = 0$:

$$\begin{aligned} \Pi_V^{\text{tot}}(s) &= -\frac{3m^2 s}{(4\pi)^2} [\pi_1(s) + \pi_0], \\ \Sigma_V^{\text{tot}}(s) &= \frac{3m^2 s}{(4\pi)^2} [\sigma_1(s) + \sigma_0], \end{aligned} \quad (\text{B5})$$

where $s = p^2/m^2$, the constants π_0 , σ_0 are arbitrary renormalization constants, depending on the subtraction point, and $\pi_1(s)$, $\sigma_1(s)$ are the explicit analytical functions

$$\begin{aligned} \pi_1(x) &= \frac{5}{8x} + \frac{1}{72} [L_a + L_b + L_c + R_a + R_b + R_c], \\ \sigma_1(x) &= \frac{1}{12} [L_g + R_g], \end{aligned} \quad (\text{B6})$$

written in terms of the logarithmic functions L_x

$$\begin{aligned} L_a(x) &= \frac{3x^3 - 34x^2 - 28x - 24}{x} \\ &\quad \times \sqrt{\frac{4+x}{x}} \log\left(\frac{\sqrt{4+x} - \sqrt{x}}{\sqrt{4+x} + \sqrt{x}}\right), \\ L_b(x) &= \frac{2(1+x)^2}{x^3} (3x^3 - 20x^2 + 11x - 2) \log(1+x), \\ L_c(x) &= (2 - 3x^2) \log(x), \\ L_g(x) &= \frac{(1+x)^2(2x-1)}{x^2} \log(1+x) - 2x \log(x) \end{aligned} \quad (\text{B7})$$

and of the rational parts R_x

$$\begin{aligned} R_a(x) &= -\frac{4+x}{x} (x^2 - 20x + 12), \\ R_b(x) &= \frac{2(1+x)^2}{x^2} (x^2 - 10x + 1), \\ R_c(x) &= \frac{2}{x^2} + 2 - x^2, \\ R_g(x) &= \frac{1}{x} + 2. \end{aligned} \quad (\text{B8})$$

2. Thermal part of J_m and $J_m^{L,T}$

The integral J_m is defined in Eq. (A13) and has the general form of Eq. (B1) with

$$f(\mathbf{k}, ik_0) = G_m(\mathbf{k}, ik_0) = \frac{1}{\epsilon_{\mathbf{k},m}^2 - k_0^2}, \quad (\text{B9})$$

having denoted by $\epsilon_{\mathbf{k},m}$ the positive square root

$$\epsilon_{\mathbf{k},m} = \sqrt{\mathbf{k}^2 + m^2}. \quad (\text{B10})$$

The thermal part, Eq. (B3), takes a contribution at the pole $k_0 = \epsilon_{\mathbf{k},m}$, yielding

$$(J_m)_{Th} = - \int \frac{d^3 \mathbf{k}}{(2\pi)^3} \left[\left(\frac{-2}{\epsilon_{\mathbf{k},m} + k_0} \right) \left(\frac{1}{e^{\beta k_0} - 1} \right) \right]_{k_0 = \epsilon_{\mathbf{k},m}}, \quad (\text{B11})$$

and denoting by $n(\epsilon)$ the Bose distribution,

$$n(\epsilon) = [e^{\beta \epsilon} - 1]^{-1}, \quad (\text{B12})$$

we obtain

$$(J_m)_{Th} = \int \frac{d^3\mathbf{k}}{(2\pi)^3} \frac{n(\epsilon_{\mathbf{k},m})}{\epsilon_{\mathbf{k},m}} = \int_0^\infty \frac{x^2 dx n(\epsilon_{x,m})}{2\pi^2 \epsilon_{x,m}}, \quad (\text{B13})$$

with the obvious notation $\epsilon_{x,m} = \sqrt{x^2 + m^2}$.

In the special case $m = 0$,

$$(J_0)_{Th} = \int_0^\infty \frac{x dx}{2\pi^2} n(x). \quad (\text{B14})$$

The thermal parts of the integrals J_m^L, J_m^T , as defined in Eq. (A27), follow immediately by replacing $f(k) \rightarrow -k_0^2 f(k)$ and $f(k) \rightarrow \frac{1}{3} k^2 f(k)$, respectively, in Eq. (B9). Following the same steps as before, the thermal parts read

$$\begin{aligned} (J_m^L)_{Th} &= - \int_0^\infty \frac{x^2 dx}{2\pi^2} \epsilon_{x,m} n(\epsilon_{x,m}), \\ (J_m^T)_{Th} &= \int_0^\infty \frac{x^4 dx}{6\pi^2} \frac{n(\epsilon_{x,m})}{\epsilon_{x,m}}. \end{aligned} \quad (\text{B15})$$

3. Thermal part of $I^{a\beta}(p)$

The integral $I^{a\beta}(p)$ is also defined in Eq. (A13) and has the general form of Eq. (B1) with

$$\begin{aligned} f(k) &= G_\alpha(k) G_\beta(p-k) \\ &= \frac{1}{(\epsilon_{\mathbf{k},\alpha}^2 - k_0^2)[\epsilon_{\mathbf{p}-\mathbf{k},\beta}^2 - (p_0 - k_0)^2]}, \end{aligned} \quad (\text{B16})$$

where $\epsilon_{\mathbf{p}-\mathbf{k},\beta} = \sqrt{(\mathbf{p}-\mathbf{k})^2 + \beta^2}$ and $-ip_0 = p_4$ is the external frequency. The poles are at $k_0 = \pm \epsilon_{\mathbf{k},\alpha}$ and $k_0 = p_0 \pm \epsilon_{\mathbf{p}-\mathbf{k},\beta}$. The residues are readily evaluated:

$$\begin{aligned} R_\alpha^\pm &= \mp \frac{1}{2\epsilon_{\mathbf{k},\alpha}} G_\beta(\mathbf{p}-\mathbf{k}, ip_0 \mp i\epsilon_{\mathbf{k},\alpha}), \\ R_\beta^\pm &= \mp \frac{1}{2\epsilon_{\mathbf{p}-\mathbf{k},\beta}} G_\alpha(\mathbf{k}, ip_0 \pm i\epsilon_{\mathbf{p}-\mathbf{k},\beta}), \end{aligned} \quad (\text{B17})$$

and we can write

$$f(\mathbf{k}, ik_0) = \sum_{\pm} \frac{R_\alpha^\pm}{k_0 \mp \epsilon_{\mathbf{k},\alpha}} + \sum_{\pm} \frac{R_\beta^\pm}{k_0 - p_0 \mp \epsilon_{\mathbf{p}-\mathbf{k},\beta}} = A_{\alpha\beta}(\mathbf{k}, \mathbf{p}-\mathbf{k}; ik_0, ip_0) + A_{\beta\alpha}(\mathbf{p}-\mathbf{k}, \mathbf{k}; ip_0 - ik_0, ip_0), \quad (\text{B18})$$

where

$$A_{\alpha\beta}(\mathbf{k}, \mathbf{p}-\mathbf{k}; ik_0, ip_0) = \frac{1}{2\epsilon_{\mathbf{k},\alpha}} \left[\frac{G_\beta(\mathbf{p}-\mathbf{k}, ip_0 + i\epsilon_{\mathbf{k},\alpha})}{k_0 + \epsilon_{\mathbf{k},\alpha}} - \frac{G_\beta(\mathbf{p}-\mathbf{k}, ip_0 - i\epsilon_{\mathbf{k},\alpha})}{k_0 - \epsilon_{\mathbf{k},\alpha}} \right]. \quad (\text{B19})$$

It can be easily shown that for any external frequency $\omega'_n = -ip_0 = 2\pi T n'$ and momentum \mathbf{p} , the integral over \mathbf{k} and the sum over $\omega_n = -ik_0 = 2\pi T n$ have the property

$$T \sum_n \int \frac{d^3\mathbf{k}}{(2\pi)^3} A_{\alpha\beta}(\mathbf{k}, \mathbf{p}-\mathbf{k}; ik_0, ip_0) = T \sum_n \int \frac{d^3\mathbf{k}}{(2\pi)^3} A_{\alpha\beta}(\mathbf{p}-\mathbf{k}, \mathbf{k}; ip_0 - ik_0, ip_0), \quad (\text{B20})$$

which follows by replacing $\mathbf{k} \rightarrow \mathbf{p}-\mathbf{k}$ and $k_0 \rightarrow p_0 - k_0$ in the integral and in the sum. Thus, we can replace in Eq. (B3)

$$\mathfrak{R}f(\mathbf{k}, ik_0) = \{\mathfrak{R}[A_{\alpha\beta}(\mathbf{k}, \mathbf{p}-\mathbf{k}; ik_0, ip_0)] + \alpha \leftrightarrow \beta\}. \quad (\text{B21})$$

Moreover, since $G_m(\mathbf{p}, ip_0) = G_m(\mathbf{p}, -ip_0)$, by inspection of Eq. (B19), we observe that $A_{\alpha\beta}(\mathbf{k}, \mathbf{p}-\mathbf{k}; -ik_0, ip_0) = A_{\alpha\beta}(\mathbf{k}, \mathbf{p}-\mathbf{k}; ik_0, -ip_0)$, so that

$$\mathfrak{R}[A_{\alpha\beta}(\mathbf{k}, \mathbf{p}-\mathbf{k}; ik_0, ip_0)] = \frac{1}{2} [A_{\alpha\beta}(\mathbf{k}, \mathbf{p}-\mathbf{k}; ik_0, ip_0) + A_{\alpha\beta}(\mathbf{k}, \mathbf{p}-\mathbf{k}; ik_0, -ip_0)]. \quad (\text{B22})$$

Hereafter, the last equation is taken as the definition of the symbol \mathfrak{R} for any generic function of ip_0 .

In Eq. (B3), the poles at $k_0 = \epsilon_{\mathbf{k},\alpha}$, $\epsilon_{\mathbf{k},\beta}$ have the residues $[-n(\epsilon_{\mathbf{k},\alpha})/\epsilon_{\mathbf{k},\alpha}] \mathfrak{R}G_\beta(\mathbf{p}-\mathbf{k}, ip_0 - i\epsilon_{\mathbf{k},\alpha})$ and $[-n(\epsilon_{\mathbf{k},\beta})/\epsilon_{\mathbf{k},\beta}] \mathfrak{R}G_\alpha(\mathbf{p}-\mathbf{k}, ip_0 - i\epsilon_{\mathbf{k},\beta})$, respectively, yielding in terms of the external frequency $\omega = p_4 = -ip_0$

$$[I^{a\beta}(\mathbf{p}, \omega)]_{Th} = \int \frac{d^3\mathbf{k}}{(2\pi)^3} \left\{ \frac{n(\epsilon_{\mathbf{k},\alpha})}{\epsilon_{\mathbf{k},\alpha}} \mathfrak{R}G_\beta(\mathbf{p}-\mathbf{k}, \omega + i\epsilon_{\mathbf{k},\alpha}) + \alpha \leftrightarrow \beta \right\}. \quad (\text{B23})$$

Finally, we observe that since $G_m(\mathbf{p}, ip_0) = G_m(\mathbf{p}, -ip_0)$, then

$$\mathfrak{R}G_\beta(\mathbf{p}-\mathbf{k}, ip_0 - i\epsilon_{\mathbf{k},\alpha}) = \frac{1}{2} [G_\beta(\mathbf{p}-\mathbf{k}, \omega + i\epsilon_{\mathbf{k},\alpha}) + G_\beta(\mathbf{p}-\mathbf{k}, \omega - i\epsilon_{\mathbf{k},\alpha})]. \quad (\text{B24})$$

The angular integral in Eq. (B23) can be evaluated exactly by writing

$$G_\alpha(\mathbf{p} - \mathbf{k}, z) = \frac{1}{g_\alpha(z, \mathbf{p}^2, \mathbf{k}^2) - 2\mathbf{p} \cdot \mathbf{k}}, \quad (\text{B25})$$

where, denoting $x = \sqrt{\mathbf{k}^2}$ and $y = \sqrt{\mathbf{p}^2}$, the function $g_\alpha(z; x^2, y^2)$ is given by

$$g_\alpha(z; y^2, x^2) = z^2 + \alpha^2 + x^2 + y^2 \quad (\text{B26})$$

and does not depend on the angles. Moreover, we observe that

$$g_\alpha(z; y^2, x^2) \pm 2xy = z^2 + \epsilon_{y \pm x, \alpha}^2, \quad (\text{B27})$$

where

$$\epsilon_{y \pm x, \alpha} = \sqrt{(y \pm x)^2 + \alpha^2}, \quad (\text{B28})$$

so that the integral over the angles can be written in terms of the function

$$L_\alpha(z; y, x) = \log \frac{z^2 + \epsilon_{y+x, \alpha}^2}{z^2 + \epsilon_{y-x, \alpha}^2} \quad (\text{B29})$$

and an elementary integration gives

$$[I^{\alpha\beta}(y, \omega)]_{Th} = \int_0^\infty \frac{x dx}{8\pi^2 y} \left\{ \frac{n(\epsilon_{x, \alpha})}{\epsilon_{x, \alpha}} \Re L_\beta(\omega + i\epsilon_{x, \alpha}; y, x) + \alpha \leftrightarrow \beta \right\}. \quad (\text{B30})$$

It might be useful to evaluate the leading behavior in the long wavelength limit $\mathbf{p} \rightarrow 0$ (i.e., $y \rightarrow 0$):

$$z^2 + \epsilon_{y \pm x, \beta}^2 = (z^2 + \epsilon_{x, \beta}^2) \left[1 \pm \frac{2xy}{z^2 + \epsilon_{x, \beta}^2} + \frac{y^2}{z^2 + \epsilon_{x, \beta}^2} \right], \quad (\text{B31})$$

$$L_\beta(z; y, x) = \frac{4xy}{z^2 + \epsilon_{x, \beta}^2} - \frac{4xy^3}{(z^2 + \epsilon_{x, \beta}^2)^2} + \frac{16x^3y^3}{3(z^2 + \epsilon_{x, \beta}^2)^3} + \mathcal{O}(y^5), \quad (\text{B32})$$

$$[I^{\alpha\beta}(y \rightarrow 0, \omega)]_{Th} \approx \int_0^\infty \frac{x^2 dx}{2\pi^2} \left\{ \frac{n(\epsilon_{x, \alpha})}{\epsilon_{x, \alpha}} \Re \frac{1}{(\omega + i\epsilon_{x, \alpha})^2 + \epsilon_{x, \beta}^2} + \alpha \leftrightarrow \beta \right\}. \quad (\text{B33})$$

Moreover, in the limit $\omega \rightarrow 0$, using Eq. (B13),

$$\lim_{\omega \rightarrow 0} \lim_{y \rightarrow 0} [I^{\alpha\beta}(y, \omega)]_{Th} = \int_0^\infty \frac{x^2 dx}{2\pi^2} \left\{ \frac{n(\epsilon_{x, \alpha})}{\epsilon_{x, \alpha}} \frac{1}{\beta^2 - \alpha^2} + \alpha \leftrightarrow \beta \right\} = \frac{(J_\alpha)_{Th} - (J_\beta)_{Th}}{\beta^2 - \alpha^2}, \quad (\text{B34})$$

in agreement with the first of Eqs. (A26). The same limit is obtained by setting $\omega = 0$ from the beginning and exploring the leading behavior when $y \rightarrow 0$.

4. Thermal part of $I_{L,T}^{\alpha\beta}(p)$

The projected integrals $I_{L,T}^{\alpha\beta}(p)$ were defined in Eq. (A14) and have the general form of Eq. (B1) with

$$f(k) = G_\alpha(k) G_\beta(p - k) \frac{k_\mu k_\nu}{c_{L,T}} P_{\mu\nu}^{L,T}(p), \quad (\text{B35})$$

where $c_L = 1$ and $c_T = 2$. The function $f(k)$ is the same found for the integral $I^{\alpha\beta}(p)$ in Eq. (B16), multiplied by a factor

$$f(k) \rightarrow f(k) \left[\frac{k_\mu k_\nu}{c_{L,T}} P_{\mu\nu}^{L,T}(p) \right]. \quad (\text{B36})$$

The new factor has no poles in the complex k_0 plane and does not depend on the masses α, β . Thus, $f(k)$ has the same pole structure of Eq. (B18) with residues multiplied by the same factor. Moreover, we observe that because of Eq. (A15), we can still exchange k and $p - k$ in the integral without affecting the multiplied factor. Then, Eq. (B21) still holds with the function $A_{\alpha\beta}$ just multiplied by the same factor of Eq. (B36), which by an explicit calculation reads

$$[k_\mu k_\nu P_{\mu\nu}^L(p)] = \frac{[(\mathbf{k} \cdot \mathbf{p})\omega + ik_0 \mathbf{p}^2]^2}{(\mathbf{p}^2 + \omega^2) \mathbf{p}^2} \quad (\text{B37})$$

and

$$\left[\frac{k_\mu k_\nu}{2} P_{\mu\nu}^T(p) \right] = \frac{1}{2} \left[\mathbf{k}^2 - \frac{(\mathbf{k} \cdot \mathbf{p})^2}{\mathbf{p}^2} \right], \quad (\text{B38})$$

to be evaluated at the poles $k_0 = \epsilon_{\mathbf{k},\alpha}$ and $k_0 = \epsilon_{\mathbf{k},\beta}$, yielding

$$\begin{aligned} [I_L^{\alpha\beta}(\mathbf{p}, \omega)]_{Th} &= \int \frac{d^3\mathbf{k}}{(2\pi)^3} \left\{ \frac{n(\epsilon_{\mathbf{k},\alpha})}{\epsilon_{\mathbf{k},\alpha}} \Re \left[\frac{((\mathbf{k} \cdot \mathbf{p})\omega + i\epsilon_{\mathbf{k},\alpha}\mathbf{p}^2)^2}{(\mathbf{p}^2 + \omega^2)\mathbf{p}^2} G_\beta(\mathbf{p} - \mathbf{k}, \omega + i\epsilon_{\mathbf{k},\alpha}) \right] + \alpha \leftrightarrow \beta \right\}, \\ [I_T^{\alpha\beta}(\mathbf{p}, \omega)]_{Th} &= \frac{1}{2} \int \frac{d^3\mathbf{k}}{(2\pi)^3} \left[\mathbf{k}^2 - \frac{(\mathbf{k} \cdot \mathbf{p})^2}{\mathbf{p}^2} \right] \left\{ \frac{n(\epsilon_{\mathbf{k},\alpha})}{\epsilon_{\mathbf{k},\alpha}} \Re G_\beta(\mathbf{p} - \mathbf{k}, \omega + i\epsilon_{\mathbf{k},\alpha}) + \alpha \leftrightarrow \beta \right\}, \end{aligned} \quad (\text{B39})$$

where the symbol \Re denotes an average over $\pm\omega$ or, equivalently, an average over $\pm i\epsilon_{\mathbf{k},\alpha}$.

The angular integrals can be evaluated exactly [38]. In the transverse projection, we can write

$$\begin{aligned} \int \frac{d^3\mathbf{k}}{(2\pi)^3} \left[\mathbf{k}^2 - \frac{(\mathbf{k} \cdot \mathbf{p})^2}{\mathbf{p}^2} \right] G_\alpha(\mathbf{p} - \mathbf{k}, z) &= \int_0^\infty \frac{x^4 dx}{4\pi^2} \int_{-1}^1 d\cos\theta \frac{1 - \cos^2\theta}{g_\alpha(z; y^2, x^2) - 2xy \cos\theta} \\ &= \int_0^\infty \frac{x^2 dx}{8\pi^2 y^2} \left[g_\alpha(z; y^2, x^2) - \frac{([g_\alpha(z; y^2, x^2)]^2 - 4x^2 y^2)}{4xy} L_\alpha(z; y, x) \right]. \end{aligned} \quad (\text{B40})$$

Then, denoting by L_α^T the transverse logarithmic function

$$L_\alpha^T(z; y, x) = (z^2 + \epsilon_{y+x,\alpha}^2)(z^2 + \epsilon_{y-x,\alpha}^2) L_\alpha(z; y, x) \quad (\text{B41})$$

and using Eq. (B27), we can write

$$[I_T^{\alpha\beta}(y, \omega)]_{Th} = - \int_0^\infty \frac{x dx}{64\pi^2 y^3} \left\{ \frac{n(\epsilon_{x,\alpha})}{\epsilon_{x,\alpha}} [\Re L_\beta^T(\omega + i\epsilon_{x,\alpha}; y, x) - 4xy(\omega^2 + y^2 + \beta^2 - \alpha^2)] + \alpha \leftrightarrow \beta \right\}. \quad (\text{B42})$$

In the longitudinal projection, the angular integration reads

$$\begin{aligned} \int \frac{d^3\mathbf{k}}{(2\pi)^3} \left[\frac{((\mathbf{k} \cdot \mathbf{p})\omega + (z - \omega)\mathbf{p}^2)^2}{\mathbf{p}^2} \right] G_\alpha(\mathbf{p} - \mathbf{k}, z) \\ &= \int_0^\infty \frac{x^2 dx}{4\pi^2} \int_{-1}^1 d\cos\theta \frac{[x\omega \cos\theta + y(z - \omega)]^2}{g_\alpha(z; y^2, x^2) - 2xy \cos\theta} \\ &= \int_0^\infty \frac{\omega^2 x dx}{32\pi^2 y^3} \left\{ \left[g_\alpha(z; y^2, x^2) + 2y^2 \left(\frac{z}{\omega} - 1 \right) \right]^2 L_\alpha(z; y, x) - 4xy g_\alpha(z; y^2, x^2) - \frac{16xy^3(z - \omega)}{\omega} \right\}. \end{aligned} \quad (\text{B43})$$

Denoting by L_α^L the longitudinal logarithmic function

$$L_\alpha^L(z; y, x) = \left[z^2 + \epsilon_{x,\alpha}^2 + y^2 \left(\frac{2z}{\omega} - 1 \right) \right]^2 L_\alpha(z; y, x), \quad (\text{B44})$$

using Eq. (B26) and observing that $\Re(z - \omega)$ vanishes when evaluated at $z = \omega \pm i\epsilon_{x,\alpha}$, we can write

$$[I_L^{\alpha\beta}(y, \omega)]_{Th} = \frac{\omega^2}{(y^2 + \omega^2)} \int_0^\infty \frac{x dx}{32\pi^2 y^3} \left\{ \frac{n(\epsilon_{x,\alpha})}{\epsilon_{x,\alpha}} [\Re L_\beta^L(\omega + i\epsilon_{x,\alpha}; y, x) - 4xy(\omega^2 + y^2 + \beta^2 - \alpha^2)] + \alpha \leftrightarrow \beta \right\}. \quad (\text{B45})$$

5. Thermal part of ∂J_m , $\partial J_m^{L,T}$, $\partial^2 J_m$ and $\partial^2 J_m^{L,T}$

The thermal parts of ∂J_m and $\partial J_m^{L,T}$ can be obtained by a simple derivative of the thermal parts of J_m and $J_m^{L,T}$, respectively, according to the definition of the integrals in Eq. (A24). For a function of $\epsilon_{x,m}$

$$\frac{\partial}{\partial m^2} = \frac{1}{2\epsilon_{x,m}} \frac{\partial}{\partial \epsilon_{x,m}} = \frac{1}{2x} \frac{\partial}{\partial x}, \quad (\text{B46})$$

so that it might be useful to integrate by parts, using Eq. (B13):

$$\begin{aligned} (\partial J_m)_{Th} &= \frac{\partial}{\partial m^2} \int_0^\infty \frac{x^2 dx}{2\pi^2} \frac{n(\epsilon_{x,m})}{\epsilon_{x,m}} \\ &= \int_0^\infty \frac{x dx}{4\pi^2} \frac{\partial}{\partial x} \left[\frac{n(\epsilon_{x,m})}{\epsilon_{x,m}} \right] \\ &= - \int_0^\infty \frac{dx}{4\pi^2} \frac{n(\epsilon_{x,m})}{\epsilon_{x,m}}. \end{aligned} \quad (\text{B47})$$

A plain further derivative gives

$$(\partial^2 J_m)_{Th} = \int_0^\infty \frac{dx}{8\pi^2} \frac{n(\epsilon_{x,m})}{\epsilon_{x,m}^3} - \frac{1}{T} J_m^{nn/\epsilon\epsilon}, \quad (\text{B48})$$

where

$$J_m^{nn/\epsilon\epsilon} = \int_0^\infty \frac{dx}{8\pi^2} \left[\frac{n(\epsilon_{x,m})n(-\epsilon_{x,m})}{(\epsilon_{x,m})^2} \right]. \quad (\text{B49})$$

By the same method, using Eq. (B15),

$$\begin{aligned} (\partial J_m^L)_{Th} &= \int_0^\infty \frac{dx}{4\pi^2} \epsilon_{x,m} n(\epsilon_{x,m}), \\ (\partial J_m^T)_{Th} &= - \int_0^\infty \frac{x^2 dx}{4\pi^2} \frac{n(\epsilon_{x,m})}{\epsilon_{x,m}} = -\frac{1}{2} (J_m)_{Th}, \end{aligned} \quad (\text{B50})$$

and by a plain further derivative

$$\begin{aligned} (\partial^2 J_m^L)_{Th} &= -\frac{1}{2} (\partial J_m)_{Th} + \frac{1}{T} J_m^{nn}, \\ (\partial^2 J_m^T)_{Th} &= -\frac{1}{2} (\partial J_m)_{Th}, \end{aligned} \quad (\text{B51})$$

where

$$J_m^{nn} = \int_0^\infty \frac{dx}{8\pi^2} n(\epsilon_{x,m})n(-\epsilon_{x,m}). \quad (\text{B52})$$

6. Thermal part of $\partial I^{\alpha\beta}(p)$

The thermal part of $\partial I^{\alpha\beta}(p)$ can be obtained by a derivative of the thermal part of $I^{\alpha\beta}(p)$, using the explicit expression of Eq. (B30)

$$[\partial I^{\alpha\beta}(y, \omega)]_{Th} = \int_0^\infty \frac{x dx}{8\pi^2 y} \left\{ \frac{\partial}{\partial \alpha^2} \mathcal{A} + \frac{\partial}{\partial \alpha^2} \mathcal{B} \right\}, \quad (\text{B53})$$

where

$$\begin{aligned} \mathcal{A} &= \frac{n(\epsilon_{x,\alpha})}{\epsilon_{x,\alpha}} \Re L_\beta(\omega + i\epsilon_{x,\alpha}; y, x), \\ \mathcal{B} &= \frac{n(\epsilon_{x,\beta})}{\epsilon_{x,\beta}} \Re L_\alpha(\omega + i\epsilon_{x,\beta}; y, x). \end{aligned} \quad (\text{B54})$$

Using $\epsilon_{x,\alpha}$ as independent variable, with $\epsilon_{x,\alpha} d\epsilon_{x,\alpha} = x dx$, we can write $x = \sqrt{\epsilon_{x,\alpha}^2 - \alpha^2}$ and eliminate the explicit dependence on x in the function \mathcal{A} . The total derivative of \mathcal{A} reads

$$\frac{d\mathcal{A}}{d\epsilon_{x,\alpha}} = \left(\frac{\partial \mathcal{A}}{\partial \epsilon_{x,\alpha}} \right)_x + \left(\frac{\partial \mathcal{A}}{\partial x} \right)_{\epsilon_{x,\alpha}} \left(\frac{dx}{d\epsilon_{x,\alpha}} \right), \quad (\text{B55})$$

and observing that

$$\left(\frac{\partial \mathcal{A}}{\partial \epsilon_{x,\alpha}} \right)_x = 2\epsilon_{x,\alpha} \left(\frac{\partial \mathcal{A}}{\partial \alpha^2} \right), \quad \left(\frac{dx}{d\epsilon_{x,\alpha}} \right) = \frac{\epsilon_{x,\alpha}}{x}, \quad (\text{B56})$$

it can be written as

$$\frac{d\mathcal{A}}{d\epsilon_{x,\alpha}} = 2\epsilon_{x,\alpha} \left(\frac{\partial \mathcal{A}}{\partial \alpha^2} \right) + \frac{\epsilon_{x,\alpha}}{x} \left(\frac{\partial \mathcal{A}}{\partial x} \right)_{\epsilon_{x,\alpha}}, \quad (\text{B57})$$

so that the first derivative in Eq. (B53) follows as

$$\frac{\partial \mathcal{A}}{\partial \alpha^2} = \frac{1}{2\epsilon_{x,\alpha}} \frac{d\mathcal{A}}{d\epsilon_{x,\alpha}} - \frac{1}{2x} \left(\frac{\partial \mathcal{A}}{\partial x} \right)_{\epsilon_{x,\alpha}}. \quad (\text{B58})$$

Moreover, observing that

$$\begin{aligned} \left(\frac{\partial \mathcal{A}}{\partial x} \right)_{\epsilon_{x,\alpha}} &= 2x \left(\frac{\partial \mathcal{A}}{\partial \epsilon_{y+x,\beta}^2} + \frac{\partial \mathcal{A}}{\partial \epsilon_{y-x,\beta}^2} \right) \\ &\quad + 2y \left(\frac{\partial \mathcal{A}}{\partial \epsilon_{y+x,\beta}^2} - \frac{\partial \mathcal{A}}{\partial \epsilon_{y-x,\beta}^2} \right), \end{aligned} \quad (\text{B59})$$

we find, explicitly,

$$\begin{aligned} \frac{1}{2x} \left(\frac{\partial \mathcal{A}}{\partial x} \right)_{\epsilon_{x,\alpha}} &= \frac{n(\epsilon_{x,\alpha})}{\epsilon_{x,\alpha}} \Re \left[\frac{1}{z_\alpha^2 + \epsilon_{y+x,\beta}^2} - \frac{1}{z_\alpha^2 + \epsilon_{y-x,\beta}^2} \right] \\ &\quad + \left(\frac{y}{x} \right) \frac{n(\epsilon_{x,\alpha})}{\epsilon_{x,\alpha}} \Re \left[\frac{1}{z_\alpha^2 + \epsilon_{y+x,\beta}^2} + \frac{1}{z_\alpha^2 + \epsilon_{y-x,\beta}^2} \right] \end{aligned} \quad (\text{B60})$$

where $z_\alpha = \omega + i\epsilon_{x,\alpha}$. On the other hand, a simple derivative gives

$$\frac{\partial \mathcal{B}}{\partial \alpha^2} = \frac{n(\epsilon_{x,\beta})}{\epsilon_{x,\beta}} \Re \left[\frac{1}{z_\beta^2 + \epsilon_{y+x,\alpha}^2} - \frac{1}{z_\beta^2 + \epsilon_{y-x,\alpha}^2} \right], \quad (\text{B61})$$

where $z_\beta = \omega + i\epsilon_{x,\beta}$. Finally, inserting Eq. (B58) in Eq. (B53) and changing the integration variable $x dx = \epsilon_{x,\alpha} d\epsilon_{x,\alpha}$ in the first term, the integral of the total derivative gives a vanishing contribution at $x = \infty$ and $x = 0$, since $L_\beta \rightarrow 0$. Collecting the other terms, we find

$$\begin{aligned} [\partial I^{\alpha\beta}(y, \omega)]_{Th} = & - \int_0^\infty \frac{dx}{8\pi^2} \frac{n(\epsilon_{x,\alpha})}{\epsilon_{x,\alpha}} \Re \left[\frac{1}{(\omega + i\epsilon_{x,\alpha})^2 + \epsilon_{y+x,\beta}^2} + \frac{1}{(\omega + i\epsilon_{x,\alpha})^2 + \epsilon_{y-x,\beta}^2} \right] + \\ & + \int_0^\infty \frac{x dx}{8\pi^2 y} \left\{ \frac{n(\epsilon_{x,\beta})}{\epsilon_{x,\beta}} \Re \left[\frac{1}{(\omega + i\epsilon_{x,\beta})^2 + \epsilon_{y+x,\alpha}^2} - \frac{1}{(\omega + i\epsilon_{x,\beta})^2 + \epsilon_{y-x,\alpha}^2} \right] - (\alpha \leftrightarrow \beta) \right\}, \quad (\text{B62}) \end{aligned}$$

where the second integral is zero if $\alpha = \beta$.

7. Thermal part of $\partial I_{L,T}^{\alpha\beta}(p)$

The thermal part of the projected integrals $\partial I_{L,T}^{\alpha\beta}(p)$ can be obtained by a derivative of the thermal part of $I_{L,T}^{\alpha\beta}(p)$, using the explicit expressions of Eqs. (B45) and (B42):

$$\begin{aligned} [\partial I_L^{\alpha\beta}(y, \omega)]_{Th} &= \frac{\omega^2}{(y^2 + \omega^2)} \int_0^\infty \frac{x dx}{32\pi^2 y^3} \left\{ \frac{\partial}{\partial \alpha^2} \mathcal{A}_L + \frac{\partial}{\partial \alpha^2} \mathcal{B}_L \right\}, \\ [\partial I_T^{\alpha\beta}(y, \omega)]_{Th} &= - \int_0^\infty \frac{x dx}{64\pi^2 y^3} \left\{ \frac{\partial}{\partial \alpha^2} \mathcal{A}_T + \frac{\partial}{\partial \alpha^2} \mathcal{B}_T \right\}, \quad (\text{B63}) \end{aligned}$$

where

$$\begin{aligned} \mathcal{A}_{L,T} &= \frac{n(\epsilon_{x,\alpha})}{\epsilon_{x,\alpha}} [\Re L_\beta^{L,T}(\omega + i\epsilon_{x,\alpha}; y, x) - 4xy(\omega^2 + y^2 + \beta^2 - \alpha^2)], \\ \mathcal{B}_{L,T} &= \frac{n(\epsilon_{x,\beta})}{\epsilon_{x,\beta}} [\Re L_\alpha^{L,T}(\omega + i\epsilon_{x,\beta}; y, x) - 4xy(\omega^2 + y^2 + \alpha^2 - \beta^2)]. \quad (\text{B64}) \end{aligned}$$

Because of the explicit dependence on α , Eq. (B58) is modified as

$$\frac{\partial \mathcal{A}_{L,T}}{\partial \alpha^2} = 4xy \frac{n(\epsilon_{x,\alpha})}{\epsilon_{x,\alpha}} + \frac{1}{2\epsilon_{x,\alpha}} \frac{d\mathcal{A}_{L,T}}{d\epsilon_{x,\alpha}} - \frac{1}{2x} \left(\frac{\partial \mathcal{A}_{L,T}}{\partial x} \right)_{\epsilon_{x,\alpha}}, \quad (\text{B65})$$

while Eq. (B61) becomes

$$\begin{aligned} \frac{\partial \mathcal{B}_L}{\partial \alpha^2} &= \frac{n(\epsilon_{x,\beta})}{\epsilon_{x,\beta}} \left\{ \Re \left[\left(\frac{1}{z_\beta^2 + \epsilon_{y+x,\alpha}^2} - \frac{1}{z_\beta^2 + \epsilon_{y-x,\alpha}^2} \right) \left(z_\beta^2 + \epsilon_{x,\alpha}^2 + y^2 \left(\frac{2z_\beta}{\omega} - 1 \right) \right)^2 + \right. \right. \\ &\quad \left. \left. + 2 \left(z_\beta^2 + \epsilon_{x,\alpha}^2 + y^2 \left(\frac{2z_\beta}{\omega} - 1 \right) \right) L_\alpha(z_\beta; y, x) \right] - 4xy \right\}, \\ \frac{\partial \mathcal{B}_T}{\partial \alpha^2} &= \frac{n(\epsilon_{x,\beta})}{\epsilon_{x,\beta}} \{ \Re [(2z_\beta^2 + \epsilon_{y-x,\alpha}^2 + \epsilon_{y+x,\alpha}^2) L_\alpha(z_\beta; y, x)] - 8xy \}, \quad (\text{B66}) \end{aligned}$$

where $z_\beta = \omega + i\epsilon_{x,\beta}$. Moreover, an explicit calculation gives

$$\begin{aligned}
-\frac{1}{2x} \left(\frac{\partial A_L}{\partial x} \right)_{\epsilon_{x,\alpha}} &= -\frac{1}{2x} \frac{n(\epsilon_{x,\alpha})}{\epsilon_{x,\alpha}} \left\{ \Re \left[4x \left(z_\alpha^2 + \epsilon_{x,\beta}^2 + y^2 \left(\frac{2z_\alpha}{\omega} - 1 \right) \right) L_\beta(z_\alpha; y, x) \right. \right. \\
&\quad \left. \left. + 2 \left(z_\alpha^2 + \epsilon_{x,\beta}^2 + y^2 \left(\frac{2z_\alpha}{\omega} - 1 \right) \right)^2 \left(\frac{x+y}{z_\alpha^2 + \epsilon_{y+x,\beta}^2} - \frac{x-y}{z_\alpha^2 + \epsilon_{y-x,\beta}^2} \right) \right] - 4y(\omega^2 + y^2 + \beta^2 - \alpha^2) \right\}, \\
-\frac{1}{2x} \left(\frac{\partial A_T}{\partial x} \right)_{\epsilon_{x,\alpha}} &= -\frac{n(\epsilon_{x,\alpha})}{\epsilon_{x,\alpha}} \left\{ \Re \left[(2z_\alpha^2 + \epsilon_{y-x,\beta}^2 + \epsilon_{y+x,\beta}^2 - 4y^2) L_\beta(z_\alpha; y, x) \right] - 4xy \right\}, \tag{B67}
\end{aligned}$$

where $z_\alpha = \omega + i\epsilon_{x,\alpha}$.

Inserting Eqs. (B65) and (B66) in Eq. (B63) and dropping the integral of the total derivative which gives a vanishing contribution, we find

$$\begin{aligned}
[\partial I_L^{\alpha\beta}(y, \omega)]_{Th} &= -\frac{\omega^2}{y^2(y^2 + \omega^2)} \int_0^\infty \frac{dx}{32\pi^2} \frac{n(\epsilon_{x,\alpha})}{\epsilon_{x,\alpha}} \Re \left[\left(\frac{1}{z_\alpha^2 + \epsilon_{y+x,\beta}^2} + \frac{1}{z_\alpha^2 + \epsilon_{y-x,\beta}^2} \right) \left(z_\alpha^2 + \epsilon_{x,\beta}^2 + y^2 \left(\frac{2z_\alpha}{\omega} - 1 \right) \right)^2 \right] + \\
&\quad + \frac{\omega^2}{y^2(y^2 + \omega^2)} \int_0^\infty \frac{dx}{16\pi^2} \frac{n(\epsilon_{x,\alpha})}{\epsilon_{x,\alpha}} [\omega^2 + y^2 + \beta^2 - \alpha^2] + \frac{\omega^2}{y^2(y^2 + \omega^2)} \int_0^\infty \frac{x^2 dx}{8\pi^2} \left[\frac{n(\epsilon_{x,\alpha})}{\epsilon_{x,\alpha}} - \frac{n(\epsilon_{x,\beta})}{\epsilon_{x,\beta}} \right] + \\
&\quad + \frac{\omega^2}{y^3(y^2 + \omega^2)} \left\{ \int_0^\infty \frac{xdx}{16\pi^2} \frac{n(\epsilon_{x,\beta})}{\epsilon_{x,\beta}} \Re \left[\left(z_\beta^2 + \epsilon_{x,\alpha}^2 + y^2 \left(\frac{2z_\beta}{\omega} - 1 \right) \right) L_\alpha(z_\beta; y, x) \right] - (\alpha \leftrightarrow \beta) \right\} + \\
&\quad + \frac{\omega^2}{y^3(y^2 + \omega^2)} \left\{ \int_0^\infty \frac{xdx}{32\pi^2} \frac{n(\epsilon_{x,\beta})}{\epsilon_{x,\beta}} \Re \left[\left(z_\beta^2 + \epsilon_{x,\alpha}^2 + y^2 \left(\frac{2z_\beta}{\omega} - 1 \right) \right)^2 \left(\frac{1}{z_\beta^2 + \epsilon_{y+x,\alpha}^2} - \frac{1}{z_\beta^2 + \epsilon_{y-x,\alpha}^2} \right) \right] - (\alpha \leftrightarrow \beta) \right\}, \\
[\partial I_T^{\alpha\beta}(y, \omega)]_{Th} &= -\frac{1}{y} \int_0^\infty \frac{xdx}{16\pi^2} \frac{n(\epsilon_{x,\alpha})}{\epsilon_{x,\alpha}} \Re L_\beta(z_\alpha; y, x) + \frac{1}{y^2} \int_0^\infty \frac{x^2 dx}{8\pi^2} \left[\frac{n(\epsilon_{x,\beta})}{\epsilon_{x,\beta}} - \frac{n(\epsilon_{x,\alpha})}{\epsilon_{x,\alpha}} \right] + \\
&\quad + \frac{1}{y^3} \left\{ \int_0^\infty \frac{xdx}{32\pi^2} \frac{n(\epsilon_{x,\alpha})}{\epsilon_{x,\alpha}} \Re [(z_\alpha^2 + \beta^2 + x^2 + y^2) L_\beta(z_\alpha; y, x)] - (\alpha \leftrightarrow \beta) \right\}, \tag{B68}
\end{aligned}$$

where, as before, $z_\alpha = \omega + i\epsilon_{x,\alpha}$ and $z_\beta = \omega + i\epsilon_{x,\beta}$. We observe that most of these integrals are antisymmetric in the mass arguments α, β and their contribution is zero if $\alpha = \beta = m$.

It is instructive to explore the leading behavior in the limit $p \rightarrow 0$. According to Eq. (A20), the longitudinal projection $\partial I_L^{\alpha\beta}$ tends to the value $\partial I_{L,0}^{\alpha\beta}$ if ω is set to zero first and the limit $y \rightarrow 0$ is studied afterwards. Setting $\omega \rightarrow 0$ in Eq. (B68), the only terms of $\partial I_L^{\alpha\beta}$ that do not vanish are those containing the factor $(2z/\omega)^2$. Observing that $z_\alpha^2 \rightarrow -\epsilon_{x,\alpha}^2$ and that, in the limit $y \rightarrow 0$,

$$\begin{aligned}
\frac{1}{z_\alpha^2 + \epsilon_{y+x,\beta}^2} + \frac{1}{z_\alpha^2 + \epsilon_{y-x,\beta}^2} &\rightarrow \frac{2}{\beta^2 - \alpha^2}, \\
\frac{1}{z_\alpha^2 + \epsilon_{y+x,\beta}^2} - \frac{1}{z_\alpha^2 + \epsilon_{y-x,\beta}^2} &\rightarrow \frac{-4xy}{(\beta^2 - \alpha^2)^2}, \tag{B69}
\end{aligned}$$

we obtain the leading behavior

$$[\partial I_{L,0}^{\alpha\beta}]_{Th} = \frac{(\partial J_\alpha^L)_{Th}}{\beta^2 - \alpha^2} + \frac{(J_\alpha^L)_{Th} - (J_\beta^L)_{Th}}{(\beta^2 - \alpha^2)^2}, \tag{B70}$$

having made use of the explicit expressions of $(J_m^L)_{Th}$, $(\partial J_m^L)_{Th}$ as reported in Eqs. (B15) and (B50). The result is in agreement with the general relations of Eq. (A28).

The transverse projection, $\partial I_T^{\alpha\beta}$, tends to a different value, $\partial I_{T,0}^{\alpha\beta}$, in the same limit. Using Eq. (B32),

$$\begin{aligned}
(z^2 + \epsilon_{x,\beta}^2 + y^2) L_\beta(z_\alpha; y, x) &\approx 4xy + \frac{16x^3 y^3}{3(z^2 + \epsilon_{x,\beta}^2)^2} + \mathcal{O}(y^5) \\
L_\beta(z_\alpha; y, x) &\approx \frac{4xy}{(z^2 + \epsilon_{x,\beta}^2)} + \mathcal{O}(y^3), \tag{B71}
\end{aligned}$$

and inserting the expansions in $\partial I_T^{\alpha\beta}$, in Eq. (B68), the terms y^{-2} cancel exactly while the leading term is of order $\sim y^0$, so that we can safely take the limit $y \rightarrow 0$. The leading term reads

$$\begin{aligned}
[\partial I_T^{\alpha\beta}(0, \omega)]_{Th} &= -\int_0^\infty \frac{x^2 dx}{4\pi^2} \frac{n(\epsilon_{x,\alpha})}{\epsilon_{x,\alpha}} \Re \frac{1}{(z_\alpha^2 + \epsilon_{x,\beta}^2)} \\
&\quad + \int_0^\infty \frac{x^4 dx}{6\pi^2} \left\{ \frac{n(\epsilon_{x,\alpha})}{\epsilon_{x,\alpha}} \Re \frac{1}{(z_\alpha^2 + \epsilon_{x,\beta}^2)^2} - (\alpha \leftrightarrow \beta) \right\}. \tag{B72}
\end{aligned}$$

The expansion holds for any value of ω , even $\omega = 0$, so that we can exchange the limits for the transverse projection. Setting $\omega = 0$ and $z_\alpha^2 = -\epsilon_{x,\alpha}^2$, we can simply write $(z_\alpha^2 + \epsilon_{x,\beta}^2) = (\beta^2 - \alpha^2)$ and the leading term reads

$$[\partial I_{T,0}^{\alpha\beta}]_{Th} = \frac{(\partial J_\alpha^T)_{Th}}{\beta^2 - \alpha^2} + \frac{(J_\beta^T)_{Th} - (J_\alpha^T)_{Th}}{(\beta^2 - \alpha^2)^2}, \quad (\text{B73})$$

having made use of the explicit expressions of $(J_m^T)_{Th}$, $(\partial J_m^T)_{Th}$ as reported in Eqs. (B15) and (B50). Again, the result is in agreement with the general relations of Eq. (A28).

On the other hand, the limits cannot be interchanged for the longitudinal projection $\partial I_L^{\alpha\beta}$ which tends to the same limit of the transverse projection, $\partial I_{T,0}^{\alpha\beta}$, if y is set to zero first and the limit $\omega \rightarrow 0$ is taken afterwards. Taking ω finite, we can write in the limit $y \rightarrow 0$

$$\Re \left[\left(\sum_{\pm} \frac{1}{z_\alpha^2 + \epsilon_{y\pm x,\beta}^2} \right) \left(z_\alpha^2 + \epsilon_{x,\beta}^2 + y^2 \left(\frac{2z_\alpha}{\omega} - 1 \right) \right)^2 \right] \approx 2(\omega^2 + y^2 + \beta^2 - \alpha^2) + 8x^2 y^2 \Re \frac{1}{(z_\alpha^2 + \epsilon_{x,\beta}^2)} + \mathcal{O}(y^4); \quad (\text{B74})$$

then, using the expansion

$$\left(\frac{1}{z_\beta^2 + \epsilon_{y+x,\alpha}^2} - \frac{1}{z_\beta^2 + \epsilon_{y-x,\alpha}^2} \right) \approx -\frac{4xy}{(z_\beta^2 + \epsilon_{x,\alpha}^2)^2} + \frac{8xy^3}{(z_\beta^2 + \epsilon_{x,\alpha}^2)^3} - \frac{16x^3 y^3}{(z_\beta^2 + \epsilon_{x,\alpha}^2)^4} + \mathcal{O}(y^5), \quad (\text{B75})$$

we can write

$$\Re \left[\left(z_\beta^2 + \epsilon_{x,\alpha}^2 + y^2 \left(\frac{2z_\beta}{\omega} - 1 \right) \right)^2 \left(\frac{1}{z_\beta^2 + \epsilon_{y+x,\alpha}^2} - \frac{1}{z_\beta^2 + \epsilon_{y-x,\alpha}^2} \right) \right] \approx \Re \left[-4xy - \frac{16xy^3(z_\beta - \omega)}{\omega(z_\beta^2 + \epsilon_{x,\alpha}^2)} - \frac{16x^3 y^3}{(z_\beta^2 + \epsilon_{x,\alpha}^2)^2} + \mathcal{O}(y^5) \right], \quad (\text{B76})$$

and finally, using Eq. (B32),

$$\Re \left[2 \left(z_\beta^2 + \epsilon_{x,\alpha}^2 + y^2 \left(\frac{2z_\beta}{\omega} - 1 \right) \right) L_\alpha(z_\beta; y, x) \right] \approx \Re \left[8xy + \frac{16xy^3(z_\beta - \omega)}{\omega(z_\beta^2 + \epsilon_{x,\alpha}^2)} + \frac{32x^3 y^3}{3(z_\beta^2 + \epsilon_{x,\alpha}^2)^2} + \mathcal{O}(y^5) \right]. \quad (\text{B77})$$

Inserting the expansions in $\partial I_L^{\alpha\beta}$, in Eq. (B68), again the negative powers of y cancel exactly. We can safely set $y = 0$ and the same identical expression of Eq. (B72) is recovered, yielding

$$[\partial I_L^{\alpha\beta}(0, \omega)]_{Th} = [\partial I_T^{\alpha\beta}(0, \omega)]_{Th} \quad (\text{B78})$$

for any finite ω , as expected in the long wavelength limit, where no special direction in space is defined, in agreement with Eq. (A20).

-
- | | |
|---|---|
| [1] A. G. Duarte, O. Oliveira, and P. J. Silva, <i>Phys. Rev. D</i> 94 , 014502 (2016). | [7] O. Oliveira and P. J. Silva, <i>Phys. Rev. D</i> 86 , 114513 (2012). |
| [2] A. Cucchieri and T. Mendes, <i>Phys. Rev. D</i> 78 , 094503 (2008). | [8] G. Burgio, M. Quandt, H. Reinhardt, and H. Vogt, <i>Phys. Rev. D</i> 92 , 034518 (2015). |
| [3] A. Cucchieri and T. Mendes, <i>Phys. Rev. Lett.</i> 100 , 241601 (2008). | [9] J. M. Cornwall, <i>Phys. Rev. D</i> 26 , 1453 (1982). |
| [4] I. L. Bogolubsky, E.-M. Ilgenfritz, M. Müller-Preussker, and A. Sternbeck, <i>Phys. Lett. B</i> 676 , 69 (2009). | [10] B. Lucini, M. Teper, and U. Wenger, <i>J. High Energy Phys.</i> 01 (2004) 061. |
| [5] D. Dudal, O. Oliveira, and N. Vandersickel, <i>Phys. Rev. D</i> 81 , 074505 (2010). | [11] P. J. Silva, O. Oliveira, P. Bicudo, and N. Cardoso, <i>Phys. Rev. D</i> 89 , 074503 (2014). |
| [6] A. Ayala, A. Bashir, D. Binosi, M. Cristoforetti, and J. Rodriguez-Quintero, <i>Phys. Rev. D</i> 86 , 074512 (2012). | [12] R. Aouane, V. Bornyakov, E.-M. Ilgenfritz, V. Mitrjushkin, M. Müller-Preussker, and A. Sternbeck, <i>Phys. Rev. D</i> 85 , 034501 (2012). |

- [13] M. Nahrgang, J. Aichelin, P. B. Gossiaux, and K. Werner, *Phys. Rev. C* **93**, 044909 (2016).
- [14] P. Castorina, V. Greco, D. Jaccarino, and D. Zappalà, *Eur. Phys. J. C* **71**, 1826 (2011).
- [15] M. Ruggieri, P. Alba, P. Castorina, S. Plumari, C. Ratti, and V. Greco, *Phys. Rev. D* **86**, 054007 (2012).
- [16] S. Plumari, W. M. Alberico, V. Greco, and C. Ratti, *Phys. Rev. D* **84**, 094004 (2011).
- [17] D. Dudal, O. Oliveira, and P. J. Silva, *Phys. Rev. D* **89**, 014010 (2014).
- [18] F. Siringo, arXiv:1509.05891.
- [19] F. Siringo, *Nucl. Phys.* **B907**, 572 (2016).
- [20] F. Siringo, *Phys. Rev. D* **94**, 114036 (2016).
- [21] F. Siringo and G. Comitini, *Phys. Rev. D* **98**, 034023 (2018).
- [22] F. Siringo, *EPJ Web Conf.* **137**, 13016 (2017).
- [23] F. Siringo, *Phys. Rev. D* **99**, 094024 (2019).
- [24] F. Siringo, *Phys. Rev. D* **100**, 074014 (2019).
- [25] G. Comitini and F. Siringo, *Phys. Rev. D* **102**, 094002 (2020).
- [26] F. Siringo, *Phys. Rev. D* **96**, 114020 (2017).
- [27] G. Comitini and F. Siringo, *Phys. Rev. D* **97**, 056013 (2018).
- [28] K. Kajantie and J. Kapusta, *Ann. Phys. (N.Y.)* **160**, 477 (1985).
- [29] U. Heinz, K. Kajantie, and T. Toimela, *Phys. Lett. B* **183**, 96 (1987); *Ann. Phys. (N.Y.)* **176**, 218 (1987).
- [30] T. H. Hansson and I. Zahed, *Nucl. Phys.* **B292**, 725 (1987).
- [31] M. E. Carrington, T. H. Hansson, H. Yamagishi, and I. Zahed, *Ann. Phys. (N.Y.)* **190**, 373 (1989).
- [32] R. Kobes, G. Kunstatter, and A. Rebhan, *Nucl. Phys.* **B355**, 1 (1991).
- [33] M. Stingl, *Z. Phys. A* **353**, 423 (1996).
- [34] P. M. Stevenson, *Nucl. Phys.* **B868**, 38 (2013).
- [35] P. M. Stevenson, *Nucl. Phys.* **B910**, 469 (2016).
- [36] N. K. Nielsen, *Nucl. Phys.* **B97**, 527 (1975).
- [37] N. K. Nielsen, *Nucl. Phys.* **B101**, 173 (1975).
- [38] U. Reinosa, J. Serreau, M. Tissier, and N. Wschebor, *Phys. Rev. D* **89**, 105016 (2014).
- [39] J.-P. Blaizot, A. Ipp, and A. Rebhan, *Ann. Phys. (Amsterdam)* **321**, 2128 (2006).
- [40] E. Braaten and R. D. Pisarski, *Phys. Rev. D* **45**, R1827 (1992).
- [41] F. Siringo, *Phys. Rev. D* **92**, 074034 (2015).

Screened massive expansion of the quark propagator in the Landau gaugeGiorgio Comitini^{1,2,*}, Daniele Rizzo^{1,†}, Massimiliano Battello^{1,‡} and Fabio Siringo^{1,2,§}¹*Dipartimento di Fisica e Astronomia “E. Majorana”, Università di Catania,
Via S. Sofia 64, I-95123 Catania, Italy*²*INFN Sezione di Catania, Via S. Sofia 64, I-95123 Catania, Italy*

(Received 1 August 2021; accepted 30 September 2021; published 19 October 2021)

The infrared behavior of the quark propagator is studied at one loop and in the Landau gauge ($\xi = 0$) using the screened massive expansion of full QCD and three different resummation schemes for the quark self-energy. The shift of the expansion point of perturbation theory, which defines the screened expansion, together with a nonstandard renormalization of the bare parameters, proves sufficient to describe the dynamical generation of an infrared quark mass also in the chiral limit. Analytically, the scale for such a mass is set by a mass parameter M , whose value is fixed by a fit to the lattice data for quenched QCD. The quark mass function $\mathcal{M}(p^2)$ is shown to be in very good agreement with the lattice results. The quark Z function, on the other hand, shows the wrong qualitative behavior in all but one of the studied resummation schemes, where its behavior is qualitatively correct, but only at sufficiently high energies.

DOI: 10.1103/PhysRevD.104.074020

I. INTRODUCTION

In the Standard Model of particle physics, the light quarks acquire their masses dynamically through two separate and complementary mechanisms. The first one is the spontaneous breaking of the electroweak gauge symmetry $U(1)_Y \times SU(2)_L$, induced by a nonvanishing vacuum expectation value (VEV) for the Higgs field. Due to the former, a quark mass M_q is generated which is proportional to the product of the quark-Higgs Yukawa coupling and the Higgs field VEV. The second mechanism is a remnant of the violation of global chiral symmetry. In this context, the violation is caused by the strong interactions and manifests itself in a nonzero VEV for the quark mass operator $\bar{\psi}\psi$, i.e., of the quark condensate, which would be constrained to vanish in the presence of chiral symmetry. In turn, the quark condensate triggers the nonvanishing of the quark mass function $\mathcal{M}(p^2)$ in the chiral limit, as can be proven by an operator product expansion (OPE) of the quark propagator. Despite being obeyed by the massless quarks only, limited to the light quarks ($M_q \ll \Lambda_{\text{QCD}}$, where Λ_{QCD} is the QCD scale), chiral

symmetry is still a good approximate symmetry of the QCD Lagrangian; the mechanism that underlies its violation leads to the dressing of the light Higgs-generated masses, greatly enhancing their effective values in the infrared (IR) regime.

Studying the origin of the quark effective masses in the IR is of paramount importance for understanding the experimentally observed hadron spectrum. This is rooted in the fact that the measured values of the light Higgs-generated masses— $M_u \approx 2.2$ MeV, $M_d \approx 4.7$ MeV, $M_s \approx 93$ MeV for the up, down, and strange quarks, respectively, [1]—do not compare well with the observed values of the (unflavored) baryon masses, which are of the order of 1 GeV. The infrared enhancement, induced by the violation of chiral symmetry, is a good candidate for filling the gap between those masses. Unfortunately, mainly because of the nonperturbative nature of dynamical mass generation, no purely analytical and fully predictive description of the latter in the framework of first principles QCD is available to date.

In the context of the strong interactions, dynamical mass generation has been an active field of research for decades now. The development of chiral perturbation theory in the 1960s and 1970s offered a framework in which the large observed masses of the hadrons could be understood to be a consequence of chiral symmetry violation. In the gauge sector, the hypothesis that the gluons might acquire an infrared mass as a result of their self-interactions was advanced by Cornwall in 1982 [2] and confirmed by lattice studies in the 2000s [3–15]. In the continuum, considerable progresses have been made by the numerical integration of integral equations [16–28], by variational methods [29–39],

*giorgio.comitini@dfa.unict.it
†daniele.rizzo@studium.unict.it
‡massimiliano.battello@gmail.com
§fabio.siringo@ct.infn.it

Published by the American Physical Society under the terms of the [Creative Commons Attribution 4.0 International license](#). Further distribution of this work must maintain attribution to the author(s) and the published article's title, journal citation, and DOI. Funded by SCOAP³.

and by physically motivated phenomenological models [40–51]. For a recent review on the subject, see Ref. [52]. The generation of a mass for the gluons is of special interest from a theoretical point of view, since gauge invariance in the framework of ordinary perturbation theory (PT) forbids the gluons to acquire a mass.

While, in principle, the failure of ordinary PT to describe the gluon’s infrared mass could be attributed to its break down at low energies, in recent years a new approach to the perturbation theory of pure Yang-Mills (YM) theory has shown that most of the nonperturbative content of the gluon dynamic—at least as far as the two-point functions are concerned—can be absorbed into a shift of the expansion point of the Yang-Mills perturbative series. This approach, termed the screened massive expansion [53–64], is a simple extension of ordinary PT, formulated in such a way as to treat the transverse gluons as massive already at tree level while leaving the total action of the theory unchanged. The screened expansion has proven to be self-consistent to one loop—since it is renormalizable and leads to an infrared-finite and moderately small running coupling constant [63]—and predictive when optimized by principles of gauge invariance [60]; it yields two-point functions which are in excellent agreement with the lattice data in the Landau gauge [60,63].

The main objective of this paper is to extend the formalism of the screened massive expansion to full QCD with one flavor of quark, with the aim of studying the infrared behavior of the quark propagator. The method was already applied in Refs. [58,59] to describe some of the low-energy features of the quark dynamics in the chiral limit; here, we refine its definition, implement some of our latest findings on the gauge sector, extend the study to nonchiral quarks, and use a new set of lattice data as a benchmark for comparison and in order to fix some of the free parameters in our expressions.

Our treatment of the quark sector closely follows what we did in pure Yang-Mills theory for the gluons; namely, we shift the expansion point of the perturbative series by introducing a new mass parameter M for the zero-order quark propagator. The motivation for the shift lies in the phenomenon of dynamical mass generation for the light quarks. As previously discussed, due to the strong interactions, at low energies the light quarks propagate with a mass which is greatly enhanced with respect to their tree-level (Lagrangian) value; since this effect cannot be captured by ordinary perturbation theory, some kind of nonordinary and nonperturbative resummation of the quark self-energy is needed in order to successfully describe the infrared quark dynamics. This is precisely what the shift does; by replacing the mass contained in the standard zero-order propagator with an enhanced mass parameter, it optimizes the expansion point of perturbation theory so that the quarks propagate with an effective infrared mass of the order of the QCD scale Λ_{QCD} , rather than with the mass

contained in the Lagrangian, which would be more relevant to the high energy regime. The same is done for the transverse gluons, which at tree level are set up to propagate with a finite nonzero mass.

The shift is performed in such a way as to leave the total action of the theory unchanged. As a result, three new two-point interaction vertices arise which are proportional to the quark mass parameter M and bare mass M_B and to the gluon mass parameter m^2 . Since the expansion cannot be carried out exclusively in powers of the coupling constant, the approach is nonperturbative in nature; nonetheless, the calculations are done using standard Feynman diagram techniques, so that the method is still perturbative in the widest sense of the word.

As we shall see in the following sections, our analysis still has major theoretical limitations. First and foremost, the value of the quark mass parameter M introduced by the shift needs to be fixed from external inputs in order to obtain definite quantitative results. At variance with pure Yang-Mills theory, where the method was optimized based on principles of gauge invariance and the redundancy in the number of free parameters was effectively eliminated (see Ref. [60] and the discussion in Sec. II), at this moment no such procedure is available for full QCD. Because of this, in order to test the strength of the screened expansion of QCD, we resort to fitting the free parameters of the expansion using the lattice data; for reasons which are discussed in a later section, the fit is done using a set of data for quenched QCD.

Our study of the quark propagator makes use of three different resummation schemes for the quark self-energy: the minimalistic, vertex-wise, and complex-conjugate schemes (to be defined in Sec. III). The first and second ones are a variation on the same theme and only differ by the number of gluon mass counterterms (i.e., two-point mass vertices, see the next section) included in the computation of the self-energy. The complex-conjugate scheme, on the other hand, uses the fully dressed gluon propagator (or, to be precise, an approximation thereof) in place of the zero-order gluon propagator as the internal gluon line of the self-energy. Each of these schemes has strengths and weaknesses which are discussed. For the moment, we anticipate that the three resulting mass functions $\mathcal{M}(p^2)$ do not show significant differences and are in very good agreement with the lattice data (provided of course that the values of the free parameters are chosen appropriately). The quark Z functions, conversely, show the wrong qualitative behavior in all but the complex-conjugate scheme; when computed using the latter, $Z(p^2)$ is qualitatively correct at sufficiently high energies, but fails nonetheless at low energies.

Ultimately, we were not able to quantitatively reproduce the lattice Z function using the method presented in this study. However, it must be kept in mind that, in the Landau gauge, the divergent part of the Z function is exactly zero at

one loop, and above 1.0–1.5 GeV the finite contribution to $Z(p^2) - 1$ is quite small, yielding an almost constant $Z(p^2) \approx 1$. Thus, the Z function seems to be very sensitive to corrections coming from higher loops [65], thermal effects [66], neglected nonperturbative terms, and—on the lattice side—even artifacts which may affect the actual result found in the numerical simulations.

This paper is organized as follows. In Sec. II, we review the setup and results of the screened expansion of pure Yang-Mills theory. In Sec. III, we formalize the screened expansion of full QCD with one flavor of quark, discuss its renormalization, and define the resummation schemes which we use for the computation of the one-loop quark self-energy. In Sec. IV, we present our results for the quark propagator, fitting the free parameters of the expansion from the lattice data. In Sec. V, we discuss our results and present our conclusions.

II. THE SCREENED MASSIVE EXPANSION OF PURE YANG-MILLS THEORY

The screened massive expansion for the gauge-fixed, renormalized Faddeev-Popov Lagrangian was developed in Refs. [53,54] and extended to finite temperature in [55–57] to full QCD in [58,59] and to a generic covariant gauge in [60,61]. Its renormalization in the Landau gauge was discussed in Refs. [62,63], where different renormalization schemes were considered and analytical expressions were reported for its beta function. The method has proven to be self-consistent and predictive when optimized by principles of gauge invariance [60,63].

In what follows, we give a brief review of the setup and main results of the screened expansion of pure Yang-Mills theory in the Landau gauge. Both of these are functional to our analysis of full QCD.

A. Setup of the method

The bare Faddeev-Popov (FP) Lagrangian for pure SU(N) Yang-Mills theory in a general covariant gauge is given by

$$\mathcal{L} = \mathcal{L}_{\text{YM},B} + \mathcal{L}_{\text{fix},B} + \mathcal{L}_{\text{FP},B}, \quad (1)$$

where

$$\begin{aligned} \mathcal{L}_{\text{YM},B} &= -\frac{1}{2} \text{Tr}(F_{B\mu\nu} F_B^{\mu\nu}), \\ \mathcal{L}_{\text{fix},B} &= -\frac{1}{\xi_B} \text{Tr}(\partial_\mu A_B^\mu \partial_\nu A_B^\nu), \\ \mathcal{L}_{\text{FP},B} &= \partial_\mu \bar{c}_B^a D_B^\mu c_B^a. \end{aligned} \quad (2)$$

Here, we have defined the bare gauge field A_B^μ as

$$A_B^\mu = A_B^{a\mu} T_a, \quad (3)$$

where the T_a 's are SU(N) generators, chosen so that

$$\text{Tr}(T_a T_b) = \frac{1}{2} \delta_{ab}. \quad (4)$$

ξ_B is the bare gauge parameter defining the covariant gauge, and $F_B^{\mu\nu}$ is the bare field-strength tensor,

$$F_B^{a\mu\nu} = \partial^\mu A_B^{a\nu} - \partial^\nu A_B^{a\mu} + g_B f_{bc}^a A_B^{b\mu} A_B^{c\nu}, \quad (5)$$

with

$$[T_a, T_b] = i f_{ab}^c T_c. \quad (6)$$

The bare covariant derivative D_B^μ acting on the ghost and antighost fields c_B^a, \bar{c}_B^a reads

$$(D_B^\mu)_c^a = \delta_c^a \partial^\mu + g_B f_{bc}^a A_B^{b\mu}. \quad (7)$$

\mathcal{L} can be renormalized by introducing suitable renormalization factors $Z_A, Z_c,$ and $Z_{A\bar{c}}$ for the gauge and ghost fields and for the coupling constant, respectively, and by defining new, renormalized gauge and ghost fields $A_\mu^a, c^a,$ and $\bar{c}^a,$ a renormalized coupling g and a renormalized gauge parameter $\xi,$ according to

$$\begin{aligned} A_B^\mu &= Z_A^{1/2} A_\mu^a, & \xi_B &= Z_A \xi, \\ c_B^a &= Z_c^{1/2} c^a, & \bar{c}_B^a &= Z_c^{1/2} \bar{c}^a, \\ g^2 &= g_B^2 \frac{Z_A Z_c^2}{Z_{A\bar{c}}^2}. \end{aligned} \quad (8)$$

In terms of the renormalized fields, the Faddeev-Popov Lagrangian reads

$$\mathcal{L} = \mathcal{L}_{\text{YM}} + \mathcal{L}_{\text{fix}} + \mathcal{L}_{\text{FP}} + \mathcal{L}_{\text{c.t.}}, \quad (9)$$

where

$$\begin{aligned} \mathcal{L}_{\text{YM}} &= -\frac{1}{2} \text{Tr}(F_{\mu\nu} F^{\mu\nu}), \\ \mathcal{L}_{\text{fix}} &= -\frac{1}{\xi} \text{Tr}(\partial^\mu A_\mu \partial^\nu A_\nu), \\ \mathcal{L}_{\text{FP}} &= \partial^\mu \bar{c}^a D_\mu c^a, \end{aligned} \quad (10)$$

and $\mathcal{L}_{\text{c.t.}}$ contains the renormalization counterterms. The renormalized field-strength tensor $F_{\mu\nu}^a$ and covariant derivative D_μ are defined as

$$\begin{aligned} F_{\mu\nu}^a &= \partial_\mu A_\nu^a - \partial_\nu A_\mu^a + g f_{bc}^a A_\mu^b A_\nu^c, \\ (D_\mu)_c^a &= \delta_c^a \partial_\mu + g f_{bc}^a A_\mu^b. \end{aligned} \quad (11)$$

We note that $\mathcal{L}_{\text{c.t.}}$ does not contain a counterterm for the gauge-fixing term \mathcal{L}_{fix} ; indeed, the Slavnov-Taylor identities ensure that the bare gauge parameter ξ_B can be

multiplicatively renormalized by the gauge field renormalization factor Z_A alone.

Ordinary perturbation theory is defined by a split of the renormalized Lagrangian,

$$\mathcal{L} = \mathcal{L}_0 + \mathcal{L}_{\text{int}} + \mathcal{L}_{\text{c.t.}}, \quad (12)$$

where $\mathcal{L}_0 = \lim_{g \rightarrow 0} \mathcal{L}$ is taken to be the noninteracting limit of \mathcal{L} ,

$$\mathcal{L}_0 = \frac{1}{2} A_\mu^a [i\Delta_{0ab}^{\mu\nu}(p)^{-1}] A_\nu^b + \bar{c}^a [i\mathcal{G}_{0ab}(p^2)^{-1}] c^b. \quad (13)$$

Here, the ordinary zero-order gluon and ghost propagators $\Delta_{0\mu\nu}^{ab}$ and \mathcal{G}_0^{ab} read

$$\begin{aligned} \Delta_{0\mu\nu}^{ab}(p) &= \frac{-i\delta^{ab}}{p^2} (t_{\mu\nu}(p) + \xi \ell_{\mu\nu}(p)), \\ \mathcal{G}_0^{ab}(p^2)^{-1} &= \frac{i\delta^{ab}}{p^2}, \end{aligned} \quad (14)$$

where $t_{\mu\nu}(p)$ and $\ell_{\mu\nu}(p)$ are the transverse and longitudinal projectors defined as

$$t_{\mu\nu}(p) = \eta_{\mu\nu} - \frac{P_\mu P_\nu}{p^2}, \quad \ell_{\mu\nu}(p) = \frac{P_\mu P_\nu}{p^2}. \quad (15)$$

The interaction term \mathcal{L}_{int} contains a three-gluon, four-gluon, and ghost-gluon interaction,

$$\mathcal{L}_{\text{int}} = \mathcal{L}_{3g} + \mathcal{L}_{4g} + \mathcal{L}_{\bar{c}cg}, \quad (16)$$

where

$$\begin{aligned} \mathcal{L}_{3g} &= -gf_{bc}^a \partial_\mu A_\nu^a A^{b\mu} A^{c\nu}, \\ \mathcal{L}_{4g} &= -\frac{1}{4} gf_{bc}^a f_{de}^a A_\mu^b A_\nu^c A^{d\mu} A^{e\nu}, \\ \mathcal{L}_{\bar{c}cg} &= gf_{bc}^a \partial^\mu \bar{c}^a A_\mu^b c^c. \end{aligned} \quad (17)$$

On the other hand, the term $\mathcal{L}_{\text{c.t.}}$ contains the field and coupling renormalization counterterms,

$$\mathcal{L}_{\text{c.t.}} = -\frac{1}{2} \delta_A \delta_{ab} p^2 t^{\mu\nu}(p) A_\mu^a A_\nu^b + \delta_c \delta_{ab} p^2 \bar{c}^a c^b + \dots, \quad (18)$$

where $\delta_A = Z_A - 1$ and $\delta_c = Z_c - 1$. In particular, the gluon field renormalization counterterm is completely transverse.

At low energies, the ordinary perturbation theory of pure YM theory is known to be inconsistent due to the presence of an IR Landau pole in the running of the strong coupling constant. Moreover, constraints due to gauge invariance—when applied in the framework of ordinary perturbation theory—prevent the generation of an IR dynamical mass for the gluons, a phenomenon which

by now has been well established mainly thanks to lattice calculations [4–15]. Addressing these issues is the main objective of the screened massive expansion.

The screened massive expansion of pure YM theory is defined by a shift of the expansion point of the Yang-Mills perturbative series, performed in such a way as to treat the transverse gluons as massive already at tree level [53,54]. Explicitly, a shifting term $\delta\mathcal{L}$ is added to the zero-order (kinetic) part of the gauge-fixed, renormalized Fadeev-Popov Lagrangian and subtracted back from its interaction part,

$$\mathcal{L}'_0 = \mathcal{L}_0 + \delta\mathcal{L}, \quad \mathcal{L}'_{\text{int}} = \mathcal{L}_{\text{int}} - \delta\mathcal{L}. \quad (19)$$

$\delta\mathcal{L}$ is chosen so that the zero-order transverse gluon propagator contained in \mathcal{L}'_0 is replaced by a massive one; in momentum space

$$\delta\mathcal{L} = \frac{1}{2} A_\mu^a(p) i [i\Delta_{mab}^{-1\mu\nu}(p) - i\Delta_{0ab}^{-1\mu\nu}(p)] A_\nu^b(-p), \quad (20)$$

where

$$\Delta_{mab}^{\mu\nu}(p) = \delta_{ab} \left\{ \frac{-it^{\mu\nu}(p)}{p^2 - m^2} + \xi \frac{-i\ell^{\mu\nu}(p)}{p^2} \right\} \quad (21)$$

is the new, massive zero-order gluon propagator. Since $\delta\mathcal{L}$ is added to and subtracted from the FP Lagrangian, the shift does not modify the full action of Yang-Mills theory. Instead, it introduces a new free mass parameter m^2 and changes the Feynman rules of YM theory in two respects. First of all, since the new zero-order Lagrangian \mathcal{L}'_0 reads

$$\mathcal{L}'_0 = \frac{1}{2} A_\mu^a [i\Delta_{mab}^{-1\mu\nu}] A_\nu^b + \bar{c}^a [i\mathcal{G}_{0ab}^{-1}] c^b, \quad (22)$$

the transverse gluons propagate with a massive propagator rather than with a massless one, see Eq. (21). Second of all, the interacting part of the Lagrangian, $\mathcal{L}'_{\text{int}}$, contains a new two-point interaction, namely,

$$-\delta\mathcal{L} = -\frac{1}{2} A_\mu^a(p) i \delta\Gamma_{gab}^{\mu\nu}(p) A_\nu^b(-p), \quad (23)$$

where the vertex $\delta\Gamma_{gab}^{\mu\nu}(p)$ is given by

$$\delta\Gamma_{gab}^{\mu\nu}(p) = -im^2 t^{\mu\nu}(p) \delta_{ab}. \quad (24)$$

We refer to the latter as the gluon mass counterterm, not to be confused with the renormalization counterterms contained in $\mathcal{L}_{\text{c.t.}}$. Neither the remaining interaction vertices—spelled out in Eq. (17)—nor the renormalization counterterms are affected by the shift.

The quantities of physical interest can be computed in the framework of the screened expansion using the Feynman rules described above. Since the vertex $\delta\Gamma_g$ is

not proportional to the coupling constant, diagrams with an arbitrary number of vertices—termed crossed diagrams if they contain at least one gluon mass counterterm—coexist at any given loop order. For this reason, the screened expansion is intrinsically nonperturbative.

The crossed diagrams can be computed as derivatives of noncrossed diagrams with respect to the gluon mass parameter. This easily follows from the equality [64]

$$\begin{aligned} & [\Delta_m(p) \cdot (\delta\Gamma_g(p) \cdot \Delta_m(p))^n]_{ab}^{\mu\nu} \\ &= \frac{-i(-m^2)^n}{(p^2 - m^2)^{n+1}} t^{\mu\nu}(p) \delta_{ab} \\ &= \frac{(-m^2)^n}{n!} \frac{\partial^n}{\partial(m^2)^n} \Delta_{mab}^{\mu\nu}(p), \end{aligned} \quad (25)$$

which is valid for every $n \geq 1$ and in any covariant gauge and carries over to the loop integrals.

Due to the massiveness of the zero-order gluon propagator in the screened expansion, new UV divergences arise in the loop integrals which are proportional to the gluon mass parameter m^2 . These divergences do not invalidate the renormalizability of the n -point functions of the theory, since they cancel as soon as crossed diagrams with a higher number of crossed vertices are taken into account [54,64]. The removal of mass divergences can (and indeed must) be adopted as a criterion for fixing the minimum number of crossed loops to be included when computing some quantity at a given loop order [54,64].

To one loop, the one-particle-irreducible (1PI) gluon polarization $\Pi_{\mu\nu}^{ab}(p)$ and ghost self-energy $\Sigma^{ab}(p^2)$ were computed from the diagrams in Fig. 1. The crossed vertices in the figure represent the gluon mass counterterm $\delta\Gamma_g$. Diagrams (1c) and (2c) in the gluon polarization are required in order to eliminate the mass divergences that arise from diagrams (1b) and (2b), respectively; they have a total of three vertices. To one loop, there are two more diagrams with the same number of vertices, namely, diagram (1d) and the crossed diagram in the ghost self-energy (top right diagram

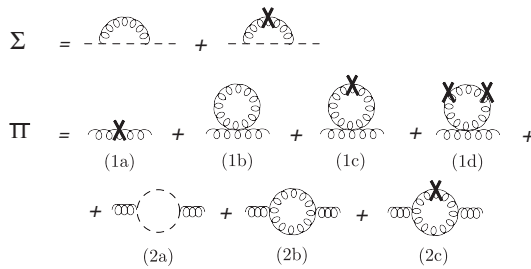


FIG. 1. Two-point graphs with no more than three vertices and no more than one loop. The cross is the transverse mass counterterm of Eq. (24) and is regarded as a two-point vertex. The renormalization counterterms are not shown in the figure.

in Fig. 1); these were also included in the one-loop calculation for consistency.

Since the shift that defines the screened expansion does not change the total action of pure YM theory, the full 1PI gluon polarization is known to be transverse by the Slavnov-Taylor identities. Therefore, we can write

$$\Pi_{\mu\nu}^{ab}(p) = \Pi(p^2) t_{\mu\nu}(p) \delta^{ab}, \quad (26)$$

where $\Pi(p^2)$ is the gluon's scalar polarization. After the resummation of the 1PI diagrams, the transverse-gluon and ghost dressed propagators $\Delta(p^2)$ and $\mathcal{G}(p^2)$ can then be expressed as

$$\begin{aligned} \Delta(p^2) &= -i[p^2 - m^2 - \Pi(p^2)]^{-1}, \\ \mathcal{G}(p^2) &= i[p^2 - \Sigma(p^2)]^{-1}, \end{aligned} \quad (27)$$

where $\Sigma(p^2)$ is the ghost self-energy. Diagram (1a) in Fig. 1 is easily shown to contribute to the gluon polarization with a constant term $\Delta\Pi = -m^2$,

$$\Pi(p^2) = -m^2 + \Pi^{(\text{loops})}(p^2), \quad (28)$$

where $\Pi^{(\text{loops})}(p^2)$ is the loop contribution to the polarization—diagrams (1b)–(2c) in Fig. 1. It is then easy to see that the tree-level mass term inherited from the shift cancels out with $\Delta\Pi$, so that the dressed propagator itself can be expressed as

$$\Delta(p^2) = -i[p^2 - \Pi^{(\text{loops})}(p^2)]^{-1}. \quad (29)$$

From the above equation it is clear that in the screened expansion, rather than being a trivial effect of the shift of the expansion point, the gluon mass must come from the loops and is thus genuinely dynamical in nature; it does not coincide with the gluon mass parameter m^2 , which at this stage is just an undetermined dimensionful scale.

Quite interestingly, the existence of a finite mass-scale in YM theory has been derived in the Gaussian approximation from first principles [56,64], but, of course, the actual value of that scale can only arise from the phenomenology, since there is no energy scale in pure YM theory. The best variational Gaussian vacuum was shown to be the vacuum of a massive gluon, and the present screened expansion emerged has the perturbative loop expansion around that best massive vacuum [56]. While fermions have also been incorporated in the Gaussian formalism in the past [67], it is not clear if the screened expansion of full QCD, as is discussed in the present paper, can also be regarded as a loop expansion around a variational Gaussian vacuum which breaks the chiral symmetry.

TABLE I. Results of the screened massive expansion of pure YM theory, obtained by imposing the gauge-parameter independence of the poles and of the phases of the residues of the gluon propagator in a general covariant gauge. From left to right: the additive renormalization constant F_0 in the Landau gauge, the adimensional position $z_0^2 = p_0^2/m^2$ of the poles of the gluon propagator in the Landau gauge, the gauge-invariant phases φ of the residues of the gluon propagator, and the gauge-invariant dimensionful positions of the poles of the propagator, assuming $m = 0.6557$ GeV in the Landau gauge (the \pm signs are independent from each other).

F_0	z_0^2	φ	p_0 (GeV)
-0.876	$0.4575 \pm 1.0130i$	± 1.262	$\pm 0.5810 \pm 0.3571i$

B. Optimization and results in the Landau gauge

In a general renormalization scheme and in the Landau gauge, the dressed gluon propagator $\Delta(p^2)$ can be expressed as

$$\Delta(p^2) = \frac{-iZ_\Delta}{p^2(F(s) + F_0)}, \quad (30)$$

where $s = -p^2/m^2$ and Z_Δ and F_0 are, respectively, a multiplicative and an additive renormalization constant.¹ The function $F(s)$ was computed to one loop and third order in the number of vertices from the diagrams in Fig. 1; its analytical expression is reported in Ref. [54]. The zero-momentum limit of $F(s)$ reads

$$F(s) \rightarrow \frac{5}{8s}(s \rightarrow 0), \quad (31)$$

so that

$$\Delta(p^2) \rightarrow \frac{i8Z_\Delta}{5m^2}(p^2 \rightarrow 0), \quad (32)$$

implying that the screened expansion's gluon propagator is indeed massive in the infrared. We reiterate that the gluon mass, as defined, for instance, and nonunivocally, by $i\Delta(0)^{-1}$, comes from the loops and is thus dynamical in nature.

Together with the gluon mass parameter m^2 , Z_Δ and F_0 are the only free parameters determining the gluon propagator in the screened expansion. The multiplicative constant Z_Δ can of course be fixed by renormalizing the propagator at some specified renormalization scale $p^2 = -\mu^2$, i.e., by requiring that

$$\Delta(-\mu^2) = \frac{-i}{-\mu^2}. \quad (33)$$

The value of the additive renormalization constant F_0 , on the other hand, was optimized and fixed in Ref. [60]

¹The strong coupling constant α_s was absorbed into the definition of Z_Δ and F_0 and makes no explicit appearance in what follows.

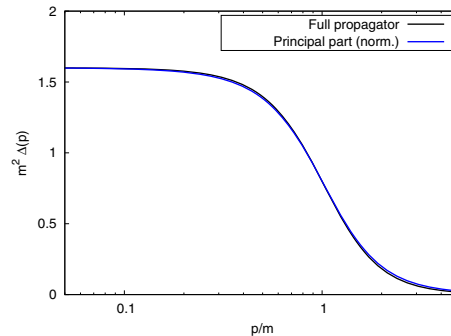


FIG. 2. Transverse gluon propagator in the Landau gauge ($\xi = 0$) and in Euclidean space, computed in the screened expansion of pure YM theory. Black line: full one-loop propagator. Blue line: principal part of the one-loop propagator, normalized by a factor of 0.945.

according to principles of gauge invariance. In more detail, it was shown that there exists a value of F_0 in the Landau gauge, namely, $F_0 = -0.876$, which, when evolved to a general covariant gauge ($\xi \neq 0$), yields gauge-invariant poles p_0^2 for the gluon propagator whose residues are also gauge invariant in phase to less than 0.3% [68–70].

In the same context (and in previous papers also, see, e.g., [55,58]), we found that the screened expansion's gluon propagator has two complex-conjugate poles, whose adimensional positions $z_0^2 = p_0^2/m^2$ and \bar{z}_0^2 were determined in [60] from first principles. The existence of complex-conjugate poles has been related in the literature to the issue of the violation of positivity of the gluon spectral function and, more generally, to that of confinement [71,72]. The poles and phases of the residues of the gluon propagator, as computed in the (optimized) screened expansion, are reported in Table I.

Of particular relevance to this paper is the fact that the principal part of the gluon propagator, i.e., the term which contains its poles, well-approximates the full propagator itself [64], provided that the former is multiplied by a factor of 0.945. This is shown in Fig. 2.

With Z_Δ and F_0 fixed, the gluon mass parameter m^2 is left as the only free parameter of the theory (at least as far as the gluon two-point function is concerned). m^2 sets the energy units for the dimensionful quantities in the theory; as such, it cannot be determined from first principles and must be fixed from phenomenology. In this respect, the gluon mass parameter plays the same role as the QCD scale Λ_{QCD} of ordinary perturbation theory.² The propagator

²For a lengthy discussion on the conceptual similarities between the gluon mass parameter m^2 and the QCD scale Λ_{QCD} , see Ref. [63], where the issue was addressed in the context of the renormalization group improvement of the screened expansion.

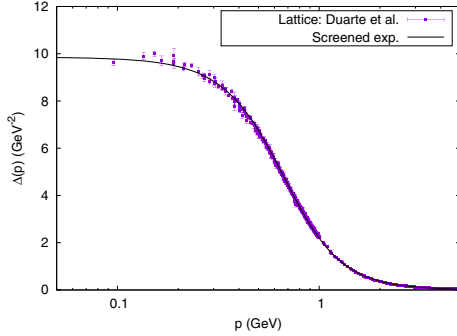


FIG. 3. Transverse dressed gluon propagator in the Landau gauge ($\xi = 0$) and in Euclidean space, computed in the screened expansion of pure YM theory by optimizing the additive renormalization constant F_0 based on principles of gauge invariance. The lattice data are taken from Ref. [15].

defined by Eq. (30), with $F_0 = -0.876$ optimized by principles of gauge invariance, was found to accurately reproduce the Euclidean lattice data of Ref. [15], provided that the energy units of the screened expansion are set by choosing $m = 0.6557$ GeV (see Fig. 3). Once the value of the gluon mass parameter is determined, the dimensionful values of the poles of the propagator can be computed; they are reported in the last column of Table I.

III. THE SCREENED MASSIVE EXPANSION OF FULL QCD

In this section, we extend the screened massive expansion to full QCD with one flavor of quarks. As we will see, our formalism is able to describe the nonperturbative generation of an infrared dynamical mass both for the chiral and the light quarks.

Our starting point is the formalism laid out in Sec. II A. After introducing the quarks in the Faddeev-Popov Lagrangian of pure Yang-Mills theory, we perform a nonordinary renormalization and split of the quark Lagrangian into a kinetic and an interaction term plus renormalization counterterms. The procedure parallels what we previously did for the gauge sector, but has a new feature, namely, the nonrenormalization of the quark's bare mass. The motivation and consistency of such a choice are discussed in Sec. III A. In Sec. III B, we define three resummation schemes for the dressed quark propagator, which differ by how the internal gluon line is treated in the quark self-energy.

A. Setup and renormalization

The Lagrangian of full QCD with one flavor of quarks is given by

$$\mathcal{L}_{\text{QCD}} = \mathcal{L} + \mathcal{L}_{q,B}, \quad (34)$$

where \mathcal{L} is the Faddeev-Popov Lagrangian of pure Yang-Mills theory—Eq. (1)—and $\mathcal{L}_{q,B}$ is the quark Lagrangian expressed in terms of the bare fields, mass, and coupling,

$$\mathcal{L}_{q,B} = \bar{\psi}_B (i\not{D}_B - M_B) \psi_B. \quad (35)$$

Here, M_B is the quark's bare mass, while D_B is the bare covariant derivative acting on the bare quark field ψ_B ,

$$D_B^\mu = \partial^\mu - ig_B A_B^{a\mu} T_a. \quad (36)$$

In order to renormalize the quark Lagrangian, we introduce a quark field renormalization constant Z_ψ such that

$$\psi_B = Z_\psi^{1/2} \psi, \quad (37)$$

where ψ is the renormalized quark field. Then, $\mathcal{L}_{q,B}$ can be expressed as

$$\mathcal{L}_{q,B} = \bar{\psi} (i\not{D} - M_B Z_\psi) \psi + \mathcal{L}_{q,\text{c.t.}}, \quad (38)$$

where D is the renormalized covariant derivative acting on the renormalized quark field,

$$D_\mu = \partial_\mu - ig A_\mu^a T_a, \quad (39)$$

with g and A_μ^a being the renormalized coupling and gluon field defined as in Sec. II A, while $\mathcal{L}_{q,\text{c.t.}}$ contains the quark's field strength and quark-gluon vertex renormalization counterterms.

At this point, if the quark is not massless (i.e., $M_B \neq 0$), one usually introduces a renormalized quark mass through a kinetic term of the form $-M_R \bar{\psi} \psi$ and includes the corresponding mass renormalization counterterm $-\delta_M \bar{\psi} \psi$ into $\mathcal{L}_{q,\text{c.t.}}$. In ordinary perturbation theory, M_R and M_B are understood to be proportional and related to each other by radiative corrections which can be computed perturbatively at any given loop order. Due to dynamical mass generation, however, in the IR the light quarks acquire a mass which is much larger than their renormalized mass M_R and non-proportional to it; indeed, the former would be nonzero (and of the order of the QCD scale Λ_{QCD}) also in the case of chiral quarks ($M_B = 0$). Clearly, choosing M_R as the mass of the zero-order propagator around which to expand the perturbative series is not optimal for the purpose of exploring the low-energy dynamics of the quark sector.

On the other hand, the situation could improve if an effective mass scale, mimicking the dynamically generated IR quark mass, was used in place of the renormalized mass M_R . Our setup, therefore, employs the following scheme. As in ordinary perturbation theory, we add to the quark Lagrangian a mass term of the form $-M \bar{\psi} \psi$. However, we do not interpret M as the renormalized counterpart of M_B . Instead, we regard the former as being a nonperturbative

mass scale arising from the low-energy dynamics of the theory and leave M_B unrenormalized. Explicitly, we rewrite the quark Lagrangian as

$$\mathcal{L}_{q,B} = \bar{\psi}(i\mathcal{D} - M)\psi + \bar{\psi}(M - M_B Z_\psi)\psi + \mathcal{L}_{q,c.t.} \quad (40)$$

and treat M and M_B as *independent* mass parameters; the difference $M_B Z_\psi - M$, which in ordinary perturbation theory would correspond to the mass renormalization counterterm δ_M , is not taken to be proportional to the coupling constant (i.e., small in the perturbative sense) nor is it regarded as fixed by the renormalization of the quark propagator. We anticipate that an appropriate choice of the diagrams to include in the one-loop quark propagator preserves the renormalizability of the theory also when using this nonstandard scheme.

The quark Lagrangian is now split into a kinetic (zero-order) term $\mathcal{L}_{q,0}$,

$$\mathcal{L}_{q,0} = \bar{\psi}(i\mathcal{D} - M)\psi, \quad (41)$$

in which M appears as the mass in the zero-order quark propagator; an interaction term $\mathcal{L}_{q,int}$,

$$\mathcal{L}_{q,int} = \bar{\psi}(g\mathbf{A}^a T_a + M - M_B Z_\psi)\psi, \quad (42)$$

which contains the quark-gluon vertex and two new quadratic terms, proportional to M and M_B ; and a renormalization term $\mathcal{L}_{q,c.t.}$,

$$\mathcal{L}_{q,c.t.} = \bar{\psi}(i\delta_\psi \mathcal{D} + g\delta_g \mathbf{A}^a T_a)\psi. \quad (43)$$

which contains the quark field strength renormalization counterterm $\delta_\psi = Z_\psi - 1$ and a renormalization counterterm δ_g for the quark-gluon vertex.

The addition and subtraction of the mass term $-M\bar{\psi}\psi$ from the quark Lagrangian parallels what we did in the gluon sector of pure Yang-Mills theory. This is best seen in the chiral limit ($M_B \rightarrow 0$), where the addition of a mass term of the form $-M_R\bar{\psi}\psi$ would be meaningless, since $M_R \propto M_B = 0$. As a nonperturbative mass parameter not directly related to M_B , M has the same status of the gluon mass parameter m in the screened expansion of YM theory and is allowed to remain finite also in the chiral limit. For this reason, we refer to M as the *chiral mass* of the quark.

As in the screened expansion of YM theory, the shift of the quark Lagrangian changes the Feynman rules of the theory. First of all, the chiral mass M now figures as the tree-level mass in the zero-order quark propagator $S_M(p)$,

$$S_M(p) = \frac{i}{\not{p} - M}. \quad (44)$$

Second of all, two new two-point vertices $\delta\Gamma_{q,1}$ and $\delta\Gamma_{q,2}$ arise in the interaction,

$$\Sigma = \text{(1a)} + \text{(1b)} + \text{(2a)} + \text{(2b)} + \text{(2c)} + \text{(2d)} + \dots$$

FIG. 4. 1PI diagrams for the screened expansion one-loop quark self-energy. The crosses denote insertions of the mass counterterms. The subscripts 1 and 2 label the vertices $\delta\Gamma_{q,1}$ and $\delta\Gamma_{q,2}$ in Eq. (45). The renormalization counterterms are not shown in the figure.

$$\delta\Gamma_{q,1}(p) = iM, \quad \delta\Gamma_{q,2}(p) = -iM_B Z_\psi. \quad (45)$$

We reiterate that in our framework these are treated as independent vertices. The quark-gluon interaction and renormalization vertices, on the other hand, are left unchanged, except for the quark mass renormalization counterterm, which must not be included in the calculation.

These Feynman rules must of course be supplied with those of the gluon sector, which were derived in Sec. II A in the context of pure YM theory. In particular, the transverse gluons propagate with a massive zero-order propagator—Eq. (21)—and a third two-point vertex, the gluon mass counterterm of Eq. (24), is included in the interaction.

As a consequence of the new Feynman rules, the screened expansion of full QCD is nonperturbative in nature. Like in pure YM theory, this is due to the two-point vertices $\delta\Gamma_g$, $\delta\Gamma_{q,1}$, and $\delta\Gamma_{q,2}$, which are proportional to the gluon and the quark mass parameters m^2 , M , and M_B , and are not taken to be proportional to the strong coupling constant.

Let us now turn our attention to how to compute the quark propagator in the new framework. The dressed quark propagator $S(p)$ can be expressed in terms of the 1PI quark self-energy $\Sigma(p)$ ³ as

$$S(p) = \frac{i}{\not{p} - M - \Sigma(p)}. \quad (46)$$

Due to the shift of the expansion point, $\Sigma(p)$ receives tree-level contributions not only from the quark field strength renormalization counterterm $\delta_\psi = Z_\psi - 1$, but also from the new vertices $\delta\Gamma_{q,1}$ and $\delta\Gamma_{q,2}$ —diagrams (1a) and (1b) in Fig. 4. We have

$$\Sigma(p) = -\delta_\psi \not{p} - M + M_B Z_\psi + \Sigma^{(\text{loops})}(p), \quad (47)$$

where $\Sigma^{(\text{loops})}(p)$ is the self-energy contribution coming from the loops. It follows that

³Not to be confused with the ghost self-energy of Sec. II A.

$$[-iS(p)]^{-1} = Z_\psi \not{p} - M_B Z_\psi - \Sigma^{(\text{loops})}(p). \quad (48)$$

As in pure YM theory, the mass M introduced by the shift of the quark Lagrangian disappears from the propagator, and the bare mass is restored at tree level, up to field-strength renormalization. In order to define the quark mass function $\mathcal{M}(p^2)$ and Z function $Z(p^2)$, we first subdivide $\Sigma^{(\text{loops})}(p)$ into a vector and a scalar term,

$$\Sigma^{(\text{loops})}(p) = \not{p}\Sigma_V(p^2) + \Sigma_S(p^2), \quad (49)$$

and then define two scalar functions $A(p^2)$ and $B(p^2)$,

$$\begin{aligned} A(p^2) &= Z_\psi - \Sigma_V(p^2), \\ B(p^2) &= M_B Z_\psi + \Sigma_S(p^2). \end{aligned} \quad (50)$$

In terms of $A(p^2)$ and $B(p^2)$, the functions $\mathcal{M}(p^2)$ and $Z(p^2)$ read

$$Z(p^2) = \frac{1}{A(p^2)}, \quad \mathcal{M}(p^2) = \frac{B(p^2)}{A(p^2)}. \quad (51)$$

Moreover, Eq. (46) can be rewritten as

$$S(p) = \frac{iZ(p^2)}{\not{p} - \mathcal{M}(p^2)}. \quad (52)$$

From Eqs. (50) and (51), we see that in the chiral limit ($M_B \rightarrow 0$), despite the absence of a tree-level mass for the quark propagator, the quark mass function $\mathcal{M}(p^2)$ does not vanish; thanks to the finiteness of the nonperturbative scale M , one finds that $\Sigma_S(p^2) \neq 0$, which makes $B(p^2) \neq 0$ and thus $\mathcal{M}(p^2) \neq 0$, also for vanishing M_B . Since $\Sigma_S(p^2)$ comes from the loops, the mass of the quark is genuinely dynamical, a feature that was already highlighted in Sec. II for the gluons in pure YM theory. For nonchiral quarks the situation is similar, the only difference being that $B(p^2)$ also contains one additional tree-level term which is proportional to the bare mass M_B of the quark. As we will see in a moment, the fact that this term is not renormalized poses no issue of consistency.

To one loop, an infinite number of diagrams contributes to the 1PI quark self-energy. These have the structure of the ordinary one-loop diagram of standard perturbation theory—diagram (2a) in Fig. 4—with an arbitrarily large number of insertions of the gluon mass counterterm $\delta\Gamma_g$ and of the quark mass counterterms $\delta\Gamma_{q,1}$ and $\delta\Gamma_{q,2}$. In order to chose a truncation scheme for this infinite series, let us have a look at the first few such diagrams.

The simplest one-loop self-energy diagram is the ordinary uncrossed loop—denoted by (2a) in Fig. 4. In a general covariant gauge, diagram (2a) has divergences in both its vector component and in its scalar component,

$$\Sigma^{(2a)}(p) = (c_{2aV}\not{p} + c_{2aS}M)\frac{2}{\epsilon} + \dots, \quad (53)$$

where c_{2aV} and c_{2aS} are $O(g^2)$ coefficients, $\epsilon = 4 - d$ is the regulator of dimensional regularization, and the dots denote finite self-energy terms. While the vector divergence can be straightforwardly absorbed into the renormalization constant Z_ψ —see the first of Eq. (50)—in order to remove the mass divergence c_{2aS} , we would need to define a renormalized mass M_R in terms of which

$$M_B = Z_\psi^{-1} \left(M_R - c_{2aS}M\frac{2}{\epsilon} + \text{scheme-dep. const.} \right), \quad (54)$$

see the second of Eq. (50). A relation like this mixes infrared entities (namely, the chiral mass M) to UV features (the divergence and the renormalization of the bare mass) with no apparent logic, aside from the mathematical convenience of it. Moreover, this type of renormalization cannot be employed in the chiral limit $M_B \rightarrow 0$, when there is no bare mass in which to absorb the divergence. For these reasons, it must be rejected.

We note that, having been introduced through a term which is added and subtracted in the Lagrangian, the mass parameter M cancels in the total action; as a consequence, any divergence proportional to M must disappear when diagrams with a different number of mass counterterms are resummed at the same loop order.

In fact, diagram (2b) in Fig. 4 is easily shown to contain the same mass divergence of diagram (2a) with an opposite sign; since the crossed quark line in the diagram can be expressed as a derivative with respect to the quark's chiral mass,

$$\frac{i}{\not{p} - M} (iM) \frac{i}{\not{p} - M} = -M \frac{\partial}{\partial M} \frac{i}{\not{p} - M}. \quad (55)$$

The self-energy contribution from diagram (2b), $\Sigma^{(2b)}(p)$, can be obtained as a derivative of $\Sigma^{(2a)}(p)$,

$$\Sigma^{(2b)}(p) = -M \frac{\partial}{\partial M} \Sigma^{(2a)}(p). \quad (56)$$

It follows that

$$\Sigma^{(2b)}(p) = -c_{2aS}M\frac{2}{\epsilon} + \dots, \quad (57)$$

that is, $\Sigma^{(2a)}(p)$ and $\Sigma^{(2b)}(p)$ have opposite mass divergences. As a consequence, the sum of diagrams (2a) and (2b) only contains a divergence in the vector component, coming entirely from $\Sigma^{(2a)}(p)$. This divergence can be shown to be the same as the one found in ordinary perturbation theory and is to be absorbed into the definition of Z_ψ , as we saw earlier.

Now, in the Landau gauge ($\xi = 0$), the divergence contained in $\Sigma^{(2a)}(p)$ is known from ordinary perturbation theory to vanish. Therefore, not only does the sum $\Sigma^{(2a)}(p) + \Sigma^{(2b)}(p)$ not contain mass divergences, but in the Landau gauge it is also fully finite. In particular, if we truncate the perturbative series to diagrams (2a) and (2b) in Fig. 4 and limit ourselves to the Landau gauge, then the term $M_B Z_\psi$ that appears in the $B(p^2)$ function—see Eq. (50)—can be taken to be a finite constant. In other words, no renormalization of divergent constants or masses is required in the screened expansion of the Landau gauge quark propagator, provided that the latter is truncated to diagrams (2a) and (2b).

On the other hand, if $\xi \neq 0$, the vector divergence in $\Sigma^{(2a)}(p) + \Sigma^{(2b)}(p)$ still needs to be absorbed into Z_ψ . For nonchiral quarks ($M_B \neq 0$), if M_B were taken to be finite, this would leave us with a divergent $M_B Z_\psi$ term inside $B(p^2)$. Therefore, for $\xi \neq 0$ and $M_B \neq 0$, a renormalized mass M_R must still be introduced, even when truncating the quark self-energy to diagrams (2a) and (2b).

It is easy to see that a renormalized mass of the form $M_R = M_B Z_\psi$ would not have the ordinary behavior of a running mass under the renormalization group (RG). Indeed, if the RG equations were employed in the scheme, M_R would run exclusively with the anomalous dimension of the quark field, rather than with the full anomalous dimension of the quark mass. This happens because we have left out one further divergent diagram from the calculation, namely, diagram (2c) in Fig. 4. The latter can be obtained from diagram (2a) by using the equality

$$\frac{i}{\not{p} - M} (-i M_B Z_\psi) \frac{i}{\not{p} - M} = M_B Z_\psi \frac{\partial}{\partial M} \frac{i}{\not{p} - M}, \quad (58)$$

which can be exploited to write

$$\Sigma^{(2c)}(p) = M_B Z_\psi \frac{\partial}{\partial M} \Sigma^{(2a)}(p). \quad (59)$$

In particular,

$$\Sigma^{(2c)}(p) = c_{2aS} M_B Z_\psi \frac{2}{\epsilon} + \dots \quad (60)$$

As we can see, diagram (2c) has a scalar divergence proportional to $M_B Z_\psi$. When the latter is summed to the tree-level term in $B(p^2)$, one finds

$$B(p^2) = M_B Z_\psi \left(1 + c_{2aS} \frac{2}{\epsilon} \right) + \dots \quad (61)$$

By simple dimensional arguments, it is easy to show that the remaining one-loop diagrams in the quark self-energy are finite. Therefore, the above expression spells out the complete divergent term of the scalar component of the

one-loop self-energy, obtained by summing the divergences of diagrams (2a) to (2c) in Fig. 4. Such a term can indeed be equated, modulo finite constants, to a renormalized mass M_R which would run like an ordinary quark mass if the RG equations were to be used, leaving us with

$$B(p^2) = M_R + \text{finite terms.} \quad (62)$$

Beyond the Landau gauge, then, consistency with the renormalization group requires us to include diagram (2c) in the calculation. In the Landau gauge, on the other hand, diagram (2c) is not needed, in principle, since to one loop the sum of diagrams (2a) and (2b) already results in a finite quark 1PI self-energy.

Despite being necessary for theoretical consistency, if the renormalized quark mass M_R is much smaller than the chiral mass M , the inclusion of diagram (2c) in the quark self-energy turns out not to be essential from a quantitative point of view. This is easily seen as follows. Let $\Sigma_f^{(2a,2b,2c)}(p)$ be the finite parts of the self-energy diagrams (2a), (2b), and (2c). Using Eqs. (56) and (59),

$$\Sigma_f^{(2b)}(p) + \Sigma_f^{(2c)}(p) = -(M - M_B Z_\psi) \frac{\partial}{\partial M} \Sigma_f^{(2a)}(p). \quad (63)$$

Modulo higher-order corrections, we can set $M_B = M_R$, $Z_\psi = 1$ in the above equation, so that

$$\Sigma_f^{(2b)}(p) + \Sigma_f^{(2c)}(p) = -(M - M_R) \frac{\partial}{\partial M} \Sigma_f^{(2a)}(p). \quad (64)$$

It is then clear that, as long as $M_R \ll M$, the contribution of diagram (2c) is completely negligible with respect to that of diagram (2b). In other words, for the light quarks, diagram (2c) can be taken to contribute only to the divergent part of the self-energy, i.e., to the renormalization of the bare mass.⁴

To summarize, in every linear covariant gauge, diagram (2b) in Fig. 4 is needed in order to remove the mass divergence in diagram (2a). This mass divergence has no counterpart in ordinary perturbation theory, since it is proportional to the quark chiral mass M . Diagram (2c) is essential to renormalize the bare mass M_B in compliance with the standard RG equations. Nonetheless, its finite part is completely negligible in the case of light quarks. Finally, in the Landau gauge the sum of diagrams (2a) and (2b)

⁴For the sake of completeness, we note that there is one catch in this argument; at high energies, the scalar part of the sum of diagrams (2a) and (2b) can be shown to vanish, see, e.g., Sec. IV A, so that, instead of being negligible, diagram (2c) actually makes up for the whole scalar self-energy. As long as we limit ourselves to low and moderate energies, this issue does not arise. At large energies, however, diagram (2c) and appropriate RG techniques are needed to account for the correct asymptotic behavior of the quark mass function.

results in a finite self-energy. Since for the light quarks diagram (2c) is quantitatively negligible, in the Landau gauge one can simply exclude it from the self-energy and interpret the free parameters M_B and Z_ψ as bare but finite quantities.

In the next section, we carry on with our analysis of the resummation of the one-loop quark propagator. Our main focus is on exploring different ways to treat the finite diagrams in Fig. 4.

B. Resummation schemes for the quark propagator

Up to this point, we have discussed the self-energy diagrams which contribute to the divergent part of the one-loop quark propagator, namely, diagrams (2a) to (2c) in Fig. 4. Using simple dimensional arguments, it is easy to show that, to one loop, other insertions of the gluon and quark two-point mass counterterms indeed yield convergent diagrams. As an example, consider diagram (2d) in Fig. 4. This diagram has a superficial degree of divergence D

$$D = d - 1 - 2 - 2 \rightarrow -1 < 0, \quad (65)$$

where the -1 and the -2 's come from the internal quark and gluon lines, respectively, making diagram (2d) UV-finite in the limit $d \rightarrow 4$. Equivalently, observe that diagram (2d) can be expressed as a derivative of diagram (2a) with respect to the gluon mass parameter m^2 ; using Eq. (25) with $n = 1$, we find that

$$\Sigma^{(2d)}(p) = -m^2 \frac{\partial}{\partial m^2} \Sigma^{(2a)}(p). \quad (66)$$

Since the divergent part of $\Sigma^{(2a)}(p)$ does not depend on m^2 , $\Sigma^{(2d)}(p)$ is again shown to be finite.

While divergent diagrams are included in the one-loop calculation based on principles of renormalizability, assessing which finite diagrams should be included as well is far more tricky. One option could be to adopt a minimalistic point of view and limit oneself to the one-loop diagrams needed for consistency, i.e., diagrams (2a) to (2b) or (2c) in Fig. 4. Yet another option could be to retain all the one-loop diagrams with a maximum of three vertices, as we did for the gluon propagator in Sec. II; in practice, this amounts to also including diagram (2d) in the self-energy. These two resummation schemes differ by how the internal gluon line is treated—explicitly, by whether the internal zero-order gluon propagator is corrected with its own mass counterterm or not. We refer to them as the minimalistic and the vertex-wise schemes, respectively. Schemes with a larger number of crossed diagrams (not shown in Fig. 4) are not considered in this paper.

In the next section, we fit and compare the results obtained in the minimalistic and vertex-wise schemes with the quenched lattice data of Ref. [73]. The reason for using

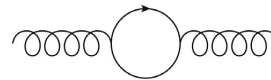


FIG. 5. Quark loop in the unquenched gluon polarization. To one loop, its inclusion affects the value of the gluon mass parameter m^2 and the position and residue of the poles of the gluon propagator.

quenched rather than unquenched lattice data is to exploit our previous results for pure YM theory and fix *ab initio* the value of the gluon mass parameter m^2 that appears in the quark propagator—thus reducing the number of free parameters to be fitted. Indeed, observe that, to one loop, the quark self-energy diagrams for the quenched and unquenched theories coincide. Hence, in principle, our results could be used for comparisons with both quenched and unquenched data. However, in the framework of the screened massive expansion, the value of the gluon mass parameter m^2 running in diagrams (2a)–(2d) (Fig. 4) can receive corrections from the quark loop in the gluon polarization (Fig. 5), which is only present in the unquenched theory. Thus, we expect the value of m^2 to be different depending on which theory (quenched or unquenched) we are trying to fit. In order to reduce the freedom in the choice of free parameters, we decide not to make a new determination of the gluon mass parameter, but rather to use the quenched lattice data for our fits. The value $m = 0.6557$ GeV was obtained in [60] by a fit of the lattice data of Ref. [15] for pure YM theory. With m fixed, the remaining free parameters of the quark propagator are the chiral mass M , the quark bare mass M_B or renormalized mass M_R , and the renormalization constants.

As we will see, the minimalistic and vertex-wise schemes are practically equivalent from the point of view of the fit, the only difference being in the values of the parameters needed to achieve the match with the lattice data. Both of them succeed in quantitatively reproducing the lattice mass function $\mathcal{M}(p^2)$ with very good precision. On the other hand, in none of the two the Z function has the behavior displayed by the lattice data; $Z(p^2)$ is found to be a decreasing function of momentum, at variance with the lattice. To one loop, such a mismatch is not unseen, having been reported for another massive model, namely, the Curci-Ferrari model of Ref. [45].

One interesting question to ask is whether higher-order or nonperturbative corrections to the internal gluon line in the quark self-energy can sensibly change the behavior of the Z function. Indeed, as we noted in the Introduction, in the Landau gauge, to one loop and at sufficiently high energies, $Z(p^2) \approx 1$, making the Z function sensitive to all kinds of contributions beyond the leading perturbative order. The near vanishing of the perturbative contribution makes the Z function a valid benchmark for investigating the role of condensates by the OPE. Indeed, the slightly increasing behavior which is observed on the lattice has been modeled

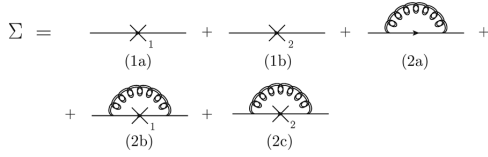


FIG. 6. 1PI diagrams for the quark self-energy in the complex-conjugate (CC) scheme. The double lines represent the fully dressed gluon propagator, which in the CC scheme is approximated by the principal part of the one-loop gluon propagator (Sec. II).

by OPE [74–76] and shown to be consistent with the existence of a dimension-2 gluon condensate of the form $\langle A^2 \rangle$. In order to explore these issues, we introduce a third resummation scheme, which we term the complex-conjugate (CC) scheme for reasons that will become apparent in a moment.

In the CC scheme, instead of only summing the zero-order gluon propagator (minimalistic scheme) or its counterterm-corrected counterpart (vertex-wise scheme), we use the fully dressed gluon propagator as the internal gluon line of the one-loop quark self-energy (see Fig. 6). Switching to the dressed gluon propagator allows us to account for the full nonperturbative dynamics of the gluon, when computing the quark propagator.

While, in principle, using the dressed propagator would require us to resum and integrate an infinite number of higher-order diagrams, in practice we know that—in pure Yang-Mills theory—the principal part of the screened expansion’s one-loop gluon propagator provides a very good approximation to the dressed propagator, modulo a multiplicative factor (see Sec. II B, in particular, Figs. 2 and 3). Therefore, in the CC scheme, we use a zero-order gluon propagator which—in Euclidean space and in the Landau gauge—reads

$$\Delta_{\mu\nu}^{(c.c.)}(p) = \left\{ \frac{R}{p^2 + p_0^2} + \frac{\bar{R}}{p^2 + \bar{p}_0^2} \right\} t_{\mu\nu}(p). \quad (67)$$

Here, p_0^2 and \bar{p}_0^2 are the complex-conjugate poles of the dressed gluon propagator (hence, the name CC scheme) in the complexified Minkowski space, and R and \bar{R} are their normalized residues. The value of the modulus $|R|$ —which depends both on the renormalization conventions for the dressed gluon propagator and on a multiplicative factor that converts between the full propagator and its principal part—does not actually affect the results for the quark propagator, provided that the free parameters are suitably redefined. Indeed, to one loop, the internal gluon line in the quark self-energy is multiplied by a factor of the strong coupling constant α_s , so that $|R|$ can be absorbed into the definition of the latter. Our convention for the definition of $|R|$ (and thus also α_s in the CC scheme) is discussed in

Sec. IV C. As for p_0^2 and the phase of R , we use the values reported in Table I (Sec. II B). These were obtained in pure Yang-Mills theory and are thus suitable for calculations in the quenched theory, in line with our discussion on the gluon mass parameter m^2 in the minimalistic and vertex-wise schemes.

As we show in Appendix B, despite the poles p_0^2 and \bar{p}_0^2 being complex, as long as the external momentum $p^2 \in \mathbb{R}$, the loop integrals in the CC scheme can be computed by employing the usual machinery of Feynman parameter integrals and gamma functions. In particular, if we denote with $\Sigma_m^{(\text{loops})}(p)$ the loop contribution to quark self-energy computed in the minimalistic scheme—diagrams (2a) to (2c) in Fig. 4—then we can express the corresponding self-energy term $\Sigma_{c.c.}^{(\text{loops})}(p)$ in the CC scheme as

$$\Sigma_{c.c.}^{(\text{loops})}(p) = R \Sigma_m^{(\text{loops})}(p)|_{m^2=p_0^2} + \bar{R} \Sigma_m^{(\text{loops})}(p)|_{m^2=\bar{p}_0^2} \quad (68)$$

or equivalently

$$\Sigma_{c.c.}^{(\text{loops})}(p) = 2\text{Re}\{R \Sigma_m^{(\text{loops})}(p)|_{m^2=p_0^2}\}. \quad (69)$$

As we will see, the Z function computed in the CC scheme indeed turns out to have a qualitatively different behavior than those computed in the minimalistic or vertex-wise scheme, closer to the one displayed by the quenched lattice data at moderately large momenta.

IV. THE QUARK PROPAGATOR IN THE LANDAU GAUGE

In this section, we report our results for the quark propagator in the Landau gauge using the screened massive expansion of full QCD in the minimalistic, vertex-wise, and complex-conjugate resummation schemes introduced in Sec. III B. As previously discussed, we use the lattice data of Ref. [73] for quenched QCD in order to test the validity of the expansion and fit the free parameters that appear in the propagator. These parameters are defined in what follows.

In general, see Eqs. (50) and (51), the quark mass and Z function can be expressed as

$$\begin{aligned} \mathcal{M}(p^2) &= \frac{M_B Z_\psi + \Sigma_S(p^2)}{Z_\psi - \Sigma_V(p^2)}, \\ Z(p^2) &= [Z_\psi - \Sigma_V(p^2)]^{-1}. \end{aligned} \quad (70)$$

Here, $\Sigma_V(p^2)$ and $\Sigma_S(p^2)$ are the vector and scalar components of the loop contribution to the quark self-energy, M_B is the quark bare mass, and Z_ψ is the quark field renormalization constant. In the Landau gauge and to one loop, as we saw in Sec. III, $\Sigma_V(p^2)$ is UV convergent. As a consequence, we can write

$$\Sigma_V(p^2) = \frac{\alpha_s}{3\pi} \sigma_V(p^2), \quad (71)$$

where $\sigma_V(p^2)$ is a finite function. Nonetheless, the value of Z_ψ still needs to be fixed. We decide to do so by renormalizing the Z function in the momentum-subtraction (MOM) scheme at a specified renormalization scale μ^2 . Namely, we set

$$Z(\mu^2) = 1 \Leftrightarrow Z_\psi - \Sigma_V(\mu^2) = 1, \quad (72)$$

or, equivalently,

$$Z_\psi = 1 + \frac{\alpha_s}{3\pi} \sigma_V(\mu^2), \quad (73)$$

where we take μ to be equal to 4 GeV. As we will see in a moment, as far as the fits are concerned, this choice is inessential to our results.

At variance with $\Sigma_V(p^2)$, the scalar component $\Sigma_S(p^2)$ can be either UV divergent or UV convergent depending on whether diagram (2c) in Figs. 4 and 6 is included or not in the self-energy, respectively. In the absence of diagram (2c), $\Sigma_S(p^2)$ can be expressed as

$$\Sigma_S(p^2) = \frac{\alpha_s}{\pi} \sigma_S(p^2), \quad (74)$$

where $\sigma_S(p^2)$ is a finite function. In particular, it follows from the first of Eq. (70) that M_B must be taken to be finite. If we now define two finite constants h_0 and k_0 ,

$$\begin{aligned} h_0 &= \frac{3\pi}{\alpha_s} Z_\psi, \\ k_0 &= \frac{\pi}{\alpha_s} M_B Z_\psi, \end{aligned} \quad (75)$$

then the mass function $\mathcal{M}(p^2)$ reads

$$\mathcal{M}(p^2) = \frac{3[k_0 + \sigma_S(p^2)]}{h_0 - \sigma_V(p^2)}. \quad (76)$$

Here, α_s and M_B have been absorbed into the definition of h_0 and k_0 .

While the exact propagator should not depend on the scale μ , apart from a renormalization factor, the approximate one-loop function $\mathcal{M}(p^2)$ still has an implicit spurious dependence on μ through the parameters h_0 , k_0 , according to Eqs. (75) and (73). Thus, the one-loop result can be optimized by a wise choice of the parameters; fixing h_0 and k_0 amounts to choosing an optimal renormalization—together with the corresponding coupling and bare mass—for the quark mass function.

As discussed in Sec. II B, for the gluon propagator such an optimization can be achieved from first principles in pure YM theory. Here, we just assume the existence of an

optimal value of the parameters and determine them by a comparison with the lattice data. Thus, h_0 and k_0 are regarded as free parameters which depend on the scale ambiguity of the loop expansion.

For our fits, we use h_0 , k_0 and the chiral mass M as the primary free parameters. It follows that our choice of the MOM scheme with $\mu = 4$ GeV as the renormalization scale has no impact on the results of the fit. What the renormalization scheme actually determines is the value of α_s , which can be computed at fixed h_0 and M by using Eq. (73) and the first of Eq. (75),

$$\alpha_s = 3\pi[h_0 - \sigma_V(\mu^2)]^{-1}. \quad (77)$$

From the above equation, α_s could be interpreted as the strong coupling constant defined at the renormalization scale $\mu = 4$ GeV. However, it must be kept in mind that the renormalization prescription we chose is fully arbitrary. Actually, if the Z function computed in the screened expansion is not well behaved, which is the case here as we have anticipated, then taking $Z(\mu^2) = 1$ as the starting point for measuring α_s could lead to meaningless values for the coupling constant. For the same reason, while, in principle, the lattice data for the Z function could be used to fit at least some of the parameters of the expansion, we instead fully rely on the lattice data for the quark mass function to perform the fit.

For completeness, we also report our results in terms of the renormalized mass M_R . As we saw in Sec. III A, the latter must be introduced as soon as diagram (2c) is included in the quark self-energy. This is due to the fact that, in the presence of said diagram, $\Sigma_S(p^2)$ contains a divergence proportional to $M_B Z_\psi$. Namely, for $N = 3$, in the minimalistic and vertex-wise schemes,⁵

$$\Sigma_S(p^2) = \frac{\alpha_s}{\pi} \left[\sigma_S(p^2) + M_B Z_\psi \frac{2}{\epsilon} \right]. \quad (78)$$

Since, when $M_R \ll M$, the finite part of diagram (2c) is negligible—see the discussion in Sec. III—the function $\sigma_S(p^2)$ in Eq. (78) can be taken to be very same as the one in Eq. (74).⁶ A renormalized mass M_R can then be defined by absorbing the mass divergence of diagram (2c) into M_B ,

$$M_R = M_B Z_\psi \left(1 + \frac{\alpha_s 2}{\pi \epsilon} \right). \quad (79)$$

With M_R as above, Eq. (76) still holds in the presence of diagram (2c), with the constant k_0 defined as

⁵For the complex-conjugate scheme see ahead, Sec. IV C.
⁶The same goes for Eq. (71); $\Sigma_V(p^2)$ is the same function both in the presence and in the absence of diagram (2c), with $\sigma_V(p^2)$ unchanged.

$$k_0 = \frac{\pi}{\alpha_s} M_R \quad (80)$$

and h_0 defined in the first of Eq. (75). Of course, whether we express our results in terms of M_B or of M_R has no quantitative impact on our fits, since these are performed using h_0 and k_0 , which as free parameters are more general than the masses and coupling themselves.

In the next sections, our focus is on quarks whose lattice masses $M_{\text{lat}} = 18, 36, 54, 72, 90$ MeV are small with respect to the QCD scale. Nonetheless, we also present some results for heavier quarks.

A. Minimalistic scheme

In the minimalistic resummation scheme, the loop diagrams included in the quark self-energy are those denoted by (2a), (2b), and, for the purpose of defining a renormalized mass M_R , (2c) in Fig. 4. The quark mass function $\mathcal{M}(p^2)$ can be expressed as

$$\mathcal{M}(p^2) = \frac{3[k_0 + \sigma_S^{(m)}(p^2)]}{h_0 - \sigma_V^{(m)}(p^2)}, \quad (81)$$

where the analytic expressions for the scalar functions $\sigma_S^{(m)}(p^2)$ and $\sigma_V^{(m)}(p^2)$ are reported in Appendix A. By

TABLE II. Fit parameters for the quark mass function $\mathcal{M}(p^2)$ in the minimalistic scheme. M_{lat}, M , and k_0 are expressed in MeV. The lattice data are taken from Ref. [73]. The asterisked row was obtained at fixed M_B , see Table III.

M_{lat}	M	h_0	k_0
18	368.6	2.132	-10.3
18*	318.1	1.791	6.0
36	330.8	1.967	14.1
54	320.0	2.073	38.1
72	330.7	2.341	62.4
90	336.9	2.504	88.6

TABLE III. Fit parameters for the quark mass function $\mathcal{M}(p^2)$ in the minimalistic scheme, in terms of α_s and M_B or M_R (renormalization scale: $\mu = 4$ GeV). M_{lat}, M, M_B , and M_R are expressed in MeV. The lattice data are taken from Ref. [73]. The asterisked row was obtained at fixed M_B .

M_{lat}	M	α_s	M_B	M_R
18	368.6	3.139	-14.4	-10.2
18*	318.1	3.542	10	6.7
36	330.8	3.322	21.5	14.9
54	320.0	3.202	55.2	38.9
72	330.7	2.935	79.9	58.3
90	336.9	2.793	106.1	78.8

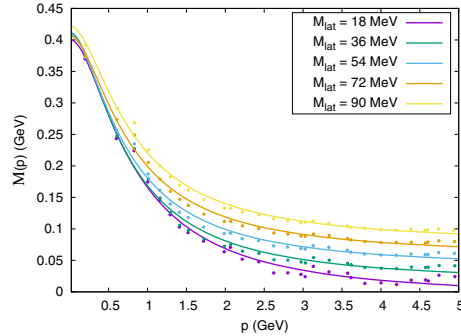


FIG. 7. Quark mass function $\mathcal{M}(p^2)$ in the Euclidean space and in the Landau gauge for different values of the lattice mass M_{lat} . Points: quenched lattice data from Ref. [73]. Curves: one-loop mass functions computed in the minimalistic resummation scheme using the parameters in Table II (equivalently, Table III).

fixing $m = 655.7$ MeV as discussed in Sec. III B and fitting the quenched lattice mass functions of Ref. [73] for the lattice masses $M_{\text{lat}} = 18, 36, 54, 72, 90$ MeV, we obtained the values of h_0 and k_0 reported in Table II. In Table III, we list the corresponding values of α_s , M_B , and M_R , computed by employing the definitions in Eqs. (73), (75), and (80).

As we can see from Fig. 7, the mass functions computed in the minimalistic scheme show a very good agreement with the lattice data. For all but one of the considered lattice masses—namely, $M_{\text{lat}} = 18$ MeV, which we discuss separately in a moment—the fitted values of the chiral mass M are found to be in the range 320–337 MeV, while the bare masses M_B are found to increase with M_{lat} , always keeping close to the latter.

The fact that $M_B \approx M_{\text{lat}}$ can be easily explained by looking at the high-momentum limit of the functions $\sigma_V^{(m)}(p^2)$ and $\sigma_S^{(m)}(p^2)$. For $p^2 \gg m^2, M^2$ we have

$$\begin{aligned} \sigma_V^{(m)}(p^2) &\rightarrow -1 - \frac{3m^2}{4p^2} + \frac{3m^2}{2p^2} \ln \frac{p^2}{m^2} \rightarrow -1, \\ \sigma_S^{(m)}(p^2) &\rightarrow \frac{2M^2}{p^2} \ln \frac{p^2}{M^2} \rightarrow 0. \end{aligned} \quad (82)$$

Therefore, in terms of M_B and α_s ,

$$\mathcal{M}(p^2) \rightarrow \frac{M_B Z_\psi}{Z_\psi + \frac{\alpha_s}{3\pi}} \approx M_B (p^2 \gg m^2, M^2), \quad (83)$$

where the approximation holds provided that the coupling is sufficiently small. The above equation shows that the scale of the high-momentum limit of the mass function is set by the bare mass M_B ; since on the lattice the same role is played by the lattice mass M_{lat} , we expect $M_B \approx M_{\text{lat}}$ as long as our function fits well the lattice data.

In the limit of vanishing momenta, regardless of the lattice mass, the data saturate to a finite value of about 350–450 MeV.⁷ The approximate independence of the saturation value from M_{lat} is expected on the basis that, in the infrared, the light quarks acquire most of their mass through the strong interactions, whose scale is much larger than the quark mass contained in the Lagrangian, and thus dominates over the latter. The mass function computed in the minimalistic scheme does reproduce this feature, provided that the chiral mass M is comparable in value for the lattice masses under consideration (as is the case in our fits).

In Table III, the value of the bare mass M_B fitted for $M_{\text{lat}} = 18$ MeV stands out for being negative (this is a direct consequence of $k_0 < 0$ in Table II). Presumably, this physically meaningless result is an artifact of the fit caused by the highly oscillatory tail of the $M_B = 18$ MeV lattice mass function; the oscillations themselves are most likely due to discretization errors, as suggested by the large error bars in the original data (see Ref. [73]). A constrained fit forcing $M_B \geq 0$ is not able to fix this issue, since, in the presence of the constraint, the fitting routine still tries to push M_B to negative values, which implies that the lower boundary of the fitting interval, namely, $M_B = 0$, is inevitably hit. Thus, no meaningful result for M_B is obtained by constraining the latter to be non-negative. Cutting the data at large momenta in order to avoid the oscillations (which begin at approximately 2.5–3 GeV), as well, would not improve the situation; since at low momenta the quark mass function is not very sensitive to the value of M_B (provided, of course, that we assume $M_B \ll M$), employing a cut dataset would make it impossible to meaningfully establish the value of the bare mass by a fit. As an alternative, to test our results, we checked that fixing the value of M_B by hand, instead of fitting it from the lattice data, still yields a mass function which—modulo oscillations—is in good agreement with the lattice. Some examples are shown in Fig. 8, where we plot the data for $M_{\text{lat}} = 18$ MeV together with our minimalistic scheme mass function. Here, M_B is set to 0, 10, 18 MeV, while the rest of the free parameters (reported in Table IV) are still obtained by fitting the data. Remarkably, as soon as the bare mass is fixed to small but positive values, the values of the parameters M and α_s obtained from the constrained fit get closer to those found for $M_{\text{lat}} = 36$ –90 MeV (Table III), further evidence that $M_B > 0$ is a more consistent choice when compared to the raw result of the fit.

Being in possession of analytic expressions which give a good description of the quark mass function in the Euclidean space, we are in a position to extend the quark propagator to the complexified Minkowski space and look for its poles p_0^2 . These are defined as the solutions to the equation

⁷Note that this value is larger for the heavy quarks, as we show later on in Fig. 10.

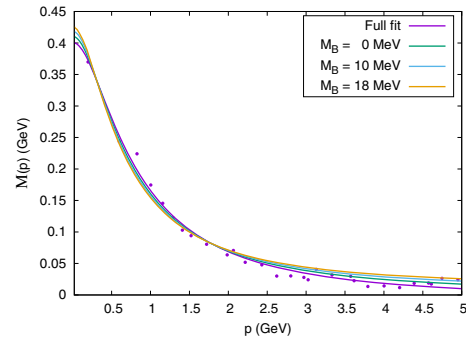


FIG. 8. $M_{\text{lat}} = 18$ MeV quark mass function in the Euclidean space and in the Landau gauge. Points: quenched lattice data from Ref. [73]. Curves: one-loop mass functions computed in the minimalistic resummation scheme. The parameters for the curves with $M_B = 0, 10, 18$ MeV are reported in Table IV; those for the curve labeled as “full fit” are reported in Table III.

$$p_0^2 - \mathcal{M}^2(p_0^2) = 0, \quad (84)$$

where the argument p^2 of the function $\mathcal{M}(p^2)$ is a complexified Minkowski momentum squared, at variance with the convention used in this section, where we used the Euclidean momentum. For all the considered lattice masses, using the parameters in Tables II and III, we found that the quark propagator has a pair of complex-conjugate poles in the variable p^2 (equivalently, two pairs in the variable $p = \sqrt{p^2}$); their positions p_0 are reported in Table V. In the literature, the existence of complex-conjugate poles has been interpreted as proof of confinement, since the imaginary part of the poles has the effect of removing the particles from the asymptotic states of the theory [55,60,71]. In the minimalistic scheme, the real part of the poles was found to be between 388 and 424 MeV, while their imaginary part is roughly half these values, having been found in the range from 174 to 194 MeV. Fixing $M_B = 10$ MeV by hand for the lattice mass $M_{\text{lat}} = 18$ MeV yields $p_0 = \pm 373.7 \pm 202.3i$ MeV, a result which is more consistent with those of the other lattice masses, when compared with the one obtained from the raw

TABLE IV. Fit parameters for the quark mass function $\mathcal{M}(p^2)$ in the minimalistic scheme, in terms of α_s and M_B or M_R (renormalization scale: $\mu = 4$ GeV), given $M_{\text{lat}} = 18$ MeV and M_B fixed to three different values. M_{lat} , M_B , M , and M_R are expressed in MeV. The lattice data are taken from Ref. [73].

M_{lat}	M_B	M	α_s	M_R
18	0	338.1	3.373	0.0
18	10	318.1	3.542	6.7
18	18	302.7	3.679	11.9

TABLE V. Poles p_0 of the quark propagator derived in the minimalistic scheme, using the parameters in Tables II and III. Both M_{lat} and p_0 are in MeV; the \pm signs in p_0 are independent from one another. The asterisked row was obtained at fixed M_B .

M_{lat}	p_0
18	$\pm 404.9 \pm 187.5i$
18*	$\pm 373.7 \pm 202.3i$
36	$\pm 388.0 \pm 194.2i$
54	$\pm 390.7 \pm 185.6i$
72	$\pm 407.7 \pm 174.9i$
90	$\pm 424.4 \pm 177.3i$

fit. Indeed, we note that $|\text{Re}(p_0)|$ increases with M_{lat} , while $|\text{Im}(p_0)|$ decreases with it. We checked that using small but positive values of M_B for $M_{\text{lat}} = 18$ MeV yields similar poles to those reported above.

In Fig. 9, we show an example of the Z function computed in the minimalistic scheme using the parameters in Table III, compared with the lattice data for a quark with mass $M_{\text{lat}} = 54$ MeV. As we can see, the behavior of $Z(p^2)$ is the complete opposite of that found on the lattice; while on the lattice the Z function increases with momentum, in the minimalistic scheme it decreases. This behavior is independent of the considered lattice mass, and we checked that it does not change if the parameters are fixed by fitting the Z function itself rather than the mass function. We believe that the mismatch with the lattice data may be due to the fact that, at least at sufficiently high energies, $Z(p^2) \approx 1$, making the Z function very sensitive to higher-order and even nonperturbative corrections. This is supported by the results we obtained in the complex-conjugate resummation scheme, which show an improved agreement at large momenta (see Sec. IV C) and by recent findings reported in Ref. [65], where the Z function is computed in

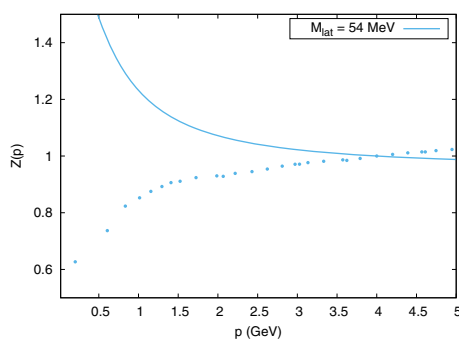


FIG. 9. Quark Z function $Z(p^2)$ in the Euclidean space and in the Landau gauge for $M_{\text{lat}} = 54$ MeV, renormalized at $\mu = 4$ GeV. Points: quenched lattice data from Ref. [73]. Curve: one-loop Z function computed in the minimalistic resummation scheme using the parameters in Table III.

the context of the Curci-Ferrari model and shown to change its behavior at two loops.

While up to this point our main focus has been on the light quarks, it may be interesting to see what happens if we try to apply the screened expansion to heavier quarks. Therefore, to end this section, we compare the minimalistic scheme mass function with the lattice data for quarks of mass $M_{\text{lat}} = 126, 181, 271$ MeV. The outcome is shown in Fig. 10; as in Fig. 7, the free parameters are fitted from the data themselves. It should be noted that when M_B becomes of the same order as M , as is the case in these fits, the approximation that we employed throughout this paper, namely, to neglect the finite part of diagram (2c) in Fig. 4, becomes less justifiable, and the diagram should be fully included in the quark self-energy. Nevertheless, it appears that the mass functions in the minimalistic scheme still manage to fit well the lattice data. As for the light quarks, the Z functions computed in the minimalistic scheme for the heavier quark do not match the lattice data and are thus not reported.

B. Vertex-wise scheme

In the vertex-wise resummation scheme, the loop diagrams included in the quark self-energy are those denoted by (2a), (2b), (2d), and, for defining a renormalized mass M_R , (2c) in Fig. 4. The quark mass function $\mathcal{M}(p^2)$ can be expressed as

$$\mathcal{M}(p^2) = \frac{3[k_0 + \sigma_S^{(v)}(p^2)]}{h_0 - \sigma_V^{(v)}(p^2)}, \quad (85)$$

where the analytic expressions for the scalar functions $\sigma_S^{(v)}(p^2)$ and $\sigma_V^{(v)}(p^2)$ are reported in Appendix A. As in Sec. IV A, we fixed $m = 655.7$ MeV and performed a fit to

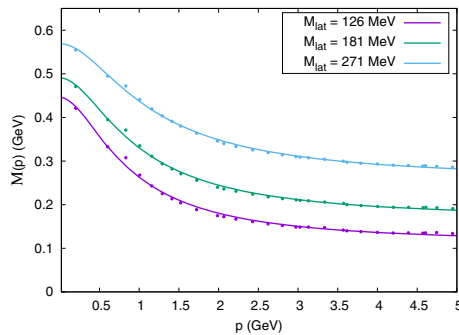


FIG. 10. Quark mass function $\mathcal{M}(p^2)$ in the Euclidean space and in the Landau gauge for larger lattice masses M_{lat} . Points: quenched lattice data from Ref. [73]. Curves: one-loop mass functions computed in the minimalistic resummation scheme. The chiral masses M are in the range 366–518 MeV, while the bare masses M_B are in the range 147–301 MeV.

TABLE VI. Fit parameters for the quark mass function $\mathcal{M}(p^2)$ in the vertex-wise scheme. M_{lat} , M , and k_0 are expressed in MeV. The lattice data are taken from Ref. [73]. The asterisked row was obtained at fixed M_B , see Table VII.

M_{lat}	M	h_0	k_0
18	268.0	2.656	-16.9
18*	197.6	2.051	6.8
36	228.7	2.418	11.5
54	221.4	2.577	40.0
72	238.4	2.977	70.1
90	249.0	3.207	102.5

the quenched lattice mass functions of Ref. [73] for the lattice masses $M_{\text{lat}} = 18, 36, 54, 72, 90$ MeV. The results of the fit are reported in Table VI, while in Table VII we list the corresponding values of α_s , M_B and M_R .

No significant change was found in the behavior of the mass and Z functions computed in the vertex-wise scheme when compared to the minimalistic scheme, the main difference between the two being the fitted values of the free parameters. For this reason, in what follows we keep the discussion to a minimum and limit ourselves to reporting our results. We refer to Sec. IVA for details.

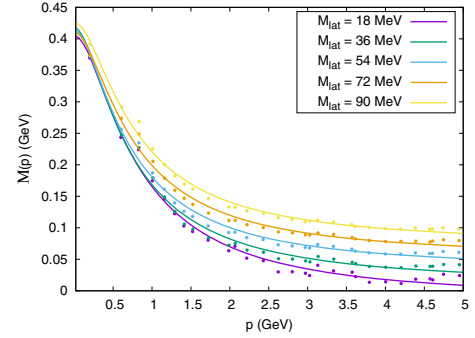
In Fig. 11, we show the mass function $\mathcal{M}(p^2)$ computed in the vertex-wise scheme together with the lattice data. As we can see, the mass functions have the same behavior as in the minimalistic scheme and fit very well the data. Like in the former scheme, the fitted values of the bare masses M_B are close to M_{lat} , as expected upon inspection of the high-momentum limit $p^2 \gg m^2, M^2$, which in the case of the vertex-wise scheme reads

$$\begin{aligned} \sigma_V^{(v)}(p^2) &\rightarrow -1 + \frac{3m^2}{2p^2} \rightarrow -1, \\ \sigma_S^{(v)}(p^2) &\rightarrow \frac{m^2}{p^2} \ln \frac{p^2}{m^2} + \frac{2M^2}{p^2} \ln \frac{p^2}{M^2} \rightarrow 0, \end{aligned} \quad (86)$$

again yielding

 TABLE VII. Fit parameters for the quark mass function $\mathcal{M}(p^2)$ in the vertex-wise scheme, in terms of α_s and M_B or M_R (renormalization scale: $\mu = 4$ GeV). M_{lat} , M , M_B , and M_R are expressed in MeV. The lattice data are taken from Ref. [73]. The asterisked row was obtained at fixed M_B .

M_{lat}	M	α_s	M_B	M_R
18	268.0	2.605	-19.1	-14.0
18*	197.6	3.128	10	6.8
36	228.7	2.788	14.3	10.2
54	221.4	2.663	46.6	33.9
72	238.4	2.393	70.7	53.4
90	249.0	2.261	95.9	73.8


 FIG. 11. Quark mass function $\mathcal{M}(p^2)$ in the Euclidean space and in the Landau gauge for different values of the lattice mass M_{lat} . Points: quenched lattice data from Ref. [73]. Curves: one-loop mass functions computed in the vertex-wise resummation scheme using the parameters in Table VI (equivalently, Table VII).

$$\mathcal{M}(p^2) \rightarrow \frac{M_B Z_\psi}{Z_\psi + \frac{\alpha_s}{3\pi}} \approx M_B(p^2 \gg m^2, M^2). \quad (87)$$

In the vertex-wise scheme, the fitted values of the chiral mass M turn out to be smaller than those reported in Sec. IVA, being found in the range 221–249 MeV. Together with the values of the coupling constant α_s , which are larger in the minimalistic scheme, this is by far the biggest difference between the two schemes.

Like in the minimalistic scheme, the bare mass M_B fitted from the lattice dataset $M_{\text{lat}} = 18$ MeV is negative. Again, as shown in Fig. 12, small but positive values of M_B yield a mass function which fits well the lattice data and whose parameters M , α_s , and M_R are closer to those extracted from the other fits (Table VII).

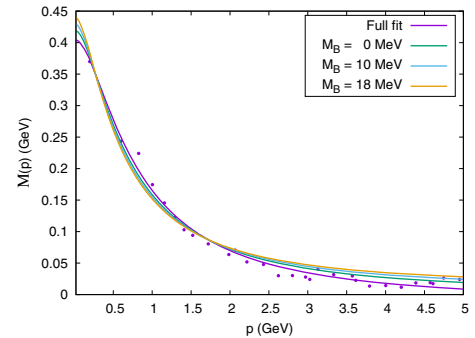

 FIG. 12. $M_{\text{lat}} = 18$ MeV quark mass function in the Euclidean space and in the Landau gauge. Points: quenched lattice data from Ref. [73]. Curves: one-loop mass functions computed in the vertex-wise resummation scheme. The parameters for the curves with $M_B = 0, 10, 18$ MeV are reported in Table VIII; those for the curve labelled as “full fit” are reported in Table VII.

TABLE VIII. Fit parameters for the quark mass function $\mathcal{M}(p^2)$ in the vertex-wise scheme, in terms of α_s and M_B or M_R (renormalization scale: $\mu = 4$ GeV), given $M_{\text{lat}} = 18$ MeV and M_B fixed to three different values. M_{lat} , M_B , M , and M_R are expressed in MeV. The lattice data are taken from Ref. [73].

M_{lat}	M_B	M	α_s	M_R
18	0	220.9	2.931	0.0
18	10	197.6	3.128	6.8
18	18	179.7	3.300	11.9

In Table IX, we report the position of the poles of the vertex-wise scheme quark propagator, obtained by using the parameters in Table VII. These have real parts in the range from 371 to 410 MeV and imaginary parts between 167 and 185 MeV, slightly less than their minimalistic scheme analogues. At variance with the minimalistic scheme, we found that $|\text{Im}(p_0)|$ is smaller for $M_{\text{lat}} = 72$ MeV than for $M_{\text{lat}} = 90$ MeV, the difference being of few MeVs. Given the generally decreasing behavior of $|\text{Im}(p_0)|$ with M_{lat} , we believe that this result maybe a glitch of the fit. Indeed, we checked that slightly changing the values of the free parameters for either of the two quark masses yields both a decreasing $|\text{Im}(p_0)|$ and mass functions which still fit well the lattice data. As for the $M_{\text{lat}} = 18$ MeV quark, if we fix M_B to 10 MeV like we did in Sec. IV A, the poles are found at $p_0 = \pm 349.2 \pm 193.1i$ MeV. Again, this result is consistent with the increasing (respectively, decreasing) behavior of $|\text{Re}(p_0)|$ (respectively, $|\text{Im}(p_0)|$) with M_{lat} , and choosing other small but positive values for M_B does not change the picture.

The Z function computed in the vertex-wise scheme, displayed in Fig. 13 for the lattice mass $M_{\text{lat}} = 54$ MeV, shows the same behavior as its minimalistic scheme counterpart, being a decreasing function of momentum. In particular, the change of scheme does not manage to solve the mismatch with the lattice data.

Finally, as in Sec. IV A, the mass functions obtained from a fit of the heavier quarks, $M_{\text{lat}} = 126, 181, 271$ MeV, see Fig. 14, are in good agreement with the lattice data, despite having neglected the finite part of diagram (2c) in Fig. 4.

TABLE IX. Poles p_0 of the quark propagator derived in the vertex-wise scheme, using the parameters in Tables VI–VII. Both M_{lat} and p_0 are in MeV; the \pm signs in p_0 are independent from one another. The asterisked row was obtained at fixed M_B .

M_{lat}	p_0
18	$\pm 387.4 \pm 180.9i$
18*	$\pm 349.2 \pm 193.1i$
36	$\pm 371.7 \pm 185.4i$
54	$\pm 375.2 \pm 177.2i$
72	$\pm 392.9 \pm 167.6i$
90	$\pm 410.8 \pm 170.2i$

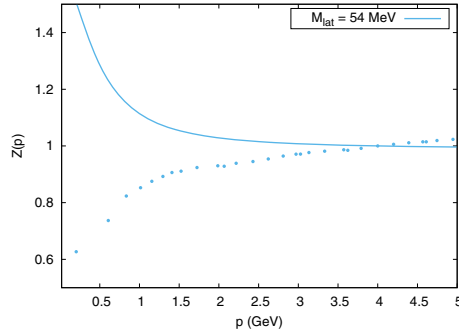


FIG. 13. Quark Z function $Z(p^2)$ in the Euclidean space and in the Landau gauge for $M_{\text{lat}} = 54$ MeV, renormalized at $\mu = 4$ GeV. Points: quenched lattice data from Ref. [73]. Curve: one-loop Z-function computed in the vertex-wise resummation scheme using the parameters in Table VII.

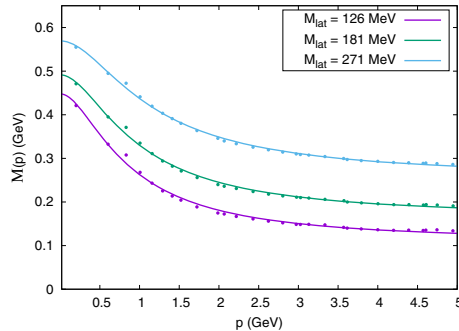


FIG. 14. Quark mass function $\mathcal{M}(p^2)$ in the Euclidean space and in the Landau gauge for larger lattice masses M_{lat} . Points: quenched lattice data from Ref. [73]. Curves: one-loop mass functions computed in the vertex-wise resummation scheme. The chiral masses M are in the range 288–472 MeV, while the bare masses M_B are in the range 136–290 MeV.

We conclude that, when used to compute the quark propagator in the Landau gauge, the minimalistic and vertex-wise resummation schemes are practically equivalent; albeit with different values of the free parameters, they both yield mass functions which are found to be in good agreement with the lattice, while not being able to reproduce the correct behavior of the lattice Z function. As we shall see in the following section, the complex-conjugate scheme offers a partial solution to the latter issue.

C. CC scheme

Before reporting the results of the fits in the complex-conjugate resummation scheme, let us address one final aspect of its definition. Recall that in the CC scheme the free gluon propagator (internal gluon line) $\Delta_{\mu\nu}^{(\text{c.c.})}(p)$ is defined modulo the absolute value of the residue R of the

corresponding dressed propagator at its poles. As discussed in Sec. III B, since to one loop $|R|$ is multiplied to the coupling constant α_s , a change in the former can be always compensated by a change in the latter. Therefore, fixing the value of $|R|$ actually amounts to choosing a definition for the coupling. In order to choose our conventions for R and α_s , let us inspect the divergences of the CC scheme. From Eq. (68) we know that, to one loop and in the Landau gauge, the only divergence that arises in the CC scheme comes from the scalar part of the quark self-energy and, in particular, from diagram (2c) in Fig. 6. Using Eq. (78), it is easy to show that in the presence of diagram (2c),

$$\Sigma_S^{(c.c.)}(p^2) = \frac{\alpha_s}{\pi} \left[\sigma_S^{(c.c.)}(p^2) + M_B Z_\psi (R + \bar{R}) \frac{2}{\epsilon} \right], \quad (88)$$

where $\Sigma_S^{(c.c.)}(p^2)$ is the scalar part of the loop self-energy in the CC scheme and

$$\sigma_S^{(c.c.)}(p^2) = R \sigma_S^{(m.)}(p^2)|_{m^2=p_0^2} + \bar{R} \sigma_S^{(m.)}(p^2)|_{m^2=\bar{p}_0^2}, \quad (89)$$

where $\sigma_S^{(m.)}(p^2)$ is the minimalistic scheme scalar function defined in Sec. IV A. As we can see, for general values of $R = |R|e^{i\theta}$, the divergence in $\Sigma_S^{(c.c.)}(p^2)$ is not the standard one-loop divergence of QCD; a factor of $(R + \bar{R}) = 2|R|\cos\theta$ appears in front of the ordinary result. This is not an inconsistency by itself. As explained in Sec. III B, the CC scheme is to be interpreted as a resummation of higher-order gluon polarization diagrams, so that the structure of its divergent part does not need to coincide with what we would expect from one-loop standard perturbation theory. Nonetheless, we can exploit the freedom in the choice of $|R|$ to make the scalar divergence look like a standard one-loop divergence. This can be achieved by setting

$$R + \bar{R} = 2|R|\cos\theta = 1. \quad (90)$$

With R normalized as such, we have that

$$\Delta_{\mu\nu}^{(c.c.)}(p) \rightarrow \frac{-it_{\mu\nu}(p)}{p^2} \quad (91)$$

in the UV ($p^2 \gg m^2$), as in standard perturbation theory. We remark that this choice is not dictated by any profound principle that needs to be satisfied in order for the scheme to be consistent. It must be interpreted as a convention by which we fix the value of the strong coupling constant α_s .

Having fully defined the CC scheme, let us now turn to the results of the fit. As in Secs. IV A and IV B, the quark mass function $\mathcal{M}(p^2)$ computed in the complex-conjugate scheme can be expressed as

$$\mathcal{M}(p^2) = \frac{3[k_0 + \sigma_S^{(c.c.)}(p^2)]}{h_0 - \sigma_V^{(c.c.)}(p^2)}, \quad (92)$$

where $\sigma_S^{(c.c.)}(p^2)$ is given by Eq. (89) and

$$\sigma_V^{(c.c.)}(p^2) = R \sigma_V^{(m.)}(p^2)|_{m^2=p_0^2} + \bar{R} \sigma_V^{(m.)}(p^2)|_{m^2=\bar{p}_0^2}, \quad (93)$$

where $\sigma_V^{(m.)}(p^2)$ has been defined in Sec. IV A. In order to fix the value of the free parameters k_0 and h_0 , we fitted the quenched lattice mass functions of Ref. [73] for the quark masses $M_{\text{lat}} = 18, 36, 54, 72, 90$ MeV, using $m = 655.7$ MeV as the gluon mass parameter. The results of the fit are reported in Tables X and XI.

In Fig. 15, we show the complex-conjugate scheme mass functions $\mathcal{M}(p^2)$ together with the lattice data. As in the minimalistic and vertex-wise schemes, our analytic functions are in very good agreement with the data. The chiral mass M is found in the range from 405 to 450 MeV, and the values of M_B increase with M_{lat} , having set $2|R|\cos\theta = 1$ makes Eqs. (82) and (83) hold also in the CC scheme. For the $M_{\text{lat}} = 18$ MeV quark, which by a raw fit, as in the previous schemes, is found to have negative bare mass, fixing M_B to small but positive values still results in a mass function which fits well the lattice data—see Table XII and Fig. 16.

TABLE X. Fit parameters for the quark mass function $\mathcal{M}(p^2)$ in the complex-conjugate scheme. M_{lat} , M , and k_0 are expressed in MeV. The lattice data are taken from Ref. [73]. The asterisked row was obtained at fixed M_B , see Tab. XI.

M_{lat}	M	h_0	k_0
18	449.9	6.294	-4.6
18*	405.9	5.467	18.2
36	406.6	5.701	49.0
54	405.2	6.166	108.0
72	431.9	7.216	176.3
90	449.8	7.801	248.3

TABLE XI. Fit parameters for the quark mass function $\mathcal{M}(p^2)$ in the complex-conjugate scheme, in terms of α_s and M_B or M_R (renormalization scale: $\mu = 4$ GeV). M_{lat} , M , M_B , and M_R are expressed in MeV. The lattice data are taken from Ref. [73]. The asterisked row was obtained at fixed M_B .

M_{lat}	M	α_s	M_B	M_R
18	449.9	1.252	-2.2	-1.8
18*	405.9	1.407	10	8.2
36	406.6	1.359	25.8	21.2
54	405.2	1.273	52.6	43.8
72	431.9	1.115	73.3	62.6
90	449.8	1.043	95.5	82.4

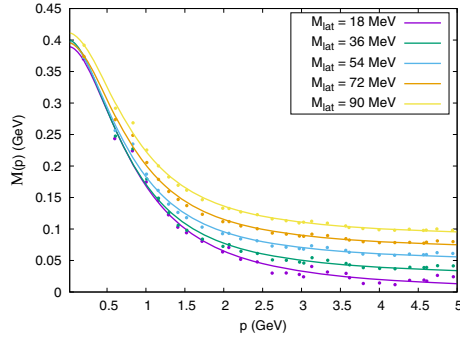


FIG. 15. Quark mass function $\mathcal{M}(p^2)$ in the Euclidean space and in the Landau gauge for different values of the lattice mass M_{lat} . Points: quenched lattice data from Ref. [73]. Curves: one-loop mass functions computed in the complex-conjugate resummation scheme using the parameters in Table X (equivalently, Table XI).

TABLE XII. Fit parameters for the quark mass function $\mathcal{M}(p^2)$ in the complex-conjugate scheme, in terms of α_s and M_B or M_R (renormalization scale: $\mu = 4$ GeV), given $M_{\text{lat}} = 18$ MeV and M_B fixed to three different values. M_{lat} , M_B , M , and M_R are expressed in MeV. The lattice data are taken from Ref. [73].

M_{lat}	M_B	M	α_s	M_R
18	0	441.6	1.279	0.0
18	10	405.9	1.407	8.2
18	18	379.5	1.519	14.4

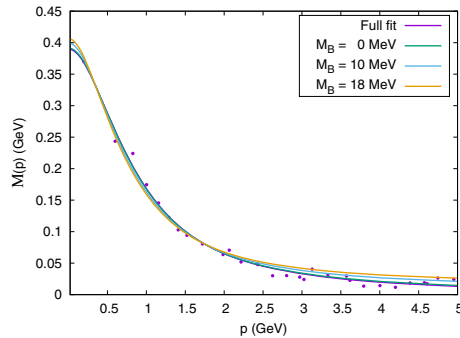


FIG. 16. $M_{\text{lat}} = 18$ MeV quark mass function in the Euclidean space and in the Landau gauge. Points: quenched lattice data from Ref. [73]. Curves: one-loop mass functions computed in the complex-conjugate resummation scheme. The parameters for the curves with $M_B = 0, 10, 18$ MeV are reported in Table XII; those for the curve labeled as “full fit” are reported in Table XI.

The CC quark propagator has a pair of complex-conjugate poles, whose positions are reported in Table XIII. With M_B fixed to example value of 10 MeV,

TABLE XIII. Poles p_0 of the quark propagator derived in the complex-conjugate scheme, using the parameters in Tables X and XI. Both M_{lat} and p_0 are in MeV; the \pm signs in p_0 are independent from one another. The asterisked row was obtained at fixed M_B .

M_{lat}	p_0
18	$\pm 448.8 \pm 167.9i$
18*	$\pm 423.8 \pm 186.0i$
36	$\pm 428.5 \pm 182.4i$
54	$\pm 434.2 \pm 172.5i$
72	$\pm 457.1 \pm 155.7i$
90	$\pm 477.7 \pm 157.6i$

$|\text{Re}(p_0)|$ is found in the range from 423 to 478 MeV, increasing with M_{lat} , while $|\text{Im}(p_0)|$ lies between 186 and 157 MeV, decreasing with it. The former are quite larger than those of the minimalistic and vertex-wise schemes, while the latter are somewhat smaller. In other words, the ratio $|\text{Im}(p_0)/\text{Re}(p_0)|$ tends to be smaller in the CC scheme in comparison to the other schemes.

Along with some differences in the fitted values of the free parameters and in the position of the quark poles, the mass functions computed in the CC scheme also show a small change in shape, when compared to their analogues in the minimalistic and vertex-wise schemes. This is displayed in Fig. 17, where we plot the mass functions obtained in the three schemes for the example value of $M_{\text{lat}} = 54$ MeV. As a result of the change, the CC scheme mass function is somewhat more suppressed in the $p \rightarrow 0$ limit. The effect, however, is very small and might not be meaningful.

The radical departure of the complex-conjugate scheme from the minimalistic and vertex-wise schemes concerns the Z function. In Fig. 18, we plot $Z(p^2)$ for the example

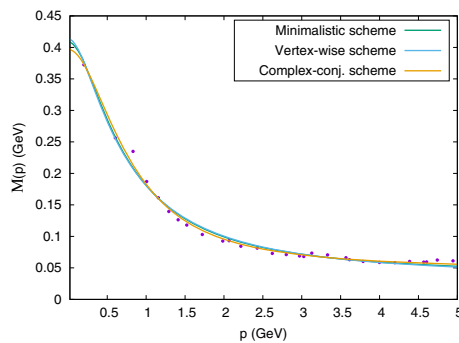


FIG. 17. Quark mass function $\mathcal{M}(p^2)$ in the Euclidean space and in the Landau gauge for $M_{\text{lat}} = 54$ MeV. Points: quenched lattice data from Ref. [73]. Curves: one-loop mass functions computed in the minimalistic, vertex-wise, and complex-conjugate resummation schemes.

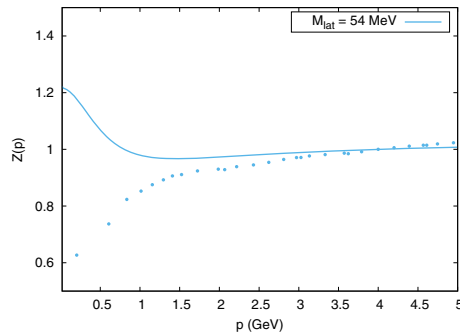


FIG. 18. Quark Z function $Z(p^2)$ in the Euclidean space and in the Landau gauge for $M_{\text{lat}} = 54$ MeV, renormalized at $\mu = 4$ GeV. Points: quenched lattice data from Ref. [73]. Curve: one-loop Z -function computed in the complex-conjugate resummation scheme using the parameters in Table XI.

value of $M_{\text{lat}} = 54$ MeV together with the lattice data. As we can see, at variance with the previous two schemes and consistent with the lattice, the CC scheme Z function increases with momentum for $p \gtrsim 1$ GeV. Moreover, above this cutoff value, our analytical expression is also in fair quantitative agreement with the lattice data.⁸ At low momenta, on the other hand, the agreement is lost, since $Z(p^2)$ changes behavior and starts to increase with decreasing p . This picture holds for any of the lattice masses considered in this section.

It appears that, at sufficiently large momenta, computing the quark Z function with the fully dressed gluon propagator (or, to be more precise, its CC scheme approximation) as the internal gluon line of the quark self-energy solves the mismatch between the screened expansion and the lattice data. As discussed in Sec. III B, this may be due to the dressed gluon propagator containing nonperturbative contributions (e.g., from the condensates, consistent with the OPE studies [74–76]) which a bare massive propagator does not.

To end this section, as we did in Secs. IV A and IV B, in Fig. 19 we compare the mass function with the lattice data for heavier quarks, $M_{\text{lat}} = 126, 181, 271$ MeV. We see that also in the CC scheme our analytic expressions fit well the data.

V. DISCUSSION

The present work was motivated by the ambitious aim of developing a reliable analytical approach to nonperturbative QCD from first principles. In this paper, important progresses have been made by the inclusion of quarks in the

⁸Observe that in Fig. 18 the Z -function is plotted on an enlarged scale: for $p > 1.0$ – 1.5 GeV the difference between the function computed in the CC scheme and the lattice data is at most around 10–20%.

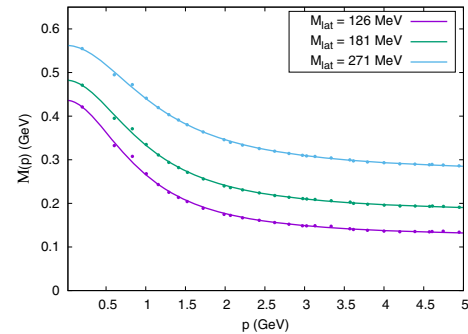


FIG. 19. Quark mass function $\mathcal{M}(p^2)$ in the Euclidean space and in the Landau gauge for larger lattice masses M_{lat} . Points: quenched lattice data from Ref. [73]. Curves: one-loop mass functions computed in the complex-conjugate resummation scheme. The chiral masses M are in the range 503–738 MeV, while the bare masses M_B are in the range 132–282 MeV.

successful framework of the screened expansion, which was first introduced for pure YM theory in [53,54]. Here, we have shown that, without any change to the gauge-fixed Faddeev-Popov Lagrangian, by a wise choice of the expansion point and by a reasonable setting of the scheme and parameters, perturbation theory gives a quantitative agreement with the available lattice data for the quark mass function—albeit in the quenched case until now. This constitutes an improvement over the results of a previous analysis, which led to an only qualitative description of the quark sector [58].

Because of the agreement which is reached with the lattice in the Euclidean space, we believe that the analytic properties of the mass function might be reliable in the whole complex plane up to moderately high energies. Thus, the explicit one-loop analytical expressions are not just good interpolation formulas, but they also unveil important analytic features of the propagators, like the existence of complex-conjugate poles, pointing to a confinement scenario which is rooted in those peculiar features which make quarks and gluons unobservable, yielding a dynamical mechanism for their exclusion from the asymptotic states.

While the existence of complex-conjugated poles might not be a direct proof of confinement [72], their existence would be ruled out if quarks were present in the asymptotic states. Actually, the usual Källén-Lehmann relations do not hold if there are complex poles, and the relative spectral densities do not satisfy the usual positivity conditions.

We must note that in Ref. [58]—which used the same formalism of the present paper, albeit in a different scheme, to study the chiral limit of QCD—the quark propagator was found to have a unique pole on the real axis. In that work, as we said, the agreement with the lattice data was only qualitative: the data themselves showed large error bars and fluctuations, so that any comparison with the analytic result could not be conclusive. Having attained a much better

match with the lattice now leads us to revisit our previous results.

Unfortunately, our main aim is far from being fully achieved yet, and, despite the good quantitative description of the quark mass function, many aspects must still be addressed. First of all, we must still find a way to fix from first principles the two spurious parameters which arise from the approximation, namely, an arbitrary additive constant which emerges from the renormalization of the one-loop quark self-energy and the ratio M/m between the quark and the gluon mass scales, which are arbitrary up to an overall choice for the energy units.

In pure YM theory, by enforcing some constraints of Becchi-Rouet-Stora-Tyutin (BRST) symmetry, like the Nielsen identities [68–70], the expansion can be optimized yielding a fully predictive method which does not require any external input and does not contain any spurious parameter [60]. In the quark sector, we still have to fix the spurious parameters by a fit of the available lattice data. While it is encouraging to see that an optimal choice of the parameters does exist which describes the quark mass function data very well for any given lattice mass, we still expect that the spurious parameters might be fixed by enforcing some constraints from first principles, like we did for pure YM theory.

Of course, if carried out by employing the Nielsen identities or similar exact methods, this program would require a fully consistent calculation for the interacting quark-gluon theory. In the present approach, we instead used the optimized parameters of pure YM theory and investigated the quark sector in a quenched approximation. Even at one loop, the existence of quarks modifies the gluon polarization by a quark loop which was not included in the gluon optimization. Thus, we expect that the removal of all spurious parameters by first principles like in [60] will require a fully consistent, unquenched calculation.

Another important issue is the truncation of the expansion, which, in the absence of a unique smallness parameter, like the coupling in ordinary perturbation theory, might appear quite arbitrary. In principle, the method allows us to carry out the calculations perturbatively, by adding higher-order corrections; however, in order to do so, a general criterion for the order-by-order truncation of the expansion is required. In this work, we have shown that the ambiguity can only arise for finite graphs, since the cancellation of spurious divergences requires a well defined set of graphs to be retained at each order. Moreover, at one loop, the residual ambiguity seems to be compensated by a change in the values of the spurious free parameters, with basically no residual effect on the quark propagator. Even in the complex plane, the pole position is quite robust, with only a few percent change when going from a truncation scheme to the other. In this respect, the weak dependence of the pole position on the resummation scheme can be regarded as an estimate of the accuracy of the method.

Despite the difficulties, the available data for light quarks remain the most important benchmark for our predictions, since the nonperturbative effects, like dynamical mass generation and chiral symmetry breaking, become less evident for heavier quarks. Nonetheless, we checked that the agreement with the data is very good even for lattice masses in the range 100–300 MeV.

A nonperturbative feature which is not captured by either the minimalistic or the vertex-wise scheme is the slightly increasing tail of the Z function shown by the lattice data. This behavior can be understood by the OPE, which predicts a powerlike behavior for $Z(p^2)$, with a coefficient proportional to the dimension-2 gluon condensate $\langle A^2 \rangle$ [77]. It is a pure nonperturbative effect which the present one-loop expansion fails to predict, unless some kind of resummation is performed; the same mismatch has been observed in other massive models, like the Curci-Ferrari model [45]. We note that, in the tail, the effects of the interactions on the lattice Z function are very small, so that $Z(p^2) \approx 1$. Thus, the observed deviations are not very relevant for the overall description of the quark propagator, which at moderately high energies is basically determined by the mass function alone. Actually, the one-loop contribution to $Z(p^2)$, too, is finite and very small, explaining why the Z function is so sensitive to higher-order corrections [65] and thermal effects [66]. In the context of the Curci-Ferrari model [65], it has been shown that the two-loop self-energy is enough to correct the behavior of the Z function over the whole momentum range.

On the other hand, the almost vanishing perturbative contributions make $Z(p^2)$ a very interesting benchmark for investigating nonperturbative effects and the role of the gluon condensate through the OPE at large energies. It is remarkable that, if the gluon line is resummed inside the one-loop quark self energy, replacing the free-gluon propagator with the dressed one-loop gluon line, an increasing Z function is found at large momenta, just where the OPE result should hold. Since the main feature of the nonperturbative resummation is the existence of complex-conjugated poles in the dressed gluon propagator, instead of the real pole of the undressed propagator, we argue that the complex gluon poles might be related with the existence of a nonvanishing gluon condensate [78].

Overall, we can say that, when optimized, the screened massive expansion provides a quantitative and analytical tool for investigating the infrared limit of the full QCD, at least in the quenched approximation. The results are very encouraging and suggest that in a fully consistent unquenched calculation, even the residual free parameters might be fixed by the general constraints of BRST symmetry, yielding a more complete analytical description of nonperturbative QCD from first principles.

ACKNOWLEDGMENTS

This research was supported in part by “Piano per la Ricerca di Ateneo—Linea di intervento 2” of the University of Catania.

APPENDIX A: QUARK SELF-ENERGY

In this Appendix, we report the relevant functions for the screened expansion’s quark propagator in the minimalistic and vertex-wise resummation schemes. As discussed in Sec. III B, the corresponding complex-conjugate scheme functions are easily derived from the minimalistic scheme; this is proven in Appendix B.

1. Diagrams (2a), (2b), and (2d)

In Euclidean space, the self-energy contribution $\Sigma^{(2a)}(p)$ due to the uncrossed quark loop, i.e., diagram (2a) in Fig. 4, can be divided into a vector and a scalar component, $\Sigma_V^{(2a)}(p^2)$ and $\Sigma_S^{(2a)}(p^2)$, as

$$\Sigma^{(2a)}(p) = i\not{p}\Sigma_V^{(2a)}(p^2) + \Sigma_S^{(2a)}(p^2). \quad (\text{A1})$$

The two components can be expressed in terms of two scalar functions $\sigma_V^{(2a)}(p^2)$ and $\sigma_S^{(2a)}(p^2)$ as

$$\begin{aligned} \Sigma_V^{(2a)}(p^2) &= \frac{\alpha_s}{3\pi} \sigma_V^{(2a)}(p^2), \\ \Sigma_S^{(2a)}(p^2) &= \frac{\alpha_s}{\pi} M \left\{ \frac{2}{\epsilon} - \ln \frac{M^2}{\bar{\mu}^2} + \sigma_S^{(2a)}(p^2) \right\}, \end{aligned} \quad (\text{A2})$$

where $\epsilon = 4 - d$ and $\bar{\mu}$ is an arbitrary scale introduced by dimensional regularization. If we define two adimensional variables s and x , representing the Euclidean momentum p^2 and the quark chiral mass M ,

$$s = p^2/m^2, \quad x = M^2/m^2, \quad (\text{A3})$$

then, the functions $\sigma_V^{(2a)}$ and $\sigma_S^{(2a)}$ can be put in the form

$$\begin{aligned} \sigma_V^{(2a)} &= C_R \ln R + C_x \ln x + C_{xs} \ln \frac{x}{x+s} + C_0, \\ \sigma_S^{(2a)} &= \frac{t}{s} \ln R - \frac{t-s-x+1}{2s} \ln x, \end{aligned} \quad (\text{A4})$$

where the coefficient functions C_R , C_x , C_{xs} , and C_0 read

$$\begin{aligned} C_R &= \frac{t}{2s^2} [(x+s)^2 + (x-s) - 2], \\ C_x &= -\frac{1}{2} C_R + \frac{1}{4s^2} [(x+s)^3 - 3(x-s) + 2], \\ C_{xs} &= -\frac{(x+s)^3}{2s^2}, \\ C_0 &= \frac{x-2}{2s} - \frac{1}{2}, \end{aligned} \quad (\text{A5})$$

while R is defined as

$$R = \frac{t-s+x-1}{t+s+x-1}. \quad (\text{A6})$$

In Eqs. (A4)–(A6), t is itself a function of s and x , defined as

$$t = \sqrt{(x+s)^2 + 2(s-x) + 1}. \quad (\text{A7})$$

The expressions reported above agree with those computed in the one-loop Curci-Ferrari model [45].

As discussed in Sec. III, diagrams (2b) and (2d) in Fig. 4 can be computed as derivatives of diagram (2a),

$$\begin{aligned} \Sigma^{(2b)}(p) &= -M \frac{\partial}{\partial M} \Sigma^{(2a)}(p), \\ \Sigma^{(2d)}(p) &= -m^2 \frac{\partial}{\partial m^2} \Sigma^{(2a)}(p). \end{aligned} \quad (\text{A8})$$

Once split into a vector and a scalar component,

$$\begin{aligned} \Sigma^{(2b)}(p) &= i\not{p}\Sigma_V^{(2b)}(p^2) + \Sigma_S^{(2b)}(p^2), \\ \Sigma^{(2d)}(p) &= i\not{p}\Sigma_V^{(2d)}(p^2) + \Sigma_S^{(2d)}(p^2), \end{aligned} \quad (\text{A9})$$

$\Sigma^{(2b)}(p)$ and $\Sigma^{(2d)}(p)$ can be expressed in terms of four scalar functions, $\sigma_{V,S}^{(2b)}(p^2)$ and $\sigma_{V,S}^{(2d)}(p^2)$,

$$\begin{aligned} \Sigma_V^{(2b)}(p) &= \frac{\alpha_s}{3\pi} \sigma_V^{(2b)}(p^2), \\ \Sigma_S^{(2b)}(p) &= \frac{\alpha_s}{\pi} M \left\{ -\frac{2}{\epsilon} + \ln \frac{M^2}{\bar{\mu}^2} + \sigma_S^{(2b)}(p^2) \right\}, \\ \Sigma_V^{(2d)}(p) &= \frac{\alpha_s}{3\pi} \sigma_V^{(2d)}(p^2), \\ \Sigma_S^{(2d)}(p) &= \frac{\alpha_s}{\pi} M \sigma_S^{(2d)}(p^2). \end{aligned} \quad (\text{A10})$$

Using Eqs. (A8) and (A2), it is easy to compute these functions as derivatives of $\sigma_V^{(2a)}$ and $\sigma_S^{(2a)}$; for diagram (2b), we have

$$\begin{aligned}\sigma_V^{(2b)} &= -M \frac{\partial}{\partial M} \sigma_V^{(2a)}, \\ \sigma_S^{(2b)} &= -\frac{\partial}{\partial M} [M \sigma_S^{(2a)}] + 2 \\ &= -\sigma_S^{(2a)} - M \frac{\partial}{\partial M} \sigma_S^{(2a)} + 2,\end{aligned}\quad (\text{A11})$$

whereas for diagram (2d)

$$\begin{aligned}\sigma_V^{(2d)} &= -m^2 \frac{\partial}{\partial m^2} \sigma_V^{(2a)}, \\ \sigma_S^{(2d)} &= -m^2 \frac{\partial}{\partial m^2} \sigma_S^{(2a)}.\end{aligned}\quad (\text{A12})$$

Note that the 2 on the right-hand side of $\sigma_S^{(2b)}$ comes from the derivative of $\ln M^2$ inside the brackets in Eq. (A2).

In what follows, we report the explicit self-energy functions computed in the minimalistic and vertex-wise resummation schemes.

2. Self-energy in the minimalistic and vertex-wise resummation schemes

Recall that in the minimalistic scheme we only keep the self-energy diagrams (2a) and (2b), whereas in the vertex-wise scheme we also include diagram (2d). Let us start from the first one.

In the minimalistic scheme, the loop contribution $\Sigma^{(m)}(p)$ to the quark self-energy is given by

$$\Sigma^{(m)}(p) = \Sigma^{(2a)}(p) + \Sigma^{(2b)}(p).\quad (\text{A13})$$

If we split $\Sigma^{(m)}(p)$ into a vector and a scalar component,

$$\Sigma^{(m)}(p) = i\not{p}\Sigma_V^{(m)}(p^2) + \Sigma_S^{(m)}(p^2),\quad (\text{A14})$$

then, $\Sigma_V^{(m)}(p^2)$ and $\Sigma_S^{(m)}(p^2)$ can be expressed in terms of two scalar functions $\sigma_V^{(m)}(p^2)$ and $\sigma_S^{(m)}(p^2)$, as

$$\begin{aligned}\Sigma_V^{(m)}(p^2) &= \frac{\alpha_s}{3\pi} \sigma_V^{(m)}(p^2), \\ \Sigma_S^{(m)}(p^2) &= \frac{\alpha_s}{\pi} M \sigma_S^{(m)}(p^2).\end{aligned}\quad (\text{A15})$$

Here,

$$\begin{aligned}\sigma_V^{(m)} &= \sigma_V^{(2a)} + \sigma_V^{(2b)}, \\ \sigma_S^{(m)} &= \sigma_S^{(2a)} + \sigma_S^{(2b)}.\end{aligned}\quad (\text{A16})$$

Going back to Eq. (A11), the derivatives with respect to M can be traded with derivatives with respect to $x = M^2/m^2$,

$$M \frac{\partial}{\partial M} = 2x \frac{\partial}{\partial x}.\quad (\text{A17})$$

Then, $\sigma_{V,S}^{(2b)}$ can be expressed as the following derivatives of $\sigma_{V,S}^{(2a)}$:

$$\begin{aligned}\sigma_V^{(m)} &= \left(1 - 2x \frac{\partial}{\partial x}\right) \sigma_V^{(2a)}, \\ \sigma_S^{(m)} &= -2x \frac{\partial}{\partial x} \sigma_S^{(2a)} + 2.\end{aligned}\quad (\text{A18})$$

A straightforward albeit tedious calculation leads to the result

$$\begin{aligned}\sigma_V^{(m)} &= C_R^{(m)} \ln R + C_x^{(m)} \ln x + C_{xs}^{(m)} \ln \frac{x}{x+s} + C_0^{(m)}, \\ \sigma_S^{(m)} &= -\frac{2x(x+s-1)}{st} \ln R - \frac{x(t-x-s+1)}{st} \ln x,\end{aligned}\quad (\text{A19})$$

where the coefficient functions $C_R^{(m)}$, $C_x^{(m)}$, $C_{xs}^{(m)}$, and $C_0^{(m)}$ read

$$\begin{aligned}C_R^{(m)} &= \frac{1}{2s^2t} \{(s-5x)[(s+x)^3 + (s^2-x^2)] - 3(s^2-x^2) \\ &\quad - 4sx - 5s - x - 2\}, \\ C_x^{(m)} &= -\frac{1}{2} C_R^{(m)} + \frac{1}{4s^2} [(s-5x)(x+s)^2 + 3(x+s) + 2], \\ C_{xs}^{(m)} &= -\frac{(x+s)^2}{2s^2} (s-5x), \\ C_0^{(m)} &= -\frac{5x+2}{2s} - \frac{1}{2}.\end{aligned}\quad (\text{A20})$$

Similarly, in the vertex-wise scheme, by including diagram (2d) to obtain the loop contribution $\Sigma^{(v)}(p)$ to the self-energy,

$$\Sigma^{(v)}(p) = \Sigma^{(2a)}(p) + \Sigma^{(2b)}(p) + \Sigma^{(2d)}(p),\quad (\text{A21})$$

we can write

$$\Sigma^{(v)}(p) = i\not{p}\Sigma_V^{(v)}(p^2) + \Sigma_S^{(v)}(p^2),\quad (\text{A22})$$

and express $\Sigma_V^{(v)}(p^2)$ and $\Sigma_S^{(v)}(p^2)$ in terms of two scalar functions $\sigma_V^{(v)}(p^2)$ and $\sigma_S^{(v)}(p^2)$,

$$\begin{aligned}\Sigma_V^{(v)}(p^2) &= \frac{\alpha_s}{3\pi} \sigma_V^{(v)}(p^2), \\ \Sigma_S^{(v)}(p^2) &= \frac{\alpha_s}{\pi} M \sigma_S^{(v)}(p^2).\end{aligned}\quad (\text{A23})$$

Clearly,

$$\begin{aligned}\sigma_V^{(v)} &= \sigma_V^{(2a)} + \sigma_V^{(2b)} + \sigma_V^{(2d)}, \\ \sigma_S^{(v)} &= \sigma_S^{(2a)} + \sigma_S^{(2b)} + \sigma_S^{(2d)}.\end{aligned}\quad (\text{A24})$$

Using the previous results for $\sigma_{V,S}^{(2b)}$, together with Eq. (A12) and

$$m^2 \frac{\partial}{\partial m^2} = -s \frac{\partial}{\partial s} - x \frac{\partial}{\partial x}, \quad (\text{A25})$$

it is easy to show that the scalar functions $\sigma_{V,S}^{(v)}$ can be computed as the following derivatives of $\sigma_{V,S}^{(2a)}$:

$$\begin{aligned} \sigma_V^{(v)} &= \left(1 - x \frac{\partial}{\partial x} + s \frac{\partial}{\partial s}\right) \sigma_V^{(2a)}, \\ \sigma_S^{(v)} &= \left(-x \frac{\partial}{\partial x} + s \frac{\partial}{\partial s}\right) \sigma_S^{(2a)} + 2. \end{aligned} \quad (\text{A26})$$

A lengthy calculation yields [58]

$$\begin{aligned} \sigma_V^{(v)} &= C_R^{(v)} \ln R + C_x^{(v)} \ln x + C_{xs}^{(v)} \ln \frac{x}{x+s} + C_0^{(v)}, \\ \sigma_S^{(v)} &= -\frac{s(2x+1) + (2x-1)(x-1)}{st} \ln \frac{R}{\sqrt{x}} + \frac{1-2x}{2s} \ln x, \end{aligned} \quad (\text{A27})$$

where the coefficient functions $C_R^{(v)}$, $C_x^{(v)}$, $C_{xs}^{(v)}$, and $C_0^{(v)}$ read

$$\begin{aligned} C_R^{(v)} &= \frac{1}{s^2 t} \{(s-2x)[(x+s)^3 + (s^2-x^2)] \\ &\quad + (s-x+1)(1-3x) + 2sx\}, \\ C_x^{(v)} &= -\frac{1}{2} C_R^{(v)} + \frac{1}{2s^2} [(x+s)^2(s-2x) + 3x-1], \\ C_{xs}^{(v)} &= -\frac{(s-2x)(x+s)^2}{s^2}, \\ C_0^{(v)} &= \frac{1-2x}{s}. \end{aligned} \quad (\text{A28})$$

APPENDIX B: LOOP INTEGRALS IN THE CC SCHEME

The complex-conjugate (CC) scheme for the quenched one-loop quark propagator is defined by the internal gluon lines in Fig. 6 being set equal to the principal part of the fully dressed gluon propagator; in Euclidean space,

$$\Delta_{\mu\nu}^{(c.c.)}(p) = \left\{ \frac{R}{p^2 + p_0^2} + \frac{\bar{R}}{p^2 + \bar{p}_0^2} \right\} \epsilon_{\mu\nu}(p), \quad (\text{B1})$$

where the values of p_0^2 , R , and of their complex conjugates \bar{p}_0^2 and \bar{R} are derived in the framework of the screened

expansion of pure Yang-Mills theory⁹ (see Sec. III B and Table I in Sec. II B).

The loop diagrams (2a) to (2c) in Fig. 6 can be computed by employing the usual machinery of Feynman parameter integrals and gamma functions. In order to see this, first note that the Feynman parameter formula

$$\frac{1}{AB} = \int_0^1 dx \frac{1}{[xA + (1-x)B]^2} \quad (\text{B2})$$

remains valid for complex A and B . As a consequence, in Euclidean space, all the loop integrals can be expressed in terms of double integrals \mathcal{I} of the form

$$\mathcal{I} = \int_0^1 dx \int \frac{d^d q}{(2\pi)^d} \frac{(q^2)^n}{(q^2 + \Delta)^2}, \quad (\text{B3})$$

where n is equal to either 0 or 1. In the above equation, at variance with the standard case,

$$\Delta = xp_0^2 + (1-x)M^2 + x(1-x)p^2 \quad (\text{B4})$$

is a complex, nonreal quantity due to p_0^2 itself being complex with $\text{Im}(p_0^2) \neq 0$ (here, we are assuming that the external momentum $p^2 \in \mathbb{R}$). The angular integration in Eq. (B3) can be readily performed, yielding

$$\begin{aligned} \mathcal{I} &= \frac{\Omega_{d-1}}{(2\pi)^d} \int_0^1 dx \int_0^{+\infty} dq q^{d-1} \frac{(q^2)^n}{(q^2 + \Delta)^2} \\ &= \frac{\Omega_{d-1}}{2(2\pi)^d} \int_0^1 dx \int_0^{+\infty} dy \frac{y^{d/2-1+n}}{(y + \Delta)^2}, \end{aligned} \quad (\text{B5})$$

where Ω_{d-1} is the volume of the $(d-1)$ -dimensional unit sphere, and on the last line, we have changed the variable of integration to $y = q^2$. The integrand in Eq. (B5) has a complex pole outside of the domain of integration, i.e., the positive real axis, at $y = -\Delta$. The integral over the y variable can be expressed as the limit

$$\int_0^{+\infty} dy \frac{y^{d/2-1+n}}{(y + \Delta)^2} = \lim_{\Lambda \rightarrow +\infty} \int_0^\Lambda dy \frac{y^{d/2-1+n}}{(y + \Delta)^2}. \quad (\text{B6})$$

We can now change the contour of integration of the definite integral on the right-hand side by setting

⁹The value of $|R|$ is actually inessential in our calculation, see Sec. III B.

$$\int_0^\Lambda dy \frac{y^{d/2-1+n}}{(y+\Delta)^2} = \oint_\gamma dy \frac{y^{d/2-1+n}}{(y+\Delta)^2} + \int_{\gamma_2} dy \frac{y^{d/2-1+n}}{(y+\Delta)^2} - \int_{\gamma_\Lambda} dy \frac{y^{d/2-1+n}}{(y+\Delta)^2}, \quad (\text{B7})$$

where $\gamma = \gamma_1 + \gamma_\Lambda + \gamma_2$ and the contours γ_1, γ_Λ , and γ_2 are displayed in Fig. 20. In particular, γ_2 is chosen so that $y \in \gamma_2$ is opposite to $-\Delta$ with respect to the origin of the complex plane. Since the integral over the closed contour γ in Eq. (B7) is zero by analyticity, we have

$$\int_0^{+\infty} dy \frac{y^{d/2-1+n}}{(y+\Delta)^2} = \lim_{\Lambda \rightarrow +\infty} \int_{-\gamma_2} dy \frac{y^{d/2-1+n}}{(y+\Delta)^2}, \quad (\text{B8})$$

where the integral over γ_Λ drops out in the limit $\Lambda \rightarrow +\infty$.¹⁰ Moreover, by construction, the argument of $y \in -\gamma_2$ satisfies $\arg(y) = \arg(\Delta)$. Therefore, we can write

$$\int_0^{+\infty} dy \frac{y^{d/2-1+n}}{(y+\Delta)^2} = (e^{i\arg(\Delta)})^{d/2-2+n} \int_0^{+\infty} dy \frac{y^{d/2-1+n}}{(y+|\Delta|)^2}. \quad (\text{B9})$$

One last change of integration variables from y to $y/|\Delta|$ leaves us with

$$\int_0^{+\infty} dy \frac{y^{d/2-1+n}}{(y+\Delta)^2} = (|\Delta|e^{i\arg(\Delta)})^{d/2-2+n} \int_0^{+\infty} dy \frac{y^{d/2-1+n}}{(y+1)^2} = \Delta^{d/2-2+n} \Gamma(d/2+n) \Gamma(2-d/2-n). \quad (\text{B10})$$

¹⁰Keep in mind that, in dimensional regularization, all the integrals are assumed to converge before the limit $d \rightarrow 4$ is taken. As a consequence, integrals at infinity such as the one over γ_Λ in Eq. (B7) can be safely set to zero.

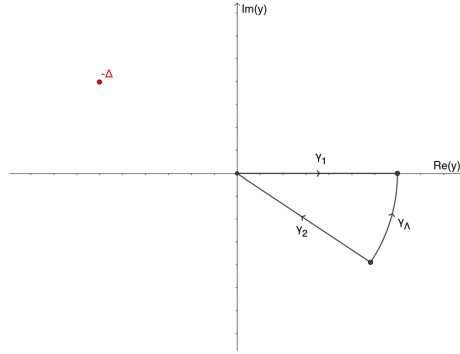


FIG. 20. Contour for the loop integrals in the CC scheme. γ_2 is chosen so that $y \in \gamma_2$ is opposite to the pole $-\Delta$ with respect to the origin of the complex plane, hence $\arg(y) = \arg(\Delta)$.

The latter is the very same result found for $\Delta \in \mathbb{R}$. Hence the integral \mathcal{I} can be computed as if Δ were a real number or, equivalently, as if p_0^2 were real.

Finally, since the diagrams for the CC scheme (Fig. 6) are identical to those of the minimalistic scheme [Fig. 4, diagrams (2a) to (2c)] except for the fact that the internal gluon propagator is made up of two terms, each multiplied by a factor of R or \bar{R} , by considering each of these two terms separately we find that


$$\Sigma_{\text{c.c.}}^{(\text{loops})}(p) = R \Sigma_{\text{m.}}^{(\text{loops})}(p)|_{m^2=p_0^2} + \bar{R} \Sigma_{\text{m.}}^{(\text{loops})}(p)|_{m^2=\bar{p}_0^2}, \quad (\text{B11})$$

where $\Sigma_{\text{c.c.}}^{(\text{loops})}(p)$ and $\Sigma_{\text{m.}}^{(\text{loops})}(p)$ are the loop contributions to the 1PI quark self-energies computed, respectively, in the CC scheme and in the minimalistic scheme, and m^2 is the gluon mass parameter introduced by the screened expansion.

- [1] P. A. Zyla *et al.* (Particle Data Group), *Prog. Theor. Exp. Phys.* **2020**, 083C01 (2020).
 [2] J. M. Cornwall, *Phys. Rev. D* **26**, 1453 (1982).
 [3] A. Sternbeck, L. von Smekal, D. B. Leinweber, and A. G. Williams, *Proc. Sci., LAT2007* (**2007**) 340.
 [4] O. Oliveira and P. Bicudo, *J. Phys. G* **38**, 045003 (2011).
 [5] A. Cucchieri and T. Mendes, *Proc. Sci., LAT2007* (**2007**) 297.
 [6] A. Cucchieri and T. Mendes, *Phys. Rev. D* **78**, 094503 (2008).
 [7] A. Cucchieri and T. Mendes, *Phys. Rev. Lett.* **100**, 241601 (2008).

- [8] A. Cucchieri and T. Mendes, *Proc. Sci., QCD-TNT09* (**2009**) 026.
 [9] I. L. Bogolubsky, E. M. Ilgenfritz, M. Muller-Preussker, and A. Sternbeck, *Phys. Lett. B* **676**, 69 (2009).
 [10] O. Oliveira and P. Silva, *Proc. Sci., LAT2009* (**2009**) 226.
 [11] D. Dudal, O. Oliveira, and N. Vandersickel, *Phys. Rev. D* **81**, 074505 (2010).
 [12] A. Ayala, A. Bashir, D. Binosi, M. Cristoforetti, and J. Rodríguez-Quintero, *Phys. Rev. D* **86**, 074512 (2012).
 [13] O. Oliveira and P. J. Silva, *Phys. Rev. D* **86**, 114513 (2012).
 [14] G. Burgio, M. Quandt, H. Reinhardt, and H. Vogt, *Phys. Rev. D* **92**, 034518 (2015).

- [15] A. G. Duarte, O. Oliveira, and P. J. Silva, *Phys. Rev. D* **94**, 014502 (2016).
- [16] A. C. Aguilar, D. Binosi, and J. Papavassiliou, *Phys. Rev. D* **78**, 025010 (2008).
- [17] A. C. Aguilar and J. Papavassiliou, *Phys. Rev. D* **81**, 034003 (2010).
- [18] A. C. Aguilar, D. Binosi, and J. Papavassiliou, *Phys. Rev. D* **89**, 085032 (2014).
- [19] A. C. Aguilar, D. Binosi, D. Ibáñez, and J. Papavassiliou, *Phys. Rev. D* **89**, 085008 (2014).
- [20] A. C. Aguilar, D. Binosi, and J. Papavassiliou, *Phys. Rev. D* **91**, 085014 (2015).
- [21] D. Binosi, L. Chang, J. Papavassiliou, and C. D. Roberts, *Phys. Lett. B* **742**, 183 (2015).
- [22] A. L. Blum, M. Q. Huber, M. Mitter, and L. von Smekal, *Phys. Rev. D* **89**, 061703(R) (2014).
- [23] M. Q. Huber, *Phys. Rev. D* **91**, 085018 (2015).
- [24] A. K. Cyrol, M. Q. Huber, and L. von Smekal, *Eur. Phys. J. C* **75**, 102 (2015).
- [25] M. Q. Huber, *Phys. Rev. D* **101**, 114009 (2020).
- [26] M. Mitter, J. M. Pawłowski, and N. Strodthoff, *Phys. Rev. D* **91**, 054035 (2015).
- [27] A. K. Cyrol, L. Fister, M. Mitter, J. M. Pawłowski, and N. Strodthoff, *Phys. Rev. D* **94**, 054005 (2016).
- [28] A. K. Cyrol, M. Mitter, J. M. Pawłowski, and N. Strodthoff, *Phys. Rev. D* **97**, 054006 (2018).
- [29] C. Feuchter and H. Reinhardt, *Phys. Rev. D* **70**, 105021 (2004).
- [30] H. Reinhardt and C. Feuchter, *Phys. Rev. D* **71**, 105002 (2005).
- [31] D. Epple, H. Reinhardt, W. Schleifenbaum, and A. P. Szczepaniak, *Phys. Rev. D* **77**, 085007 (2008).
- [32] M. Quandt, H. Reinhardt, and J. Heffner, *Phys. Rev. D* **89**, 065037 (2014).
- [33] F. Siringo and L. Marotta, *Eur. Phys. J. C* **44**, 293 (2005).
- [34] F. Siringo, *Mod. Phys. Lett. A* **29**, 1450026 (2014).
- [35] F. Siringo, *Phys. Rev. D* **88**, 056020 (2013).
- [36] F. Siringo, *Phys. Rev. D* **89**, 025005 (2014).
- [37] F. Siringo, *Phys. Rev. D* **90**, 094021 (2014).
- [38] F. Siringo, *Phys. Rev. D* **92**, 074034 (2015).
- [39] F. Siringo, arXiv:1507.05543.
- [40] D. Zwanziger, *Nucl. Phys.* **B323**, 513 (1989).
- [41] X. Li and C. M. Shakin, *Phys. Rev. D* **71**, 074007 (2005).
- [42] L. Baulieu, D. Dudal, M. S. Guimaraes, M. Q. Huber, S. P. Sorella, N. Vandersickel, and D. Zwanziger, *Phys. Rev. D* **82**, 025021 (2010).
- [43] M. Tissier and N. Wschebor, *Phys. Rev. D* **82**, 101701(R) (2010).
- [44] M. Tissier and N. Wschebor, *Phys. Rev. D* **84**, 045018 (2011).
- [45] M. Pelaez, M. Tissier, and N. Wschebor, *Phys. Rev. D* **90**, 065031 (2014).
- [46] M. A. L. Capri, A. D. Pereira, R. F. Sobreiro, and S. P. Sorella, *Eur. Phys. J. C* **75**, 479 (2015).
- [47] M. A. L. Capri, D. Fiorentini, M. S. Guimaraes, B. W. Mintz, L. F. Palhares, S. P. Sorella, D. Dudal, I. F. Justo, A. D. Pereira, and R. F. Sobreiro, *Phys. Rev. D* **92**, 045039 (2015).
- [48] D. Dudal, J. A. Gracey, S. P. Sorella, N. Vandersickel, and H. Verschelde, *Phys. Rev. D* **78**, 065047 (2008).
- [49] D. Dudal, S. P. Sorella, N. Vandersickel, and H. Verschelde, *Phys. Rev. D* **77**, 071501(R) (2008).
- [50] D. Dudal, S. P. Sorella, and N. Vandersickel, *Phys. Rev. D* **84**, 065039 (2011).
- [51] F. A. Machado, arXiv:1601.02067.
- [52] M. Q. Huber, *Phys. Rep.* **879**, 1 (2020).
- [53] F. Siringo, arXiv:1509.05891.
- [54] F. Siringo, *Nucl. Phys.* **B907**, 572 (2016).
- [55] F. Siringo, *Phys. Rev. D* **96**, 114020 (2017).
- [56] G. Comitini and F. Siringo, *Phys. Rev. D* **97**, 056013 (2018).
- [57] F. Siringo and G. Comitini, *Phys. Rev. D* **103**, 074014 (2021).
- [58] F. Siringo, *Phys. Rev. D* **94**, 114036 (2016).
- [59] F. Siringo, *EPJ Web Conf.* **137**, 13016 (2017).
- [60] F. Siringo and G. Comitini, *Phys. Rev. D* **98**, 034023 (2018).
- [61] F. Siringo, *Phys. Rev. D* **99**, 094024 (2019).
- [62] F. Siringo, *Phys. Rev. D* **100**, 074014 (2019).
- [63] G. Comitini and F. Siringo, *Phys. Rev. D* **102**, 094002 (2020).
- [64] G. Comitini, arXiv:1910.13022.
- [65] N. Barrios, J. A. Gracey, M. Peláez, and U. Reinosa, arXiv:2103.16218.
- [66] O. Oliveira and P. J. Silva, *Eur. Phys. J. C* **79**, 793 (2019).
- [67] F. Siringo, *Phys. Rev. D* **86**, 076016 (2012).
- [68] N. K. Nielsen, *Nucl. Phys.* **B97**, 527 (1975); **B101**, 173 (1975).
- [69] R. Kobes, G. Kunstatter, and A. Rebhan, *Phys. Rev. Lett.* **64**, 2992 (1990).
- [70] J. C. Breckenridge, M. J. Lavelle, and T. G. Steele, *Z. Phys. C* **65**, 155 (1995).
- [71] M. Stingl, *Z. Phys. A* **353**, 423 (1996).
- [72] Y. Hayashi and K.-I. Kondo, *Phys. Rev. D* **103**, L111504 (2021).
- [73] W. Kamleh, P. O. Bowman, D. B. Leinweber, A. G. Williams, and J. Zhang, *Phys. Rev. D* **71**, 094507 (2005).
- [74] E. R. Arriola, P. O. Bowman, and W. Broniowski, *Phys. Rev. D* **70**, 097505 (2004).
- [75] B. Blossier, P. Boucaud, M. Brinet, F. De Soto, Z. Liu, V. Morenas, O. Pène, K. Petrov, and J. Rodríguez-Quintero, *Phys. Rev. D* **83**, 074506 (2011).
- [76] C. Wang, Y. Bi, H. Cai, Y. Chen, M. Gong, and Z. Liu, *Chin. Phys. C* **41**, 053102 (2017).
- [77] P. Boucaud, F. De Soto, J. P. Leroy, A. Le Yaouanc, J. Micheli, H. Moutarde, O. Pène, and J. Rodríguez-Quintero, *Phys. Rev. D* **74**, 034505 (2006).
- [78] A. Cucchieri, D. Dudal, T. Mendes, and N. Vandersickel, *Phys. Rev. D* **85**, 094513 (2012).

Nielsen identities in screened theoriesFabio Siringo^{1,*} and Giorgio Comitini^{1,2,†}¹*Dipartimento di Fisica e Astronomia dell'Università di Catania, INFN Sezione di Catania, Via S. Sofia 64, I-95123 Catania, Italy*²*KU Leuven Campus Kulak Kortrijk, Department of Physics, Etienne Sabbelaan 53 bus 7657, 8500 Kortrijk, Belgium* (Received 9 August 2022; accepted 17 October 2022; published 26 October 2022)

One-loop explicit expressions are derived for the gluon Nielsen identity in the formalism of the screened massive expansion for Yang-Mills theory. The gauge-parameter-independence of the poles and residues is discussed in a strict perturbative context and, more generally, in extended resummation schemes. No exact formal proof was reached by the approximate resummation schemes, but some evidence is gathered in favor of an exact invariance of the phase, consistently with previous numerical studies.

DOI: [10.1103/PhysRevD.106.076014](https://doi.org/10.1103/PhysRevD.106.076014)**I. INTRODUCTION**

Confinement and dynamical mass generation are among the most important open problems of contemporary physics. The quantum field theories which describe the interactions of quarks and gluons, QCD and pure Yang-Mills theory, are believed to be fully consistent theories, at all scales, containing a dynamical cutoff in the IR. But unfortunately, we are still far from a full understanding of the confinement mechanism which seems to be somehow related to the dynamical generation of almost all the mass which is observed in the universe. Lattice and continuous studies [1–47] have ruled out the existence of a Landau pole and supported the existence of a finite coupling, which is not too large even deep in the IR. On the other hand, the important role of the analytic properties of the Green functions, and their relation with the dynamics, is still largely unexplored because of the breakdown of ordinary perturbation theory and of the lack of alternative analytical tools in the continuous.

Quite recently, by a change of the expansion point, a new perturbative approach has been developed [48–58], a *screened massive expansion* which is perfectly sound in the IR and has the usual merits of ordinary perturbation theory: calculability, analytical outputs and a manifest description of the analytic properties in the complex plane. The method gives direct and quantitative predictions for the

poles of the gluon propagator which appear as complex conjugated polar singularities [50,56,57].

The existence of complex conjugated poles was predicted by several models, like the refined Gribov-Zwanziger model [59–63], and their deep effects on the dynamical properties of the gluon and on the confinement of color have been discussed by many authors [64–67]. Moreover, a pair of complex conjugated poles invalidates the existence of the Källén-Lehmann representation [68], raises important questions on the correct analytic continuation of the gluon propagator and jeopardizes the analytic properties of Dyson-Schwinger equations, unless some compensation arises from the unknown structure of the exact vertices [69].

On the physical meaning of the complex poles there are different, contrasting, opinions. A recent formal approach [67] has embraced the view that the complex poles would emerge from unphysical zero-norm states which should be removed from the Hilbert space, giving rise to a confinement mechanism. However, the formal removal of quarks and gluons from the physical states does not seem a satisfying solution for the problem of confinement, which would miss a more physical and dynamical explanation. Moreover, according to that formal approach, the analytic continuation of the gluon propagator does not exist [67], raising serious issues on the physical content of the theory.

A more physical approach [56,65] relies on the idea that quarks and gluons do exist, as internal degrees of freedom of the theory, but their phenomenological appearance is damped by a very short lifetime which confines them. In that view, the complex poles would play a physical dynamical role in confinement, besides having to do with the dynamical mass which is observed in the IR. That approach is corroborated by the discovery that, not only the poles, but even the phases of the complex residues appear

*fabio.siringo@ct.infn.it

†giorgio.comitini@dfa.unict.it

Published by the American Physical Society under the terms of the Creative Commons Attribution 4.0 International license. Further distribution of this work must maintain attribution to the author(s) and the published article's title, journal citation, and DOI. Funded by SCOAP³.

to be gauge-parameter-independent. The whole principal part of the gluon propagator seems to be gauge invariant: the phase of the residue is found to change less than 3×10^{-3} when the gauge parameter goes from $\xi = 0$ to $\xi = 1.2$ [52]. On the other hand, in a modified Källén-Lehmann representation, in presence of zero-norm states, the phase of the residues could be the direct consequence of a complex spectrum, and the invariance of the phase could be itself related to the gauge invariance of the spectrum.¹ The same principal part seems to give the main contribution to a dimension-two condensate [70] and to the short-range linear raising potential which emerges from the Fourier transform of the propagator at the leading order. Thus, many arguments would favor the gauge invariance of the phase of the residues if the gluons are believed to be confined but still physical degrees of freedom. Here, by “physical” we mean that the zero-norm states and their complex energies might play a role as intermediate steps in the building of physical excitations, like in the i -particle scenario of Ref. [71].

From a formal point of view, a proof of gauge invariance would require the study of the Nielsen identities [72–74], exact identities which determine the gauge dependence of the propagator in a covariant gauge. The identities are a direct consequence of the Becchi-Rouet-Stora-Tyutin (BRST) symmetry which is displayed by the Faddeev-Popov Lagrangian of QCD and Yang-Mills theories. There is a growing interest in the role of the Nielsen identities for determining the properties of the propagators in a generic covariant gauge [75] and for their explicit numerical evaluation [76].

In this paper, the Nielsen identity for the gluon propagator is evaluated by an explicit one-loop calculation in the framework of a screened perturbative expansion. Here, our primary interest is in the screened massive expansion, but the explicit one-loop expressions might be useful for other screened theories, like the Curci-Ferrari model [77–83]. Moreover, the result can be pushed beyond a strict one-loop expansion by some resummation of infinite classes of graphs.

Because of the soft breaking of BRST which occurs in the screened expansion at any fixed order, the Nielsen identities are not expected to be fulfilled at one loop in our framework. Nonetheless, it is instructive to explore how the results change when going from the strictly perturbative expressions to those obtained by an approximate resummation of the internal gluon lines. The detailed study of the analytic properties of the latter seems to suggest that the phase might be exactly invariant, as expected both numerically [52] and by physical arguments—if the gluon

principal part is to play a genuine physical role on the dynamics of the strong interactions. Thus, enforcing the pole and phase invariance turns out to be a consistent criterion for the optimization of the screened expansion from first principles, as was done in [52] with remarkably good results.

Besides the perturbative, partially resummed, context, we are still not able to provide an exact formal proof for the invariance of the phases of the residues.

This paper is organized as follows: the massive screened expansion is briefly reviewed in Sec. II, in order to fix the notation; in Sec. III the Nielsen identity for the gluon propagator is derived and its relation with the polarization function is discussed; in Sec. IV the explicit one-loop expression of the identity is derived by the screened expansion; in Sec. V the one-loop result is discussed both in the perturbative context and by using different resummation schemes. A detailed account of the explicit steps leading to the evaluation of the one-loop graphs is reported in the Appendix.

II. THE SCREENED EXPANSION

The massive, *screened* expansion was first developed in Refs. [48,49] and related to the Gaussian effective potential in Refs. [41,42]. It is based on a change of the expansion point of ordinary perturbation theory.

In the pure gauge sector, the gauge-fixed Lagrangian can be written as

$$\mathcal{L} = \mathcal{L}_{\text{YM}} + \mathcal{L}_{\text{fix}} + \mathcal{L}_{\text{FP}}, \quad (1)$$

where \mathcal{L}_{YM} is the Yang-Mills term

$$\mathcal{L}_{\text{YM}} = -\frac{1}{2} \text{Tr}(\hat{F}_{\mu\nu} \hat{F}^{\mu\nu}), \quad (2)$$

\mathcal{L}_{FP} is the ghost term arising from the Faddeev-Popov determinant and \mathcal{L}_{fix} is a covariant gauge-fixing term,

$$\mathcal{L}_{\text{fix}} = -\frac{1}{\xi} \text{Tr}[(\partial_\mu \hat{A}^\mu)(\partial_\nu \hat{A}^\nu)]. \quad (3)$$

Usually, the total action is split as $S_{\text{tot}} = S_0 + S_I$ where the quadratic part can be written as

$$S_0 = \frac{1}{2} \int A_{a\mu}(x) \delta_{ab} \Delta_0^{-1\mu\nu}(x, y) A_{b\nu}(y) d^4x d^4y \\ + \int \bar{c}_a(x) \delta_{ab} \mathcal{G}_0^{-1}(x, y) c_b(y) d^4x d^4y, \quad (4)$$

while the interaction contains the three terms

$$S_I = \int d^d x [\mathcal{L}_{gh} + \mathcal{L}_3 + \mathcal{L}_4], \quad (5)$$

¹As discussed in Ref. [67], the existence of zero-norm states gives rise to complex conjugated eigenvalues if the Hamiltonian is Hermitian. Complex residues follow from the existence of a complex spectrum even if we *assume* that the Hamiltonian is Hermitian.

which read

$$\begin{aligned}\mathcal{L}_3 &= -gf_{abc}(\partial_\mu A_{a\nu})A_b^\mu A_c^\nu, \\ \mathcal{L}_4 &= -\frac{1}{4}g^2 f_{abc}f_{ade}A_{b\mu}A_{c\nu}A_d^\mu A_e^\nu, \\ \mathcal{L}_{gh} &= -gf_{abc}(\partial_\mu \bar{c}_a)c_b A_c^\mu.\end{aligned}\quad (6)$$

In Eq. (4), Δ_0 and \mathcal{G}_0 are the standard free-particle propagators for gluons and ghosts, respectively, and their Fourier transforms are

$$\begin{aligned}\Delta_0^{\mu\nu}(p) &= \Delta_0(p)[t^{\mu\nu}(p) + \xi \mathcal{L}^{\mu\nu}(p)], \\ \Delta_0(p) &= \frac{1}{-p^2}, \quad \mathcal{G}_0(p) = \frac{1}{p^2},\end{aligned}\quad (7)$$

having used the transverse and longitudinal projectors

$$t_{\mu\nu}(p) = g_{\mu\nu} - \frac{p_\mu p_\nu}{p^2}, \quad \mathcal{L}_{\mu\nu}(p) = \frac{p_\mu p_\nu}{p^2}.\quad (8)$$

The screened massive expansion is obtained by a change of the quadratic expansion point, adding a transverse mass term to the quadratic part of the action and subtracting it again from the interaction, thus leaving the total action unchanged.² We add and subtract the action term

$$\delta S = \frac{1}{2} \int A_{a\mu}(x) \delta_{ab} \delta\Gamma^{\mu\nu}(x, y) A_{b\nu}(y) d^4x d^4y, \quad (9)$$

where the vertex function $\delta\Gamma$ is a shift of the inverse propagator,

$$\delta\Gamma^{\mu\nu}(x, y) = [\Delta_m^{-1\mu\nu}(x, y) - \Delta_0^{-1\mu\nu}(x, y)], \quad (10)$$

and $\Delta_m^{\mu\nu}$ is a new massive free-particle propagator,

$$\Delta_m^{\mu\nu}(p) = \Delta_m(p)t^{\mu\nu}(p) + \frac{\xi}{-p^2} \mathcal{L}^{\mu\nu}(p), \quad (11)$$

with a massive transverse component

$$\Delta_m(p) = \frac{1}{-p^2 + m^2}.\quad (12)$$

Adding that action term is equivalent to substituting the new massive propagator $\Delta_m^{\mu\nu}$ for the old massless one $\Delta_0^{\mu\nu}$ in the quadratic part.

Of course, in order to leave the total action unaffected by the change, we must include the new interaction vertex, $\delta\Gamma$, among the standard interaction terms. Dropping all color indices in the diagonal matrices and inserting Eqs. (7) and (11) into Eq. (10), the vertex is just the transverse mass shift of the quadratic part,

²This is actually done after renormalizing the Lagrangian. The details can be found e.g., in [53].

$$\delta\Gamma^{\mu\nu}(p) = m^2 t^{\mu\nu}(p).\quad (13)$$

The proper gluon polarization Π and ghost self-energy Σ can then be evaluated, order by order, by perturbation theory. In all Feynman graphs the internal gluon lines are replaced by the massive free-particle propagator $\Delta_m^{\mu\nu}$ while the new two-point vertex can be regarded as a new (transverse) mass counterterm, $\delta\Gamma^{\mu\nu}$, to be inserted in order to compensate the shift of the quadratic term in the action. The new two-point vertex is usually represented by a cross, like other counterterms, and we will refer to the graphs with one or more crosses as *crossed* graphs.

Since the total gauge-fixed FP Lagrangian is not modified and because of gauge invariance, the longitudinal polarization is known exactly and is zero, so that the total polarization is transverse,

$$\Pi^{\mu\nu}(p) = \Pi(p)t^{\mu\nu}(p), \quad (14)$$

and the (exact) dressed propagators read

$$\begin{aligned}\Delta_{\mu\nu}(p) &= \Delta(p)t_{\mu\nu}(p) + \Delta^L(p)\mathcal{L}^{\mu\nu}(p), \\ \mathcal{G}^{-1}(p) &= p^2 - \Sigma(p),\end{aligned}\quad (15)$$

where the transverse and longitudinal parts are given by

$$\begin{aligned}\Delta^{-1}(p) &= -p^2 + m^2 - \Pi(p), \\ \Delta^L(p) &= \frac{\xi}{-p^2}.\end{aligned}\quad (16)$$

At tree level, the polarization is given by the counterterm $\delta\Gamma$ of Eq. (13), so that the tree-term $\Pi_{\text{tree}} = m^2$ just cancels the mass in the dressed propagator Δ of Eq. (16), giving back the standard free-particle propagator of Eq. (7).

Summing up the loops, the transverse dressed propagator can be written as

$$\Delta(p) = [-p^2 - \Pi_{\text{loop}}(p)]^{-1}, \quad (17)$$

where $\Pi_{\text{loop}}(p) = \Pi(p) - m^2$ is the sum of the transverse part of all the polarization graphs containing loops (that is, excluding the tree-level term).

The diverging integrals are made finite by dimensional regularization and can be evaluated in the Euclidean space, by setting $d = 4 - 2\epsilon$. An important feature of the massive expansion is that the crossed graphs cancel all the spurious diverging mass terms exactly, so that no mass renormalization is required. At one-loop, as shown in Refs. [48,49,52], in the $\overline{\text{MS}}$ scheme, the diverging part of the proper transverse polarization can be written as

$$\Pi_{\text{loop}}^\xi(p) = -p^2 \frac{Ng^2}{(4\pi)^2 \epsilon} \left(\frac{13}{6} - \frac{\xi}{2} \right), \quad (18)$$

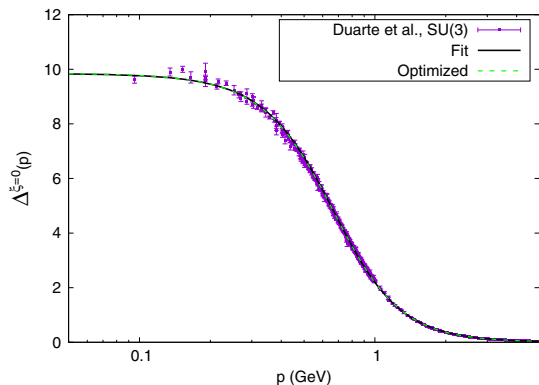


FIG. 1. The one-loop gluon propagator computed in the Landau gauge ($\xi = 0$) within the framework of the fixed-scale screened massive expansion, together with the lattice data of Ref. [18]. Free fit (solid black curve) and optimized calculation (green dashed curve). The energy scale is set by taking $m \approx 0.65$ GeV.

which is the same identical result of standard perturbation theory [84].

As usual, the diverging part can be canceled by wave function renormalization, by subtraction at an arbitrary point. Of course, a finite term $\sim \text{const.} \times p^2$ arises from the subtraction and cannot be determined in any way: it depends on the regularization scheme and on the arbitrary renormalization scale μ , so that its actual value remains somehow arbitrary. When the coupling is absorbed into an overall finite multiplicative renormalization constant for the propagator and the gluon mass m is used to fix the energy scale of the theory (see [49] for details), such a term is left as the only spurious free parameter of the approximation.

The fixed-scale approach, as opposed to its RG-improved counterpart [53], has the advantage of providing analytical expressions which are in excellent agreement with the lattice data below 2 GeV—see Fig. 1 (solid black curve)—and can be easily continued to the whole complex plane [50,52,55,56]. The success of the method would suggest that, in the infrared, a mere constant, inserted in the factor of p^2 in Eq. (18), can mimic the effects of higher-order terms.

The agreement can be achieved from first principles by using a sort of optimization by variation of the renormalization scheme, a method that was proven to be very effective for the convergence of the expansion [85,86]. In this framework, the $\text{const.} \times p^2$ term—or, equivalently in MOM-like schemes, the dimensionless subtraction scale μ/m —, is fixed by requiring that some properties related to gauge invariance, and more precisely the gauge invariance of the poles and phases of the residues, are satisfied by the approximate one-loop expression of the gluon propagator [52,54]. When such properties are enforced [52], the optimized one-loop analytical expression again provides

an excellent agreement with the lattice, as shown in Fig. 1 (dashed green curve).

The gauge invariance of the gluon poles [73] is an exact property which easily follows from the BRST invariance of the Yang-Mills Lagrangian. Using the BRST symmetry, a Nielsen identity [72]

$$\frac{\partial}{\partial \xi} \frac{1}{\Delta(p)} = 2\mathcal{F}(p) \left[\frac{1}{\Delta(p)} \right]^2, \quad (19)$$

where $\mathcal{F}(p)$ is the transverse component of another Green function (more on this in the next section), can be derived [74]. Since the Yang-Mills Lagrangian is not modified as a whole by our shift of the expansion point, we know that, provided that the BRST symmetry is not broken non-perturbatively, a sufficiently accurate approximation of the gluon propagator must have gauge-invariant poles.

Nonetheless, due to the soft breaking of BRST symmetry caused by the introduction of a mass term in the kinetic and interaction terms of the Lagrangian, the gluon propagator computed in the screened expansion does not automatically fulfill such a constraint, for general values of the free parameters. The poles of the gluon propagator were found to be complex [49], coming in a complex-conjugate pair at $p^2 = p_0^2, (p_0^2)^*$, with $\text{Im}(p_0^2) \neq 0$. While the poles, being the solution of the ξ -dependent equation $\Delta^{-1}(p, \xi) = 0$, can in general depend on the gauge parameter ξ , the free parameters of the expansion—that is, the constant in the $\text{const.} \times p^2$ term and the gluon mass parameter m^2 itself—can be tuned with the gauge so as to make the poles ξ -independent [52], thus complying with the Nielsen identities. The additional requirement that the *phase* of the residues be gauge-invariant was found to be sufficient to fix the value of the spurious free constant in the Landau gauge [52] and yielded a gluon propagator which is remarkably close to the free fit obtained from the lattice data, and to the lattice results themselves.

While the gauge invariance of the poles is a trivial consequence of the Nielsen identities, and must hold even when the poles are complex, the gauge invariance of the phase of the residues is less obvious. As discussed in Ref. [52], because of the square on the right-hand side of Eq. (19), the phase of the complex residues is invariant *if* the Green function \mathcal{F} does not have a pole at the same position as the gluon propagator $\Delta(p)$.

Thus, the discovery of Ref. [52], that the gauge invariance of the phase of residues (in the complex plane) provides an optimal agreement with the lattice data (in the Euclidean space), might lead to two different interpretations: either the function \mathcal{F} has no poles at the same position as the gluon propagator, and the gauge invariance of the phase of the gluon residues is an exact property, or the change of the phase with the gauge is an accidentally small higher-order effect which is not seen at one-loop. Actually, due to the arbitrariness in the renormalization of

the gluon residue, there is also a third possibility, which will be discussed in the next section.

A more detailed analysis of the point motivates the explicit derivation of the Nielsen identity, Eq. (19), in the special context of the screened expansion. This will be the content of the next two sections.

III. THE NIELSEN IDENTITIES

The Nielsen identities [72] are a set of equations which determine the gauge dependence of the exact Green functions of a gauge theory. They can be derived using BRST symmetry, under the hypothesis that the latter is not broken in the vacuum. For the propagators of QCD, the identities were fully discussed and derived by a functional method in Ref. [74]. In that work, a detailed calculation was reported for the explicit one-loop identities, in the framework of standard perturbation theory.

In this section, we give a quite straightforward derivation of the identities and discuss their relation with the polarization function. A detailed derivation of the explicit one-loop expressions, in the framework of the screened massive expansion, will be discussed in the next section.

We start by reintroducing the Nakanishi-Lautrup auxiliary field B_a in the Yang-Mills action and writing the gauge-fixing term in Eq. (3) as

$$\mathcal{L}_{\text{fix}} = \frac{\xi}{2} B_a B_a + B_a (\partial \cdot A_a). \quad (20)$$

Integrating out the Nakanishi-Lautrup field is equivalent to solving the equation of motion $B_a = -(\partial \cdot A_a)/\xi$.

When expressed in terms of the B -field, the total Yang-Mills Lagrangian satisfies the usual BRST invariance property

$$\delta_\theta \mathcal{L} = 0, \quad (21)$$

where

$$\begin{aligned} \delta_\theta A_a^\mu &= \theta D^\mu c_a, \\ \delta_\theta \bar{c}_a &= \theta B_a, \\ \delta_\theta c_a &= -\frac{g}{2} f^{abc} \theta c_b c_c, \\ \delta_\theta B_a &= 0, \end{aligned} \quad (22)$$

and θ is a Grassmann parameter.

The field B also determines the gauge-parameter dependence of the total Lagrangian, since the derivative of the latter with respect to ξ is given by

$$\frac{\partial \mathcal{L}}{\partial \xi} = \frac{1}{2} B_a B_a. \quad (23)$$

Using Eq. (23), the average $\langle \mathcal{O} \rangle$ of any operator \mathcal{O} ,

$$\langle \mathcal{O} \rangle = \frac{\int \mathcal{O} \exp(i \int \mathcal{L})}{\int \exp(i \int \mathcal{L})}, \quad (24)$$

is easily seen to satisfy

$$\begin{aligned} \frac{\partial}{\partial \xi} \langle \mathcal{O} \rangle &= \left\langle \mathcal{O} \left(i \int \frac{\partial \mathcal{L}}{\partial \xi} \right) \right\rangle - \langle \mathcal{O} \rangle \left\langle \left(i \int \frac{\partial \mathcal{L}}{\partial \xi} \right) \right\rangle \\ &= \frac{i}{2} \left\langle \mathcal{O} \int B_a B_a \right\rangle. \end{aligned} \quad (25)$$

The last equality follows from Eq. (23) and from the Slavnov-Taylor identity

$$0 = \langle \delta_\theta (\bar{c}_a B_a) \rangle = \langle \delta_\theta \bar{c}_a B_a \rangle = \langle B_a B_a \rangle, \quad (26)$$

which holds provided that the vacuum is BRST-invariant, so that

$$\langle \delta_\theta \mathcal{O}' \rangle = 0 \quad (27)$$

for any operator \mathcal{O}' .

For the case of the exact gluon propagator

$$\Delta_{ab}^{\mu\nu}(x, y) = -i \langle A_a^\mu(x) A_b^\nu(y) \rangle, \quad (28)$$

we can denote by $2\mathcal{F}$ the Green function

$$\begin{aligned} 2\mathcal{F}_{ab}^{\mu\nu}(x, y) &= \frac{\partial}{\partial \xi} \Delta_{ab}^{\mu\nu}(x, y) \\ &= \frac{1}{2} \int d^4 z \langle A_a^\mu(x) A_b^\nu(y) B_c(z) B_c(z) \rangle, \end{aligned} \quad (29)$$

or in a more compact notation

$$\frac{\partial \Delta}{\partial \xi} = \frac{1}{2} \left\langle AA \int B^2 \right\rangle = 2\mathcal{F}. \quad (30)$$

Denoting by $\Gamma = -\Delta^{-1}$ the two-point vertex function, the Nielsen identity for Γ reads

$$\frac{\partial \Gamma}{\partial \xi} = \Delta^{-1} \cdot \frac{\partial \Delta}{\partial \xi} \cdot \Delta^{-1} = \Gamma \cdot (2\mathcal{F}) \cdot \Gamma, \quad (31)$$

where the dot products are functional products which become ordinary products when the Fourier transform is taken.

Strictly speaking, Eq. (31) becomes the Nielsen identity only when an independent and direct evaluation of the Green function \mathcal{F} is provided by the Slavnov-Taylor identities, as shown below. While the Green function \mathcal{F} seems to have two gluon legs (hence a double gluon pole in the Fourier transform) in Eq. (29), one of the legs is eaten up as a result of BRST symmetry, so that according to Eq. (31) the Fourier transform of the function \mathcal{F} has a single pole at most. This follows from the Slavnov-Taylor identity

$$0 = \langle \delta_\theta(AA\bar{c}B) \rangle = \langle (Dc)A\bar{c}B \rangle + \langle A(Dc)\bar{c}B \rangle + \langle AAB\bar{B} \rangle, \quad (32)$$

which yields

$$2\mathcal{F}_{ab}^{\mu\nu}(x, y) = -\frac{1}{2} \left[\int d^4z \langle D^\mu c_a(x) A_b^\nu(y) \bar{c}_c(z) B_c(z) \rangle + (x \leftrightarrow y, a \leftrightarrow b) \right]. \quad (33)$$

The equivalence of the function \mathcal{F} in Eq. (33) and in Eq. (29) is the core of the Nielsen identity for the gluon propagator.

The presence of a single gluon leg in Eq. (33) ensures that at least one of the two Γ factors survives on the right-hand side of Eq. (31) and that a zero occurs at the pole position $p = p_0$ in the derivative of the Fourier transforms:

$$\left[\frac{\partial \Gamma}{\partial \xi} \right]_{p=p_0} = \left[\frac{\partial \Pi}{\partial \xi} \right]_{p=p_0} = 0 \quad \text{if } \Gamma(p_0) = 0. \quad (34)$$

As a consequence, the position of the pole is gauge-parameter-independent in the exact gluon propagator, as can be explicitly seen from the equations

$$\begin{aligned} 0 &= \frac{d}{d\xi} \Gamma(p_0^2(\xi), \xi) \\ &= \frac{\partial \Gamma}{\partial \xi}(p_0^2(\xi), \xi) + \frac{\partial \Gamma}{\partial p^2}(p_0^2(\xi), \xi) \frac{dp_0^2}{d\xi}(\xi) \\ &= \frac{\partial \Gamma}{\partial p^2}(p_0^2(\xi), \xi) \frac{dp_0^2}{d\xi}(\xi) \Rightarrow \frac{dp_0^2}{d\xi} = 0, \end{aligned} \quad (35)$$

given that in order for Γ to have a zero at p_0^2 , $(\partial \Gamma / \partial p^2)_{p_0}$ must be finite. Here, a transverse projection is understood for all the functions, since the longitudinal parts are known exactly and, in that case, the invariance of the pole is trivial, being the longitudinal pole unshifted from $p = 0$ in any gauge.

The discovery that the phase of the complex residue may be gauge-invariant [52] has led to the claim that the Green function \mathcal{F} might have no pole at all in $p = p_0$. Then, the double zero on the right-hand side of Eq. (31) due to the Γ 's would be enough for ensuring that

$$\frac{\partial}{\partial \xi} \left[\frac{\partial \Gamma}{\partial p^2} \right]_{p=p_0} = 0, \quad (36)$$

yielding a proof of gauge invariance for the residue [52], see ahead. Going back to Eq. (31), the claim is equivalent to assuming that the derivatives $\partial \Gamma / \partial \xi$ and $\partial \Pi / \partial \xi$ have a double zero at the pole position.

Actually, the invariance of the *modulus* of the residue would not make much physical sense, since the modulus is

defined up to an arbitrary—potentially gauge-dependent—real renormalization factor. What emerged in Ref. [52] was the invariance of the *phase* of the residue, which would be enforced by a weaker condition: denoting by $R = |R| \exp(i\theta)$ the complex residue at the pole $p^2 = p_0^2$, the transverse projection of the two-point function reads

$$\Gamma(p^2) = (p^2 - p_0^2) \frac{e^{-i\theta}}{|R|} + \dots, \quad (37)$$

and because of the gauge invariance of the pole p_0 , the logarithmic derivative gives

$$\frac{\partial \theta}{\partial \xi} = -\text{Im} \left[\frac{1}{\Gamma} \frac{\partial \Gamma}{\partial \xi} \right]_{p=p_0} = -\text{Im}[(2\mathcal{F})\Gamma]_{p=p_0}, \quad (38)$$

where the second equality follows from Eq. (31) and a transverse projection is understood in all the functions on the right hand side. Thus, the vanishing of the imaginary part, on the right-hand side, would be enough for ensuring that the phase is invariant.

While the invariance of the modulus of the residue seems to be unnecessary in view of renormalization, the invariance of the phase makes sense in presence of complex poles: the phase determines the shape of the principal part of the propagator—which, as shown in [52], makes up for the largest contribution to $\Delta(p)$ —and has an effect on all related observable objects, like the Fourier transform of the propagator which at large momenta could be seen as a short-distance approximation for the quark-quark potential. On the other hand, the invariance of the phase has always been expected whenever the pole and residue were real, since then, trivially, $\theta = 0$ for any ξ .

It is instructive to explore the content of Eq. (29) in terms of diagrams of the screened expansion and, more generally, of perturbation theory. We will be interested in the Fourier transform

$$2\delta_{ab}\mathcal{F}^{\mu\nu}(p) \equiv 2\mathcal{F}_{ab}^{\mu\nu}(p, -p), \quad (39)$$

where

$$\begin{aligned} 2\mathcal{F}_{ab}^{\mu\nu}(p, q) &= (2\pi)^4 \delta^{(4)}(p+q) \\ &= 2 \int d^4x d^4y \mathcal{F}_{ab}^{\mu\nu}(x, y) e^{ip \cdot x + iq \cdot y}. \end{aligned} \quad (40)$$

We first recover, by the equations of motion,

$$\langle B_a A_b^\mu \rangle = -\frac{1}{\xi} \langle (\partial \cdot A_a) A_b^\mu \rangle, \quad (41)$$

yielding the exact result

$$\int d^4x e^{ip \cdot x} \langle B_a(0) A_b^\mu(x) \rangle = \frac{-ip_\nu}{\xi} i\Delta_{ab}^{\nu\mu}(p) = \frac{\delta_{ab} p^\mu}{-p^2}, \quad (42)$$

which is valid to all orders [74] because of Eq. (16). All graphs contributing to the right hand side of Eq. (29) can be obtained by the insertion of the two-point local vertex B_a^2 in the graphs of the gluon propagator. At tree level, there is only one term given by the product $\langle AB \rangle \langle BA \rangle$ with a symmetry factor of 2, yielding

$$2\mathcal{F}^{\mu\nu}(p) = \left[\frac{p^\mu}{-p^2} \right] \left[\frac{-p^\nu}{-p^2} \right] = -\frac{p^\mu p^\nu}{p^4}. \quad (43)$$

Inserting this longitudinal term in Eq. (31), together with the exact longitudinal part $\Gamma^{\mu\nu} = \ell^{\mu\nu} p^2 / \xi$, the identity is easily seen to be satisfied exactly. Thus, we predict that all loop contributions to \mathcal{F} must be transverse [74]. In fact, this is the case, since they can all be derived by insertion of a vertex $\int B^2$ in all graphs for the gluon polarization, which is transverse.

In more detail, denoting by $\pi^{(n)}$ a polarization graph with n internal gluon lines, all the corresponding graphs for the function \mathcal{F} , in Eq. (29), are obtained by substituting the longitudinal term $\langle AB \rangle \langle BA \rangle$ for one of the n internal gluon lines and restoring the external gluon legs. The inserted longitudinal term is just the tree-level graph for $2\mathcal{F}$ and is equal to $\Delta^L \ell^{\mu\nu} / \xi = \partial \Delta_m^{\mu\nu} / \partial \xi$ according to Eqs. (11), (16) and (43). Thus, we are just replacing a gluon line by its longitudinal part, divided by ξ . Now, this is precisely what we get by taking the derivative $\partial \pi^{(n)} / \partial \xi$. Summing over n , we get a direct proof of Eq. (29), since the dependence on ξ is in the internal lines, while the external legs are projected on the transverse polarization and do not depend on ξ . This argument holds both for the screened expansion ($m \neq 0$) and for standard perturbation theory ($m = 0$), since it only depends on the transversality of the exact gluon polarization.

While the content of Eq. (29) is trivial in terms of diagrams, its equivalence to Eq. (33) is not immediate and there is no one-to-one correspondence of diagrams. Eq. (33) follows from the overall BRST symmetry of the Lagrangian and the equivalence to Eq. (29) holds for the exact functions. As shown in Ref. [74], in ordinary perturbation theory, if both functions are correctly expanded in powers of the coupling, they must agree at any finite order. On the other hand, the addition and subtraction of a gluon mass term that defines the screened massive expansion causes the soft breaking of BRST invariance at any finite order. Thus, we expect the Nielsen identities not to hold perturbatively in the screened expansion. This does not imply, however, that the screened expansion's gluon poles are not gauge-invariant. As discussed in the last section, the freedom in the choice of the spurious free parameters is still enough to enforce their invariance, once an explicit expression for the gluon propagator has been obtained at finite order.

At any finite order, deviations from the exact BRST symmetry are a *measure* of the accuracy of the truncated

expansion [52,54,55]. Thus, it is not a case that the screened expansion gives an excellent agreement with the lattice data when optimized by the constraints of pole (and phase) invariance, since these are the conditions which minimize the deviations between one-loop and exact results.

On the other hand, we might wonder if the gauge-invariance of the phase of the residue is an exact property of Yang-Mills theory. To date, we have not been able to reach a formal proof. For what concerns the screened expansion, due to the previously discussed soft breaking of BRST invariance, the perturbative expression for $\partial\theta/\partial\xi$ cannot be trusted as is at any finite order. Nonetheless, a nonperturbative resummation of the gluon graphs in the Nielsen identity might give us hints as to whether the phase is really invariant. This will be discussed in Sec. V.

IV. ONE LOOP EXPLICIT CALCULATION

The Green function \mathcal{F} , in Eq. (33), can be directly evaluated in the framework of the screened massive expansion, order by order. Here, we give the explicit result up to one-loop.

At tree level, there is only one graph contributing to Eq. (33) which factors as $\langle (\partial^\mu c) \bar{c} \rangle \langle BA^\nu \rangle$ yielding

$$2\mathcal{F}^{\mu\nu}(p) = -(-ip^\mu) \left(\frac{i}{p^2} \right) \left(\frac{-p^\nu}{-p^2} \right) = -\frac{p^\mu p^\nu}{p^4} \quad (44)$$

in agreement with the exact result in Eq. (43). There are no crossed graphs at tree level because any insertion of the transverse mass vanishes in the longitudinal tree term. As discussed above, since Eq. (44) gives the whole longitudinal contribution, the sum of all higher order terms must be transverse. In fact, the uncrossed one-loop graphs which contribute to Eq. (33) are the first three pairs reported in Fig. 2, and each pair gives a pure transversal term. More generally, all loop graphs occur in pairs, with the structure displayed in Fig. 3, arising from the splitting of the covariant derivative in two terms,

$$D^\mu c_a = \delta_{ab} \partial^\mu c_b + gf_{abc} A_b^\mu c_c, \quad (45)$$

and from the insertion of a ghost-gluon vertex ($\bar{c}Ac$) in the first of these. The expressions of the graphs of type (1) and (2) have the following general form, respectively,

$$\begin{aligned} 2\mathcal{F}_{ab(1)}^{\mu\nu}(p) &= -i \langle (\partial^\mu c_a) (gf_{def} \partial_a \bar{c}_d A_e^\alpha c_f) \cdots \rangle \\ &= (-ip^\mu) \left(\frac{1}{p^2} \right) (ip_\alpha) gf_{aef} \int \Delta_{meg}^{\alpha\beta} \cdots, \\ 2\mathcal{F}_{ab(2)}^{\mu\nu}(p) &= - \langle (gf_{aef} A_e^\mu c_f) \cdots \rangle \\ &= -gf_{aef} \int \Delta_{meg}^{\mu\beta} \cdots, \end{aligned} \quad (46)$$

and their sum is a manifestly transverse contribution

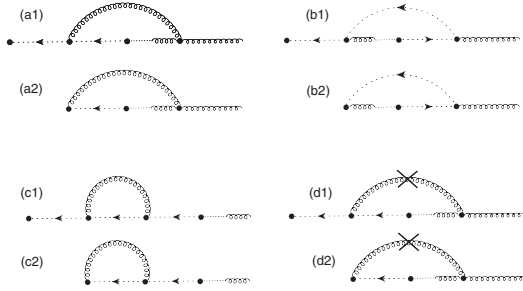


FIG. 2. One-loop graphs contributing to the function \mathcal{F} , as defined in Eq. (33), in the screened expansion. The mixed line is the longitudinal function $\langle BA \rangle$, while the solid cross is the transverse mass counterterm.

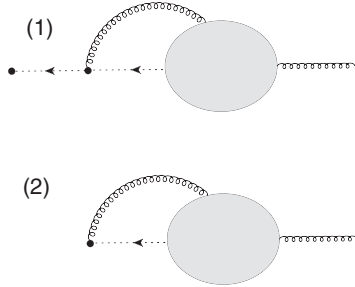


FIG. 3. General structure of each pair of graphs contributing to the function \mathcal{F} in Eq. (33). For each pair, the sum of graph (1) and graph (2) gives a transversal term, as shown in Eqs. (46) and (47).

$$2\mathcal{F}_{ab(1+2)}^{\mu\nu}(p) = \left(g_a^\mu - \frac{p^\mu p_\alpha}{p^2} \right) g f_{eaf} \int \Delta_m^{\alpha\beta} \dots \quad (47)$$

As we said, these three pairs give the transverse one-loop contribution for any expansion with a mass in the free propagator, Δ_m . While our main interest is on the screened massive expansion of Sec. II, their explicit expressions might be of some interest for other theories, like Curci-Ferrari model in the Landau gauge. We must mention that, in massive theories, there is a class of anomalous graphs, not shown in Fig. 2, contributing to the longitudinal part of \mathcal{F} . These arise from polarization insertions in the external gluon leg of the longitudinal tree-level graph. While individual polarization terms might have a nonvanishing longitudinal part in massive theories, their exact resummation is zero in the screened massive expansion, ensuring that the tree-level term still provides the total longitudinal contribution, as required by the BRST symmetry. Thus, we might neglect the anomalous terms entirely.

The third pair of graphs in Fig. 2, (c1) and (c2), have a longitudinal leg on the right side. Then, their sum is zero according to Eq. (47), because of the transverse projector

coming from the loops on the left. The second pair, graphs (b1) and (b2), are basically the same as in the standard perturbation theory, since no massive propagator occurs in the loop. The only difference arises from the bare gluon leg on the right side, which must be replaced by the massive free propagator Δ_m in the screened expansion. The first pair, graphs (a1) and (a2), differs from the standard result because of the internal massive gluon line. The explicit calculation is straightforward and the detailed steps are reported in the appendix. The sum of all the uncrossed one-loop graphs can be written as

$$2\mathcal{F}^{\mu\nu}(p) = \frac{g^2 N}{64\pi^2} \frac{t^{\mu\nu}(p)}{p^2 - m^2} F(-p^2/m^2), \quad (48)$$

where the diverging function $F(s)$, with $s = -p^2/m^2$, is regularized by setting $d = 4 - 2\epsilon$ and reads

$$F(s) = \frac{2}{\epsilon} - 3L(s) + \log(s) - 2\xi + \text{const.}, \quad (49)$$

while the logarithmic function $L(s)$, which is derived in Eq. (A34), can be recast as

$$L(s) = -\frac{1}{3s} + \left(1 - \frac{1}{s} + \frac{1}{3s^2} \right) \log s + \left[\left(s + 1 - \frac{1}{s} + \frac{1}{3s^2} \right) \log \left(1 + \frac{1}{s} \right) - 1 \right] \quad (50)$$

and shows the leading behavior $L(s) \sim \log s$ in the limit $s \rightarrow \infty$, which occurs when the mass is set to zero in order to recover the result of standard perturbation theory. Actually, as shown in the appendix, graphs (a) and (b) agree with the known results in that limit [74]. Moreover, in the same limit, the diverging part can be checked by a direct comparison with the explicit one-loop diverging term of the polarization, which is well known and is reported in Eq. (18). By a direct calculation of the derivative and by inserting it in Eq. (31), with the tree-level two-point function, $\Gamma(p) = p^2$, the diverging part of the transverse one-loop function \mathcal{F} reads

$$\begin{aligned} 2\mathcal{F} &= \frac{1}{\Gamma^2} \frac{\partial \Gamma}{\partial \xi} = \frac{1}{\Gamma^2} \frac{\partial \Pi}{\partial \xi} \\ &\sim \left[\frac{1}{p^2} \right]^2 \left[-p^2 \frac{Ng^2}{(4\pi)^2} \left(\frac{-1}{2\epsilon} \right) \right] \\ &= \frac{g^2 N}{64\pi^2} \frac{1}{p^2} \left[\frac{2}{\epsilon} \right], \end{aligned} \quad (51)$$

in perfect agreement with Eqs. (48) and (49). That is important for the renormalization of the function \mathcal{F} , since all the divergences must be absorbed by the wave function renormalization of the gluon propagator in order to make

sense of the Nielsen identity, Eq. (31), when the finite, renormalized propagator is considered.

It is instructive to see how the divergence cancels in the renormalized functions. In the $\overline{\text{MS}}$ scheme, the wave function renormalization constant Z_A follows from the divergence of the polarization in Eq. (18) and reads

$$Z_A = 1 + \frac{g^2 N}{(4\pi)^2} \left[\frac{1}{\epsilon} \right] \left(\frac{13}{6} - \frac{\xi}{2} \right), \quad (52)$$

while the logarithmic derivative of the renormalized (transverse) vertex function, $\Gamma^R = Z_A \Gamma$, can be written as

$$\begin{aligned} \frac{1}{\Gamma^R} \frac{\partial \Gamma^R}{\partial \xi} &= \frac{1}{Z_A} \left(\frac{\partial Z_A}{\partial \xi} \right) + \frac{1}{\Gamma} \frac{\partial \Gamma}{\partial \xi} \\ &= -\frac{g^2 N}{2(4\pi)^2} \left[\frac{1}{\epsilon} \right] + \frac{g^2 N}{64\pi^2} F(s) \\ &= \frac{g^2 N}{64\pi^2} \left[F(s) - \frac{2}{\epsilon} \right], \end{aligned} \quad (53)$$

where the second term in the second line arises from the Nielsen identity, Eq. (31), and from the insertion of the one-loop result, Eq. (48), neglecting higher order terms. According to Eqs. (37) and (38), the real and imaginary part of the logarithmic derivative are the gauge-parameter derivative of the modulus and phase, respectively, of the residue. They are made finite by the subtraction of the diverging term which occurred in Eq. (49). But, while the modulus still depends on an arbitrary (real) constant which arises from the subtraction and regularization schemes, as it should, the phase of the residue is finite anyway and does not depend on the renormalization up to higher order corrections. In fact, we can write

$$\frac{\partial \theta}{\partial \xi} = -\text{Im} \left[\frac{1}{\Gamma} \frac{\partial \Gamma}{\partial \xi} \right]_{p_0} = \left(\frac{g^2 N}{64\pi^2} \right) \text{Im}[F\Gamma\Delta_m]_{p_0}, \quad (54)$$

where p_0 is the pole position and, neglecting higher order corrections, Γ can be taken at tree level, so that $\Gamma\Delta_m \approx -1$, which is real. Thus, when computing the derivative of the phase, we can drop all constants and real additive terms in the one-loop function F , which simplifies as

$$F(s) \rightarrow \log(s) - 3L(s). \quad (55)$$

At one loop, in principle, there are other graphs contributing to F in the screened expansion: the crossed graphs which contain one or more insertions of the transverse mass counterterm, such as diagrams (d1) and (d2) in Fig. 2. These are higher order graphs by vertex counting, but still one-loop if the powers of g^2 are considered. Thus, their inclusion must be discussed in the framework of the detailed approximation scheme which is used. For instance, the inclusion of an infinite set of graphs with any number of

mass counterterms is equivalent to a Dyson resummation of the constant polarization term $\Pi = m^2$. The effect is that, in any gluon line, the massive gluon propagator is replaced by the bare massless one, restoring the ordinary standard perturbation theory. That is not what we would aim to, of course. The inclusion of a finite number of mass counterterms, up to a given order, turned out to be the best choice for canceling the spurious divergences without falling into a trivial resummation [49]. Here, no spurious divergence is found and the inclusion of a finite number of crossed graphs will be discussed case by case.

The crossed graphs can be easily evaluated by derivatives of the standard one-loop graphs [48–50]. For instance, the fourth pair of graphs in Fig. 2, graphs (d1) and (d2), contain one insertion of the transverse mass counterterm in the internal gluon line which is replaced by the transverse chain $\Delta_m \cdot m^2 \cdot \Delta_m$

$$\begin{aligned} \frac{1}{-p^2 + m^2} &\rightarrow \frac{1}{-p^2 + m^2} m^2 \frac{1}{-p^2 + m^2} \\ &= -m^2 \frac{\partial}{\partial m^2} \left[\frac{1}{-p^2 + m^2} \right]. \end{aligned} \quad (56)$$

Thus, after amputating the external leg, the inclusion of the crossed graphs (d1) and (d2) follows from the corresponding uncrossed graphs, (a1) and (a2), as

$$\Gamma_m \mathcal{F}_{(a)} + \Gamma_m \mathcal{F}_{(d)} = \left(1 - m^2 \frac{\partial}{\partial m^2} \right) [\Gamma_m \mathcal{F}_{(a)}]. \quad (57)$$

That is equivalent to replacing the logarithmic function $L(s)$ with a new function $L^C(s)$ in Eqs. (49) and (55), defined as

$$L^C(s) = \left(1 + s \frac{\partial}{\partial s} \right) L(s) - 1, \quad (58)$$

where the added constant, -1 , arises from the derivative of $1/\hat{\epsilon}$ according to Eq. (A16). The explicit calculation yields

$$\begin{aligned} L^C(s) &= \frac{1}{3s} - \frac{4}{3(1+s)} + \left(1 - \frac{1}{3s^2} \right) \log s \\ &+ \left[\left(2s + 1 - \frac{1}{3s^2} \right) \log \left(1 + \frac{1}{s} \right) - 2 \right]. \end{aligned} \quad (59)$$

The manifest leading behavior $L^C(s) \sim L(s) \sim \log s$, in the limit $s \rightarrow \infty$, confirms that the contribution of the crossed graphs is zero in the limit $m \rightarrow 0$.

V. DISCUSSION

We would like to discuss the invariance properties of the principal part of the gluon propagator. Our starting point is Eq. (54), which gives the explicit one-loop gauge dependence for the phase of the residue at the pole of the gluon propagator, as computed in the screened expansion by the

Nielsen identities. With $\Delta_m \Gamma = -1$ at tree level, the identity simplifies as

$$\frac{\partial \theta}{\partial \xi} = -\text{Im} \left[\frac{1}{\Gamma} \frac{\partial \Gamma}{\partial \xi} \right]_{p_0} = -\left(\frac{g^2 N}{64\pi^2} \right) \text{Im}[F]_{p_0}. \quad (60)$$

As previously discussed, since BRST invariance is broken in the screened expansion at any finite order, we may expect $\text{Im}[F]_{p_0}$ to be different from zero even if the phase were exactly gauge-invariant. This is indeed the case, as we show in Fig. 4 by plotting the $\text{Im}\{F(-p^2/m^2)\} = 0$ contour in the complex p -plane. We find a continuous line of zeros for the imaginary part, but quite far away from the pole position (asterisk-shaped point in the figure), which was found at $p_0/m = 0.8857 + 0.5718i$ in Ref. [52] by the optimized one-loop expansion. The line does not cross the pole, but we would not expect that to happen at one-loop.

Inserting a finite number of mass counterterms in the internal gluon lines would not change the result too much. For instance, by including the crossed graphs (d1) and (d2) we obtain, by Eq. (59), the contour plot shown in Fig. 5. Again, we find a line of zeros, but the distance from the pole is even larger.

A more accurate approximation of the exact result would consist in the resummation of all the one-loop polarization insertions in the internal gluon line. This would be equivalent to replacing the bare gluon propagator Δ_m with the one-loop function $-\Gamma(p)^{-1}$ inside the integrals in graphs (a1) and (a2), so that, in addition, the diagrams themselves would contain information on the position of the poles. The one-loop function $\Gamma(p^2)$ is known analytically, but the integrals would be prohibitive. On the other hand, they can be easily evaluated if the propagator is

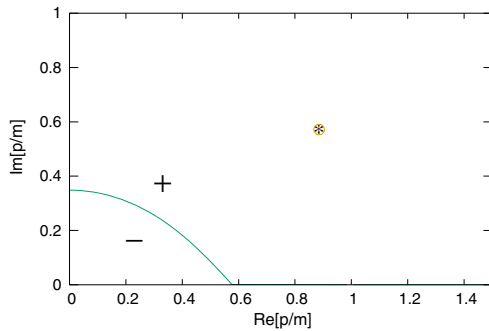


FIG. 4. Contour plot of the equation $\text{Im}\{F(-p^2/m^2)\} = 0$ in the complex plane of p , in units of m . The asterisk is the gluon pole p_0 , $\text{Re}[p_0/m] = 0.8857$, $\text{Im}[p_0/m] = 0.5718$, as found in Ref. [52]. A continuous line of zeros is found for the imaginary part of F . Because of the symmetry $F(-p^2/m^2) = F(-p^2/m^2)^*$, only the first quadrant is shown. The plain Eq. (55) is used for the calculation, without any insertion of crossed graphs or resummations.

approximated by its principal part,

$$\Delta_P(p) = -\frac{R}{p^2 - p_0^2} - \frac{R^*}{p^2 - (p_0^*)^2}, \quad (61)$$

as was done in Ref. [58] to study the infrared behavior of the quark propagator. The principal part $\Delta_P(p)$ is the largest contribution to the one-loop gluon propagator of Fig. 1, and by a slight renormalization it provides a very good approximation of the exact propagator in the IR [52]. It is also equivalent to the leading order propagator of the refined Gribov-Zwanziger effective theory [59–63].

In graphs (a1) and (a2), an approximate resummation of all the polarization insertions in the internal gluon line can be achieved very easily, without having to evaluate new integrals, by replacing $\Delta_m \rightarrow \Delta_P$ under the sign of integral and using a trick which was discussed in Ref. [58]. Using the linearity of the one-loop graphs, the result follows by analytic continuation of the mass parameter m in the complex plane. If we denote by Δ_{p_0} a bare propagator Δ_m with the mass m replaced by p_0 , then the principal part can be written as

$$\Delta_P = \frac{1 + i \tan \theta}{2} \Delta_{p_0} + \frac{1 - i \tan \theta}{2} \Delta_{p_0^*}, \quad (62)$$

where as before θ is the phase of the residue and the overall normalization of Δ_P is fixed so that $\Delta_P(p) \sim \Delta_m(p)$ in the UV, thus ensuring that the divergent part of the integral does not change. Denoting by $s_0 = p_0^2/m^2$ the adimensional pole position, we can then define a modified resummed logarithmic function L^R as

$$L^R(s) = \frac{1 + i \tan \theta}{2} L(s/s_0) + \frac{1 - i \tan \theta}{2} L(s/s_0^*), \quad (63)$$

to replace the function $L(s)$ in Eq. (55). A rigorous proof of the procedure is given in Ref. [58].

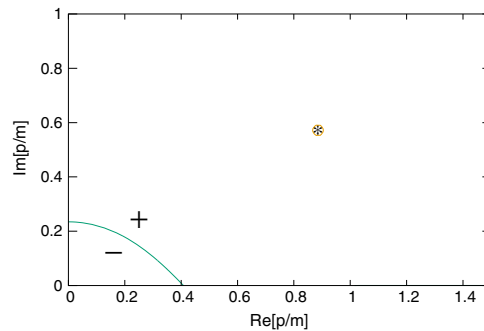


FIG. 5. Same as Fig. 4, but with the inclusion of the crossed graphs (d1) and (d2). Equation (59) is used for the calculation instead of Eq. (50).

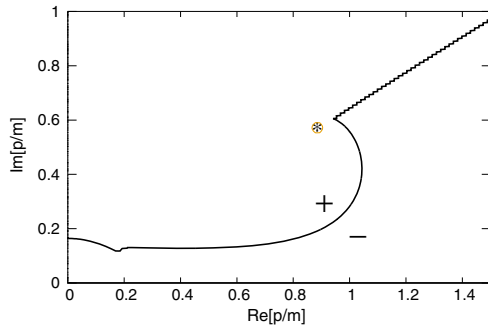


FIG. 6. Same as Fig. 4, but with a full resummation of the internal gluon line by the principal part, according to Eq. (63), which is used for the calculation instead of Eq. (50). The wavy line is a branch cut where the function changes sign without crossing the zero.

The analytic properties of the function F change dramatically when the internal gluon line is replaced by the principal part, with complex poles, using Eq. (63) instead of Eq. (50) in Eq. (55). As shown in Fig. 6, the line of zeros of the imaginary part is strongly modified and reaches a point very close to the pole. In more detail, the line of zeros merges with a branch cut which—albeit not clearly visible in the plot—originates at the pole itself. In the figure, the branch cut is depicted as a wavy line, along which the function changes sign without going to zero.³

The branch cut is explained by the existence of a logarithmic divergence at the pole. In Fig. 7, this logarithmic divergence is displayed by plotting the function $\text{Im}[F]$ with the real part $\text{Re}[p/m]$ kept fixed at the pole value, $\text{Re}[p_0/m] = 0.8857$, while changing the imaginary part, $\text{Im}[p/m]$, across the pole, which occurs at $\text{Im}[p_0/m] = 0.5718$. The logarithmic divergence arises from the divergence of $L(s)$ at $s = -1$ in Eq. (50); it follows the pole and moves to $s = -s_0$ in Eq. (63), as L gets replaced by L^R .

The divergence does not spoil the invariance of the pole, since it is anyways canceled by the zero of Γ in Eq. (31). On the other hand, at the level of the derivative $\partial\theta/\partial\xi$, the phase of the residue would receive an unphysical diverging term if the logarithm were not compensated by an extra zero at the pole. In other words, if the branch cut is a true feature of the exact result, then the Nielsen identity for the phase is well-defined only if the exact line of zeros reaches the pole. We may then expect that vertex and higher order corrections, when included, would drive the imaginary part of F toward an exact zero at p_0 , in order to reconcile the identity with the expectation of a finite phase change for the residue. The vanishing of the derivative of the phase would then follow.

³As such, the branch cut should not be viewed as being part of the contour $\text{Im}\{F(-p^2/m^2)\} = 0$, of course.

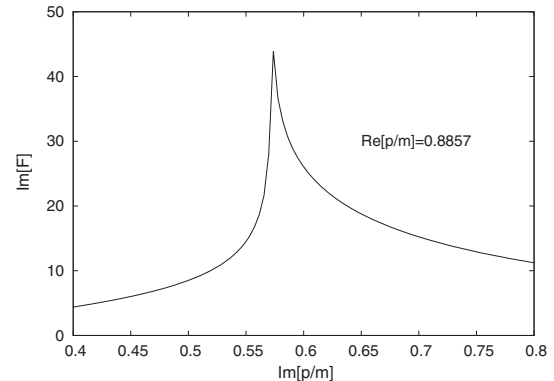


FIG. 7. Logarithmic divergence of the function F at the pole, according to the resummation scheme of Eq. (63). The imaginary part, $\text{Im}\{F(-p^2/m^2)\}$ is evaluated by Eq. (63) as a function of $\text{Im}(p/m)$ across the pole, with $\text{Re}p/m$ kept fixed at the pole value, $\text{Re}p/m = 0.8857$.

More generally, if the logarithmic divergence were genuine—with no zero to tame it in F —the diverging phase would be the sign of a branch point at the zero of Γ . p_0 would not then be a true pole of the propagator, and the steps which led to Eqs. (38) and (54) would be invalidated. The Nielsen identity would still hold, but its relation to the phase would be lost, because there would not be a well-defined residue in the first place. Of course, in this scenario, the gluon propagator would have no principal part at all, which is in contrast with what was found by the screened expansion at one loop. This is quite unlikely, if we look at the excellent agreement which is found with the lattice data in Fig. 1.

At the same time, it has been recently shown that without a knowledge of the exact vertex structure, nothing can prevent a wild proliferation of unphysical branch cuts, order by order, when complex-conjugated poles are present in the propagator [69]. Thus, the logarithmic divergence and associated branch cut might just be a consequence of the missing resummation of vertex corrections. In the complete absence of a logarithmic divergence at p_0 , $\text{Im}[F]_{p_0}$ would be finite with a line of zeros passing remarkably close to it. Thus, again, our resummed results point to either the derivative $\partial\theta/\partial\xi$ being exactly zero, or at least to it being very small.

We are far from having reached a formal proof of the vanishing of the gauge-derivative of the phase, of course. Nonetheless, we argue that the exact gauge-parameter-independence of the phase θ is the only reasonable assumption which could avoid any conflict between the exact Nielsen identity and the results of the screened expansion. Were the conflict an artifact of the expansion itself, we argue that there are good indications from our results that the derivative of the phase is at least very small, if not exactly zero.

ACKNOWLEDGMENTS

This research was supported in part by the Istituto Nazionale di Fisica Nucleare (INFN), SIM national project, and by the “Linea di intervento 2” of the University of Catania, Department of Physics and Astronomy, project HQCDyn.

APPENDIX: ONE-LOOP GRAPHS

1. Graphs (a1) and (a2)

The first graph, (a1) in Fig. 2, reads

$$2\mathcal{F}_{ab}^{\mu\nu}(p) = -(-ip^\mu) \left(\frac{i}{p^2} \right) p_\alpha g f_{dac} \int \frac{d^4k}{(2\pi)^4} i\Delta_m^{\alpha\beta}(k) [g f_{dcb} V_{\beta\sigma\lambda}(p, k)] \left[\frac{i}{(k-p)^2} \right] \left[\frac{(p-k)^\sigma}{(p-k)^2} \right] i\Delta_m^{\lambda\nu}(p), \quad (\text{A1})$$

where the three-gluon vertex structure is

$$V_{\beta\sigma\lambda}(p, k) = g_{\beta\sigma}(p-2k)_\lambda + g_{\sigma\lambda}(k-2p)_\beta + g_{\lambda\beta}(k+p)_\sigma, \quad (\text{A2})$$

while the ghost and mixed propagators are $\langle c\bar{c} \rangle = i/p^2$ and $\langle BA^\mu \rangle = p^\mu/p^2$, respectively, according to Eqs. (7) and (42). The massive gluon propagator Δ_m was defined in Eq. (11). As a countercheck of sign consistence we can use the Slavnov-Taylor identity $0 = \langle \delta_\theta(A_\mu \bar{c}) \rangle = \langle (D_\mu c) \bar{c} \rangle + \langle A_\mu B \rangle$ leading to $\langle A_\mu B \rangle = -\langle (\partial_\mu c) \bar{c} \rangle = -(-ip_\mu)(i/p^2) = -p_\mu/p^2$ as $g \rightarrow 0$. The sum over color indices gives $f_{dac} f^{dcb} = -N\delta_{ab}$ and dropping the delta

$$2\mathcal{F}^{\mu\nu}(p) = -ig^2 N \frac{p^\mu p_\alpha}{p^2} \int \frac{d^4k}{(2\pi)^4} \Delta_m^{\alpha\beta}(k) V_{\beta\sigma\lambda}(p, k) \frac{(p-k)^\sigma}{(p-k)^4} \Delta_m^{\lambda\nu}(p). \quad (\text{A3})$$

According to Eq. (47), the sum of the first pair of graphs, (a1) and (a2) in Fig. 2, can be written as

$$2\mathcal{F}_{(a1+a2)}^{\mu\nu}(p) = ig^2 N t_a^\mu(p) \Delta_m^{\lambda\nu}(p) \int \frac{d^4k}{(2\pi)^4} \Delta_m^{\alpha\beta}(k) V_{\beta\sigma\lambda}(p, k) \frac{(p-k)^\sigma}{(p-k)^4}, \quad (\text{A4})$$

and by a bit of algebra

$$2\mathcal{F}_{(a1+a2)}^{\mu\nu}(p) = -g^2 N t_a^\mu(p) I^\alpha_\lambda(p) \Delta_m^{\lambda\nu}(p), \quad (\text{A5})$$

where the integral $I^\alpha_\lambda(p)$ is

$$I^\alpha_\lambda(p) = i \int \frac{d^4k}{(2\pi)^4} \frac{\Delta_m^{\alpha\beta}(k)}{(p-k)^4} [k^2 t_{\beta\lambda}(k) - p^2 t_{\beta\lambda}(p)]. \quad (\text{A6})$$

We need the transverse part of the integral to be inserted in Eq. (A5). Thus, replacing $t_{\beta\lambda}(p)$ by $g_{\beta\lambda}$ and using the identity

$$\frac{1}{k^2(k^2-m^2)} = \frac{1}{m^2} \left[\frac{1}{k^2-m^2} - \frac{1}{k^2} \right], \quad (\text{A7})$$

the integral reads

$$I_{a\lambda}(p) = \frac{m^2-p^2}{m^2} J_{a\lambda}(p, m) + \frac{p^2}{m^2} J_{a\lambda}(p, 0) + \xi p^2 K_{a\lambda}(p), \quad (\text{A8})$$

where

$$J_{a\lambda}(p, m) = -i \int \frac{d^4k}{(2\pi)^4} \frac{k^2 g_{a\lambda} - k_\alpha k_\lambda}{[(k-p)^2]^2 (k^2-m^2)},$$

$$K_{a\lambda}(p) = i \int \frac{d^4k}{(2\pi)^4} \frac{k_\alpha k_\lambda}{[(k-p)^2 k^2]^2}. \quad (\text{A9})$$

By Feynman parametrization and neglecting odd terms in the numerator, the first integral splits as

$$J^\alpha_\lambda(p, m) = \tilde{J}^\alpha_\lambda(p, m) + p^2 t^\alpha_\lambda(p) J(p, m), \quad (\text{A10})$$

where

$$\tilde{J}^\alpha_\lambda(p, m) = 2 \int_0^1 x dx \int \frac{d_E^4 q}{(2\pi)^4} \frac{(q^2 \delta^\alpha_\lambda - q^\alpha q_\lambda)}{(q^2 + M_{x,m}^2)^3},$$

$$J(p, m) = -2 \int_0^1 x^3 dx \int \frac{d_E^4 q}{(2\pi)^4} \frac{1}{(q^2 + M_{x,m}^2)^3}, \quad (\text{A11})$$

and the integrals are in the Euclidian space where q_α is defined, while the mass function $M_{x,m}^2$ is

$$M_{x,m}^2 = (1-x)[m^2 - xp^2]. \quad (\text{A12})$$

By the same notation, dropping a longitudinal term, the integral $K_{\alpha\lambda}$ reads

$$K^{\alpha}_{\lambda}(p) = (3!) \int_0^1 x(1-x) dx \int \frac{d^4 q}{(2\pi)^4} \frac{q^{\alpha} q_{\lambda}}{(q^2 + M_{x,0}^2)^4}. \quad (\text{A13})$$

The integral \tilde{J} is evaluated by dimensional regularization with $d = 4 - 2\epsilon$ and an arbitrary scale factor $\mu^{2\epsilon}$

$$\tilde{J}^{\alpha}_{\lambda}(p, m) = 2\delta^{\alpha}_{\lambda} \left(\frac{d-1}{d}\right) \int_0^1 x dx \frac{\mu^{2\epsilon}}{2^{d-1} \pi^{d/2} \Gamma(d/2)} (M_{x,m})^{d-4} \times \frac{\Gamma(d/2+1)\Gamma(2-d/2)}{2\Gamma(3)}, \quad (\text{A14})$$

yielding

$$\begin{aligned} \int_0^1 x dx &= \frac{1}{2} \\ \int_0^1 x \log(1-x) dx &= -\frac{3}{4} \\ \int_0^1 x \log(1+sx) dx &= \frac{1}{2} \left[L_1(s) - \frac{1}{2} \right] \\ \int_0^1 \frac{sx^3}{(1-x)(1+sx)} dx &= \frac{s}{1+s} \left[\lim_{\eta \rightarrow 0} \int_0^{1-\eta} \frac{x^2}{(1-x)} dx - \int_0^1 \frac{x^2}{(1+sx)} dx \right] \\ &= \frac{s}{1+s} \left[L_2(s) - \frac{3}{2} - \log \eta + \mathcal{O}(\eta) \right], \end{aligned} \quad (\text{A18})$$

where the limit $\eta \rightarrow 0$ must be taken at the end of the calculation in order to deal with the spurious IR divergence which arises in the first integral of the last line. The logarithmic functions L_1, L_2 are defined as

$$\begin{aligned} L_1(s) &= \frac{1}{s} + \frac{s^2-1}{s^2} \log(1+s), \\ L_2(s) &= \frac{1}{s^2} - \frac{1}{2s} - \frac{1}{s^3} \log(1+s), \end{aligned} \quad (\text{A19})$$

where the variable s is the Euclidean squared momentum $s = -p^2/m^2$ in units of the mass parameter m . Inserting these explicit expressions, the integrals \tilde{J}, J and K read

$$\tilde{J}^{\alpha}_{\lambda}(p, m) = \frac{3\delta^{\alpha}_{\lambda}}{32\pi^2} \int_0^1 x dx \left[\frac{1}{\hat{\epsilon}} - \frac{2}{3} - \log \frac{M_{x,m}^2}{m^2} \right], \quad (\text{A15})$$

where the diverging part is

$$\frac{1}{\hat{\epsilon}} = \frac{1}{\epsilon} - \gamma + \log \frac{4\pi\mu^2}{m^2}, \quad (\text{A16})$$

while $J(p, m)$ and $K^{\alpha}_{\lambda}(p)$ are finite in the UV,

$$\begin{aligned} J(p, m) &= -2 \int_0^1 x^3 dx \left[\frac{1}{32\pi^2} \frac{1}{M_{x,m}^2} \right], \\ K^{\alpha}_{\lambda}(p) &= \frac{(3!)\delta^{\alpha}_{\lambda}}{4} \int_0^1 x(1-x) dx \left[\frac{1}{(3!)8\pi^2} \frac{1}{M_{x,0}^2} \right]. \end{aligned} \quad (\text{A17})$$

The remaining integrals are elementary:

$$\begin{aligned} \tilde{J}^{\alpha}_{\lambda}(p, m) &= \frac{3\delta^{\alpha}_{\lambda}}{64\pi^2} \left[\frac{1}{\hat{\epsilon}} + \frac{4}{3} - L_1(s) \right] \\ p^2 J(p, m) &= \frac{2}{32\pi^2} \left(\frac{s}{1+s} \right) \left[L_2(s) - \frac{3}{2} - \log \eta \right] \\ p^2 K^{\alpha}_{\lambda}(p) &= -\frac{\delta^{\alpha}_{\lambda}}{32\pi^2}. \end{aligned} \quad (\text{A20})$$

We observe that, in the limit $s \rightarrow \infty$, which is equivalent to $m \rightarrow 0$, the logarithmic functions $L_1(s), L_2(s)$ have the asymptotic behavior

$$\begin{aligned} L_1(s) &= \log(s) + \frac{2}{s} + \mathcal{O}(s^{-2}), \\ L_2(s) &= -\frac{1}{2s} + \mathcal{O}(s^{-2}) \rightarrow 0. \end{aligned} \quad (\text{A21})$$

Then, we can write

$$(1+s)\tilde{J}^\alpha_\lambda(p,m) - s\tilde{J}^\alpha_\lambda(p,0) = \delta_\lambda^\alpha \frac{3}{64\pi^2} \left[\frac{1}{\hat{\epsilon}} + \frac{4}{3} - (1+s)L_1(s) + s \log s \right],$$

$$(1+s)p^2 J(p,m) - sp^2 J(p,0) = \frac{4}{64\pi^2} [sL_2(s)]. \quad (\text{A22})$$

Because of the transverse projector in Eq. (A5), we can replace $t^\alpha_\lambda(p)$ by δ^α_λ in Eq. (A10) and insert it in Eq. (A8) which reads

$$I^\alpha_\lambda(p) = \frac{\delta_\lambda^\alpha}{64\pi^2} \left[\frac{3}{\hat{\epsilon}} - 3(1+s)L_1(s) + 3s \log s + 4sL_2(s) - 2\xi + 4 \right]. \quad (\text{A23})$$

Finally, the first pair of graphs, (a1) and (a2) in Fig. 2, give the pure transverse sum

$$2\mathcal{F}^{\mu\nu}_{(a1+a2)}(p) = \frac{g^2 N}{64\pi^2} \frac{t^{\mu\nu}(p)}{p^2 - m^2} \left[\frac{3}{\hat{\epsilon}} - 3(1+s)L_1(s) + 3s \log s + 4sL_2(s) - 2\xi + 4 \right]. \quad (\text{A24})$$

We notice the presence of the transverse part of the bare massive propagator $\Delta_m(p)$, as a factor which arises from the external gluon leg. As a check, in the limit $m \rightarrow 0$, which is equivalent to $s \rightarrow \infty$, we recover the same result—modulo irrelevant constants—that was found in Ref. [74] by standard perturbation theory, namely

$$[2\mathcal{F}^{\mu\nu}_{(a1+a2)}(p)]_{m=0} = \frac{g^2 N}{64\pi^2} \frac{t^{\mu\nu}(p)}{p^2} \times \left[\frac{3}{\hat{\epsilon}} - 3 \log(-p^2/m^2) - 2\xi - 4 \right]. \quad (\text{A25})$$

2. Graphs (b1) and (b2)

The second pair of graphs, (b1) and (b2) in Fig. 2, have no internal gluon lines and there are no masses in the internal propagators. Thus, the result is the same as for standard perturbation theory, apart from the external bare gluon line. As a check of consistence, here we recover the explicit result of Ref. [74] by our notation. The graph (b1) gives

$$2\mathcal{F}^{\mu\nu}_{ab}(p) = -(-ip^\mu) \left(\frac{i}{p^2} \right) p_\alpha g f^{dac} \int \frac{d^4 k}{(2\pi)^4} \left[-\frac{(p-k)^\alpha}{(p-k)^2} \right] \times \left[\frac{i}{k^2} \right] \left[\frac{i}{(p-k)^2} \right] [k_\lambda g f^{bcd}] i\Delta_m^{\lambda\nu}(p), \quad (\text{A26})$$

and dropping the δ_{ab} which arises from the sum over color indices

$$2\mathcal{F}^{\mu\nu}(p) = -ig^2 N \frac{p^\mu p_\alpha}{p^2} \int \frac{d^4 k}{(2\pi)^4} \frac{(p-k)^\alpha k_\lambda}{(p-k)^4 k^2} \Delta_m^{\lambda\nu}(p). \quad (\text{A27})$$

According to Eq. (47), the sum of the second pair of graphs, (b1) and (b2) in Fig. 2, can be written as

$$2\mathcal{F}^{\mu\nu}_{(b1+b2)}(p) = ig^2 N t^\mu_\alpha(p) \Delta_m^{\lambda\nu}(p) \int \frac{d^4 k}{(2\pi)^4} \frac{(p-k)^\alpha k_\lambda}{(p-k)^4 k^2} = g^2 N t^\mu_\alpha(p) T^\alpha_\lambda(p) \Delta_m^{\lambda\nu}(p), \quad (\text{A28})$$

where, dropping a longitudinal term, the integral $T^\alpha_\lambda(p)$ is

$$T^\alpha_\lambda(p) = -i \int \frac{d^4 k}{(2\pi)^4} \frac{k^\alpha k_\lambda}{(p-k)^4 k^2}. \quad (\text{A29})$$

By Feynman parametrization and, again, neglecting odd and longitudinal terms, the integral can be evaluated in the Euclidean space and reads

$$T^\alpha_\lambda(p) = 2 \int_0^1 x dx \int \frac{d^d q}{(2\pi)^d} \frac{q^\alpha q_\lambda}{(q^2 + M_{x,0}^2)^3} = \left(\frac{1}{d-1} \right) \tilde{J}^\alpha_\lambda(p,0). \quad (\text{A30})$$

By dimensional regularization, adding the factor $(d-1)^{-1} \approx (1/3)(1+2\epsilon/3)$ and using the asymptotic behavior of $L_1(s)$, Eq. (A21), the integral follows from the first line of Eq. (A20),

$$T^\alpha_\lambda(p) = \frac{\delta_\lambda^\alpha}{64\pi^2} \left[\frac{1}{\hat{\epsilon}} + 2 - \log(s) \right], \quad (\text{A31})$$

and by insertion in Eq. (A28) we obtain the final result

$$2\mathcal{F}^{\mu\nu}_{(b1+b2)}(p) = -\frac{g^2 N}{64\pi^2} \frac{t^{\mu\nu}(p)}{p^2 - m^2} \left[\frac{1}{\hat{\epsilon}} - \log(-p^2/m^2) + 2 \right], \quad (\text{A32})$$

which agrees with Ref. [74], apart from the denominator, $p^2 - m^2$, which arises from the external gluon leg and is replaced by the bare denominator, p^2 , in the standard perturbation theory.

3. Total one-loop contribution

The sum of all the uncrossed one-loop graphs in Fig. 2 gives

$$2\mathcal{F}^{\mu\nu}(p) = \frac{g^2 N}{64\pi^2} \frac{t^{\mu\nu}(p)}{p^2 - m^2} \left[\frac{2}{\hat{\epsilon}} - 3L(-p^2/m^2) + \log(-p^2/m^2) - 2\xi - 6 \right], \quad (\text{A33})$$

where the logarithmic function $L(s)$ is defined as

$$\begin{aligned} L(s) &= (1+s)L_1(s) - s \log s - 2 - \left[\frac{4s}{3}L_2(s) + \frac{2}{3} \right] \\ &= \frac{1+s}{s} + \frac{(1+s)(s^2-1)}{s^2} \log(1+s) - 2 - s \log s - \frac{4}{3} \left[\frac{1}{s} - \frac{1}{s^2} \log(1+s) \right] \end{aligned} \quad (\text{A34})$$

and has the leading behavior $L(s) \sim \log s$ in the limit $s \rightarrow \infty$ or $m \rightarrow 0$.

In the limit $m \rightarrow 0$, modulo an irrelevant constant, we recover the result of standard perturbation theory [74]

$$[2\mathcal{F}^{\mu\nu}(p)]_{m=0} = \frac{g^2 N}{64\pi^2} \frac{t^{\mu\nu}(p)}{p^2} \left[\frac{2}{\hat{\epsilon}} - 2 \log(-p^2/m^2) - 2\xi - 6 \right]. \quad (\text{A35})$$

-
- [1] J. M. Cornwall, *Phys. Rev. D* **26**, 1453 (1982).
 - [2] C. W. Bernard, *Nucl. Phys.* **B219**, 341 (1983).
 - [3] J. F. Donoghue, *Phys. Rev. D* **29**, 2559 (1984).
 - [4] O. Philipsen, *Nucl. Phys.* **B628**, 167 (2002).
 - [5] O. Oliveira and P. Bicudo, *J. Phys. G* **38**, 045003 (2011).
 - [6] A. C. Aguilar and A. A. Natale, *J. High Energy Phys.* **08** (2004) 057.
 - [7] D. Binosi, L. Chang, J. Papavassiliou, and C. D. Roberts, *Phys. Lett. B* **742**, 183 (2015).
 - [8] A. Cucchieri and T. Mendes, *Proc. Sci.*, LAT2007 (2007) 297.
 - [9] A. Cucchieri and T. Mendes, *Phys. Rev. D* **78**, 094503 (2008).
 - [10] A. Cucchieri and T. Mendes, *Phys. Rev. Lett.* **100**, 241601 (2008).
 - [11] A. Cucchieri and T. Mendes, *Proc. Sci.*, QCD-TNT09 (2009) 026.
 - [12] I. L. Bogolubsky, E. M. Ilgenfritz, M. Muller-Preussker, and A. Sternbeck, *Phys. Lett. B* **676**, 69 (2009).
 - [13] O. Oliveira and P. Silva, *Proc. Sci.*, LAT2009 (2009) 226.
 - [14] D. Dudal, O. Oliveira, and N. Vandersickel, *Phys. Rev. D* **81**, 074505 (2010).
 - [15] A. Ayala, A. Bashir, D. Binosi, M. Cristoforetti, and J. Rodriguez-Quintero, *Phys. Rev. D* **86**, 074512 (2012).
 - [16] O. Oliveira and P. J. Silva, *Phys. Rev. D* **86**, 114513 (2012).
 - [17] G. Burgio, M. Quandt, H. Reinhardt, and H. Vogt, *Phys. Rev. D* **92**, 034518 (2015).
 - [18] A. G. Duarte, O. Oliveira, and P. J. Silva, *Phys. Rev. D* **94**, 014502 (2016).
 - [19] A. C. Aguilar, D. Binosi, and J. Papavassiliou, *Phys. Rev. D* **78**, 025010 (2008).
 - [20] A. C. Aguilar and J. Papavassiliou, *Phys. Rev. D* **81**, 034003 (2010).
 - [21] A. C. Aguilar, D. Binosi, and J. Papavassiliou, *Phys. Rev. D* **89**, 085032 (2014).
 - [22] A. C. Aguilar, D. Binosi, and J. Papavassiliou, *Phys. Rev. D* **91**, 085014 (2015).
 - [23] C. S. Fischer, A. Maas, and J. M. Pawłowski, *Ann. Phys. (Amsterdam)* **324**, 2408 (2009).
 - [24] A. L. Blum, M. Q. Huber, M. Mitter, and L. von Smekal, *Phys. Rev. D* **89**, 061703 (2014).
 - [25] M. Q. Huber, *Phys. Rev. D* **91**, 085018 (2015).
 - [26] A. K. Cyrol, M. Q. Huber, and L. von Smekal, *Eur. Phys. J. C* **75**, 102 (2015).
 - [27] J. Braun, H. Gies, and J. M. Pawłowski, *Phys. Lett. B* **684**, 262 (2010).
 - [28] J. Braun, A. Eichhorn, H. Gies, and J. M. Pawłowski, *Eur. Phys. J. C* **70**, 689 (2010).
 - [29] L. Fister and J. M. Pawłowski, *Phys. Rev. D* **88**, 045010 (2013).
 - [30] F. Siringo, *Phys. Rev. D* **90**, 094021 (2014).
 - [31] F. Siringo, *Phys. Rev. D* **92**, 074034 (2015).
 - [32] P. Watson and H. Reinhardt, *Phys. Rev. D* **82**, 125010 (2010).

- [33] P. Watson and H. Reinhardt, *Phys. Rev. D* **85**, 025014 (2012).
- [34] E. Rojas, J. de Melo, B. El-Bennich, O. Oliveira, and T. Frederico, *J. High Energy Phys.* **10** (2013) 193.
- [35] F. Siringo, *Mod. Phys. Lett. A* **29**, 1450026 (2014).
- [36] F. Siringo, *Phys. Rev. D* **89**, 025005 (2014).
- [37] F. Siringo, *Phys. Rev. D* **88**, 056020 (2013).
- [38] C. Feuchter and H. Reinhardt, *Phys. Rev. D* **70**, 105021 (2004).
- [39] H. Reinhardt and C. Feuchter, *Phys. Rev. D* **71**, 105002 (2005).
- [40] M. Quandt, H. Reinhardt, and J. Heffner, *Phys. Rev. D* **89**, 065037 (2014).
- [41] F. Siringo, arXiv:1701.00286.
- [42] G. Comitini and F. Siringo, *Phys. Rev. D* **97**, 056013 (2018).
- [43] A. Cucchieri, T. Mendes, and E. M. Santos, *Phys. Rev. Lett.* **103**, 141602 (2009).
- [44] A. Cucchieri, T. Mendes, and E. M. S. Santos, *Proc. Sci., QCD-TNT09* (2009) 009.
- [45] A. Cucchieri, T. Mendes, G. M. Nakamura, and E. M. Santos, *Proc. Sci., FACESQCD2010* (2010) 026.
- [46] P. Bicudo, D. Binosi, N. Cardoso, O. Oliveira, and P. J. Silva, *Phys. Rev. D* **92**, 114514 (2015).
- [47] F. Gao, S.-X. Qin, C. D. Roberts, and J. Rodriguez-Quintero, *Phys. Rev. D* **97**, 034010 (2018).
- [48] F. Siringo, arXiv:1509.05891.
- [49] F. Siringo, *Nucl. Phys.* **B907**, 572 (2016).
- [50] F. Siringo, *Phys. Rev. D* **94**, 114036 (2016).
- [51] F. Siringo, *EPJ Web Conf.* **137**, 13016 (2017).
- [52] F. Siringo and G. Comitini, *Phys. Rev. D* **98**, 034023 (2018).
- [53] G. Comitini and F. Siringo, *Phys. Rev. D* **102**, 094002 (2020).
- [54] F. Siringo, *Phys. Rev. D* **100**, 074014 (2019).
- [55] F. Siringo, *Phys. Rev. D* **99**, 094024 (2019).
- [56] F. Siringo, *Phys. Rev. D* **96**, 114020 (2017).
- [57] F. Siringo and G. Comitini, *Phys. Rev. D* **103**, 074014 (2021).
- [58] G. Comitini, D. Rizzo, M. Battello, and F. Siringo, *Phys. Rev. D* **104**, 074020 (2021).
- [59] D. Dudal, J. A. Gracey, S. P. Sorella, N. Vandersickel, and H. Verschelde, *Phys. Rev. D* **78**, 065047 (2008).
- [60] M. A. L. Capri, D. Dudal, A. D. Pereira, D. Fiorentini, M. S. Guimaraes, B. W. Mintz, L. F. Palhares, and S. P. Sorella, *Phys. Rev. D* **95**, 045011 (2017).
- [61] D. Dudal, O. Oliveira, and N. Vandersickel, *Phys. Rev. D* **81**, 074505 (2010).
- [62] D. Dudal, M. S. Guimaraes, and S. P. Sorella, *Phys. Rev. Lett.* **106**, 062003 (2011).
- [63] D. Dudal, O. Oliveira, and P. J. Silva, *Ann. Phys. (Amsterdam)* **397**, 351 (2018).
- [64] M. Stingl, *Phys. Rev. D* **34**, 3863 (1986); **36**, 651(E) (1987).
- [65] M. Stingl, *Z. Phys. A* **353**, 423 (1996).
- [66] Y. Hayashi and K-I Kondo, *Phys. Rev. D* **101**, 074044 (2020).
- [67] Y. Hayashi and K-I Kondo, *Phys. Rev. D* **103**, L111504 (2021).
- [68] F. Siringo, *EPJ Web Conf.* **137**, 13017 (2017).
- [69] J. Horak, J. M. Pawłowski, and N. Wink, arXiv:2202.09333.
- [70] Ph. Boucaud, F. De Soto, J. Rodriguez-Quintero, and S. Zafeiropoulos, *Phys. Rev. D* **96**, 098501 (2017).
- [71] L. Baulieu, D. Dudal, M. S. Guimaraes, M. Q. Huber, S. P. Sorella, N. Vandersickel, and D. Zwanziger, *Phys. Rev. D* **82**, 025021 (2010).
- [72] N. K. Nielsen, *Nucl. Phys.* **B97**, 527 (1975); **B101**, 173 (1975).
- [73] R. Kobes, G. Kunstatter, and A. Rebhan, *Phys. Rev. Lett.* **64**, 2992 (1990).
- [74] J. C. Breckenridge, M. J. Lavelle, and T. G. Steele, *Z. Phys. C* **65**, 155 (1995).
- [75] A. C. Aguilar, D. Binosi, and J. Papavassiliou, *Phys. Rev. D* **91**, 085014 (2015).
- [76] M. Napetschnig, R. Alkofer, M. Q. Huber, and J. M. Pawłowski, *Phys. Rev. D* **104**, 054003 (2021).
- [77] M. Tissier and N. Wschebor, *Phys. Rev. D* **82**, 101701(R) (2010).
- [78] M. Tissier and N. Wschebor, *Phys. Rev. D* **84**, 045018 (2011).
- [79] M. Pelaez, M. Tissier, and N. Wschebor, *Phys. Rev. D* **90**, 065031 (2014).
- [80] U. Reinosa, J. Serreau, M. Tissier, and N. Wschebor, *Phys. Rev. D* **89**, 105016 (2014).
- [81] U. Reinosa, J. Serreau, M. Tissier, and N. Wschebor, *Phys. Rev. D* **96**, 014005 (2017).
- [82] M. Pelaez, U. Reinosa, J. Serreau, M. Tissier, and N. Wschebor, *Phys. Rev. D* **96**, 114011 (2017).
- [83] M. Pelaez, U. Reinosa, J. Serreau, M. Tissier, and N. Wschebor, *Rep. Prog. Phys.* **84**, 124202 (2021).
- [84] M. E. Peskin and D. V. Schroeder, *An Introduction to Quantum Field Theory* (CRC Press, Boca Raton, 1996).
- [85] P. M. Stevenson, *Nucl. Phys.* **B868**, 38 (2013); **B910**, 469 (2016).
- [86] P. M. Stevenson, *Renormalized Perturbation Theory and Its Optimization by the Principle of Minimal Sensitivity* (World Scientific, Singapore, 2022).

Bibliography

- [AB98] D. Atkinson and J. C. R. Bloch, *QCD in the infrared with exact angular Integrations*, Mod. Phys. Lett. **A13**, 1055 (1998), URL <https://doi.org/10.1142/S0217732398001121>.
- [ABB⁺12] A. Ayala, A. Bashir, D. Binosi, M. Cristoforetti, and J. Rodríguez-Quintero, *Quark flavour effects on gluon and ghost propagators*, Phys. Rev. **D86**, 074512 (2012), URL <https://doi.org/10.1103/PhysRevD.86.074512>.
- [ABC⁺22] Y. Aoki, T. Blum, G. Colangelo, S. Collins, M. Della Morte, P. Dimopoulos, S. Dürr, *et al.*, *FLAG Review 2021*, Eur. Phys. J. **C82**, 869 (2022), URL <https://doi.org/10.1140/epjc/s10052-022-10536-1>.
- [ABD⁺04] C. Aubin, C. Bernard, C. DeTar, J. Osborn, S. Gottlieb, E. B. Gregory, D. Toussaint, *et al.*, *Light hadrons with improved staggered quarks: Approaching the continuum limit*, Phys. Rev. **D70**, 094505 (2004), URL <https://doi.org/10.1103/PhysRevD.70.094505>.
- [ABP08] A. C. Aguilar, D. Binosi, and J. Papavassiliou, *Gluon and ghost propagators in the Landau gauge: Deriving lattice results from Schwinger-Dyson equations*, Phys. Rev. **D78**, 025010 (2008), URL <https://doi.org/10.1103/PhysRevD.78.025010>.
- [ABP16] A. C. Aguilar, D. Binosi, and J. Papavassiliou, *The gluon mass generation mechanism: A concise primer*, Front. Phys. **11**, 111203 (2016), URL <https://doi.org/10.1007/s11467-015-0517-6>.
- [ADJ⁺14] C. Alexandrou, V. Drach, K. Jansen, C. Kallidonis, and G. Koutsou, *Baryon spectrum with $N_f = 2+1+1$ twisted mass fermions*, Phys. Rev. **D90**, 074501 (2014), URL <https://doi.org/10.1103/PhysRevD.90.074501>.
- [ADK22] C. Amsler, T. DeGrand, and B. Krusche, *Quark model*, Review of Particle Physics – Prog. Theor. Exp. Phys. **2022**, 083C01 (2022), URL <https://doi.org/ptep/ptac097>.
- [ADSF⁺22] A. C. Aguilar, F. De Soto, M. N. Ferreira, J. Papavassiliou, F. Pinto-Gómez, C. D. Roberts, and J. Rodríguez-Quintero, *Schwinger mechanism for gluons from lattice QCD* (2022), URL <https://arxiv.org/abs/2211.12594>.
- [AEF⁺06] Y. Aoki, G. Endrődi, Z. Fodor, S. D. Katz, and K. K. Szabó, *The order of the quantum chromodynamics transition predicted by the standard model of particle physics*, Nature **443**, 675 (2006), URL <https://doi.org/10.1038/nature05120>.

- [AII⁺09] S. Aoki, K.-I. Ishikawa, N. Ishizuka, T. Izubuchi, D. Kadoh, K. Kanaya, Y. Kuramashi, *et al.*, *2+1 flavor lattice QCD toward the physical point*, Phys. Rev. **D79**, 034503 (2009), URL <https://doi.org/10.1103/PhysRevD.79.034503>.
- [AK17] C. Alexandrou and C. Kallidonis, *Low-lying baryon masses using $N_f = 2$ twisted mass clover-improved fermions directly at the physical pion mass*, Phys. Rev. **D96**, 034511 (2017), URL <https://doi.org/10.1103/PhysRevD.96.034511>.
- [AN04] A. C. Aguilar and A. A. Natale, *A dynamical gluon mass solution in a coupled system of the Schwinger-Dyson equations*, J. High Energy Phys. **2004**, 057 (2004), URL <https://doi.org/10.1088/1126-6708/2004/08/057>.
- [AP06] A. C. Aguilar and J. Papavassiliou, *Gluon mass generation in the PT-BFM scheme*, J. High Energy Phys. **2006**, 012 (2006), URL <https://doi.org/10.1088/1126-6708/2006/12/012>.
- [AP08] A. C. Aguilar and J. Papavassiliou, *Power-law running of the effective gluon mass*, Eur. Phys. J. **A35**, 189 (2008), URL <https://doi.org/10.1140/epja/i2008-10535-4>.
- [BBB⁺75] B. C. Barish, J. F. Bartlett, D. Buchholz, T. Humphrey, F. S. Merritt, F. J. Sciulli, L. Stutte, *et al.*, *Measurement of neutrino and antineutrino total cross sections at high energy*, Phys. Rev. Lett. **35**, 1316 (1975), URL <https://doi.org/10.1103/PhysRevLett.35.1316>.
- [BBB⁺79] D. P. Barber, U. Becker, H. Benda, A. Boehm, J. G. Branson, J. Bron, D. Buikman, *et al.*, *Discovery of three-jet events and a test of Quantum Chromodynamics at PETRA*, Phys. Rev. Lett. **43**, 830 (1979), URL <https://doi.org/10.1103/PhysRevLett.43.830>.
- [BBB⁺15] J. A. Bailey, A. Bazavov, C. Bernard, C. M. Bouchard, C. DeTar, D. Du, A. X. El-Khadra, *et al.*, *$|V_{ub}|$ from $B \rightarrow \pi \ell \nu$ decays and $(2+1)$ -flavor lattice QCD*, Phys. Rev. **D92**, 014024 (2015), URL <https://doi.org/10.1103/PhysRevD.92.014024>.
- [BBC⁺12] A. Bazavov, T. Bhattacharya, M. Cheng, C. DeTar, H.-T. Ding, S. Gottlieb, R. Gupta, *et al.*, *Chiral and deconfinement aspects of the QCD transition*, Phys. Rev. **D85**, 054503 (2012), URL <https://doi.org/10.1103/PhysRevD.85.054503>.
- [BBC⁺15] P. Bicudo, D. Binosi, N. Cardoso, O. Oliveira, and P. J. Silva, *The lattice gluon propagator in renormalizable ξ gauges*, Phys. Rev. **D92**, 114514 (2015), URL <https://doi.org/10.1103/PhysRevD.92.114514>.
- [BBD⁺14] A. Bazavov, T. Bhattacharya, C. DeTar, H.-T. Ding, S. Gottlieb, R. Gupta, P. Hegde, *et al.*, *Equation of state in $(2+1)$ -flavor QCD*, Phys. Rev. **D90**, 094503 (2014), URL <https://doi.org/10.1103/PhysRevD.90.094503>.
- [BBDS⁺14] P. Boucaud, M. Brinet, F. De Soto, V. Morénas, O. Pène, K. Petrov, and J. Rodríguez-Quintero, *Three-gluon running coupling from lattice QCD at $N_f = 2 + 1 + 1$: a consistency check of the OPE approach*, J. High Energy

- Phys. **2014**, 086 (2014), URL [https://doi.org/10.1007/JHEP04\(2014\)086](https://doi.org/10.1007/JHEP04(2014)086).
- [BBG⁺79] R. Brandelik, W. Braunschweig, K. Gather, V. Kadansy, K. Lübelmeyer, P. Mättig, H.-U. Martyn, *et al.*, *Evidence for planar events in e^+e^- annihilation at high energies*, Phys. Lett. **B86**, 243 (1979), URL [https://doi.org/10.1016/0370-2693\(79\)90830-X](https://doi.org/10.1016/0370-2693(79)90830-X).
- [BBG⁺80] R. Brandelik, W. Braunschweig, K. Gather, V. Kadansy, F. J. Kirschfink, K. Lübelmeyer, H.-U. Martyn, *et al.*, *Evidence for a spin-1 gluon in three-jet events*, Phys. Lett. **B97**, 453 (1980), URL [https://doi.org/10.1016/0370-2693\(80\)90639-5](https://doi.org/10.1016/0370-2693(80)90639-5).
- [BBG⁺11] W. Bietenholz, V. Bornyakov, M. Göckeler, R. Horsley, W. G. Lockhart, Y. Nakamura, H. Perlt, *et al.*, *Flavor blindness and patterns of flavor symmetry breaking in lattice simulations of up, down, and strange quarks*, Phys. Rev. **D84**, 054509 (2011), URL <https://doi.org/10.1103/PhysRevD.84.054509>.
- [BBL⁺01] F. D. R. Bonnet, P. O. Bowman, D. B. Leinweber, A. G. Williams, and J. M. Zanotti, *Infinite volume and continuum limits of the Landau-gauge gluon propagator*, Phys. Rev. **D64**, 034501 (2001), URL <https://doi.org/10.1103/PhysRevD.64.034501>.
- [BBLW00] F. D. R. Bonnet, P. O. Bowman, D. B. Leinweber, and A. G. Williams, *Infrared behavior of the gluon propagator on a large volume lattice*, Phys. Rev. **D62**, 051501 (2000), URL <https://doi.org/10.1103/PhysRevD.62.051501>.
- [BCD⁺69] E. D. Bloom, D. H. Coward, H. DeStaebler, J. Drees, G. Miller, L. W. Mo, R. E. Taylor, *et al.*, *High-energy inelastic $e-p$ scattering at 6° and 10°* , Phys. Rev. Lett. **23**, 930 (1969), URL <https://doi.org/10.1103/PhysRevLett.23.930>.
- [BCD⁺80] W. Bartel, D. Canzler, T. Cords, P. Dittmann, R. Eichler, R. Felst, D. Haidt, and S. Kawabata, *Observation of planar three-jet events in e^+e^- annihilation and evidence for gluon bremsstrahlung*, Phys. Lett. **B91**, 141 (1980), URL [https://doi.org/10.1016/0370-2693\(80\)90680-2](https://doi.org/10.1016/0370-2693(80)90680-2).
- [BCF⁺80] H. Behrend, C. Chen, J. Field, U. Guempel, V. Schröder, H. Sindt, W. Apel, *et al.*, *Topology of hadronic e^+e^- annihilation events at 22 and 34 GeV CM energy*, Phys. Lett. **B110**, 329 (1980), URL [https://doi.org/10.1016/0370-2693\(82\)91266-7](https://doi.org/10.1016/0370-2693(82)91266-7).
- [BCK17] P. A. Baikov, K. G. Chetyrkin, and J. H. Kühn, *Five-loop running of the QCD coupling constant*, Phys. Rev. Lett. **118**, 082002 (2017), URL <https://doi.org/10.1103/PhysRevLett.118.082002>.
- [BDD⁺78] P. C. Bosetti, H. Deden, M. Deutschmann, P. Fritze, H. Grässler, F. J. Hasert, J. Morfin, *et al.*, *Analysis of nucleon structure functions in CERN bubble chamber neutrino experiments*, Nucl. Phys. **B142**, 1 (1978), URL [https://doi.org/10.1016/0550-3213\(78\)90399-1](https://doi.org/10.1016/0550-3213(78)90399-1).

- [BDDP⁺11] C. Bernard, C. DeTar, M. Di Pierro, A. X. El-Khadra, R. T. Evans, E. D. Freeland, E. Gámiz, *et al.*, *Tuning Fermilab heavy quarks in 2 + 1 flavor lattice QCD with application to hyperfine splittings*, Phys. Rev. **D83**, 034503 (2011), URL <https://doi.org/10.1103/PhysRevD.83.034503>.
- [BDMO14] Z. S. Brown, W. Detmold, S. Meinel, and K. Orginos, *Charmed bottom baryon spectroscopy from lattice QCD*, Phys. Rev. **D90**, 094507 (2014), URL <https://doi.org/10.1103/PhysRevD.90.094507>.
- [BFK⁺69] M. Breidenbach, J. I. Friedman, H. W. Kendall, E. D. Bloom, D. H. Coward, H. DeStaebler, J. Drees, *et al.*, *Observed behavior of highly inelastic electron-proton scattering*, Phys. Rev. Lett. **23**, 935 (1969), URL <https://doi.org/10.1103/PhysRevLett.23.935>.
- [BGG⁺79] C. Berger, H. Genzel, R. Grigull, W. Lackas, F. Raupach, A. Klovning, E. Lillestöl, *et al.*, *Evidence for gluon bremsstrahlung in e^+e^- annihilations at high energies*, Phys. Lett. **B86**, 418 (1979), URL [https://doi.org/10.1016/0370-2693\(79\)90869-4](https://doi.org/10.1016/0370-2693(79)90869-4).
- [BGG⁺80] C. Berger, H. Genzel, R. Grigull, W. Lackas, F. Raupach, A. Klovning, E. Lillestöl, *et al.*, *A study of multi-jet events in e^+e^- annihilation*, Phys. Lett. **B97**, 459 (1980), URL [https://doi.org/10.1016/0370-2693\(80\)90640-1](https://doi.org/10.1016/0370-2693(80)90640-1).
- [BGPR21] N. Barrios, J. A. Gracey, M. Peláez, and U. Reinosa, *Precision QCD propagators with dynamical quarks from the Curci-Ferrari model*, Phys. Rev. **D104**, 094019 (2021), URL <https://doi.org/10.1103/PhysRevD.104.094019>.
- [BHL⁺04] P. O. Bowman, U. M. Heller, D. B. Leinweber, M. B. Parappilly, and A. G. Williams, *Unquenched gluon propagator in Landau gauge*, Phys. Rev. **D70**, 034509 (2004), URL <https://doi.org/10.1103/PhysRevD.70.034509>.
- [BHL⁺07] P. O. Bowman, U. M. Heller, D. B. Leinweber, M. B. Parappilly, A. Sternbeck, L. von Smekal, A. G. Williams, *et al.*, *Scaling behavior and positivity violation of the gluon propagator in full QCD*, Phys. Rev. **D76**, 094505 (2007), URL <https://doi.org/10.1103/PhysRevD.76.094505>.
- [BIMPS09] I. L. Bogolubsky, E.-M. Ilgenfritz, M. Müller-Preussker, and A. Sternbeck, *Lattice gluodynamics computation of Landau-gauge Green's functions in the deep infrared*, Phys. Lett. **B676**, 69 (2009), URL <https://doi.org/10.1016/j.physletb.2009.04.076>.
- [Bjo69] J. D. Bjorken, *Asymptotic sum rules at infinite momentum*, Phys. Rev. **179**, 1547 (1969), URL <https://doi.org/10.1103/PhysRev.179.1547>.
- [BLLY⁺12] P. Boucaud, J.-P. Leroy, A. Le Yaouanc, J. Micheli, O. Pène, and J. Rodríguez-Quintero, *The infrared behaviour of the Pure Yang-Mills Green functions*, Few-Body Syst. **53**, 387 (2012), URL <https://doi.org/10.1007/s00601-011-0301-2>.
- [BLS95] J. C. Breckenridge, M. J. Lavelle, and T. G. Steele, *The Nielsen identities for the two-point functions of QED and QCD*, Z. Phys. **C65**, 155 (1995), URL <https://doi.org/10.1007/BF01571316>.

- [BLYL⁺01] P. Boucaud, A. Le Yaouanc, J. P. Leroy, J. Micheli, O. Pène, and J. Rodríguez-Quintero, *Testing the Landau gauge operator product expansion on the lattice with a $\langle A^2 \rangle$ condensate*, Phys. Rev. **D63**, 114003 (2001), URL <https://doi.org/10.1103/PhysRevD.63.114003>.
- [BMMP10] V. G. Bornyakov, V. K. Mitrjushkin, and M. Müller-Preussker, *SU(2) lattice gluon propagator: continuum limit, finite-volume effects and infrared mass scale m_{IR}* , Phys. Rev. **D81**, 054503 (2010), URL <https://doi.org/10.1103/PhysRevD.81.054503>.
- [BnLB12] R. A. Briceño, H.-W. Lin, and D. R. Bolton, *Charmed-baryon spectroscopy from lattice QCD with $N_f=2+1+1$ flavors*, Phys. Rev. **D86**, 094504 (2012), URL <https://doi.org/10.1103/PhysRevD.86.094504>.
- [BP69] J. D. Bjorken and E. A. Paschos, *Inelastic electron-proton and γ -proton scattering and the structure of the nucleon*, Phys. Rev. **185**, 1975 (1969), URL <https://doi.org/10.1103/PhysRev.185.1975>.
- [BP92] E. Braaten and R. D. Pisarski, *Simple effective Lagrangian for hard thermal loops*, Phys. Rev. **D45**, R1827 (1992), URL <https://doi.org/10.1103/PhysRevD.45.R1827>.
- [BPRW20] N. Barrios, M. Peláez, U. Reinosa, and N. Wschebor, *The ghost-antighost-gluon vertex from the Curci-Ferrari model: two-loop corrections*, Phys. Rev. **D102**, 114016 (2020), URL <https://doi.org/10.1103/PhysRevD.102.114016>.
- [BRS75] C. Becchi, A. Rouet, and R. Stora, *Renormalization of the abelian Higgs-Kibble model*, Commun. Math. Phys. **42**, 127 (1975), URL <https://doi.org/10.1007/BF01614158>.
- [BRS76] C. Becchi, A. Rouet, and R. Stora, *Renormalization of gauge theories*, Ann. Phys. **98**, 287 (1976), URL [https://doi.org/10.1016/0003-4916\(76\)90156-1](https://doi.org/10.1016/0003-4916(76)90156-1).
- [BTB⁺10] A. Bazavov, D. Toussaint, C. Bernard, J. Laiho, C. DeTar, L. Levkova, M. B. Oktay, *et al.*, *Nonperturbative QCD simulations with 2 + 1 flavors of improved staggered quarks*, Rev. Mod. Phys. **82**, 1349 (2010), URL <https://doi.org/10.1103/RevModPhys.82.1349>.
- [Cal70] C. G. Callan, *Broken scale invariance in scalar field theory*, Phys. Rev. **D2**, 1541 (1970), URL <https://doi.org/10.1103/PhysRevD.2.1541>.
- [CDF⁺15] M. A. L. Capri, D. Dudal, D. Fiorentini, M. S. Guimaraes, I. F. Justo, A. D. Pereira, B. W. Mintz, *et al.*, *An exact nilpotent non-perturbative BRST symmetry for the Gribov-Zwanziger action in the linear covariant gauge*, Phys. Rev. **D92**, 045039 (2015), URL <https://doi.org/10.1103/PhysRevD.92.045039>.
- [CDF⁺16a] M. A. L. Capri, D. Dudal, D. Fiorentini, M. S. Guimaraes, I. F. Justo, B. W. Mintz, L. F. Palhares, *et al.*, *More on the non-perturbative Gribov-Zwanziger quantization of linear covariant gauges*, Phys. Rev. **D93**, 065019 (2016), URL <https://doi.org/10.1103/PhysRevD.93.065019>.

- [CDF⁺16b] M. A. L. Capri, D. Dudal, D. Fiorentini, M. S. Guimaraes, I. F. Justo, A. D. Pereira, B. W. Mintz, *et al.*, *A local and BRST-invariant Yang-Mills theory within the Gribov horizon*, Phys. Rev. **D94**, 025035 (2016), URL <https://doi.org/10.1103/PhysRevD.94.025035>.
- [CDG⁺05] M. A. L. Capri, D. Dudal, J. A. Gracey, V. E. R. Lemes, R. F. Sobreiro, S. P. Sorella, and H. Verschelde, *Study of the gauge invariant, nonlocal mass operator $\text{Tr} \int d^4x F_{\mu\nu}(D^2)^{-1} F_{\mu\nu}$ in Yang-Mills theories*, Phys. Rev. **D72**, 105016 (2005), URL <https://doi.org/10.1103/PhysRevD.72.105016>.
- [CDG⁺18] M. A. L. Capri, D. Dudal, M. S. Guimaraes, A. D. Pereira, B. W. Mintz, L. F. Palhares, and S. P. Sorella, *The universal character of Zwanziger's horizon function in Euclidean Yang-Mills theories*, Phys. Lett. **B781**, 48 (2018), URL <https://doi.org/10.1016/j.physletb.2018.03.058>.
- [CDI⁺10] N. H. Christ, C. Dawson, T. Izubuchi, C. Jung, Q. Liu, R. D. Mawhinney, C. T. Sachrajda, *et al.*, *η and η' mesons from lattice QCD*, Phys. Rev. Lett. **105**, 241601 (2010), URL <https://doi.org/10.1103/PhysRevLett.105.241601>.
- [CDK⁺16] B. Colquhoun, R. J. Dowdall, J. Koponen, C. T. H. Davies, and G. P. Lepage, *$B \rightarrow \pi \ell \nu$ at zero recoil from lattice QCD with physical u/d quarks*, Phys. Rev. **D93**, 034502 (2016), URL <https://doi.org/10.1103/PhysRevD.93.034502>.
- [CDM⁺18] A. Cucchieri, D. Dudal, T. Mendes, O. Oliveira, M. Roelfs, and P. J. Silva, *Faddeev-Popov matrix in linear covariant gauge: First results*, Phys. Rev. **D98**, 091504 (2018), URL <https://doi.org/10.1103/PhysRevD.98.091504>.
- [CDP⁺17] M. A. L. Capri, D. Dudal, A. D. Pereira, D. Fiorentini, M. S. Guimaraes, B. W. Mintz, L. F. Palhares, *et al.*, *Non-perturbative aspects of Euclidean Yang-Mills theories in linear covariant gauges: Nielsen identities and a BRST invariant two-point correlation function*, Phys. Rev. **D95**, 045011 (2017), URL <https://doi.org/10.1103/PhysRevD.95.045011>.
- [CF76] G. Curci and R. Ferrari, *On a class of Lagrangian models for massive and massless Yang-Mills fields*, Nuovo Cim. **A32**, 151 (1976), URL <https://doi.org/10.1007/BF02729999>.
- [CF94] M. Consoli and J. H. Field, *Effective gluon mass and the determination of α_s from J/ψ and Υ branching ratios*, Phys. Rev. **D49**, 1293 (1994), URL <https://doi.org/10.1103/PhysRevD.49.1293>.
- [CF97] M. Consoli and J. H. Field, *Relativistic versus gluon mass effects: the role of $1/Q$ corrections in quarkonia decays*, J. Phys. **G23**, 41 (1997), URL <https://doi.org/10.1088/0954-3899/23/1/004>.
- [CFG⁺16] M. A. L. Capri, D. Fiorentini, M. S. Guimaraes, B. W. Mintz, L. F. Palhares, and S. P. Sorella, *Local and renormalizable framework for the gauge-invariant operator A_{\min}^2 in Euclidean Yang-Mills theories in linear covariant gauges*, Phys. Rev. **D94**, 065009 (2016), URL <https://doi.org/10.1103/PhysRevD.94.065009>.

- [CFHV17] K. G. Chetyrkin, G. Falcioni, F. Herzog, and J. A. M. Vermaseren, *Five-loop renormalisation of QCD in covariant gauges*, J. High Energ. Phys. **2017**, 179 (2017), URL <https://doi.org/10.1007/JHEP10%282017%29179>.
- [CFPS17] M. A. L. Capri, D. Fiorentini, A. D. Pereira, and S. P. Sorella, *Renormalizability of the Refined Gribov-Zwanziger action in the linear covariant gauges*, Phys. Rev. **D96**, 054022 (2017), URL <https://doi.org/10.1103/PhysRevD.96.054022>.
- [CLS22] A. Ceccucci, Z. Ligeti, and Y. Sakai, *CKM quark-mixing matrix*, Review of Particle Physics – Prog. Theor. Exp. Phys. **2022**, 083C01 (2022), URL <https://doi.org/ptep/ptac097>.
- [CM08] A. Cucchieri and T. Mendes, *Constraints on the IR behavior of the gluon propagator in Yang-Mills theories*, Phys. Rev. Lett. **100**, 241601 (2008), URL <https://doi.org/10.1103/PhysRevLett.100.241601>.
- [CMM08] A. Cucchieri, A. Maas, and T. Mendes, *Three-point vertices in Landau-gauge Yang-Mills theory*, Phys. Rev. **D77**, 094510 (2008), URL <https://doi.org/10.1103/PhysRevD.77.094510>, 0803.1798.
- [CNZ99] K. G. Chetyrkin, S. Narison, and V. I. Zakharov, *Short-distance tachyonic gluon mass and $1/Q^2$ corrections*, Nucl. Phys. **B550**, 353 (1999), URL [https://doi.org/10.1016/S0550-3213\(99\)00167-4](https://doi.org/10.1016/S0550-3213(99)00167-4).
- [Col84] J. C. Collins, *Renormalization*, Cambridge University Press (1984), URL <https://doi.org/10.1017/CB09780511622656>.
- [Com19] G. Comitini, *Perturbation theory of non-perturbative Yang-Mills theory: A massive expansion from first principles*, Thesis for the Master's Degree in Physics (2019), URL <https://arxiv.org/abs/1910.13022>.
- [Cor82] J. M. Cornwall, *Dynamical mass generation in continuum quantum chromodynamics*, Phys. Rev. **D26**, 1453 (1982), URL <https://doi.org/10.1103/PhysRevD.26.1453>.
- [CRBS21] G. Comitini, D. Rizzo, M. Battello, and F. Siringo, *Screened massive expansion of the quark propagator in the Landau gauge*, Phys. Rev. **D104**, 074020 (2021), URL <https://doi.org/10.1103/PhysRevD.104.074020>.
- [Cre85] M. Creutz, *Quarks, Gluons and Lattices*, Cambridge University Press (1985), URL <https://doi.org/10.1017/9781009290395>.
- [CS18] G. Comitini and F. Siringo, *Variational study of mass generation and deconfinement in Yang-Mills theory*, Phys. Rev. **D97**, 056013 (2018), URL <https://doi.org/10.1103/PhysRevD.97.056013>.
- [CS20] G. Comitini and F. Siringo, *One-loop RG improvement of the screened massive expansion in the Landau gauge*, Phys. Rev. **D102**, 094002 (2020), URL <https://doi.org/10.1103/PhysRevD.102.094002>.
- [CvEP⁺18] M. A. L. Capri, D. M. van Egmond, G. Peruzzo, M. S. Guimaraes, O. Holanda, S. P. Sorella, R. C. Terin, *et al.*, *On a renormalizable class of gauge fixings for the gauge invariant operator A_{min}^2* , Ann. Phys. **390**, 214 (2018), URL <https://doi.org/10.1016/j.aop.2018.01.009>.

- [Cza05] M. Czakon, *The four-loop QCD beta-function and anomalous dimensions*, Nucl. Phys. **B710**, 485 (2005), URL <https://doi.org/10.1016/j.nuclphysb.2005.01.012>.
- [CZB⁺20] Z.-F. Cui, J.-L. Zhang, D. Binosi, F. De Soto, C. Mezrag, J. Papavassiliou, C. D. Roberts, *et al.*, *Effective charge from lattice QCD*, Chin. Phys. **C44**, 083102 (2020), URL <https://doi.org/10.1088/1674-1137/44/8/083102>.
- [DCMG⁺19] M. Di Carlo, G. Martinelli, D. Giusti, V. Lubicz, C. T. Sachrajda, F. Sanfilippo, S. Simula, *et al.*, *Light-meson leptonic decay rates in lattice QCD + QED*, Phys. Rev. **D100**, 034514 (2019), URL <https://doi.org/10.1103/PhysRevD.100.034514>.
- [DD06] T. DeGrand and C. DeTar, *Lattice Methods for Quantum Chromodynamics*, World Scientific (2006), URL <https://doi.org/10.1142/6065>.
- [DDHH12] R. J. Dowdall, C. T. H. Davies, T. C. Hammant, and R. R. Horgan, *Precise heavy-light meson masses and hyperfine splittings from lattice QCD including charm quarks in the sea*, Phys. Rev. **D86**, 094510 (2012), URL <https://doi.org/10.1103/PhysRevD.86.094510>.
- [DEJ⁺11] J. J. Dudek, R. G. Edwards, B. Joó, M. J. Peardon, D. G. Richards, and C. E. Thomas, *Isoscalar meson spectroscopy from lattice QCD*, Phys. Rev. **D83**, 111502 (2011), URL <https://doi.org/10.1103/PhysRevD.83.111502>.
- [DFF⁺08] S. Dürr, Z. Fodor, J. Frison, C. Hoelbling, R. Hoffmann, S. D. Katz, S. Krieg, *et al.*, *Ab initio determination of light hadron masses*, Science **322** (2008), URL <https://doi.org/10.1126/science.1163233>.
- [DFP⁺19] D. Dudal, C. P. Felix, L. F. Palhares, F. Rondeau, and D. Vercauteren, *The BRST-invariant vacuum state of the Gribov-Zwanziger theory*, Eur. Phys. J. **C79**, 731 (2019), URL <https://doi.org/10.1140/epjc/s10052-019-7235-0>.
- [dGHH⁺79a] J. G. H. de Groot, T. Hansl, M. Holder, J. Knobloch, J. May, H. P. Paar, P. Palazzi, *et al.*, *Comparison of moments from the valence structure function with QCD predictions*, Phys. Lett. **B82**, 292 (1979), URL [https://doi.org/10.1016/0370-2693\(79\)90759-7](https://doi.org/10.1016/0370-2693(79)90759-7).
- [dGHH⁺79b] J. G. H. de Groot, T. Hansl, M. Holder, J. Knobloch, J. May, H. P. Paar, P. Palazzi, *et al.*, *Inclusive interactions of high-energy neutrinos and antineutrinos in iron*, Z. Phys. **C1**, 143 (1979), URL <https://doi.org/10.1007/BF01445406>.
- [dGHH⁺79c] J. G. H. de Groot, T. Hansl, M. Holder, J. Knobloch, J. May, H. P. Paar, P. Palazzi, *et al.*, *QCD analysis of charged-current structure functions*, Phys. Lett. **B82**, 456 (1979), URL [https://doi.org/10.1016/0370-2693\(79\)90266-1](https://doi.org/10.1016/0370-2693(79)90266-1).
- [DGS⁺08] D. Dudal, J. A. Gracey, S. P. Sorella, N. Vandersickel, and H. Verschelde, *Refinement of the Gribov-Zwanziger approach in the Landau gauge: Infrared propagators in harmony with the lattice results*, Phys. Rev. **D78**, 065047 (2008), URL <https://doi.org/10.1103/PhysRevD.78.065047>.

- [DKL⁺19] C. DeTar, A. S. Kronfeld, S.-h. Lee, D. Mohler, and J. N. Simone, *Splittings of low-lying charmonium masses at the physical point*, Phys. Rev. **D99**, 034509 (2019), URL <https://doi.org/PhysRevD.99.034509>.
- [DL89] A. Donnachie and P. V. Landshoff, *Gluon condensate and pomeron structure*, Nucl. Phys. **B311**, 509 (1989), URL [https://doi.org/10.1016/0550-3213\(89\)90165-X](https://doi.org/10.1016/0550-3213(89)90165-X).
- [DM20] T. De Meerleer, *Non-abelian Landau-Khalatnikov-Fradkin transformations and dynamically massive linear covariant gauges*, Ph.D. thesis (2020), URL <https://lirias.kuleuven.be/handle/123456789/660289>.
- [DOS16] A. G. Duarte, O. Oliveira, and P. J. Silva, *Lattice gluon and ghost propagators, and the strong coupling in pure SU(3) Yang-Mills theory: Finite lattice spacing and volume effects*, Phys. Rev. **D94**, 014502 (2016), URL <https://doi.org/10.1103/PhysRevD.94.014502>.
- [DOV10] D. Dudal, O. Oliveira, and N. Vandersickel, *Indirect lattice evidence for the Refined Gribov-Zwanziger formalism and the gluon condensate $\langle A^2 \rangle$ in the Landau gauge*, Phys. Rev. **D81**, 074505 (2010), URL <https://doi.org/10.1103/PhysRevD.81.074505>.
- [DSV11] D. Dudal, S. P. Sorella, and N. Vandersickel, *Dynamical origin of the refinement of the Gribov-Zwanziger theory*, Phys. Rev. **D84**, 065039 (2011), URL <https://doi.org/10.1103/PhysRevD.84.065039>.
- [DSVV08] D. Dudal, S. P. Sorella, N. Vandersickel, and H. Verschelde, *New features of the gluon and ghost propagator in the infrared region from the Gribov-Zwanziger approach*, Phys. Rev. **D77**, 071501(R) (2008), URL <https://doi.org/10.1103/PhysRevD.77.071501>.
- [DvERV22] D. Dudal, D. M. van Egmond, U. Reinosa, and D. Vercauteren, *Polyakov loop, gluon mass, gluon condensate, and its asymmetry near deconfinement*, Phys. Rev. **D106**, 054007 (2022), URL <https://doi.org/10.1103/PhysRevD.106.054007>.
- [DVS03] D. Dudal, H. Verschelde, and S. P. Sorella, *The anomalous dimension of the composite operator A^2 in the Landau gauge*, Phys. Lett. **B555**, 126 (2003), URL [https://doi.org/10.1016/S0370-2693\(03\)00043-1](https://doi.org/10.1016/S0370-2693(03)00043-1).
- [Dys49] F. J. Dyson, *The S Matrix in Quantum Electrodynamics*, Phys. Rev. **75**, 1736 (1949), URL <https://doi.org/10.1103/PhysRev.75.1736>.
- [Dys52] F. J. Dyson, *Divergence of perturbation theory in quantum electrodynamics*, Phys. Rev. **85**, 631 (1952), URL <https://doi.org/10.1103/PhysRev.85.631>.
- [Fey69a] R. P. Feynman, *The behavior of hadron collisions at extreme energies*, Proc. III Intern. Conf. on High Energy Collisions p. 237 (1969), URL https://doi.org/10.1007/978-94-009-3051-3_25.
- [Fey69b] R. P. Feynman, *Very high-energy collisions of hadrons*, Phys. Rev. Lett. **23**, 1415 (1969), URL <https://doi.org/10.1103/PhysRevLett.23.1415>.

- [Fey98] R. P. Feynman, *Statistical Mechanics: A Set of Lectures*, CRC Press (1998), URL <https://doi.org/10.1201/9780429493034>.
- [FGM71] H. Fritzsche and M. Gell-Mann, *Light cone current algebra*, Proc. Intern. Conf. on Duality and Symmetry in Hadron Physics p. 317 (1971), URL <https://arxiv.org/abs/hep-ph/0301127>.
- [FGM72] H. Fritzsche and M. Gell-Mann, *Current algebra: Quarks and what else?*, Proc. XVI Intern. Conf. on High Energy Physics p. 135 (1972), URL <https://arxiv.org/abs/hep-ph/0208010>.
- [FGML73] H. Fritzsche, M. Gell-Mann, and H. Leutwyler, *Advantages of the color octet gluon picture*, Phys. Lett. **B47**, 365 (1973), URL [https://doi.org/10.1016/0370-2693\(73\)90625-4](https://doi.org/10.1016/0370-2693(73)90625-4).
- [Fie94] J. H. Field, *Are gluons massive?*, Int. J. Mod. Phys. **A9**, 3283 (1994), URL <https://doi.org/10.1142/S0217751X94001291>.
- [Fie02] J. H. Field, *Phenomenological analysis of gluon mass effects in inclusive radiative decays of the J/ψ and Υ* , Phys. Rev. **D66**, 013013 (2002), URL <https://doi.org/10.1103/PhysRevD.66.013013>.
- [FIK⁺15] J. M. Flynn, T. Izubuchi, T. Kawanai, C. Lehner, A. Soni, R. S. Van de Water, and O. Witzel, *$B \rightarrow \pi \ell \nu$ and $B_s \rightarrow K \ell \nu$ form factors and $|V_{ub}|$ from $2+1$ -flavor lattice QCD with domain-wall light quarks and relativistic heavy quarks*, Phys. Rev. **D91**, 074510 (2015), URL <https://doi.org/10.1103/PhysRevD.91.074510>.
- [FK72] J. I. Friedman and H. W. Kendall, *Deep inelastic electron scattering*, Ann. Rev. Nucl. Sci. **22**, 203 (1972), URL <https://doi.org/10.1146/annurev.ns.22.120172.001223>.
- [FP67] L. D. Faddeev and V. Popov, *Feynman diagrams for the Yang-Mills field*, Phys. Lett. **B25**, 29 (1967), URL [https://doi.org/10.1016/0370-2693\(67\)90067-6](https://doi.org/10.1016/0370-2693(67)90067-6).
- [GDK⁺11] E. B. Gregory, C. T. H. Davies, I. D. Kendall, J. Koponen, K. Wong, E. Follana, E. Gámiz, *et al.*, *Precise B , B_s , and B_c meson spectroscopy from full lattice QCD*, Phys. Rev. **D83**, 014506 (2011), URL <https://doi.org/10.1103/PhysRevD.83.014506>.
- [GIRM12] E. B. Gregory, A. C. Irving, C. M. Richards, and C. McNeile, *Study of the η and η' mesons with improved staggered fermions*, Phys. Rev. **D86**, 014504 (2012), URL <https://doi.org/10.1103/PhysRevD.86.014504>.
- [GL10] C. Gattringer and C. B. Lang, *Quantum Chromodynamics on the Lattice*, Springer (2010), URL <https://doi.org/10.1007/978-3-642-01850-3>.
- [GLT⁺18] D. Giusti, V. Lubicz, C. Tarantino, G. Martinelli, C. T. Sachrajda, F. Sanfilippo, S. Simula, *et al.*, *First lattice calculation of the QED corrections to leptonic decay rates*, Phys. Rev. Lett **120**, 072001 (2018), URL <https://doi.org/10.1103/PhysRevLett.120.072001>.

- [GM61] M. Gell-Mann, *The Eightfold Way: A Theory of Strong Interaction Symmetry*, California Institute of Technology – Synchrotron Laboratory (1961), URL <https://doi.org/10.2172/4008239>.
- [GM64] M. Gell-Mann, *A schematic model of baryons and mesons*, Phys. Lett. **8**, 214 (1964), URL [https://doi.org/10.1016/S0031-9163\(64\)92001-3](https://doi.org/10.1016/S0031-9163(64)92001-3).
- [GML54] M. Gell-Mann and F. E. Low, *Quantum electrodynamics at small distances*, Phys. Rev. **95**, 1300 (1954), URL <https://doi.org/10.1103/PhysRev.95.1300>.
- [GP17] L. Giusti and M. Pepe, *Equation of state of the $SU(3)$ Yang–Mills theory: A precise determination from a moving frame*, Phys. Lett. **B769**, 385 (2017), URL <https://doi.org/10.1016/j.physletb.2017.04.001>.
- [GPRT19] J. A. Gracey, M. Peláez, U. Reinosa, and M. Tissier, *Two loop calculation of Yang-Mills propagators in the Curci-Ferrari model*, Phys. Rev. **D100**, 034023 (2019), URL <https://doi.org/10.1103/PhysRevD.100.034023>.
- [Gra03] J. A. Gracey, *Three loop \overline{MS} renormalization of the Curci-Ferrari model and the dimension two BRST invariant composite operator in QCD*, Phys. Lett. **B552**, 101 (2003), URL [https://doi.org/10.1016/S0370-2693\(02\)03077-0](https://doi.org/10.1016/S0370-2693(02)03077-0).
- [Gre64] O. W. Greenberg, *Spin and unitary-spin independence in a paraquark model of baryons and mesons*, Phys. Rev. Lett. **13**, 598 (1964), URL <https://doi.org/10.1103/PhysRevLett.13.598>.
- [Gri78] V. N. Gribov, *Quantization of non-abelian gauge theories*, Nucl. Phys. **B139**, 1 (1978), URL [https://doi.org/10.1016/0550-3213\(78\)90175-X](https://doi.org/10.1016/0550-3213(78)90175-X).
- [GSZ01] F. V. Gubarev, L. Stodolsky, and V. I. Zakharov, *On the significance of the vector potential squared*, Phys. Rev. Lett. **86**, 2220 (2001), URL <https://doi.org/10.1103/PhysRevLett.86.2220>.
- [GW73] D. J. Gross and F. Wilczek, *Ultraviolet behavior of non-abelian gauge theories*, Phys. Rev. Lett. **30**, 1343 (1973), URL <https://doi.org/10.1103/PhysRevLett.30.1343>.
- [GZ01] F. V. Gubarev and V. I. Zakharov, *Emerging phenomenology of $\langle A_{min}^2 \rangle$* , Phys. Lett. **B501**, 28 (2001), URL [https://doi.org/10.1016/S0370-2693\(01\)00085-5](https://doi.org/10.1016/S0370-2693(01)00085-5).
- [HAB⁺75] G. Hanson, G. S. Abrams, A. M. Boyarski, M. Breidenbach, F. Bulos, W. Chinowsky, G. J. Feldman, *et al.*, *Evidence for jet structure in hadron production by e^+e^- annihilation*, Phys. Rev. Lett. **35**, 1609 (1975), URL <https://doi.org/10.1103/PhysRevLett.35.1609>.
- [HK19] Y. Hayashi and K.-I. Kondo, *Complex poles and spectral function of Yang-Mills theory*, Phys. Rev. **D99**, 074001 (2019), URL <https://doi.org/10.1103/PhysRevD.99.074001>.
- [HK20] Y. Hayashi and K.-I. Kondo, *Complex poles and spectral functions of Landau gauge QCD and QCD-like theories*, Phys. Rev. **D101**, 074044 (2020), URL <https://doi.org/10.1103/PhysRevD.101.074044>.

- [HKN93] F. Halzen, G. Krein, and A. A. Natale, *Relating the QCD pomeron to an effective gluon mass*, Phys. Rev. **D47**, 295 (1993), URL <https://doi.org/10.1103/PhysRevD.47.295>.
- [HMTZ19] S. Heinemeyer, M. Mondragón, N. Tracas, and G. Zoupanos, *Reduction of couplings and its application in particle physics*, Phys. Rept. **814**, 1 (2019), URL <https://doi.org/j.physrep.2019.04.002>.
- [HN65] M. Y. Han and Y. Nambu, *Three-triplet model with double SU(3) symmetry*, Phys. Rev. **139**, B1006 (1965), URL <https://doi.org/10.1103/PhysRev.139.B1006>.
- [HRU⁺17] F. Herzog, B. Ruijl, T. Ueda, J. A. M. Vermaseren, and A. Vogt, *The five-loop beta function of Yang-Mills theory with fermions*, J. High Energy Phys. **2017**, 90 (2017), URL [https://doi.org/10.1007/JHEP02\(2017\)090](https://doi.org/10.1007/JHEP02(2017)090).
- [HRZ22] J. Huston, K. Rabertz, and G. Zanderighi, *Quantum Chromodynamics*, Review of Particle Physics – Prog. Theor. Exp. Phys. **2022**, 083C01 (2022), URL <https://doi.org/10.1093/ptep/ptac097>.
- [HSL22] S. Hashimoto, S. R. Sharpe, and J. Lahio, *Lattice Quantum Chromodynamics*, Review of Particle Physics – Prog. Theor. Exp. Phys. **2022**, 083C01 (2022), URL <https://doi.org/ptep/ptac097>.
- [HvS13] M. Q. Huber and L. von Smekal, *On the influence of three-point functions on the propagators of Landau gauge Yang-Mills theory*, J. High Energy Phys. **2013**, 149 (2013), URL <https://doi.org/10.1007/JHEP04%282013%29149,1211.6092>.
- [IFL10] B. L. Ioffe, V. S. Fadin, and L. N. Lipatov, *Quantum Chromodynamics: Perturbative and Nonperturbative Aspects*, Cambridge University Press (2010), URL <https://doi.org/10.1017/CB09780511711817>.
- [IM97] M. Istvan and G. Münster, *Quantum Fields on a Lattice*, Cambridge University Press (1997), URL <https://doi.org/10.1017/CB09780511470783>.
- [IMPS⁺07] E.-M. Ilgenfritz, M. Müller-Preussker, A. Sternbeck, A. Schiller, and I. L. Bogolubsky, *Landau gauge gluon and ghost propagators from lattice QCD*, Braz. J. Phys. **37**, 193 (2007), URL <https://doi.org/10.1590/S0103-97332007000200006>.
- [ISI09] T. Iritani, H. Suganuma, and H. Iida, *Gluon-propagator functional form in the Landau gauge in SU(3) lattice QCD: Yukawa-type gluon propagator and anomalous gluon spectral function*, Phys. Rev. **D80**, 114505 (2009), URL <https://doi.org/10.1103/PhysRevD.80.114505>.
- [IZ06] C. Itzykson and J. Zuber, *Quantum Field Theory*, McGraw-Hill (2006).
- [JA90] C.-R. Ji and F. Amiri, *Perturbative QCD analysis of pion and kaon form factors and pair production in photon-photon collisions using a frozen coupling constant*, Phys. Rev. **D42**, 3764 (1990), URL <https://doi.org/10.1103/PhysRevD.42.3764>.

- [JP97] R. Jackiw and S.-Y. Pi, *Seeking an even-parity mass term for 3-D gauge theory*, Phys. Lett. **B403**, 297 (1997), URL [https://doi.org/10.1016/S0370-2693\(97\)00520-0](https://doi.org/10.1016/S0370-2693(97)00520-0).
- [Kas92] B. M. Kastening, *Renormalization group improvement of the effective potential in massive ϕ^4 theory*, Phys. Lett. **B283**, 287 (1992), URL [https://doi.org/10.1016/0370-2693\(92\)90021-U](https://doi.org/10.1016/0370-2693(92)90021-U).
- [KBL⁺05] W. Kamleh, P. O. Bowman, D. B. Leinweber, A. G. Williams, and J. Zhang, *Fat link irrelevant clover overlap quark propagator*, Phys. Rev. **D71**, 094507 (2005), URL <https://doi.org/10.1103/PhysRevD.71.094507>.
- [KG06] J. I. Kapusta and G. Gale, *Finite-Temperature Field Theory: Principles and Applications*, Cambridge University Press (2006), URL <https://doi.org/10.1017/CB09780511535130>.
- [KO78a] T. Kugo and I. Ojima, *Manifestly covariant canonical formulation of the Yang-Mills field theories I: General formalism*, Prog. Teor. Phys. **60**, 1869 (1978), URL <https://doi.org/10.1143/PTP.60.1869>.
- [KO78b] T. Kugo and I. Ojima, *Manifestly covariant canonical formulation of Yang-Mills theories physical state subsidiary conditions and physical S-matrix unitarity*, Phys. Lett. **B73**, 459 (1978), URL [https://doi.org/10.1016/0370-2693\(78\)90765-7](https://doi.org/10.1016/0370-2693(78)90765-7).
- [KO79a] T. Kugo and I. Ojima, *Local covariant operator formalism of non-abelian gauge theories and quark confinement problem*, Prog. Teor. Phys. Suppl. **66**, 1 (1979), URL <https://doi.org/10.1143/PTPS.66.1>.
- [KO79b] T. Kugo and I. Ojima, *Manifestly covariant canonical formulation of the Yang-Mills field theories II: SU(2) Higgs-Kibble Model with spontaneous symmetry breaking*, Prog. Teor. Phys. **61**, 294 (1979), URL <https://doi.org/10.1143/PTP.61.294>.
- [KO79c] T. Kugo and I. Ojima, *Manifestly covariant canonical formulation of the Yang-Mills field theories III: Pure Yang-Mills theories without spontaneous symmetry breaking*, Prog. Teor. Phys. **61**, 644 (1979), URL <https://doi.org/10.1143/PTP.61.644>.
- [KPP97] F. Karsch, A. Patkós, and P. Petreczky, *Screened perturbation theory*, Phys. Lett. **B401**, 69 (1997), URL [https://doi.org/10.1016/S0370-2693\(97\)00392-4](https://doi.org/10.1016/S0370-2693(97)00392-4).
- [KW71] J. Kuti and V. F. Weisskopf, *Inelastic lepton-nucleon scattering and lepton pair production in the relativistic quark-parton model*, Phys. Rev. **D4**, 3418 (1971), URL <https://doi.org/10.1103/PhysRevD.4.3418>.
- [Lau66] B. Lautrup, *Canonical quantum electrodynamics in covariant gauges*, Mat. Fys. Medd. Dan. Vid. Selsk. **35**, 1 (1966).
- [Lav91] M. Lavelle, *Gauge-invariant effective gluon mass from the operator-product expansion*, Phys. Rev. **D44**, R26 (1991), URL <https://doi.org/10.1103/PhysRevD.44.R26>.

- [LLOWL10] L. Liu, H.-W. Lin, K. Orginos, and A. Walker-Loud, *Singly and doubly charmed $J = 1/2$ baryon spectrum from lattice QCD*, Phys. Rev. **D81**, 094505 (2010), URL <https://doi.org/10.1103/PhysRevD.81.094505>.
- [LM15] H.-W. Lin and H. B. Meyer, *Lattice QCD for Nuclear Physics*, Springer (2015), URL <https://doi.org/10.1007/978-3-319-08022-2>.
- [LMM⁺05] E. G. S. Luna, A. F. Martini, M. J. Menon, A. Mihara, and A. A. Natale, *Influence of a dynamical gluon mass in the pp and $\bar{p}p$ forward scattering*, Phys. Rev. **D72**, 034019 (2005), URL <https://doi.org/10.1103/PhysRevD.72.034019>.
- [LMMS16] T. Luthe, A. Maier, P. Marquard, and Y. Schroder, *Towards the five-loop beta function for a general gauge group*, J. High Energ. Phys. **2016**, 127 (2016), URL [https://doi.org/10.1007/JHEP07\(2016\)127](https://doi.org/10.1007/JHEP07(2016)127).
- [LMQ22] T. M. Liss, F. Maltoni, and A. Quandt, *Top quark*, Review of Particle Physics – Prog. Theor. Exp. Phys. **2022**, 083C01 (2022), URL <https://doi.org/ptep/ptac097>.
- [LS70] C. H. Llewellyn Smith, *Current-algebra sum rules suggested by the parton model*, Nucl. Phys. **B17**, 277 (1970), URL [https://doi.org/10.1016/0550-3213\(70\)90165-3](https://doi.org/10.1016/0550-3213(70)90165-3).
- [LS71] C. H. Llewellyn Smith, *Inelastic lepton scattering in gluon models*, Phys. Rev. **D4**, 2392 (1971), URL <https://doi.org/10.1103/PhysRevD.4.2392>.
- [LS88] M. J. Lavelle and M. Schaden, *Propagators and condensates in QCD*, Phys. Lett. **B208**, 297 (1988), URL [https://doi.org/10.1016/0370-2693\(88\)90433-9](https://doi.org/10.1016/0370-2693(88)90433-9).
- [LSWP98a] D. B. Leinweber, J. I. Skullerud, A. G. Williams, and C. Parrinello, *Asymptotic scaling and infrared behavior of the gluon propagator*, Phys. Rev. **D60**, 094507 (1998), URL <https://doi.org/10.1103/PhysRevD.60.094507>.
- [LSWP98b] D. B. Leinweber, J. I. Skullerud, A. G. Williams, and C. Parrinello, *Gluon propagator in the infrared region*, Phys. Rev. **D58**, 031501(R) (1998), URL <https://doi.org/10.1103/PhysRevD.58.031501>.
- [LW96] J. Liu and W. Wetzel, *Gluon-mass effects in quarkonia decays, e^+e^- annihilation and the scalar glueball current*, University of Heidelberg pre-print HD-THEP-96-47 (1996), URL <https://arxiv.org/abs/hep-ph/9611250>.
- [MBB⁺72] G. Miller, E. D. Bloom, G. Buschhorn, D. H. Coward, H. DeStaebler, J. Drees, C. L. Jordan, *et al.*, *Inelastic electron-proton scattering at large momentum transfers and the inelastic structure functions of the proton*, Phys. Rev. **D5**, 528 (1972), URL <https://doi.org/10.1103/PhysRevD.5.528>.
- [MLB22] A. V. Manohar, L. P. Lellouch, and R. M. Barnett, *Quark masses*, Review of Particle Physics – Prog. Theor. Exp. Phys. **2022**, 083C01 (2022), URL <https://doi.org/ptep/ptac097>.
- [MN00] A. Mihara and A. A. Natale, *Dynamical gluon mass corrections in heavy quarkonia decays*, Phys. Lett. **B482**, 378 (2000), URL [https://doi.org/10.1016/S0370-2693\(00\)00546-3](https://doi.org/10.1016/S0370-2693(00)00546-3).

- [MOU13] C. Michael, K. Ottnad, and C. Urbach, η and η' mixing from lattice QCD, Phys. Rev. Lett. **111**, 181602 (2013), URL <https://doi.org/10.1103/PhysRevLett.111.181602>.
- [MP71] G. Myatt and D. H. Perkins, *Further observations on scaling in neutrino interactions*, Phys. Lett. **B34**, 542 (1971), URL [https://doi.org/10.1016/0370-2693\(71\)90676-9](https://doi.org/10.1016/0370-2693(71)90676-9).
- [MPPS19] B. W. Mintz, L. F. Palhares, G. Peruzzo, and S. P. Sorella, *Infrared massive gluon propagator from a BRST-invariant Gribov horizon in a family of covariant gauges*, Phys. Rev. **D99**, 034002 (2019), URL <https://doi.org/10.1103/PhysRevD.99.034002>.
- [MW11] D. Mohler and R. M. Woloshyn, *D and D_s meson spectroscopy*, Phys. Rev. **D84**, 054505 (2011), URL <https://doi.org/10.1103/PhysRevD.84.054505>.
- [NAI+13] Y. Namekawa, S. Aoki, K.-I. Ishikawa, N. Ishizuka, K. Kanaya, Y. Kuramashi, M. Okawa, *et al.*, *Charmed baryons at the physical point in 2+1 flavor lattice QCD*, Phys. Rev. **D87**, 094512 (2013), URL <https://doi.org/10.1103/PhysRevD.87.094512>.
- [Nak66] N. Nakanishi, *Covariant quantization of the electromagnetic field in the Landau gauge*, Prog. Teor. Phys. **35**, 1111 (1966), URL <https://doi.org/10.1143/PTP.35.1111>.
- [Nat09] A. A. Natale, *QCD phenomenology with infrared finite SDE solutions*, PoS **QCD-TNT09**, 031 (2009), URL <https://doi.org/10.22323/1.087.0031>.
- [Ne'61] Y. Ne'eman, *Derivation of strong interactions from a gauge invariance*, Nucl. Phys. **26**, 222 (1961), URL [https://doi.org/10.1016/0029-5582\(61\)90134-1](https://doi.org/10.1016/0029-5582(61)90134-1).
- [Nie75] N. K. Nielsen, *On the gauge dependence of spontaneous symmetry breaking in gauge theories*, Nucl. Phys. **B101**, 173 (1975), URL [https://doi.org/10.1016/0550-3213\(75\)90301-6](https://doi.org/10.1016/0550-3213(75)90301-6).
- [Oji78] I. Ojima, *Observables and quark confinement in the covariant canonical formalism of Yang-Mills theory*, Nucl. Phys. **B143**, 340 (1978), URL [https://doi.org/10.1016/0550-3213\(78\)90029-9](https://doi.org/10.1016/0550-3213(78)90029-9).
- [OS12] O. Oliveira and P. J. Silva, *The lattice Landau gauge gluon propagator: Lattice spacing and volume dependence*, Phys. Rev. **D86**, 114513 (2012), URL <https://doi.org/10.1103/PhysRevD.86.114513>.
- [Pan68] W. K. H. Panofsky, *Electromagnetic interactions: Low q^2 electrodynamics; elastic and inelastic electron (and muon) scattering*, Proc. XIV Int. Conf. on High Energy Physics p. 23 (1968), URL <https://www.slac.stanford.edu/pubs/slacpubs/0500/slac-pub-0502.pdf>.
- [PEMP14] M. Padmanath, R. G. Edwards, N. Mathur, and M. Peardon, *Spectroscopy of triply charmed baryons from lattice QCD*, Phys. Rev. **D90**, 074504 (2014), URL <https://doi.org/10.1103/PhysRevD.90.074504>.

- [Per72] D. H. Perkins, *Neutrino interactions*, Proc. XVI Int. Conf. on High Energy Physics p. 189 (1972), URL <https://www.slac.stanford.edu/econf/C720906/papers/v4p189.pdf>.
- [Pol73] H. D. Politzer, *Reliable perturbative results for strong interactions?*, Phys. Rev. Lett. **30**, 1346 (1973), URL <https://doi.org/10.1103/PhysRevLett.30.1346>.
- [PP80] G. Parisi and R. Petronzio, *On low energy tests of QCD*, Phys. Lett. **B94**, 51 (1980), URL [https://doi.org/10.1016/0370-2693\(80\)90822-9](https://doi.org/10.1016/0370-2693(80)90822-9).
- [PRCB15] P. Pérez-Rubio, S. Collins, and G. S. Bali, *Charmed baryon spectroscopy and light flavor symmetry from lattice QCD*, Phys. Rev. **D92**, 034504 (2015), URL <https://doi.org/10.1103/PhysRevD.92.034504>.
- [PRS⁺17] M. Peláez, U. Reinosa, J. Serreau, M. Tissier, and N. Wschebor, *Small parameters in infrared quantum chromodynamics*, Phys. Rev. **D96**, 114011 (2017), URL <https://doi.org/10.1103/PhysRevD.96.114011>.
- [PRS⁺21a] M. Peláez, U. Reinosa, J. Serreau, M. Tissier, and N. Wschebor, *Spontaneous chiral symmetry breaking in the massive Landau gauge: realistic running coupling*, Phys. Rev. **D103**, 094035 (2021), URL <https://doi.org/10.1103/PhysRevD.103.094035>.
- [PRS⁺21b] M. Peláez, U. Reinosa, J. Serreau, M. Tissier, and N. Wschebor, *A window on infrared QCD with small expansion parameters*, Rep. Prog. Phys. **84**, 124202 (2021), URL <https://doi.org/10.1088/1361-6633/ac36b8>.
- [PS85] O. Piguet and K. Sibold, *Gauge independence in ordinary Yang-Mills theories*, Nucl. Phys. **B253**, 517 (1985), URL [https://doi.org/10.1016/0550-3213\(85\)90545-0](https://doi.org/10.1016/0550-3213(85)90545-0).
- [PS95] M. E. Peskin and D. V. Schroeder, *An Introduction to Quantum Field Theory*, CRC Press (1995), URL <https://doi.org/10.1201/9780429503559>.
- [PTW13] M. Peláez, M. Tissier, and N. Wschebor, *Three-point correlation functions in Yang-Mills theory*, Phys. Rev. **D88**, 125003 (2013), URL <https://doi.org/10.1103/PhysRevD.88.125003>.
- [PTW14] M. Peláez, M. Tissier, and N. Wschebor, *Two-point correlation functions of QCD in the Landau gauge*, Phys. Rev. **D90**, 065031 (2014), URL <https://doi.org/10.1103/PhysRevD.90.065031>.
- [PTW15] M. Peláez, M. Tissier, and N. Wschebor, *Quark-gluon vertex from the Landau gauge Curci-Ferrari model*, Phys. Rev. **D92**, 045012 (2015), URL <https://doi.org/10.1103/PhysRevD.92.045012>.
- [Ric74] B. Richter, $e^+e^- \rightarrow \text{hadrons}$, Proc. XVII Int. Conf. on High Energy Physics p. IV (1974), URL <https://www.slac.stanford.edu/pubs/slacpubs/1250/slac-pub-1478.pdf>.
- [Rot97] H. J. Rothe, *Lattice Gauge Theories*, World Scientific (1997), URL <https://doi.org/10.1142/5674>.

- [RST15] U. Reinosa, J. Serreau, and M. Tissier, *Perturbative study of the QCD phase diagram for heavy quarks at nonzero chemical potential*, Phys. Rev. **D92**, 025021 (2015), URL <https://doi.org/10.1103/PhysRevD.92.025021>.
- [RSTT17] U. Reinosa, J. Serreau, M. Tissier, and A. Tresmontant, *Yang-Mills correlators across the deconfinement phase transition*, Phys. Rev. **D95**, 045014 (2017), URL <https://doi.org/10.1103/PhysRevD.95.045014>.
- [RSTW14] U. Reinosa, J. Serreau, M. Tissier, and N. Wschebor, *Yang-Mills correlators at finite temperature: a perturbative perspective*, Phys. Rev. **D89**, 105016 (2014), URL <https://doi.org/10.1103/PhysRevD.89.105016>.
- [RSTW15a] U. Reinosa, J. Serreau, M. Tissier, and N. Wschebor, *Deconfinement transition in $SU(2)$ Yang-Mills theory: a two-loop study*, Phys. Rev. **D91**, 045035 (2015), URL <https://doi.org/10.1103/PhysRevD.91.045035>.
- [RSTW15b] U. Reinosa, J. Serreau, M. Tissier, and N. Wschebor, *Deconfinement transition in $SU(N)$ theories from perturbation theory*, Phys. Lett. **B742**, 61 (2015), URL <https://doi.org/10.1016/j.physletb.2015.01.006>.
- [RSTW16] U. Reinosa, J. Serreau, M. Tissier, and N. Wschebor, *Two-loop study of the deconfinement transition in Yang-Mills theories: $SU(3)$ and beyond*, Phys. Rev. **D93**, 105002 (2016), URL <https://doi.org/10.1103/PhysRevD.93.105002>.
- [RSTW17] U. Reinosa, J. Serreau, M. Tissier, and N. Wschebor, *How nonperturbative is the infrared regime of Landau gauge Yang-Mills correlators?*, Phys. Rev. **D96**, 014005 (2017), URL <https://doi.org/10.1103/PhysRevD.96.014005>.
- [RSVdW22] J. L. Rosner, S. L. Stone, and R. S. Van de Water, *Leptonic decays of charged pseudoscalar mesons*, Review of Particle Physics – Prog. Theor. Exp. Phys. **2022**, 083C01 (2022), URL <https://doi.org/ptep/ptac097>.
- [SB51] E. E. Salpeter and H. A. Bethe, *A relativistic equation for bound-state problems*, Phys. Rev. **84**, 1232 (1951), URL <https://doi.org/10.1103/PhysRev.84.1232>.
- [SBB⁺75] R. F. Schwitters, A. M. Boyarski, M. Breidenbach, F. Bulos, G. J. Feldman, G. Hanson, D. L. Hartill, *et al.*, *Azimuthal asymmetry in inclusive hadron production by e^+e^- annihilation*, Phys. Rev. Lett. **35**, 1320 (1975), URL <https://doi.org/10.1103/PhysRevLett.35.1320>.
- [SC18] F. Siringo and G. Comitini, *The gluon propagator in linear covariant R_ξ gauges*, Phys. Rev. **D98**, 034023 (2018), URL <https://doi.org/10.1103/PhysRevD.98.034023>.
- [SC21] F. Siringo and G. Comitini, *Thermal extension of the screened massive expansion in the Landau gauge*, Phys. Rev. **D103**, 074014 (2021), URL <https://doi.org/10.1103/PhysRevD.103.074014>.
- [SC22a] F. Siringo and G. Comitini, *Analytic continuation and physical content of the gluon propagator* (2022), URL <https://arxiv.org/abs/2210.11541>.

- [SC22b] F. Siringo and G. Comitini, *Nielsen identities in screened theories*, Phys. Rev. **D106**, 076014 (2022), URL <https://doi.org/10.1103/PhysRevD.106.076014>.
- [Sch51] J. Schwinger, *On the Green's functions of quantized fields*, PNAS **37**, 452 (1951), URL <https://doi.org/10.1073/pnas.37.7.452>.
- [Sch62a] J. Schwinger, *Gauge invariance and mass*, Phys. Rev. **125**, 397 (1962), URL <https://doi.org/10.1103/PhysRev.125.397>.
- [Sch62b] J. Schwinger, *Gauge invariance and mass II*, Phys. Rev. **128**, 2425 (1962), URL <https://doi.org/10.1103/PhysRev.125.397>.
- [SIMPS05] A. Sternbeck, E.-M. Ilgenfritz, M. Müller-Preussker, and A. Schiller, *Towards the infrared limit in $SU(3)$ Landau gauge lattice gluodynamics*, Phys. Rev. **D72**, 014507 (2005), URL <https://doi.org/10.1103/PhysRevD.72.014507>.
- [Sir15a] F. Siringo, *Perturbation theory of non-perturbative QCD* (2015), URL <https://arxiv.org/abs/1507.05543>.
- [Sir15b] F. Siringo, *Perturbative study of Yang-Mills theory in the infrared* (2015), URL <https://arxiv.org/abs/1509.05891>.
- [Sir16a] F. Siringo, *Analytic structure of QCD propagators in Minkowski space*, Phys. Rev. **D94**, 114036 (2016), URL <https://doi.org/10.1103/PhysRevD.94.114036>.
- [Sir16b] F. Siringo, *Analytical study of Yang-Mills theory in the infrared from first principles*, Nucl. Phys. **B907**, 572 (2016), URL <https://doi.org/10.1016/j.nuclphysb.2016.04.028>.
- [Sir17a] F. Siringo, *The dark side of the propagators: exploring their analytic properties by a massive expansion*, EPJ Web of Conferences **137**, 03021 (2017), URL <https://doi.org/10.1051/epjconf/201713703021>.
- [Sir17b] F. Siringo, *Dispersion relations for unphysical particles*, EPJ Web of Conferences **137**, 13017 (2017), URL <https://doi.org/10.1051/epjconf/201713713017>.
- [Sir17c] F. Siringo, *Quasiglueon lifetime and confinement from first principles*, Phys. Rev. **D96**, 114020 (2017), URL <https://doi.org/10.1103/PhysRevD.96.114020>.
- [Sir17d] F. Siringo, *Universal scaling of gluon and ghost propagators in the infrared*, EPJ Web of Conferences **137**, 13016 (2017), URL <https://doi.org/10.1051/epjconf/201713713016>.
- [Sir19a] F. Siringo, *Calculation of the non-perturbative strong coupling from first principles*, Phys. Rev. **D100**, 074014 (2019), URL <https://doi.org/10.1103/PhysRevD.100.074014>.
- [Sir19b] F. Siringo, *Yang-Mills ghost propagator in linear covariant gauges*, Phys. Rev. **D99**, 094024 (2019), URL <https://doi.org/10.1103/PhysRevD.99.094024>.

- [Sla72] A. A. Slavnov, *Ward identities in gauge theories*, *Theor. Math. Phys.* **10**, 99 (1972), URL <https://doi.org/BF01090719>.
- [SO04] P. J. Silva and O. Oliveira, *Gribov copies, lattice QCD and the gluon propagator*, *Nucl. Phys.* **B690**, 177 (2004), URL <https://doi.org/10.1016/j.nuclphysb.2004.04.020>.
- [SO10] P. J. Silva and O. Oliveira, *Unquenching the Landau gauge lattice propagators and the Gribov problem*, *PoS Lattice2010*, 287 (2010), URL <https://doi.org/10.22323/1.105.0287>.
- [SOBC14] P. J. Silva, O. Oliveira, P. Bicudo, and N. Cardoso, *Gluon screening mass at finite temperature from the Landau gauge gluon propagator in lattice QCD*, *Phys. Rev.* **D89**, 074503 (2014), URL <https://doi.org/10.1103/PhysRevD.89.074503>.
- [Sym70] K. Symanzik, *Small-distance behaviour analysis and power counting*, *Commun. Math. Phys.* **18**, 227 (1970), URL <https://doi.org/10.1007/BF01649434>.
- [Tay69] R. E. Taylor, *Inelastic electron-proton scattering in the deep continuum region*, *Proc. IV Int. Symp. on Electron Photon Interactions at High Energies* p. 251 (1969), URL <https://slac.stanford.edu/pubs/slapubs/0500/slac-pub-0677.pdf>.
- [Tay71] J. C. Taylor, *Ward identities and charge renormalization of the Yang-Mills field*, *Nucl. Phys.* **B33**, 436 (1971), URL [https://doi.org/10.1016/0550-3213\(71\)90297-5](https://doi.org/10.1016/0550-3213(71)90297-5).
- [TW10] M. Tissier and N. Wschebor, *Infrared propagators of Yang-Mills theory from perturbation theory*, *Phys. Rev.* **D82**, 101701 (2010), URL <https://doi.org/10.1103/PhysRevD.82.101701>.
- [TW11] M. Tissier and N. Wschebor, *An infrared safe perturbative approach to Yang-Mills correlators*, *Phys. Rev.* **D84**, 045018 (2011), URL <https://doi.org/10.1103/PhysRevD.84.045018>.
- [Tyu75] I. V. Tyutin, *Gauge invariance in field theory and statistical physics in operator formalism*, Preprint of the P. N. Lebedev Physical Institute N. 39 (1975), URL <https://arxiv.org/abs/0812.0580>.
- [Ver95] H. Verschelde, *Perturbative calculation of non-perturbative effects in quantum field theory*, *Phys. Lett.* **B351**, 242 (1995), URL [https://doi.org/10.1016/0370-2693\(95\)00338-L](https://doi.org/10.1016/0370-2693(95)00338-L).
- [VKVAV01] H. Verschelde, K. Knecht, K. Van Acoleyen, and M. Vanderkelen, *The non-perturbative groundstate of QCD and the local composite operator A_μ^2* , *Phys. Lett.* **B516**, 307 (2001), URL [https://doi.org/10.1016/S0370-2693\(01\)00929-7](https://doi.org/10.1016/S0370-2693(01)00929-7).
- [vRVL97] T. van Ritbergen, J. A. M. Vermaseren, and S. A. Larin, *The four-loop beta-function in Quantum Chromodynamics*, *Phys. Lett.* **B**, 379 (1997), URL [https://doi.org/10.1016/S0370-2693\(97\)00370-5](https://doi.org/10.1016/S0370-2693(97)00370-5).

- [vSHA97] L. von Smekal, A. Hauck, and R. Alkofer, *The infrared behavior of gluon and ghost propagators in Landau gauge QCD*, Phys. Rev. Lett. **79**, 3591 (1997), URL <https://doi.org/10.1103/PhysRevLett.79.3591>.
- [VSV97] H. Verschelde, S. Schelstraete, and M. Vanderkelen, *Nonperturbative calculation of the mass-gap in the Gross-Neveu model*, Z. Phys. **C76**, 161 (1997), URL <https://doi.org/10.1007/s002880050540>.
- [Wei95] S. Weinberg, *The Quantum Theory of Fields*, vol. 1, Cambridge University Press (1995), URL <https://doi.org/10.1017/CB09781139644167>.
- [Wei96] S. Weinberg, *The Quantum Theory of Fields*, vol. 2, Cambridge University Press (1996), URL <https://doi.org/10.1017/CB09781139644174>.
- [Wil69] K. G. Wilson, *Non-Lagrangian models of current algebra*, Phys. Rev. **179**, 1499 (1969), URL <https://doi.org/10.1103/PhysRev.179.1499>.
- [Wil74] K. G. Wilson, *Confinement of quarks*, Phys. Rev. **D10**, 2445 (1974), URL <https://doi.org/10.1103/PhysRevD.10.2445>.
- [YM54] C. N. Yang and R. Mills, *Conservation of isotopic spin and isotopic gauge invariance*, Phys. Rev. **96**, 191 (1954), URL <https://doi.org/10.1103/PhysRev.96.191>.
- [ZBDS⁺19] S. Zafeiropoulos, P. Boucaud, F. De Soto, J. Rodríguez-Quintero, and J. Segovia, *The strong running coupling from the gauge sector of Domain Wall lattice QCD with physical quark masses*, Phys. Rev. Lett. **122**, 162002 (2019), URL <https://doi.org/10.1103/PhysRevLett.122.162002>.
- [Zim70] W. Zimmermann, *Lectures on elementary particles and quantum field theory*, vol. 1, MIT Press (1970).
- [Zim85] W. Zimmermann, *Reduction in the number of coupling parameters*, Commun. Math. Phys. **97**, 211 (1985), URL <https://doi.org/10.1007/BF01206187>.
- [Zwa89] D. Zwanziger, *Local and renormalizable action from the Gribov horizon*, Nucl. Phys. **B323**, 513 (1989), URL [https://doi.org/10.1016/0550-3213\(89\)90122-3](https://doi.org/10.1016/0550-3213(89)90122-3).
- [Zwe64a] G. Zweig, *An $SU(3)$ model for strong interaction symmetry and its breaking*, CERN Report No. 8182/TH. 401 (1964), URL <https://cds.cern.ch/record/352337>.
- [Zwe64b] G. Zweig, *An $SU(3)$ model for strong interaction symmetry and its breaking II*, CERN Report No. 8419/TH. 412 (1964), URL <https://cds.cern.ch/record/570209>.

A note on the figures

Most of the figures displayed in Chapters 3 and 4 were reproduced from the published papers already cited in the introductions to those chapters and within the text (see Appendix C).

Acknowledgments

Although it is a (bad) habit of mine not to write acknowledgments in theses, this one would feel especially incomplete if I didn't express gratitude to the people without whom I would never have made it this far.

First and foremost, I would like to thank my parents for their unwavering support throughout these last years of Ph.D., and long before them for that matter. It is truly hard for me to imagine what person I would be today without their kindness and affection.

Then, I would like to thank Fabio Siringo for the supervision and opportunities he provided me with since we started working on the Screened Massive Expansion. It feels like yesterday I entered his office seeking for a research topic for my Bachelor's thesis, and here we are now, years later, still looking for ways to make QCD work.

Furthermore, I would like to thank David Dudal both for his supervision on the Dynamical Model and for being a terrific host during the months spent in Kortrijk as part of the joint Ph.D. between Catania and Leuven. Despite the complications due to the pandemic, he managed to make me feel at home while being miles away.

Last, but absolutely not least, I need to express my gratitude to Cinzia for having had the patience to bear with me during these last few months. I am sorry I was not there at critical times, when you needed it the most. I will never be able to repay you enough for your understanding.